BNL--52262

DE91 004920

Fourth Workshop on Experiments and Detectors for a Relativistic Heavy Ion Collider

July 2-7, 1990

Edited by M. Fatyga and B. Moskowitz

BROOKHAVEN NATIONAL LABORATORY
ASSOCIATED UNIVERSITIES, INC.
UPTON, LONG ISLAND, NEW YORK 11973

UNDER CONTRACT NO. DE-AC02-76CH00016 WITH THE
UNITED STATES DEPARTMENT OF ENERGY

Printed in the United States of America
Available from
National Technical Information Service
U.S. Department of Commerce
5285 Port Royal Road
Springfield, VA 22161

NTIS price codes:
Printed Copy: A21; Microfiche Copy: A01

PREFACE

These are the Proceedings of the Fourth Workshop on Experiments and Detectors for a Relativistic Heavy Ion Collider (RHIC), held at Brookhaven National Laboratory on July 2 - 7, 1990. This has been a particularly important workshop for the RHIC program, given the earlier announcement that the BNL RHIC project had been included in the President's proposed FY1991 budget as a new construction item. A call for letters of intent for RHIC experiments was formally issued by the BNL Director's Office at the annual AGS User's Meeting in May, and was repeated at the RHIC Workshop. Approximately 180 physicists from around the world attended the workshop, with the main goal of forming collaborations to prepare and submit letters of intent.
The presentations given at the workshop naturally divide themselves into four categories: theory, the study groups devoted to a single topic ,the RHIC R & D projects, and the experimental working groups.

The study groups, with the names of the conveners in parentheses, were:

- Collision Regions at RHIC: Beam Crossing Geometries, Layout of Experimental Areas, and Radiation Environment (A. Stevens)
- Monte Carlo Simulation of Interactions and Detectors (O. Hansen)
- Proton-Nucleus Interactions at RHIC (R. Ledoux)
- The Physics of Very Intense Electromagnetic Fields in the Collision of Ultrarelativistic Heavy Ions (M. Fatyga)

The experimental working groups, with the names of the conveners in parentheses, were:

- A Modular Array for RHIC Spectra (W. Busza)
- High p_t Photons, Charged Particles, Jets and High Mass e+e- Pairs at RHIC (P. Braun-Munzinger)
- Elastic Cross-section Measurements at RHIC (W. Guryn)
- Two-Arm Lepton Spectrometer (R.Hayano and M.J.Tannenbaum)
- A Particle and Jet Production Experiment at RHIC (J. Harris)
- A 4π Tracking TPC Spectrometer for RHIC (S. Lindenbaum)
- Open Focusing Spectrometer (S. Nagamiya and D. Lissauer)
- Dimuon Working Group (G. Young)

On behalf of the Organizing Committee we wish to thank all of the conveners, contributors and participants for making this a very exciting and successful workshop. Special thanks go to all of those who helped in organizing the workshop, in particular, Bonnie Sherwood, Patricia Tuttle, Isabelle Harrity and Marie Gavigan. Thanks also go out to

the BNL Staff Services, especially Patrick Glynn, for providing food and drink during a holiday week.
The help of the BNL Graphics and Illustration Department in preparing these proceedings for publication, and the assistance of Ziping Chen in the cover design, are most gratefully acknowledged.

Mirek Fatyga

Bruce Moskowitz

(editors)

TABLE OF CONTENTS


LAW

Fourth Workshop

on

Experiments and Detectors for a

Relativistic Heavy Ion Collider

July 2-7, 1990

Brookhaven National Laboratory

Advisory Board:

H.Gutbrod GSI, Darmstadt

M.Gyulassy LBL

R.Hayano U.Tokyo

J.Harris LBL

T.Humanic U.Pittsburgh

B.Jacak LANL

G.London CEN – Saclay

T.Matsui MIT

H.Satz CERN

P.Seyboth MPI, Munich

J.Stachel Stony Brook

G.Young ORNL

W.Zajc Columbia U.

Organizing Committee:

T.Ludlam (Chairman), B.Sherwood (Secretary),

C.Dover, M.Fatyga, B.Moskowitz, M.Sakitt.

LIST OF PARTICIPANTS
RHIC WORKSHOP
July 2-7, 1990

Y. Akiba, Univ. of Tokyo
N. Amelin, Univ. of Bergen
B.A. Andersson, SUNY at Stony Brook
S.H. Aronson, BNL
Z.J. Azzam, MIT
A.J. Baltz, BNL
D.R. Beavis, BNL
P.D. Beery, Univ. of Calif. - Riverside
R. Belliwied, SUNY at Stony Brook
O. Benary, BNL
C.A. Bertulani, Univ. Fed. do Rio de Janeiro
N. Biswas, Notre Dame Univ.
G. Blanar, LeCroy Corp.
J.G.J. Boissevain, LANL
P. Bond, BNL
P. Braun-Munzinger, SUNY at Stony Brook
H.C. Britt, LLNL
W. Busza, SLAC
A.S. Carroll, BNL
J. Carroll, LBL
C-S. Chan, BNL
C. Chasman, BNL
Z. Chen, BNL
J. Chiba, KEK, Tsukuba
S-U. Chung, BNL
W.E. Cleland, Univ. of Pittsburgh
T.M. Cormier, Texas A&M Univ.
M. Danos, Nat'l. Inst. for Standards & Technology
G. David, SUNY at Stony Brook
R.R. Debbe, BNL
O. Dietzsch, BNL
H. Enyo, Kyoto Univ.
J.R. Erskine, U.S. DOE
A. Etkin, BNL
M. Fatyga, BNL
K. Foley, BNL
D. Fox, LANL
L. Frankfurt, Leningrad Nucl. Phys. Inst.
S-Y. Fung, Univ. of Calif. - Riverside
A. Gavron, LANL
A. Goldhaber, SUNY at Stony Brook
M. Goldhaber, BNL
H.A. Gordon, BNL
S.V. Greene, Yale Univ.
W. Guryn, BNL
S.E. Gushue, BNL
H-A. Gustafsson, Univ. of Lund
L.J. Gutay, Purdue Univ.
H.H. Gutbrod, CERN
R.W. Hackenburg, BNL
H. Hahn, BNL
C. Halliwell, Chicago, Ill.
T. Hallman, Johns Hopkins Univ.
H. Hamagaki, BNL
O. Hansen, BNL
J.W. Harris, LBL
R.S. Hayano, Univ. of Tokyo
S. Hayashi, BNL
T.K. Hemmick, Yale Univ.
D.L. Hendrie, U.S. DOE
S.F. Heppelmann, Penn State Univ.
A. Hershcovitch, BNL
J.C. Hill, Iowa State Univ.
A.S. Hirsch, Purdue Univ.
T.J. Humanic, Univ. of Pitts.
B.V. Jacak, LANL
P.M. Jacobs, LBL
K. Kadija, Inst. Ruder Boskovic
S.H. Kahana, BNL
J.H. Kang, Univ. of Calif. - Riverside
W.L. Kehoe, MIT
R. Klanner, DESY
D. Kovar, U.S. DOE
M.A. Kramer, BNL, CCNY
K. Kurita, Columbia Univ.
R.J. Ledoux, MIT
S-Y. Lee, BNL
M.J. Leitch, LANL
P. Levai, Duke Univ.
S.J. Lindenbaum, BNL, CCNY
D.A. Lissauer, BNL
R.S. Longacre, BNL
W.A. Love, BNL
T.W. Ludlam, BNL
L. Madansky, Johns Hopkins Univ.
C.F. Maguire, CNR, Vanderbilt Univ.
S. Majewski, CEBAF
M. Masera, Torino
T. Matsui, MIT
P.L. McGaughey, LANL
R. McGrath, SUNY at Stony Brook

LIST OF PARTICIPANTS
(continued)
RHIC WORKSHOP
July 2-7, 1990

B.A. Mecking, CEBAF
Y. Miake, BNL
J.T. Mitchell, Yale Univ.
T.W. Morris, BNL
R.J. Morse, MIT
W. Morse, BNL
B.E. Moskowitz, BNL
B. Mueller, Duke Univ.
G.S. Mutchler, Rice Univ.
S. Nagamiya, Nevia Labs., Columbia
K. Nakai, KEK, Tsukuba
C.J. Naudet, LBL
T. Nayak, Nevis Labs.
J.W. Norbury, Rider College
E.J. O'Brien, BNL
F.E. Obenshain, ORNL
G. Odyniec, LBL
D.L. Olson, LBL
S. Ozaki, BNL
J. Piekarz, Fermilab
R.D. Pisarski, BNL
F. Plasil, ORNL
E. Platner, BNL
V.A. Polychronakos, BNL
A.M. Poskanzer, LBL
S.D. Protopopescu, BNL
C.A. Pruneau, BNL
J. Rafelski, Univ. of Arizona
L.P. Remsberg, BNL
M.J. Rhoades-Brown, BNL
C.R. Richardson, U.S. DOE
H.G. Ritter, LBL
L. Roberts, Boston Univ.
G.R. Roche, LBL
B. Rubin, Nevis Labs.
A.G. Ruggiero, BNL
S. Saini, ORNL
M. Sakitt, BNL
H. Sakurai, Univ. of Tokyo, BNL
A.K. Sambaburti, BNL
N.P. Samios, BNL
H. Sano, Osaka Univ.
A.C. Saulys, BNL
R.P. Scharenberg, Purdue Univ.
L.S. Schroeder, LBL
P.A. Seidl, LBL
R.K. Seto, Nevis Labs. Columbia
P.F. Seyboth, Max-Planck Inst.
B. Shivakumar, Yale Univ.
E. Shuyrak, BNL
W.E. Sondheim, LANL
B.K. Srivastava, Purdue Univ.
J. Stachel, SUNY at Stony Brook
S.G. Steadman, MIT
G.S.F. Stephans, MIT
A.J. Stevens, BNL
M. Strickman, Leningrad Nucl. Inst.
D. Strottman, LANL
T. Sugitate, Hiroshima Univ.
T. Suzuki, Riken, Linac Lab.
J. Symons, LBL
M. Takagui, BNL
H. Takai, BNL
M. Tanaka , BNL
M.J. Tannenbaum, BNL
J. Thomas, LLNL
T.G. Throwe, BNL
M.L. Tincknell, ORNL
T.L. Trueman, BNL
I. Tserruya, CERN
J.H. VanDijk, BNL
A.J. VanGinneken, Fermilab
F. Videbaek, BNL
B. Wadsworth, MIT
F. Wang, Columbia Univ.
X.N. Wang, LBL
Y. Wang, Nevis Labs.
L.S. Waters, SUNY at Stony Brook
H.E. Wegner, BNL
G.D. Westfall, Michigan State Univ.
H.H. Wieman, LBL
W.J. Willis, CERN
K.L. Wolf, Texas A&M Univ.
C. Woody, BNL
J. Wu, ORNL
Y. Wu, Nevis Labs., Columbia
N. Xu, SUNY at Stony Brook
B.T. Yost, LeCroy Corp.
G.R. Young, ORNL
W.A. Zajc, Nevis Labs., Columbia
K. Zhao, BNL

RHIC WORKSHOP
Physics Department Auditorium, Bldg. 510
July 2-7, 1990
AGENDA

Monday, July 2
8:15 - 9:00 Registration

Morning Session (Chairman, P. Bond)

9:00	Welcome	N.P. Samios
9:15	Overview of RHIC	S. Ozaki
9:45	Letters of Intent	T.L. Trueman
10:00	Physics at RHIC	E. Shuryak
10:45	Break	
11:00	Issues and Plans for the Workshop	T. Ludlam
11:30	Brief reports from the Study Groups:	
	- Simulation Group	O. Hansen
	- Collision Regions	A. Stevens
	- Proton-Nucleus	R. Ledoux
	- EM Interactions	M. Rhoades-Brown
12:15	Lunch	

Afternoon Session (Chairman, T. Ludlam)

1:30 - 5:00 Presentations by Convenors of Experimental Working Groups. (20 minutes each)

W. Busza
S. Lindenbaum
L. Gutay
M. Tannenbaum
P. Braun-Munzinger
S. Nagamiya
G. Young
J. Harris
R. Hayano
W. Guryn

5:00 - 6:00 Working Group Sign-up session: Lobby of Auditorium

Working Groups Meet.

Tuesday, July 3

9:00 - 10:30	Theory Presentations (Chairman W. Busza)	
	1. J/ψ Production	T. Matsui
	2. Di-Lepton Production	R. Pisarski
10:30 - Noon	Working Groups meet	
	Simulation group has working lunch.	
1:30 - 6:00	Detector R&D Presentations (Chairman L. Schroeder)	
	(25 min. each: 18 min. + discussion)	
	Cleland	
	Seidl	
	O'Brien	
	Polychronakos	
	Platner	

Ritter
Wadsworth
Alley
Young
Nagamiya

Tuesday Evening Working groups meet, if desired.
Detector Advisory Committee meets. (closed session)

Wednesday, July 4

9:00 - 10:30 Theory Presentations (Chairman H.C Britt)
1. Jets in Heavy Ions — X.N. Wang
2. Flavor Flow and QGP: Contact between Theory and Experiment — J. Rafelski

10:45 - 12:15 Study Group Presentations (Chairman F. Plasil)
- Proton/Nucleus — R. Ledoux
- EM Interactions — M. Fatyga
- Collision Regions — A. Stevens
- KEK Collider Workshop — J. Chiba

12:15 - 1:30 Lunch at Cafeteria

Wednesday Afternoon Working Groups Meet

Wednesday Evening Free

Thursday, July 5

9:00 - 10:30 Theory Presentations (Chairman A. Poskanzer)
1. Parton Distributions in Hard Nuclear Collisions — M. Strickman
2. QCD Treatment of Nuclear Collisions at RHIC Energies — B. Mueller

10:45 - Noon Working Groups Meet

Thursday Afternoon Working Groups Meet

Thursday Evening
5:15 Cocktails - Lobby at Berkner Hall (Compliments of AUI)
6:00 Banquet - Cafeteria
8:00 Cavani String Quartet at Berkner Hall

Friday, July 6

Totally Free for Working Group Meetings

Saturday Morning, July 7 (Chairman H. Gutbrod)

9:00 - 9:45	Closing remarks by BNL and RHIC Project management; discussion.
10:00 - 12:30	Progress reports by Experimental Working Groups

---

Theory Talks

Contents:

Physics at RHIC

E.V. Shuryak

Physics Department
Brookhaven National Laboratory
Upton, New York 11973

ABSTRACT

This Introductory talk contains a brief discussion of future experiments at RHIC related to physics of superdense matter. In particular, we consider the relation between space-time picture of the collision and spectra of the observed secondaries. We discuss where one should look for QGP signals and for possible manifestation of the phase transition. We pay more attention to a rather new topic: hadron modification in the gas phase, which is interesting by itself as a collective phenomenon, and also as a precursor indicating what happens with hadrons near the phase transition. We briefly review current understanding of the photon physics, dilepton production, charm and strangeness and J/ψ suppression. At the end we try to classify all possible experiments.

1. Introduction

Starting this Introductory talk at the 4-th RHIC Workshop, I should probably not go into detailed discussions of the QCD-based theory of excited hadronic matter which has essentially inspired the RHIC project. These theoretical expectations, especially phase transitions into the so–called quark-gluon plasma (QGP) have been discussed in a number of reviews[1]. I am sure their main ideas are known to participants of the workshop, at least all of them probably have the RHIC Conceptual Design Book[2].

Facing our experimental colleagues who came to Brookhaven with intentions of discussing RHIC detectors, I should probably not go into discussion of either current results of BNL and CERN experiments, or their interpretation, and I will do so only if it is relevant for RHIC. Many interesting ideas were suggested during the last decade, some of them are in agreement with observations, but we are still very far from real understanding of exact

properties of excited matter produced in these experiments. For discussions the reader may see proceedings of latest Quark Matter conferences[3] and previous RHIC Workshops[4].

Planning a completely new round of experiments, we have to formulate once more their main goals and select the main observables. Now we have to face difficult questions of priority and the feasibility of different experiments. Certainly it is not an easy task, especially for such a potentially rich field as "RHIC physics", but now we have to do our best. Many of the important questions are still open and we have to formulate them now, as homework for the next workshop.

Let me start with one very general remark, looking at RHIC physics in wider perspective. Nowdays, when all branches of science are becoming more and more specialised, we witness surprising phenomenon in physics of strong interactions. Two communities, a part of the high energy one doing hadronic physics and nuclear physicists, are obviously merging. RHIC is the most important example of such trend, but it is not the only one: one can just pick up a volume of Nucl. Phys. B and A (or Phys. Rev. C and D) to become convinced that many papers in them discuss essentially the same physics. However, such convergence after decades of independent existence is probably not so surprising, if we formulate the main goal of all this activity as: "Understanding QCD".

In fact, two more communities also address the same questions. I mean (unfortunately, not so numerous) theorists, trying to understand QCD as quantum field theory, and also "numerical experimentalists" working with lattice gauge theory. These people have formulated a more specific goal as a reasonable first step: "To understand the structure of the QCD vacuum". Indeed, studying any complicated quantum system, one should probably begin with its ground state.

However, experiments can only work with excitations. Those can be divided into two main categories: "microscopic" and "macroscopic" ones, depending on whether the total energy or energy density is fixed. The former is traditional "particle physics", doing hadronic spectroscopy and reactions, while at RHIC we hope to study the latter ones. But why do we need to study macroscopic excitations?

The reason is simple: we hope that they are simpler to understand. Pions, nucleons and other hadrons are but collective excitations, like phonons in solids. Therefore, in order to understand their spectra, scattering amplitudes etc. we have to know many

details about the structure of matter. However, melting of solids into some liquid can be predicted, without much knowledge, from general considerations. Quite similarly, general considerations suggest that at temperatures above about 200 MeV, the QCD vacuum is "melted", changing its properties and a completely new phase of matter is expected. One of the main goals of RHIC is to test this prediction of QCD.

In connection to this, let me discuss one point from the history of physics. About a century ago people faced the strange world of atoms. As we now know, the key to it was quantum mechanics. And we also know (and should explain it to curious students), this key was found in a strange way: instead of working on the simplest atoms and their spectra, some people have concentrated on a kind of side problem, that of "black body radiation". They have made nice experiments, and in the fit to these data the Planck constant was first introduced. Was it a logical development or just an occasional event?

I think it was very much logical: free field in the cavity is indeed much simpler than atoms, that is why Planck could guess the answer. Also to measure the energy density of the "excited vacuum" (as we will call it now) at given T was indeed simpler than to work with individual photons.

In many respects, we now have a similar situation in non-perturbative QCD. Its best quantitative prediction available is probably the lattice measurements of the energy density $\epsilon(T)$. It is very difficult to calculate accurately such quantities like the proton mass, and nobody knows how to calculate pp cross section at high energies. Therefore, we cannot compare accurate measurements of these quantities with the theory. So, if theorists cannot calculate what experiments have already measured, new experiments are needed to measure what they can do.

These general considerations have practical consequences. We hope that AA collisions, producing "macroscopic" excited systems, are easier to understand than pp collisions. Let me discuss this point in greater detail, for it always creates a lot of confusion.

We do not have a real theory of pp collisions. There exist only some models, fitting the pp data with several parameters. We hope the picture of color strings breaking, etc. is correct, but it is still far from being a solid fact. Of course, we use the "event generators"based on these models in order to get some ideas of what to expect in the AA case, but certainly we are not making these experiments in order to test their predictions. (By

the way, most of these models are certainly flexible enough to fit practically any data to appear. But, unfortunately, their parameters do not have any direct connection to the fundamental theory, so I do not think much understanding will come out of such fit. We have had plenty of examples of such kinds before.)

In other words, coming from *pp* to AA we are not looking for additional complications: on the contrary, we hope that the macroscopic system is insensitive to many details of the dynamics (e.g., of the initial wave function of colliding nucleons) and is therefore much simpler. The main hope is that we will manage to extract quantities like equation of state (EOS) in a model-independent way, and then compare it with accurate predictions of QCD.

Completing the introduction, one more general comment about connection of *pp* and AA collisions. Many people have defined "new phenomena" in AA as something radically different from what is seen in *pp*. However, such an attitude is a little bit dangerous. What we are going to do is to make systematic studies of this new field without any prejudice. We are not looking for miracles, and, after all, nucleons are made out of the same quarks and gluons.

Let me give an example, explaining what I mean. CERN experiments with ^{16}O, ^{32}S beams have produced about the same p_t spectra as the *pp* ones. Some people were discouraged saying that "nothing new is observed". That is certainly wrong: now theorists should determine why *pp* spectra happened to be of such shape that rescattering of secondaries (which are by no means negligible) does not change them.

2. Main goals of RHIC experiments

Let me formulate the main goals of RHIC experiments as follows:

1. Produce as macroscopic system of hadrons as possible;
2. Perform detailed studies of properties of hadronic matter at energies densities $\epsilon < \epsilon_0$ (about 1 GeV/fm^3);
3. Study matter properties at the highest available energy densities ($\epsilon \gtrsim 3$ GeV/fm^3) and check whether it is indeed the QGP.
4. Study hard processes and initial thermolisation.

5. Study properties of the phase transition region (the value of T_c, the first or the second order, etc.);

Note, that these topics are listed in order of increasing difficulty. Let me make some general comments about all of them.

The point (1) is no longer a problem if RHIC is built: at central Au Au collisions several thousands of pions will be produced. At breakup the size of this system is expected to be 20 – 30 fm. At the stage just preceeding breakup this system is certainly larger than mean free paths of particles, so there is little doubt that macroscopic considerations are relevant for its description. In terms of multiplicity, it is a significant step forward from present BNL and CERN experiments. (By the way, the future LHC project can hardly increase dn/dy significantly, for it grows with energy only logarithmically.)

Comments for the point (2): hadronic phase takes most of the space-time volume available, with energy density changing from about 1 to 0.03 GeV/fm^3. This field was not studied much in the past, but potentially it is at least as rich as nuclear physics (only that nuclear matter is mainly fermionic and this one mainly consists of mesons). Many interesting phenomena are expected here: in particular, mesons become quasiparticles, modified in matter. Detection of these modifications is certainly one of the most interesting ways of testing whether we really approach chiral phase transition. We come to that in sections 6 and 7.

Looking for QGP we have to rely on "penetrating probes", photons and dileptons (see sections 9, 10). Their production rates are calculable with reasonably good accuracy, so we have some estimates of the expected yields. J/ψ and in particular ψ' suppression is also important in this respect, although many complicated phenomena may affect it (see section 12).

Hard collisions of partons, then the so–called higher twist effects (parton rescattering) etc. until initial approximate parton thermolisation is a separate field of investigation. We discuss it in section 14.

I put point (5) above, although at the moment it is difficult to indicate what particular measurements (if any) can be sensitive to the phase transition region. Some speculation can be found in section 8.

3. Space-time picture of the collisions

All general discussions of heavy ion collisions inevitably start with space-time evolution of the system and the values of parameters involved at its different stages. Let me also define four characteristic time values (having in mind Au Au 100*100 GeV collisions):

1. $\tau_{\rm passing} \sim R/\gamma \sim 1/10$ fm.
2. $\tau_{\rm mixing} \sim 0.3 - 1$ fm.
3. $\tau_{\rm p.t.} \sim 2 - 4$ fm.
4. $\tau_{\rm breakup} \sim 30$ fm.

During the time $\tau_{\rm passing}$ two Lorentz-contracted nuclei pass each other, the energy density is huge $\epsilon \sim 30$ GeV/fm^3, but most of the partons just move ahead, with only rare hard collisions taking place.

By definition, $\tau_{\rm mixing}$ is the (proper) time, at which scattering probability of co-moving quarks and gluons become of the order O(1). Optimists (including myself[6]) use perturbative estimates for gg scattering and get lower value, while more conservative people use the Bjorken guess of 1 fm. Depending on that, we may say that "matter" in more or less equilibrated form appears at RHIC at energy density not larger than 10-3 GeV/fm^3. Still we have chances to see the QGP.

However, it does not exist long, and already at $\tau_{\rm p.t.}$ indicated above we come to the "mixed phase". Therefore, a gluon may happen to be scattered about 10 times in QGP, but a quark may be scattered just several times. Certainly simple estimates of QGP kinetics in Ref. 6 should be made much more detailed. Perturbative QCD provides estimates for all possible types of processes, not only of rescattering of partons, but also of their production and recombination. B. Muller with collaborators has started "partonic cascades" for RHIC, and I hope at the next workshop we will have more detailed ideas of how well equilibrated QGP can really be.

One more important comment. If we indeed have strong first order transition, the system comes to mixed phase in ordinary sense, a mixture of two phases. If not (and the latest lattice results show it is most probably the case), it is mixed in the sense that none of the simple description (in hadronic or quark language) is valid here. In this region the equation of state is such, that increasing the energy density by a large factor we increase

temperature very little (if any). The physical reason for that is that the number of effective degrees of freedom is rapidly changing under these conditions, so most of the energy density change is related to it. We return to this point below.

At $\tau_{\rm breakup}$ hadrons become independent, and this stage corresponds to the energy density $\epsilon \sim .03$ GeV/fm^3. In other terms, each pion occupies a volume of about 6-8 fm^3, as nucleons in nuclear matter. Although pions interact weaker than nucleons, and although they still have temperature of about 120 MeV or so, even at this point it is not exactly the ideal gas of pions, as it is often assumed. It is obviously not so at more dense hadronic matter, probably it is much more like liquid[5].

Summarising, we have expanding matter with the energy density changing by about two orders of magnitude! Certainly, it is a very rich field for investigations, but let me add one more "experimental dimension" to it. One experimental year (10^7 sec) is about 10^{13} central collisions, which puts limitations on what we can observe.

4. Different stages versus different kinematic regions

While trying to understand how all these stages of matter evolution are connected to observed spectra of secondaries, people often use the following assumptions:

1. Particles emitted at certain stage with temperatures T have momenta of the order T.
2. Thermal spectra are always exponential, with the slope given by the corresponding temperature T.

As we will show shortly, due to expansion of the system both are not exactly true, and the difference is of importance for planned experiments.

The space-time picture of the collision is complicated enough, and in order to come to some conclusions we have to simplify it. One radical way of understanding all this[6] is to view the whole process in terms of "temperature history". Assuming local thermal equilibrium we may describe all properties of matter by one variable T. It is still a function of space and time, but the probablity of any reaction of interest P per collision can be put in the following form:

$$P = \int d^4x W_{\rm reaction}(x) = \int F(T)\, W_{\rm reaction}(T)\, dT$$

where universal function $F(T)$, the so–called "temperature profile", cont ins all information about the space-time evolution. The function $W_{\rm reaction}(T)$ depends on "matter properties" and can be considered separately.

I do not have here a place to derive any formulae, but I want to explain what these functions look like and the implications this has to the experiments at RHIC. The typical shape of the "temperature profile" $F(T)$ (incorporating our understanding of expansion and E.O.S.) has three main components:

1. Huge peak near the break-up temperature where most of the secondaries become free, with strongly decreasing tail toward larger T, like T^{10} (the power comes essentially from the E.O.S. of the pion gas);
2. a peak at critical temperature T_c, where the system spends much more time than at any other value (this statement is true independent of whether or not we indeed have mixed phase and first order transition);
3. QGP region, in which $F(T)$ falls further as T^7 till the value of the initial temperature T_i, above which there is no equilibrium and the concept of T is meaningless.

Summarising: $F(T)$ is the strongly decreasing function of T: powers involved are large. Now we look for another ingredient of our integral $W_{\rm reaction}(T)$ which, on the contrary, is typically a rapidly increasing function of T. For example, production of dilepton with invariant mass M goes as $dW/dM \sim M^{3/2}\exp(-M/T)$, and similar Boltzmann factor appears in production of a photon or a hadron with large transverse momentum, etc.

The central point: their product shows a very sharp peak at some T. This observation leads to several important conclusions. First, observing e.g. dileptons with given mass M, we actually probe the matter at a very specific stage of its evolution, namely at $T(M) = M/b$ where b is a constant. The interplay of rapid expansion and strong Boltzmann factor suppression results in very strong suppression of both earlier or later stages.

Second, the ratio b of the observed M, p_t and relevent T is not of the order one, as one may naively guess (see point 1 at the beginning of this section). It actually depends on the process, but usually it is about 6 for QGP and 9 for hadronic phase. Therefore, if we are interested in particles emitted e.g. at phase transition ($T = 200$ MeV), we have to

look at M, p_t as big as 1.2-1.8 GeV. The hottest stage at RHIC is expected to correspond to $T_i = 300 - 400$ MeV: from our simple "rule of thumb" given above, we get that QGP component should be dominant at M, p_t about 2–3 GeV. Detailed evaluation of various processes (including direct parton scattering, such as the Drell-Yan reaction for dileptons) more or less confirmed this simple estimate.

Third, after integration over the temperature history we do not get simple thermal exponential spectra (point 2 above), but have instead spectra which have rather power-like behaviour. (The only exception is the "mixed phase" contribution, which should really give exponential ones, with $\exp(-p_t/T_c)$.)

Summarising this discussion, going down in probablity we actually travel from the final toward the initial stages of evolution of the system. On the way we meet contributions of various components. Is it possible to separate them experimentally? Can one notice any changes in the production mechanism, as he scans the kinematical region? In particular, is it possible to reveal the exponential contribution corresponding to T_c, among so many others? Future experiments will try to answer these questions.

5. Mean p_t and collective flow at RHIC

Transverse collective flow of excited matter is certainly the most obvious method to measure the equation of state, pressure versus energy density $p(\epsilon)$. In this audience I probably should not remind about the complicated history, describing how this idea was put into reality at BEVALAC energies.

However, at higher energies the situation with observability of the flow is much more difficult. Even if one takes the original Landau model, with naive equation of state $p = (1/3)\epsilon$, it was shown by Milekhin in the '60's that expansion affect $< p_t >$ very little, it grows with energy, but only as $s^{1/12}$.

Later it was realised[7,8] that when one approaches the phase transition region the equation of state becomes very "soft" ($p \ll \epsilon$), so even much smaller flow velocity is expected unless the initial energy density significantly exceeds that needed for QGP formation.

Explicit calculations of hydro expansion with the bag-model type EOS[9] gave predictions shown in Fig. 1(a). The existence of some plateau in its middle is the consequence of softness of EOS in the "mixed phase".

Independence of mean p_t on E_t or multiplicity was indeed observed by CERN experiments. The first data which (I hope) show some QGP flow are TEVATRON data which were first discussed in Lenox. Now this group has much better data for identified secondaries[10], see Fig. 1(b) . Selecting large multiplicity events in 1.8 TeV $p\bar{p}$ interaction, they have shown that $< p_t >$ of heavier secondaries start to grow with multiplicity, if N_c exceeds about 100. The shape of their observed dependence is provocatively similar to hydro calculations. These events indeed correspond to very high initial energy density, much exceeding critical ones for QGP formation. (Note also, that such growth is contrary to the obvious kinematic effects, as well as the "mini-jet" type models for the large p_t tail: small jets in few GeV e^+e annihilation are very poor in nucleons and lambdas, so their production should rather affect mesonic spectra, not baryonic ones as observed.)

Can these effects be studied at RHIC? The standard event has $(1/A)dn/dy \sim 3$, and selecting special Au-Au events we can, perhaps, go to twice larger values. Comparing this to the theoretical predictions and data given above, one can see that this is still essentially smaller than what is needed for significant flow and smaller than those reached at TEVATRON. However, if the statement about "no flow" can be made strong enough at RHIC, it will be very important.

Of course, this question should be studied in cascades first, but I think Au-Au collisions will not fluctuate much. Also, as we need for the flow large energy density and not necessarily very big systems (let me remind here, that flow is caused not just by pressure, but by the pressure gradient), it is probably also reasonable to try pp mode at RHIC (or, maybe He-He?), using an extra few orders of magnitude in the number of collisions for triggering for much stronger fluctuations.

6. Spectra at smallest p_t and physics of the "pion liquid"

Whether or not QGP will be produced at RHIC, there certainly will be thousands of pions per event. At break-up these hadronic systems will reach radii 20-30 fm, so they are significantly larger than the heaviest nuclei. In some sense this is "another nuclear physics", only with mesons instead of baryons and density decreasing with time. We expect collective effects like common potential well, so familiar in nuclear context. Certainly, properties of this kind of matter should be investigated.

In the past, hadronic matter at finite temperatures has not been studied much, as it was considered to be the "known and next-to-trivial physics". However, recent theoretical development as well as data from CERN and Brookhaven has shown it is very far from being correct. In particular, it was expected theoretically that at the breakup this matter is nothing else but ideal pion gas, taken at the breakup temperature T_f. This assumption was not a bad approximation for p_t spectra of secondaries seen in pp collisions, (although one should not expect it to work in this case because the system is not really macroscopically large). Applying these ideas to AA collisions, at much higher multiplicities, one might expect them to work even better. And still, experimental data for AA collisions obtained by WA80 and HELIOS (as well as recent data from E810 at BNL) have seen the unpredicted enhancement of very soft pions, with small p_t. This phenomenon, known as "soft pion puzzle", shows that we have to understand a lot even about rather dilute pion gas.

Recently interest in such a system from the theoretical point of view was much increased, in particular to its thermodynamics[11,13]. The results essentially supported observations made long ago[12] that $\epsilon(T) \sim T^6$, not T^4. Also kinetics of particle scattering in it was studied[14], and it was realised that pions, kaons and perhaps nucleons in such matter are rather good quasiparticles in the sense that they are not absorbed too strongly. Third, the real part of the "mass operators" (or, rather energy operators, for they depend on the momentum in respect to matter in the non-trivial way) is not in all cases that small, so renormalization of such quasiparticles may in many cases be very important.

Summarising conclusions of these studies: pion matter is far from being the ideal gas, but is rather a liquid in which strong attractive interaction among secondaries plays an essential role[5]. Having density comparable to nuclear density or larger, mesons in this

matter develop collective potential similar to nuclear one. The only important difference is that this potential is strongly momentum-dependent. However, just like in ordinary liquid, particles have difficulties if they try to leave the system, and this makes important observable effects.

In order to explain what type of collective potential is built–in by the pion-pion interaction, let us first recollect some general facts about the pions. They are the lightest hadrons because they are Goldstone modes, the remnants of spontaneously broken symmetry. If u, d quarks are massless, pions should be massless too, exactly for the same reason as e.g. acoustical phonons. Another consequence of their Goldstone nature: in the "chiral world" with massless quarks, the pions with $k \to 0$ cannot interact with anything. (Exactly due to this fact, acoustical phonons propagate distances much larger than molecule free paths, thus we can hear each other.)

This means that the discussed collective potential cannot be strong at low momenta. However, at larger momenta it becomes substantial, especially when two pions can form ρ meson. This potential is negative below the resonance, but positive above it (a phenomenon well known e.g. in the physics of low energy neutron). Thus, the resulting quasipion dispersion curve at large T may develop a secondary dip, as in the famous dispersion curve of elementary excitations in liquid He^4. At breakup temperatures 120-140 MeV it is just "flat" up to momenta of the order of 300 MeV, which means that in this momentum range the pion energy does not change much. (Explicit calculations of this effect are now in progress.)

Now we return to the "soft pion puzzle". Several explanations of this observation were suggested. One of them is related to small T at break-up, say 50-100 MeV, supplemented by significant transverse flow[15]. We think this is contradictory to pion gas kinetics and to interferometry, giving us not that big size of the system at breakup. Another suggested explanation, due to the positive pion chemical potential[16] claims to have a kinetic explanation, but that was not explicitly demonstrated. One more explanation is the resonance decays[17], but this is essentially the same physics as discussed above (if the system lifetime exceeds that of the resonances, that language should be used).

Pion modification plus boundary phenomena discussed above can provide a semi-quantitative explanation of the soft pion component at small p_t[5]. Climbing out of the

potential well, the outgoing pion reduces its momenta, and if the dispersion curve is flat at low momenta, large phase space inside corresponds to soft outgoing pions. Monte Carlo simulations[5] have demonstrated very effective production of nearly stopping pions, which roughly correspond to data. Another consequence of the collective attractive potential is that some pions are reflected from the boundary which makes the system lifetime longer. This can be checked by interferometry, also it is very important for photon production, discussed in the next section.

7. Restoration of chiral symmetry and modification of other hadrons at non-zero temperatures

In this section we try to look at modification of hadronic "quasiparticles" in wider perspective, connecting it with what is expected to happen to them at the chiral restoration phase transition. We will especially concentrate on possible experimental signatures of these modifications.

In the first approximation, one may start with the naive constituent quark model, and say that roughly speaking mesonic and baryonic masses are nothing else but 2 or 3 "constituent quark masses". As these masses are related to chiral symmetry breaking too, one may expect that at $T = T_c$ all masses of hadrons turn to zero. The simplest scenario[18] is that all mass scales are the same, therefore

$$m_{\rm hadrons}(T) \sim f_\pi(T) \sim |\langle\psi\psi\rangle(T)|^{1/3} \sim \left(1 - T^2/T_c^2\right)^{1/6}.$$

In the second approximation[19] we discuss why all mesons are not alike. This is essentially due to instanton-induced interaction between quarks and anti-quarks. For example, η^0 is so heavy because this interaction is repulsive, while the pion is so light because it is attractive. Asking what happens to these effects at higher T, one gets a simple answer: instantons are suppressed at high T (see Ref. 1). Let me speculate, that these phenomena which are first order in the instanton density, should disappear earlier than effective mass (proportional to its smaller power). If so, then first all meson masses come together, and only later their masses all come down. In particular, η^0 mass is expected to decrease faster than that of "normal" mesons like ρ, ω, ϕ. For pion we have the competition of two trends, and chiral perturbation theory gives even slight increase

$m_\pi(T)/m_\pi(0) = 1 + T^2/48F_\pi^2 + ...$[20], in agreement with this hypothesis. However, such a shift takes place (if at all) only at small momenta of the pions.

In the third (and, at the moment, the most realistic) approximation we take into account the effects of resonance interaction, ρ in the $\pi\pi$ case, K^* in the $K\pi$ case, etc. It is much stronger and it produces significant attractive potential. These effects are now investigated in detail.

But how can one observe all that? I think the best case is the ϕ meson. There are several reasons for this:

(i) ϕ lifetime is about 45 fm/c, which is comparable to the expected lifetime of hadronic fireball in heavy ion collisions. It means that (unlike J/ψ) there should be a significant fraction of ϕ decaying inside the matter. Kaon modification, to be discussed below, makes this conclusion even stronger.

(ii) The ϕ mass is just a bit above the double kaon mass, but still its dominant decay mode is the KK one. Therefore, its modification is very sensitive to relative shifts of dispersion curves of ϕ and K. (this point was also independently made by R. Pisarski)

(iii) ϕ has isospin zero, and pion scattering at low energies is proportional to isospin. No strong resonances, decaying into $\phi - \pi$ are known. So we expect ϕ to be modified less than K. If the K mass goes up a little as suggested above, the main decay channel of ϕ is blocked, if it goes down, Γ_ϕ is much enhanced.

(iv) Two modes of ϕ decay, the KK and e^+e^- ones, are measurable, so one can directly check whether the branching ratio is different from that in the vacuum. (This point was suggested by D. Lissauer in a discussion.)

(v) With good enough resolution, one may also look for the changes of the ϕ peak in invariant dilepton mass: modifications in question should produce some change in the peak shape, and its shift by few MeV. Unfortunately, we do not really know much about $\pi\phi$ interaction, and there are no resonances strongly coupled to this channel, so it is difficult to estimate what exactly should happen.

Summarising, I suggest the following. Let us consider the central region and $p_t \lesssim 600$ MeV. Such ϕ should decay into two K, each with momentum $p_t \lesssim 300$ Mev in the matter rest frame. It means they are most strongly affected by $K\pi$ interaction via K^* resonance, and this creates negative shift in energy of the order of 20-40 MeV (dependent on density).

If so, ϕ decay rate is increased significantly, by factor 3, thus nearly all of them decay inside the matter, the peak is shifted and widened, etc. If one increases p_t of ϕ, this effect should come away, for we are far off K . (Moreover, for relative collision energies above the resonance, the scattering amplitude changes sign and induces repulsive potential!)

The next interesting candidate is ω meson. Its width in vacuum is 8.5 MeV, so it again has a lifetime comparable to those of the excited hadronic system. But inside matter its width should be essentially increased. There are two reasons for that:

(i) Induced radiation. If the quantum state for the outgoing pion is occupied (the probablity for that is $n(E) = [\exp(E/T) - 1]^{\Gamma_1}$), transition is inhanced by $(1 + n(E))$. Omega decays into three pions, so there are three such factors: as a result its width nearly doubles. (This consideration is discussed as a pedagogical example in my book[1]).

(ii) Each pion gets in average $m_\omega/3$ in energy, but with the pion modification included it corresponds to somewhat larger pion momenta. As a result, there is more phase space and respectively another factor enhancing ω decay in matter.

I hope it is quite possible to measure ω width with few MeV accuracy, and notice this modification.

Other resonances, e.g. ρ, are also interesting (note that in this case the produced pions may be modified stronger, but it is two-body decay, less influenced by phase space.) Speaking about other hadrons such as nucleons, hyperons or ρ mesons, one should remember, that these are not Goldstone modes and therefore their significant modifications in the pion gas can take place even for zero momenta. However, recent studies of the nucleon modification[21] showed that the nucleon mass is shifted only by about 10 MeV up at $T = 150$ MeV, while its imaginary part at this T is already about 100 MeV.

Summarising this section, I can say that near chiral symmetry restoration temperature T_c all hadronic excitations are modified strongly. However, most space-time the system spends at much less dense matter, essentially the pion gas. Still some "precursor" modifications of π, K, ϕ, ω mesons in matter can, in principle, be observed. We look forward to hear from our experimental colleagues which of them are feasible in the proposed detectors.

8. Spectra of secondary hadrons

Rapidity distribution of secondaries, especially of nucleons, is too controversial a topic to be discussed now in such a short time. But even considering p_t spectra, we certainly have several components with different production mechanisms. We observe a superposition of hadrons (and quarks, fragmenting into hadrons), "evaporated" during the whole history of the system. Even for a very big system, with really significant suppression of surface effects compared to volume ones, one can see all of them just by going a little bit further in p_t, because cross sections drop significantly there and even a small factor in front is not fatal, providing the mechanism can give larger p_t particles.

Roughly speaking, p_t spectra of pions should contain the following components:

(i) a peak at small $p_t < 200MeV$, related to pion collective interaction;

(ii) pions with larger p_t, not modified by matter but evaporated at temperatures in the whole interval $T_f - T_c$;

(iii) contribution of the mixed phase which is difficult to describe except that it should contain $\exp(-p_t/T_c)$;

(iv) evaporation of quarks and gluons from QGP ("thermal jets"), fragmenting to hadrons later;

(v) products of jet fragmentation.

I will not go into detailed discussion here, but just adopt a very pragmatic experimental point of view, namely, ask whether one can separate all these contributions on a purely experimental basis, without using any theory.

One possible way of attempting that was suggested by O.V.Zhirov[22] many years ago. He has differentiated spectra and plotted "local slopes" $T_{\rm eff}^{-1} = d\log(d\sigma/dp_t^2)/dM_t$ versus $M_t = (p_t^2 + m^2)^{1/2}$. He indeed found two regions of growing $T_{\rm eff}$ separated by some funny "plateau" ($T_{\rm eff} = {\rm const}(M_t)$) in various hadronic reactions studied at ISR. I will not speculate here about the interpretation of these phenomenona, but certainly they demonstrate that some different mechanisms are responsible for different parts of spectra. I think this example teaches us that if we get p_t spectra in AA collisions of comparable quality, we can shed some light on the underlying mechanisms by using this idea.

Unfortunately, existing CERN and BNL data are not yet at such level of accuracy. Let me demonstrate the best I could do with a rather sophisticated analysis I recently attempted myself. The idea is to get "temperature profile" $F(T)$ from the pion p_t spectra[5], writing it as a convolution of $F(T)$ with the thermal spectum. In practice, it was written as four terms with different temperatures, taken with fixed step. The results are shown in Fig. 2. Being perhaps too optimistic, I see some enhancement in the bin with $T = 225$ MeV (close to expected T_c) if AA data are compared to pp ones.

(One comment is probably needed here. Most experimentalists just smile when I show this figure: they say I see enhancement as one-point effect. Actually it is not: just look at the error bars, they are small exactly because it was obtained from the fit to many data points in real spectra. But let me also confess that I present this provocative picture on purpose: it is a challenge to experimentalist to supply us with data good enough for such a sophisticated analysis.)

9. Photon physics

There are three regions of interest in the photon physics, depending on the photon p_t: (i) 1-100 MeV; (ii) 2-4 GeV; (iii) 5-15 GeV; which we consider subsequently. At the end of this section we also consider double photon production.

We have concluded above that the observed spectra consist of several components with completely different production mechanisms. In the case of photons we have to add one more important contributions: bremsstrahlung, dominating in the domain of soft processes. This, in turn, we divide into two parts: (i) radiation from initial nuclei and their forward-moving fragments; (ii) radiation from outgoing secondaries.

The former is coherent radiation of all nucleons sensitive to the (much discussed) "stopping" properties of the collision: this forward-peaked radiation is due to the fact that outgoing currents are less than ingoing ones. The second one in the soft photon limit should be proportional to multiplicity, and in general the corresponding spectra are simply connected with the spectra of charged secondaries. One may find estimates of these contributions in Ref. 23.

One may say that these estimates are but a simple exercise in electrodynamics and that one cannot learn much from their experimental check. However, we have to understand the soft photon physics for the following reasons. First of all, at the moment all existing observations of soft photons[24] report significant excess over the theoretical expectations. Certainly, this should be checked in case we are really missing something.

The second reason: their emission is indeed described by classical electrodynamics in wide energy range, but simple bremsstrahlung from outgoing secondaries is the main effect only if the photon energies ω are small compared to inverse lifetime of the radiating system. If this is not true, radiation from the excited system contibutes as well, and this is very interesting.

Indeed, let me consider simple model of the dilute pion gas near breakup. Still pions are rescattering there, say via ρ meson. Any scattering is some change in the current, so it contributes to radiation. If these contributions can be added incoherently, we have a term proportional to the number of pion rescatterings. Certainly, it would be very interesting to measure it. The exact boundary (as a function of the photon energy) where we can or cannot add radiations from different rescatterings provides information on space-time evolution near breakup. Certainly we welcome such information too as a valuable "second check" after pion interferometry. Discussion of these topics with estimates in the "quasipion" model can be found in Ref. 5.

Unfortunately, experimentally this soft photons physics is considerably restricted in the small "window" below the huge background due to π^0 decay (say, for photon p_t less then 70 MeV). Can one really see something interesting there, other than trivial bremsstrahlung?

The answer may be positive, especially for very large systems. Indeed, the signal we are looking for is proportional to the number of pions times the number of rescatterings per pion. The second factor is expected to be few tens in Au-Au collisions, so it is certainly is not small correction to bremsstrahlung. Existing data[24](however questionable they are) seems to show nearly quadratic dependence on multiplicity which is consistent with the importance of interparticle interactions.

Coming to the second "window", we start with the comment that production of the "penetrating probes", direct photons and dileptons, was suggested as the best signal for QGP formation already in the first paper on this subject[6]. Explicit calculations[6,25] differ

slightly in details, but use the same model of ideal QGP with the lowest order cross sections for $qq \to \gamma g$, $qg \to \gamma q$ processes. All of them agree that these photons should be looked for using another "window" at p_t about 2–4 GeV, where they presumably dominate both over hadronic decays and hard "Compton scattering" $qg \to \gamma$. Estimates done by Kajantie and Hwa also included bremsstrahlung-type processes in which photon is emitted by a quark moving in the same direction. They did not emphasize it, but from their results it seems to follow that these effects are not important in this window. Actual experiments in this p_t region (so far done in pp collisions, mainly at ISR) also proved that no hadrons seem to be much correlated with photon, even in hard processes.

Comparison between various production mechanisms is discussed by P. Braun-Munziger at this workshop, so the interested reader should look at his compilation. My only comment is that neither background from hadronic decays nor photon production from the hadronic matter are not yet really calculated, and this is one of our hometasks. It is important in order to realize how low in p_t we should go, in search of an interesting signal.

Unfortunately, not much can be said on this point from the experimental side. WA80 has recently looked for direct photons in nuclear collisions up to $p_t = 2$ GeV/c, but did not find them there (as expected). Efforts to go further are continuing.

Now we come to the last kinematic region (iii), that of hard photons. The main idea of this kind of physics is: "photon is a jet without fragmentation". Therefore, observation of hard photon is the ideal trigger for hard "Compton scattering". If it is observed, then we know that a quark with about the same p_t is going in the opposite direction. Two-arm experiments based on this idea were done at ISR. Trying to answer the question "what happens with a quark in very dense matter", one may repeat them, comparing pp and AA cases. At such momenta and in a heavy ion environment it is probably impossible to see jets by calorimeters, as it was possible at ISR, so one has to look for large p_t hadrons. Therefore, we cannot check the balance of p_t, but can only measure to which extent photons and recoil hadrons are in the same plane. Whether it is a good measure of quark rescattering or not, deserves further study.

A few words about direct photon pairs. There was one experiment at ISR[27] which was able to see this phenomenon. The rate is about 4 times larger than for dileptons, but background is more difficult. However, matching both is interesting: if we have only

quark-antiquark annihilation in both cases, the ratio is fixed. Simplicity of the prediction makes these difficult experiments probably sufficiently interesting.

10. Dileptons

We have already discussed ϕ,ω physics above, and we return to J/ψ below, so in this section "dileptons" are those produced not in direct hadronic decays, that is, not in the peaks in dilepton invariant mass M.

Generally speaking, production mechanisms of dileptons are about the same as for photons. For example, for the smallest mass (M about 2 m_e) it is certainly two–photon collisions, and for the largest M it is the hard Drell-Yan annihilation process. But dileptons are more informative, for they have not only total p_t, but also invariant mass M and angular distribution. All this information, if experimentally available, can certainly shed some light on the production mechanism.

The first interesting "window" I think is at M about $2m_\pi$, connected with physics of the pion annihilation threshold. Gale and Kapusta[26] were the first to suggest it in another context, in low energy nuclear reactions in which pion modification inside nuclear matter were considered. Recently, motivated by the "soft pion puzzle" considered above, there were a number of suggestions like non-zero chemical potential[16] or modification of the pion dispersion curve[5]. Both predict significant enhancement of pions with energy near $2m_\pi$. Unfortunately, there is huge background from hadronic decays etc., so it very questionable whether one really can see this enhancement.

The second region of interest is "between ϕ and J/ψ" in invariant mass, where QGP signal was first suggested[6]. Detailed calculations were done by many authors, let me present here Fig. 3 from Ref. 28. (Most people have probably already seen it several times: it is the most complete one. The problem is that it is somewhat more optimistic then expectations for RHIC conditions, where initial temperature is not expected to be so high.) A recent review on the subject can be found in Ref. 29. I think the conclusions drawn from this picture still need some comments. First, DY curve traditionally goes with its famous K-factor about 2, not yet incorporated into the QGP calculation (for discussion of radiation correction in QGP see Ref. 46. Second, nucleon structure functions at larger

x are used. However, $M = 2$ GeV corresponds to $x_1 \sim x_2 \sim 0.01$, and here shadowing is already important in nuclear structure functions. This shifts the ratio QGP/DY up by another factor 2, so I think all dileptons below J/ψ are mostly of "thermal" origin.

Distinquishing two production mechanisms is in principle easy: one should measure angular distribution of the pair compared to beam axis. DY give $(1 + \cos^2\theta)$, while QGP gives isotropic distribution. Another possibility is connected with p_t distribution of the dilepton. Thermal production gives $\langle p_t^2 \rangle$ about $2MT$, or growthing p_t with M, while DY suggests constant value of the parton p_t, modified slightly by QCD radiative corrections.

One more important comment: experimentally it is also possible not to look for "back to back" pairs, but for small M and large p_t. In other terms, we may look for annihilation of quarks going transverse to the beam. I think DY is less competing here, also the background Dalitz decays are less important in such kinematics. Therefore, in this case we probably have a better chance to see "thermal dileptons".

Another important thing to do is to go to very small M and match "virtual photon production" to that of real photons. Consistency between both sets of data, with their completely different backgrounds etc. is a non-trivial test.

Unfortunately, I do not have much to say about present experimental situation. NA38 dilepton data are still not presented in absolute normalisation form, and (as far as I know), the dilepton continuum seen by them was not really analysed. Much better data (in particular, with heavy ion beams) are needed, in order to get reliable information about the hottest stages of the collisions.

And last (but not least): dileptons outside peaks have huge background from Dalitz decays. Thus, it is not good to have magnetic field everywhere and just throw away soft particles: it will then lead to many false dileptons. A lot of Monte Carlo is needed here, in order to understand where it is not hopeless to look for "thermal dileptons".

11. Production of new flavors

Enhanced production of new types of quarks, charmed and strange ones, in the plasma phase has been repeatedly emphasised starting from the very first works on the subject[1]. It was suggested to be a very nice "thermometer", similar to the one used by doctors, sensitive to the highest temperature of the process. However, this thermometer needs a careful grading.

For charm the theoretical situation is simpler, for both direct processes (mainly gg collisions) and those in QGP seem to be under better theoretical control. But experimental observation of charmed hadrons is next to impossible, especially in the heavy ion environment. The only hope (or, may be, danger) is connected with semileptonic decays of charmed hadrons. Just at p_t about few GeV this produces a serious source of leptons, thus we have to understand it anyway. For doing this it is important to have at least one detector, capable not only of comparing "same charge lepton pairs" to "opposite charge" ones, as is done traditionally, but also of looking for, say "opposite charge $e\mu$ pairs" in a single event.

The theoretical situation with charm production was recently discussed in Ref. 30, with the conclusion that at RHIC charm production in QGP still does not dominate over direct gg process. (The latter gives about 3 charmed hadrons per Au-Au collision at RHIC!) Still there remain some open questions, like charm production in QGP plasma in more-than-two gluon collisions. Also one should keep in mind, that gluonic structure functions of nuclei at such small x are actually unknown, and can be significantly "screened" compared to extrapolations from larger x and pp data, used in these works. I think we more detailed studies of "partonic cascades" (which is quite possible to do in perturbative QCD framework) can provide more reliable estimates of total charm production at RHIC. If we find additional mechanisms to increase charm production by factor 5 or so, it will reach the equilibrium density of charm in QGP.

Now we switch to the strangeness production. Here the situation is quite the opposite: the current experimental situation is becoming more interesting, now there are data on

production of $K, \phi, \Lambda, \Sigma, \bar{\Sigma}, \Xi, \bar{\Xi}$, although some of them are still in very restricted kinematics. At the same time, understanding of these data still remains very poor. (I briefly return to this point below.)

I think at RHIC the situation with strangeness will be much simpler than it is at AGS. The reason for this is based on the observation known for some time (see review Ref. 31 and references therein), that perturbative processes in QGP (especially $gg \to ss$) lead to strangeness equilibration time τ_s which is pretty short, about 3 fm/c at T_c and 1 fm/c at $T = 400$ MeV (about T_i expected at RHIC) . One new idea, pointing in the s me direction, was recently suggested in Ref. 32. These authors argue that if gluons obtain large effective mass above $2m_s$ one has direct decay of the gluon $g \to s\bar{s}$. If so, it makes τ_s even few times shorter.

Therefore, strangeness equilibration time is presumably smaller than system lifetime at such temperatures so one hope strangeness equilibration in QGP will take place. If so, an admixture of strange quarks can be calculated from simple equilibrium formulae for QGP.

Now, can this strangeness be annihilated at a later hadronic stage, when the system becomes cooler? Estimates have shown that it cannot be a significant effect. As a result, we do expect at RHIC much higher ratios of say $\bar{\Lambda}/\bar{p}$, or $\bar{\Xi}/\bar{p}$ Ref. 31 than observed in the pp case (or in nuclear collisions at AGS). Another good measure of the strange quark admixture is $\phi/(\omega + \rho)$ ratio.

Although it is not stricly related to the topic of this talk, let me briefly say why I find present situation with strangeness so confusing. Let me start with experimental observations at low energies. Significant strangeness enhancement is seen in antiproton annihilation on nuclei at energies as low as 4 GeV,[33] where particle spectra show in this case, temperature as low as 60 MeV, so the excitation energy density is orders of magnitude smaller than in QGP. (Nevertheless, some authors[34] still ascribe it to QGP production.) Another important fact is that strangeness production starts to grow in nuclear collisions already at AGS energies, or already in hadronic matter. For example, K^+/π^+ ratio increases from about .04 (pp or pBe at such energies) to about .2 in Si-Au collisions[37].

If one uses equilibrium thermodynamics and K^+, K^-, Λ data at AGS[38], he gets $T = 100$ MeV, $n_B = .1$ fm^{-3}. But it certainly cannot be true, for ordinary processes in hadronic

matter cannot keep strangeness in equilibrium at such low temperatures, even lower ones than those seen in p_t spectra. Therefore, we certainly have a non-equilibrium situation, and have to study kinetics of strangeness production in hadronic matter. Unfortunately, in literature one can find quite different estimates for strangeness production rates. Some people[35] use large cross section $\sigma(\pi\pi \to K\bar{K})$ of the order of 3 mb. On the contrary, in Ref. 36 it is argued, that the standard one-meson exchange model gives for this cross section estimates about ten times smaller. If so, the ordinary hadronic cascades do not explain these numbers.

An interesting point made in Ref. 36 is that production of strangeness is very sensitive to meson modification in matter. The simplest effect (in fact, not discussed in this paper, but considered above) is that attraction between pions (or modified dispersion curve) leads to essentially larger pion density at the same temperature. This by itself can increase the rate by more than one order of magnitude near T_c. The second effect is that in hot matter the kaon mass is expected to be shifted. In pure pion gas we argued above that the shift is a small increase, but according to Ref. 36, the interaction to nucleons (and there are many nucleons at AGS energies in the matter) is more important and this makes m_K smaller. If so, it can much enhance the K production rate, for it contains $\exp(-2m_K/T)$. Similar shift in m_ρ makes the process $\rho\rho \to K\bar{K}$ also very important[36]. Concluding, we have to understand rates of strangeness production in hadronic matter (even in a rather dilute one) much better, in order to explain the whole bulk of low energy data.

Coming now to the situation with strangeness in CERN experiments. We have a set of new data, with ratios like $\bar{\Xi}/\Xi = 0.43 \pm 0.07$ (WA85), $\bar{\Lambda}/\Lambda$ about 1/4, Λ/K_s about 2 (NA35), etc. It was recently noticed by C. Dover[40], that they all can be more or less described by equilibrium thermodynamics of hadronic gas, now at $T = 200$ MeV and $\mu_B = 180$ MeV, $\mu_s = 45$ MeV. (Note, that here we have one parameter, not three: the first is taken from the observed slope of p_t distribution, and two others are related by strangeness and baryon number conservations, so it is very nontrivial fit.) The question is then, does it really mean that we have strangeness equilibration in hadronic phase, or is this agreement occasional, and is it just an interplay of much higher production rates with small lifetime of the plasma, so that in QGP strangeness equilibration was not reached.

As for the ϕ enhancement recently observed by NA38, we have to warn the reader, that they correspond to high p_t, well above 1 GeV. If one adopts an "evaporation" scenario for this p_t region, he finds that the main effect here is probably the larger mean free path for ϕ relative to ρ, ω mesons in the pion gas, so that ϕ can be "evaporated" from inside and its enhancement may be just a volume-to-surface effect[39]. Again, a direct check is to do the same at small p_t. Also, it is interesting to make the system larger using lead beam, and see whether enhancement is changed.

Concluding this section, let me emphasize that non-perturbative QCD is only now approaching the question of flavor mixing, both in the vacuum, in hadrons and at non-zero temperature. One may hope that till the RHIC operation time we will learn much more about it.

12. J/ψ suppression

The original idea of Matsui and Satz[41] was that color forces are screened in QGP, so that for the c quarks no bound states remain in the resulting effective potential. NA38 experiments indeed found such suppression, but exact interpretation of this observation still remains a matter of dispute. Not going into it in details, I only outline existing possibilities and make some comments, related to future RHIC experiments.

My first theoretical comment is that this statement depends on the particular value of the c quark mass. Therefore, it is not exactly true that such suppression is "a signal of color deconfinement", but rather a measure of the screening radius. Say, if we will be able to see Υ suppression as well, we will have stronger limit on that. But the screening length is also extremely important: experimental demonstration that it is indeed small means, in practice, that we have found QGP!

However, as one wants to understand whether the observed J/ψ suppression is indeed due to QGP, a lot of questions arise. The obvious question is whether J/ψ can be "split" into a pair of charmed hadrons in hot hadronic matter[43]. In order to answer it one may use the idea suggested by Karsch and Petronzio[42]: J/ψ can jump out of the "hot spot" if its p_t is large enough $> P_c$, where $P_c = M_\psi(\tau^2_{\rm QGP}/\tau^2_\psi - 1)^{1/2}$. And indeed, at $p_t > 2GeV$ the observed suppression disappears. Taken literally, it means that the plasma lifetime

τ_{QGP} only slightly exceeds the J/ψ formation time τ_ψ. This seems strange, a kind of "fine tuning", also usually people assumed τ_ψ to be small, 1/2 - 1 fm/c, and it is not clear why plasma lifetime should be so small too. Thus, I would not say data are so naturally explained by QGP suppression.

However, these data seem to rule out hadronic mechanism of suppression even stronger. In such a scenario one obtains suppression till much larger p_T (remember, the system size at breakup is as big as about 8 fm, so it is not easy to jump out of it).

Another possible reason for more J/ψ at larger p_t is "initial stage rescattering" of the gluons, producing the charmed quarks[44]. It got support from recent FNAL experiments E772 in which similar suppression in pA collisions were observed.

One more possibility (M. Strikman, private communication) is based on the old observation at ISR that about 40% of J/ψ seems to come from χ radiative decays. There is a significant difference betweem J/ψ and χ size: the latter is believed to have nearly as big cross section as the pion. Can it be that it is actually χ, not J/ψ that is absorbed? Data on ψ^0suppression (it is similar in size to χ) can tell us more on that. (By the way, NA38 data gives a hint that $\psi^0$is suppressed nearly completely.) Unfortunately, the cross section drops by about two orders for ψ^0, so luminosity (including that in the RHIC project) does not really allow us to say much about its production.

Some of these questions will presumably be clarified by future experiments with Pb, Au beams at CERN and BNL prior to RHIC. In this case we certainly have larger plasma lifetime τ_{QGP}, so if the QGP suppression idea is right, this suppression should persist in this case up to essentially higher p_t. If the initial gluon rescattering or χ absorption is the case, we will see no big differences between O^{16} and heavy ion collisions.

13. Interferometry at RHIC

At a previous RHIC workshop interferometry was discussed very nicely by W.A. Zajc[45], so I really add only a few comments on this issue.

First of all, what size of the source at breakup is expected at RHIC (Au-Au collisions)? Naive extrapolations from existing data with $R \sim (dN/dy)^a, a = 1/3 - 1/2$ gives R=20-30 fm. As the momentum difference at which interference is seen should be about 1/R, it

makes it rather difficult to work with the typical p_t pions and it is better to use as soft pions as possible. This by itself probably implies a specialized detector.

Second, is this number interesting? Yes, it is, and even existing CERN data on the source size (which are not yet really very accurate) has already played an important role. In partucular, the measures R about 8 fm may appear large, but it is not so if one calculates the density of particles. It has already ruled out a scenario in which pion gas can be cooled to such low T as 50-100 MeV.

The density of pions at breakup is sensitive to pion modification quite significantly. Attraction among them increases the density, and I think lower value R about 20 fm is preferable. At the same time, these effects make it more difficult for the pion to leave the system, so the lifetime becomes longer. Whether it is the case or not, we will learn from interferometry.

One more important point which was not discussed much in recent years is a possibility to try interferometry with pions with p_t about 0.5-1 GeV. It may appear crazy in view of what was just said above, but on the other hand these pions are probably produced at earlier stages, where R is still of the order of the size of colliding nuclei (about 5 fm), and also the lifetime is only few fm/c. (What kind of detector is needed for that should probably be discussed. I think it may be some hole in the detector with its part put farther, or a section with especially good segmentation.)

14. Initial thermalisation and jets

Discussion of jets at RHIC was made in Ref. 47, and I cannot add anything valuable to it. Let me only briefly discuss the region between QGP and initial hard scattering, which is potentially very interesting.

People working in perturbative QCD predicted a huge number of "mini-jets" of energies 1-2 GeV at RHIC, and at the same time they said that "there will be no quark-gluon plasma". But it is easy to see that these predicted gluons will be thermolised very soon, in less than 1 fm/c, so these "mini-jets" are nothing else but the plasma.

Of course, we need a more quantitative theory of what is going to happen at the initial stage of the collision. I think one can do a lot of work in this direction, using the

well-developed perturbative QCD. After the first estimates of quark and gluon mean free paths[6] people for a long time discussed methodical questions like how to incorporate the color field into the kinetic equation etc., and only recently have first attempts been made to make straigtforward Monte Carlo with quarks and gluons (see the talk by B. Mueller in this proceedings). I think that still not all necessary features are incorporated in this approach. In particular, reactions which diminish the number of partons (say, $3 \rightarrow 2$) are not included, so in this approach they will multiply like cockroaches. Another problem is that subsequent collisions are not really completely incoherent (one should add amplitudes, not cross sections). But all this can well be included, remaining in perturbative QCD.

One more difficult question is that we know initial conditions only partly, from structure functions, which are one-particle distribution without correlations. However, one may hope that such details are not important for such global quantities like thermolisation time, although it may affect some reaction rates.

Experimentally it is very difficult to look for jets with just several GeV in p_t in RHIC environment. Still one may try correlation of say two high p_t hadrons to look for them. But let me express here the main idea of this type of physics anyway. If one sees two jets (or jets and the photon) with well balanced p_t, he says it is a hard collision which took place at one point. If it is completely unbalanced by another jet (which means it is balanced by nearly all secondaries together), we call it "evaporation" from matter, or jet absorption.

15. Classification of the experiments

This section is a kind of a summary, in which experiments are classified according to the kinematical regions studied and physical problems addressed. One should not of course mix "experiments" in this meaning with detectors: the latter should certainly be as universal as possible. In fact, there is a general feeling that it is probably a correlation of several signals, not just one of them, which will allow to reveal reliably enough the complicated physical phenomena we are going to study at RHIC.

1. Physics of hadronic matter

• Pion spectra at typical p_t. Soft pion enhancement, its dependence on multiplicity, atomic number and rapidity.

• Composition of secondaries: strangeness and antibaryons.

• Exact form of low-p_t spectra of heavier secondaries (especially antiprotons and Λ's, if possible). Analysis for possible manifestation of collective flow. Dependence on multiplicity (or rather local dN/dy). Selection of special events (may be even in pp or He He modes).

• Interferometry using the soft pions. System size and lifetime versus multiplicity. Interferometry with kaons.

• Search for ϕ and ω modification. Measurements of both KK and e^+e modes of the former with the test of branching. Precise (up to few MeV) measurements of their masses and widths in dilepton mode.

• Soft photons (p_t below π^0 decay background limit). Test of bremstrahlung predictions, search for possible signal due to multiple pion rescattering.

• Soft dileptons. Very small invariant masses: matching to real photons. Studies of whether one can see pion annihilation below Dalitz decay background.

2. Physics of QGP

• Hadronic spectra at p_t about 1-3 GeV. Accurate measuremets of slopes. Composition of secondaries.

• Possible measurements of interferometric correlations between these particles (measurements of the size of their source: the size of colliding nuclei or more?).

• Dileptons outside resonance, either with $M = 1 - 3$ GeV, or small mass but p_t of such magnitude. Angular distribution (polarization of virtual photon). $e - \mu$ pairs as a charm signal.

• Direct photons with p_t about 2-4 GeV.

• J/ψ and ψ suppression. (The latter, definitely only with some luminosity increase.) Dependence on p_t, multiplicity, atomic number.

3. Hard trigger experiments

• Spectrum of hadrons with $p_t > 5$ GeV.

• Search for jets, whatever its definition in RHIC environment can be.

• Direct photons with maximal possible p_t.

• Study of the opposite side correlation: how p_t is compensated, by a jet, or all system reacts as a whole?

4. Experiment with high multiplicity trigger

(At RHIC Au Au collisions one may skip about 5-6 orders in probablity of the events, and still have about a thousand of them, presumably enough to answer these questions.)

• What the spectra looks like in these events, in particular mean p_t?

• What is the particle composition in these special events?

• Is the size and lifetime of the system different?

Certainly, these types of experiments need quite different detectors. For example, for # 1 one does not need large solid angle (there are so many particles anyway), but needs very high resolution (for interferometry and resonances). # 2 presumably needs strong field (to get rid of the soft component), and reasonably big solid angle, especially for dileptons (pairs are wide enough in angle, also rates are small). Hard trigger (# 3) should probably be two-arm ones, while "special events" (# 4) need large solid angle, to take maximal information from such events. And still, it is better to have all features in one detector, to the degree it is practically possible.

As a parting remark let me say that certainly my list is far from complete (in particular, I said nothing about forward region, fragmentation, stopping, etc). Maybe my experimental considerations are too naive. But this is the topic of this workshop, and I hope at the end of this week we will know much better what people want to do at RHIC.

REFERENCES

1. E.V. Shuryak, Phys. Rep. 61 (1980) 72, 115 (1984) 152. The QCD Vacuum, Hadrons and the Superdense Matter, World Scientific 1988;
   D.J. Gross, R.D. Pisarsky and L.G. Yaffe, Rev. Mod. Phys. 53 (1981) 43;
   B. Muller, Lecture Notes in Physics 225, (Springer-Verlag 1985);
   J. Cleymans, R.V. Gavai and E. Suchonen. Phys. Rep. C130 (1986) 217;
   "Quark-gluon plasma", Advanced Series on Directions in High Energy Physics Vol.6, ed.R.Hwa, WSPC, Singapore 1990..
2. Conceptual design of RHIC, BNL report, 1989..
3. Proceedings of Quark Matter '88, Nordkirhen, Z. Phys. C. 38 (1988);
   Proceedings of Quark Matter '89, Lenox, Nucl. Phys. A498 (1989);
   Proceedings of Quark Matter '90, , Nucl. Phys. (in press)..

4. Proceedings of the Second Workshop on Experiments and Detectors for RHIC, LBL-24604, Berkeley 1987. Proceedings of the Third Workshop on Experiments and Detectors for RHIC, BNL 52185, Brookhaven 1988..
5. E.V. Shuryak, Pion modification in hot hadronic matter and "ultrasoft" phenomena in high energy collisions, CERN-TH-5386/89 and "L. Van Hove Festschrift", World Scientific, (1990). Physics of the pion liquid, BNL–44522, 1990, Phys.Rev.D, in press..
6. E.V. Shuryak,Phys. Lett. 78B (1978) 150, Yad. Fis. 28 (1978) 796..
7. E.V. Shuryak and O.V. Zhirov, Phys. Lett. 89B (1980) 253.
8. L. Van Hove, Z. Phys. C21 (1983) 93.
9. M. Kataja, P.V. Ruuskanen, L.D. McLerran and H. von Gersdorff, Phys. Rev. D34 (1986) 2755.
10. T. Alexopoulos et al., Phys. Rev. Lett. 64 (1990) 991;
F. Turkot, Talk at Quark Matter '90, Menton, 1990.
11. P. Gerber and H. Leutwyler, Bern Univ. preprint BUTP-88/30 (Nucl.Phys., in press).
12. E.V. Shuryak, Jad. Fis. (Sov. J. of Nucl. Phys.) 16 (1972) 395.
13. G.M. Welke, R. Venugopalan and M. Prakash, The speed of sound in an interacting pion gas, SUNY-NTG-90-20.
14. E.V. Shuryak, Phys. Lett. 207B (1988) 345;
J.L. Goity and H. Leutwyler, Bern University Preprint 1990.
15. K.S. Lee, U. Heinz and E. Schnedermann, Search for collective... preprint TPR-90-18, Regensburg, submitted to Zeit. Phys. C.
16. M. Kataja and P.V. Ruuskanen, University of Jyvaskyla preprint 1/90, January 1990.
17. G.E. Brown, J. Stachel and G.M. Welke, Hot and Cool Baryons and Cool Pions in Relativistic Heavy Ion Reactions, preprint of SUNY, Stony Brook 1990.
18. G.E. Brown, Matter under extreme conditions, SUNY-NTG-90-13.
19. E.V.Shuryak, Talk at "Quark Matter" conference, Menton 1990. (To be published in Nucl.Phys.).
20. J. Gasser and H. Leutwyler, Phys. Rep. 87 (1982) 79..
21. H. Leutwyler and A. Smilga, BERN University preprint, 1990.
22. O.V. Zhirov, Nontrivial variation of p_t slope: a good separation of the production mechanisms, preprint INP 81-31, Novosibirsk 1981 (unpublished)..
23. R.N. Cahn, Phys. Rev. 110 (1973) 247.
24. P.V. Chliapnikov et al., Phys. Lett. 141B (1984) 276;
U. Gurlach, (HELIOS coll.) Proc. of 24–th Int. Conf. High. Energy Phys., Munich 1988;
W.J. Willis, Nucl. Phys. A478 (1988) 151C;
J. Schukraft, (HELIOS coll.) Talk at 7th Int. Conf. Quark Matter '88, Lenox, Massachusetts 1988.
25. R.C. Hwa and K. Kajantie, Phys. Rev. D32 (1985) 1109.
26. C. Gale and J. Kapusta, Phys. Rev. C35 (1987) 2107;
L.H. Xia et al., Nucl. Phys. A485 (1988) 721;

J. Kapusta, Talk at HIPAGS Workshop, BNL, March 1990.

27. T. Akesson et al., (AFS colloboration) Z. Phys. C32 (1986) 491.
28. K. Kajantie, M. Kataja, L. McLerran and P.V. Ruuskanen, Phys. Rev. D34 (1986) 794.
29. P.V. Ruuskanen, in "Quark-gluon plasma", Advanced Series on Directions in High Energy Physics Vol.6, ed. R. Hwa, WSPC, Singapore 1990. Also Invited Talk at 7-th "Quark Matter", Menton, 1990.
30. A. Shor, Phys. Lett. 215B (1988) 375, 233B (1989) 231.
31. P. Koch, B. Muller and J. Rafelski, Phys. Rep. 142 (1986) 167;
H.C. Eggers and J. Rafelski, Strangeness and QGP: Aspects of Theory and Experiment. Arizona Univ. preprint AZPH-TH/90-28.
32. T.S. Biro, P. Levai and B. Muller, Strangeness production with "massive" gluons, Durham, NC, 1990.
33. K. Miyano et al., Phys. Rev. Lett. 53 (1984) 1725 and later preprints.
34. J. Rafelski, Phys. Lett. 207B (1988) 371.
35. J. Kapusta and A. Mekjian, Phys. Rev. C33 (1986) 1304.
36. C.M. Ko, Z. Wu, L.H. Xia, G.E. Brown, Proceedings of the HIPAGS Workshop, BNL, March 1990.
37. Y .Miake, Talk at HIPAGS Workshop, BNL, March 1990.
38. J. Cleymans, Invited talk at 7-th "Quark Matter", Menton 1990.
39. P. Koch, Invited talk at 7-th "Quark Matter", Menton 1990.
40. C.B. Dover, Theoretical Overview of RHIC Physics, talk at Annual Meeting of the AGS users group, BNL-44621, May 1990.
41. T. Matsui and H. Satz, Phys. Lett. 178b (1986) 416.
42. F. Karsch and R. Petronzio, Z. Phys. C37 (1988) 627;
M.C. Chu and T. Matsui, Phys. Rev. D37 (1988) 1851.
43. J. Ftacnik, P. Lichard and J. Pisut, Phys. Lett. B207 (1988) 194;
S. Gavin, M. Gyulassy and A. Jackson, Phys. Lett. 207B (1988) 257.
44. S. Gavin and M. Gyulassy, Phys. Lett. 214B (1988) 241;
J. Hufner, Y. Kurihara and H.J. Pirner, Phys. Lett. 215B (1988) 218;
J.P. Blaizot and J.Y. Ollitrault, Phys. Lett. 217B (1989) 392.
45. W. Zajc, Invited talk at Second RHIC Workshop, BNL 1988, and 7-th "Quark Matter", Menton 1990.
46. R. Baier, B. Pire and D. Schiff, Phys. Rev. 38D (1988) 2814;
T. Altherr, P. Aurenche and T. Becherrawy, Nucl. Phys. B315 (1989) 436;
A. Mahlin, Dilepton spectrum from QGP in second Born approximation, ITP-89-72E, Kiev 1989.
47. F.E. Paige, Invited talk at Third RHIC Workshop, BNL 1988.

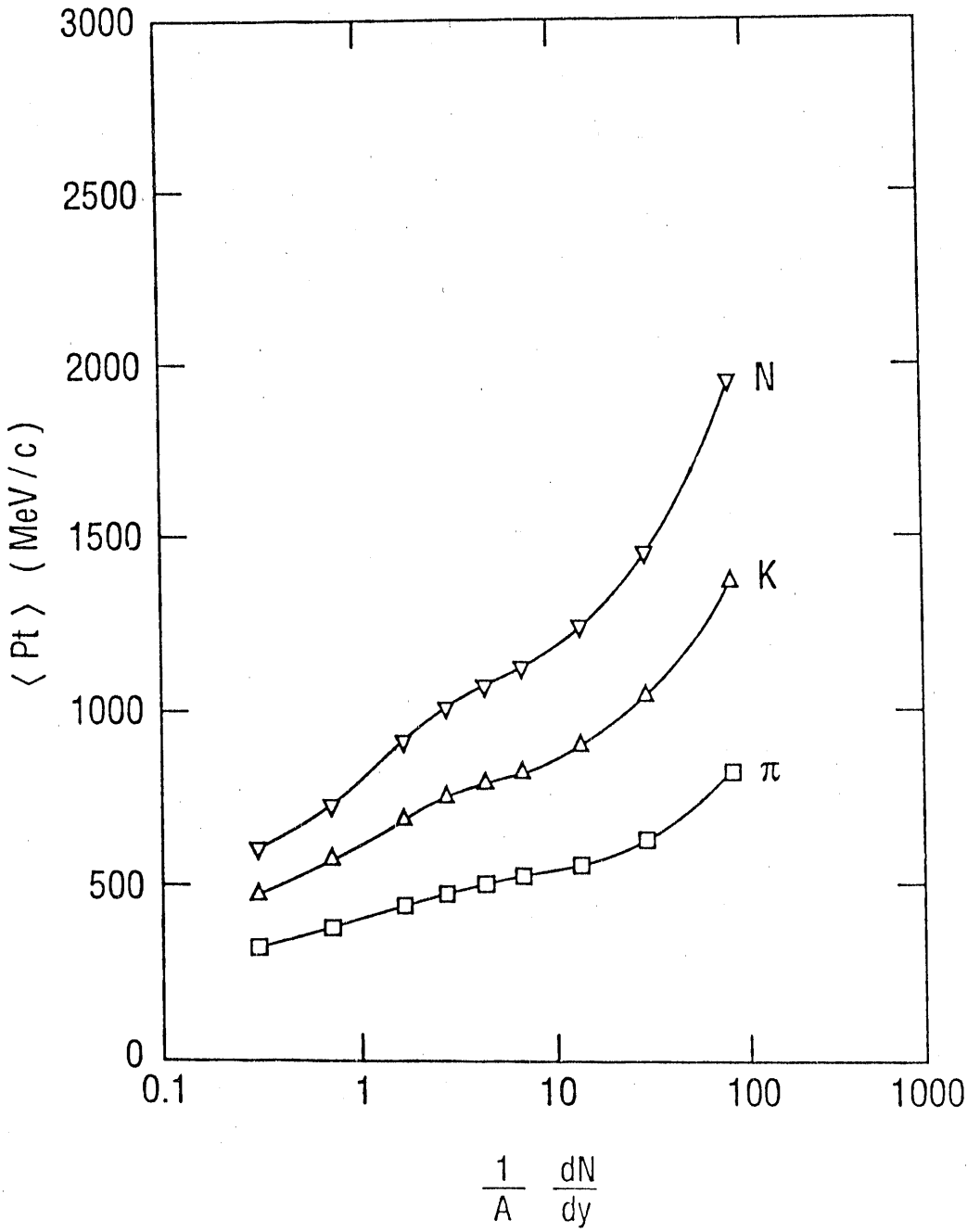

Fig. 1(a): Mean transverse momenta of various secondaries versus dN/dy (effective energy density). Hydrodynamics with phase transition[9].

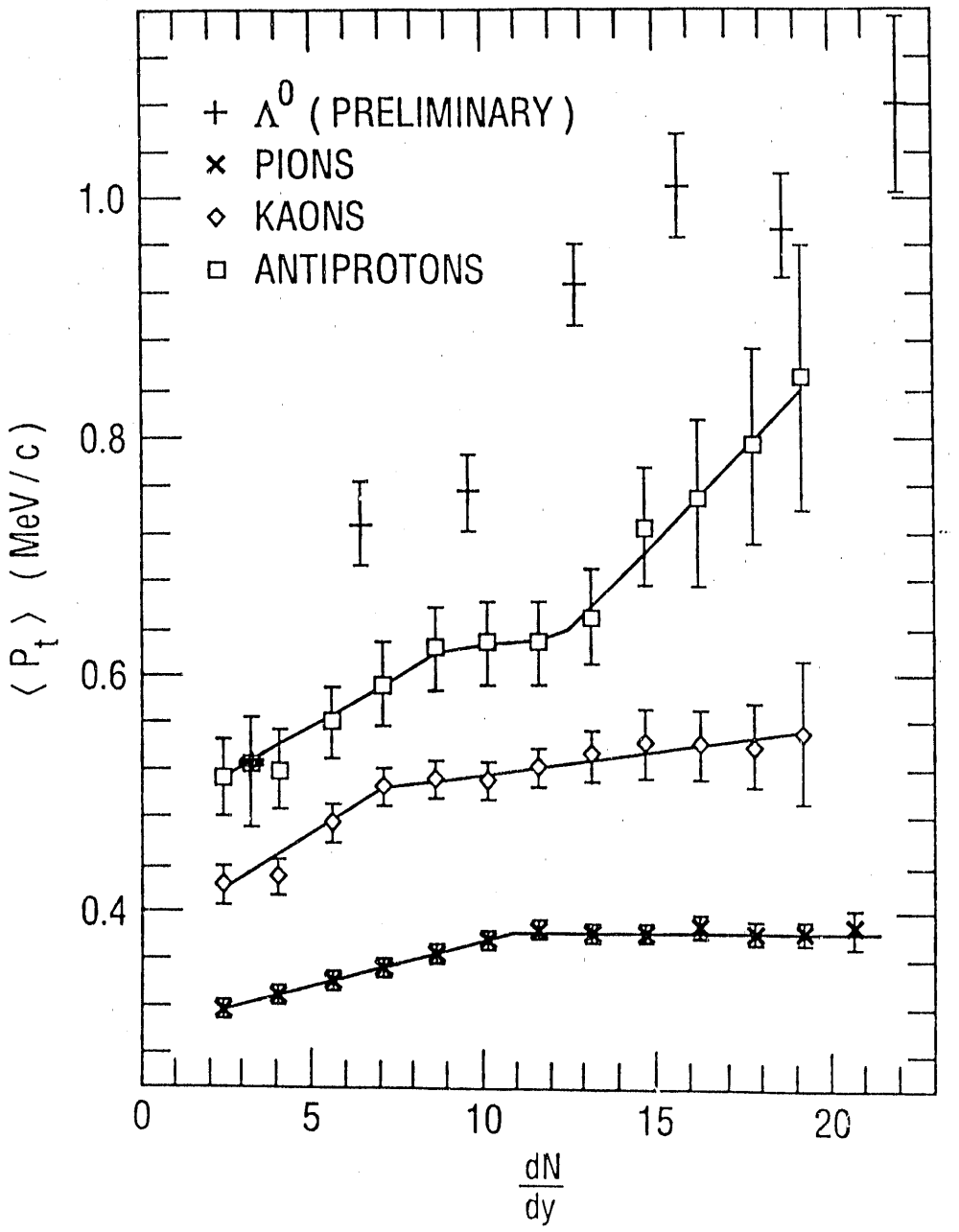

Fig. 1(b): Mean transverse momenta of various secondaries versus dN/dy (effective energy density) FNAL data[10]

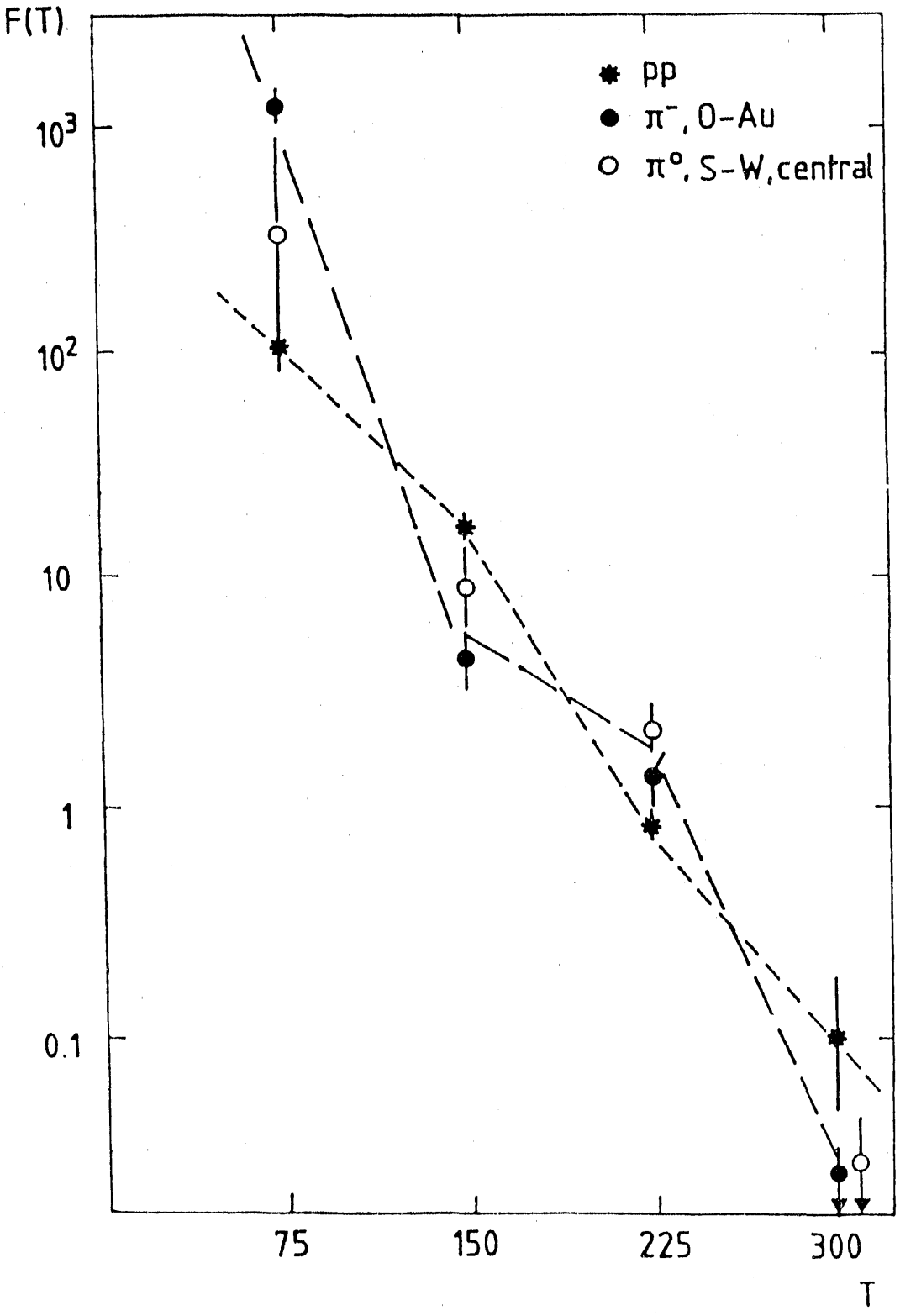

Fig. 2: The temperature profile function $F(T)$ versus temperature (for comparison, each spectrum is normalised to one), from[5]. The open and closed points correspond to WA80 and HELIOS data for reactions indicated, while stars represent the pp data from ISR.

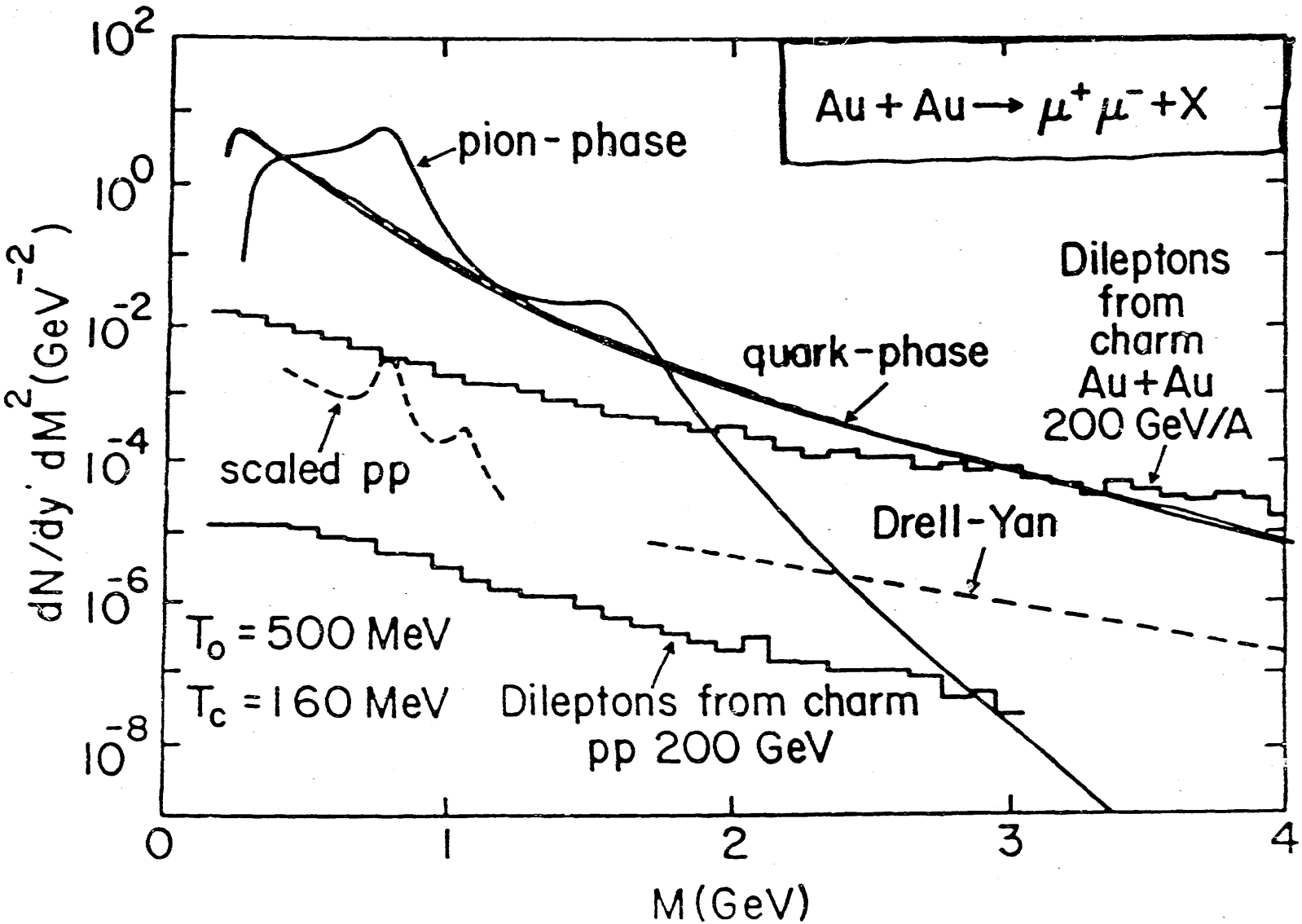

Fig. 3: Dilepton invariant mass spectrum at Au-Au collisions at RHIC coming from various sources. Pion phase and QGP contributions are from[28], charm decays from[30].

Flavor Flow From Quark Gluon Plasma

Johann Rafelski

Department of Physics, University of Arizona Tucson AZ 85721

In this lecture presented at the July 1990 RHIC-BNL-Workshop I discuss diverse hadronic observable of the reactions between relativistic heavy ions related to the production and flow of flavor, and its significance for the observation and identification of quark-gluon matter. This discussion in particular includes a brief survey of our current understanding of the strange particle signature of quark gluon plasma.

1 Looking For Quark Gluon Plasma

The inherent difficulty of the study of Quark-Gluon matter is its expected fleeting presence when two heavy nuclei collide. Therefore, an important element in theoretical investigation of relativistic heavy ion collisions has been the identification of observable of this new state of matter. We must from outset realize that an observable can be either 'characteristic' and/or 'descriptive'. A characteristic measurement would tell us unequivocally that some time during the nuclear interaction quark-gluon matter has been formed. A descriptive observable will not necessarily be characteristic, but should allow us to study the properties of the quark-gluon matter phase, if we can with certainty assume its formation.

First I note that we can in principle measure as function of rapidity and transverse mass the following simple hadronic observable:

- the yield of charge;
- the yield of baryon number;
- the yield of strange particles and in particular that of:
  - single strange particles ($\bar{s}q, s\bar{q}, \bar{s}qq, s\bar{q}\bar{q}$),
  - multi strange baryons ($ssq, \bar{s}\bar{s}\bar{q}, sss, \bar{s}\bar{s}\bar{s}$),
  - ϕ-meson yield ($\bar{s}s$),
  - HBT correlations of strange particles,
  - strange exotica.

In order to present a comprehensive and complete description of the diverse processes occurring, a theoretical interpretation of the data must necessarily account for details of the collision dynamics. This information is at present not available for the energies accessible at RHIC and theoretical models are by necessity dependant on a number of assumptions, in absence of a truly fundamental approach to the collision dynamics. Furthermore, there are additional uncertainties related to carrying through a simulation of the collision dynamics involving a possible phase transformation. Thus it is of essence for the discussion here presented that initial RHIC experiments determine:

- the "stopping power" of the constituent quarks in the colliding nuclei, as measured by the rapidity distribution of the electrical charge;
- the baryon number stopping power of the nuclear medium, as measured conveniently by rapidity distribution of (strange) baryons;

- the entropy produced in the collision, as measured e.g. by the particle multiplicity, in particular pion to baryon ratio as function of rapidity;
- the characteristic "temperature", as measured e.g. by the slopes of transverse mass spectra;

The primary observable we address here is the strange quark flavor and in addition to the above I would like to see a measurement of:

- the high density, above-equilibrium nature of the over saturated strangeness phase space density, which is noted for by the abundance of multistrange baryons and in particular their anomalous abundance enhancement as compared to singly strange antibaryons, which in turn are enhanced as compared to antiprotons produced; and
- the overabundance of strangeness flavor as measured by overabundance of strange particles produced in A–A collisions compared to p–p and p–A reactions;
- kaon HBT correlations, which should show a smaller source than pionic HBT size of the fireball.

The remainder of this lecture is organized as follows: Next, I explain why strangeness flow is viewed as an observable of quark-gluon matter. This is followed by a brief consideration of lessons from the present strangeness data.

2 Why Flavor – Strangeness?

I proposed about ten years ago [1,2] strangeness as an observable of quark-gluon matter. Following on early equilibrium considerations it became soon apparent that strangeness production must be treated in a kinetic approach [3]. Furthermore, in a review prepared for QM'82 [4] I noted "..measurement of production cross section of strange antibaryons could be already quite helpful in the observation of the phase transition.....Measurement of the relative K^+/K^- yield, while indicative for the value of the chemical potential (in hadronic gas phase) may carry less specific information about the plasma. The K/π ratio may indeed also contain relevant information - however it will be more difficult to decipher the message ...it appears that otherwise quite rare multistrange hadrons will be enhanced ... hence we should search for the rise of the abundance of particles like $\Xi, \bar{\Xi}, \Omega, \bar{\Omega}, \phi$ and perhaps highly strange pieces of baryonic matter (strangeletts), rather than in the K-channels. It seems that such experiments would uniquely determine the existence of the phase transition to quark gluon plasma..." This is in a shell nut my position today, though in the elapsed decade the initial simple ideas have undergone a substantial evolution [5,6] and have come under intense scrutiny, see Ref.[7] and references therein.

I think that those who have been critical of "strangeness" have never taken time to study the detailed ideas related to flavor (strangeness) flow, of which the simplest point of view I have quoted myself above. It seems indeed that we have just gone more than 8 years back, as in the strangeness review at QM'90 we can read (see [7]) "Strangeness has been proposed as a signal for quark- gluon plasma formation in RHI collisions. Subsequent to the original proposal several papers appeared which considerably weakened (hic) the early claims (which???) made for strangeness production in heavy ion collisions (references follow from 1985,1986,1988 addressing the question what Kaons can tell us or not..). Representative of several I (J.Cleymans) quote...'...we conclude that there is no natural large difference in flavor composition between the ...QGP and an *equilibrium* hadron gas' ". Clearly, the key which the experimentalists working presently in the field well comprehended and which eludes many theorists, most recently Cleymans, Satz, Suhonen, von Oertzen [8], is not how much strangeness there is, but *what happens to the strange and antistrange quarks*, and how this compares with control data e.g. from p-A collisions.

Clearly, the interest to measure strangeness is there even discounting all theoretical controversy, as every experimentalist hopes to see a spectacular phenomenon, a 'smoking gun' of the phase transition. Interest

in observing strange particles also derives from the second objective of experiments involving relativistic nuclear collisions, the study of equations of state of highly excited nuclear matter. Namely, even without the formation of quark-gluon phase, that is in case that the collision proceeds via the intermediate stage of a fireball consisting only of highly excited hadron gas, the strange particle flow provides essential information about the properties of matter under extreme conditions. However, the relation between observable particle spectra and the equation of state presents many difficulties of detail, and much theoretical modeling will be required; for quark-gluon phase these difficulties are compounded as the observable of a quark-gluon state can be seen only after undergoing a phase transition back into a hadronic form. The phasetransition in turn depends on the equations of state. Hence the study of strange particles emanating from collisions at conditions believed not to lead to quark-gluon phase is extremely important as it helps us understand the backgrounds to the quark-gluon phase signatures, at the same time as we learn about *confined* nuclear matter.

A comprehensive survey of the status of the theory of strange particle production and evolution in hadronic collisions before 1985 can be found in ref.[5]. The progress of experiments and theory has been recorded at the Tucson HMIC meeting [6]. An update has been recently prepared by Eggers et al. [9].

2.1 Strange signatures of quark-gluon plasma

Let us consider the situation in some more detail: as is apparent several experimental options for the study of the flavor–strangeness signal of QGP in heavy ion collisions are available. The most obvious measurement is the determination of the multiplicity of various strange hadrons, often represented as ratios to reduce the influence of the experimental bias (trigger). In this class of measurements, however, components originating from all the different production processes are included; for example, strange hadrons may be formed in

- initial high energy hadronic collisions,
- inside the QGP,
- during QGP hadronization,
- in the final expanding hadron gas,
- rescattering from spectator nuclear matter,

or, if the QGP is not formed at all, during the various (equilibrium and non-equilibrium) stages of a hadron gas fireball. This means that the QGP strangeness signal must be evaluated in relation to proton nucleus reactions and detailed conventional wisdom cascade calculations.

Somewhat more specific approach to identify strangeness signal of QGP is to measure strange particle rapidity and transverse energy or momentum spectra. The above mentioned distinct physical processes normally emit particles into different windows of rapidity or transverse energy, making it possible to select particles from a specific process by introducing appropriate cuts in the differential cross section data. Transverse energy spectra are often divided into separate, although overlapping, regions in which a specific physical process dominates [10]. This conjecture is supported by the fact that ratios of different particle species vary strongly with $m_\perp$. At low $m_\perp$, one finds particles formed in the rescattering of the spectator nucleons. At slightly higher $m_\perp$, particles produced in the hadron gas, which decoupled at the freeze-out temperature of the fireball are dominant. Particles emitted with moderately high $m_\perp$ originate from hot and dense form of matter, conceivably the early QGP. A number of mechanisms can be responsible for this sector of the particle abundance. For example in Ref. [11] two processes were considered: in the first a quark or diquark from the high-momentum tail of the QGP strikes the phase boundary. It than may create a $q\bar{q}$ pair e.g. via string-breaking and so a high $m_\perp$ meson or baryon is emitted in such a micro-jet process. Alternatively, a baryon or meson like cluster in the QGP leaves the

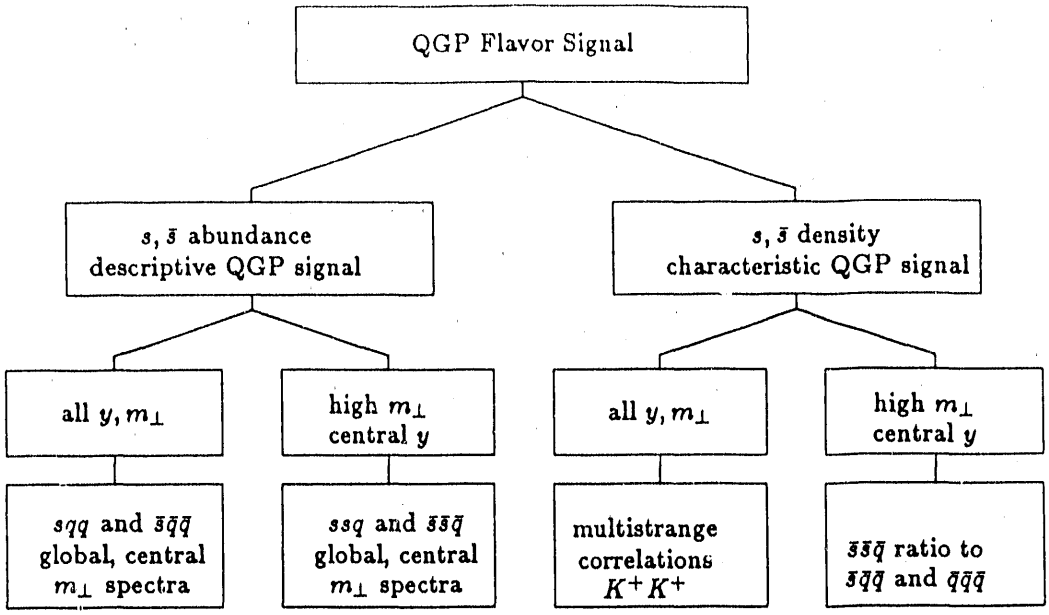

Figure 1: Strange particle quantities for diagnosis of QGP

QGP in unison. In particular it follows from this consideration and the high $\bar{s}$ density that the differential measurement of multistrange antibaryons should have a good (QGP) signal to (HG) noise ratio. If such multistrange antibaryon yields can be analyzed in terms of their transverse and longitudinal flow, the signature for new phenomena will be clear.

From this discussion it is clear that the most interesting part of the particle spectrum involves central rapidity, median (e.g. 1-5 GeV/c) transverse momenta. To sum up the different ways of measuring strangeness, a schematic diagram is shown in Figure 1.

2.1.1 Arguments for strangeness as a QGP observable

The correlated factors why strange particles possess a priori a distinct diagnostic function of the behavior of highly excited nuclear matter and are well suited as a signal distinguishing quark-gluon phase from the hadron gas are as follows:

1. near flavor symmetry for antiquarks $\bar{s}, \bar{u}, \bar{d}$ in all conditions (baryon rich and baryon poor),
2. strongly differing production rates in different phases and strangeness mass thresholds which are of the same magnitude as temperature;
3. extremely high $s\bar{s}$–quark pair density in the quark-gluon phase.
4. the predicted strange antibaryon abundance is greater than background p-p ISR results.

We now discuss in more detail each of these points.

1. Anti-flavor symmetry: Recent BNL and CERN experiments indicate that up to currently available energies the fireball usually has a sizable baryon number and therefore a relatively large baryo-chemical potential μ_B. This means that, for quark-gluon phase in chemical equilibrium, the number of light anti-quarks is suppressed. Deconfined strange and antistrange quarks, on the other hand, are not affected by μ_B and so are suppressed in quark-gluon phase only by their non zero mass. Consequently, but provided that strangeness production has saturated the available phase space, the abundance of antiquarks $\bar{u}, \bar{d}, \bar{s}$ will be nearly equal. In baryon free region, as possibly established at RHIC, this flavor symmetry of

hadronic particles is also in part a result of the fragmentation of the numerous gluons.

2. Production rates and thresholds: Rates for production of $s\bar{s}$ pairs in the quark-gluon phase were often calculated, the latest reference being [9]. The strangeness production time constant in the quark-gluon phase is of the order of 10^{-23} s, while in hadronic gas phase it is 10 to 30 times slower [12] at the same temperature and baryo-chemical potential. This difference is mainly due to the presence of gluons in QGP and different reaction thresholds. The typical time scale for the creation and decay of a fireball can be estimated as the time to traverse, say, a distance of 15 fm i.e. $\simeq 5 \times 10^{-23}$ s, and so strangeness in a thermal hadronic gas will not likely reach equilibrium values, contrary to quark-gluon phase expectations. Thus we expect that any kinetic description of strangeness production involving the usual hadronic particles will give a total strange particle yield significantly below the limits obtained from an equilibrium picture of hadronic gas fireballs. The most accessible reaction (if allowed) is usually the creation of a ΛK or $K\bar{K}$ pair and requires at least 700 MeV. In the quark- gluon phase, on the other hand, the threshold is given by the rest mass of the strange-antistrange quark pair, i.e. only $2m_s \simeq 350$ MeV. This difference between the two thresholds though insignificant at the initial high energies, is noticeably impacting the time scale of strangeness production in a "thermalized " glob of hadronic matter. It is anticipated that at RHIC temperatures of 250 ± 50 MeV will be reached. Here I note the trivial, though important point that in general strangeness production occurs in the numerous rescattering processes, not in the highly energetic initial parton-parton collisions. From this we expect in particular substantial enhancement of strangeness in Nucleus-Nucleus collisions, as compared to scaled p-Nucleus yield, (this subject to the validity of the hypothesis of formation of a hadronic fireball of any 'texture'). I recall here, however, the discussion of Koch and Rafelski [13] concerning the abundance of strangeness in regular hadronic interactions. It was found so close to the expected equilibrium abundance, that it seems as if quark-gluon plasma like phase were formed, permitting to saturate the available strangeness phase space in most hadronic collisions. However, Wróblewski [14] determined that regular hadronic interactions are about three times less effective in making strange flavor as compared to light flavors. Since QGP based estimates lead me to expect flavor symmetry in QGP, some strangeness enhancement must be expected in comparison to p-A scaled result.

3. $s\bar{s}$–density: Even at the time of hadronization, $s\bar{s}$ density (now half as high as at it peak) is about 0.4 strange particle pairs per fm^3. As consequence, most of baryons and antibaryons emerging is strange, and non- strange nucleons are expected to be only 20% of the total baryon–antibaryon abundance [5]. In the hadronic gas phase, by contrast, all antibaryons are suppressed, particularly those with high (anti)strangeness content [5], leading to the expectation that quark-gluon phase be distinguishable from hadronic gas phase by relatively enhanced numbers of anti-strange hadrons [1,4]. This argument, initially developed for baryon rich quark-gluon matter remains valid without change at RHIC energies at central rapidity region, i.e. in the central fireball. As detailed calculations [5] have shown. there is an abundance anomaly expected for strange antibaryons arising primarily from the enormous strange pair density in thequark-gluon matter.

4. Expected direct reaction 'background' It is helpful to consider the magnitude of backgrounds expected for the multi strange (anti) baryons. The $\bar{\Xi}/\bar{Y}$ ratio seen at ISR at $\sqrt{s} = 63$ GeV is only 0.06 ± 0.02 in the central rapidity region [15]. The expected quark-gluon matter result at RHIC is predicted to be ten times greater [5], or even up to 50 times greater [11], at relatively high $m_\perp$. The parallel ratio $\bar{Y}/\bar{N}$ is 0.27 ± 0.02 as measured in the same experiment at ISR, my expectation is that $\bar{Y}/\bar{N}|_{plasma} \sim 2 \pm 0.5$. We thus see that both $\bar{\Xi}/\bar{Y}$ and the $\bar{Y}/\bar{N}$ ratios a interesting, with the former being characteristic of the new form of matter, as it is more difficult to imagine how an enhancement along the theoretical QGP prediction could be made otherwise.

In conclusion: The enormous strangeness pair density to be expected in RHIC–QGP is in my opinion the main experimental objective of flavor based RHIC experiments. This property of the QGP state is particularly interesting, since the primary production mechanism of strangeness is by gluons present

in the deconfined phase. Measurement of strangeness density removes interpretational ambiguities, related to our present ignorance of reaction dynamics, in attempting a comparison of the respective *total* strangeness content of quark-gluon phase and hadronic gas phase, as enhancement of quark-gluon phase strangeness may be diluted by the geometry of the ensemble of collisions and can be argued away on the basis of the perpetual ignorance of the lifetime of the hypothetical hadronic gas phase fireball. Thus strange particle abundance per se, though perhaps most interesting 'barometer' and 'thermometer' of the quark-gluon matter phase, is to be employed to study QGP properties only once the high strangeness density has been established.

2.1.2 Paths to observe multistrange (anti) baryons

Even though at RHIC the "common knowledge" is that the central rapidity region is baryon free, I will not assume here this prejudice and hence refer to the (strange) anti-baryons, which are characteristic for QGP irrespective of the degree of stopping of the baryon number. However, practically every point discussed applies both to baryon flow in baryon free region, and it is of preference if both strange baryons and antibaryons are measured. I will assume that any detector aiming at the measurement of baryon flow will permit the observation and measurement of the charged decay 'V' of the neutral $\bar{\Lambda}$ particles. The decaying $\bar{\Lambda}$ particles originate in part in the (rapid) electromagnetic decays of the $\bar{\Sigma}^0$ particles. All anticascades ultimately become $\bar{\Lambda}$, while only half of all anti-hyperons $\bar{Y}$ will be in the $\bar{\Lambda}$-decay chain, of which 64.2% are giving they typical 'V' decay pattern. Assuming full acceptance for the 'visual' detector for all V's, the total sample of all seen V-events is

$$N_V = 0.642\bar{Y}(\frac{1}{2} + \frac{\bar{\Xi}}{\bar{Y}}) \tag{1}$$

and, should the abundance ratio $\bar{\Xi}/\bar{Y} \sim 1/2$, we see that half of the observed V's would be associated with the primordial $\bar{\Xi}$ abundance.

The difficulty is that the observable $\Xi^-, \bar{\Xi}^+$ decay over a significantly shorter path ($c\tau = 4.92$ cm)than Λ ($c\tau = 7.89$ cm), making necessary a novel detector directly outside the beam pipe. This poses particular instrumental problems, related both to the interface between the two detectors, but more significantly, to the need for extremely high resolution in view of the enormous multiplicity of charged particles, in which the occasional cascade 'kink' has to be searched for. Probably this path to the measurement of multi strange (ant) baryons will be ultimately attempted. However, I would like to draw attention to an alternate approach [16]: in order to find out how many $\bar{\Lambda}$ descend from the cascade decay all that is needed is the measurement of the longitudinal $\bar{\Lambda}$ polarization.
There is a significant difference in this polarization of the $\bar{\Lambda}$ descending from the weak $\bar{\Xi}$ decays. The weak decay polarizes the $\bar{\Lambda}$-spin longitudinally, the mean value of its helicity being given by the decay asymmetry parameter $\alpha_{\bar{\Xi}}$. In the subsequent weak $\bar{\Lambda}$ decay this polarization is effectively 'analyzed'. The practical approach is to consider the so-called up-down asymmetry of the $\bar{\Lambda}$ decay with reference to the plane normal to the $\bar{\Lambda}$-momentum, i.e., to measure how often in the $\bar{\Lambda}$ rest frame the antiproton appears 'above' as compared to 'below', with respect to a plane normal to the direction of $\bar{\Lambda}$-momentum.

The simple criterion which determines the up-down asymmetry is identified boosting the antiproton momentum to the $\bar{\Lambda}$ rest frame and considering S, the vector product between $\bar{\Lambda}$-momentum and $\bar{p}$-momentum. I obtain:

$$S := \vec{P}_{\bar{\Lambda}} \cdot \vec{P}_{\bar{p}}/P_{\bar{\Lambda}}^2 = E_{\bar{p}}/E_{\bar{\Lambda}} = \begin{cases} \text{positive for up} \\ \text{negative for down} \end{cases} \tag{2}$$

Here we have, as usual, $\vec{P}_{\bar{\Lambda}} = \vec{P}_{\bar{p}} + \vec{P}_{\pi}$ for the respective particle momenta and similarly for their energies $E = \sqrt{m_i^2 + P_i^2}$. At this point, I note that the longitudinal polarization considered here is of entirely different origin and nature than the transverse polarization of $\bar{\Lambda}$ associated with hadronic formation processes of these particles. Multiple scattering in the hadronic gas cannot create longitudinally polarized

$\bar{\Lambda}$ out of primordial transverse polarization. However, the longitudinal polarization will be influenced by spin rotation in a magnetic field.

This up/down asymmetry is given by [16]:

$$\frac{N_u - N_d}{N_u + N_d} = \frac{1}{2}\alpha_{\bar{\Lambda}} \wp_{\bar{\Lambda}}, \tag{3}$$

where $\wp_{\bar{\Lambda}}$ is the $\bar{\Lambda}$ polarization and is equal to the α_{Ξ} decay parameter. This polarization is analyzed by the $\alpha_{\bar{\Lambda}}$ decay parameter. The different values of the parameters found in the data tables are: $\alpha_{\Lambda} = -\alpha_{\bar{\Lambda}} = 0.642 \pm 0.013$; $\alpha_{\bar{\Xi}^0} = -\alpha_{\Xi^0} = 0.413 \pm 0.022$; and $\alpha_{\bar{\Xi}^+} = -\alpha_{\Xi^-} = 0.455 \pm 0.015$. The total up-down asymmetry of all V-events is

$$\frac{N_u - N_d}{N_u + N_d} = \frac{N_{\Xi}}{N_{\bar{Y}}} \frac{1}{2} \alpha_{\Lambda} \alpha_{\Xi}, \tag{4}$$

where we have included the relative abundance of all polarized $\bar{\Lambda}$ to the total abundance of V's: $N_{\Xi}/N_{\bar{Y}} = (2\bar{\Xi}/\bar{Y})/(1 + 2\bar{\Xi}/\bar{Y})$. With $\bar{\Xi}/\bar{Y}$ in the range 1/2(resp. 1/3) we expect a negative up-down asymmetry of 14% (resp. 11%). For the 'normal' value $\bar{\Xi}/\bar{Y} \sim 0.06$ there is the hardly observable asymmetry of only 1.6%. Hence observation of the longitudinal polarization is QGP specific!
I further note that $\bar{\Omega}$ weak decays have a negligible influence over the particle abundances and, in particular, their polarizations, since $\bar{\Omega}$, Ω are at least five times less abundant than $\bar{\Xi}$, Ξ [5] and their decay asymmetry parameter ("polarizer" capability) is 5-20 times weaker (depending on the decay channel). The fact that some $\bar{Y}$, $\bar{\Xi}$ are descendants of strong decays of $\bar{Y}(1385)$, $\bar{\Xi}(1530)$, etc. is also of no consequence, as abundances of these particles has been considered part of $\bar{Y}$ resp. $\bar{\Xi}$ abundance.

2.1.3 Gluons in plasma

The key role played by gluons in making high strangeness density an important observable is self-evident. Not only do gluons produce strangeness flavor dominantly (see below) but more importantly they provide the key distinction between the quark-gluon phase and the hadron gas. The high gluon abundance and density in the plasma impacts the entire history of the plasma state, in particular also the process of hadronization at the end of the quark-gluon phase lifetime, in which appreciable strangeness production occurs again. Indeed, strangeness can be considered a signal for gluons in the quark-gluon phase. We will briefly summarize here the expectations about the gluonic component in the plasma. We note that since gluons do not carry electrical charge, but only the strong charge, they can be observed (indirectly of course) only by suitable measurement of strongly interacting particles.

Including a first-order perturbative effect [17] the gluon number density can be estimated from the equilibrium density as

$$\rho_g \ (\mathrm{fm}^{-3}) = 1.04 \left(\frac{T}{160 \ \mathrm{MeV}} \right)^3 \left(1 - \frac{15\alpha_s}{4\pi} \right) \tag{5}$$

giving for a typical temperature of 200 MeV a value of 0.55 fm^{-3} for $\alpha_s = 0.6$ and 0.8 fm^{-3} for $\alpha_s = 0.5$. For a quark-gluon phase volume with radius 4 - 5 fm, we therefore have 200–300 gluons. Note also that this density rises as the cube of the temperature. Because gluons can be created and annihilated easily in interactions with other gluons and light quarks, the gluon density closely follows the evolution of temperature in the course of the quark-gluon phase lifetime. The equilibrium gluon energy density is

$$\varepsilon_g = \frac{8\pi^2}{15} T^4 \left(1 - \frac{15\alpha_s}{4\pi} \right) \tag{6}$$

and the gluon partial pressure is

$$P_g \ (\mathrm{GeV.\ fm}^{-3}) = \frac{1}{3}\varepsilon_g = 0.15 \left(\frac{T}{160 \ \mathrm{MeV}} \right)^4 \left(1 - \frac{15\alpha_s}{4\pi} \right) \tag{7}$$

which for $T = 200$ MeV and $\alpha_s = 0.6$ yields 100 MeV fm^{-3} and forms the major component of the quark-gluon phase pressure. (The total quark-gluon phase pressure must, of course, be larger than both the vacuum pressure $B^{1/4}$ and the pressure of the hadron gas surrounding it.)

Gluons also play a major role in the dynamics of the quark-gluon phase-hadronic gas phase transition: they carry much of the quark-gluon phase entropy, contributing an entropy density of about

$$\begin{aligned} \sigma_g(\,\mathrm{fm}^{-3}) &= \frac{32\pi^2}{45} T^4 \left(1 - \frac{15\alpha_s}{4\pi}\right) \\ &= 3.76 \left(\frac{T}{160\mathrm{MeV}}\right)^3 \left(1 - \frac{15\alpha_s}{4\pi}\right) \end{aligned} \tag{8}$$

which for $T = 200$ MeV and $\alpha_s = 0.6$ is 2 units per fm^3 (3.6 units per gluon). This large amount of entropy plays a major role in the hadronization phase transition, forcing gluons to fragment into quarks.

2.2 Strangeness production in the quark-gluon phase

Since the time scale in a typical nucleus-nucleus collision is very short, the strangeness content of both quark-gluon phase and hadronic gas phase cannot *a priori* be assumed to be in equilibrium: it is necessary to determine explicitly the rate of strangeness production in both phases. The key result was obtained in the work of Rafelski and Müller [3]. The plasma initially contains very few, if any, strange quarks as those produced in pre-quark-gluon phase direct hadron-hadron reactions will generally be at higher rapidity than the fireball. Essentially all the $s\bar{s}$ production is therefore dominated by collisions of the central gluons, which in a first approximation can be assumed to be in a practically thermal distribution; light quark-antiquark collisions, it turns out, play only a minor role. Therefore the time evolution of strangeness density during the production process is only a function of temperature and not of the baryo-chemical potential. I will give here a brief sketch of the theory of strangeness production and show how strangeness density grows with time.

The t-averaged cross sections for strangeness production are shown [9] in Figure 2. At this point it seems that both glue and quark induced processes are of comparable magnitude. However, as we will just see the statistical factors entering the thermal average will strongly favor the gluon induced processes: there are simply more glue-glue than quark-antiquark collisions of suitable quantum number in plasma. In order to identify the energy range contributing to the production of strangeness, it is useful to write the production rate as an integral over the differential rate dA/ds [9]:

$$A_i = \int_{4m^2}^{\infty} ds\, (dA_i/ds) = \int_{4m^2}^{\infty} ds\, \bar{\sigma}_i(s)\, P_i(s) \qquad i = g, q \tag{9}$$

The weight function $P_g(s)ds$ is the number of (gluon) collisions within the interval $(s, s + ds)$ per unit time per unit volume, with a similar interpretation for $P_q(s)$. In a thermal system:

$$P_g(s) = \int \frac{d^3p_a}{(2\pi)^3 E_a} \frac{d^3p_b}{(2\pi)^3 E_b} \frac{s}{2} \delta[s - (p_a + p_b)^2] \frac{1}{2} g_g^2 f_g(p_a) f_g(p_b) \tag{10}$$

In principle, non-equilibrium momentum distribution functions should be used for f_g, presumably evolving from the structure functions of the incoming reacting hadrons towards their equilibrium forms. However, because of the high gluon-gluon cross sections, this should happen very quickly [18,19]. In first approximation, one can therefore use the (thermal and chemical) Fermi and Bose equilibrium distributions. In Figure 3, the product of the weight functions $P_g(s)$ and $P_q(s)$ with the respective cross sections is plotted for $T = 250$ MeV and $m = 170$ MeV. In one case, $\alpha_s = 0.6$, in another, the running coupling constant was used with $\Lambda = 200$ MeV. Note that most $s\bar{s}$ pairs are made at $\sqrt{s} \simeq 0.5$ GeV, giving at least some

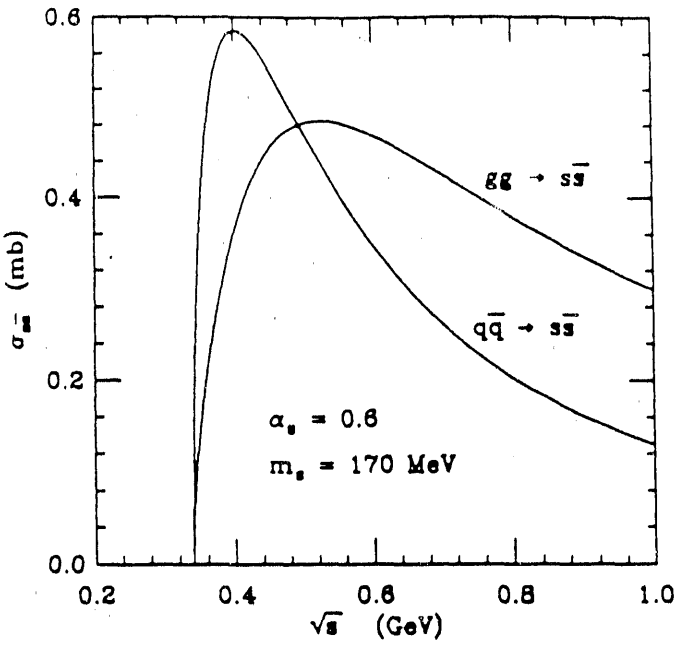

Figure 2: t-averaged strangeness production cross sections for $\alpha_s = 0.6$, $m = 170$ MeV

credence to the use of perturbative QCD, and in particular the value $\alpha_s = 0.6$ selected.

In Figure 4, the time evolution of the density of strange quarks in quark-gluon phase is shown ($\alpha_s = 0.6, m_s = 170$ MeV). As expected, there is a strong threshold effect at temperatures around 150 MeV. A similar calculation which included an expansion model of the fireball [5] showed that the strong dependence of $s\bar{s}$ production on the temperature also implies that the strangeness abundance freezes out with a value characteristic of the highest temperatures reached during the collision. No significant strangeness annihilation occurs during the fireball expansion.

3 Lessons From Present Experimental Results on Strangeness

I will focus here on the aspects of current experimental work instructive to the described developments, giving only a schematic interpretation. The experimental method employed to determine the enhancement is to compare the yield of strange particles as a function of the inelasticity of the interaction. In order to demonstrate the kind of analysis we will have to implement for RHIC experiments let me now consider a hypothetical quark-gluon phase fireballs as being at the origin of the latest results in strangeness production. I consider the *experimental* situation as it presents itself in May 1990, following on the Quark Matter '90 meeting. In all BNL and CERN experiments reported so far strangeness enhancement by a factor 2 ± 0.5 has indeed been seen, but can not be taken without prejudice to be a signal of quark-gluon plasma.

In this discussion I will use experimental results to estimate the value of the temperature and chemical potential at which the strange particles are likely to have been born and will try to determine if there is any glaring inconsistency of the present data with such a hypothesis. Alas, as we will see, total strangeness data of from BNL can not point to a particular phase of matter, much as expected. Nevertheless, in order to test the consistency, rather than two parameters (T, μ_B) we must consider three quantities characterising the average thermodynamical properties of the fireball, e.g.:

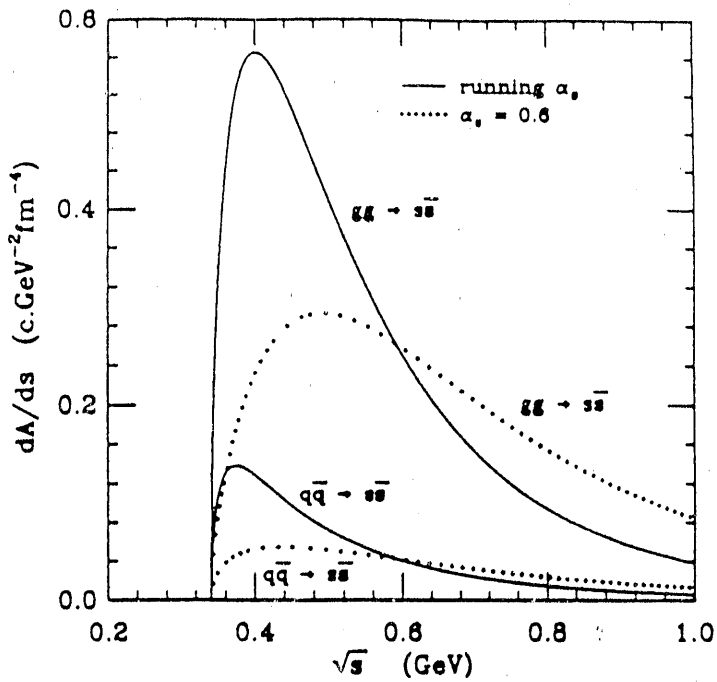

Figure 3: Differential production rate $dA/ds = P(s)\bar{\sigma}(s)$, with T =250 MeV and $m = 170$ MeV, for gluons and $q\bar{q}$ pairs, with $\mu_B = 400$ MeV. Solid lines are for running α_s with $\Lambda = 200$ MeV, dotted lines for $\alpha_s = 0.6$.

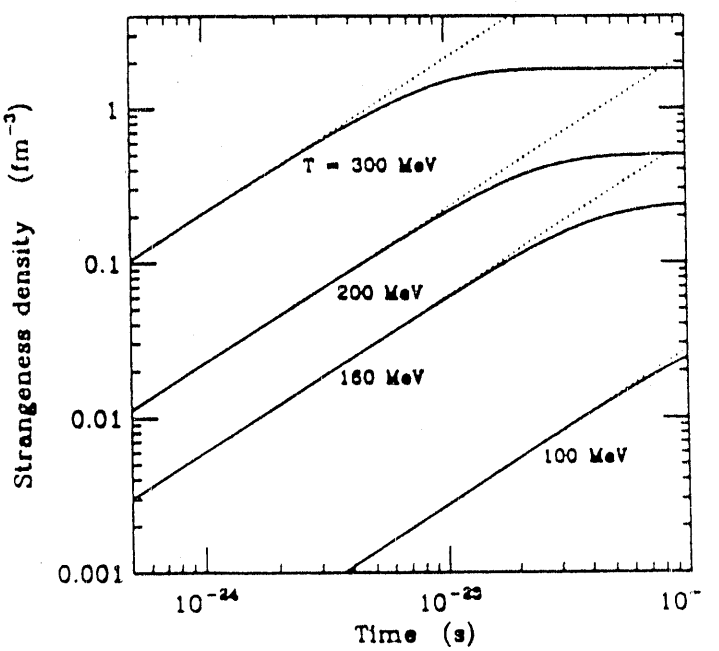

Figure 4: Time evolution of the strange quark density in quark-gluon phase for different values of the ternperature. Dashed lines: no $s\bar{s}$ annihilation.

1. The temperature T, as obtained directly from particle transverse energy spectra. Here we must take care to distinguish the projectile and target rapidity regions from the central region which of greatest interest to us here. For most particles with large cross sections such as pions, the observed slopes of transverse mass particle spectra provide us with the temperature T^H at freeze-out of the particular particle species in the hadron gas. However, strange particles can exhibit higher temperatures as their interaction length is larger. For the thermal picture to be applicable, a similar temperature should be found in the corresponding rapidity spectrum.

2. As a direct measure of the baryo-chemical potential, we can consider the entropy per baryon S/B, which we assume here to be mostly produced during the initial stages of the nuclear collision. During the subsequent, in particular hydrodynamical evolution of the quark-gluon phase or hadronic gas phase, no entropy is produced and the baryon number is also constant. For the case of the perturbative QCD equation of state, constant-S/B implies $T \propto \mu$ with a determined constant [20]. The value of entropy per baryon reached in the reaction is obtained under the assumption that a gas of nucleons and pions dominates all central fireball secondaries (counting all mesons as pions, all baryons as nucleons) [21]:

$$\frac{S}{B} \simeq \frac{S_N}{B} + \frac{S_\pi}{\langle n_\pi \rangle} \frac{\langle n_\pi \rangle}{B} \tag{11}$$

   where the entropy per pion is about 4.05 and the entropy per nucleon outside of the degeneracy region is $S/B = 2.5 + (m_N - \mu_B)/T$.

3. The baryo-chemical potential μ_B^H in the (final stage) hadron gas phase can be determined conveniently from the K^+/K^- or K_s/Λ ratios, which are sensitive to μ_B^H [22], because of large strangeness exchange cross sections which rapidly establish the so-called relative chemical equilibrium between different species of strange particles. This is true even if absolute chemical equilibrium is not attained for strangeness in thehadronic gas phase [5]. If the values of T and μ_B^H do not disagree to much with the entropy based QGP constraint (see above), this can be taken as a first indication that we are possibly close to the quark-gluon phase.

3.1 BNL - RHI results

There are two experiments at BNL measuring strange particle spectra, of which the more ambitious TPC-based E810 has just begun to collect data [23], while the magnetic spectrometer experiment E802 has essentially completed its data taking [24]. Both experiments see an appreciable strangeness signal in 14.6 A GeV/c Si–Au collisions (the beam rapidity is 3.44), with a central collision trigger. The common result of both experiments is that strange particles have a rather "thermal" shape in the central rapidity region, and that the temperature is in the vicinity of 150 MeV, but with a statistical error which is presently 15 MeV. While E810 expects to measure the abundances of diverse multi strange baryons and antibaryons in the near future, experiment E802 provides already today precise data on ratio of meson abundances [24]. Additional data including in particular the antiproton spectra has recently been presented at the BNL-HIPAGS workshop [25]. It therefore seems justified to assess the results of E802 with a simple fireball model in mind. We will need just the most naive of the pictures for further discussion: the tube model of the nucleus-nucleus collision leads to the formula for the number of participating target nucleons $A_t = 1.5 A_{\rm projectile}^{2/3} A_{\rm target}^{1/3}$ predicts $A_t \simeq 80$ for the Si–Au case and hence a total baryon content of the fireball $B \simeq 108$. This corresponds to a theoretical rapidity $y_{lab} \simeq 1.23$ for a fireball made out of $(A_p + A_t)$ nucleons, closely corresponding to the experimentally inferred central rapidity $y = 1.2$. This assumes complete stopping so that the accessible CM energy $\sqrt{s} = 261$ GeV is mostly transferred into the internal excitation of the fireball,suggesting an energy content of 2.42 Gev per baryon, less energy in excitation of spectator matter.

From rapidity particle densities we can now derive the central pion to baryon ratio: for $1.1 < y < 1.6$, the proton rapidity density dN/dy is 16.2 ± 0.3, implying a baryon rapidity density 38 ± 0.7 (given the baryon to proton ratio of 2.35 in the tube model for Si-Au collisions). Both the π^+ and π^- rapidity

density is quoted at 16 ± 1. Allowing for an equal number of neutral pions the pion central rapidity density is 48 ± 1.8. This results in a pion to baryon ratio 1.25 ± 0.05. For $T \simeq 125$ MeV (observed pion temperature), the pion gas entropy per pion is $\simeq 4.3$, and hence the pion entropy per baryon is 5.4 units of entropy. This implies that we are still in a rather degenerate nuclear gas phase, and hence the entropy contribution of baryon gas is, relatively speaking, small. For $\mu_B = 840, T = 125$ MeV, the baryon gas contributes about 3.7 units of entropy, while at $\mu_B = 500, T = 150$ MeV we have 5.4 units additional entropy. Hence we are at $S/B \simeq 8 - 10$, the lower value for the higher range of baryo-chemical potential.

The observed relative abundance $K^+/\pi^+ = 0.203 \pm 0.019$ is obtained by ignoring the possible distortions of the low energy spectra due to 'low energy' phenomena; both K and π spectra are extrapolated assuming the Boltzmann form controlled by the fireball properties. Similarly, the K-ratio $K^-/K^+ = 0.19 \pm 0.03$ is found - with same limitations as described above. The question now is if these results on particle ratios, temperature, and other inferred fireball properties are consistent with the assumption of a particular phase of hadronic matter and the above constraints. Before beginning this discussion we note that the first of the particle ratios is indeed a lower limit, in the sense that whatever the reaction mechanism, we do not expect to saturate the strangeness phase space fully, and hence the preliminary *equilibrium* picture we develop should predict a larger value than is actually observed.

Let us first make the hypothesis that hadronic gas was made [26]. I fix the K^-/K^+-ratio at 0.2. There are two options:

- I take T = 125 MeV as the freeze out temperature. I infer following Koch et. al [22] a value of baryo-chemical potential of 520 MeV; the expected K^+/π^+ ratio is about 0.26, allowing for pions from Δ-decays, and assuming that the strangeness phase space has been saturated.
- Taking instead as basis the strange particle temperature T= 150 MeV (under the tacit assumption that pion spectra are distorted by Δ decays and rescattering on spectator matter) the K - ratio implies a slightly lower baryo-chemical potential of just below 500 MeV and the K^+/π^+ ratio is slightly higher at 0.334.

Thus with the proviso that 'only' 80, resp. 60% of the strangeness phase space is saturated both temperature hadronic gas scenario seems fully consistent with the data, with the exception that we do not understand how so much strangeness could be made by hadronic gas processes. At this point I note that this discussion disagrees in its detail with Ref. [8], which assumes fully saturated strangeness phase space. Therefore a rather low temperature is found, incompatible with the transverse spectra, or said differently (allowing for flow effects), with the mean energy per particle. Interestingly, the difference between our (and Lévai's [26]) analysis and Ref. [8] is the predicted d/p ratio which is highly sensitive to the entropy per baryon: assuming to much strangeness, additional pions are needed in order to 'dilute' the strange particle abundance, an effect which I estimate at about 3 units of entropy per baryon. By implication the expected value for Ref. [8] of the $d/p = 0.05$, our discussion suggests 2 - 3 times larger value.

For both above considered choices T, μ_B, the energy per baryon, which in this region of parameters is mainly controlled by the K^-/K^+-ratio, turns out to be below 1.9 GeV. To get a slightly higher value, as it may seem required within the simple fireball model presented above, we should have set the Kaon ratio to a larger value, allowing for an unseen low energy fraction of K^-. Taking a value 0.25 at $T = 150$ MeV would lead to energy per baryon somewhat above 2 GeV and at the same time a π^+/p ratio near 1.3, in agreement with the value reported at central rapidity.

Next, let us see how the data fare under the assumption of quark-gluon plasma phase. Naturally, the advantage of this assumption is that we have little difficulty swallowing the saturation of strangeness phase space, thanks to the described rapid strangeness production. Furthermore it turns out that in region of $(\mu_B, T) = (850, 130)$ MeV there would be a similar amount of entropy in the quark-gluon phase, as in the hadronic gas phase at $(\mu_B, T) = (500, 150)$ MeV. The supposition is that in the phase transition of the isolated glob some reheating from about 130 to 150 MeV takes place, and there is corresponding

reduction of the chemical potential. As any pre - transition emission from the plasma would in such environment be covered by the soft component of the hadronic gas phase, we should not expect any visible quark matter effects in kaon spectra. Thus solely from the observation of singly strange particles we can not make a definitive statement about the presence of QGP in nuclear collisions at BNL. However, it is interesting to note that the BNL conditions are near to the baryon-rich quark-gluon phase domain. This conjecture is supported by the recent finding of antiproton multiplicity [25], which in the central rapidity region is less than one part in thousand of the proton multiplicity.

But presently the only argument one could make in favor of QGP at Brookhaven is that the values of the parameters estimated above imply that even at BNL energies strangeness production in the quark-gluon phase will be rapid and will nearly saturate the available phase space. It is therefore most interesting to look at BNL for strange antibaryons, which without quark-gluon phase formation should hardly be produced at these energies. Given the suppression of antiprotons, which is expected for a baryon-rich fireball consisting of either hadronic gas phase or quark-gluon phase, observation of a *greater* strange antibaryon yields would strongly suggest that already at BNL energies this state of matter may be formed. It is to be hoped that the results from experiment E810 will allow us to conclude this issue.

3.2 CERN - RHI results

At CERN the available energy is much greater and ranges from 60 up to 200 GeV per nucleon. However, the laboratory has not taken full advantage of the available machine resources as yet, by limiting its main experimental runs to the highest available energy. In the asymmetric reactions such as the S–W collisions studied by WA85 [27] there is the advantage over the S–S collisions studied by NA35 [28] of the much greater baryon number stopping. But there are difficulties in interpreting the data, which are associated with overlap of the different kinematic regions (target, central and projectile). In this regard, one has here in principle less of a problem than at BNL since the rapidity window is almost twice as large as at BNL: the projectile rapidity at 200 A GeV/c is 6, compared to 3.4 for BNL. The particular advantage of the S–S data is the symmetry of the kinematics, permitting a much better understanding of particle flows. The disadvantage is the likely presence of significant transparency at 200 GeV per nucleon. However, the central rapidity region is 3 (for symmetric collisions), making a particle in the laboratory very fast. Consequently an experiment similar to E802 is impossible, as the time of flight does not permit particle identification. Thus the small aperture spectrometer experiment at CERN, NA34, is concentrating on the target fragmentation region. In view of the currently available results and this discussion it would seem that it would be of considerable advantage to study the symmetric S–S collisions at lowest available CERN energy, viz. 60 A GeV, in expectation of the lead beam run initially at a similar energy.

Points of importance to our work in the most recent results of NA35 are:

- The Λ–$\bar{\Lambda}$ rapidity distribution, which shows two pronounced peaks within the projectile and target rapidity regions, an indication of a severe depletion in the central region. This shows that much of the Λ signal derives from re-scattering in the baryon rich projectile and target fragmentation region.
- The $\bar{\Lambda}$ multiplicity is sharply confined to the central region $y = 3 \pm 0.5$. The rate of $\bar{\Lambda}$ production in S–S collisions is about 120 times greater than in p–p collisions (the error quoted is large). The per trigger event multiplicity of $\bar{\Lambda}$ is given to be 1.5! This (120-fold) enhancement has to be confronted with the 36-fold enhancement of the negatively charged tracks (i.e. pions). This truly surprising result cannot even remotely be explained by cascading in hadronic gas, as the probability of $\bar{\Lambda}$ formation is decreasing during the moderation of the beam energy.
- The general strangeness flavor production is up by a factor 2.5 on top of the factor 36 for negatives: the K/π-ratio at mid-rapidity $y = 3$ is 0.15, to be compared to 0.06 for similar energy p–p system.

All these results remind us of the quark-gluon phase. Unfortunately, we do not have comparable data on production of $\bar{p}$ or $\bar{\Xi}$ and thus cannot conclude that the expected systematic signal of quark-gluon phase has been found. The lack of data on the essential $\bar{p}$ and $\bar{\Xi}$ production is being filled by the large aperture Ω'-spectrometer WA85 experiment, which has presented the first results from the study of S–W collisions at 200 A GeV. Because of complex Monte Carlo studies required to understand the relative sensitivity of the experiment to $\bar{\Lambda}$ and $\bar{\Xi}$, this ratio is not known as yet, though WA85 has already reported first observation of $\bar{\Xi}$. The following has now been reported by WA85 [27]:

- The temperature (inverse slope) of negatives, Λ and $\bar{\Lambda}$ is the same and is 227 MeV, i.e. higher than the temperature seen in S–S collisions. Because of the greater stopping expected, this result can be taken as a confirmation that the highest energy and baryon densities were reached in this experiment. Unfortunately, we cannot determine the baryo- chemical potential for this experiment as yet, nor can we determine the entropy per baryon. To this end we would need data on kaon (K_s), pion (negatives) and also positive particle (protons and positive kaons) spectra in relation to the strange baryons and antibaryons.
- The yield of both Λ and $\bar{\Lambda}$ per negative track in the central rapidity region $2.4 < y < 2.65$ is enhanced by a factor 1.7 in comparison to the control p–W data. Both enhancements are similar and the ratio of Λ to $\bar{\Lambda} \simeq 0.2$ does not change.
- There seems to be an enhancement in the anticascade to cascade ratio in S–W collisions ($\sim 0.43 \pm 0.07$) as compared to the control p–W run ($\sim 0.27 \pm 0.06$). Clearly, more statistics are needed to reconfirm this result. Also, it is important to know by how much the $\bar{\Xi}/\bar{\Lambda}$ ratio is enhanced in S–W reactions with reference to p–W reactions.

In CERN data, we hence once again see a clear strangeness enhancement, accompanied now by a highly significant enhancement of strange antibaryon yield. We cannot imagine how to interpret this data other than in terms of quark-gluon plasma. However, the data are still fragile at the level of only a few standard deviations, and require some improvement in the statistics. Also, we need a more complete evaluation of all available data in order to be able to give more detailed characterization of the conditions reached in the S–W and S–S collisions.

3.3 Concluding comments

Without a substantial interaction between experiment and theory, the most spectacular measurements remain, especially in this subject matter without much concrete insight. The situation is further complicated by numerous superficial if not wrong publications (as exemplified above) relating to the subject, as well as the process of "reinventing the wheel", which so often leads not only to the repetition of the old mistakes. The particular reason why flavor flow experiments are very attractive in the beginning of any nuclear collider operation is the fact that the high expected strangeness production allows event by event analysis. Even if event rate should initially be small, strangeness will be clearly visible. The experiments suggested here are based on the following key observations:

1. At sufficiently high energy densities, heavy ion collisions may lead to formation of a deconfined phase of strongly interacting nuclear matter, the quark-gluon phase, in which flavor symmetry is partially restored and strangeness becomes abundant. The full event characterization is needed to fix the thermodynamic variables of essence for the basic understanding of reaction kinematics needed in understanding (strange) particle flows.
2. Compared to a hadron gas, in quark-gluon phase strangeness is produced faster and strangeness density is greatly higher. Also, strangeness is produced in quark-gluon phase almost totally by glue-glue processes. Uncertainty about the hadronization process makes global strangeness measurements less attractive as a signal of quark-gluon phase than observation of specific (multi)strange particles.

3. Anomalous (large) strange and multistrange antibaryon multiplicities can be viewed as the clearest signal that something unusual is happening in central collisions, particularly when viewed in specific windows of $(p_\perp, y)$.

4. Multistrange antibaryons can provide crucial information as they are predominantly formed in phase space regions characterized by a very high strangeness density.

5. As the theory of strangeness production and hadronization relies on key parameters of QCD, these will become accessible to measurement in heavy-ion collision induced reactions, through the measurement of diverse flavor and particle flows and detailed comparison of experiment with theory.

Acknowledgement I would like to thank G. Odyniec, S. Lindenbaum and L. Madanski for their interest in this work and pertinent comments about important experimental aspects. I thank T. Ludlam for his kind hospitality at BNL.

References

[1] J. Rafelski and R. Hagedorn, in: Statistical Mechanics of Quarks and Hadrons, ed. H. Satz, North Holland, Amsterdam 1981

[2] J. Rafelski, in: Workshop on Future Relativistic Heavy Ion Experiments, eds. R. Bock, R. Stock, GSI 81-6, Darmstadt 1981

[3] J. Rafelski and B. Müller, Phys. Rev. Lett. **48**,1066 (1982); **56**,2334(E) (1986)

[4] J. Rafelski, "Strangeness in Quark Gluon Plasma", S. Afr. J. Phys. **6**,37 (1983)

[5] P. Koch, B. Müller and J. Rafelski, Phys. Rep. **142**,167 (1986)

[6] "Hadronic Matter in Collision 1988", held in Tucson, Arizona, October 6-12, 1988; World Scientific, 1989, eds. P. Carruthers and J. Rafelski

[7] J. Cleymans, "Strangeness Production in Relativistic Ion Collisions - Theoretical Review", UCT-TP 142/90, to appear in proceedings of QM'90 meeting, Menton, France, May 1990.

[8] J. Cleymans, H. Satz, E. Suhonen and D.W. von Oertzen, Phys. Lett. **242B**,111 (1990)

[9] H.C. Eggers and J. Rafelski, "Strangeness and Quark Gluon Plasma: Aspects of Theory and Experiments", Preprint AZPH-TH/90-28, submitted to J. Mod. Phys.

[10] E. Shuryak, in this volume

[11] J. Rafelski and M. Danos, Phys. Lett. **192B**,432 (1987)

[12] P. Koch and J. Rafelski, Nucl. Phys. **A444**,678 (1985)

[13] P. Koch and J. Rafelski, S. Afr. J. Phys. **9**,8 (1986)

[14] A. Wróblewski, Act. Phys. Pol. **B16**,379 (1985)

[15] T. Akesson et al. [ISR-Axial Field Spectrometer Collaboration], Nucl. Phys. **B246**,1 (1984)

[16] M. Jacob and J. Rafelski Phys. Lett. **190B**,173 (1987)

[17] S.A. Chin, Phys. Lett. **78B**,552 (1978):

[18] S. Mrówczyński and J. Rafelski, Phys. Rev. **C40**,1077 (1989)

[19] B. Müller, in this volume

[20] J. Rafelski and A.L. Schnabel, in: Conference on Intersections between Particle and Nuclear Physics, Rockport 1988, AIP# 176; J. Rafelski and A.L. Schnabel, Phys. Lett. **207B**,6 (1988)

[21] N.K. Glendenning and J. Rafelski, Phys. Rev. **C31**,823 (1985)

[22] P. Koch, J. Rafelski and W. Greiner, Phys. Lett. **123B**,151 (1983)

[23] S.E. Eiseman et al. [E810 collaboration], "Neutral V production with 14.6 x A GeV/c Silicon Beams", BNL-44716, submitted to Phys. Lett. B

[24] T. Abbott et al. [E802 collaboration], Phys. Rev. Lett. **54**,847 (1990)

[25] J.B. Costales [E802 Collaboration], HIPAGS Workshop, Brookhaven, March 1990

[26] P. Lévai, B. Lukács and J. Zimányi, J. Phys. **G16**,1019 (1990)

[27] N.J. Narjoux et al. [WA85 Collaboration], Lecture at Quark Matter '90, Menton, France, May 7–11, 1990
D. Evans et al. [WA85 Collaboration], Lecture at Quark Matter '90, Menton, France, May 7–11, 1990
E. Quercigh, in: "Hadronic Matter in Collision 1988", World Scientific, 1989, eds. P. Carruthers and J. Rafelski

[28] R. Stock et al. [NA35 Collaboration], Lecture at Quark Matter '90, Menton, France, May 7–11, 1990
H. Ströbele et al. [NA35 Collaboration], Lecture at Quark Matter '90, Menton, France, May 7–11,1990

Space-Time Quark-Gluon Cascade for R.H.I.C.

K. GEIGER AND B. MÜLLER

Department of Physics, Duke University

Durham, NC 27706, U.S.A.

1. Introduction

In order to provide a numerical simulation of the time evolution of ultrarelativistic heavy ion collisions we have formulated a fully relativistic space-time approach based on a parton cascade model. This model hopefully sets the stage for a detailed and realistic study of heavy ion collisions on the microscopic level of the dynamics of quark and gluon interactions within the framework of QCD. For earlier work in this direction see D. H. Boal, [1].

Ultimately, the goal is to make predictions for, e.g., the thermalization time-scale and the energy densities associated with the quarks and gluons in the central region of the nuclear collision system. Of major importance will be to analyze whether the system will temporarily form a quark-gluon plasma during the time of collision.

Such a study is of fundamental importance, insofar as some of the most essential questions regarding the experimental search for the formation of a quark gluon plasma in ultrarelativistic nuclear collisions are, first, whether the energy densities achievable in such reactions will be sufficiently large to force the transition, second, whether the duration of the high density phase is sufficiently long to allow for an approach to thermal phase

space equilibrium, and finally, whether there are characteristic signatures that for the identification of an actual occurrence of such a transition.

2. Hadron Collisions at large and intermediate $p_\perp$

The picture of a nuclear collision as a cascade of independent parton-parton collisions is based on two fundamental assumptions, namely, the short range of (hard and semi-hard) parton-parton interactions, and, the factorization of parton scattering and hadronization process. There is no doubt that the first assumption is questionable in the presence of a dense medium, but at high energies it should be much better satisfied for a parton cascade than for a cascade of nucleons with an internal size of 1 fm. The second assumption has been extensively tested in 'large $p_\perp$' (large angle) scatterings of individual hadrons. Theoretically it is known to hold for "inclusive" processes, but it is often found to be approximately valid also in semi-exclusive processes.

To illustrate these concepts, let us first review how they apply to an inclusive reaction between individual hadrons. We consider the reaction

$$A + B \longrightarrow C + X, \tag{1}$$

where A, B are two colliding hadrons, C is the detected particle and X symbolizes all other particles that may have been produced but which are not observed. At high energies, this is a typical 'large $p_\perp$' process, where the particle C has a high momentum perpendicular to the $A - B$ axis. Kinematically we have the situation shown in Fig. 1.

The transverse momentum is defined as $p_\perp = |\vec{p}_C| \cdot \sin\theta$, where θ is the scattering angle with respect to the $A - B$ axis. Furthermore

$$\begin{aligned} s &= (p_A + p_B)^2, \\ t &= (p_A - p_C)^2 = -\sqrt{s}\, p_\perp \cot\frac{\theta}{2}, \\ u &= (p_B - p_C)^2 = -\sqrt{s}\, p_\perp \tan\frac{\theta}{2}. \end{aligned} \tag{2}$$

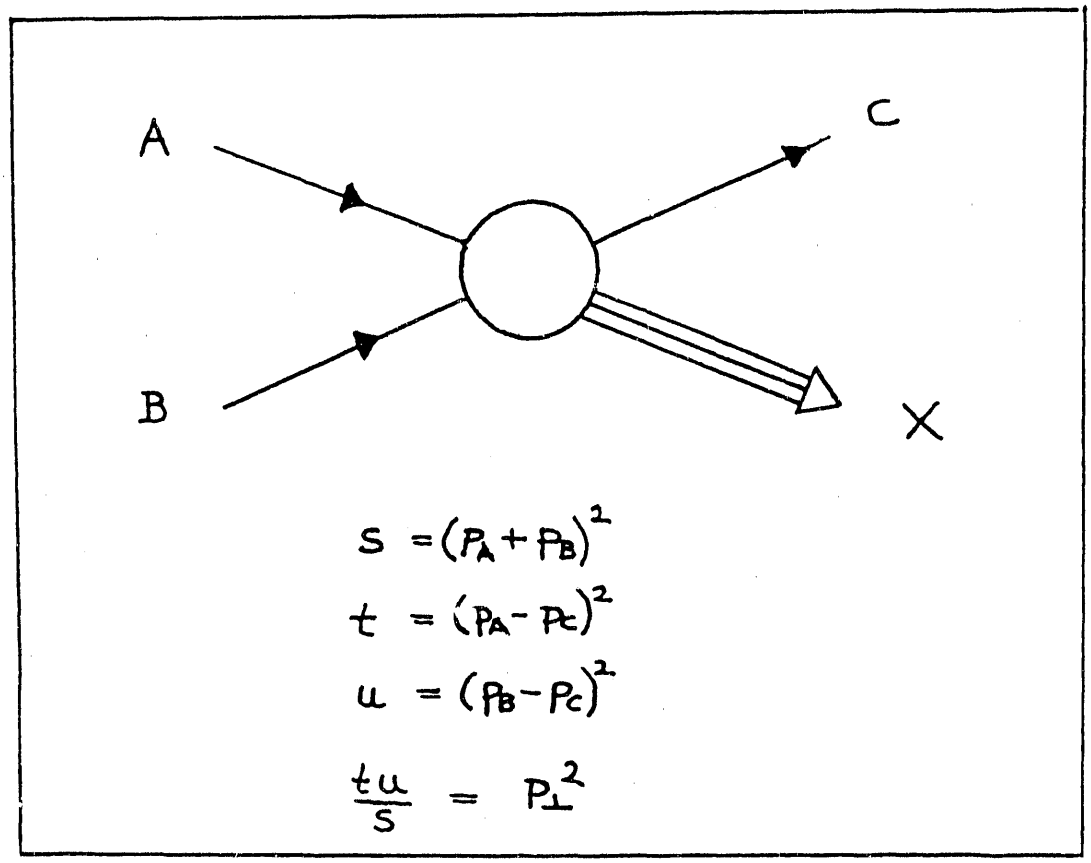

Fig. 1: The process $A + B \to C + X$

If $s, t, u, p_\perp^2$ and M_X^2 (the missing mass of all the nonobserved particles in $A+B \to C+X$) are all large, i.e. larger than $m_{A,B,C}^2$, then one may hope that no intrinsic mass scales are governing the dynamics and that the basic scattering can be represented as in Figure 2.

The essential hypotheses of this picture are:

a) Soft fragmentations $A \to a, \ldots$, $B \to b, \ldots$ occur, where the partons $a, b \ldots$ carry finite fractions $x_a, x_b \ldots$ of the momenta of the initial nuclei A, B.

b) All the large $p_\perp$ scattering arises from the hard parton- parton scattering $ab \to cd$.

c) Recombinations $c \to C \ldots$, $d \to X$ happen such that the final hadron C is carrying

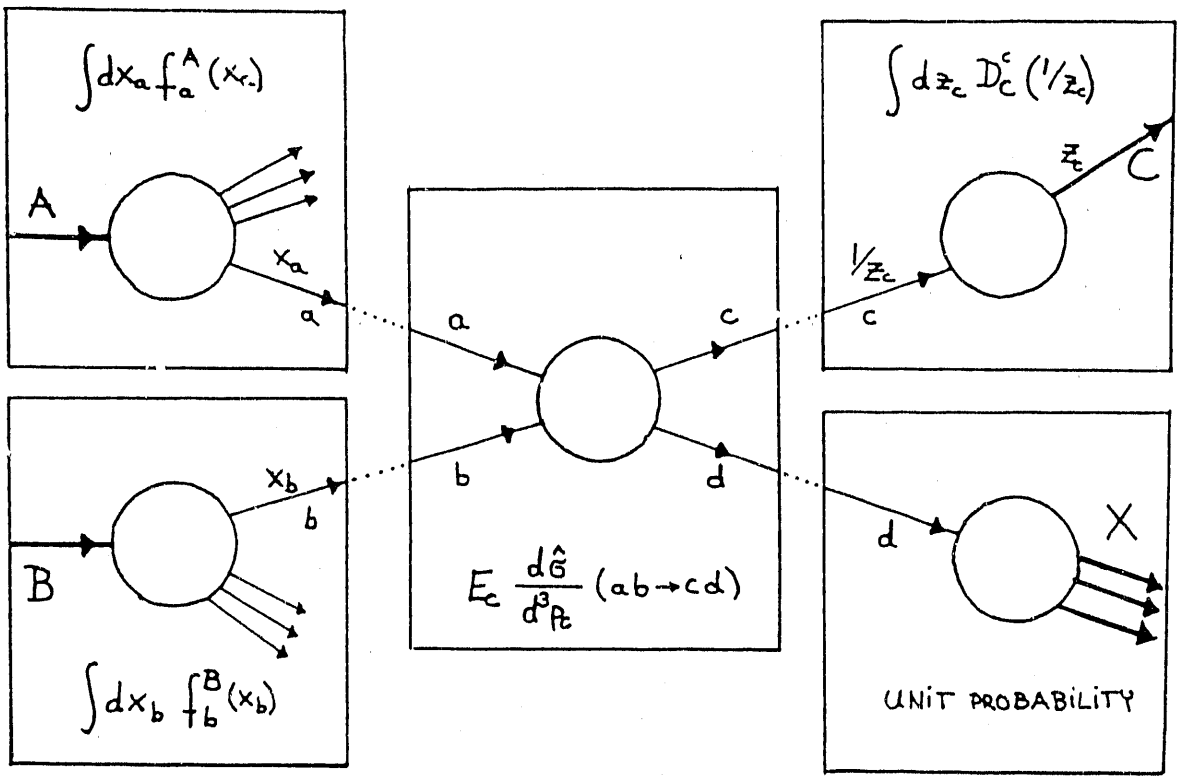

Fig. 2: The reaction $A+B \to C+X$ at large $p_\perp$ arising as a result of fragmentations $A \to a\ldots, B \to b\ldots$, hard scattering of constituents $ab \to cd$, and recombinations $c \to C\ldots, d \to X$ (hadrons).

off a finite fraction z_c of the momentum of parton c, and similarly for all the nn-detected hadrons X.

The inclusive cross section for $A + B \to C + X$ can then be represented in the form

$$E_C \frac{d\sigma}{d^3p_C}(AB \to CX) = \sum_{a,b} \int_0^1 dx_a \int_0^1 dx_b f_a^A(x_a, Q^2) f_b^B(x_b, Q^2) \cdot$$
$$\cdot \sum_d \left[E_c \frac{d\hat{\sigma}}{d^3p_c}(ab \to cd) \right] \cdot \int_0^1 dz_c D_C^c\left(\frac{1}{z_c}, Q^2\right) \cdot 1, \qquad (3)$$

where a, b, c, d specify the parton types (gluons, $u, d, s\ldots$ quarks), x_a, x_b are the fractions of momenta of A, B carried by the partons a, b and $f_a^A(x_a, Q^2), f_b^B(x_b, Q^2)$ are the prob-

ability distributions of the parton flavors in x_a, x_b, which depend also on the momentum transfer Q^2 in the collision (scaling violations). Furthermore $d\hat{\sigma}/d^3p_c$ is the differential cross section for the parton-parton scattering process $ab \to cd$, z_c is the fraction of the parton c momentum carried off by the hadron c and $\mathcal{D}_C^c(1/z_c, Q^2)$ is the 'fragmentation function', which is the probability distribution of the final hadron C in z_c.

Thus, we require three ingredients to describe the hadron hadron collision (1) at large $p_\perp$:

a) The parton distribution functions f_a^A, f_b^B, which describe the structure of A, B in terms of their parton distributions,

b) The parton-parton cross sections $d\hat{\sigma}/d^3p_c$ for all types of $2 \to 2$ scattering processes,

c) The fragmentation functions D_C^c, which describe the probability that the detected hadron C takes a fraction z_c of the leading partons momentum, thus, the momentum composition of C in terms of parton momenta.

The structure functions a) and the fragmentation functions c) contain essential non-perturbative QCD effects and cannot be derived from perturbation theory. However, the momentum distributions of partons in hadrons, i.e. the structure functions $f_j^h(x, Q^2)$ are very well probed in deep inelastic eN-scattering in the range $10^{-3} \lesssim x \lesssim 1$ at specific Q^2. Similarly, the fragmentation functions $D_h^j(z, Q^2)$ can be measured in $e^+e^- \to$ jets or in $eN \to$ jets for a broad range of z and fixed Q^2. With these data, for some particular Q^2, the charge of $f_j^h(x, Q^2)$ and $D_h^j(z, Q^2)$ with Q^2 can then be calculated by means of the evolution equations (see e.g. [2],[3],[4]).

$$\begin{aligned} \frac{d\, f_i^h(x, Q^2)}{d(\ln Q^2)} &= \alpha_s(Q^2) \int_x^1 \frac{dy}{y} \sum_j f_j^h(y, Q^2) \cdot P_{j \to i}\left(\frac{x}{y}\right) \\ \frac{d\, D_h^i(z, Q^2)}{d \ln Q^2} &= \alpha_s(Q^2) \int_z^1 \frac{dy}{y} \sum_j D_h^j\left(\frac{z}{y}, Q^2\right) P_{j \to i}(y), \end{aligned} \tag{4}$$

where the $P_{j \to i}\left(\frac{x}{y}\right)$ are the 'splitting functions'. These appear as the lowest order expres-

sions for the variation per unit Q^2 of the probability for finding the parton i in parton j with a fraction x/y of the parent parton momentum ($y > x$).

From these evolution equations one can determine the parton distributions f_g^j and the fragmentation functions D_h^j for sufficiently large values of Q^2, provided they are known (i.e. measured) at some value Q_0^2. Finally, the remaining ingredient b), the cross sections $d\hat{\sigma}/d^3p_c$ ($ab \rightarrow cd$), can be calculated in QCD perturbation theory, if Q^2 is large enough ($Q^2 \gtrsim 1 - 2\mathrm{GeV}^2$) and the strong coupling $\alpha_s(Q^2)$ between the partons becomes sufficiently small.

Thus, putting it all together it is possible to calculate the inclusive cross section for $A + B \rightarrow C + X$ from Eq. (3). For a more detailed presentation see e.g. [2],[3] and references therein.

3. Dynamics of relativistic nuclear collisions

In order to describe the dynamics of a highly relativistic nuclear collision within the picture outlined in the previous section (i.e. in accordance with Eq. (3) and Fig. 2), we have formulated a parton cascade model to simulate the time evolution of such a reaction.

Basically, we 'solve' Eq. (3) by means of a Monte Carlo sampling method, i.e. by simulating many collision events on the computer and taking their average.

How do we simulate such a nuclear collision?

The goal is to find a realistic description based on the fundamental QCD-interaction of quarks and gluons, with a maximum of calculable theoretical input, supplemented by a minimum of experimental data (e.g. the structure functions), where our limited present knowledge of strong interactions requires.

Clearly a fully relativistic space-time description is necessary. As a guideline we use the picture of hadron interactions, sketched in the previous section, and incorporate the factorization of the reaction in the three essential elements, namely, fragmentation of

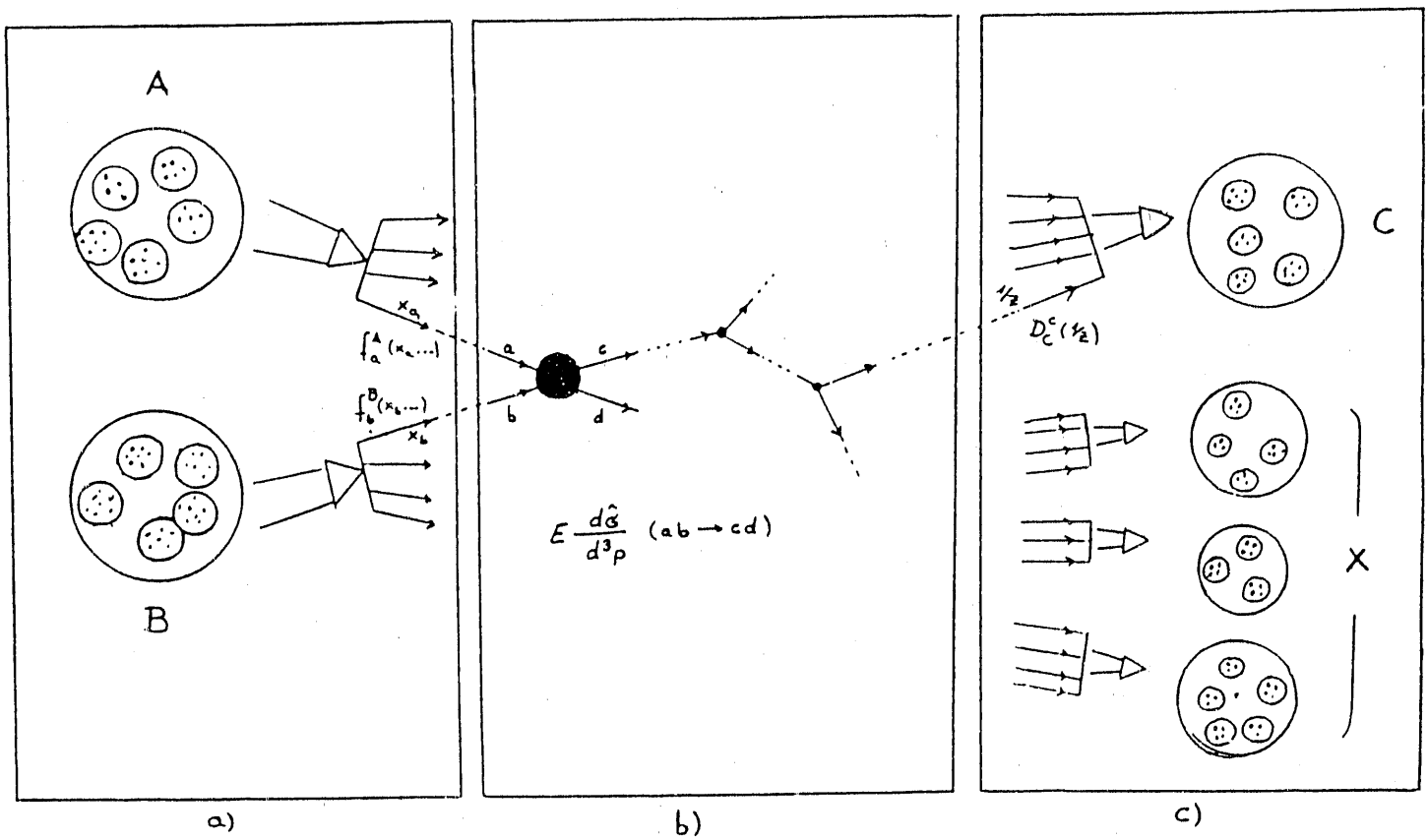

Fig. 3: The three essential building blocks of our dynamical description of a nuclear collision $A + B \rightarrow \ldots$:

a) Initialization with parton distributions in the nucleons of the colliding nuclei A, B according to the structure functions f_a^A, f_b^B.

b) Collision of the nuclei, described in terms of the space-time evolution of parton cascades, governed by elementary parton-parton collisions and parton decays.

c) Hadronization occurs after a certain thermalization time and is controlled by the fragmentation functions D_C^c yielding the final hadron states and momentum distributions.

partons from the colliding nuclei, parton-parton collisions and recombination into final hadrons (c.f. Fig. 2, Eq. (3)). Such an approach would then allow for a study of ultrarelativistic nuclear collisions on the microscopic level of the dynamics of quarks and gluons, both in momentum space and configuration space.

The model we employed is a parton cascade evolution. The concept (illustrated in Fig. 3a)-c)) is the following:

We consider central collisions of two highly relativistic nuclei $A + B \rightarrow \ldots$ in their center of mass (CM) frame.

In accordance with the three-stage picture, the model consists of three building blocks

a) Initialization (fragmentations of A and B into partons, (Fig. 3a)),

b) Parton collisions and parton decays (parton cascades, (Fig. 3b)),

c) Hadronization (formation of final state hadrons, (Fig. 3c)).

In the following we will describe the details of these elements.

a) Initialization:

The nucleons of the two colliding nuclei A and B are assigned initial positions randomly throughout the volume of A, respectively B.

The nucleons themselves are pictured as ensembles of partons (i.e. valence quarks, sea quarks and gluons). Since the structure functions $f_a^A(x,Q^2)$, $f_b^B(x,Q^2)$ are the probability distributions of the parton flavours in $x = p_{\text{parton}}/p_{\text{hadron}}$, the fractional distributions of the initial momenta of A and B among their constituent partons will be given by $x_a f_a^A(x,Q^2)$ and $x_b f_b^B(x_b,Q^2)$. Thus, the partons of A and B are randomly assigned fractions x_a, x_b of the CM-momentum per nucleon according to the distributions

$$x f_i^N(x,Q^2), \qquad \begin{cases} N & = \text{proton, neutron} \\ i & = \text{gluons, valence quarks, sea quarks,} \end{cases} \tag{5}$$

from which the longitudinal momenta $p_{\parallel} = x \cdot p_N$ were determined. The explicit forms of the $xf(x,Q^2)$ that we use, are shown in Fig. 4. They are the $EHLQ$ structure functions

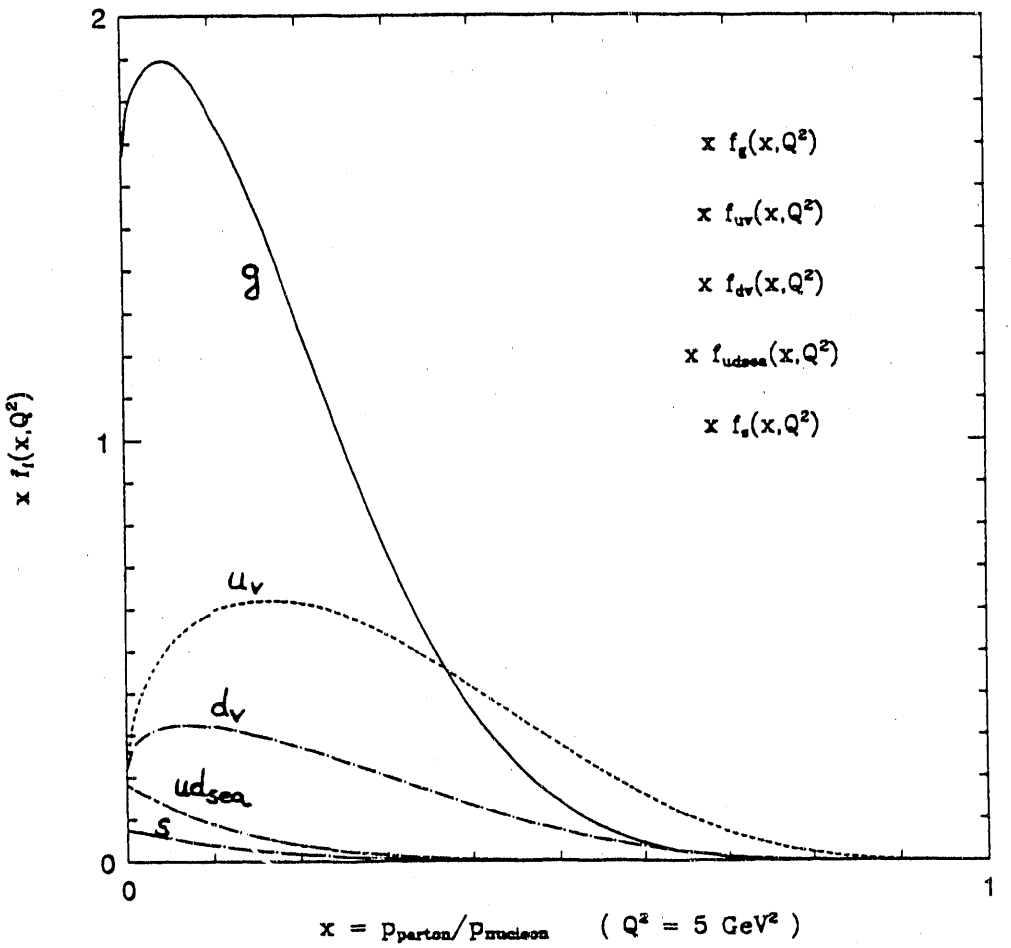

Fig. 4: Structure Functions $xf_j(x, Q^2)$ for Sampling Longitudinal Momenta of Initial Partons.

in the parametrization of Eichten et al. [5]. So far we assumed that the parton structure of the nuclei A and B are well represented by simple superposition of their nucleons' structure functions. A more realistic description (which we plan to implement) is to include 'shadowing' and 'EMC-type' effects [11] that modify this simple picture.

The transverse momenta $p_\perp$ of the partons are sampled from a normal distribution with zero mean value and variance of 0.18 GeV [1]. This transverse momentum spread

results essentially from the partons 'Fermi motion', which is due to the fact that they are confined within the radius of a nucleon (of the order of 0.5-1 fm). Thus, by the uncertainty principle, the partons must have a momentum spread of $\Delta p \simeq \hbar/(0.5\text{fm}) \simeq 0.4$ GeV transverse to the nucleon's direction. The corresponding $p_\perp$-distribution is found to be approximately a normal distribution, roughly indepdendent of $s = (E_A + E_B)^2$ and Q^2.

The positions of the partons in configuration space are randomly chosen within a sphere of radius $r_N = 1$ fm around the nucleons CM positions. These positions are then boosted into the CM frame of the initial nuclei A, B, which establishes the strongly Lorentz contracted shape of the nuclei as viewed in the CM frame (see Fig. 8).*

Each parton is therefore described by its flavor f, its coordinates $\vec{r}$ in configuration space (the CM frame of A and B), its four momentum $p = (E, \vec{p})$ and its restmass m.

b) Collision:

Once the initialization is complete, the time development (described in discrete time steps of the nuclear collision starts. In each timestep the flavor f, position $\vec{r}$, energy E, momentum $\vec{p}$ and virtual mass M_v (which the parton can acquire through off shell scattering as described below) are stored for each parton. These quantities are updated after each time step. Since we incorporate particle creation processes, the number of partons will increase with time, and we need to consider partons with all possible flavors $f = g, u, d, s, \overline{u}, \overline{d}, \overline{s}$. Heavier quarks c, b are not taken into account at this time.

The evolution of the collision now proceeds as cascades of partons and is described as follows:

---

* The informed reader may wonder whether this is correct because it was shown sometime ago that a moving object would look rotated, and not contracted, if viewed by an observer at rest. However, this is not what is shown in Fig. 8. The positions of the particles are plotted as if they would be instantaneously seen by a multitude of syncronized local observers, not by a single distant observer.

The partons propagate along classical trajectories until they collide. 'Internal' parton collisions, i.e. very soft collisions between almost colinear partons are ignored if the total energy of the pair is $\sqrt{\hat{s}} \leq 1$ GeV, (quantities with a 'hat' i.e. $\hat{s}, \hat{t}, \hat{u}, \hat{\sigma}$ etc. refer to the partons).

To decide, whether in a given time step a collision between two partons occurs, the total cross sections $\hat{\sigma}$ for parton-parton scatterings are used to define a specific area of interaction. If the distance of closest approach of the two trajectories (defined as the point where the product of relative velocity and separation of the parton pair under consideration is zero) is within this area of interaction, then a collision occurs (i.e. if $|\vec{r}_1 - \vec{r}_2|_{\min} < R_{\hat{\sigma}} \equiv \sqrt{\hat{\sigma}/\pi}$.)

The cross sections we use are evaluated from the lowest order $2 \rightarrow 2$ processes of QCD. The relevant processes are depicted in Fig. 5, the corresponding amplitudes for the case of massless partons are summarized in Ref. [6]. In order to avoid the Coulomb-like singularity of the scattering amplitudes at small four momentum transfer $\hat{t}$, between the partons, the cross sections were set equal to a constant below a cutoff momentum $p_0 \equiv \sqrt{-\hat{t}_0} = 0.5$ GeV. However, since we will also take into account 'off-shell' scattering, we generalized the cross-sections for massless partons to include also virtually massive partons.

Once a collision occurs between a specified parton pair (1,2) the nature of the process (cf. Fig. 5) has to be chosen. For example, for the scattering of two gluons, where there are the four processes

$$gg \rightarrow gg, u\bar{u}, d\bar{d}, s\bar{s}, \tag{6}$$

we sample the type of process and thus the type of outgoing partons according to the relative probabilities (depending on $\hat{s} = (p_1 + p_2)^2$). Notice that, beside ordinary scattering $gg \rightarrow gg$, there is the possibility of producing particles of different flavor via $gg \rightarrow q\bar{q}$.

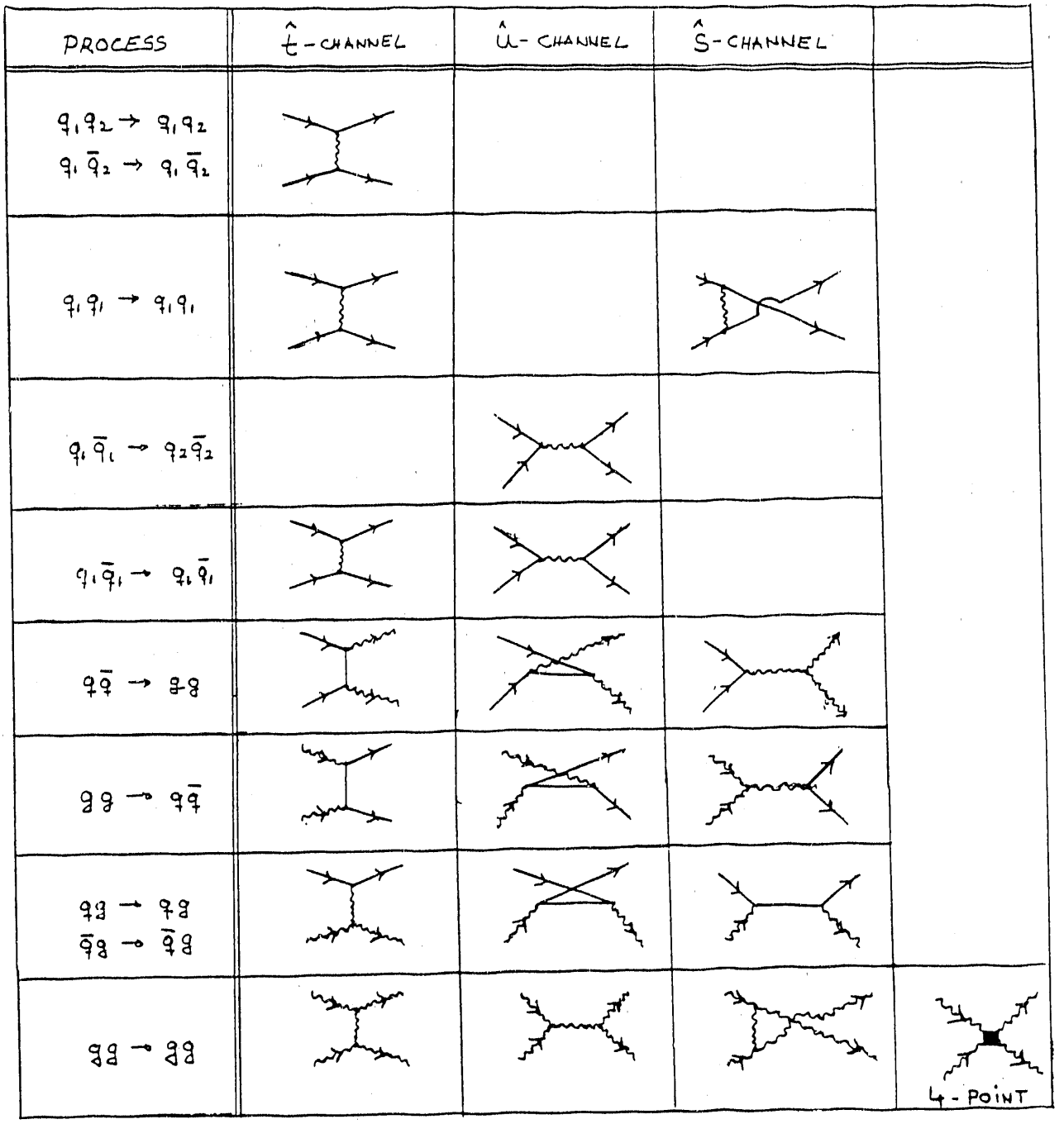

Fig. 5: Lowest order diagrams to evaluate the cross sections for parton-parton scattering processes. Shown are the $\hat{t}, \hat{u}, \hat{s}$ channel contributions. For $gg \to gg$ in addition there is the four point vertex.

Similarly for $q\bar{q}$-scattering we have to choose from

$$q\bar{q} \rightarrow u\bar{u}, d\bar{d}, s\bar{s}, gg. \tag{7}$$

Next the partons (3,4) that emerge from a collision are distributed in $\hat{t} = (p_1 - p_3)^2$ and $\hat{u} = (p_1 - p_4)^2$, or equivalently in scattering angle θ and invariant masses M_3^2, M_4^2.

The distribution in mass corresponds to 'off-mass shell' scattering and effectively includes higher order QCD diagrams. For example, for the scattering of a quark and a gluon the outgoing quark line is not necessarily that of a 'free' quark but possibly connected to another vertex, as illustrated in Fig. 6. In this case the quark obtains a virtual mass M_v. Its square M_v^2 is defined as the inverse squared quark-propagator since

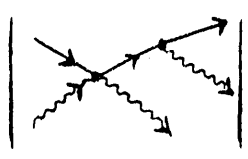

$$\propto \frac{1}{p^2 - m^2} \equiv \frac{1}{M_v^2}. \tag{8}$$

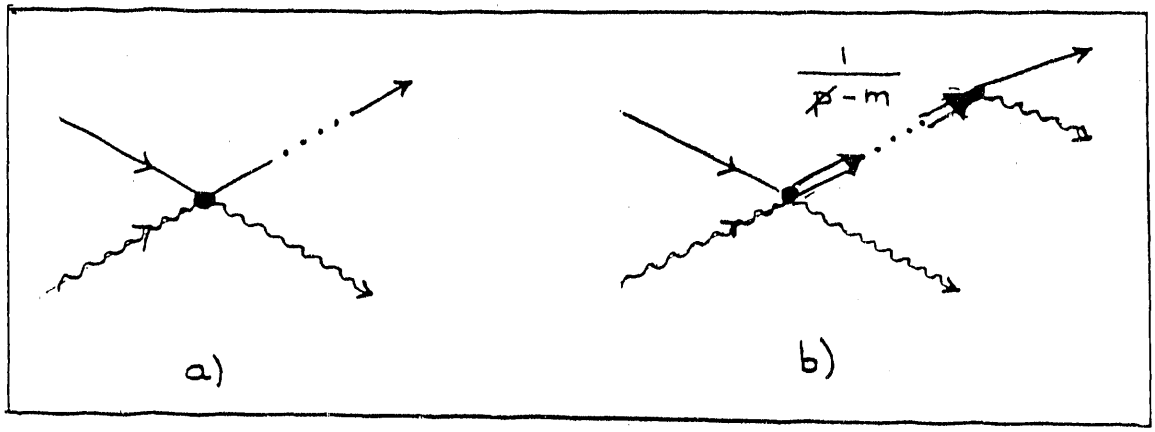

Fig. 6: Scattering of a quark and a gluon, a) with the outgoing quark on mass shell, b) with the outgoing quark scattered off mass shell, resulting in a virtual mass.

The invariant mass distribution, which determines the degree of how far the partons are off mass shell, can be calculated from QCD. Since the magnitude of the partons

virtual masses corresponds to their lifetime, the invariant masses are determined by the decay probabilities of the partons. These probabilities are given by the splitting functions $P_{j\to j_1 j_2}(z)$ for the decay of parton j into new partons j_1, j_2 which carry off fractions z and $(1-z)$ respectively of the summed energy and momentum of parton j. The invariant mass distribution one then obtains, is (see Ref. [7]).

$$f(t,t_c) = \frac{\alpha_s(t)}{2\pi t}\cdot\gamma_j(z_c)\cdot\pi_j(t,t_c) \tag{9a}$$

where $t \equiv M_v^2$, $j = q, g$ and

$$\pi_j(t,t_c) = \left(\frac{\alpha_s(t)}{\alpha_s(t_c)}\right)^{d_j} \tag{9b}$$

$$d_j = 2\gamma_j(z_c)/\beta_0 \tag{9c}$$

$$\gamma_j(z_c) = \int_{z_c}^{1-z_c} P_{j\to all}(z)dz \tag{9d}$$

$$\alpha_s(t) = \frac{4\pi}{\beta_0 \log(Q^2/\Lambda^2)}, \tag{9e}$$

$$\beta_0 = 11 - 2/3 n_f. \tag{9f}$$

The function $\pi_j(t,t_c)$ in (9b) is the probability that the parton j of invariant Mass $t = M_v^2$ decays only into 'unresolvably' soft partons until its invariant mass M^2 has been degraded to $t_c = \mu_c^2$. We will use both, an invariant mass cutoff $t_c = \mu_c^2$ and a cutoff in z at z_c. Partons with $M^2 < \mu_c^2$ are considered not to decay and to propagate freely until the next time step. Also we treat partons with $z < z_c$ as unresolvably soft, as explained after equation (13). The invariant mass cutoff t_c and the cutoff in z at z_c are necessary in order to avoid the production of an infinite number of very soft partons.

According to this picture with partons possibly being off mass shell, we choose the scattering angle and the invariant masses of the outgoing partons (3 and 4) from probability distributions which are determined by the differential cross section for the specific process sampled before,

$$\frac{d\hat{\sigma}(\hat{s},\hat{t},\hat{u})}{d\hat{t}} = \frac{d\hat{\sigma}(\hat{s},\cos\theta,M_3,M_4)}{d(\cos\theta)dM_3^2 dM_4^2}. \tag{10}$$

When a parton has been scattered off mass shell, it can 'decay', which means it can either radiate off a gluon (Bremstrahlung) or, if it is a gluon, it can also produce a $q\bar{q}$-pair (cf. Fig. 7).

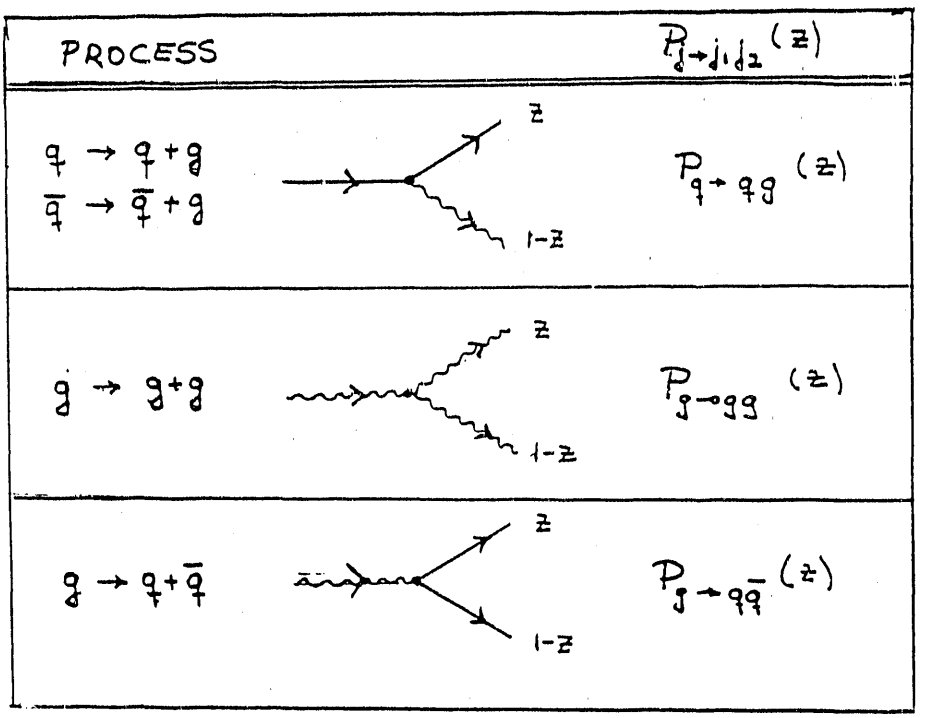

Fig. 7.: Basic QCD diagrams, for splitting processes of quarks and gluons described by the corresponding splitting functions $P_{j\to j_1 j_2}(z)$.

These decays occur with a lifetime $\Delta\tau$, determined by the degree to which the partons are off-mass shell,

$$\Delta\tau \sim \frac{1}{\Delta E} \sim \frac{(E+|\vec{p}|)}{M_v^2}. \tag{11}$$

where M_v^2 is the squared virtual mass of the decaying parton.

The processes illustrated in Fig. 7 are described by the 'splitting functions' $P_{j\to j_1 j_2}(z)$ which are defined as

$$P_{j\to j_1 j_2}(z) = \frac{z(1-z)}{2} \sum_{\substack{\text{spin}\\ \text{color}}} \frac{|V_{j\to j_1 j_2}|^2}{k_\perp^2}. \tag{12}$$

As mentioned before, they are essentially the lowest order probability densities for the splitting process $j \rightarrow j_1 j_2$ with products j_1, j_2 carrying off fractions $z = p_{j_1}/p_j$ and $(1-z) = p_{j_2}/p_j$ of the energy momentum of j. Furthermore, $k_\perp$ is the transverse momentum spread between j_1 and j_2 with respect to the direction of $\vec{p}_j$. It depends on the squared virtual mass M_v^2 of j via

$$k_\perp^2 = z(1-z) \cdot M_v^2. \tag{13}$$

In each time step, for every parton that is off mass shell it is checked, whether it decays or not. Since the distribution $\pi_j(t, t_c)$ in (9b) gives the probability for a parton j with invariant mass $t = M_v^2$ to emit only unresolvably soft radiation we generate a random number r between 0 and 1 and decide, if $r < \pi_j(t = M_v^2, t_c)$ then the parton will only emit unresolvably soft radiation and propagates freely to the end of the timestep. On the other hand, if $r > \pi_j(t = M_v^2, t_c)$, then it is allowed to decay.

If the parton decays in a given time step Δt is produces two new partons which carry off fractions z and $(1-z)$, respectively, of its summed energy and momentum according to the corresponding splitting function. In addition, the decay products receive momenta $\vec{k}_\perp$ and $-\vec{k}_\perp$, respectively, transverse to the direction of the decaying partons momentum. The magnitude of $|\vec{k}_\perp|$ is sampled from the appropriate $k_\perp$-distribution for the process under consideration.

In case of quark or antiquark the splitting process is clearly determined. However, in case of a gluon we have four competing processes

$$g \rightarrow gg, u\bar{u}, d\bar{d}, s\bar{s}, \tag{14}$$

and the nature of the actual process by which it decays is sampled according to the relative probabilities, determined by the splitting functions.

If the parton does not decay in this time step, it continues to propagate and can either decay in a later time step or may scatter with another parton before it decays.

Thus, the space-time evolution of the nuclear system proceeds by means of parton cascades and parton showers, described by elementary parton-parton collisions and parton decays calculated from QCD.

Since the computer code is still in the process of development, we will present only a few preliminary results. We considered a central collision of two equal nuclei with their center of mass chosen as the reference frame. For the initialization, three valence quarks, five gluons and no seaquarks were assigned to each nucleon according to the structure functions (5) so that the gluons carried about 50% of the nucleon's momenta on the valence quarks the other half. The contribution of seaquarks is known to be comparatively small in the region $0.02 \leq x \leq 1$ and was neglected so far. For Q^2, occurring in the structure functions (5), we took an average value depending on the collision rate of partons for the chosen CM energy of the initial nuclei ($Q^2 \approx 5$ GeV^2).

The size of time steps was taken to be 0.05 fm, small enough to resolve the density of parton collisions and decays.

We took a running coupling constant

$$\alpha_s(Q^2) = \frac{12\pi}{(33 - 2n_f)\log(Q^2/\Lambda^2)} \tag{15}$$

with $n_f = 3$, $\Lambda = 0.2$ GeV. The value of Q^2 is determined by the momentum transfer, i.e. the kinematics of each individual parton-parton collision.

For the rest masses of the quarks we took

$$m_u = m_d = 0, \quad m_s = 0.15 \text{ GeV}. \tag{16}$$

In Fig. 8 we show the time evolution of a $(A = 32)+(A = 32)$ collision in the CM frame of the nuclei at a total energy of 1280 GeV, corresponding to an $E_{\rm CM}$=20 GeV/nucleon. The series of pictures are a cut through the $z - x$ plane in configuration space from $t = 0$, corresponding to the initialization of the nuclei, until $t = 10$ fm. Fig. 9 shows the dN/dy

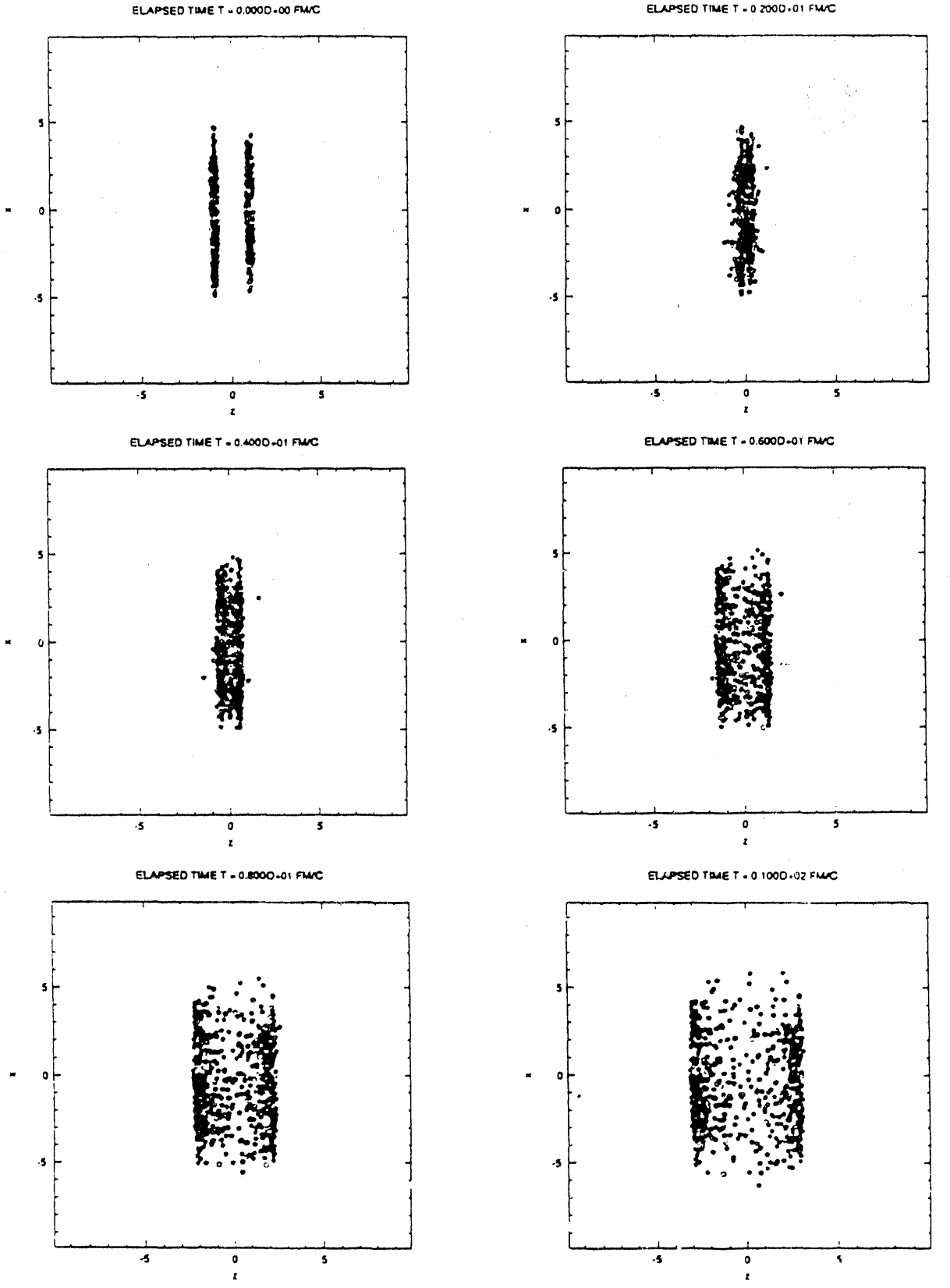

Fig. 8: Time evolution of a $(A = 32) + (A = 32)$ central collision at $E_{cm} = 20$ GeV/nucleon, in configuration space, viewed from the CM frame of the initial nuclei.

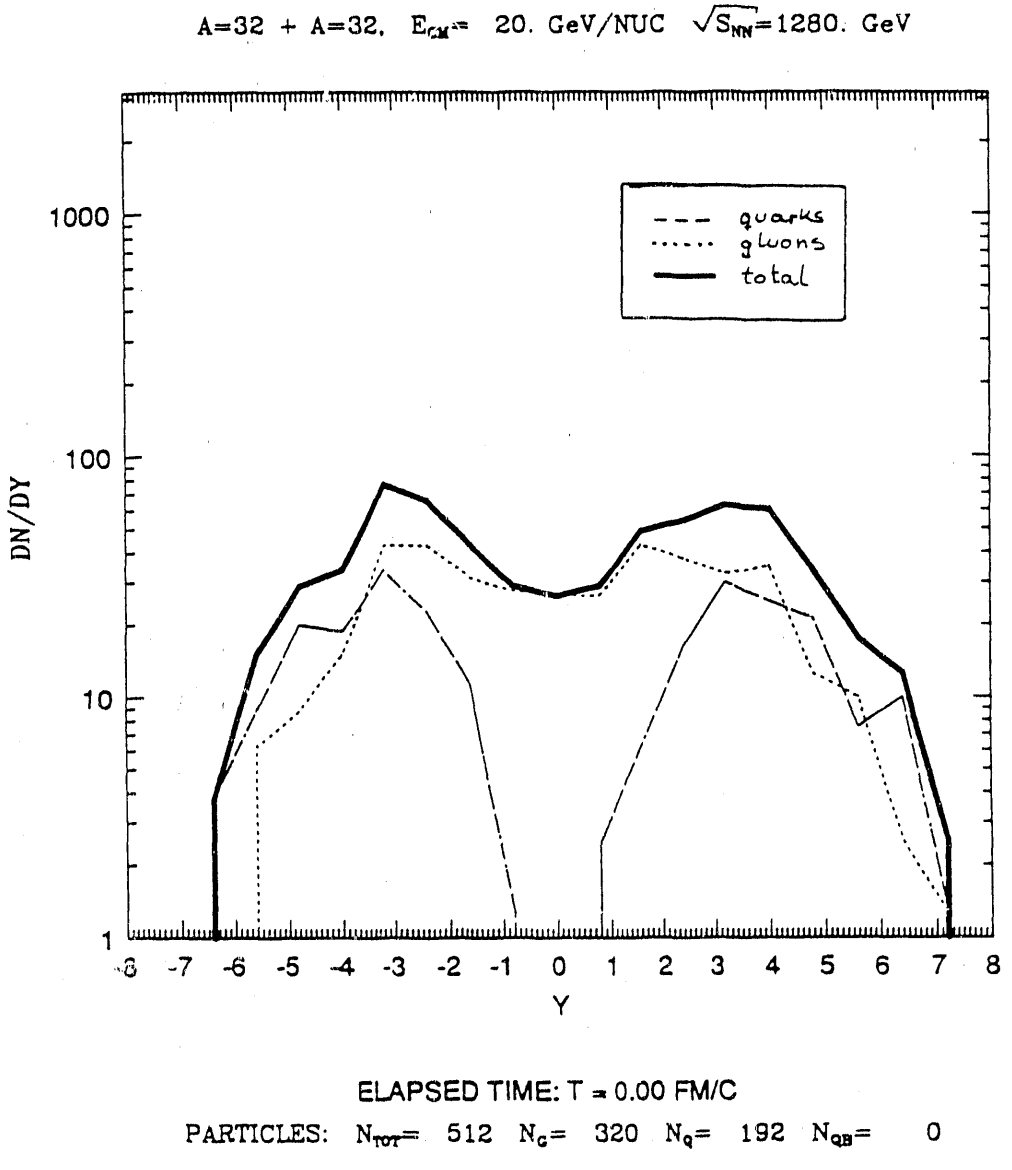

Fig. 9: dN/dy distribution of partons (only valence quarks and gluons, seaquarks are neglected so far) for $(A = 32) + (A = 32)$ collision at time $t = 0$.

distribution (i.e. the number of partons per rapidity interval) for the initial stage. The full line is the total distribution (gluons and quarks), the dotted and dashed lines

represent the individual contributions of gluons and quarks, respectively. The two peaks at $y \simeq \pm 3.7$ correspond to the rapidity of the initial nuclei. While the quarks are absent in the center around $y = 0$ and form two peaks around the nuclear rapidities, the gluons have a much broader distribution and are strongly present around $y = 0$. This is due to the dominance of gluons in the structure functions at small values of the scaling variable x, corresponding to small longitudinal momenta and thus to small values of rapidity y (c.f. Fig 3). As mentioned, seaquarks have been neglected so far. Their contribution should fill up a bit the gap in the dN/dy-distribution of the valence quarks around $y = 0$ since the seaquarks appear in the structure functions only at very small x, corresponding to $y \simeq 0$.

The time evolution of this dN/dy distribution (not shown here) shows a strong enhancement in the central rapidity region due to production of new, hard partons with relatively large transverse momentum.

c) Hadronization

After a certain time, the majority of partons has radiated off most of their energy, and the system is expected to thermalize locally. At this stage, non-perturbative effects become essential and the picture of hard parton-parton interaction governing the nuclear dynamics ceases to be valid. For example, when the average energy per parton falls below a critical value E_c the number of soft partons, characteristic for the confinement regime, increases drastically. At this point of time hadronization mechanisms become important.

Up to now we have not formulated a realistic model description of this third stage of the nuclear collision (c.f. Fig. 3c). In nuclear collisions the situation is complicated by the competition between rescattering and fragmentation of partons. We propose to treat the parton fragmentation along the lines of the Field Feynman approach [8]. Rescat-

tering and/or fragmentation of a parton will be determined on a random basis. When the system has become sufficiently dilute, so that rescattering events become rare, we will allow the remaining partons to hadronize or to recombine into hadrons, in the spirit of a fragmentation-recombination model developed earlier in the context of strangeness production in ultrarelativistic nuclear collisions [9].

An alternative description of the hadronization process is to use the results from the parton cascade calculation (stopped at a certain time, when the momentum distribution of partons starts to become thermalized) as an input for a hydrodynamical computation, an approach which is reasonable for a thermal distribution. This would then allow for a rather different analysis of the hadronization stage and e.g. the resulting momentum distributions of the observed final hadrons.

4. Future Improvements

Besides detailed tests and analyses of the results of the program at its present stage, we want to include, and explore the effects of several important aspects that have been neglected or not completely worked out so far in our parton cascade calculations:

a) The initial nucleons contain not only valence quarks but also sea quarks, whose distributions are well known experimentally. This contribution is especially important in the case of strange quarks, for which there is no valence quark contribution, and for antiquarks generally.

b) The apparent parton distributions depend on the momentum transfer in an individual parton-parton collision as mentioned in Section 2. The change in the distribution functions, as described by the evolution equations (4) is particularly drastic for sea quarks and gluons where no conservation law restrincts the shape of the distribution, and for small values of the scaling variable x. This effect may play an important role in the central rapidity region at very high energies [10], where it could facilitate the

formation of a baryon free region of high energy density.

c) The nuclear structure functions differ from a simple superposition of nucleonic structure functions by 'shadowing', 'EMC-type' effects and effects of Fermi motion [11]. These corrections combined with the improvements a) and b) will be taken into account and their influence will be tested in future calculations [12].

d) Electromagnetic processes such as $gg \rightarrow \gamma q$, $q\bar{q} \rightarrow e^+e^-$, $\mu^+\mu^-$ etc. could easily be included in the calculation.

e) We will allow for a competition between parton rescattering and hadronization, which may occur through fragmentation or recombination of partons. A parton that has not scattered for a time t_h (in the comoving reference frame) will be allowed to hadronize. The magnitude of t_h will determine whether an equilibrated parton phase (quark gluon plasma) can form or whether the partons hadronize before equilibration occurs. Observables which are sensitive to the size of t_h can then be considered as signatures of the quark gluon plasma.

References

[1] D. H. Boal, *Phys. Rev.* **C33**, 2206 (1986).

[2] P. D. B. Collins, A. D. Martin, "Hadron Interactions", Adam Hilger Publ. (1984).

[3] F. E. Close, "An Introduction to Quarks and Partons", Academic Press (1979).

[4] G. Altarelli, G. Parisi, *Nucl. Phys.* **B126**, 198 (1977).

[5] E. Eichten, I. Hinchliffe, K. Lane, C. Quigg, *Rev. Mod. Phys.* **56**, 579, (1984).

[6] R. Cutler, D. Sivers, *Phys. Rev.* **D17**, 196 (1978).

[7] R. D. Field, 'Applications of Perturbative QCD', *Frontiers in Physics,* Vol. 77, 196 (1978).

[8] R. D. Field, R. P. Feynman, *Phys. Rev.* **D15**, 2590 (1977);
R. P. Feynman, R. D. Field, G. C. Fox, *Nucl. Phys.* **B136**, 1 (1978).

[9] P. Koch, B. Müller, J. Rafelski, *Phys. Rep.* **152**, 167 (1985).

[10] A. H. Mueller, *Nucl Phys.* **A498**, 41c (1989).

[11] M. Strickman, contribution to the RHIC Detector Workshop, BNL, July 1990.

[12] K. Geiger, S. Hauger, B. Müller, to be published.

LBL-29390

Jets in Relativistic Heavy Ion Collisions*

Xin-Nian Wang† and Miklos Gyulassy

Nuclear Science Division, Mailstop 70A-3307
Lawrence Berkeley Laboratory
University of California, Berkeley, CA 94720 USA

Abstract

Several aspects of hard and semihard QCD jets in relativistic heavy ion collisions are discussed, including multiproduction of minijets and the interaction of a jet with dense nuclear matter. The reduction of jet quenching effect in deconfined phase of nuclear matter is speculated to provide a signature of the formation of quark gluon plasma. HIJING Monte Carlo program which can simulate events of jets production and quenching in heavy ion collisions is briefly described.

*This work was supported by the Director, Office of Energy Research, Division of Nuclear Physics of the Office of High Energy and Nuclear Physics of the U.S. Department of Energy under Contract No. DE-AC03-76SF00098.

†Presented at the Workshop on Experiments and Detectors for RHIC, July 2–7, 1990, Brookhaven National Laboratory, and to be published in the proceedings

1 Introduction

The state of hot and dense matter which could consist of deconfined quarks and gluons has only been a theoretical topic for more than a decade until the notable experiments of relativistic heavy ion collisions[1] at CERN and BNL, which at least give us some respectable feeling, if not understanding, of what is happening in these heavy ion interactions. With the results from these experiments and the accompanying controversy on whether quark gluon plasma(QGP) is created, we are now looking forward to the experiments at Relativistic Heavy Ion Collider(RHIC). At $\sqrt{s} = 200$ GeV/n, one would expect that hard parton scattering or jet production becomes important, since it has already played a major role in every aspect of $p\bar{p}$ collisions at S$p\bar{p}$S energies[2]. However, in heavy ion collisions nuclear effect on the jets must also come in. First, due to the large number of binary collisions in heavy ion interactions, the number of jets produced will also be large. It is estimated[3] that half of the transverse energy in a central $U + U$ collision at RHIC comes from minijets. Second, the involvement of many nucleons and the particle production in the central rapidity region over a large transverse space will give rise to the effect of initial state and final state interations on the jets production, the former resulting in the Cronin effect[4] and the later causing jet quenching in hadronic matter.

The problem of jet quenching is particularly interesting in heavy ion collisions. Unlike J/Ψ supression or strangeness enhancement, the original rate for jet production and its p_T distribution can be reliably calculated by perturbative QCD which agrees well with experiments in pp or $p\bar{p}$ collisions[5]. With some modeling[6,7], the fragmentation of these jets in free space into hadrons can also be well understood. Since the hard partons are created before the other soft interactions or the formation of QGP if possible, they must travel through the dense matter produced in the collision. Therefore, jets could serve as an external probes of the nucleus-nucleus collisions. Previous calculations[8]-[10] of the final state interactions of jets in nu-

clear collisions considered the enhanced acoplanarity of jets as a probe of multiple scattering in dense matter. Unfortunately, the initial state interactions also give rise to large acoplanarity and as emphasized in Ref. [9,10], increased acoplanarity is expected to occur in both confined and deconfined phases of dense matter. However, a sudden change accompanied by the phase transition, especially a reduction, in the energy loss of the jet when it interacts with the dense matter would be an outstanding effect[11]. Then jet quenching could provide us a viable signal of the formation of QGP. Futhermore, the effect of jet production and quenching on particle production is also important. To provide a conventional picture of the problem, we developed HIJING Monte Carlo program which uses perturbative QCD to simulate jet production in nucleus-nucleus collisions. The interactions of jets with the excited strings then provide the mechanism for jet quenching.

2 Jets Production in Nucleon-nucleon Collisions

We first briefly review jet production in hadronic interactions. In nucleon-nucleon collisions, one can calculate the cross section of hard parton scatterings as[12]

$$\frac{d\sigma_{jet}}{dP_T^2 dy_1 dy_2} = \sum_{a,b} x_1 x_2 \Big[f_a(x_1, P_T^2) f_b(x_2, P_T^2) d\sigma^{ab}(\hat{s}, \hat{t}, \hat{u})/d\hat{t} + f_b(x_1, P_T^2) f_a(x_2, P_T^2) d\sigma^{ab}(\hat{s}, \hat{u}, \hat{t})/d\hat{t} \Big] (1 - \frac{\delta_{a,b}}{2}), \qquad (1)$$

where the summation runs over all parton species, y_1,y_2 are the rapidities of the scattered partons and x_1,x_2 are the fractions of momentum carried by the initial partons and they are related by $x_1 = x_T(e^{y_1} + e^{y_2})/2$, $x_2 = x_T(e^{-y_1} + e^{-y_2})$, $x_T = 2P_T/\sqrt{s}$. This calculation as shown in Fig. 1[13] agrees with experiments very well for different range of P_T and $\sqrt{s}$. Due to the background of soft interactions, it becomes more and more experimentally difficult to detect the jets with small P_T,whose production rates given by Eq. 1 are, however, the largest. Therefore, even

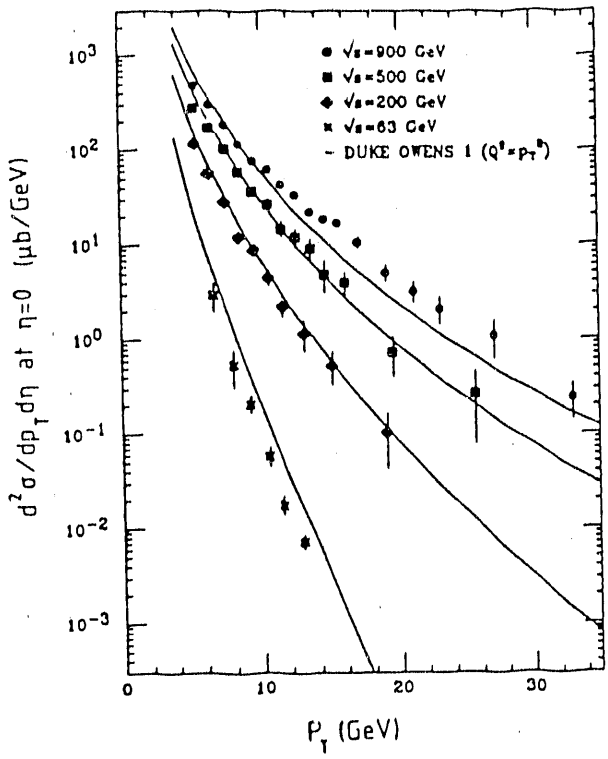

Fig. 1 Inclusive jet cross section at $\eta = 0$ for different values of $\sqrt{s}$, taken from Ref. [13].

though not directly observable, minijets whose P_T still validate the perturbative QCD have been shown to be dominant in hadronic interactions and the correponding multiparticle production[14].

We can calculate the total inclusive jet cross section by integrating Eq. 1 with a low P_T cutoff P_0,

$$\sigma_{jet} = \int_{P_0^2}^{s/4} dP_T^2 dy_1 dy_2 \frac{1}{2} \frac{d\sigma_{jet}}{dP_T^2 dy_1 dy_2}. \tag{2}$$

Since the dominant minijets have relatively small energy, we can assume that they are independently produced. Therefore, the average number of minijets production(*i.e.* pairs of minijets) for a hadron-hadron collision at impact parameter b is $\sigma_{jet} A(b)$, where $A(b)$ is partonic overlap function between the two hadrons. In terms of semiclassical probabilistic model[15], the probability for multiple minijets

production is then

$$g_j(b) = \frac{[\sigma_{jet}A(b)]^j}{j!}e^{-\sigma_{jet}A(b)}. \tag{3}$$

Similarly, we can also represent the soft interactions by an inclusive cross section σ_{soft} which, unlike σ_{jet}, can only be determined phenomenologically. Then the total inelastic cross section of the hadron-hadron collision is,

$$\sigma_{in} = \int d^2b[1 - e^{-\sigma_{soft}A(b)}]e^{-\sigma_{jet}A(b)} + \int d^2b \sum_{j=1}^{\infty} \frac{[\sigma_{jet}A(b)]^j}{j!}e^{-\sigma_{jet}A(b)}, \tag{4}$$

where the first term is the cross section for only soft interactions and the second is the cross section for at least one hard with or without soft interactions. After summation, the above equation becomes

$$\sigma_{in} = \int d^2b[1 - e^{-(\sigma_{soft}+\sigma_{jet})A(b)}]. \tag{5}$$

Using eikonal approximation, we can also calculate the total cross section σ_{tot}. By assuming $P_0 = 2$ GeV, which is the lowest cutoff one can have for Duke and Owens[16] parametrization of structure function and requires a constant σ_{soft} at high energies, we found[17] as shown in Fig. 2 that the production of minijets describes well the increase of σ_{tot} and the violation of geometrical scaling.

Following the same arguement, we can calculate the particle distribution[17][19] in the case of minijets production,

$$\begin{aligned} \sigma_{in}E\frac{d^3P(n)}{d^3p} &= \int d^2b[1 - e^{-\sigma_{soft}A(b)}]e^{-\sigma_{jet}A(b)}E\frac{d^3P_s(n)}{d^3p} \\ &\quad + \int d^2b \sum_{j=1}^{\infty} \frac{[\sigma_{jet}A(b)]^j}{j!}e^{-\sigma_{jet}A(b)}E\frac{d^3P_j(n)}{d^3p}, \end{aligned} \tag{6}$$

where $Ed^3P_s(n)/d^3p$ is the invariant distribution for particles from soft interactions, $Ed^3P_j(n)/d^3p$ is for particles from j number of jets and the accompanying soft

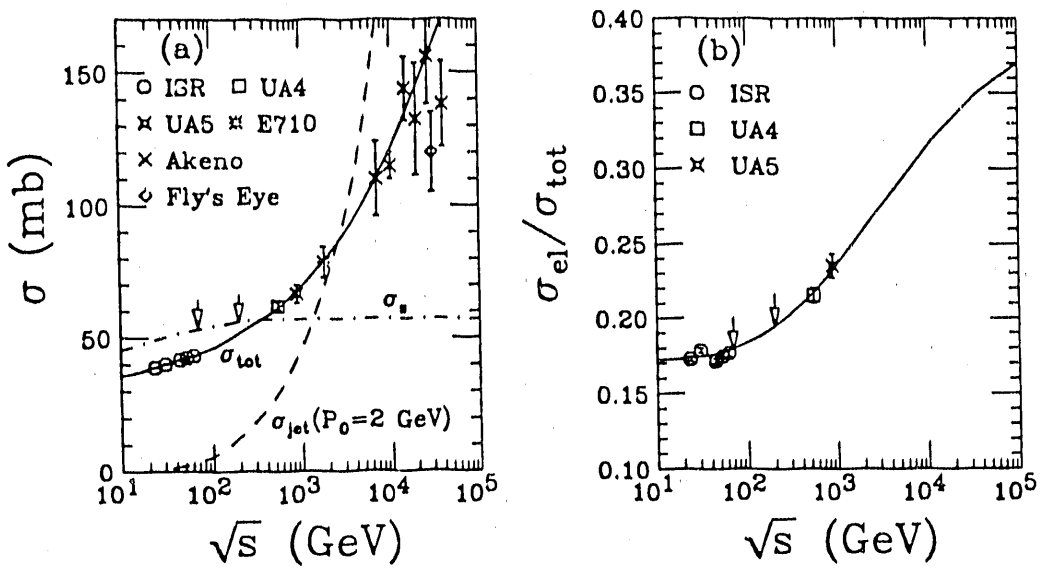

Fig. 2 (a) The calculated cross sections,σ_{tot}(solid line),σ_{jet}(dashed line) and σ_s(dot-dashed line) versus $\sqrt{s}$. (b)σ_{el}/σ_{tot} versus $\sqrt{s}$. See references of the data in Ref [17].

interaction. Using the information from e^+e^- annihilation experiments for particle production of jets and the geometrical branching model[18] for the soft particle production, we can calculate the multiplicity distributions in pp and $p\bar{p}$ collisions[17], as shown in Fig.3,4. The non-log increase of average multiplicity and broadening of the distribution with energy or KNO scaling violation are clearly attributed to jets production. Furthermore, the correlation between $<p_T>$ and multiplicity n can also be calculated[19], as shown in Fig.5, and jets production again explains why $<p_T>$ increases with n and the over all increase of $<p_T>$ with energy. One point needs special attention here. As explained in Ref. [19], the first increase of $<p_T>$ with n is due to the change of ratio between the probabilities of soft and hard interactions. However, when one increases n to some very large numbers, he might have biased the events to those of large P_T jets production, which could give a large $<p_T>$ of the total charged particles. Since experiments[20] at the Fermilab

Tevatron collider have already seen such large $<p_T>$ values which give a second

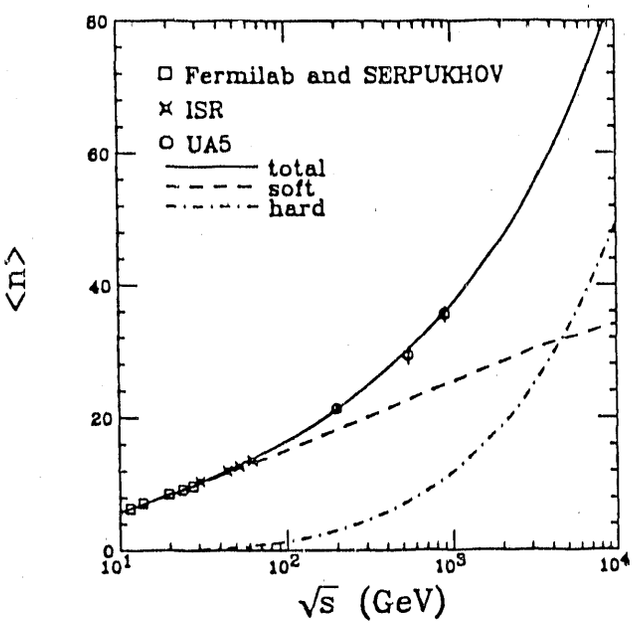

Fig. 3 The average charged multiplicities in pp or $p\bar{p}$ collisions. The solid line is for total charged particles, dashed line for particles from soft production and dotdashed line for particles from jets. See Ref. [17] for data references.

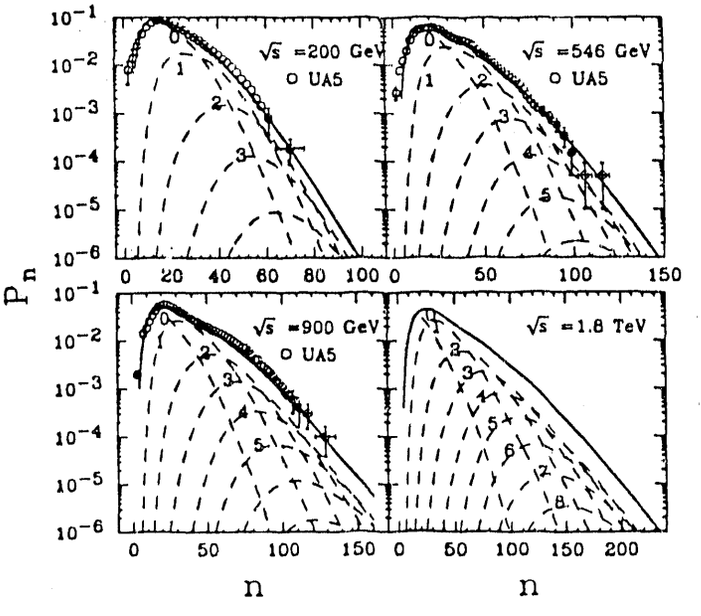

Fig. 4 The multiplicity distributions in $p\bar{p}$ collisions (solid lines). The dashed lines are contributions from events with j=0,1,2,...jets production. See Ref. [17] for data references.

rise of the correlation curve, it is necessary to look at the structure of those events with large n. If a non-neglibible fraction of these events have large P_T jets, then van Hove's scenario[21] of a rise-plateau-rise structure in $<p_T>$ and n correlation can not serve as a clean signal of QGP formation.

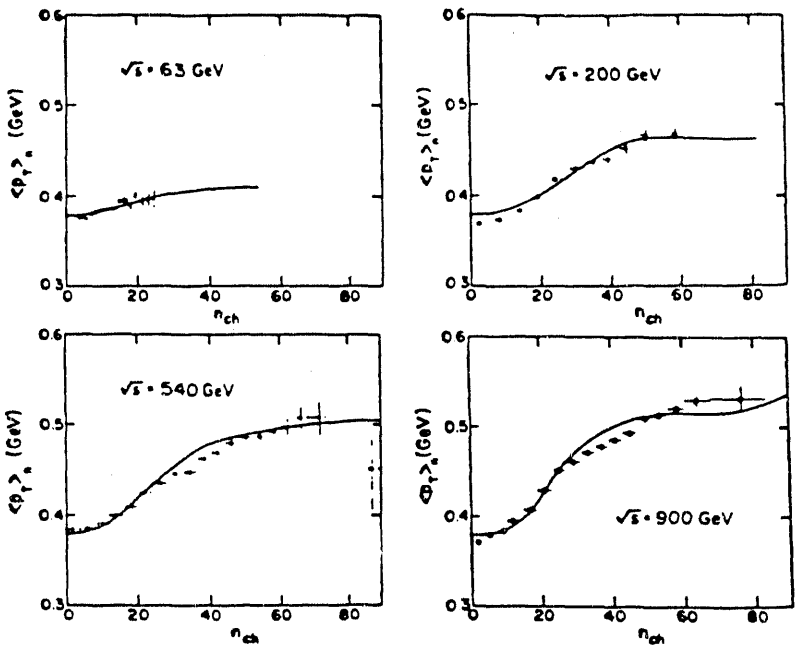

Fig. 5 Calculated $<p_T>$ versus n from Ref. [19].

3 Jets Production in Nucleus-nucleus Collisions

Similar to nucleon-nucleon collisions, one can have the number of jets production in a nucleus-nucleus collision as

$$dN(b) = T_{AB}(b) d\sigma_{jet}^{NN}, \tag{7}$$

where $T_{AB}(b)$ is the overlap function of nuclei A and B at impact parameter b which is essentially the number of binary nucleon-nucleon collisions. This calculation is straight forward and one can show that jet production rate is much higher than in

nucleon-nucleon collisions. What we are most interested now is the nulcear effect on the jets production. Basically, there are two aspects of the nuclear effect, one being the initial state interactions and the other being final state interactions. The effects of initial state interactions include the shadowing effect and the Cronin effect which have been thoroughly studied in many experiments. The final state interactions are then more sensitive to the property of the dense matter that a jet has to go through. It is the difference between the energy losses of a jet when it travels through a QGP and a hadronic matter that we hope to signal the QCD deconfinement transition.

Let us first look at the energy loss of a jet when it propagates through nuclear matter in e^-A scatterings. In such scatterings, the jets produced in the e^-N collision have to interact with the other target nucleons and then be attenuated on their way out. For jet energies $\nu = E_e - E_{e'} \sim 10$ GeV, data from SLAC[23] on e^-Sn indicates a substantial nuclear suppression of hadrons produced with fractional energies $x \gtrsim 0.1$. On the other hand, EMC data[24] show that jet quenching in nuclei is virtually absent for $\nu > 20$ GeV. Three mechanisms for the suppression of large x hadrons are studied[22] on the basis of a phase space extension of the Lund string model[7] and the resultant ratio of the fragmentation functions in e^-A and e^-N for two different jet energies are shown in Fig.6[22] together with the data[23,24]. The G-curves assume a zero formation length(distance from jet production point to hadron formation point) and the final hadron cascading. They best fit the data for $\nu = 10$ GeV, but can not account for the rapid onset of jet transparency beyond $\nu \gtrsim 20$ GeV. The C-curves also have hadron cascading but with a constituent formation length $\ell_c \sim x(1-x)L$, where $L = \nu/\kappa$ is the overall hadronization length scale and $\kappa \sim 1$ GeV/fm is the string tension. This scheme however underestimates the large suppression of small $x \sim 0.1$ hadrons in e^-Sn for 10 GeV jets. The third mechanism represented by S-curves, which assumes color string flip when the end-point partons of a string interact with a nucleon, is most consistent with the

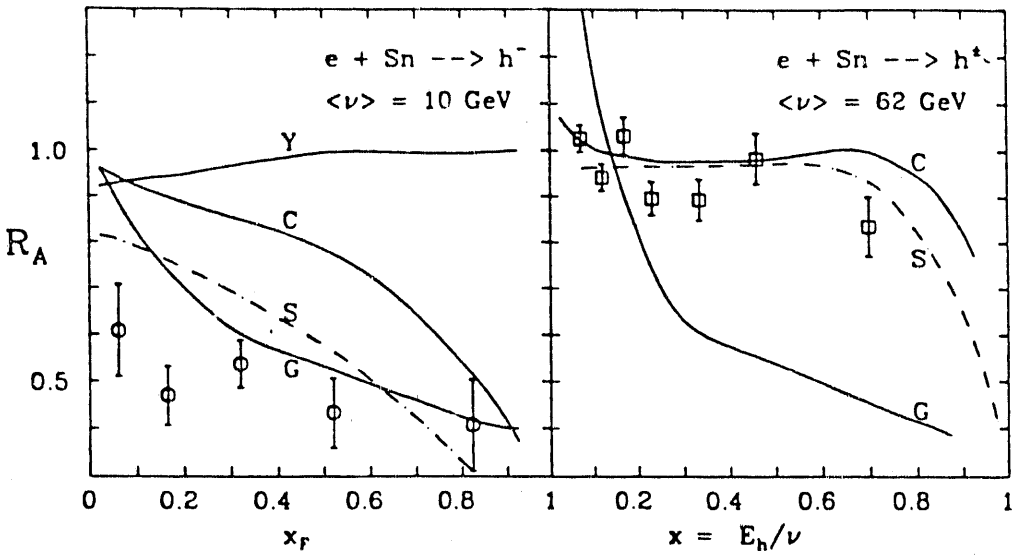

Fig. 6 The ratio $R_A(x)$ for Sn targets at $<\nu>$=10 GeV and $<\nu>$=62 GeV, taken from Ref. [22].

available data among the three schemes. In this string flip model, the hadrons from the leading string always form outside the nucleus and hence do not suffer final state cascading. When the leading string emerges from the nucleus its energy has been reduced by κR due to the kinematic rearrangement of string end points. Therefore, the jets have

$$(dE/dx)_H \equiv \kappa_H = \kappa \tag{8}$$

when they travel through nuclear matter.

In a QGP, the string flip scenario breaks down because the string between two color charges does not exist any more. The source of energy loss for jets in a QGP can only come from the collisions with the other partons in the thermalized system. It was first estimated by Bjorken[25] that such energy loss for a quark of

energy E in an ideal quark gluon plasma at a temperature T is

$$(dE/dx)_Q \approx 6\alpha_s^2 T^2 \ln(4ET/M^2)e^{-M/T}(1+M/T), \tag{9}$$

where $M \sim gT$ is an infrared cutoff on the order of Debye mass. The energy loss for gluons is expected to be 9/4 larger. A full calculation[26] of dE/dx via finite temperature perturbative QCD only shows a slight correction to the above result. The magnitude of the energy loss is clearly very sensitive to the effective coupling constant α_s. Recent QCD lattice studies[27,28] of the static heavy $q\bar{q}$ potential indicate that the coupling strength of heavy quarks is quite small, $\alpha \approx 0.1$, just above $T_c \sim 200$ MeV. A possible reduction of the static string tension just below T_c is also indicated[28]. While these results all refer to static interactions in dense matter, they may suggest the possibility that both the dynamic coupling in Eq.9 in the plasma phase and the string tension in Eq.8 in the mixed phase is also small. For $E \sim 20$ GeV jets in a plasma at temperature $T \sim 250$ MeV, a value of $\alpha_s \lesssim 0.2$ would imply that $(dE/dx)_Q \lesssim 0.4$ GeV/fm. This energy loss is significantly smaller than the energy loss $(dE/dx)_H = \kappa \approx 1$ GeV in the confined phase via the string flip model[22]. Eventually at very high temperaturs the collisional energy loss will increase with T^2. But hydrodynamic studies[29,30] show that a QGP system will spend most of its expansion time in the mixed phase, where there may be a moderate reduction of dE/dx.

Taking into account of the expansion of a QGP, the total energy loss of a jet when it is out of the system is then,

$$\Delta E_a(r,\phi) \approx C_a \int_0^{\tau_f(r,\phi)} d\tau dE(\tau)/dx, \tag{10}$$

where C_a is the color factor such that $C_q = 1$ and $C_g = 9/4$, r is the initial

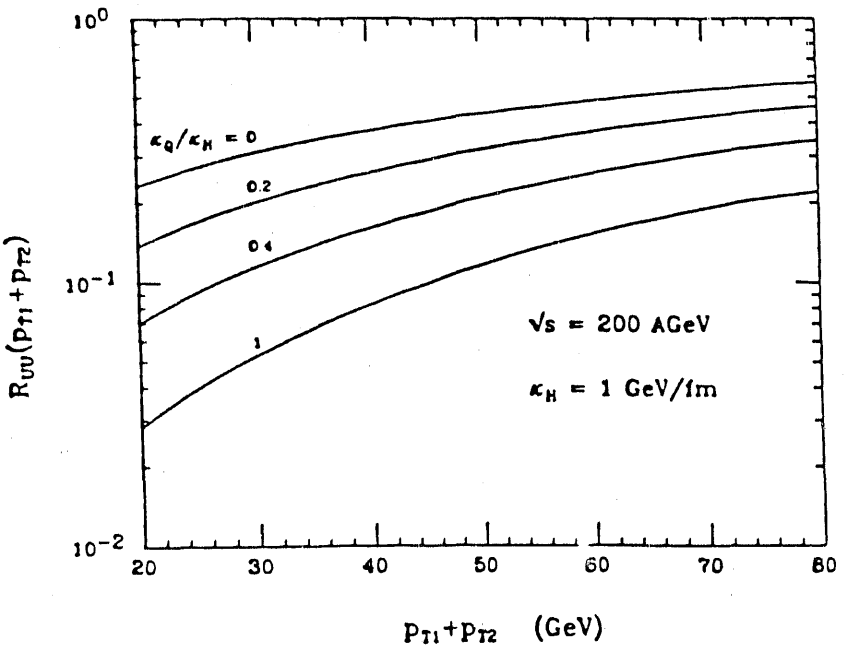

Fig. 7 Dijet reduction factor for central $U+U$ collisions at $\sqrt{s}$ =200 GeV/n as a function of the dijet energy $E = P_{T1} + P_{T2}$, for different values of κ_Q/κ_H assuming κ_H =1 GeV/fm.

transverse coordinate, ϕ the azimuthal angle of the jet and $\tau_f(r,\phi)$ the escape time. Assuming only Bjorken[31] scaling longitudinal expansion and a Bag model equation of state[31], one can find the time dependence of $dE(\tau)/dx$ and get the reduction rate of jet production at fixed P_T by averaging over the initial coordinates (r,ϕ)[22],

$$R_{AA}(E) = \frac{\sigma^{jet}(E)_{quenching}}{\sigma^{jet}(E)_{no-quenching}}. \tag{11}$$

In the plasma phase, the temperature decreases as $T(\tau)/T_c = (\tau_Q/\tau)^{1/3}$. According to Eq. 9, $dE/dx \approx \kappa_Q(\tau_Q/\tau)^{2/3}$, denoting the energy loss in the plasma phase by κ_Q. Fig.7 shows the calculated reduction factors for central $U+U$ collisions as a fucntion of the dijet energy at $\sqrt{s}$ = 200 GeV/n. The Bag model parameters were chosen such that T_c = 190 MeV, B = 0.5 GeV/fm^3, ϵ_Q = 2.5 GeV/fm^3, and ϵ_H = 0.5 GeV/fm^3. The initial conditions for these calculations were assumed to

be $\tau_0 = 1$ fm/c and

$$\epsilon_0 = \epsilon_s A^{1/3} + \epsilon_h A^{2/3}, \tag{12}$$

where the energy density due to soft processes is $\epsilon_s \approx 0.5$ GeV/fm^3 and the energy density due to semi-hard minijets is $\epsilon_h(\sqrt{s} = 200) \approx 0.08$ GeV/fm^3[3]. Note that the overall magnitude of jet quenching in heavy nuclei is quite large, reducing the expected number of jets by around an order of magnitude. The quenching is also very sensitive to the ratio of dE/dx in the two phases.

Because jet quenching depends on the size of the dense matter and the energy of the jet, one should consider the reduction factor for fixed A and dijiet energy E, but varing the c.m. energy $\sqrt{s}$ or the initial energy density ϵ_0. If the reduction factor is plotted as a function of ϵ_0, we would see an increases in R_{AA} as illustrated in Fig. 8, where $U + U$ is considered. In obtaining Fig. 8, the low bound of the correlation of thermalization time with initial temperature $\tau_0 \gtrsim 1/T_0$ is taken, with $T_0^4 \approx (\epsilon_0 - B)/12$. We note that for reduced energy loss in plasma phase transition

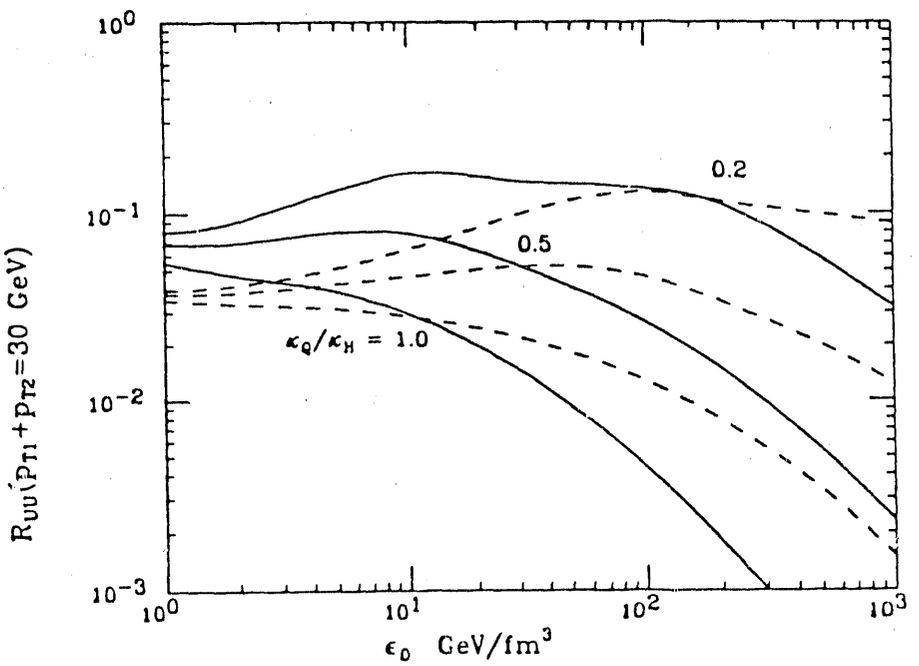

Fig. 8 Dijet reduction factor for central $U + U$ collisions at $\sqrt{s}$ =200 GeV/n for dijet energy $E = 30$ GeV as a function of the initial energy density ϵ_0 assumin a thermalization time $\tau_0 = 1/T_0$(solid lines) and $\tau_0 = 1/3T_0$(dashed lines).

there should be a period of increase in R_{AA} with ϵ_0 just above ϵ_Q. If we assume the estimation of the initial energy density ϵ_0 by Eq. 12 and a linear increase of ϵ_h with $\sqrt{s}$, we could see such an increase in the energy range of $\sqrt{s} = 20 \sim 200$ GeV but only for $A = 45 \sim 90$. For smaller nuclei, ϵ_Q can never be achieved and for larger nuclei we would miss the phase transition point where dE/dx might be small.

4 HIJING Monte Carlo Program

In nucleus-nucleus collisions, there are larger number of jets production than in nucleon-nucleon interactions. One would expect that it is easier to study the jets. However, as we have mentioned before, among the numerous jets most of them have relatively small P_T of a few GeV, characterizing that of minijets. These minijets then will have large background in the E_T distribution of the events. The continuation from minijets to high P_T jets will make the detection of dijets very difficult. To estimate the background of the minijets and to study the overall effect of jets production is our main purpose to develope HIJING Monte Carlo program for nucleus-nucleus collisions at high energy. The program also tries to study jet quenching in hadronic matter and its effect on the particle production.

The genealogy of the Monte Carlo programs related to HIJING stems from Lund/JETSET[7] which was developed for jet fragmentation in e^+e^- annihilation. From there emerged two programs for hadronic interactions. FRITIOF[32] considered that the hadronic interactions in hadron-hadron,hadron-nucleus and nucleus-nucleus collisions can be described by the excitation of the strings formed between the leading quarks and diquarks(or anti-quarks). Later on, it also took into account of the Glauber geometry for nuclear collisions which was introduced first in the ATTILA[33] version and the soft radiation was also considered[34]. The philosophy of PYTHIA[35] however is to employ perturbative QCD as much as possible in hadron-hadron interactions. It uses Eq. 1 to simulate multiple hard or semi-hard

parton interactions and conducts initial and final state radiation. The final partons are connected as strings and fragmented via Lund/JETSET. What we have done in HIJING is basically to combine FRITIOF and PYTHIA together to simulate multiple jets production in nucleus-nucleus collisions and consider the effect of initial and final state interaction of the scattered partons. Therefore HIJING contains:

1. The Glauber geometry of nuclear interactions. The probability of inelastic nucleon-nucleon collisions is described by eikonal formalism in Eq. 5.

2. FRITIOF soft excitation and soft radiation. We also have a low p_T cutoff for the radiation to aviod producing jet-like gluons.

3. Multiple jets production which could also include the production of two hard jets of fixed P_T with initial and final state radiation.

4. Jet quenching mecahnism.

5. JETSET hadronization.

6. Shadowing effect and multiple initial state interactions are also going to be included.

Our scheme of multiple jets production is based on Eq. 3, which determines the number of jets produced per nucleon-nucleon collision. Then PYTHIA is call to determine the four-momentum and flavors of the scattered partons. After each call of PYTHIA the initial momenta of scatterd partons are subtracted from the incident nucleons. Each nucleon-nucleon collision is also accompanied by FRITIOF soft excitations. Finally the accumulated partons which have been scattered are linked with the valence partons and soft radiations are performed. The fragmentation of the strings is via JETSET.

In principle, the interaction of jets with the excited hadronic matter must be considered in a space-time evolution picture. A large P_T gluon jet must begin to

fragment on its way to interact with an excited string which also have to break up. The jet will lose its energy and therefore be quenched by stretching the string which links it with other partons. The interaction or string flip only happens between the reduced jet and a section of the excited string. This scheme of jet quenching, however, can not be realized now in HIJING due to the limited computer power. We have adopted an approximate scheme in which we do not consider the space-time evolution. We determine the interaction point via

$$dP = \frac{dr}{\lambda_s} e^{-r/\lambda_s}, \tag{13}$$

where λ_s is the mean free path of the jet interaction, r is the distance the jet has travelled after the last interaction. Then we subtract κr from the jet's energy and add a gluon kink with the same amount of energy to the excited string that the jet interacts with. We continue the procedure until the jet is out of the whole excited system or the jet's energy is below the cutoff for the jet production.

One must be reminded that the calculations we present here are very preliminary. In order to investigate the background of minijets and how it will affect the detection of high P_T jets, we show in Fig. 9 the lego plot of the transverse energy E_T of two central $Au + Au$ events, one with minijets production and one without. In addition, two jets with $P_T = 40$ GeV are also added in each event. Each cell of the plots has $\delta\eta = 0.2$ and $\delta\phi = 13°$. In the event without minijets, the two high P_T jets stand out very well. When minijets are included, the background and the fluctuation are quite large even though the two jets with $P_T = 40$ GeV can still be detectable. However, for P_T=20 GeV or less the fluctuation of the background will be comparable to the signal of the jets. It can be estimated that for a central $Au + Au$ collision at RHIC, there could be about 6 jets with $P_T \approx 5$ GeV. Even though one could manage to detect a single jets with such P_T, it is not trivial to find so many dijets

at the same time. For the bulk effects of multiple minijets we show the rapidity

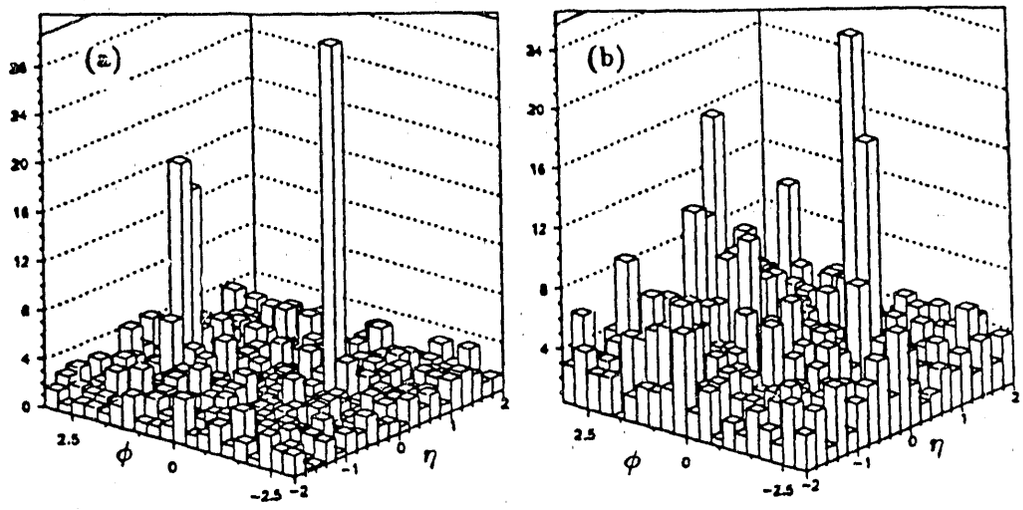

Fig. 9 Lego plot of the transverse energy distribution in central $Au + Au$ collisions at $\sqrt{s}$ =200 GeV/n (a)without and (b)with minijets production.

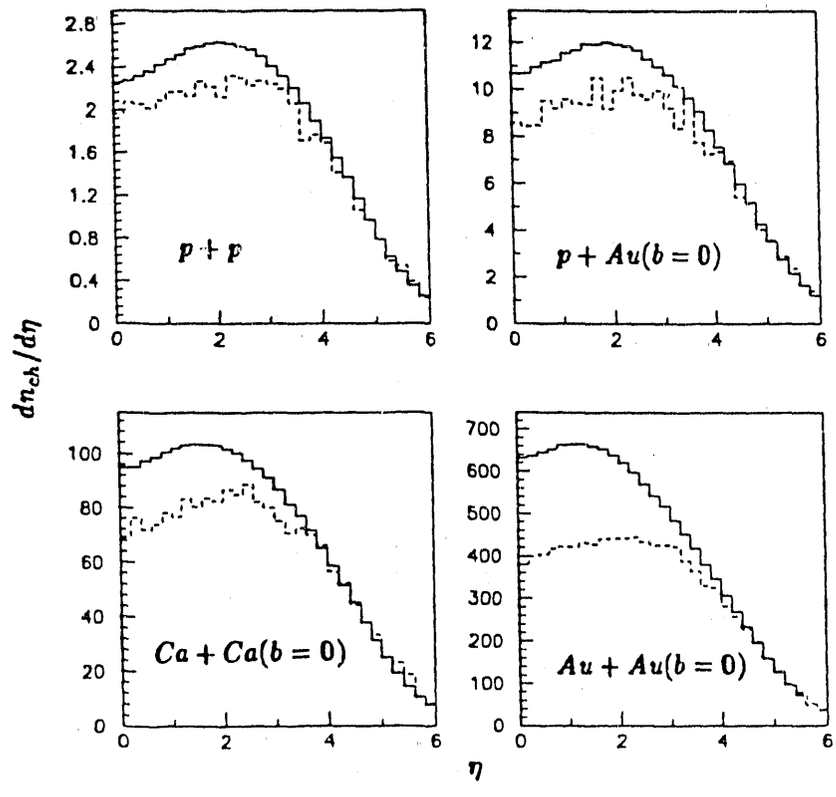

Fig. 10 Rapidity distributions of charged particles in $p+p$, central $p+Au$, $Ca+Ca$, and $Au + Au$ collisions at $\sqrt{s}$ =200 GeV/n.

distributions of charged particles in Fig. 10 for $p+p$, central $p+Au$,$Ca+Ca$ and $Au+Au$ collisions at $\sqrt{s}=200$ GeV/n. The dashed lines are the same plots without jets production. We note that the contributions to particle production from jets becomes more important for heavier nuclei. For $Au+Au$ collisions, almost half of the charged particles come from the fragmentation of jets which are about 400 in number. These results are in agreement with the estimates of Ref. [3]. When one goes to even higher energy, at $\sqrt{s}=2$ TeV of the proposed LHC for example, the contribution from minijets production will become the dominant effect as shown in Fig. 11. Of cause, the effect of shadowing will reduced the number of minijets and the initial multiple parton interaction will increase the P_T of the scattered partons.

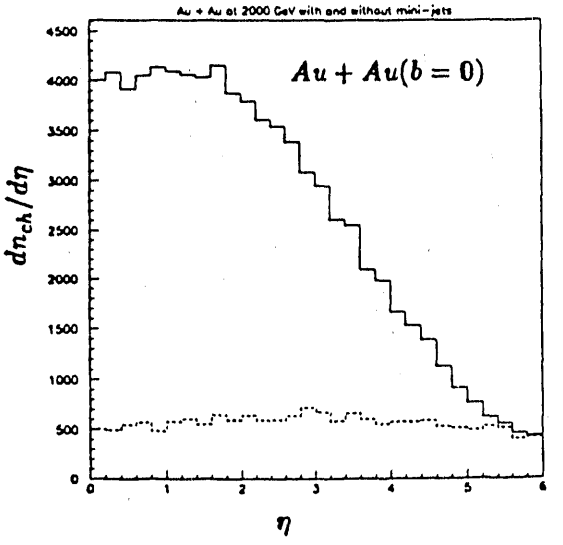

Fig. 11 Rapidity distributions of charged particles in central $Au+Au$ collisions at $\sqrt{s}$ =2000 GeV/n.

As we have noticed that numerous minijets will complicate the detection of high P_T jets especially those with $P_T \lesssim 20$ GeV. However, we are most interested in these jets because they are most affected by jet quenching from the study of e^-A interaction. Since jets are finally represented by large p_T secondary hadrons, we can study the inclusive p_T distribution of hadrons as a supplement to the study of jet properties. In Fig. 12, we show the p_T distribution of charged particles from central $Au+Au$ collisions at $\sqrt{s}=200$ GeV. The solid histogram is for the case

when jets are quenched via interactions while the dashed histogram is for the case

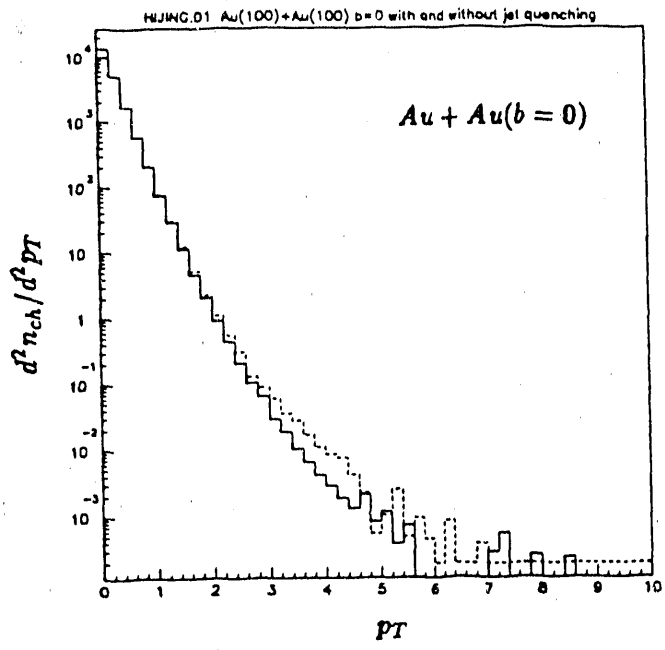

Fig. 12 Transverse momentum distributions of charged particles in central $Au+Au$ collisions at $\sqrt{s}$ =200 GeV/n with(solid line) and without(dashed line) jet quenching.

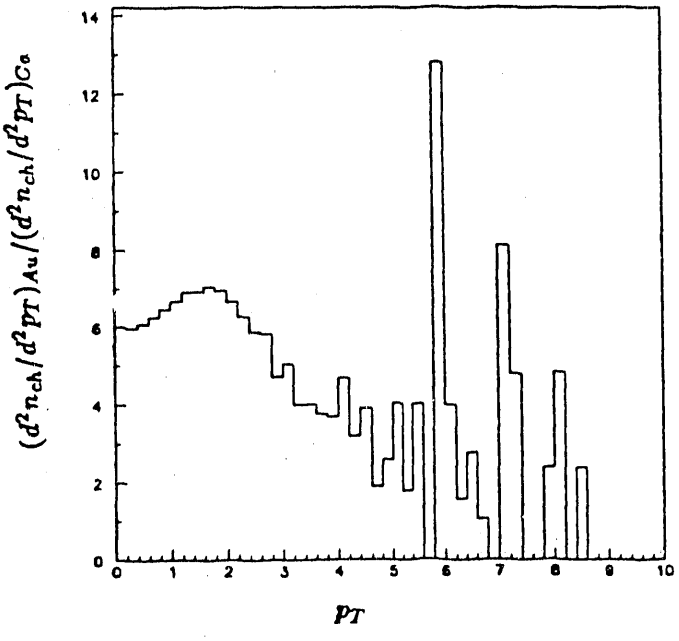

Fig. 13 The ratio of p_T distribution of charged particles in central $Au + Au$ over that in $Ca + Ca$ collisions at $\sqrt{s}$ =200 GeV/n.

that has no final state interactions between jets and the excited strings. We note that jet quenching indeed suppresses the production of high p_T hadrons and should also enhance hadrons at small p_T. To look at the effects of jet quenching more closely, one should compare the p_T distribution of heavy nucleus interaction with that of lighter nucleus or nucleon-nucleon collision for the best result, because in the later case jet quenching should be smaller than the formal one. Fig. 13 shows our calculation of the ratio between the p_T distribution of charged particles from central $Au + Au$ collisions and that of central $Ca + Ca$. It indeed shows some enhancement of particle production at $p_T \sim 2$ GeV and a substantial suppression at large p_T. If initial state interaction are taken into account, Cronin effect will compensate the suppression via jet quenching at high p_T and one would see an increase of the ratio again. Similarly to the discussion at the end of last section, one should also investigate the variation of the ratio with energy at fixed p_T where jet quenching is most prominent. HIJING will give a constant ratio at all energies because the only energy dependence in HIJING is cancelled out. If any form of variation of the ratio with energy, especially like the one in Fig. 8, are to be observed, something beyond the conventional understanding of HIJING must have happend.

5 Conclusions and Remarks

We have discussed the effect of hard or semi-hard parton scatterings in heavy ion collisions at RHIC energy and beyond. Due to their calculable production rate, hard jets can serve as external probes of the excited nuclear matter in relativistic heavy ion collisions. HIJING Monte Carlo program which is near completion can provide us with the conventional production of QCD jets and their quenching. We motivated that a noval reduction of energy loss dE/dx for a jet in a dense matter near QCD phase transition T_c would result in an abnormal behavior of the jets production rate. By studying the suppression factor of jets in heavy nucleus-nucleus collisions and

its energy variation we could get some information about the state of the excited nuclear matter and hopefully to indentify the formation of quark gluon plasma.

We would like to thank B. Andersson, M. Bloomer, J. W. Harris, R. C. Hwa, P. Jacobs, S. Nagamiya, R. D. Pisarski, M. Plümer, A. Poskanzer and other colleagues for their helpful discussions. Some topics presented here were studied in collaboration with M. Plümer and R. C. Hwa.

References

[1] See reviews in Nucl. Phys. **A498**, 1c–628c(1989), the Proceedings of the Seventh International Conference on Ultra-Relativistic Nucleus-Nucleus Collisions, edited by G. Baym, P. Braun-Munzinger and S. Nagamiya.

[2] C. Albajar,*et al.*, Nucl. Phys. **B309**, 405(1988); W. M. Geist,*et al.*, CERN preprint CERN-EP/89-159(submitted to Phys. Rep.).

[3] K. J. Eskola, K.Kajantie and J. Lindfors, Nucl. Phys. **B323**, 37(1989).

[4] Cronin *et al.*, Phys. Rev. **D11**, 3105(1975).

[5] G. Arnison *et al.*, Phys. Lett. **B172**, 461(1986); and the referenced therein.

[6] R. D. Field and R. P. Feynman, Nucl. Phys. **B136**, 1(1978).

[7] B. Andersson, G. Gustafson, G. Ingelman and T. Sjöstrand, Phys. Rep. **97**, 31(1983).

[8] D. A. Apple, Phys. Rev. **D33**, 717(1986).

[9] J. P. Blaizot and L. D. Mclerran, Phys. Rev. **D34**, 2739(1986).

[10] M. Rammerstorfer and U. Heinz, Phys. Rev. **D41**, 306(1990).

[11] M. Gyulassy and M. Plümer, Phys. Lett. **B243**, 432(1990).

[12] E. Eichten, I. Hinchliffe and C. Quigg, Rev. Mod. Phys. **56**, 579(1984).

[13] A. R. Norton, in *Multiparticle Production*, proceedings of Shandong Workshop, edited by R. C. Hwa and Q. B. Xie(World Scientific, Singapore, 1988).

[14] X. N. Wang, Preprint report No. LBL-28789, to be published in Phys. Lett. B.

[15] P. l'Heureux *et al.*, Phys. Rev. **D32**, 1681(1985); L. Durand and H. Pi, Phys. Rev. Lett. **58**, 303(1987); R. C.Hwa, Phys. Rev. **D37**, 1830(1988).

[16] D. W. Duke and J. F. Owens, Phys. Rev. **D30**, 49(1984).

[17] X. N. Wang, Preprint report No. LBL-28790, to be published in Phys. Rev. **D**.

[18] W. R. Chen and R. C. Hwa, Phys. Rev. **D36**, 760(1987); W. R. Chen, R. C. Hwa and X. N. Wang, *ibid.* **38**, 3394(1988); R. C. Hwa and X. N. Wang, *ibid.* **39**, 2561(1989); X. N. Wang and R. C. Hwa, *ibid.* **39**, 2573(1989); R. C. Hwa and X. N. Wang, *ibid.* **40**, xxxx(1990).

[19] X. N.Wang and R. C. Hwa, Phys. Rev. **D39**, 187(1989).

[20] T. Alexopoulos *et al.*, Phys. Rev. Lett. **60**, 1622(1988); **64**, 991(1990).

[21] L. Van Hove, Phys. Lett. **B118**, 138(1982).

[22] M. Gyulassy and M. Plümer, Preprint LBL-27605, Nucl. Phys. **B** in press.

[23] L. S. Osborne *et al.*, Phys. Rev. Lett. **40**, 1624(1978).

[24] P. B. Renton *et al.*, Nucl. Physics Lab., Oxford, Preprint Ref.55/88; European Muon Collaboration, A. Arvidson *et al.*, Nucl. Phys. **B246**, 381(1984); Report at the High Energy Physics Conference, Munich 1988.

[25] J. D. Bjorken, Fermilab preprint Pub-82/59-THY(1982).

[26] M. H. Thoma and M. Gyulassy, Preprint LBL-

[27] F. Karsch and H. W. Wyld, Phys. Lett. **B213**, 505(1988); F. Karsch, Nucl. Phys. **B**(Proc. Suppl.)9, 357(1989).

[28] M. Gao(Columbia Univ. Group), Nucl. Phys. **B**(Proc. Suppl.)9, 368(1989).

[29] H. von Gersdorff, L. Mclerran,M. Kataja and P. V. Ruuskanen, Phys. Rev. **D34**, 794(1986); **D34**, 2755(1986)

[30] X. N. Wang and R. C. Hwa, Phys. Rev. **D35**, 3409(1987).

[31] J. D. Bjorken, Phys. Rev. **D27**, 140(1983); M. Gyulassy and T. Matsui, Phys. Rev. **D29**, 419(1984).

[32] B. Andersson, G. Gustafson and B. Nilsson-Almqvsit, Nucl. Phys. **B281**,289(1987); B. Nilsson-Almqvist and E. Stenlund, Comp. Phys. Comm. **43**, 387(1987).

[33] M. Gyulassy, Proceedings of Eighth Balaton Conference on Nuclear Physics,(edited by Z. Fodor, KFKI, Budapest, 1987); CERN preprint CERN-TH-4794/87(1987).

[34] G. Gustafson and U. Pettersson, Nucl. Phys. **B306**, 746(1988).

[35] T. Sjöstrand and M. van Zijl, Phys. Rev. **D36**, 2019(1987).

Parton distributions in hard nuclear collisions

LEONID FRANKFURT[†], MARK STRIKMAN[†], and SIMONETTA LIUTI[‡]

† *Department of Physics, University of Illinois at Urbana-Champaign, 1110 West Green Street, Urbana, IL 61801.*)*

‡ *INFN, Viale Regina Elena 299, I-00161 Roma, Italy*

Abstract. Current calculations of nuclear shadowing for parton distributions are reviewed. The analysis of μA data is performed using exact QCD sum rules for the total momentum and baryon charge of nuclei. The evidence is found for an overall enhancement of G_A in nuclei (>4% for A≫1). Combined with the calculation of nuclear shadowing at small x, our analysis indicates enhancement of valence quark and gluon fields in nuclei for x ~ 0.1 of about 10(20)% for A=40(A=∞), as well as suppression of sea at least for x<0.1 and of valence quarks at x<0.02. It is also pointed out that due to scaling violation small shadowing observed in the Drell-Yan data at x=0.04 and $\langle Q^2 \rangle \sim 25 GeV^2$ corresponds to much larger shadowing for sea at the Q^2 range probed by NMC. Implications for disentangling the origin of nuclear forces are discussed. We emphasize also that this physics leads to significant differences between effective parton distributions which enter into description of peripheral and central nuclear collisions.

1. Introduction

Recent years observe resurrection of experimental and theoretical interest in the nuclear shadowing phenomenon in deep inelastic scattering off nuclei (for a review of these studies see[1,2,3]). To large extent this is due to the borderline character of this phenomenon - between reasonably well understood perturbative QCD and poorly understood nonperturbative QCD. On the pragmatic level, the interest in small x parton distributions arises from the necessity to take into account the difference of parton distributions in free nucleons and in nuclei in modeling hard interactions with nuclei (Note that to model collisions at RHIC energies one has to know parton distributions at $x \geq 10^{-3}$).

The aim of this talk are to describe the current level of calculations of small x parton distributions in nuclei, and to demonstrate that nuclear effects lead to significant depletion of parton distributions in nuclei at x<0.01 (by a factor ~ 2 in heavy

* On leave of absence from Leningrad Inst. of Nuclear Physics

** presented by M.Strikman

nuclei) and to a related enhancement of valence quark and gluon distributions at x~0.1 (by a factor ~1.2 for heavy nuclei).These effects lead also to an even bigger difference between parton distributions which enter into the description of peripheral and central nuclear collisions.

2. Shadowing of parton distributions at small x.

The above mentioned specific properties of low x parton distributions stems from the old observation [4] that in the $x\to 0$, $\nu\to\infty$ limit, the longitudinal component of the mean distance, $2r_\mu$, between the points where γ^* is absorbed and emitted becomes large in the nucleus rest frame:

$$z=(\vec{q}\vec{r})/|\vec{q}| \approx 1/2m_N x,\ r_t^2 \sim 1/Q^2 \qquad (1)$$

In QCD, shadowing is the leading twist effect, originating from nonperturbative QCD. Therefore the main problem is to calculate parton distributions at small x and $Q_0^2\sim$ 1 - 2 GeV^2. The main idea of calculating nuclear shadowing is to use *"a flanking maneuver"* - to work in the nucleus rest frame, i.e. "the antipartonic reference frame", using the experience of strong interaction physics, and at the final step to interpret the calculated structure functions which are invariant under Lorentz boosts using the QCD parton language. It is natural to start with the Gribov representation for σ_{γ^*N}. In QCD one has to modify it in order to take into account that configurations in the γ^* wave function with different transverse separation of color have different interaction cross section (which is roughly proportional to the transverse area, S, occupied by color if this size is smaller than the typical hadronic scale):[2]

$$\sigma_{\gamma^*A}(Q^2,\nu)=\frac{\alpha}{3\pi}\int_0^\infty \frac{R(M^2)M^2\,dM^2}{(M^2+Q^2)^2}\int dS\,\sigma^{(S)}_{"M^2"A}(Q^2,\nu),\ \text{for } x \ll 1/4R_A m_N. \qquad (2)$$

Here $R(M^2)=\sigma(e^+e^-\to\text{hadrons})/\sigma(e^+e^-\to\mu^+\mu^-)$. In QCD the wave function of γ^* with $M^2 \geq M_0^2 \sim(1.5\text{-}2)\,\text{GeV}^2$ is dominated by quark-antiquark jets (the effect of gluon emission can be separately taken into

account).It is easy to demonstrate by a quantum mechanics calculation that for $q\bar{q}$ jets aligned along $\vec{q}$ ($|k_{qt}|=|k_{\bar{q}t}|< k_{ot}$, where k_{ot} is the typical parton transverse momentum) the transverse separation is $\Delta y_t \sim 2/(m_q^2+k_{ot}^2)^{1/2}$, i.e. it is similar to the light mesons one, while for nonaligned jets with $k_t \sim Q$, the transverse separation is small: $\Delta y_t \sim 1/Q$. Thus we can approximate the high mass contribution in eq.2 as a sum of two terms: aligned jets, which are shadowed essentially as normal hadrons, and nonaligned jets which in the first approximation are not shadowed:[2,5]

$$\sigma_{\gamma^*A}(Q^2,\nu)=\lambda A\sigma_{\gamma^*N}+\frac{\alpha}{3\pi}\int_{M_o^2}^{\infty}\frac{R(M^2)M^2\,dM^2}{(M^2+Q^2)^2}\,\sigma_{\text{"aligned jet"}A}\,3k_{ot}^2/M^2, \qquad (3)$$

for $x<1/4R_Am_N$. Here the first and second terms correspond to the contribution of nonaligned and aligned jets respectively. Taking $\sigma_{\text{"aligned jet"}N} \sim \sigma_{\rho N}$, and $k_{ot}^2 \sim 0.2$ GeV^2, one finds by using eq.3 for A=1, $\lambda \approx 0.3$-0.4. Eq.3 provides an extension to QCD of the original parton idea of Bjorken[6]. A new element introduced by QCD is a possibility to understand "the mysterious mechanism which aligns the vector dominant "jets" along virtual photon direction"[6] as a consequence of color screening. As a result, differenly from the parton model, it is possible to calculate the absolute value of the soft contribution to $\sigma_{\gamma^*A}(Q^2)$.

Eq.3 predicts that at $Q^2 \gg m_\rho^2$ and $x \ll x_A=1/4m_NR_A$ σ_{γ^*A} is noticeably shadowed for large A:

$$\frac{A_{eff}}{A} = (1-\lambda)\frac{\sigma^{tot}_{\text{"aj"}A}}{A\sigma^{tot}_{\text{"aj"}N}} + \lambda \approx 1.3\,A^{-0.18}\,(1-\lambda)+\lambda \qquad (4)$$

for A>10 and $\sigma^{tot}_{\text{"aj"}N} \approx \sigma^{tot}_{\rho N} \approx 25$ mb. Note that in eqs.3,4 shadowing for the interaction of the small size components of γ^* with nuclei is neglected. This is an definitely oversimplification of the real picture since even for configurations in γ^* with $\sigma_{eff}=$ 10mb a noticeable shadowing is present for the interaction with heavy nuclei at small impact parameters. We will return to the discussion of this point in the end of the talk.

Within the Glauber approach one can generalize eq.3 to include the x-dependence of nuclear shadowing [5] :

$$\frac{A_{eff}(x,Q_0^2)}{A} = \lambda + \frac{1}{A\,\sigma_{\gamma^*N}} \frac{\alpha}{3\pi}\int_{M_0^2}^{\infty} \frac{R(M^2)M^2\,dM^2}{(M^2+Q^2)^2}\,\sigma_{\text{"aligned jet"}A}^{3k_{ot}^2/M^2} \tag{5}$$

$$x\left\{A\sigma_{\text{"aj"}N} - \frac{1}{2}\,\mathrm{Re}\,\sigma^2_{\text{"aj"}N}\int d^2b\,dz_1dz_2\rho_A(b,z_1)\rho_A(b,z_2)\vartheta(z_2-z_1)\right.$$

$$\left. x\,\exp\left(-iq_{\parallel}^{(M)}(z_1-z_2)\right)\exp\left(-\frac{1}{2}\,\sigma_{\text{"aj"}N}\int_{z_1}^{z_2}\rho_A(b,z')dz'\right)\right\}.$$

Here $\rho_A(r)$ is the nucleon density in a nucleus normalized according to $\int\rho_A(r)d^3r=A$, and $q_{\parallel}^{(M)}=(Q^2+M^2)/2\nu$ accounts for the nonconservation of energy in the $\gamma^* \to M$ transition.

Eq.5 provides a reasonable description of the current small x data.[5] Similar results for nuclear shadowing were obtained recently in models with somewhat different inputs[7,8], thus illustrating that within the Glauber approach shadowing is mostly sensitive to the size of the nucleus and to the elementary cross section.

One can demonstrate[2] that at small x essential longitudinal distances for all parton distributions (sea and valence quarks, gluons) are given by eq.1. Consequently similar shadowing is expected in these channels for low x and Q^2 of few GeV^2.

3. *Enhancement of parton distributions at x~0.1 and scaling violation effects*

Let us now consider implications of these shadowing effects for higher values of x($x \sim 0.1$) which correspond to the kinematics where essential longitudinal distances in deep inelastic processes in the nucleus rest frame are comparable with mean internucleon distances in nuclei - r_{NN}:

$$r_{NN} = 1.7\text{fm} > 1/(2m_N x) > r_N = 0.6\text{fm} \tag{6}$$

At the first step of our analysis we use only exact QCD sum

rules (7),(8) for the parton distributions in nuclei. While at the second step we add information from calculations of nuclear shadowing at small x briefly described above.The sum rules for the baryon charge, and the total nucleus momentum conservation ca ı be written as :

$$\int_0^A \frac{1}{A} V_A(\tilde{x},Q^2)\,d\tilde{x} \; - \int_0^1 V_N(x,Q^2)\,dx = 0, \qquad (7)$$

$$\int_0^A \frac{1}{A}\tilde{x}\Big(G_A(\tilde{x},Q^2)+V_A(\tilde{x},Q^2)+S_A(\tilde{x},Q^2)\Big)\,d\tilde{x} - \int_0^1 x\Big(G_N(x,Q^2)+V_N(x,Q^2)+S_N(x,Q^2)\Big)\,dx = 0. \qquad (8)$$

Here G,V,S are the gluon,valence and sea parton distributions and $\tilde{x}=AQ^2/2m_Aq_0=Am_N/m_Ax$. These equations are valid for $Q^2>Q_0^2\sim 2$ GeV^2.

We use the NMC data[3] for Ca for the ratio of the second moments of F_{2Ca} and F_{2D} and the exact QCD sum rule (5) in order to calculate the ratio of momentum fractions carried by gluons in Ca and in a free nucleon, γ_G(Ca).Neglecting the change of the gluon momentum in D and possible change of the strange sea we find [9]:

$$\gamma_G(\mathrm{Ca}) = (2.31 \pm 0.35 \pm 0.50)\% \qquad (9)$$

By including these effects γ_G(Ca) would increase by 0.2-0.7%.For A~200 an overall enhancement of G_A is estimated to be >4%.Since for small x, $G_A(x,Q^2)$ is expected to be shadowed, the enhancement of $G_A(x,Q^2)$ in nuclei is likely to be concentrated at $0.03<x<0.15$ where it can exceed 10(20)% for A=40(A=∞) and $Q^2\sim Q_0^2$ (Fig.1).Indications of an enhancement of $G_A(x,Q^2)$ in this x range where reported in [10].

It seems now that we somewhat underestimate depletion of G_A by assuning $\sigma_{\text{"alignedjet"}N}$ ~ const at $x \to 0$. More natural behaviour at $x\le 10^{-2}$ is $\sigma_{\text{"aligned jet"}N} \sim 1/x^{\varepsilon}$, where $\varepsilon\approx 0.08$ as observed for cross sections of soft hadron processes. Besides, λ should decrease at $x \to 0$ since more configurations in the wave function of γ^* are shadowed at $x \to 0$.

Using QCD evolution equations and the above estimate of the gluon enhancement we find that $R_{\bar{q}}(x,Q^2) \equiv \bar{q}_A(x,Q^2)/A\bar{q}_N(x,Q^2)-1$ increases for x=0.04 between $Q^2=3\mathrm{GeV}^2$ (corresponding to the NMC measurements of F_{2A}/F_{2D}) and $Q^2=25$ GeV^2 by at least a factor ~2 (Fig.2).Using the QCD Aligned Jet Model(QAJM)[2,5] to calculate

$8R_{\bar{q}}(x,Q^2)$, we find results for Ca to be in a reasonable agreement with recent Drell-Yan data.[11] *Thus we conclude -small shadowing for $\bar{q}_A$ observed in [11] for x~0.04 and $Q^2>16GeV^2$ corresponds to much larger shadowing for $Q^2\sim Q_0^2$.*

The presence of shadowing for sea at $x\leq 0.1$ implies a considerable enhancement of $V_A(x\sim 0.1,Q^2)$ $(R_V(x,Q^2)-1\approx 0.1(0.2)$ for $A=40(A=\infty))$ which, when combined with the baryon charge sum rule (5) implies a considerable shadowing of the valence quark distribution at $x<0.03$,is in line with the prediction of [12,2,5](Fig.3).

Note also, that shadowing of small k_t $q\bar{q}$ configurations in the γ^* wave function leads to an enhancement of relative contribution of large k_t $q\bar{q}$ configurations. Thus the distribution over k_t in the small x parton wave function of nuclei should broaden as the atomic number increases. Since for A~ 200 the contribution of soft configurations drops by a factor ~3, the increase of $\langle k_t\rangle$ with A at small x may be rather strong.Quantitative estimates of this effect will be presented elsewhere.

To summarize, current data are consistent with the parton fusion scenario first suggested in[12]: all parton distributions are shadowed at small x, while at larger x only valence quark and gluon distributions are enhanced.Consequently the EMC effect at $x < 0.15$ is dominated by effects related to shadowing. Note also that the original fusion scenario[13] (which was also assumed in[7,8])according to which momentum fractions carried by sea quarks and gluons in nuclei remain the same as in a free nucleon is hardly consistent with deep inelastic and Drell-Yan data. The pion model of the EMC effect and the so called energy binding models (which are closely related to the pion models) are also in a clear conflict with the Drell-Yan data[11].

4. Possible implications for internucleon forces

Let us briefly consider the dynamical ideas that may be consistent with the emerging picture of the small $x(x\leq 0.1)$ parton structure of nuclei.In the nucleus rest frame the $x\approx 0.1$ region corresponds to a possibility for the virtual photon to interact with two nucleons which are at distances of about 1 fm (cf.eq.6).

But at these distances quark and gluon distributions of different nucleons may overlap. So, in analogy with the pion model of the EMC effect, the natural interpretation of the observed enhancement of gluon and valence quark distributions is that intermediate range internucleon forces are a result of interchange of quarks and gluons. Within such a model, screening of the color charge of quarks and gluons would prevent any significant enhancement of the meson field in nuclei(which is ruled out by the data[11]). Such a picture of internucleon forces does not necessarily contradict the experience of nonrelativistic nuclear physics. Really in the theoretical description of high energy processes where quark and gluon degrees of freedom can be excited it is impossible to integrate them out to obtain chiral a Lagrangian which seems relevant for the existence of nuclei. On the contrary in the low energy processes where such integration seems possible the exchange of quarks(gluons) between nucleons may be equivalent within the dispersion representation over the momentum transfer, to the exchange of a group of few mesons. Another(the same?!) option is that the discussed change of parton distributions is a consequence of the difference between structure functions of bound and free nucleons.Both options suggest "melting" of nucleon degrees of freedom with the increase of nucleon density, i.e. the tendency to phase transition in superdense nuclear matter,e.g. in the cores of neutron stars.

It's also worth emphasizing that the deduced above comparatively large(≥20%) enhancement of valence quark and gluons in infinite nuclear matter for $x\approx 0.1$ should lead to a comparable change of bound nucleon properties, for example to a change of the bound nucleon elastic form factors at intermediate Q^2(though not to a noticeable change of the radii or of large Q^2 asymptotes).

Thus we conclude: investigation of the nuclear structure functions at $1/2m_N x \sim r_{NN}$ ($x\sim 0.1$) may provide new information on dense(superdence?!) nuclear matter. Direct mesurement of valence and gluon nuclear distributions are badly needed,eg. Drell-Yan pair production in $\pi^{\pm}A, \bar{p}A$ scattering, production of leading $\pi^{\pm}(h^{\pm})$ in the current fragmentation region in μA scattering, production of direct photons,etc (see [2] for the list of options). New type of information can be obtained also by searching for correlations between current and target fragmentation regions.

5. Impact parameter dependence of nuclear parton distributions

In the case of nuclear collisions one usually compares characteristics of events corresponding to central and to peripheral collisions. It is evident from the above discussion that the effective nuclear parton distributions at fixed impact parameter b, $p_A(b,x,Q^2)$, which enter into the description of these collisions, are different for peripheral and for central collisions. Really for peripheral collisions $p_A(b\approx R_A,x,Q^2) \approx p_N(x,Q^2)$ since shadowing is a correction, while for central collisions shadowing and hence antishadowing effects are somewhat larger than for inclusive parton distributions $p_A(x,Q^2)$. The effect of shadowing for small x ($1/2m_N x \gg 2R_A$) and given b can be written as (for $p_A=S_A,G_A$)

$$\frac{p_A(b,x,Q^2)}{p_A(x,Q^2)} = \lambda + (1-\lambda)\frac{2(1-\exp(-\frac{1}{2}\sigma_{"aj"N}\,T_A(b)))}{\sigma_{"aj"N}\,T_A(b)}, \qquad (10)$$

where

$$T_A(b)=\int\rho_A(b,z)dz \qquad (11)$$

It was demonstrated in[5] that in the shadowing region the shape of the x-dependence of $p_A(x,Q^2)/p_N(x,Q^2)-1$ is a rather weak function of A, for A>10. Consequently it may be reasonable for modeling hard nuclear collisions, to use for $p_A(b,x,Q^2)$ the parton distribution of a nucleus B with

$$p_B(x\to 0,Q^2)/p_N(x\to 0,Q^2)=p_A(b,x\to 0,Q^2)/p_N(x\to 0,Q^2).$$

For heavy nuclei where $p_A(b\sim 0,x\to 0,Q^2)/p_N(x\to 0,Q^2)$ is slightly smaller than $p_A(x\to 0,Q^2)/p_N(x\to 0,Q^2)$, one can use the following approximation:

$$p_A(b,x,Q^2)-1 = \frac{p_A(b,x\to 0,Q^2)/p_N(x\to 0,Q^2)-1}{p_A(x\to 0,Q^2)/p_N(x\to 0,Q^2)-1}\,(p_A(x,Q^2)-1) \qquad (12)$$

At present sufficiently accurate data exist only for A≤40, so for the time being, we suggest to use for modeling $p_A(b,x,Q^2)$ the parameterizations for Ca which are presented in the Appendix though scaled according to eqs.10-12.

References.

1. T.H.Bauer,R.D.Spital,D.R.Yennie and F.M.Pipkin,Rev.Mod.Phys. 50,261(1978).
2. L.L.Frankfurt and M.I.Strikman, Phys.Rep.160,235(1988).
3 U.Landgraf,review talk at PANIC XII,June 1990.
4. B.L.Ioffe,Phys.Lett.,B30,123(1968), V.N.Gribov,B.L.Ioffe,and I.Ya.Pomeranchuk,Yad.Fiz. 2,768(1965).
5. L.L.Frankfurt and M.I.Strikman, Nucl.Phys.B316,340(1989).
6. J.D.Bjorken,Proc. 1971 Intern.Conf.on Electron and Photon Int.at High Energies,282,Cornell University Press, J.D.Bjorken and J.Kogut,Phys.Rev.28,1341(1973).
7. S.J.Brodsky and H.J.Lu,Phys.Rev.Lett.64,1342 (1990).
8. V.I.Zakharov and N.N.Nikolaev,MPI-PAE/Th11/90.
9. L.L.Frankfurt,M.I.Strikman,and S.Liutti,Phys.Rev.Lett. in press.
10. M.de Jong, talk at PANIC XII,June 1990.
11. D.M.Alde et al.,Phys.Rev.Lett.64,2479(1990).
12. L.L.Frankfurt and M.I.Strikman, Sov.J.Yad.Fiz.41,485(1985).
13. V.I.Zakharov and N.N.Nikolaev,Phys.Lett.B55,397(1975).

Figure Captions

Fig.1 Ratio $R \equiv R_G(x,Q^2) = (2/A)G_A(x,Q^2) / G_D(x,Q^2)$ plotted vs. x, for different values of Q^2; full line: $Q^2 = 2$ GeV^2, dot-dashed line: $Q^2 = 15$ GeV^2

Fig.2 Ratio $R = (2/A)\,\bar{u}_A(x,Q^2) / \bar{u}_D(x,Q^2)$ plotted vs. x, for different values of Q^2. Notations as in Fig.1. Experimental data from Ref.11.

Fig.3 Ratios $R(x,Q_o^2) = (2/A)F_2^A(x,Q_o^2) / F_2^D(x,Q_o^2)$ (dashed line), $R \equiv R_V(x,Q_o^2) = (2/A)V_A(x,Q_o^2)/V_D(x,Q_o^2)$ (full line) and $R \equiv R_S(x,Q_o^2) = (2/A)S_A(x,Q_o^2)/S_D(x,Q_o^2)$ (dot-dashed line) in ^{40}Ca. All curves have been obtained at $Q_o^2 = 2$ GeV^2. The low x behaviour ($x \leq x_{sh}$) corresponds to the predictions of the QAJM of Refs.2 and 5; the antishadowing pattern (i.e. a 10% enhancement in the valence channel whereas no enhancement in the sea, leading to a less then 5% increase of F_2^A at $x \approx 0.1 \div 0.2$), has been evaluated within the present approach by requiring that sum rules (7) and (8) are satisfied. Experimental data are from Ref.3 (diamonds) and Ref.11 (squares), the latter representing the sea quarks ratio R_S (cf. Fig.2). The theoretical curves are located below the data at small x, due to the high experimental values of Q^2: $\langle Q^2 \rangle = 14.5$ GeV^2, in Ref.3 and $\langle Q^2 \rangle = 16$ GeV^2 in Ref.11, respectively.

Appendix

In order to make easier quantitative calculations, the x and A dependence of the ratios between the nuclear valence and gluon distributions and the free nucleon ones have been parametrized as follows:

$$R(x,q^2)= \frac{1}{(c_1-c_2)}\{c_1\exp(-\alpha\ (x-x_o)) \ - c_2\exp(-\beta\ (x-x_o))\} \qquad (A1)$$

where $R = R_G, R_V$. For ^{40}Ca and $Q^2 \equiv Q_o^2 = 2\ GeV^2$, we found

$c_1 = 1.125 \qquad c_2 = 0.125 \qquad \alpha = 0.5 \qquad \beta = 27.5$

when $R = R_G$ and

$c_1 = 1.125 \qquad c_2 = 0.125 \qquad \alpha = 0.6 \qquad \beta = 30.0$

when $R = R_V$. In both cases x_o represents the value of x at which R_G and R_V cross unity, given by $x_o = 0.04$. Moreover, the above parametrizations were obtained by requiring that the baryon and momentum sum rules are satisfied within the accuracy of $\approx 0.05\%$ at $Q^2 \equiv Q_o^2 = 2\ GeV^2$, such requirement being naturally fulfilled at higher values of Q^2 by letting eq.A1 evolve according to QCD evolution equations. Note that the range in which eq.A1 applies is given by $0 \leq x \leq 0.4$; nevertheless it can be used in the evolution equations also at $x \geq 0.4$, without noticeably affecting the $x \leq 0.2$ region discussed in this contribution. The dependence of the ratio R upon A, which is governed in principle by the nuclear density (see eq.7 in Ref.5), has been parametrized for $x \rightarrow 0$ in the following way[2,5]: $R \equiv R_G = a_G\ A^{-\gamma}(1-\lambda) + \lambda$, with $a_G = 1.3$, $\gamma = 0.18$, $\lambda = 0.4$ and $A \geq 10$; $R \equiv R_V = a_V(A/A_V)^{-v}$, with $a_V = 0.7$, $v = 0.33$, $A_V = 12$ and $A \geq 10$. Such parametrizations have shown to give reasonable results (see figs. 2 and 3), and can thus be properly extended, at higher values of x also.

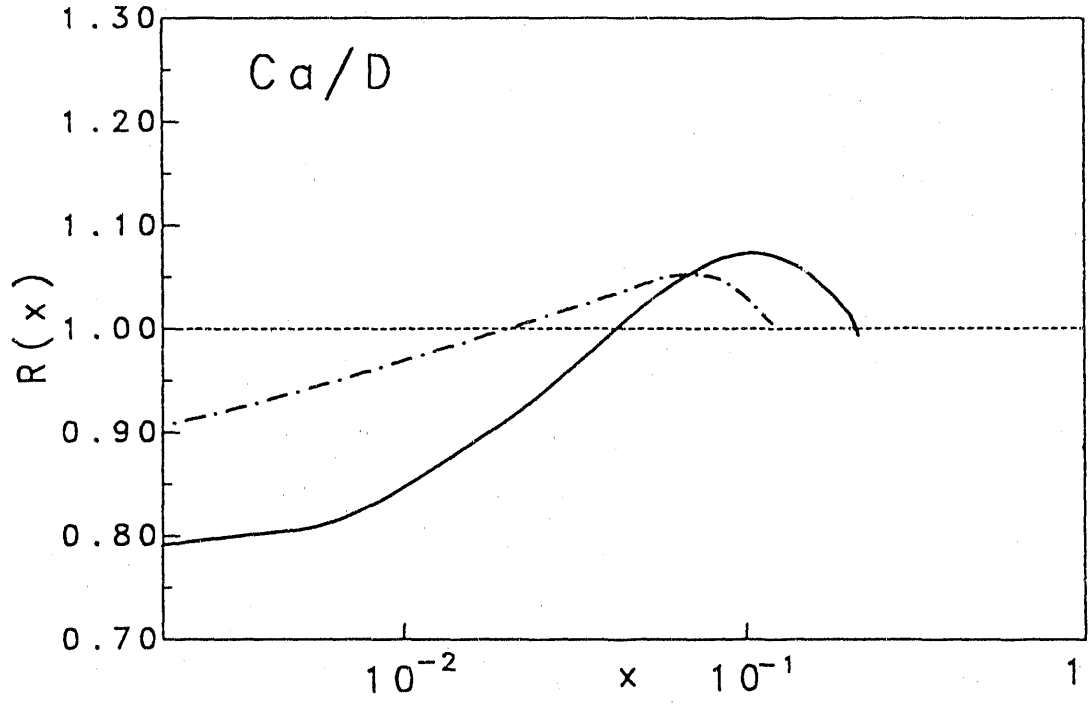
Ca/D
1.30
1.20
1.10
1.00
0.90
0.80
0.70
R(x)
10^{-2}
x
10^{-1}
1

Fig.1

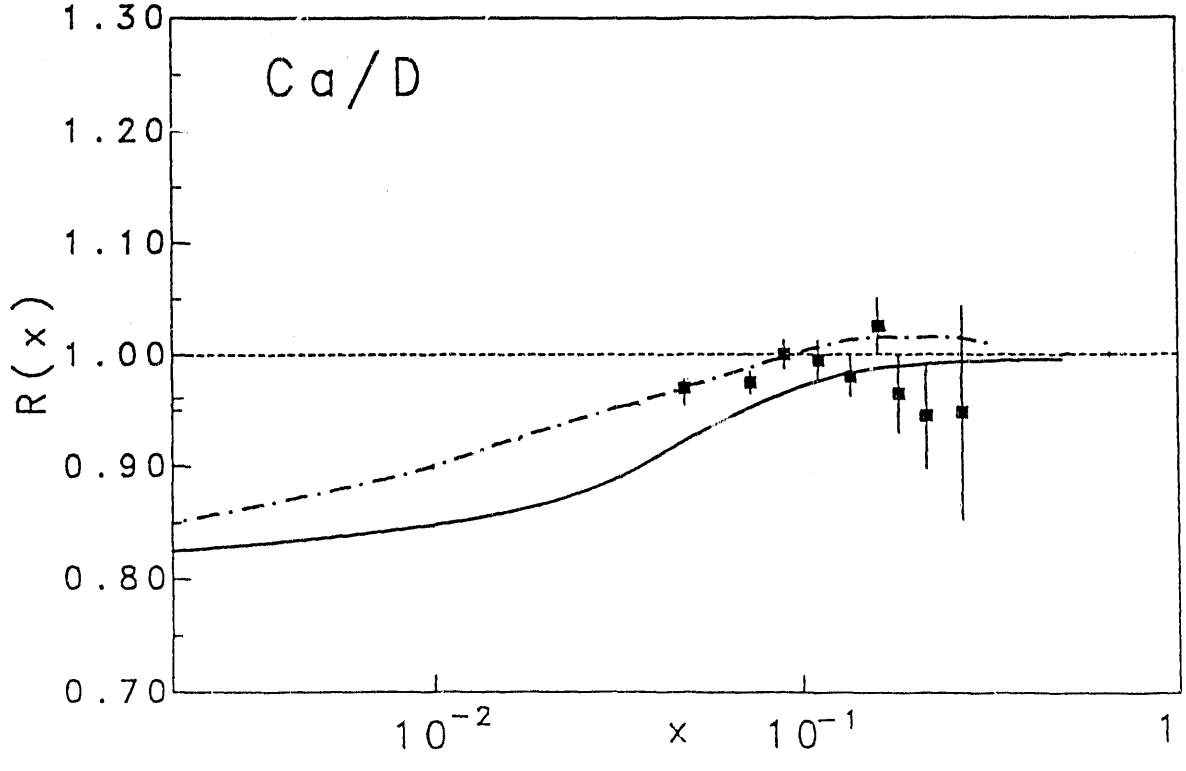
Ca/D
1.30
1.20
1.10
1.00
0.90
0.80
0.70
R(x)
10^{-2}
x
10^{-1}
1

Fig.2

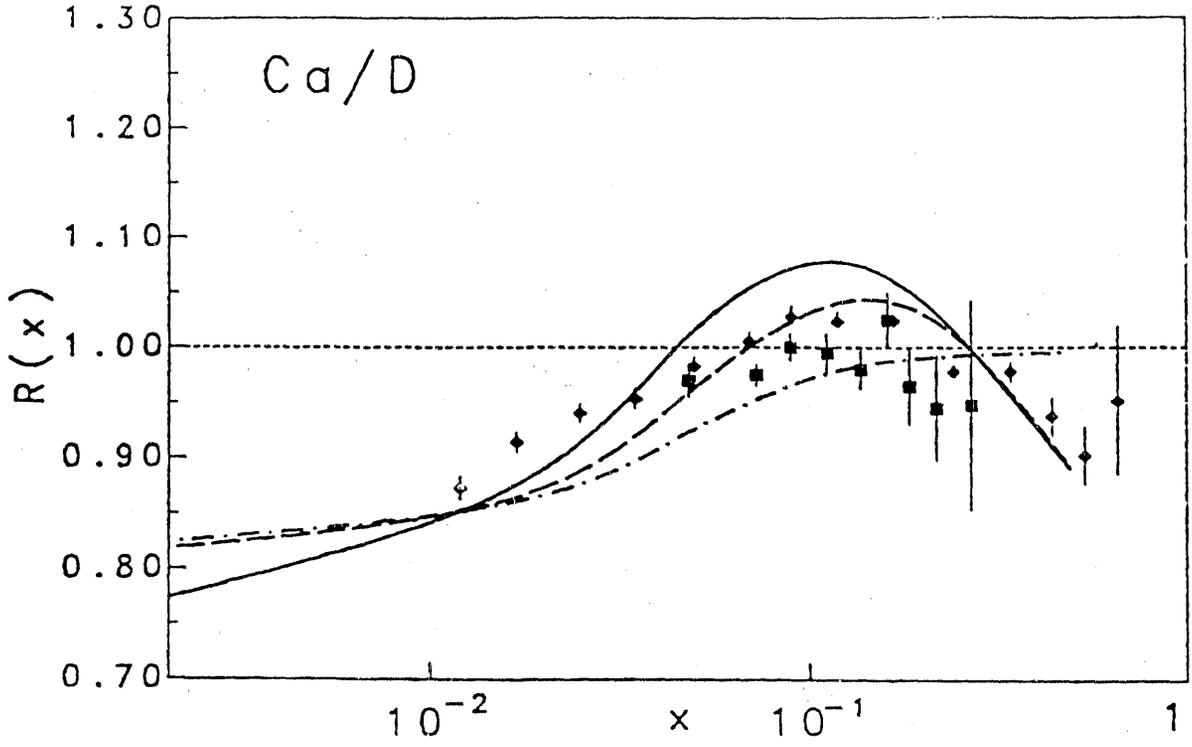

Fig.3

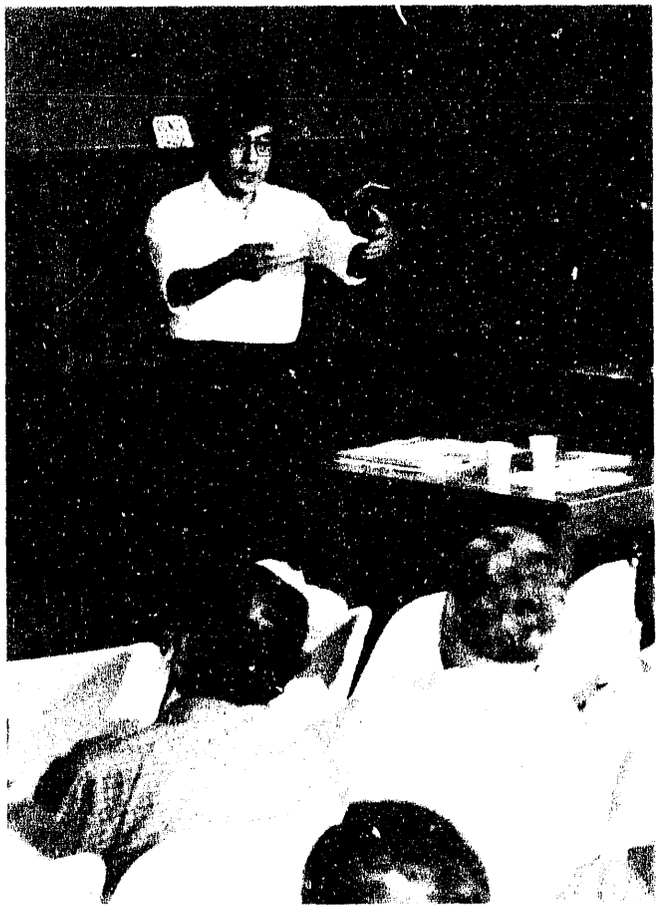

Reports of Experimental Working Groups

Contents:

* Not a working group during the workshop (a contribution received after the workshop).

** A contribution relevant to the di-muon working group, not a report of the working group.

A note from the editors.

Experimental working groups were convened with an intent to work on Letters of Intent for experiments at RHIC. Some groups chose not to submit a contribution to the proceedings of the workshop due to a short deadline for a submission of Letters of Intent.

The List of Experimental Working Groups.

- A Modular Array for RHIC Spectra (W. Busza)
- High p_t Photons, Charged Particles, Jets and High Mass e+e- Pairs at RHIC (P. Braun-Munzinger)
- Elastic Cross-section Measurements at RHIC (W. Guryn)
- Two-Arm Lepton Spectrometer (R. Hayano – merged with the group convened by M. Tannenbaum)
- A Particle and Jet Production Experiment at RHIC (J. Harris)
- A 4π Tracking TPC Spectrometer for RHIC (S. Lindenbaum)
- Open Focusing Spectrometer (S. Nagamiya and D. Lissauer)
- Dimuon Working Group (G. Young)

Concept for an Experiment on Particle and Jet Production at Midrapidity*

J.W. Harris,[7] M. Bloomer,[7] P. Brady,[1] J. Carroll,[2] S.I. Chase,[7] W. Christie,[7] J. Cramer,[12] E. Friedlander,[7] D. Greiner, [7] C. Gruhn,[7] M. Gyulassy,[7] T. Hallman,[4] E. Hjort,[10] G. Igo,[2] P. Jacobs,[7] K. Kadija,[13] D. Keane,[5] L. Madansky,[4] C. Naudet,[7] D. Nygren,[7] G. Odyniec,[7] D. Olson,[7] G. Paic,[13] A. Poskanzer,[7] G. Rai,[7] H.G. Ritter,[7] R. Scharenberg,[10] L.S. Schroeder,[7] P. Seidl,[7] P. Seyboth,[8] D. Shy,[7] R. Stock,[3] T.J.M. Symons,[7] L. Teitelbaum,[7] M.L.Tincknell,[9] H. Van Hecke,[6] X.N. Wang,[7] R. Welsh,[4] W. Wenzel,[7] H. Wieman,[7]and K.L. Wolf [11]

[1] University of California, Davis, California 95616, U.S.A.
[2] University of California, Los Angeles, California 90024, U.S.A.
[3] University of Frankfurt, D-6000 Frankfurt am Main 90, West Germany.
[4] The Johns Hopkins University, Baltimore, Maryland 21218, U.S.A.
[5] Kent State University, Kent, Ohio 44242, U.S.A.
[6] Los Alamos National Laboratory, Los Alamos, New Mexico, U.S.A.
[7] Lawrence Berkeley Laboratory, Berkeley, California 94720, U.S.A.
[8] Max Planck Institute for Physics, Munich, West Germany
[9] Oak Ridge National Laboratory, Oak Ridge, Tennessee, U.S.A.
[10] Purdue University, West Lafayette, Indiana 47907, U.S.A.
[11] Texas A&M University, College Station, Texas 77843, U.S.A.
[12] University of Washington, Seattle, Washington 98195, U.S.A.
[13] Rudjer Boskovic Institute, 41001 Zagreb, Yugoslavia

Abstract

The concept for an experiment to study global event signatures of Quark Gluon Plasma formation and to investigate the propagation of jets through strongly interacting matter at high density is presented. Both event-by-event and inclusive measurements of physical observables can be made at midrapidity over a large solid angle ($|\eta| < 1$) with full azimuthal coverage ($\Delta\phi = 2\pi$) and azimuthal symmetry. The detection system consists of a vertex detector and time projection chamber (TPC) inside a solenoidal magnet for tracking, momentum analysis and particle identification; a time-of-flight system surrounding the TPC for particle identification at higher momenta; and electromagnetic and hadronic calorimetry to measure and trigger on jets and the transverse energy of events.

I. Physics

A. Overview

The aim of this experiment is to search for event signatures of Quark-Gluon Plasma (QGP) formation and investigate the behavior of strongly interacting matter at high energy density. The experiment utilizes two aspects of hadron production that

* The author list includes all those who have contributed to the concept of this experiment. This is not necessarily the same as those who will be on the Letter of Intent.

are fundamentally new at RHIC. These are correlations between *global observables on an event-by-event basis* and the use of *hard scattering of partons* as a probe of the properties of high density nuclear matter. The event-by-event measurement of global observables - such as temperature, flavor composition, collision geometry, reaction dynamics, and energy or entropy fluctuations - is possible because of the very high charged-particle multiplicity densities ($dn_{ch}/d\eta \approx 2000$) expected in nucleus-nucleus collisions at RHIC. Furthermore, measurable jet yields at RHIC will allow investigations using hard QCD processes.

Correlations between observables on an event-by-event basis can be used to isolate potentially interesting event types. A systematic study of particle and jet production would be useful over a range of colliding nuclei from pp through AA, over a range of impact parameters from peripheral to very central, and over the range of energies available at RHIC. The experiment would momentum analyze and identify charged particles (π^+, π^-, K^+, K^-, p, $\bar{p}$, d, $\bar{d}$), as well as various neutral strange particles (K^o, ϕ, Λ, $\bar{\Lambda}$) via their charged-particle decay modes. High $p_\perp$ jets could be identified and measured event-by-event using segmented electromagnetic and hadronic calorimetry.

B. Products of Hard QCD Processes

The goal of studying products of hard QCD processes is to gain an understanding of the propagation of quarks and gluons in dense nuclear matter, hot hadronic matter and quark matter. Various calculations have predicted that the propagation of quarks and gluons through matter depends strongly upon properties of the matter.[1,2,3,4,5] A comparison of the measured yields and energies of products of hard QCD scattering processes in nucleus-nucleus collisions with predictions for their propagation through nuclear, hadronic and quark matter should furnish valuable information on the composition of the matter in these collisions.

High $p_\perp$ Jets

Hard parton-parton collisions will occur within the first fm/c of the start of the nucleus-nucleus collision process.[6,7] To be observed at midrapidity, products of a single hard parton-parton scattering (dijets) must traverse distances of several fermi through high density matter in a nucleus-nucleus collision. The energy loss of these propagating quarks and gluons is predicted[5,8] to be very sensitive to the medium. Passage through hadronic or nuclear matter is predicted to result in a dampening and broadening of jets, whereas in the case of a QGP a transparency and enhanced

---

1 J.D. Bjorken, Fermilab Report 82/59/59-THY (1982).

2 J. Appel, Phys. Rev. D33 (1986) 717.

3 J.P. Blaizot and L.D. McLerran, Phys. Rev. D34 (1986) 2739.

4 M. Rammersdorfer and U. Heinz, Phys. Rev. D41 (1990) 306.

5 M. Gyulassy and M. Pluemmer, Lawrence Berkeley Laboratory Report LBL-28531 (1990), submitted to Phys. Lett. B.

6 E.V. Shuryak in Proceedings of this Workshop.

7 T. Matsui in Proceedings of this Workshop.

8 X.N. Wang in Proceedings of this Workshop.

yield is expected relative to the damped case. The yield of jets should be measured as a function of the transverse energy of the jet. The jet events can be correlated with other event observables to deduce information on the dynamics of the collision process. The jet studies require systematic measurements of pp interactions in addition to heavier mass systems. Systematics as a function of impact parameter for heavier systems are also particularly important.

The jet production rates at RHIC have been calculated.[9] For Au ions at 200 GeV/n and a luminosity of 2×10^{26} $cm^{-2}sec^{-1}$, the expected singles rates for jets are approximately 3×10^4, 60 and 1 per day for $p_\perp > 20$, 40 and 60 GeV/c, respectively. These rates are somewhat independent of the mass of the beam when the luminosities as a function of the beam mass are taken into consideration.

Mini-Jets and High $p_\perp$ Tails of Distributions

Mini-jets are expected to be copiously produced in collisions at RHIC.[10,11] As is the case for high $p_\perp$ jets, the yield and topology of mini-jets is expected to be strongly influenced by the state of the high density medium through which they propagate.[12] However, direct measurement of mini-jets is virtually impossible due to their large opening angle and to the strongly varying background, at large particle densities, relative to the mini-jet energies. Thus, it is important to study the degree of fluctuation of the transverse energy and multiplicity as a function of rapidity and azimuthal angle ($d^2E_\perp/dyd\phi$) of individual events, which should be strongly affected by the mini-jets.[8,13] Likewise, the yield and spectrum of individual hadrons at $p_\perp > 3$ GeV/c would also be affected by modification of the jets and mini-jets by the medium. However, it should be emphasized that the single particle cross sections fall off more rapidly as a function of $p_\perp$, i.e. with $\sigma_{inv} \sim p_\perp^{-8}$, than the jet cross sections,[14] which fall off as $\sigma_{inv} \sim p_\perp^{-5}$.

C. Particle Production

Particle Spectra and Yields

The transverse momentum ($p_\perp$) distributions of charged particles can be measured and studied inclusively with high statistics for effects such as collective radial flow[15] at low $p_\perp$, critical temperature[16] at intermediate $p_\perp$, and mini-jet attenuation[8] at high $p_\perp$. Comparison of these spectra for pp and AA as a function of impact parameter is important. Large unexplained differences in spectral shapes

---

[9] T. Ludlam, L. Madansky and F. Paige, Proc. of LBL Workshop on detectors for Relativistic Nuclear Collisions, ed. L.S. Schroeder, Lawrence Berkeley Laboratory Report LBL-18225 (1984) 115.

[10] K. Kajantie, P.V. Landshoff and J. Lindfors, Phys. Rev. Lett. 59 (1987) 2527.

[11] K.J. Eskola, K. Kajantie and J. Lindfors, Nucl. Phys. B323 (1989) 37.

[12] P.V. Landshoff, Nucl. Phys. A498 (1989) 217; X.N. Wang, Lawrence Berkeley Laboratory Report LBL-28790 (1990), submitted to Phys. Rev. D.

[13] X.N. Wang, Lawrence Berkeley Laboratory Report LBL-28789 (1990), submitted to Phys. Lett. B.

[14] see W. Geist et al., CERN/EP Report 89-159 (1989) to be published in Phys. Rep. (1990).

[15] P.V. Ruuskanen, Z. Phys. C38 (1988) 219.

[16] L. Van Hove, Phys. Lett. 118B (1982) 138; K. Redlich and H. Satz, Phys. Rev. D33 (1986) 3747.

have been measured in pp, αα and higher mass nucleus-nucleus collisions at the CERN ISR and SPS.[17,18] At RHIC, because of the high multiplicities in central nucleus-nucleus events, the slope of the $p_\perp$ distribution for pions and the $\langle p_\perp \rangle$'s for pions and kaons can be determined event-by-event. Thus, individual events can be characterized by temperature to search for events with extremely high temperature, predicted[19] to result from deflagration of a QGP. Displayed in Fig. 1 are two spectra generated from Boltzmann distributions with T = 150 and 250 MeV each containing 1000 pions. This is the average number of pions of a given charge sign expected in the acceptance $|\eta| < 1$ of this experiment for central Au + Au collisions. The slopes of spectra with T = 150 and 250 MeV can easily be discriminated at the single event level. Fig. 2a shows the standard deviation in measuring $\langle p_\perp \rangle$ as a function of the charged particle multiplicity measured in a single event. From Fig. 2a it can be seen that the determination of $\langle p_\perp \rangle$ for pions and that for kaons (for 200 charged kaons per event in the acceptance) can be made very accurately on the single event basis in this experiment.

The difference between the $p_\perp$ spectra obtained for Λ and $\bar{\Lambda}$ or p and $\bar{p}$ should be indicative of the distribution in phase space of valence quarks originating from the initial nucleons of the target and projectile. The amount of net charge and net baryon number, which are proportional, reveals the stopping power of quarks and determines the baryo-chemical potential $\mu_B(y)$ in the medium.[20]

Fluctuations in Energy, Entropy and Transverse Momentum

The large energy, entropy and multiplicity densities at midrapidity in central collisions allow event-by-event measurement of fluctuations in the transverse energy ($E_\perp$), entropy and flavor flow of different types of particles as a function of $p_\perp$, rapidity and azimuthal angle. They also allow measurements of local fluctuations in $p_\perp$ as a function of rapidity and azimuthal angle. The study of these fluctuations may reveal aspects of the existence and hadronization of a QGP.[21] In addition, inclusive measurements of the $E_\perp$ and multiplicity distibutions at midrapidity provide information on the energy and matter densities, respectively.

Flavor Composition

One of the first predictions of signatures for the existence of a QGP was an enhancement in the production of strange particles[22] resulting from chemical

---

[17] W. Bell et al., Phys. Lett. 112B (1982) 271; A. Karabarbounis et al., Phys. Lett. 104B (1981) 75; A.L.S Angelis et al., Phys Lett. 116B (1982) 379.

[18] J.W. Harris et al., Nucl. Phys. A498 (1989) 133c.

[19] E V.Shuryak and O.V. Zhirov, Phys. Lett. B89 (1980) 253; E.V. Shuryak and O.V. Zhirov, Phys. Lett. B171 (1986) 99.

[20] R. Anishetty, P. Koehler and L. McLerran, Phys. Rev. D22 (1980) 2793; W. Busza and A.S. Goldhaber, Phys. Lett. 139B (1984) 235; S. Date, M. Gyulassy and H. Sumiyoshi, Phys. Rev. D32 (1985) 619.

[21] M. Gyulassy, Nucl. Phys. A400 (1983) 31c; L. Van Hove, Z. Phys. C27 (1985) 135.

[22] R. Hagedorn and J. Rafelski, Phys. Lett. 97B (1980) 180; J. Rafelski and B. Mueller, Phys. Rev. Lett. 48 (1982) 1066; P. Koch, B. Mueller and J. Rafelski, Phys. Rep. 142 (1986) 167.

equilibrium of a system of quarks and gluons. A measurement of the K/π ratio provides information on the relative concentration of strange/nonstrange quarks, i.e. $<(s + \bar{s})/(u + \bar{u} + d + \bar{d})>$. This has been suggested[23] as a diagnostic tool to differentiate between hadronic gas, QGP formation and the role of the expansion velocity. This ratio can be measured very accurately on an inclusive basis and with sufficient accuracy event-by-event to classify the events for cross-correlations with other event observables.This can be seen in Fig. 2b where the standard deviation of the measured K/π ratio event-by-event is plotted as a function of the charged particle multiplicity measured in the event.

The production cross section of φ-mesons can be measured inclusively from the decay $\phi \Rightarrow K^+ + K^-$. Measurement of the yield of the φ, which is an $\bar{s}s$ pair, places a more stringent constraint on the origin of the observed flavor composition[24] than the K/π ratio and is expected to be more sensitive to the presence of a QGP.

Measurement of the multiplicities of Λ, $\bar{\Lambda}$ and multiply-strange baryons requires detection of secondary decay vertices. Due to the short decay lengths, a vertex detector close to the beam axis is necessary for these measurements. The measurements provide a better determination of the strange/nonstrange quark ratio than the K/π ratios. Like the φ, multiply-strange baryons are more sensitive to the existence of a QGP[25] than singly-strange particles.

Particle Correlations (Bose-Einstein and Speckle Interferometry)

Correlations between identical bosons provide information on the freezeout geometry,[26] the expansion dynamics[27] and possibly the existence of a QGP.[28] These correlations can be measured on an event-by-event basis for like-sign charged pions and on an inclusive basis for like-sign charged kaons and pions. With high statistics over many events the dependence of the source parameters as a function of the transverse momentum components of the particle pairs will be measured. On an event-by-event basis the source parameters can be determined from the pion correlations and correlated with other event observables. Displayed in Fig. 2c are the number of like-sign pion pairs in a single event as a function of the measured charged-particle multiplicity in the event. The two-pion correlation statistics for a single central Au + Au event at RHIC will be similar to the accumulated statistics published in most papers on the subject. However, since pion source sizes may be as large as 30 fm., the correlation in momentum space will be limited to very small differences in momentum of the pion pair. This could make event-by-event analysis of such large source sizes extremely difficult, due to the limited pair statistics

---

[23] N.K. Glendenning and J. Rafelski, Phys. Rev. C31 (1985) 823; K.S. Lee, M.J. Rhoades-Brown and U. Heinz, Phys. Rev. C37 (1988) 1452.

[24] A. Shor, Phys. Rev. Lett. 54 (1985) 1122.

[25] J. Rafelski, Phys. Rep. 88 (1982) 331.

[26] F.B. Yano and S.E. Koonin, Phys. Lett. B78 (1978) 556; K. Kolehmainen and M. Gyulassy, Phys. Lett. B180 (1986) 203; A. Bamberger et al., Phys. Lett. B203 (1988) 320; B. Andersson and W. Hofmann, Phys. Lett. B169 (1986) 364.

[27] A. Bamberger et al., Phys. Lett. B203 (1988) 320; R. Stock, University of Frankfurt Preprint (1990).

[28] S. Pratt, Phys. Rev. D33 (1986) 1314; G. Bertsch, M. Gong and M. Tohyama, Phys. Rev. C37 (1988) 1896 and G. Bertsch MSU Preprint (1988).

at small momentum differences. It also places stringent constraints on the two particle-track resolution. To supplement the two-particle correlation data, higher particle number correlations can also be analyzed.

Inclusive measurement of KK correlations should complement the $\pi\pi$ correlation data since K's are expected to freeze out earlier[29] during expansion than the π's. Also, depending upon the baryo-chemical potential and the existence of a QGP, the K^+ and K^- are expected to freeze out at different times.[29] Furthermore, the KK correlation is less affected by resonance decays after hadronic freeze-out than the pion correlations[30], thus making interpretation of the KK correlation data easier.

With the high pion density in phase space, unique to RHIC, a novel aspect of multi-pion clustering analogous to optical speckle interferometry[31] should be observable for the first time.[32] These "speckles" are a collective multi-particle effect which leads to macroscopic structure in phase space. They may offer information on the hadronic source which is complementary to that deduced from traditional Bose-Einstein pair correlation analysis. However, prior to any interpretation of "speckle interferometry" data, significant theoretical progress on the Coulomb multiparticle corrections is necessary,

Expansion Dynamics

Anti-deuterons and heavier anti-nuclei can result from the coalescence of combinations of $\bar{p}$ and $\bar{n}$ during expansion when the antinucleon density reaches freezeout density. The "coalescence ratio" $< \bar{d} > / < \bar{p} >^2$ not only depends on the dynamics of source expansion (radial flow, temperature, etc.) at this stage but also on the source size, which reduces this ratio with increasing radius. This observable can provide information complementary to the particle correlation analysis.[33]

Correlations between Event Observables

It should be emphasized that the capability of characterizing events in terms of the values of observables measured event-by-event is unique to this experiment. Events can be characterized by their temperature, flavor content, source size, transverse energy density, multiplicity density, entropy density and degree of fluctuations. Events with extreme values of these observables may be of special interest.

II. Detecting and Measuring Jets at RHIC

Various methods of generating jet events, studying properties of jets and measuring jets in nucleus-nucleus collisions at RHIC have been investigated.

---

[29] K.S Lee, M.J. Rhoades-Brown and U. Heinz, Phys. Rev. C37 (1988) 1463.

[30] M. Gyulassy and S. S. Padula, Lawrence Berkeley Laboratory Report LBL-26077 (1988).

[31] A. Labeyrie in Progress in Optics, ed. E. Wolf, North-Holland Publishing Co., Amsterdam Vol. 14 (1976).

[32] W.A. Zajc, Phys. Rev. D35 (1987) 3396.

[33] S. Mrowczynski, Regensburg Report (1990) to be published in Phys. Lett.

Displayed in Fig.3a is a 40 GeV dijet event generated by Isajet [34] for a $\sqrt{s}$ = 200 GeV pp collision as viewed by the calorimeters in $E_\perp$ vs ϕ and η space. The two jets are easily identified and their energies and directions measured. When this same hard parton-parton scattering is mixed into a $\sqrt{s}$ = 200 GeV/n Au + Au event, generated by the Lund/Fritiof nucleus-nucleus code[35] at impact parameter b = 0, the resulting plot of $E_\perp$ vs ϕ and η in the calorimeters is shown in Fig. 3b. Jets in the background of a central Au + Au event are qualitatively more difficult to find and measure. The CDF jet-finding algorithm[36] was used to study the feasibility of identifying and measuring jets in collisions at RHIC. The results are summarized in Fig. 4. Displayed in Fig. 4a are the efficiencies for finding one and both jets of a pair in the nucleus-nucleus background as a function of the $E_\perp$ of the jet. The efficiencies increase as the $E_\perp$ of the jet increases. Displayed in Fig. 4b is the measured $E_\perp$ of the jet as a function of the $E_\perp$ of the jet known from the simulation. The measured $E_\perp$ is extracted from the background by subtraction of the average background $E_\perp$ from the locus of the jets determined from the jet-finder. The error bars shown in Fig. 4b are the standard deviations of the measurements, without effects of detector resolution. Displayed in Fig. 4c are the standard deviations for determination of ϕ , η , and $E_\perp$ for jets in the simulations. The jet energies can be well determined on the average, but fluctuations of the background increase the error in the measurements over those measured in pp interactions. Determination of the jet direction is less affected by the background and the accuracy less important than the jet $E_\perp$ determination. Precise determination of $E_\perp$ is critical because of the steeply falling jet cross section as a function of jet $E_\perp$.

Some of the problems associated with jet finding may be solved by improvement and careful tuning of the jet-finding algorithms, particularly the energy determination, for the nucleus-nucleus environment. Likewise, careful consideration of the function and design of the calorimetry is necessary to improve the jet energy signal/background. Perhaps the most complicated and most important effect is that of misidentifying fluctuations of the soft background as jets. This requires further investigation.

Wang and Gyulassy have developed a code to simulate nucleus-nucleus collisions at RHIC using as a basis the Pythia code[37] for pp interations plus inclusion of the nucleus-nucleus geometry. Partons are propagated through the matter in the collision and their energy loss is calculated depending upon the type of matter traversed (partonic, hadronic or QGP). Results from these simulations exhibit a strong attenuation of jets and mini-jets in hadronic matter. The attenuation decreases dramatically for traversal of deconfined matter (QGP). The results of the calculations are very much dependent upon the dynamics of the collisions, but the effects are largest at midrapidity. A detailed study of the effects of mini-jet and jet attenuation on the transverse energy measured in calorimetry is underway.

---

[34] F.E. Paige and S.D. Protopopescu, ISAJET, Brookhaven National Laboratory Report BNL-37066 (1985).

[35] B. Andersson et al., Nucl. Phys. B281 (1987) 289.

[36] F. Abe et al., Phys. Rev. Lett. 62 (1989) 613

[37] T. Sjostrand and M. van Zijl, Phys. Rev. D36 (1987) 2019.

Effects on the jet energy resolution of momentum cutoffs due to magnetic fields, absorption and subdivision of the measured energy into electromagnetic and hadronic fractions have been investigated using the Pythia simulation code. These calculations indicate that independent determination of EM or hadronic energy alone is insufficient for accurate jet energy determination, due mainly to the low particle statistics (10-15) in the jet. The primary source of fluctuations of the background is minijets.

The use of both jets in a dijet event allows better identification. Furthermore, measuring the dijet momentum balance provides additional information which may be useful in determining the presence of a QGP. A measurement of the two-jet differential cross section for nucleus-nucleus collisions may in itself be of interest to understanding the parton fragmentation functions in hadronic matter.

III. Layout of Experiment

A. Overview

The physics goals were used to specify the design of the experiment. The experiment consists of tracking, particle identification and calorimetry at midrapidity over a large solid angle ($|\eta| < 1$) with full azimuthal coverage ($\Delta\phi = 2\pi$) and azimuthal symmetry. The detection system consists of a vertex detector to locate the primary and secondary vertices and a time projection chamber inside a solenoidal magnet for tracking, momentum analysis and particle identification; a time-of-flight system surrounding the TPC to extend particle identification to higher momenta than achievable using dE/dx alone; and electromagnetic and hadronic calorimetry to measure and trigger on jets and the transverse energy of events. A diagram of the experiment is shown in Fig. 5.

B. Magnetic Field

The magnet is a solenoid with uniform magnetic field along the beam direction. This magnet design is chosen for complete azimuthal symmetry and high tracking accuracy. A field strength of 0.5 Tesla provides adequate resolution for momenta as high as 10 GeV/c with only modest spiralling of low $p_\perp$ particles. With a TPC inner radius of 0.5 m. the acceptance extends to transverse momenta as low as 40 MeV/c. The magnetic coil radius is 2 m. and the radius of the yoke 4 m., both 8m. in length. The magnet is a room temperature design which minimizes the coil thickness.

C. Charged Particle Tracking System

Momentum analysis and particle identification of all charged particles at midrapidity are necessary to achieve the physics goals of the experiment. The tracking should operate in conditions at higher than the maximum track density, $dn_{ch}/dy \approx 1500$, and multiplicity, $n_{ch} = 3000$, in the $|\eta| < 1$ acceptance of the experiment expected for central Au + Au collisions. Momentum resolution of $\Delta p/p < 0.01$ at $p = 0.1$ GeV/c is required by two-particle correlations, and $\Delta p/p < 0.02$ at $p = 10$ GeV/c is necessary to accurately measure spectra at high $p_\perp$ and particles from mini-jets and jets. Particle identification of pions/kaons/protons over momenta $p < 3$ GeV/c and measurement of decay particles from secondary vertices should be

possible. An additional constraint on the tracking resolution specified by the particle identification resolution is $\Delta p/p = (0.01 \times p)$ for $p < 3$ GeV/c. It is anticipated that the momentum resolution for high $p_\perp$ can be improved by further design, optimization and integration of the tracking detectors.

Time Projection Chamber (TPC)

The TPC consists of two sections each 2.5 m long as shown in Fig. 5. Ionization will drift to two end-caps, located on the outer ends. Each end-cap is instrumented with 75,000 pads, each of dimension 8mm x 20mm. Each pad receives 512 time samples. Singly-charged particles with $p_\perp < 40$ MeV/c spiral inside the inner TPC radius of 50 cm. and do not reach the TPC. Particles with 40 MeV/c $< p_\perp <$ 150 MeV/c spiral inside the TPC and most exit the end-caps. Particles with $p_\perp > 150$ MeV/c traverse the TPC and exit the outer edge at radius 200 cm. Details of the TPC design can be found in Table 1.

The gas inside the TPC is expected to be neon in order to reduce multiple scattering which dominates the momentum resolution at low momentum. The momentum resolution is displayed in Fig. 6a for the low momenta and Fig. 6b for the high momentum range of the experiment. These were calculated for the TPC using neon gas, without vertex determination. The momentum resolution at high momentum is dictated by the two track resolution at the outer radius of the TPC for two tracks close in both momentum and coordinate space.

Vertex Detector (VTX)

The function of the Vertex Detector, coupled with the TPC, is to locate the position of the primary interaction vertex, to improve the momentum resolution for high momentum tracks and to locate secondary vertices with approximately 1mm accuracy. The VTX must be able to provide three dimensional space points and vectors for traversing tracks with high spacial resolution. These tracks can be linked to tracks measured in the TPC. To cover $|\eta| < 1$ the VTX is located at a radius of approximately 0.1 m. from the beam and has a length of 0.5 m.,as shown in Fig. 5.

The design of the VTX depends upon developments in silicon detector technology.[38,39] It should be cylindrical in shape and either a multilayer pixel detector or a superlayer strip detector with stereo layers. Silicon technology should be able to provide a detector with approximately 300,000 pixels of size $1mm^2$ per layer. The VTX must be of low mass so as to minimize secondary particle production, secondary interactions and multiple scattering.

D. Time-of-Flight (TOF) Detector System

To supplement the particle identification capability of the TPC, which is mainly at momenta $p < 0.8$ GeV/c, a TOF system is used. This extends the particle identification up to approximately 2-3 GeV/c in momentum depending upon the particle. A summary of the specifications of the TOF system is provided in Table 2. The particle

---

[38] S. Parker, Nucl. Instr. Meth. A275 (1989) 494.

[39] "SSC Detector R&D Proposal: Development of Technology for Pixel Vertex Detector," D. Nygren - spokesperson (1989).

identification that can be achieved with the TPC - TOF system combination is displayed in Fig. 7. The region outside the largest semi-circle (3σ separation) constitutes the allowed region. The calculations assume a 2 m. flight path and σ = 170 ps for the entire TOF system. With a slightly improved time resolution (σ = 100 ps) the TPC-TOF combination would meet the overall requirements for particle identification. At a distance of 2 m. from the beam, the TOF system with a 6 cm^2 pixel size and 100,000 pixels has a maximum occupancy factor of 2 percent.

The TOF system has not been designed. A TOF system that operates in the magnetic field is preferred. Due to the high segmentation (100,000), lower cost detector systems than presently available must be developed.

E. Midrapidity Calorimeters

The primary purpose of the midrapidity calorimeters is to measure and trigger on high $p_\perp$ jets and the transverse energy of events. The calorimeters consist of separate electromagnetic and hadronic sections with a lateral segmentation of $\Delta\phi$ = 10° and $\Delta\eta$ = 0.1, for a total of 720 towers. The inner diameter will be 2.5 m. and outer diameter 3.8 m. Fig. 5 displays the calorimetry relative to the other detectors in the experiment. The necessity to measure precisely the transverse energies suggests the use of a compensated calorimeter with a linear response down to low energies. Corrections to the calorimeter measurements for distortions of the trajectories of charged particles in the magnetic field can be made using the tracking data.

Hadronic

The hadronic calorimetry consists of Pb/scintillator sandwich (1 cm. Pb, 2 mm. plastic scintillator) with energy resolution of approximately $0.35\text{-}0.40/\sqrt{E}$. The modules are designed to point towards the interaction vertex region and are 6 interaction lengths deep. The lateral segmentation may change after more extensive simulations are completed.

Electromagnetic

The design of the electromagnetic (EM) calorimeters has yet to be determined. It should be noted that an appreciable fraction of the deposited energy is in low energy charged pions. There is little or no difference in shower profiles for charged pions vs EM showers for these low incident energies. The effect of the magnetic field must be considered in the design. The most straightforward choice for the EM calorimeters is to utilize a section of the same Pb/scintillator sandwich structures which form the hadronic section. The EM section would be approximately 0.3 to 1.2 interaction lengths thick, depending upon the jet resolution and calorimeter simulations. In practice, a compensated section with the same response as the hadronic section produces a system which is much easier to construct and calibrate than a high resolution EM section. The EM energy resolution is expected to be approximately $0.22/\sqrt{E}$.

For better jet energy resolution the burden rests on the design of the EM section which must operate in high background. The effect of the lateral segmentation and

energy resolution of the EM section of the calorimetry requires more investigation. A lateral segmentation identical to that of the hadronic segmentation will be simulated.

F. Intermediate Rapidity ($1 < |\eta| < 5$) Detectors

The region $|\eta| > 1$ is presently unspecified. An extension of the calorimetry to $|\eta| < 1.5 - 2$ is being considered to improve the definition of jets. Since jets are observed to spread energy over a region of pseudorapidity (η) and azimuthal angle (ϕ) of size approximately $\sqrt{(\Delta\eta^2 + \Delta\phi^2)} = 1$ about the direction of the jet, edge effects are minimized by calorimeter coverage extending beyond $|\eta| = 1$. For event characterization, full calorimeter coverage is preferred. Likewise, there are similar event characterization arguments for expanding the charged particle multiplicity coverage to include the region $1 < |\eta| < 5$. Insights into these possibilities are being sought from simulations.

G. Triggering

The triggering scheme is still being developed. A three level trigger is anticipated. The first level trigger will consist of decisions at the "hardware" level. Several parallel triggers are expected at this level - multiplicity, $E_\perp$, forward energy, total energy and various ratios of these quantities. First level decisions are made in less than a μsecond. The TPC readout and digitization of counters commence on this trigger. The second level trigger is decided in tens of μseconds. It could consist of topological configurations of interest from the detectors, such as single jets, back-to-back jets, or fluctuations of various observables. The third level trigger operates on a timescale of milliseconds up to seconds. It should consist of trackfinding, momentum reconstruction, particle identification and data compression. It should be noted that the various parallel triggers will be prioritized such that triggers with the smallest cross sections can receive priority interupts.

H. Spectator Calorimeter

A spectator calorimeter to measure the forward energy at rapidities near that of the beam must be developed. This is a detector that might be common to all experiments. The forward energy information from a spectator calorimeter can be correlated with the midrapidity calorimeters to characterize events by the centrality of the nucleus-nucleus collisions.

I. Data Acquisition Rates

At present the maximum expected data acquisition rates for this experiment range from 1 central Au + Au interaction per second to 10 minimum bias Au + Au interactions per second, limited by data acquisition and storage rates. The event size for central Au + Au collisions is expected to be 80 MB. After reduction by the maximum filling factor expected for the TPC (10%) this becomes 8 MB per event. It is possible that with some developments in data reduction and compression the data rate could be increased, as much as tenfold.

J. Data Acquisition Philosophy

The goals of this experiment require data acquisition utilizing a range of projectiles (from protons to Au), available beam energies and impact parameters. It is expected that longer data acquisition periods will be necessary for studies of jet production in p + p, Au + Au and an intermediate mass system. Furthermore, the data acquisition requirements of this experiment are inherently different from those of experiments which measure observables with small cross sections. Those experiments will require data accumulation with a fixed projectile and energy for as long as possible.

Acknowledgements

The authors wish to thank N.K. Glendenning, A. Shor, G. Young, T. Ludlam, W. Geist, R. Kadel, S. Nagamiya, W. Carithers, J. Siegrist, M. Shapiro, B. Jacak and L. Van Hove for interesting and helpful discussions. This work was supported in part by the Director, Office of Energy Research, Division of Nuclear Physics of the Office of High Energy and Nuclear Physics of the U.S. Department of Energy under contract DE-AC03-76SF00098.

Appendix - RHIC Detector R&D Projects

Several detector R&D projects are necessary for the success of this concept. One project, already funded, is to develop *Integrated TPC Electronics* which includes preamp, shaper, analog storage and ADC on a single integrated circuit. Development of high resolution (σ ~ 100 ps) time-of-flight detectors, which are inexpensive compared to the cost of photomultiplier tubes, is important when considering 100,000 channels of detectors. In addition, possible operation in a magnetic field has led to consideration of *Pestov Spark Counters* and *Silicon Avalanche Diodes* for development. A project is underway to study the feasibility of a *High Track Pair Resolution TPC* which uses a parallel plate avalanche readout with resistive mesh to increase the two-track resolution, possibly tenfold. To be able to increase the data acquisition rate *Online Data Compression* via specialized hardware for track processing and analysis will be pursued. The development of a *Vectoring Vertex Detector* is necessary for this and possibly other RHIC experiments. Either a pixel vertex detector system or one with silicon superlayer strips will be developed. The calorimetry must be designed and the *Calorimeter Readout* optimized for use in this experiment. Various readout techniques, for example the use of wavelength shifter (WS) bars or WS fiberoptics, will be investigated. For calibration of the TPC a unique *3-D TPC Laser Calibration System*, utilizing time modulation of ultraviolet laser light to produce three-dimensional space points of ionization in the TPC, will be developed.

Tables

Table 1. TPC Detector Specifications

Tracking - Time Projection Chamber

Two Sections	
Uniform field (solenoid)	B = 0.5 T
Inner radius	0.5 m
Outer radius	2.0 m
Length of each section	2.5 m
# pads at each of 2 endcaps	75,000
Pad size	8mm x 20 mm
Tracking accuracy	100 μm
Time samples	512
Drift time	50 μsec
Maximum interaction rates	10^4 /sec Au-Au, 10^6 /sec p-p

Table 2. Time-of-Flight Detector Specifications

Time-of-Flight

Radius	2 m
Area	60 m^2
Cell occupancy	< 0.02
Pixel size	6 cm^2
Channels required	100,000
Time resolution	< 100 psec
Channel dead-time	< 1 msec

Figures

Figure Captions

1. Simulation of $dn/dp_\perp$ vs.$p_\perp$ for an event generated using a Boltzmann distribution with 1000 pions. The curves correspond to single events generated with T = 150 MeV and 250 MeV, as labelled.

2. As a function of the charged-particle multiplicity measured in an event are plotted a) the standard deviation of $p_\perp$, b) the standard deviation of the ratio K/π (assuming $\langle K/\pi \rangle = 0.1$) and c) the number of like-sign pion pairs. A central Au + Au

event at RHIC is expected to produce 2000 charged particles (1000 pions of each charge) into the acceptance of this experiment.

3. a) A plot of $dE_\perp$ vs ϕ and η of a 40 GeV dijet event generated by Isajet for a $\sqrt{s}$ = 200 GeV pp collision. b) A plot of $dE_\perp$ vs ϕ and η for the same hard parton-parton scattering mixed into a $\sqrt{s}$ = 200 GeV/n Au + Au event, generated at impact parameter b = 0 by the Lund/Fritiof nucleus-nucleus code. A lateral segmentation of $\Delta\phi = 10°$ and $\Delta\eta = 0.1$ for the calorimetry is assumed. No effects of detector resolution have been input into this calculation.

4. a) The efficiency for finding dijets in a simulation using the CDF jet-finding algorithm plotted as a function of the transverse energy $E_\perp$ of the jet. A lateral segmentation of $\Delta\phi = 10°$ and $\Delta\eta = 0.1$ of the calorimeters is assumed. The 400 events were generated using the Lund/Fritiof model for $\sqrt{s}$ = 200 GeV/n Au + Au at impact parameter b =0 and superimposing dijets generated with Isajet at the same incident energy. Plotted are the efficiencies for finding one jet of the pair $\varepsilon_{1,2}$ and both jets of the pair ε_2. Also plotted is a point for the efficiency for finding jets in a pp event with the same code. No detector resolution has been input into the calculation. b) The measured transverse energy $E_\perp$ of the jet as a function of the actual transverse energy $E_\perp$ of the jet for the same sample of events. c) The standard deviations in determining the azimuthal angle ϕ, pseudorapidity η and transverse energy $E_\perp$ of the jet as a function of the jet transverse energy $E_\perp$.

5. Conceptual layout of the experiment. See text for description.

6. Momentum resolution for two ranges of momenta.

7. Particle identification using a combination of energy loss and time-of-flight.[40] Displayed is the time difference and energy loss difference between pairs of particles (K-p, K-π, π-p). The 3 lines correspond to the 3 types of particle pairs considered. The momentum of the particles is given along each line. The semi-circles correspond with increasing radii to 1, 2 and 3σ separation, respectively. The region outside the semi-circles represents the allowed-region. The calculations assume 2 m. flight path and 170 ps time resolution for the time-of-flight system.

---

[40] H.G. Pugh, G. Odyniec, G. Rai and P. Seidl, Lawrence Berkeley Laboratory Report LBL-22314 (1986).

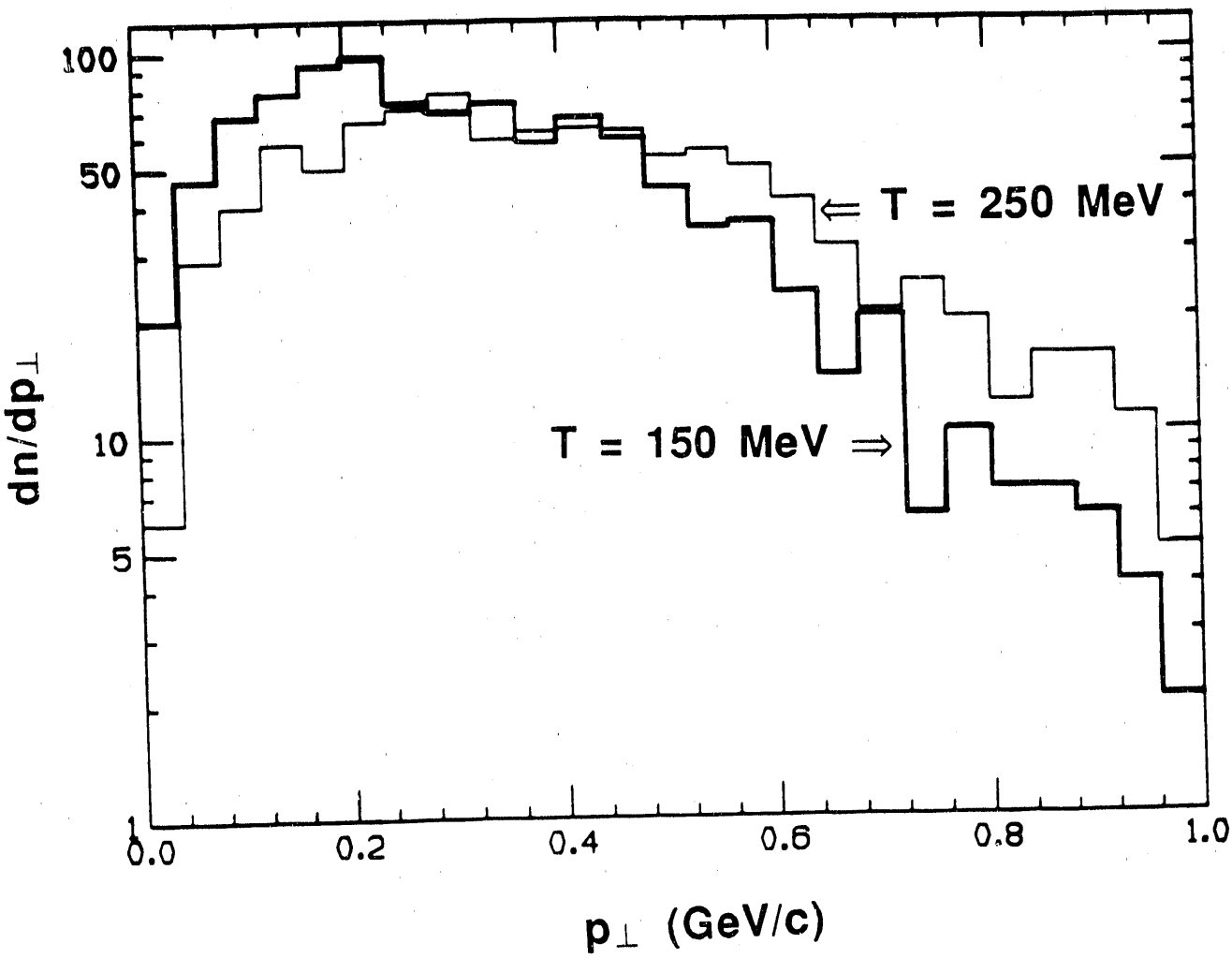

Fig. 1

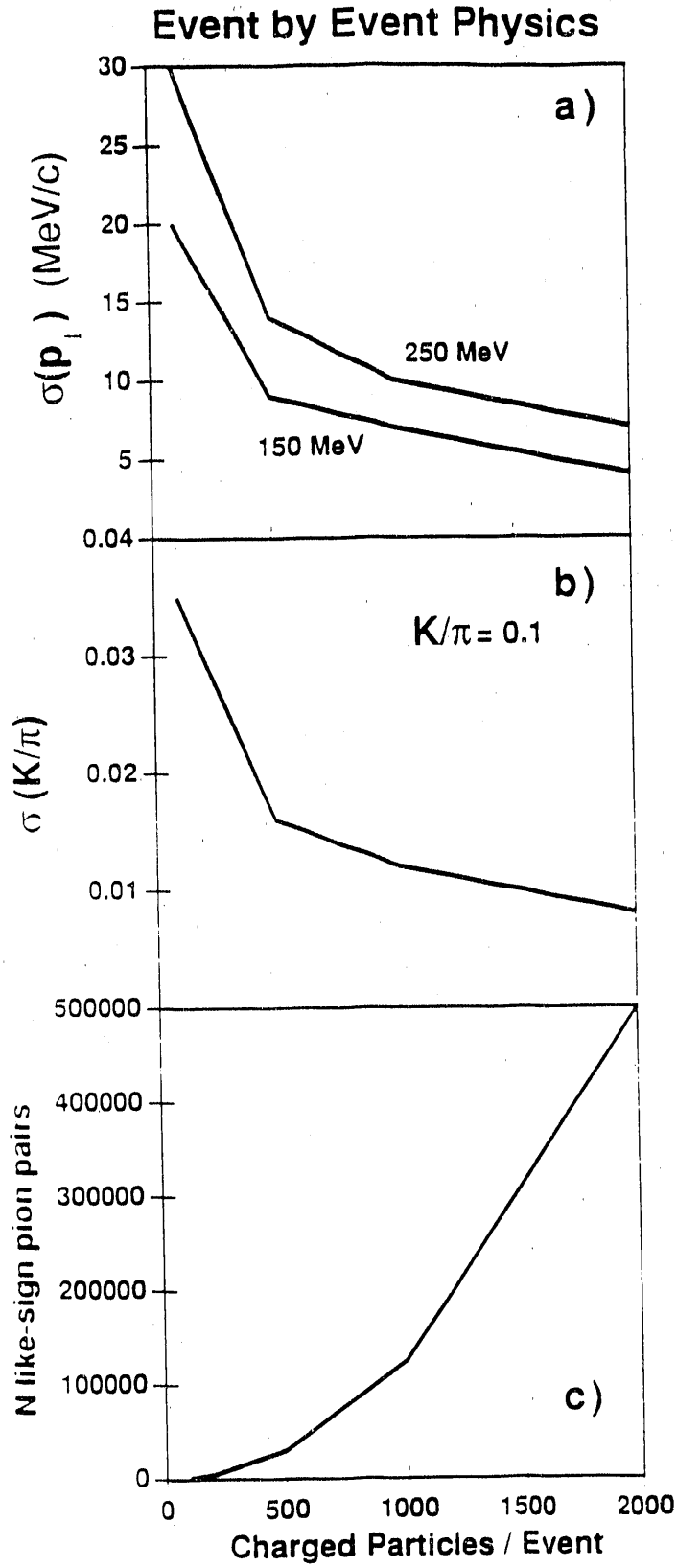
Event by Event Physics
a)
b)
c)
250 MeV
150 MeV
K/π = 0.1
σ(p_t) (MeV/c)
σ (K/π)
N like-sign pion pairs
Charged Particles / Event
30
25
20
15
10
5
0.04
0.03
0.02
0.01
500000
400000
300000
200000
100000
0
0
500
1000
1500
2000

Fig. 2

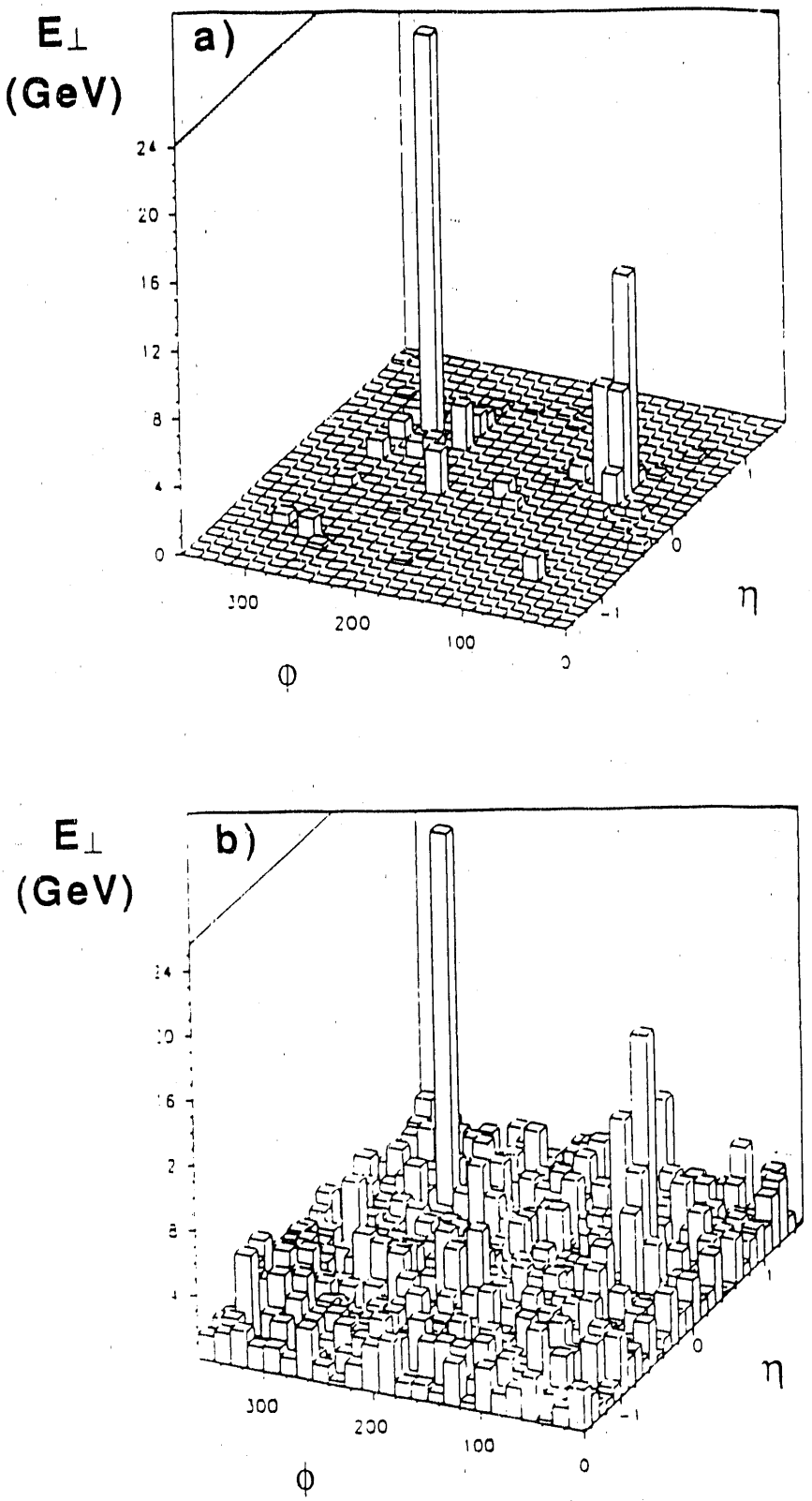
E⊥
(GeV)
a)
24
20
16
12
8
4
0
300
200
100
0
Φ
1
0
-1
η
E⊥
(GeV)
b)
300
200
100
0
ϕ
1
0
-1
η

Fig. 3

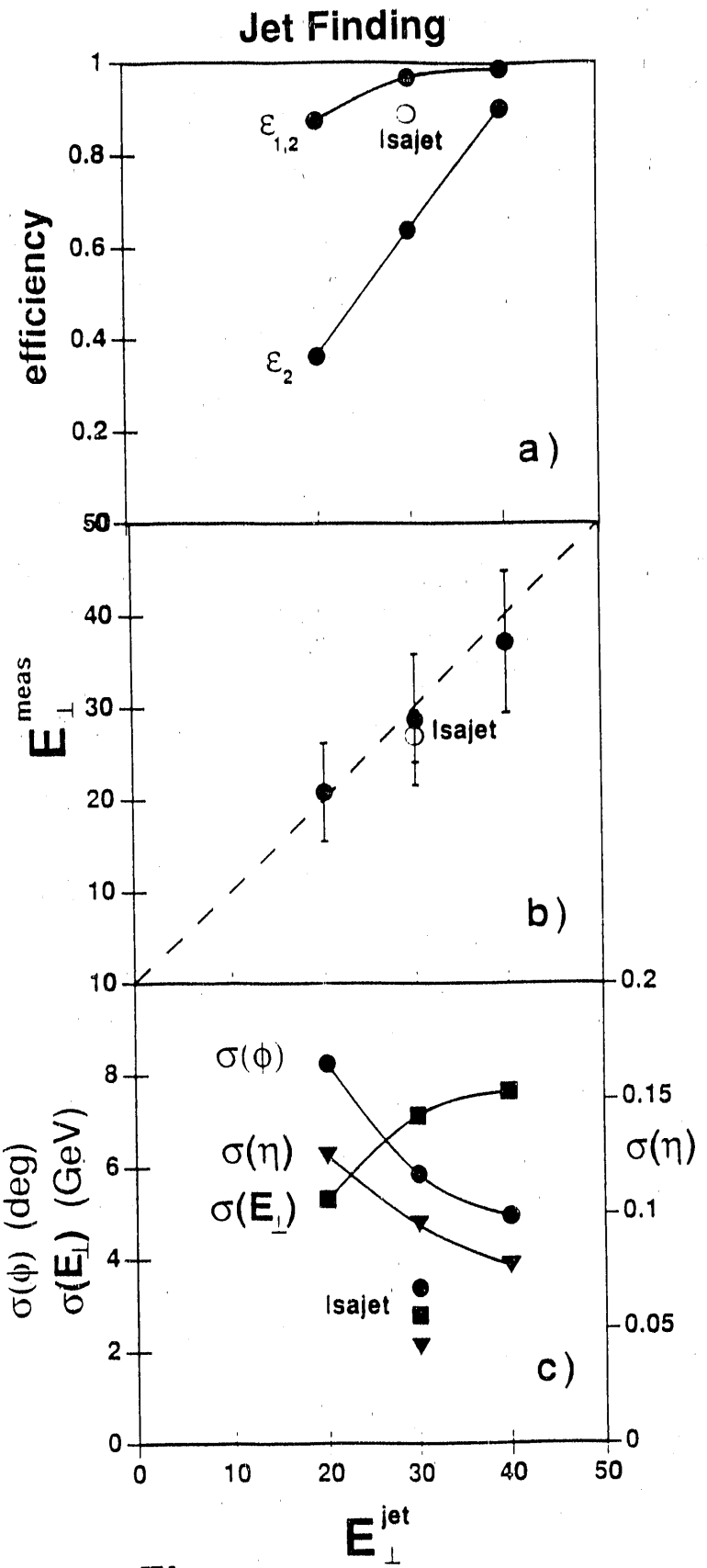
Jet Finding
efficiency
$\varepsilon_{1,2}$
ε_2
Isajet
a)
$E_\perp^{meas}$
Isajet
b)
$\sigma(\phi)$ (deg)
$\sigma(E_\perp)$ (GeV)
$\sigma(\phi)$
$\sigma(\eta)$
$\sigma(E_\perp)$
Isajet
c)
$\sigma(\eta)$
$E_\perp^{jet}$

Fig. 4

RHIC Experiment on Particle and Jet Production

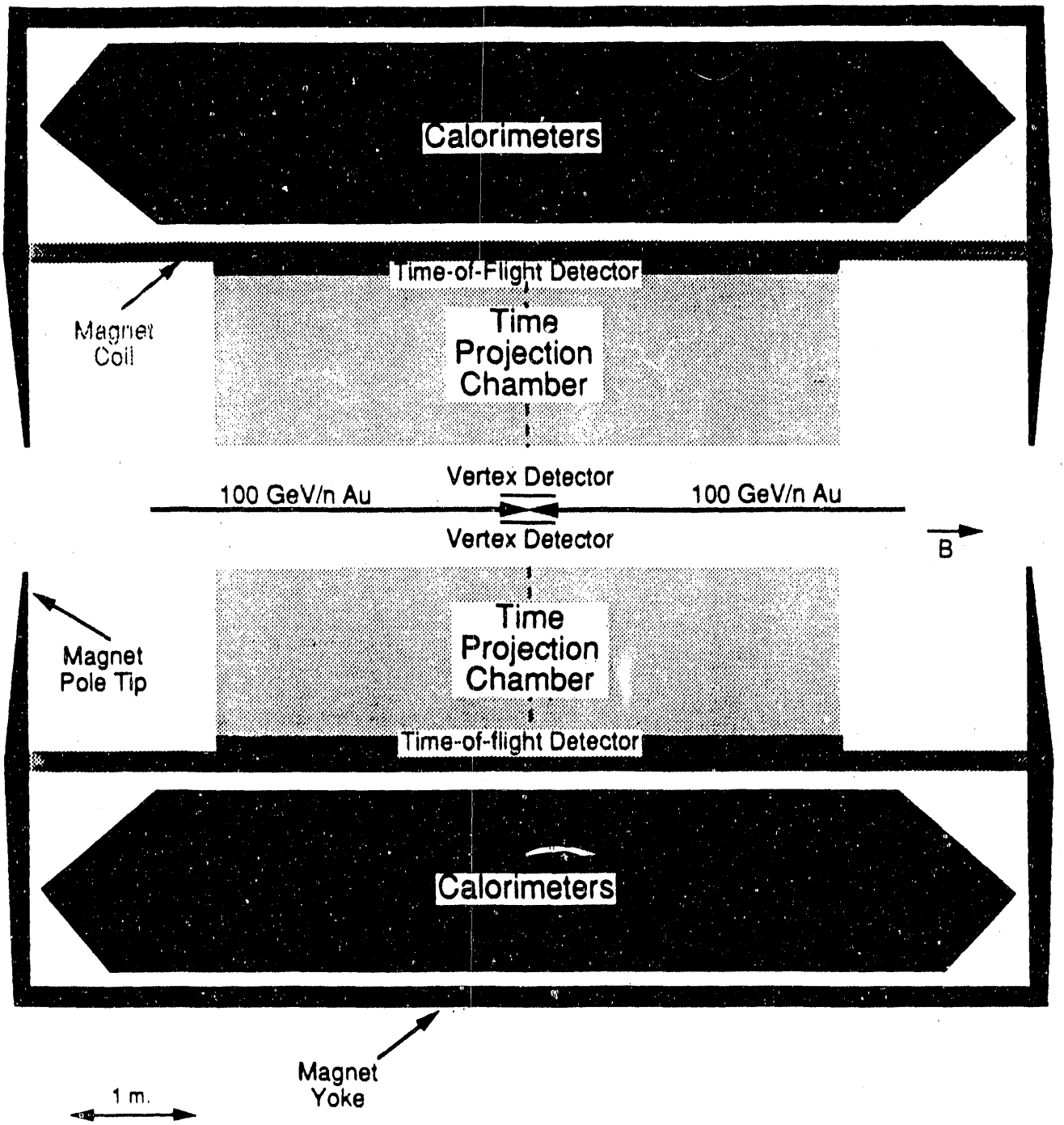

Fig. 5

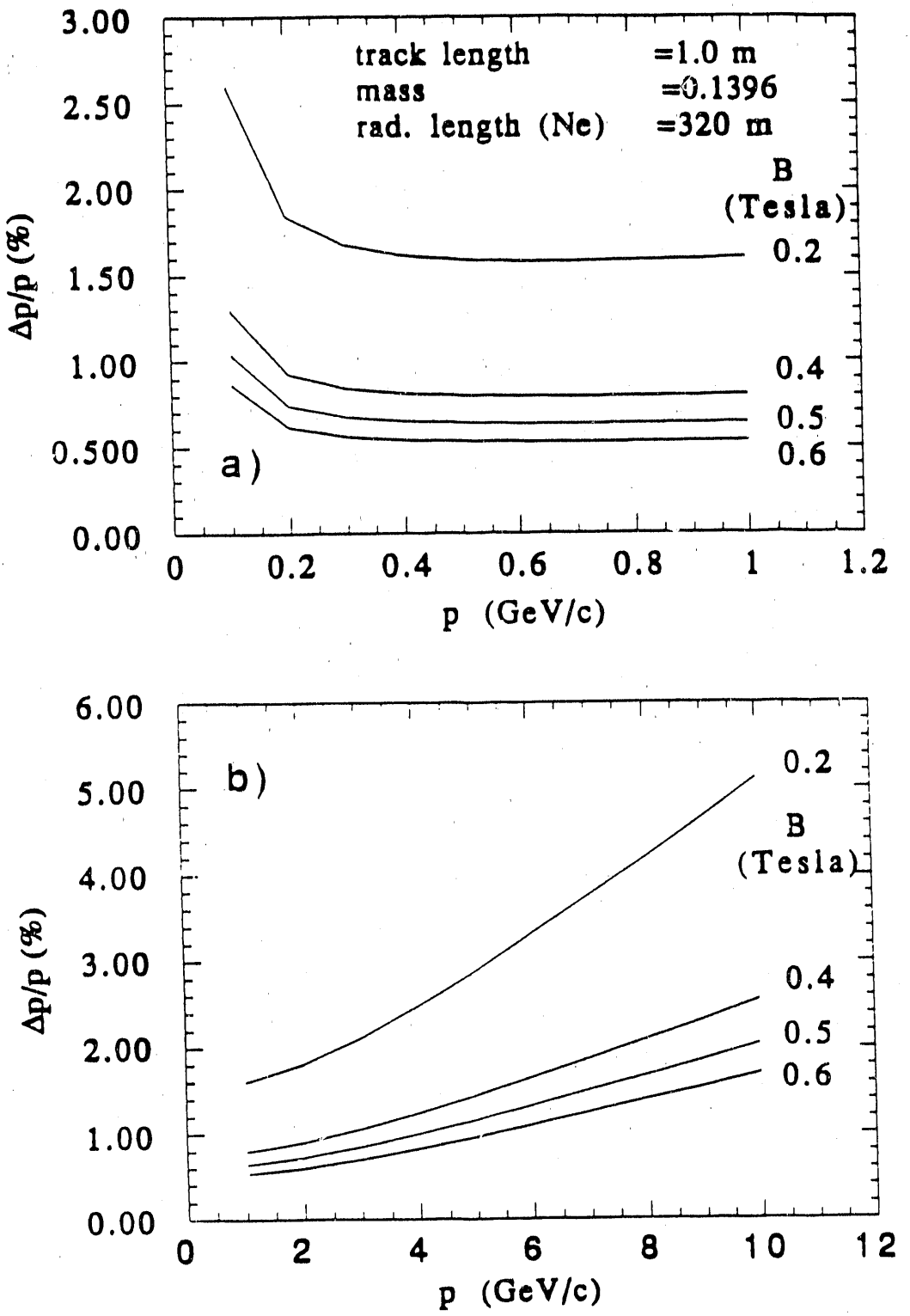
Momentum Resolution
track length =1.0 m
mass =0.1396
rad. length (Ne) =320 m
B
(Tesla)
0.2
0.4
0.5
0.6
a)
b)
Δp/p (%)
p (GeV/c)
3.00
2.50
2.00
1.50
1.00
0.500
0.00
0
0.2
0.4
0.6
0.8
1
1.2
6.00
5.00
4.00
3.00
2.00
1.00
0.00
2
4
6
8
10
12

Fig. 6

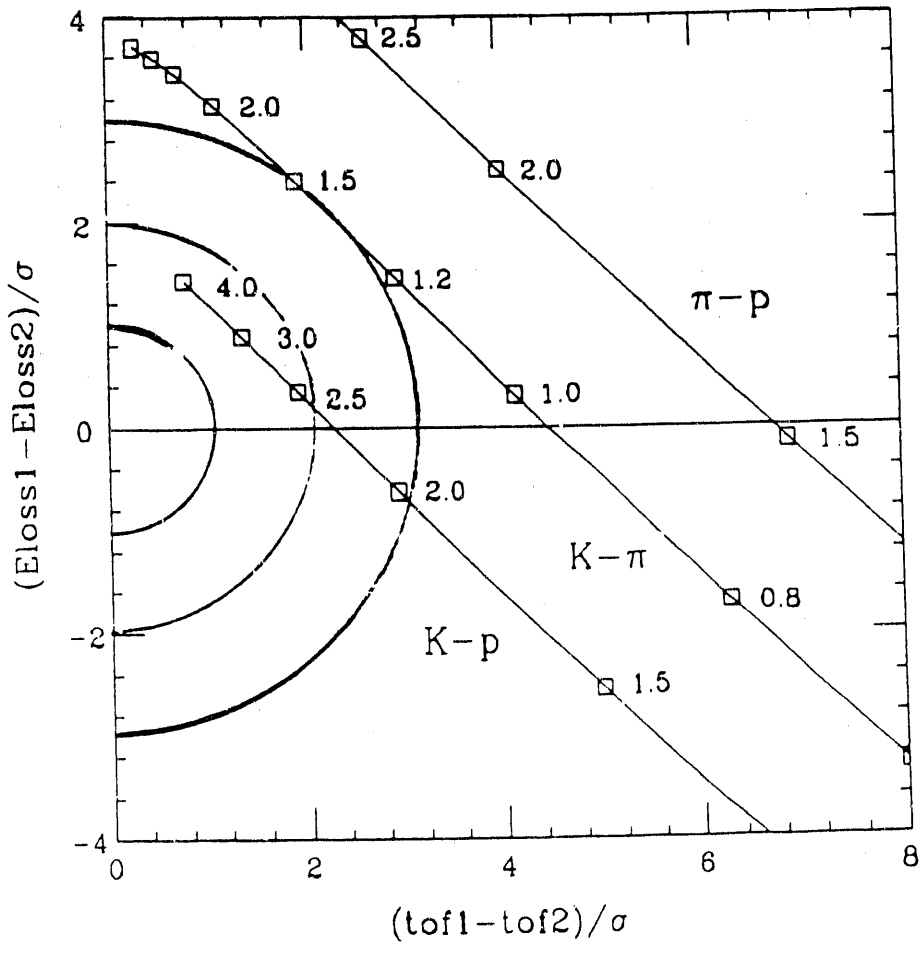
4
2
0
-2
-4
0
2
4
6
8
(Eloss1−Eloss2)/σ
(tof1−tof2)/σ
2.5
2.0
1.5
2.0
1.2
4.0
3.0
2.5
1.0
1.5
2.0
0.8
1.5
π−p
K−π
K−p

Fig. 7

Two-Arm Electron/Photon Spectrometer Collaboration

R.S. Hayano+, H. Sakurai
University of Tokyo
Y. Akiba, H. Hamagaki, Y. Tanaka
Institute for Nuclear Study (INS), University of Tokyo
J. Chiba
National Laboratory for High Energy Physics (KEK)
H. En'yo
Kyoto University
H. Sano
Osaka University
T. Sugitate
Hiroshima University
S. Hayashi, M. Tanaka, M.J. Tannenbaum++
Brookhaven National Laboratory
G. Roche
LBL/Clermont-Fd University

+) Convener
++) Local contact

Introduction

With the advent of RHIC, the study of nuclear matter will enter a new realm of extreme conditions of temperature and density. An exciting possibility is that the colliding nuclei will interact sufficiently to come to equilibrium so that the energy of the incident beams will be dissipated by compression and heating in the large volume of nuclear matter. Under such conditions, it is expected that the system will undergo a phase transition from a state of nucleons containing bound quarks and gluons to a state of deconfined quarks and gluons, in chemical and thermal equilibrium, covering nearly the entire volume of the colliding nuclei, a volume much larger than the characteristic hadronic length scale. This new state of matter is called the Quark Gluon Plasma, or Quark Matter [1][2].

It is possible that the QGP will become self-evident when just a few ultra high energy central nuclear collisions are observed. A more likely outcome is that the existence of the QGP will have to be determined from a comprehensive and systematic set of experimental data exhibiting several striking signatures "which can be interpreted in a unified way as manifestations of QGP production"[3].

The signatures proposed for the QGP include both hadronic and leptonic modes. For instance, chemical and thermal equilibrium are tested by measuring the temperature ($< p_T >$) and relative abundance of identified charged hadrons[4][5]. The existence of a phase transition may be inferred[6][7] from the variation of the temper-

ature with increasing particle or energy density, dn/dy or $dE_T/d\eta$, correlated with large fluctuations in these densities in a limited region of rapidity ($\sim$ 1 unit), on an event-by-event basis. Identical particle interferometry [8] may be used to estimate the size of the thermalized QGP. Lepton pairs are important in at least two ways: low-p_T, low-mass lepton pairs are a probe of the thermal equilibrium of the system and of the transition temperature[9]; while J/Ψ production (suppression)[10] is a probe of the deconfinement and Debye screening of color charge in the QGP. "Jet quenching" may be another example of a process that demonstrates deconfinement[11] and jet effects can probably be observed at RHIC by measurement of one or a few leading high p_T hadrons[12], or by direct single photon production[13].

In order to discover and prove the existence of the QGP, it would seem desirable to have a detector which is sensitive to as many of the proposed "signatures" as possible, so that they could all be observed and turned on and off in a predictable, reproducible, controllable and unified way. By emphasizing an open geometry experiment, optimized for detecting low-mass, low-p_T electron-positron pairs, we believe that a reasonably comprehensive measurement of the majority of the QGP signatures can be obtained.

Overview

The main focus of this working group was to design a detector system which is capable of measuring soft low-mass e^+e^- pair ($M_{e^+e^-}$) production from $\sim$ 4 GeV/c^2 down to a few hundred MeV/c^2 in the central rapidity region, together with associated hadron charged multiplicity and transverse neutral energy of the event. The soft dilepton production in this mass range and direct photon production are expected to be a sensitive *penetrating probe* to study the properties of the high energy density matter (hot hadron gas, mixed phase, and QGP) created in the heavy-ion collisions at RHIC[9].

The measurement of low-mass e^+e^- pair production with low p_T, is a nontrivial task due to the overwhelmingly large combinatorial background from π^0 and η Dalitz decays. The key to the successful measurement of the low-mass continuum is to effectively reject Dalitz-decay pairs. This requires an identification of e^+e^- pairs with relatively small ($\theta < 10^o$) opening angles *before* they enter a magnetic volume.

The detector system we studied during the workshop is schematically depicted in Fig.1. It has two identical arms on both sides of the beam pipe (each covering $-0.2 < \eta < 0.2$, $-20^o < \phi < 45^o$), has a gas ring-imaging Čerenkov (RICH) counter [1] on each arm. The RICH counters are placed close to the beam pipe, in a field-free region, and are used to identify electrons and to reject small-angle e^+e^- pairs.

Charged particle tracking starts at 1.5 m from the collision diamond. Each arm has a time projection chamber (TPC) placed in an H-type dipole magnet. The expected number of charged particles entering each arm is about 80 (for central Au+Au

[1]The use of segmented ($\sim$ 2000 segmentation) non-imaging Čerenkov detector is also being studied.

collisions).

Behind the tracking volumes, we propose to install highly-segmented high-resolution electromagnetic calorimeters. The calorimeters provide additional electron identification power, and can be also used to study γ, π^0 and η spectra.

Another major issue is the ability to trigger on electrons of a minimum p_T and e^+e^- pairs of a minimum invariant mass in real time. This would involve a first level trigger on a cluster in the EM calorimeter followed by a second or higher level trigger in which the cluster would be correlated with an electron track identified with the RICH.

Physics Motivation and Goals

The following probes are proposed to study systematically the high energy density matter in the central region together with associated charged hadron multiplicity $dN^{\pm}/dy$ and also the transverse neutral energy flow $dE_T^0/d\eta$:

1. Di-electron Production ($0.3 \leq M_{e^+e^-} \leq 4$ GeV/c^2)

- Yield of low-mass, low-p_T e^+e^- pair production ("anomalous" production, QGP enhancement – the rate is proportional to the square of $dN^{\pm}/dy$),
- Vector mesons (ρ, ω, ϕ (yield and mass shift of which the latter may be related to the chiral symmetry restoration[14]) and J/Ψ) production (distortion of the spectra and melting).

2. Direct Photon Production

- Single photon (excess at low and high p_T, γ/π ratio, associated particles),
- Diphoton production (back-to-back) at high p_T.

3. Charm Production

- Single electron production (e/π ratio, excess at low p_T?),
- Associated charm ($D\bar{D}$) production with a high p_T electron trigger.

4. Jet Production

- Away-side jet tagged with a high p_T photon,
- A high p_T π^0 as a leading particle in a jet.

5. Identified Hadron p_T Spectra

- Neutral hadrons (π^0, η) (with the EM calorimeter),
- Charged hadrons ($\pi^{\pm}$, $K^{\pm}$, $p^{\pm}$, ..)

Brief Description of detector components

Tracking -

Tracking starts at 1.5 m from the collision diamond. Each spectrometer arm has a dipole magnet with the maximum strength of 1 T-m, a TPC inside the magnet. High-resolution drift chambers (projective readout) will be placed at the entrance of the magnet, and at 1m behind the magnet.

The TPC is our primary pattern recognition device; the drift chambers, which have better spatial resolution and better two-track separation as compared to the TPC, are used to achieve good momentum resolution ($\delta p/p < 0.5\%$ at 1 GeV/c).

Electron-pair reconstruction and Dalitz-decay rejection

Electrons are identified by a gas RICH counter which fills the volume between the diamond and the magnet. Electron track candidates found by the RICH counters are matched to the tracks reconstructed in the TPC, and are further verified by the electromagnetic calorimeter placed at $R = 3.6$ m. An overall e/π separation of 10^{-5} to 10^{-4} should be achievable with this scheme.

It will be shown in the following that Dalitz decay background events from π^0 and η decays can be effectively rejected if we throw away an electron track associated with an adjacent positron track.

RICH Optics (very preliminary) -

The RICH counter will consist of a mirror system and a photon readout system. They will be installed in a container, filled with suitable radiator gas at 1 atm. The RICH counter is installed in front of the magnet placed at R=1.5m. In the current design summarized below, the mirror is placed at 1.3m from the diamond, and the radiator length is about 1m; the expected number of detected photoelectrons per single track is $10 \sim 15$.

number of mirror:	2 modules / arm (plane symmetry at z=0)
mirror curvature:	1700mm
mirror position:	1300mm from the beam axis.
coverage angle:	$\Delta\theta = 20$ degrees / module, and
	$\Delta\phi = 65$ degrees.
tilt angle:	16 degrees.
number of detectors:	2 modules / arm (plane symmetry at z=0)
detector size:	400mm $\times$ 500mm / module
detector position:	550mm from the beam axis

RICH Optical readout

One of the possible RICH readout methods is to use a multi-anode PMT tube with fine-mesh-dynodes. In near future, UV-sensitive multi-anode tubes with the following specifications should become available:

outer dimensions	120mm square
sensitive area	100mm square
no. of anodes	10×10
	40×40 maximum
window	UV glass (>180nm)
material	$3.5mm^t$ window and $16\mu m$ Cu foil$\times$ no. of dynodes
no. of dynodes	16
thickness	about 70mm
amplification	2×10^6 w/o field

Single-photon sensitivity of such tubes and its applicability to RICH readout is our high-priority R&D project for RHIC.

EM Calorimeter

A highly-segmented electromagnetic calorimeter will be placed at $R = 3.6$ m; the area covered is about 8 m^2/arm, each segmented into about 5000 blocks of crystals, such as PbF_2. In Fig.2, we show a result of a Monte Carlo simulation which demonstrates the π^0 reconstruction capability of the EM calorimeter. The choice of the calorimeter crystal is an important R&D subject.

Global event characterization

A coarse-segmentation electromagnetic barrel calorimeter covering $0 < |\eta| < 2$, and a coarse-segmentation electromagnetic endcap calorimeter covering $2 < |\eta| < 4$ will be used as our global event characterization device. Conventional lead-scintillator scheme appears to be sufficient.

Optional forward spectrometer

Since there is an open space in the forward ($1 < |\eta| < 4$) region, addition of a forward spectrometer to measure charged particle single spectra is being considered.

Expected performance of the proposed detector

Electron-pair reconstruction and Dalitz-decay rejection -

An extensive Monte Carlo study on the electron-pair reconstruction efficiency and Dalitz-decay rejection efficiency was done. We assumed a Au+Au central collision,

and included both π^0 and η Dalitz decays (the η rate was assumed to be 8% of the π^0 rate). Decays of ρ, ω and ϕ were also included in the simulated events.

The distribution of the opening angles between the Dalitz-decay e^+e^- pairs is peaked at small angles. We found that if we discard an electron/positron if there is a Čerenkov hit within a cone angle of 15°, we can improve the signal-to-noise ratio of the e^+e^- pair measurement by a factor 35 (at 1 GeV/c^2) with only 30% loss in the true-pair reconstruction efficiency.

In Fig.3, we show the e^+e^- pair invariant mass spectrum without Dalitz decay rejection (dashed histogram), and with rejection (solid histogram), plotted in 10 MeV bins. The statistics corresponds to about 2×10^7 Au+Au central collisions. The discrete peaks of ω and ϕ decays are clearly visible.

Overlaid, we show in Fig.3 two curves; the solid curve is the estimated pair continuum from QGP (Kajantie et al.[9], for initial temperature; T_0 = 500MeV, and critical temperature; T_c = 160MeV), and the dashed curve is the magnitude of the *anomalous* continuum enhancement observed so far in various measurements[15].

The $M_{e^+e^-}$ acceptance of the detector system is shown in Fig.4 (we assumed that $d\sigma/dydM_T \propto M_T \exp(-M_T/T)$ with T = 160 MeV).

A note on the "two-photon" e^+e^- pairs

It was shown at the workshop by M.Rhoades-Brown that a large number of e^+e^- pairs should emerge from relativistic heavy-ion collisions. It is our great concern whether or not the "two-photon" pairs can become an important background to our lepton-pair measurement.

A rough estimate of the number of single electrons with $p_T > 10$ MeV (lower-energy electrons can be safely neglected because they are below the gas Čerenkov threshold) which appear in our detector acceptance, is about 500/sec. If this occurs randomly, this is no threat to our e^+e^- measurement. If, on the other hand, central collisions always lead to multiple-pair production, and more than 1 electrons/positrons with $p_T >> 10$ MeV are ejected into our detector acceptance, overkilling of true events should result. This problem still needs much study.

Performance summary

The following table shows a summary of the expected performance of the proposed detector:

Pseudo rapidity range	$-0.2 < \eta < 0.2$
ϕ coverage	$-20° < \phi < 45°$, two arms
Single-particle momentum resolution	$\frac{\delta p}{p} = 0.5\%$ at 1 GeV/c
Single-particle acceptance	17 % / η
Charged particle multiplicity / arm	$\sim$ 80 (Au+Au central)
e^+e^- pair acceptance$^+$	0.7 % at J/Ψ, 0.4 % at $\phi(1020)$
e^+e^- pair mass resolution	7 MeV at 1 GeV/c^2
Dalitz-pair suppression	1/35 at $M_{e^+e^-} = 1.0$ GeV/c^2
e^+e^- pair S/N at 1 GeV	0.01 (Anomalous pair, without Dalitz rejection)
	0.5 (Anomalous pair, with Dalitz rejection)
	0.3 (QGP a la Kajantie, without Dalitz rejection)
	15 (QGP a la Kajantie, with Dalitz rejection)
J/Ψ yield	20/ day (Au+Au, $L = 5 \times 10^{26}$)
ϕ yield	60 / day (Au+Au, $L = 5 \times 10^{26}$)

+) Event rate = $L \times B\frac{d\sigma}{dy} \times Acceptance$

Major R&D Items

1. Čerenkov detector RICH or segmented Čerenkov?, Čerenkov optics (mirror, image size), and photon detector.
2. EM Calorimeter Study of crystals (CsI and PbF_2) and readout - PMT and diode.
3. TPC Read-out plane fabrication and readout electronics cost reduction.
4. Trigger and data-acquisition system to correlate a cluster in the EM calorimeter with an electron track identified with the RICH.

References

[1] W.J. Willis in Proceedings of the XVI International Conference on High Energy Physics, Chicago-Batavia, Ill., USA, 1972, eds. J.D. Jackson and A. Roberts (NAL, Batavia, Ill. 1973), Vol. 4, pp 321-331. Note particularly the suggestion attributed to G. Cocconi on page 323 that "new states of matter might be produced when hadrons could be concentrated at high densities for a sufficiently long time"

[2] Proceedings of the Eighth International Conference on Ultra-Relativistic Nucleus-Nucleus Collisions–Quark Matter 1990, eds. J. P. Blaizot, C. Gerschel, B. Pire and A. Romana, to appear as a special issue of Nuclear Physics A; and previous proceedings in this series: see also J.C. Collins and M.J. Perry, Phys. Rev. Lett. 34 (1975) 1353: N. Cabibbo and G. Parisi, Phys. Lett. 59B (1975) 67

[3] L. Van Hove, Nucl. Phys. A461 (1987) 3c

[4] J. Rafelski and B. Muller, Phys. Rev. Lett. 48 (1982) 1066

[5] T. Matsui, B. Svetitsky and L. McLerran, Phys. Rev. D34 (1986) 2047

[6] L. Van Hove, Phys. Lett. 118B (1982) 138

[7] L. Van Hove, Z. Phys. C21 (1983) 93

[8] G. Goldhaber, S. Goldhaber, W. Lee and A. Pais, Phys. Rev. 120 (1960) 300

[9] R. Hwa and K. Kajantie, Phys. Rev. D32 (1985) 1109; K. Kajantie, J. Kapusta, L. McLerran and A. Mekjian Phys. Rev. D34 (1986) 2746

[10] T. Matsui and H. Satz, Phys. Lett. B178 (1986) 416

[11] M. Gyulassy and M. Plümer, LBL-28531, February 22, 1990; see also T. Ludlam, L. Madansky, and F. E. Paige, Proceedings of the 1984 LBL Workshop on Detectors for Relativistic Nuclear Collisions, (L. Schroeder, ed.), LBL-18825, p.115 (1984).

[12] Frank E. Paige, Proceedings of the Third Workshop On Experiments and Detectors for a Relativistic Heavy Ion Collider (RHIC), (B. Shivakumar and P. Vincent, eds.), BNL-52185, p.49 (1988); see also CCOR Collaboration, A. L. S. Angelis, et al., Physica Scripta 19 (1979) 116

[13] M. Diakonou et al., Phys. Lett. 87B (1979) 292; 91B (1979) 296; A. L. S. Angelis, et al., Phys. Lett. 94B (1980) 106

[14] E. Shuryak, Proceedings of the Eighth International Conference on Ultra-Relativistic Nucleus-Nucleus Collisions–Quark Matter 1990, eds. J. P. Blaizot, C. Gerschel, B. Pire and A. Romana, to appear as a special issue of Nuclear Physics A

[15] P. Glaessel and H.J. Specht, Proceedings of the 1985 RHIC Workshop on Experiments for a Relativistic Heavy Ion Collider, (P.E. Haustein and C.L. Woody eds.), BNL-51921, p.149 (1985).

Figure Captions

Fig.1 (a) Top view and (b) end view of the two-arm electron pair spectrometer.

Fig.2 A Monte-Carlo result of the two-photon invariant-mass spectrum (Au+Au, central collision), with E_T cut at 1 GeV to each photon.

Fig.3 The e^+e^- pair invariant mass spectrum without Dalitz decay rejection (dashed histogram), and with rejection (solid histogram), plotted in 10 MeV bins. The statistics corresponds to about 2×10^7 Au+Au central collisions. The discrete peaks are ω and ϕ decays. The solid curve is the estimated pair continuum from QGP (Kajantie et al.[9], for initial temperature; $T_0 = 500$MeV, and critical temperature; $T_c = 160$MeV), and the dashed curve is the magnitude of the *anomalous* continuum enhancement observed so far in various measurements[15].

Fig.4 e^+e^- pair acceptance of the detector system for a magnet field of 5 kG over 1.5 meters of the magnetic volume, under the assumption that $d\sigma/dydM_t \propto M_t \exp(-M_t/T)$ with $T = 160$ MeV).

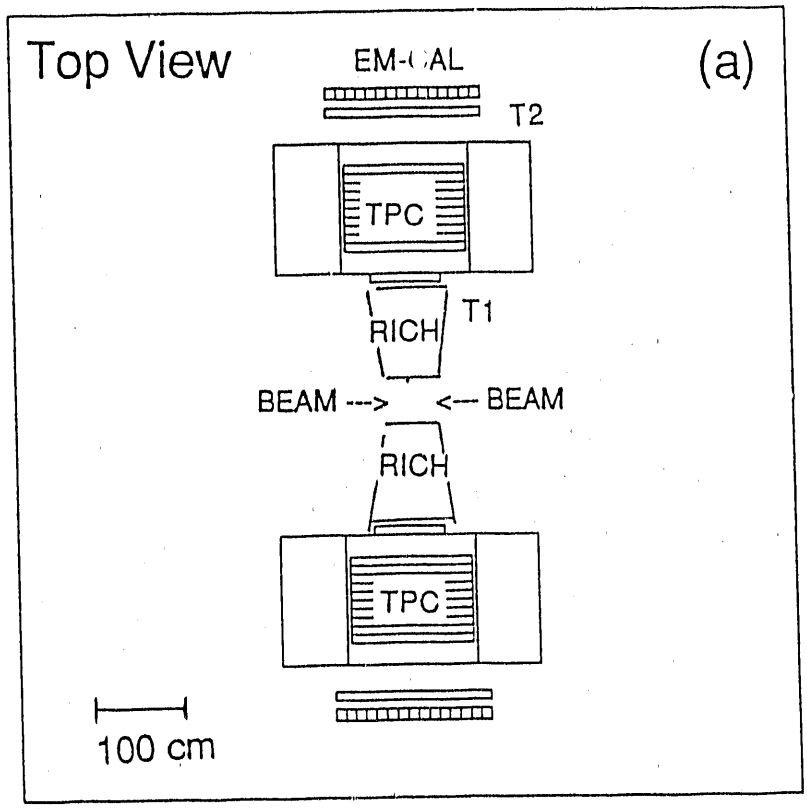
Top View
(a)
EM-CAL
T2
TPC
RICH
T1
BEAM --->
<--- BEAM
RICH
TPC
100 cm

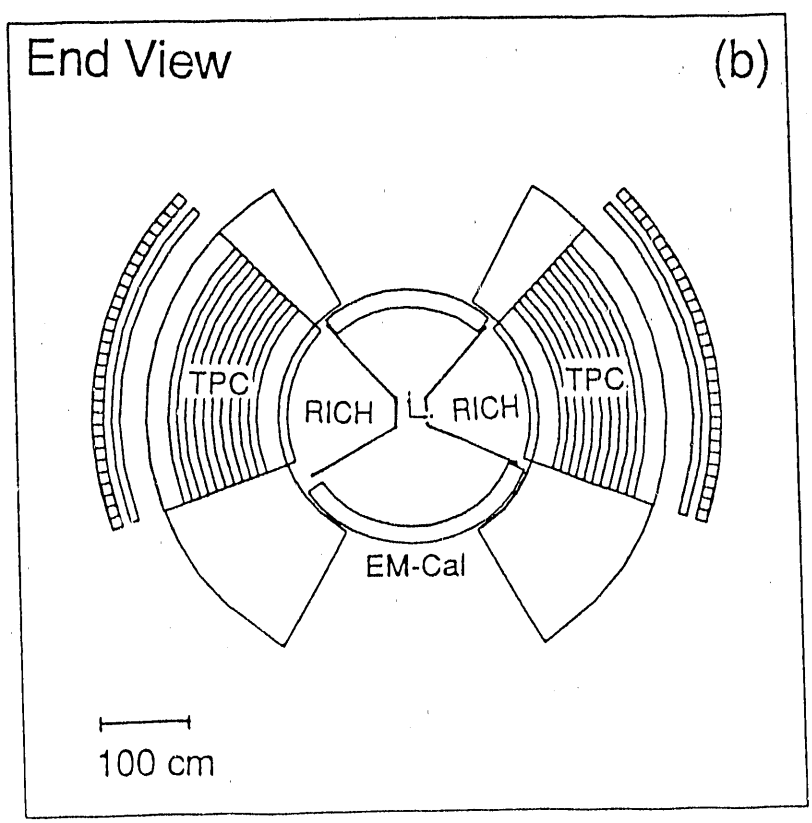
End View
(b)
TPC
RICH
RICH
TPC
EM-Cal
100 cm

Fig. 1

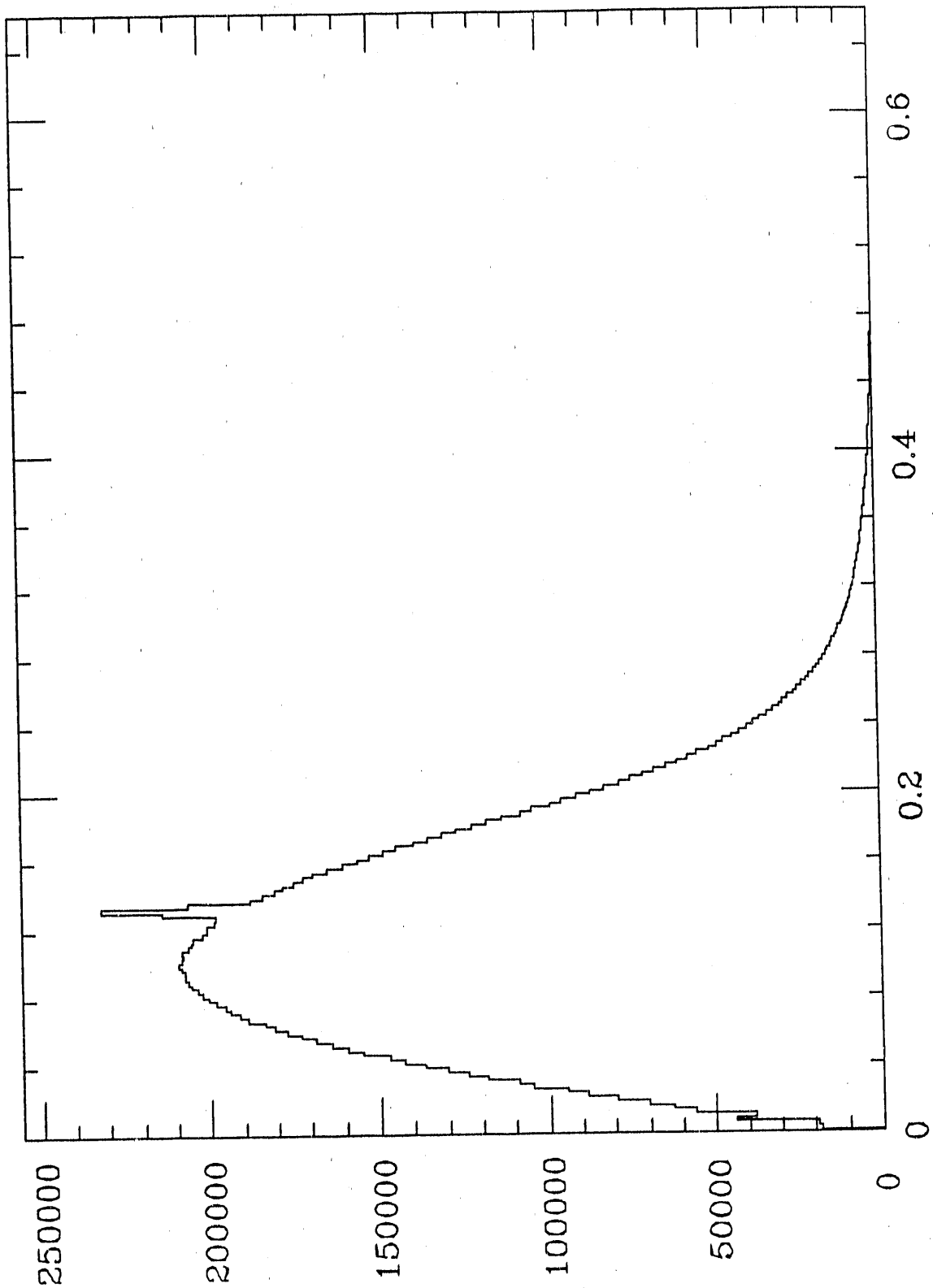

Fig. 2

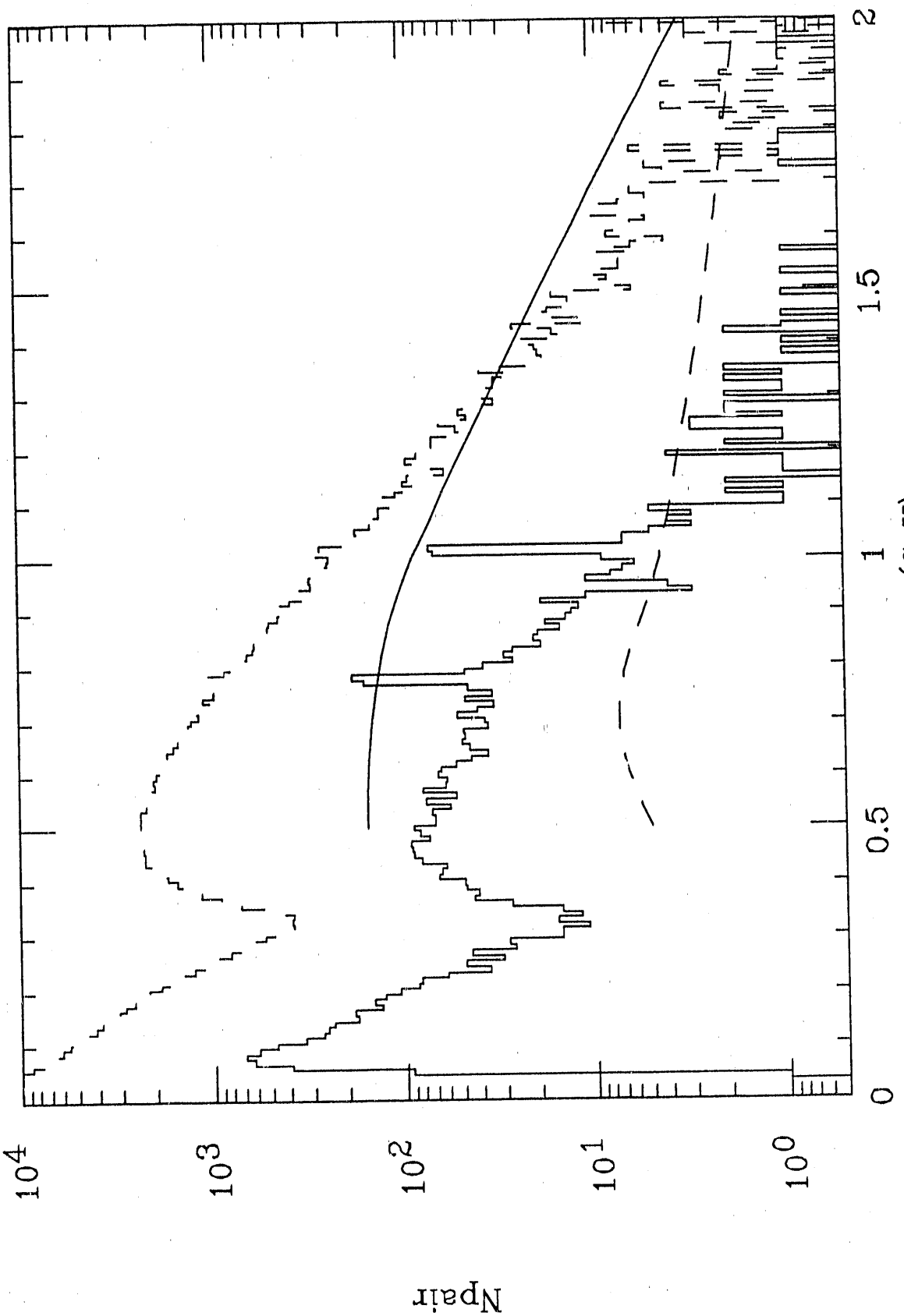

Fig. 3

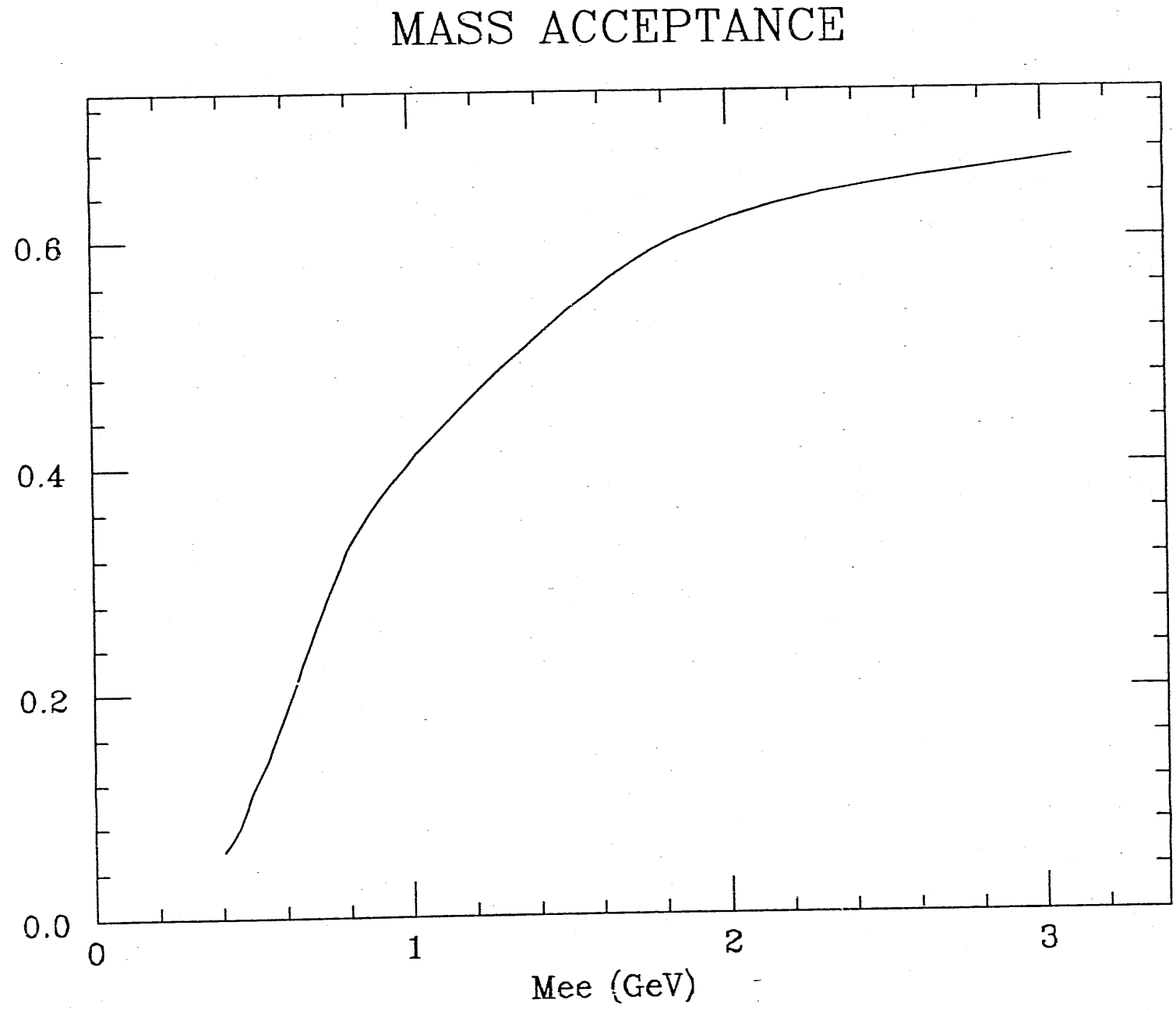

Fig. 4

TOTAL and ELASTIC pp CROSS SECTIONS AT RHIC

W. Guryn, M. Sakitt and A. Sambamurti

Physics Department,
Brookhaven National Laboratory, Upton NY 11973

and

S. Y. Lee

Accelerator Development Department,
Brookhaven National Laboratory, Upton NY 11973

and

S. Majewski

Physics Department, CEBAF, Newport News VA 23606

ABSTRACT

We have examined the feasibility of studying elastic proton-proton (pp) scattering at $\sqrt{s} = 500$ GeV, in the small angle scattering hall at RHIC. The requirements for the intersection region and the detector are described. The lattice configuration and the angular coverage of the detector will allow the simultaneous study of all three regions that characterize elastic scattering, namely the Coulomb dominated region, the Coulomb-hadronic interference region and the hadronic dominated region.

This manuscript has been authored under contract number DE-AC02-76CH00016 with the U.S. Department of Energy. Accordingly, the U.S. Government retains a non-exclusive, royalty-free license to publish or reproduce the published form of this contribution, or allow others to do so, for U.S. Government purposes.

Motivation

RHIC presents the opportunity to measure several basic parameters in low momentum transfer pp collisions at center of mass energies up to 500 GeV. These parameters include :

(i) the total and elastic cross sections, σ_{tot} and σ_{el}.

(ii) the ratio of the real to the imaginary part of the forward elastic scattering amplitude, ρ.

(iii) the nuclear slope parameter of the pp elastic scattering, b.

(iv) the structure of the differential elastic cross section $d\sigma_{el}/dt$.

While these parameters have been measured for $p\bar{p}$ interactions up to center of mass energies $\sqrt{s} = 2$ TeV, the pp measurements are available only up to $\sqrt{s} = 63$ GeV. It is of interest to compare pp and $p\bar{p}$ interactions by extending the pp measurements to the highest possible energies.

We summarize the results for elastic scattering which are discussed in greater detail in Refs. [1]-[6]. The differential elastic pp cross section is given by

$$\frac{d\sigma_{el}}{dt} = \pi |f_c + f_h|^2 \tag{1}$$

where f_c and f_h are the Coulomb and the hadronic amplitudes respectively.
The spin independent hadronic amplitude f_h is usually parametrized as

$$f_h = \left(\frac{\sigma_{tot}}{4\pi}\right)(\rho + i)\, exp\left(-\frac{1}{2}b|t|\right) \tag{2}$$

The Coulomb amplitude f_c is given by

$$f_c = 2\alpha G^2(t) \times \left(\frac{exp(i\alpha\phi)}{|t|}\right) \tag{3}$$

where α is the fine structure constant, $G(t)$ is the proton electromagnetic form factor and ϕ is the Coulomb phase, which is

$$\phi = ln\left(\frac{0.08}{|t|}\right) - 0.577. \tag{4}$$

The dependence of the differential elastic cross section $d\sigma/dt$ on t can be divided into 3 regions; the Coulomb, the interference and the hadronic regions. At low t, the Coulomb

term dominates and $d\sigma/dt$ has a $(1/t^2)$ dependence. As t increases, the interference between the Coulomb and hadronic contributions becomes maximal. Finally the hadronic contribution dominates and $d\sigma/dt$ falls off exponentially.

The total cross section is related to the differential elastic cross section by applying the optical theorem,

$$\sigma_{tot}^2 = \left(\frac{16\pi (hc)^2}{1+\rho^2} \right) \frac{d\sigma_{el}}{dt}|_{t=0}. \tag{5}$$

From general considerations of unitarity and analyticity, the difference in the total pp and $p\bar{p}$ cross section is predicted to tend to zero at large values of s

$$\sigma_{tot}\,(p\bar{p}) - \sigma_{toi}\,(pp) \rightarrow 0, \tag{6}$$

and the rate at which the pp total cross section increases is limited by the Froissart bound,

$$\sigma_{tot}\,(s) < \frac{1}{m_\pi^2} log^2 s. \tag{7}$$

The UA4 collaboration has measured σ_{tot}, σ_{el} and ρ in $p\bar{p}$ collisions at $\sqrt{s} = 540$ GeV [6]. Their measurement of $\rho = 0.24 \pm 0.04$, which is higher than the predicted value of $\rho = 0.15$, suggests that the total cross sections rise more rapidly with energy than that expected from extrapolations from low energy measurements. Some models which have tried to account for this discrepancy predict that the pp and $p\bar{p}$ total cross sections diverge at very high energies. It has been pointed out that pp measurements at $\sqrt{s} = 500$ GeV could help to differentiate between the models [1],[2].

Finally there are some speculative topics which could prove promising. The possibility of having polarized proton beams at RHIC would allow measurements of spin dependent effects in small angle scattering. Low momentum transfer AA collisions are interesting but are complicated by contributions from poorly understood processes such as low mass electron pair production and nuclear excitations. We are consulting theorists on the above matters.

Experimental Technique

In this section we sketch the technique that we intend to use. A more detailed discussion may be found in Refs. [5]-[8].

For forward elastic scattering we have

$$t = -4p^2 sin^2\,(\theta/2) \approx -p^2\theta^2 \tag{8}$$

where p is the beam momentum and θ is the scattering angle. Using the known parameters of the accelerator lattice, one can calculate the deflection y^* and the scattering angle θ_y^* at the interaction point knowing the deflection y and the angle θ_y at another point. For example, at a point where the phase advance from the interaction point is Ψ and the betatron function is β, y is given by

$$y = \sqrt{\left(\frac{\beta}{\beta^*}\right)}[cos\,(\Psi) + \alpha^* sin\,(\Psi)]y^* + \sqrt{(\beta\beta^*)}sin\,(\Psi)\,\theta_y^* \tag{9}$$

where α^* is the derivative of the betatron function at the interaction point. We have considered a lattice configuration such that α^* is zero. If the value of Ψ is an odd multiple of $\pi/2$, the above expression simplifies to

$$y = \sqrt{(\beta\beta^*)}sin\,(\Psi)\,\theta_y^*. \tag{10}$$

Therefore, if the detector is located at a point where the phase advance is an odd multiple of $\pi/2$, the scattering angle is determined just from the measurement of the displacement alone. When the above condition is satisfied, rays that are parallel to each other at the interaction point are focussed onto a single point at the detector.

At $\sqrt{s}$ = 500 GeV , the hadronic and Coulomb amplitudes are equal in magnitude when t $\approx$ 1.1x10^{-3} GeV^2. This corresponds to a scattering angle of 0.13 mrad, which sets the scale for measuring the interference between the Coulomb and the hadronic terms.

In practice, the observed scattering angle has to be larger than the angular spread of the beam σ_{θ_y} at the collision point

$$\sigma_{\theta_y} = \sqrt{\frac{\epsilon}{6\pi\beta^*}} \tag{11}$$

where ϵ is the 95% emittance and β^* is the betatron function at the interaction point. Thus a large betatron function is required at the interaction point. The magnitude of the betatron function β^* determines the size of the beam spot σ_y, which is given by

$$\sigma_y = \sqrt{\frac{\epsilon\beta^*}{6\pi}}. \tag{12}$$

The detectors are placed at suitable points along the lattice inside thin walled re-entrant vessels ("Roman pots"), whose insertion can be controlled remotely. During injection, the pots are moved away from the beam. After the beams stabilize, the pots are moved closer to the beam. Events are selected by requiring a coincidence of two counters on opposite sides of the interaction point, which experience has shown leads to a clean trigger. The longitudinal position of the collision point is determined from time of flight measurements.

We intend to measure $d\sigma/dt$ over all three regions simultaneously. Since the Coulomb contribution is calculable, the parameters can be determined without having to normalize to the luminosity or the total cross section.

The Intersection Region

In the RHIC lattice configuration, the horizontal and vertical betatron functions, $\beta_x(s)$ and $\beta_y(s)$, are related by the expression,

$$\beta_x(s) = \beta_y(-s), \tag{13}$$

where s is the longitudinal distance from the interaction point. This constrains the allowed values of vertical and horizontal betatron functions. Although β^* can be set as high as 700 m, $\beta^* = 200$ m appears to be a reasonable operating point. In our preliminary study, we have assumed that that $\beta_x^* = \beta_y^* = 200$ m. Fig. 1 shows the horizontal and vertical betatron functions. Fig. 2a(b) shows two curves. The first curve is the 6σ width (height) of the beam in the interaction region. The second curve shows the horizontal (vertical) displacement of a particle from the axis when the scattering angle is 0.1 mr. The 90^o and 270^o phase change occur at about 100 m and 140 m from the interaction point i.e. the Q4-Q5 and the Q8-Q9 locations. Fig. 2 shows that the beam and the scattered particle

are well separated when the phase change is 90°. It also suggests that scattering angles as low as 0.08 mrad can be measured. We will position Roman pots at about 100 m and somewhat closer to increase the t coverage (see discussion below). As the systematic errors for measurements made in the vertical plane are different from those that are made in the horizontal plane, we intend to make measurements in both planes. In this preliminary lattice configuration, the 90° phase change in the horizontal and vertical planes do not occur at the same point. This could complicate the measurement of the scattering angle. We are therefore pursuing a more detailed study of the lattice configuration. It should be pointed out that the length of the Q6 quadupole in this intersection should be about 1.5 m instead of 1.13 m to achieve a value of $\beta^* = 200$ m.

The aperture of the first quadrupole magnet limits the maximum angle that can be measured by the detector described above to 0.6 mrad ($t \approx 20\times10^{-3}$ GeV^2). While this is adequate to measure ρ and σ_{tot}, it is desirable to extend the angular coverage to larger angles so that the structure in the differential elastic cross section $d\sigma_{el}/dt$ can be studied. We are examining ways of placing detectors within a reentry pipe in the straight section between quadrupoles Q3 and Q4 for measuring scattering angles up to about 1.5 mrad and in the intersection region for measuring angles greater than 1.5 mrad.

The maximum luminosity for pp interactions with this lattice configuration will be about 2×10^{29} cm^{-2}sec^{-1}. However, the cross sections for low angle scattering are large and we could run at lower luminosity. The UA4 collaboration took data at a luminosity of 2×10^{26} cm^{-2}sec^{-1} [6].

The Detector

We propose to use arrays of scintillating fibers as the detector elements. Scintillating fibers are fast, resistant to radiation damage, robust and convenient to operate and calibrate. An inexpensive detector with the required segmentation can be constructed from fibers. Each Roman pot will contain six planes of fibers and a trigger scintillator. The active area of the detector in each Roman pot will be about 32 x 32 mm^2.

Currently scintillating fibers of size less than 1mm and resistant to radiation damage up to 10 Mrads are available. We are considering rectangular 0.4 mm (active) x 1.0 mm fibers. The narrower side (0.4 mm) will face the incoming particle. We believe that the 1

mm depth will produce 4-6 primary photoelectrons, which is sufficient for detection [**3**] . The fibers will be arranged in "ribbons" consisting of 64 32 mm long fibers, (the effective width of each fiber will be 0.5 mm when the contributions from the cladding, glue, black paint etc. are included) to give a 32 $\times$ 32 mm^2 detector size. Each fiber will optically isolated from its neighbor. For sufficient accuracy and redundancy, we are considering six planes; two vertical, two horizontal, and two oriented at an angle of $\pm 45^o$ to the vertical (U and V planes). The centers of the two horizontal (vertical) planes can be staggered by 0.25 mm to improve the position resolution. The U and V fiber planes will consist of 90 45 mm long fibers each to cover the active 32 x 32 mm^2 area.

Each scintillating fiber will be optically coupled to a plastic fiber and each plastic fiber will be read out independently by a channel of a multianode photomultiplier tube [9]. The combined length of the scintillating fiber and the optical fiber will be about 25 cm, which corresponds to an attenuation length of less than 0.25. At this time we are considering multianode tubes made by Hamamatsu and Philips. They are sufficiently compact and the cross talk between the channels for the Amperex tube is about 5% [**10**]. Electronic cross talk is reported to be greatly reduced in a new Hamamatsu photomultiplier tube type R4135-01 [**11**].

We estimate the total number of channels to be about 6400 or 100, 64 channel multianode PMTs. The signals from the PMTs will be fed directly to discriminators and to TDCs. The timing information will be required to locate the interaction point and to reject backgrounds. The collision point can be located to within 15 cm if the time resolution of the trigger scintillator is 0.5 ns. Hits from either the beam halo or beam gas interactions in general do not satisfy the trigger requirement of a rough coincidence between upstream and downstream counters. For further background rejection, we will cover the central region with small scintillator counters to detect inelastic collisions and veto them.

Conclusions

(1) The experiment measures some basic parameters which are of topical interest. It is inexpensive and fits in well with the RHIC program. We are pursuing a detailed design and will submit a Letter of Intent.

(2) Although the experiment is feasible with present technology, given the long lead time, we anticipate that advances in detector technology could improve the performance. Therefore we plan to pursue R & D, particularly in scintillating fibers and multianode photomultiplier tubes.

(3) We are studying the parameters of the intersection region, the resolution and precision of the detector, and the backgrounds.

(4) We are considering applications to AA scattering. However, more work is required to understand the contributions from low energy pair production and nuclear excitation effects at low momentum transfer.

References

[1] A. Martin, Proc. of International Conference on Elastic and Diffractive Scattering edited by M. M. Block and A.R. White (1989), 1-8.

[2] R. Cahn, Proc. of the 7th Topical Workshop on Proton-Antiproton Collider Physics (1988), 108-114.

[3] M.M. Block and R.N. Cahn, Rev. Mod. Phys. **57** (1985) 563.

[4] M.M. Block and R.N. Cahn, Phys Lett. **188B** (1987) 143.

[5] J. Orear, Proc. of the 7th Topical Workshop on Proton-Antiproton Collider Physics (1988), 83.

[6] D. Bernard et al., Phys. Lett. **198B** (1987) 583.

[7] J. Marx and R. Rajka, Proc. of the 1975 ISABELLE Summer Study Vol. II 204-233.

[8] R. Battison et al., NIM **A238** (1985) 35.

[9] G. Comby and R. Meunier, NIM **A269** (1988) 246.

[10] B. Esmeijer, Philips, private communication.

[11] M. Ratner, Hamamatsu, private communication.

Figure Captions

(1) The horizontal and vertical betatron functions, (β_x) and (β_y), in the small angle scattering hall intersection region. β_x, β_y are depicted by continuous and dotted lines respectively. β^* is chosen to be 200 m.

(2a) The horizontal displacement of a particle from the axis when the scattering angle is 0.1 mr. The beam momentum is 250 GeV/c and the beam emittance $\epsilon_N = 20\pi$ mm-mrad. The dotted curve depicts the 6σ width of the beam.

(2b) The vertical displacement of a particle from the axis when the scattering angle is 0.1 mr. The dotted curve depicts the 6σ height of the beam.

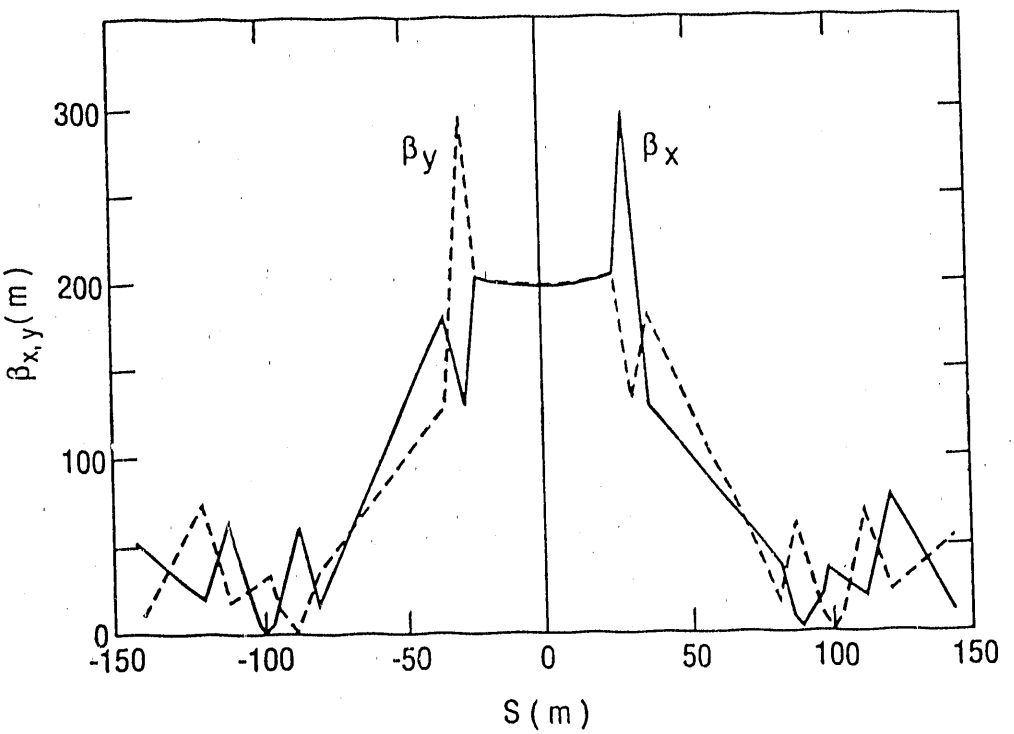

FIGURE 1.

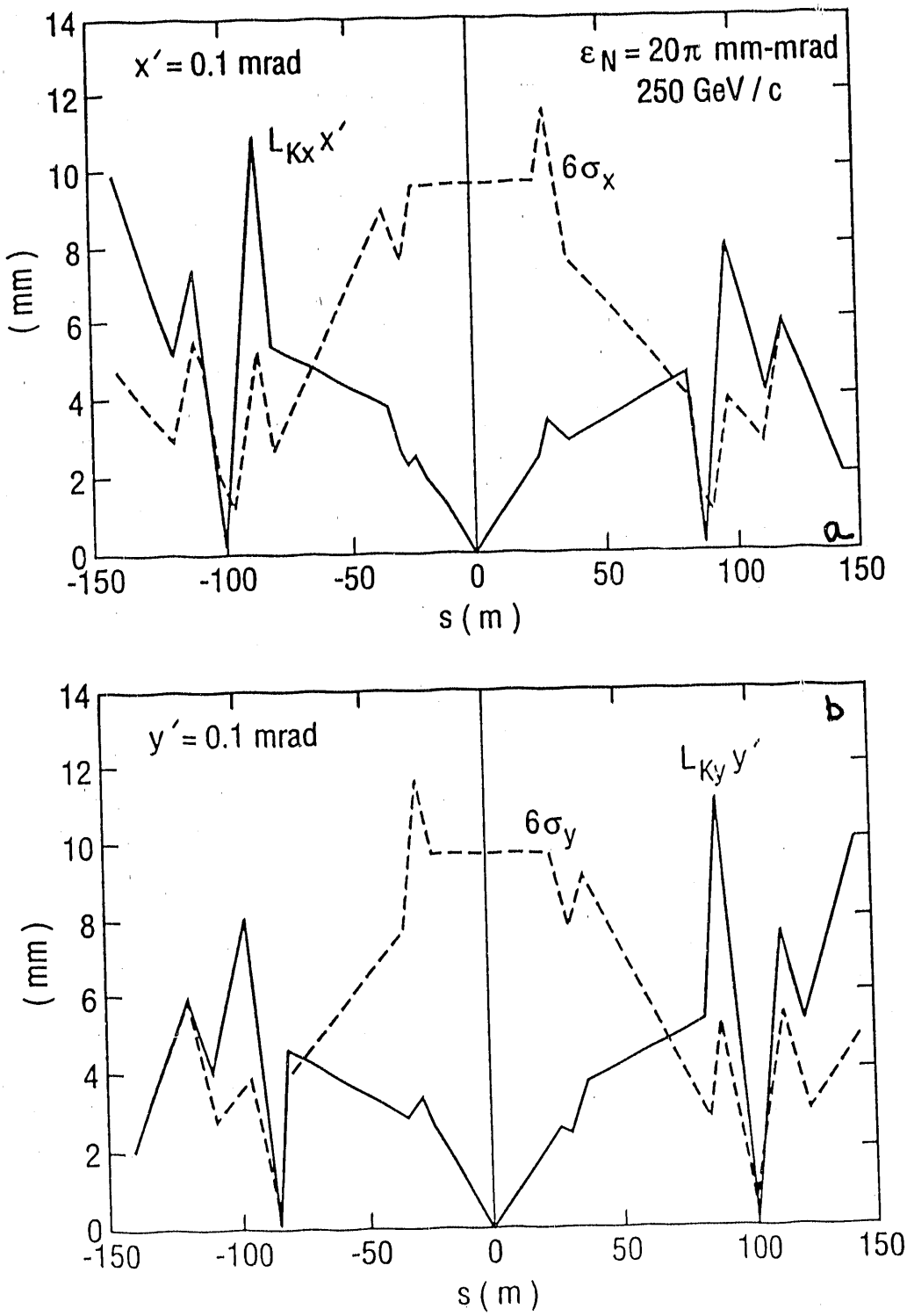
x′ = 0.1 mrad
$\varepsilon_N = 20\pi$ mm-mrad
250 GeV / c
$L_{Kx}x'$
$6\sigma_x$
(mm)
s (m)
a
y′ = 0.1 mrad
$L_{Ky}y'$
$6\sigma_y$
b

FIGURE 2

A 4π TRACKING TPC MAGNETIC SPECTROMETER FOR RHIC*

Convenors Report: S.J. Lindenbaum

Experimental Collaboration:

G. Danby, S.E. Eiseman, A. Etkin, K.J. Foley, R.W. Hackenburg,
R.S. Longacre, W.A. Love, T.W. Morris, E.D. Platner, A.C. Saulys and J.H. Van Dijk
Brookhaven National Laboratory, Upton, New York 11716

S.J. Lindenbaum
Brookhaven National Laboratory and City College of New York

C.S. Chan, M.A. Kramer and K. Zhao
City College of New York, New York, NY 10031

N. Biswas, P. Kenney and J. Piekarz
University of Notre Dame, Notre Dame, IN 46556

D.L. Adams, S. Ahmad, B.E. Bonner, J.A. Buchanan, C.N. Chiou,
J.M. Clement, M.D. Corcoran, T. Empl, H.E. Miettinen, G.S. Mutchler,
J.B. Roberts and J. Skeens
Rice University, Houston, TX 77251

PHYSICS OBJECTIVES

The primary physics objective of the 4π TPC magnetic spectrometer proposal[1-3] is to search for the Quark-Gluon Plasma. In previous workshops we have discussed what the possible hadronic signatures of such a state of matter would be. Succinctly, the QGP is a direct prediction of non-perturbative QCD. Therefore the question of the existence of this new state of matter bears directly on the validity of non-perturbative QCD. However, since non-perturbative QCD has never been established, it is apparent that what may await us is a host of new phenomena that will go beyond the standard model.

* This research was supported by the US Department of Energy under Contract Nos. DE-AC02-76CH00016, DE-AC02-83ER40107, DE-FG05-87ER40309 and the National Science Foundation.

In order to maximize the probability of observing new phenomena, the apparatus is designed to cover nearly 4π solid angle and to track and measure the momentum of individual particles produced in the collision. In addition the spectrometer will incorporate particle identification by measuring dE/dx and time-of-flight for the tracked particles. These capabilities should enable us to recognize the hadronic signals associated with the formation of a QGP, and to very likely establish its properties if it is produced at a sufficient rate.

The following list of what we hope to measure summarizes our physics objectives.

1. We will track and measure the momentum over nearly 4π of the charged particles emanating from $A + A$ and $A + A'$ collisions where A, A' range from protons to Gold.
2. We will identify charged particles by time-of-flight and dE/dx in a TPC Magnetic Spectrometer. We will be able to separate π/K/p up to $\approx$ 2.7 GeV/c and $(\pi + K)/p$ or $\bar{p}$ up to 4.5 GeV around the central region ($\mid \Delta Y \mid \approx 2$ for $p, \bar{p}$, $\mid \Delta Y \mid \approx 2.5$ for K^+, K^- and $\mid \Delta y \mid \approx 3$ for $\pi^+\pi^-$.
3. If strange and antistrange quark production is enhanced at higher momenta, we will be able to identify fast Λ, $\bar{\Lambda}$, and K^0's in each event. Future vertex detectors could allow the identification of slower $\Lambda\bar{\Lambda}, K^0$ and possibly other long lived particles.
4. The proposed techniques will allow the search for correlations of various signals from any unusual events to indicate the properties of the mechanisms involved. It is important to note that the enormous amount of information we obtain from each event will act as powerful constraints on its interpretation. In parallel we will generate predictions of what to expect from conventional effects by extensive simulations with cascade and other conventional models.

This program of physics goals can be most efficiently met by the type of spectrometer being proposed here.

WORKSHOP OBJECTIVES AND ACTIVITIES

The collaboration plans to submit a Letter of Intent this fall for a first round RHIC experimental program. Therefore the group's activities during this workshop were concentrated on expanding and improving the existing proposal.

A 4π tracking TPC magnetic spectrometer for RHIC was proposed by various members of this collaboration in all three prior RHIC workshops.[1-3] Figure 1 shows the configuration primarily considered in the prior two workshops with the addition of the time-of-flight walls described later. It consists of a central TPC, 5 meters along the beam by 5 meters wide by 2.8 meters high located inside a 5KG window frame dipole magnet. A 40 cm high by 40 cm wide region* around the beam was omitted from the TPC since track densities in some cases were considered too high to be handled at smaller distances. This central TPC will have dE/dx capability. The two end TPC's shown will track but not measure dE/dx since it is not considered useful for the generally higher momentum tracks entering there.

* This 40 cm region may be extended in the vertical direction into a slab over the beam interaction region at the height of the TPC for various practical purposes.

A dipole magnet was selected as the most practical and economical way of covering a large solid angle while maintaining good momentum resolution for forward and backward going particles.

The AGS BNL, CCNY and RICE E-810 experimental program at the AGS has provided valuable experience in TPC construction, operation, pattern recognition and data analysis. In many respects AGS E-810 serves as a valuable prototype program for this RHIC proposal. In addition, BNL/CCNY/LBL/Rice have engaged in a RHIC TPC R&D program. A Notre Dame group joined the collaboration so that the collaboration now consists of the BNL/CCNY/Notre Dame/Rice personnel listed on the first page.

THE MAIN TOPICS CONSIDERED IN THIS WORKSHOP

1. Time-of-flight walls to extend the particle identification range and there-by enhance the rapidity coverage of the TPC system.
2. Consideration of various dipole configurations to best accommodate experimental arrangements and time-of-flight.
3. Methods of incorporating the dipole in the RHIC accelerator ring with the generous assistance of S.Y. Lee.
4. Monte Carlo simulations to evaluate detector performance and optimize its design.
5. Consideration of which experimental halls can be used to house this detector system and some practical considerations in regard to its assembly and maintenance.
6. Finally, we considered what questions remain to be worked on.

TIME-OF-FLIGHT SYSTEM FOR PARTICLE IDENTIFICATION

It was felt that $\sigma \approx 75$ picoseconds time resolution although somewhat optimistic at present should be realizable for RHIC. This opinion was presented by others at the workshop.[4]

Figure 2 shows β vs. momentum in GeV/c for π, K, and p for a length of 9M and $\sigma = 75ps$. Each particle curve is accompanied by $\pm 3\sigma$ bands. It is then assumed that when these bands overlap for two particles they are no longer effectively identifiable.

With this criterion we find π, K and p are individually separable up to about 2.7 GeV/c. Protons and anti-protons are separable from the other two particles up to about 4.5 GeV/c. When combined with our dE/dx particle identification in the central TPC we cover rapidity ranges of $\Delta Y \approx \pm 3$ for pions, $\Delta y \approx \pm 2.5$ for kaons and $\Delta y \approx \pm 2$ for protons and antiprotons. Only pseudorapidities can be determined for particles with larger rapidities. The particle separations quoted above can be achieved with a time resolution of $\sigma = 105$ps if the requirement is relaxed to 2σ (95% C.L.). The final choice of design will probably be driven by cost rather than ultimate time resolution technically feasible.

CONSIDERATION OF VARIOUS DIPOLE CONFIGURATIONS

Figures 3a and 3b show the configuration of the time-of-flight walls with the additional open dipole magnet options considered. The configurations considered attempt to optimize their general usefulness and extend particle ID and thus rapidity coverage for individual particles. At the same time the TOF system should contain $\approx 20,000$ channels to keep the occupancy at $\lesssim 10\%$ and also contain costs. The time-of-flight walls will be placed around the beam in sections. These new magnet options will be further investigated. Their

advantage is that openness is preserved for future use. Their disadvantage is that the better uniformity and probably lower cost of a window frame dipole will be compromised.

In any event the magnet should be built in a symmetrical manner so that RHIC accelerator correcting magnets can be designed simply. In this regard the dipole may be the simplest for the RHIC designers. It should be noted that the time-of-flight walls are positioned to measure the particles going out the forward and back ends of the dipoles. Our Monte Carlo simulations indicate that this is where they will be most necessary to extend the rapidity range coverage. However we can of course in principle redeploy some of them in the open arrangements in the wide angle region if for any reason we decide to identify faster charged particles in these regions.

MATCHING THE DIPOLE TO RHIC

S.Y. Lee has designed a system for matching our 2.5 Tesla meter dipole magnet into RHIC. This system and some of its characteristics are shown in Fig. 4. S.Y. Lee is of the opinion that this procedure is feasible and forsees no problems.

MONTE CARLO SIMULATIONS

For our Monte Carlo simulations we have developed two new event generators. The first is a cascade generator called RHIC EVENT. We use the HIJET approach with the following important modifications:

1. We included all relevant conservation laws, and conserved quantum numbers (energy, momentum, charge, baryon number, and strangeness).
2. In order to attain the generally expected flat central plateau and proton fragmentation peaks the stopping power was reduced phenomenologically by allowing each colliding nucleon to fragment each time it hits by losing ≈ 3 units of rapidity (the width of the fragmentation region) which then goes into fragmentation. The remainder proceeds as a particle for additional collisions. This led to flat central plateaus and proton fragmentation peaks.

Thus we simulate what is generally expected at RHIC. When we get RHIC data this approach will be modified as indicated. At RHIC energies the effects of secondary interactions is being worked on in a program called HADGAS.

We have also developed a program called RHIC PLASMA EVENT. We considered the case of 100 GeV per nucleon gold on 100 GeV per nucleon gold. We tag a region of impact parameter $\pm$ 1.25 fermis and allow the nucleons in this tagged region to produce a QGP bubble of the Van Hove type, around y = 0 in the cms, and allow it to break up according to the model described below. This program models as plasma bubble breakup according to the work of P. Koch, M. Mueller and J. Rafaelski.[5] The particle production probabilities depend on the critical temperature and the gluon fragmentation function. Simple combinatoric weights are used to produce particles according to these probabilities with a momentum distribution of that of the critical temperature (chosen as $\approx$ 170 MeV). About 6% of the available energy was thus allowed to go into plasma. This is a reasonably conservative guess. However the changes in RHIC EVENT behavior the plasma bubble introduces can of course be scaled up or down according to the percentage of plasma selected. The results of RHIC EVENT (cascade without plasma) and RHIC PLASMA EVENTS (RHIC EVENT + 6% plasma) are shown for π^- or π^+ in Figs. 5a and 5b.

Figure 5b shows dN/dy for an average over 10 RHIC EVENTS to show the nature of the cascade plateau with good statistics. Figure 5a shows a single RHIC PLASMA EVENT with actual counts on the left scale and dN/dy on the right scale.

Our TPC system with the time-of-flight wall would allow a rapidity range of $\Delta y \approx \pm 3$ for pions to be detected and thus this phenomena would be clearly observed. Figure 6a shows one RHIC PLASMA EVENT for K^+ or K^-. Figure 6b shows an average of ten RHIC EVENTS (cascade), revealing an even more striking rapidity peak for the plasma over the cascade. Our TPC system with the time-of-flight wall would allow a rapidity range of $\Delta y \approx \pm\ 2.5$ for kaons to be detected.

Figure 7a shows one RHIC PLASMA EVENT for $\bar{p}$. Figure 7b shows an average of ten RHIC EVENTS (cascade) for $\bar{p}$, again revealing a striking rapidity peak for the plasma over the cascade. For $\bar{p}$ and p we can detect the rapidity range $\Delta y \approx \pm 2$. Figure 8a shows one RHIC PLASMA EVENT for p. Figure 8b shows an average of ten RHIC EVENTS (cascade) for p. The upper event clearly shows a central peak accompanied by two fragmentation peaks. Although we could detect the central peak with $\Delta y \approx \pm 2$ we would not see the fragmentation peaks.

Of course moving multi-bubbles would spread these peaks but the total number of extra particles would tend to remain about the same. There could be fluctuations in which considerably more or considerably less plasma is created. However, one should note that assuming that signals of this nature survive in a sufficient number of events we expect it would be very difficult to explain them without a Quark-Gluon Plasma.

The ability of our apparatus to see a great deal of detail is an advantage in a new field, since no one can be sure what will occur when the experiments are performed. If there are fast enough $\Lambda, \bar{\Lambda}$ or K^0's we should be able to observe them. However one of our planned future projects, a close in vertex detector should if it materializes allow the detection of slow $\Lambda, \bar{\Lambda}$ and K^0's. It also possible in that case that we may see $\Xi^- \rightarrow \Lambda\pi^-$ and $\Omega^- \rightarrow \Lambda K^-$. Our proposed apparatus has great potential for observing the unexpected which may well in the end be its greatest virtue.

Simulation of RHIC 100 GeV Per Nucleon Au on Au

During the workshop we addressed the question of helical tracks which spiral in the 5 KG magnet for momenta of $p \lesssim 0.25 GeV/c$. The result is shown for 10% of the tracks in Fig. 9. Since the TPC essentially sees in 3D, we found the helical spiraling did not cause a problem. In fact with the 500,000 channels of readout we plan we estimated that only $\approx 1\%$ of the available pixels were occupied.

Before discussing other prior simulations a description of the TPC's is in order.

THE TPC'S

The magnet is filled with TPC modules at atmospheric pressure, occupying the entire volume except for a region 30 cm wide by 80 (or more) cm high centered around the beam pipe.* This TPC (TPC1) is read out by a conventional anode wire and cathode pad system like that used for the original PEP-4 TPC. In this case, however, the readout is located over the two pole faces of the dipole. A full meter of track is measured for polar angles

* A vertex detector of suitable resolution is anticipated to be placed within this region.

greater than 15° from the beam axis. The pseudorapidity interval covered is $-2 < \eta < 2$. For most of the volume at least 100 energy loss samples will be made for each track. For tracks at small angles to the field lines momentum is not well measured.

Two other TPC's (TPC2) are located outside the magnet at each end to measure the small angle tracks. They cover the angular range from about 4° to the beam out to 24° (pseudorapidity from 1.5 to 3.5 and -1.5 to -3.5). These detectors use the short anode wire readout scheme developed for AGS Experiment 810, which gives better two-track separation but yields no usable dE/dx information. Anode wire spacing of 2.5 mm is used arranged in rows 5 cm apart. The angle and position measurements in TPC2 will enable the reconstruction of the track, measurement of momentum and assignment to the primary vertex of these tracks.

TPC READOUT ELECTRONICS

TPC1 has a $50m^2$ readout area (read out top and bottom for speed) covered with closely spaced anode wires and cathode pads underneath arranged in rows locally roughly perpendicular to the average track direction with 0.5 cm pads on 0.5 cm centers.* TPC1 requires about a half million channels of readout electronics each capable of recording multiple sets of measurements of time and pulse height (up to 16 segments of 8 amplitude samples each). The device should separate hits in the time dimension which are 0.2 cm apart so the bin size should correspond to 1 mm. This requires 10 or 11 bits of time resolution. The result is to divide the volume of the TPC into about a billion cells and to present each track with the equivalent of 150 detector planes each with pixels $0.2cm \times 1.5cm$ (assuming 3 pads corresponds to the pixel length).

The track density $d\sigma/d\Omega$ is estimated to be ≈ 400 in the central region at RHIC even for the 6% plasma events. As shown in Fig. 10 we have successfully handled track density twice this at 40 cm from the target in AGS E-810 where the pixel size is approximately the same. For an approximately constant dN/dy the hits per pixel are approximately constant at a constant distance from the RHIC beam pipe. Therefore we believe we can handle the rates at 40 cm from the RHIC beam.

We have estimated that in the very unlikely event that all the available energy in a 100 GeV Au and Au collision goes into plasma, track densities $\approx$ a factor of six higher than we have considered could occur. Thus we could in these events separate tracks at distances $\sim$ 1 meter and still have sufficient path length to do dE/dx. A similar statement applies to other possible high density fluctuations.

In order to implement such a large fast sampling analog and time measuring system, work is under way to develop large scale integration elec tronics utilizing the concept of the segmentable analog memory. At the 1987 RHIC Workshop the basic design of a chip set was acheived.[2] It was based on a low noise, low power amplifier shaper chip and a segmented analog memory chip each having 8 channels per IC (Fig. 11). The amplifier design is straight-forward and should not require high priority for prototyping. The analog memory was based on an adaptation of an LBL development by Nygren and Kleinfelder. Design changes were made to implement the segmented memory function. This is important because desparisfying or compacting the data on the fly is mandatory

* The arrangement of the cathode pads can be customized as desired.

in a system of 5×10^5 channels. It is also important to reduce memory size to minimize power consumption and silicon cost. This design reached the point that prototype chips could have been produced. Subsequently the process used in this design has been replaced by a more advanced process so a redesign is required. In order to verify the efficacy of this concept it is important to proceed with prototype production, test and evaluation. Most likely several iterations of the chip will be required for debugging and optimization.

A prototype chip run through MOSIS costs about $10,000. A conservatve estimate of the manpower and equipment to successfully develop such a chip is 5 or more man years and several hundred thousand dollars for computer and software systems, test facilities, interfaces etc. At the end of this effort, however, is the prospect of very low production costs estimated to lead to $\approx$ $10.00 per channel for the readout electronics.

The two modules of TPC2 each have $5m \times 1m$ area readout on top and bottom for a total of $20m^2$. Since no dE/dx measurement is contemplated in TPC2, 20 rows each with elements on 2.5 mm spacing should suffice (equivalent pixel figured at $2 \times 7.5mm$). This requires an additional 160,000 channels of electronics which needs to record only the drift time.

DATA ACQUISITION FROM THE TPC

Organizing and compressing time and amplitude sampling information from a half million pads raises some challenging issues. The raw uncompacted data from TPC1 produces $> 10^9$ bytes of information, $> 99\%$ of which are samples empty of relevant information. Therefore the first strategy is to record, even temporarily, as little of the empty samples as possible at the front end of the electronics chain. It is proposed at this level, to reduce the empty samples by a factor of 100-200 using the concept of the segmentable analog memory. This will leave analog data encompassing the time samples that have been triggered by an analog threshold detection.

The next level of compaction is to fit the analog samples in time yielding another factor of two or three. These two levels of compaction can be accomplished with electronics mounted on the TPC, reducing the event size to 2 - 5 MB for further processing. Higher levels of organization would be done remotely from the TPC. Electronic systems for these first two levels of compaction would be organized in 1000-2000 serial links to this external processing system.

TPC TRACK RECOGNITION

Track reconstruction efficiency for the proposed RHIC TPC was estimated by analyzing the plasma events using an existing TPC reconstruction program from AGS E-810. GEANT was used to convert the HIJET events into hits in the TPC padrows. Each hit was then converted into a simulated TPC readout taking into account Landau fluctuations, ion drift time and diffusion, and readout electronics characteristics. Background noise was added, and a randomly distributed. 5% of the readout channels were assumed dead. A readout signal was generated based on the expected amplifier characteristics. The resulting detection efficiency for individual hits was $\approx$ 90%.

The simulated readouts were then analysed by the track reconstruction program developed for AGS E-810. The E-810 TPC is rectangular with parallel readout pad rows. The proposed RHIC TPC1 will have segments whose padrows are oriented in different

directions to optimize track reconstruction. In order to use the existing program to investigate the track recognition efficiency for a segmented TPC system, the proposed RHIC TPC was simulated with three different configurations.

90° Chamber:	100 cm by 140 cm by 200 cm TPC centered at $(X, Y, Z) = 90, 70, 0$ cm relative to the beam intersection point; readout plane normal to X (beam along Z).
0° Chamber:	100 by 140 by 200 at 90, 70, 150 cm; readout plane normal to Z.
30° Chamber:	similar to 0° chamber, but with readout planes rotated 30 degrees

Efficiencies were computed for correctly reconstructing tracks which spanned ten or more padrows. Overall efficencies achieved in the 0, 30, and 90 degree chambers were, respectively, 94%, 98%, and 95% for positive tracks; 97%, 81%, and 90% for negative tracks.

Using the configuration which gave the highest efficiency for a given pseudorapidity region, the efficiency for tracks with at least ten hits is greater than 95% in the pseudorapidity range $| \eta | < 2$.

MOMENTUM RESOLUTION

The momentum resolution in the TPC1 detector will be dominated by multiple scattering and can be estimated by comparing the momentum of the reconstructed track with the generated momentum. For this comparison only tracks that spanned 25 or more padrows were used. The fraction of tracks with $\Delta P/P < 5\%$ was 74%, 83%, and 85% for the 0, 30, and 90 degree chambers, respectively. The fraction with $\Delta P/P < 10\%$ was 87%, 95%, and 94%. The average momentum resolution was about 2%. It is anticipated that the cathode pad readout in TPC1 will give better momentum resolution than this present simulation predicts. The average angular resolution is about 10 mrad.

Due to the generally higher momentum of the tracks the momentum resolution of TPC2 will be dominated by measurement accuracy. An estimated position resolution of 1 mm leads to an angle resolution in TPC2 of about 3 mrad and a momentum resolution $\Delta p/p = .01P(GeV/c)$.

TPC ACCEPTANCE

The GEANT program tracked all charged particles (assuming their identity was known) through the detector shown in Fig. 12. Hits were recorded as the tracks passed over pad rows. If a particle decayed, no further hits were recorded. Figure 12 is a GEANT plot of the hits from a small fraction ($\approx 2\%$) of the tracks from one central event in the proposed TPC. Because of the larger number of tracks involved it is difficult to produce a presentable figure of a full RHIC event. The pattern recognition results are based on complete events, of course. The track was defined as "accepted" for momentum measurement

if there were 10 separate hits recorded.The particle was "accepted" for particle identification if there were 80 cm or more of track samples recorded. The resultant acceptance is indicated in the following table.

CENTRAL EVENT ACCEPTANCES

$\|Y\|$ Range	Tracks	TPC1 > 10 hits	TPC1 Particle I.D.	TPC2 > 10 hits
0 to 1	445	95.0%	81.8%	3.9%
1 to 2	513	88.3	81.7	33.7
2 to 3	497	35.8	19.7	84.1
3 to 4	384	0	0	70.6
above 4	266	0	0	16.9
PLASMA EVENT ACCEPTANCES				
0 to 1	1284	88.6	74.1	4.3
1 to 2	556	86.4	80.1	29.4
2 to 3	433	35.9	20.6	85.9
3 to 4	335	0	0	72.0
above 4	279	0	0	16.1

TPC1 is quite efficient for $\mid Y \mid < 2$ and TPC2 complements the acceptance for larger Y where it is quite efficient. It should be noted that the above simulations assume particles are identified. In reality when we combine dE/dx and time-of-flight particle identification the rapidity ranges the TPC detector system can effectively cover are $\Delta y \approx \pm 3$ for pions, $\Delta y \approx \pm 2.5$ for kaons, and $\Delta y \approx \pm 2$ for $\bar{p}$ and p. At rapidities of larger magnitude only the pseudorapidities can be determined.

PARTICLE IDENTIFICATION

Particle identification is of particular importance for the aforementioned physics goals. In Fig. 13 is plotted the momentum spectrum for π's, K's and protons in the central rapidity region. As has been demonstrated by PEP4, the TPC is particularly effective in separating particles by ionization loss in the region between 100 and 700-1500 MeV/c depending on the particle species; see Fig. 14. It should be noted that clear π/μ separation is possible below 100 MeV/c. π/K/p separation is obtained between 100 MeV/c and 700 MeV/c, $p/(K^+ + \pi^+)$ to > 1000 MeV/c and deuterons to 1500 MeV/c. There are narrow bands of electron contamination (see Fig. 14). One should note that PEP-4 operates at a pressure of $\approx$ 5 atmospheres but we have a length of about 2.5 times greater so that the particle identification capabilities should be approximately comparable. Extending π/K/p separation to as low a momentum as possible imposes difficult requirements on electronics dynamic range. A dynamic range of 50:1 is required to distinguish K's from p's down to 100 MeV/c although π/K separation should work to 50 MeV/c. With a nominal 100 cm of sampled track (100 cm of gas) the sigma of truncated mean samples at minimum ionization is 5-6%. In order that the sampling granularity does not materially reduce this resolution, minimum ionization should be more than 5 times the least significant bit of the digitizer.

Thus to cover 50 times minimum, 8 bits of dynamic range is essential (10 bits would be more comfortable). The effort in progress mentioned in "readout electronics" has as a goal a dynamic range of 10 bits. dE/dx is the major element in our particle ID since it covers the high track density low momentum central region where prominant hadronic plasma signals are expected. However in order to extend our rapidity coverage in the non-central regions with higher momentum cascade particles we have in this workshop added $\approx 20,000$ channels of time-of-flight as discussed previously.

QED ELECTRONS

Before and during the workshop Mark Rhoades Brown[6] reported on e^+e^- pairs produced by heavy ion beams in the crossing region is proportional to the production cross section σ = constant $\times (Z_1\alpha)^2(Z_2\alpha)^2$. Obviously Au and Au is the worst case. For $\gamma = 100$ Gold on Gold he obtained $\sigma_{e^+e^-} = 3.36 \times 10^4$ barns. This now seems to be about the consensus cross section for perturbative calculations. $L = 2 \times 10^{26} cm^{-2} sec^{-1}$ for Au on Au beams in RHIC. The event rate is $L\sigma_{e^+e^-} \approx 7 \times 10^6$ events per second for $L = 2 \times 10^{26} cm^{-2} sec^{-1}$. For 28μ sec "on time" of our TPC the event rate $\rightarrow \approx 200$ events per second. However from his distribution curves for $P_{\|}$, approximately 14 slow single electrons would, he calculated,[7] enter our TPC. Allowing for non-unitary effects this could be ~ 50. They would be concentrated near the 40 cm distance from the beam pipe and due to drift they would be uniformly distributed in the vertical direction. Therefore we consider this to be a manageable problem. However we will keep an eye on this effect.

THE TRIGGERING SYSTEM AND OTHER DETECTORS

A small calorimeter surrounding the beam pipe and subtending a pseudorapidity range from 4 to 5 will measure an energy that depends on the impact parameter of the collision. A large plane device located just behind the central TPC which measures multiplicity will give a more direct measurement of the interest of the event as far as TPC response is concerned. Count information from the TOF counters can also be used as a trigger element. Note that the region 80cm wide by 80cm (or more) high immediately around the interaction region is available for insertion of a special device capable of dealing with the very large track densities. Such a device would have to have very low mass, of course, to avoid compromising the TPC.

COMPUTATION AFTER TRIGGERING

For 100 GeV $\times$ A Au on 100 GeV $\times$ A Au, the inelastic event rate $\approx \sigma L \approx 6.8 \times 10^{-24} \times 2 \times 10^{26} \approx 1400$ per sec. The trigger reduces the rate by $\approx$ a factor of 100. Pattern recognition would take about 0.5 sec per track on VAX780 based on AGS 810 experience.

Thus $\approx 14 \times 4,000 \times 0.5 \rightarrow \approx 28$ KiloVAX780 to process as we run. Approximately 20 KiloVAX780 should be sufficient when allowing for percentage on time. We now can get one 780 equivalent for < \$1,000. We expect to gain a factor ~ 5 or better when RHIC is available, so $\approx$ \$4M is sufficient. We plan to improve the trigger, and all run time will not be analyzed so allowing $\approx$ \$3M - \$4M for computing should be reasonable.

COST ESTIMATES

Cost estimates were made for the TPC Magnetic Spectrometer system and published in the LBL Workshop.[2] Salaries of the collaboration, EDIA and contingency were not included. The total cost estimated for the window frame magnet, TPC system, trigger system, and computer system was 18.5 million dollars. The time-of- flight wall we have added at this workshop is expected to increase the costs by about 5 million dollars.

A cost estimate will be included with the Letter of Intent.

EXPERIMENTAL HALLS

This detector can be installed in either the wide angle (Fig. 15) or the major facility hall (Fig. 16) without significant modification to the halls. Use of the narrow angle hall or the open region would require major reconstruction and will not be pursued. A preliminary look at the possibility of moving the magnet and attached detectors in order to simplify assembly and maintenance of the system indicates that it will not be a major difficulty, and is being studied further.

AGS E-810 PROGRESS ON TPC SYSTEM

The success of the AGS E-810 TPC Program is a clear indication that we have the appropriate expertise for this project.

The experimental arrangement for AGS E-810 is shown in Fig. 17. The AGS E-810 TPC system consists of three modules of twelve anode rows each. They are placed along the beam in the MPS 5KG magnet (Fig. 17) with the Si ion beams passing through the TPC to provide large solid angle coverage. We have been able to handle 5,000 to 10,000 Si ions per AGS pulse passing directly through the center of the TPC. When the booster becomes available at AGS to accelerate Au ions it will become necessary to deaden the beam area unless one chooses to run at rates of a few hundred incident Au ions per pulse. The anode readout wires are 25μ gold-plated tungsten 1 cm long rows parallel to the beam direction. There are 10 wires to the inch between cathode structures. A gate which opens only when events of interest occur is included for operation at high ion beam rates ($\sim 1/2\ 10^4$/pulse).

14.5 GeV/c $\times$ A Si on Au events with up to 90 tracks were reconstructed with good pattern recognition efficiencies. The event shown in Fig. 18 contains 68 tracks including a Λ. Clear Λ and K^0 peaks were obtained. About 700 single Λ events were obtained for 14.5 GeV/c Si $\times$ A on Au events during a running period of about one day. Over 50 double Λ events were observed, and 2 triple Λ events were observed (see Fig. 19). These experiments were described in references 8-10.

dN/dy distributions for negative tracks assuming they were pions were obtained and dN/dy for protons was obtained approximately by subtracting negatives from positives (see Fig. 20). Temperatures were estimated for the various particles.[9] About an order of magnitude more data was obtained for various targets ranging from Si to Tungsten in the most recent Heavy Ion run. This data is currently under analysis. A Physics Letters B on the Λ and K^0_s data is in press.[10]

SUMMARY

1. A 4π tracking TPC magnetic spectrometer for RHIC has been proposed by members of this collaboration in all four RHIC Workshops.
2. During this workshop the only basic change was the addition of time-of-flight walls to enhance particle ID and thus increase the rapidity ranges covered. We also considered various open dipole options.
3. S.Y. Lee designed a system to match our dipole into the RHIC ring.
4. The BNL/CCNY/Notre Dame/Rice collaboration believes this proposal will allow a sensitive search for a Quark-Gluon Plasma and possibly other new phenomena which go beyond the standard model.
5. Recent successes with the BNL/CCNY/Rice experimental program in AGS E-810 has demonstrated that the collaboration has the expertise required for such a project. This has been further enhanced by a successful RHIC R&D program for developing a TPC at RHIC.[11] A summary of this is given in Table I.
6. The BNL/CCNY/Notre Dame/Rice collaboration plans to submit a Letter of Intent this fall for a first round RHIC experimental program with a device of this type. Therefore at the Workshop we concentrated on preparing for this.

REFERENCES

1. (a) S.J. Lindenbaum and L. Schroeder. Large Magnetic Spectrometer. *RHIC Workshop: Experiments for a Relativistic Heavy Ion Collider, April 15-19, 1985*, P.E. Haustein and C.L. Woody, Editors, pp. 211-252 (Brookhaven National Laboratory, Upton, New York, 1985). See Part II by S.J. Lindenbaum, pp. 227-252.
2. S.J. Lindenbaum. An Approximately 4π Tracking Magnetic Spectrometer for RHIC. *Proc. of the Second Workshop on Experiments and Detectors for a Relativistic Heavy Ion Collider (RHIC), Lawrence Berkeley Laboratory, Berkeley, California, May 25-29, 1987*, Editors, Hans George Ritter and Asher Shor, pp. 146-165 (Lawrence Berkeley Laboratory, 1988).
3. S.J. Lindenbaum. A 4, Tracking Magnetic Spectrometer for RHIC. *Proc. of the Third Workshop on Experiments and Detectors for a Relativistic Heavy Ion Collider (RHIC), Brookhaven National Laboratory, July 11-22, 1988*, B. Shivakumar and P. Vincent, Editors, pp. 82-96 (Brookhaven National Laboratory, BNL 52185).
4. S. Nagamiya, talk presented at this workshop.
5. P. Koch, M. Mueller and J. Rafaelski, Phys. Reports C142, 176 (1986).
6. Mark Rhoades Brown, talk presented at this workshop.
7. Mark Rhoades Brown, private communication.
8. A.C. Saulys (for the E-810 Collaboration). V^0 Production with 14.5 GeV/c Silicon Beams. *Proc. of the Heavy Ion Physics at AGS Workshop, Brookhaven National Laboratory, March 5-7, 1990* (to be published); W.A. Love (for the E-810 Collaboration). AGS Silicon Gold Collisions Measured in the E-810 TPC. *Proc. of the Heavy Ion Physics at AGS Workshop, Brookhaven National Laboratory, March 5-7, 1990* (to be published).
9. W.A. Love (for the E-810 Collaboration). Silicon Ion Interactions Measured in the E-810 TPC at the AGS. *Proc. of Quark Matter 90, Menton, France, 7-11 May 1990*, (to be published in a special issue of Nuclear Physics A).
10. S.E. Eiseman et al. Neutral V Production with 14.6 × A GeV/c Silicon Beams. Phys. Lett. B (in press).
11. E.D. Platner, talk presented at this conference.

FIGURE CAPTIONS

Fig. 1 Horizontal section (containing the beam) of the previous[2,3] experimental arrangement. The central TPC (TPC1) is in the 5KG window frame magnet (field vertical). The external TPC's (TPC2) is only shown on the right side, but the left side contains these also. Trigger calorimeters (between $\mid n \mid = 4 - 5$) and trigger multiplicity counters (beyond TPC near yoke) are not shown. The time-of-flight arrays have been added in this workshop.

Fig. 2 Beta vs. momentum in GeV/c for π, K, p for a length of 9mm with TOF $\sigma = 75ps$. Each curve is accompanied by 3σ bands.

Fig. 3a Horizontal section (contining the beam) of an open dipole option with time-of-flight walls. The left side external TPC (TPC2) and trigger elements are not shown.

Fig. 3b Open dipole option with time-of-flight walls. The opening is in the central region. The left side external TPC (TPC2) and trigger elements are not shown.

Fig. 4 Design by S.Y. Lee for matching our 2.5 Tesla meter magnet into the RHIC ring.

Fig. 5a π^+ or π^- counts and dN/dy vs. Y for one central RHIC PLASMA EVENT.

Fig. 5b The average π^+ or $\pi^- dN/dy$ vs. Y for 10 central RHIC EVENTS.

Fig. 6a K^+ and K^- counts and dN/dy vs. Y for one central RHIC PLASMA EVENT.

Fig. 6b The average K^+ or $K^- dN/dy$ vs. Y for 10 central RHIC EVENTS.

Fig. 7a $\bar{p}$ counts and dN/dy vs. Y for one central RHIC PLASMA EVENT.

Fig. 7b The average $\bar{p} dN/dy$ for 10 central RHIC EVENTS.

Fig. 8a p counts and dN/dy vs. Y for one central RHIC PLASMA EVENT.

Fig. 8b The average $p\ dN/dy$ for 10 central RHIC EVENTS.

Fig. 9 10% of the spiraling tracks with $p < 0.25 GeV/c$ are shown for clarity. The simulation used 100% of the tracks. Since the TPC detects 3-dimensional points, there is no significant confusion.

Fig. 10 $dN/d\Omega$ vs. θ measurements obtained in AGS E-810.

Fig. 11 RHIC TPC on chamber electronics. There are 256 channels per hybrid.

Fig. 12 2% of the tracks generated in a $100 GeV \times A$ Au on a $100 GeV \times A$ Au central collision. Since the TPC detects in 3D it can handle the actual track density.

Fig. 13 Calculated momentum spectrum for $\pi^{\pm}, K^{\pm}$ and p in the central region.

Fig. 14 dE/dx(KeV/cm) vs. momentum (GeV/c). This data was obtained in the PEI'4/9 TPC.

Fig. 15 The TPC detector is shown in the wide angle hall. The time-of-flight walls are not shown.

Fig. 16 The TPC detectors is shown in the major facility hall. The time-of-flight walls are not shown.

Fig. 17 The experimental arrangement for AGS E-810 showing the TPC system in the MPS 5-meter-long 5KG magnet.

Fig. 18 A 68 track 14.5 GeV/c $\times$ A Si on Au track event containing a Λ. (a) With all tracks shown; (b) with Λ only.

Fig. 19 A triple Λ event.

Fig. 20 Pseudorapidity distribution of charged tracks from central collsions.

Fig. 21 Rapidity distribution of pions (circles) and protons (triangles) from central collisions. Proton data are scaled one decade for clarity.

Table I

TPC R & D PROGRAM
1990 PROGRESS AND FUTURE GOALS

Progress	Goals
Electronics assembly method found and tested (260 contacts). Developed elastic interconnect devices.	Develop multilayer circuit boards for chips under development.
Constructed cathode pad endcap assembly for test chamber	Fully assembled test TPC.
Gas system designed for accurately mixing a variety if gases.	Completion of gas system.
Three-dimensional field mapping program development including acquisition of 387SX computer and MATHCAD software.	Completion of field mapping program and testing against actual chamber configuration.
Laser system review of existing lasers and multipliers.	Purchase of laser system and integration with test chamber.
Review of amplifier-shapers suitable for a RHIC TPC.	Acquisition of chips and test and evaluation. Installation of chips on assembly PC's. Test on TPC.
Review of existing memory chip properties as tested by others.	Acquisition of memory chips and test and evaluation. Installation of memories on assembly PC's. Test on TPC. Design of segmented memory version. Prototype production. Test and evaluation at BNL. Installation on assembly PC's.
Design IC test facility.	Acquire test electronics - includes waveform generator, digital oscilloscope and appropriate computer interfaces. Acquire computer suitable as driver and data acquisition for these instruments and TPC tests.

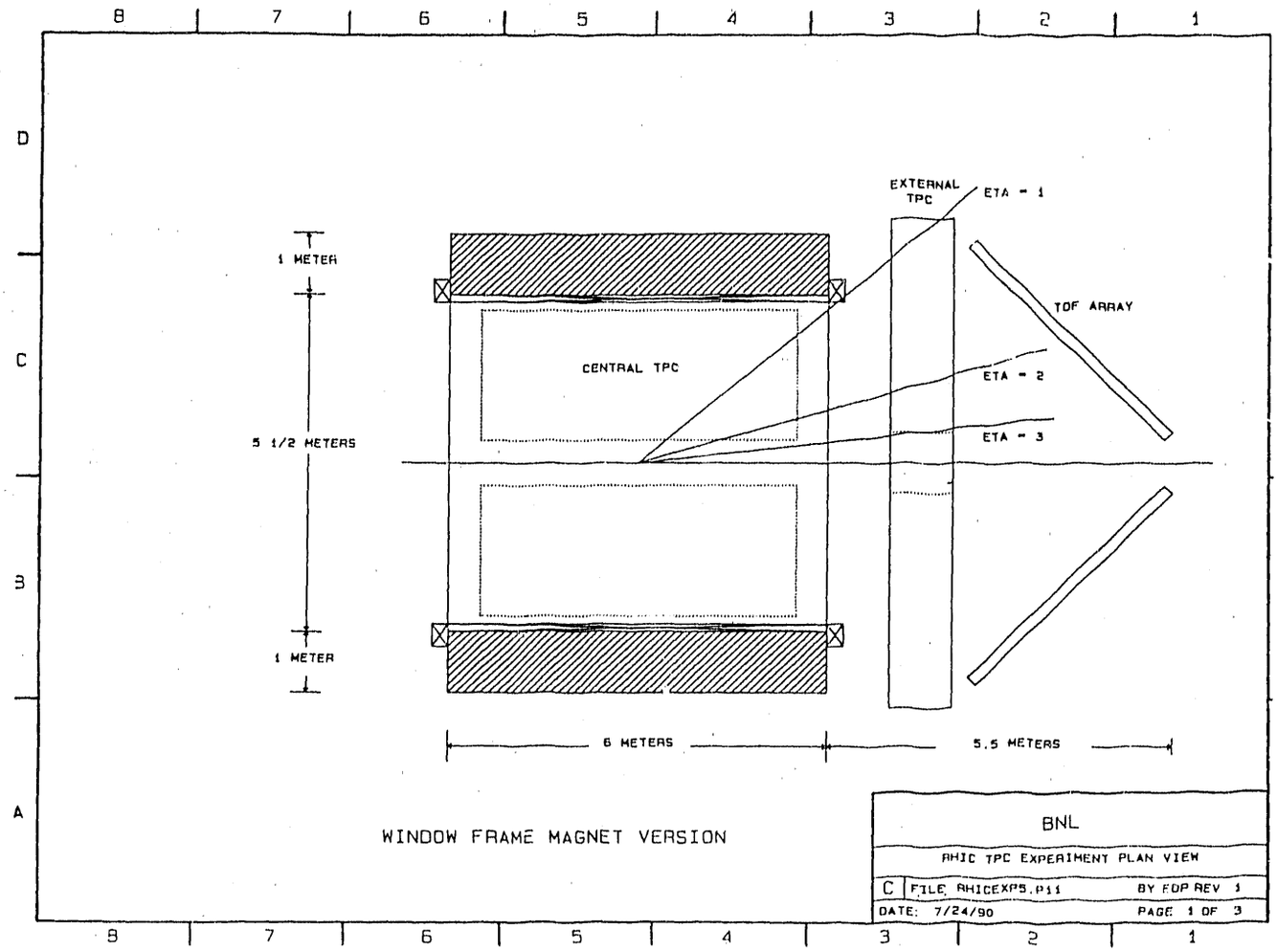
8
7
6
5
4
3
2
1
D
C
B
A
1 METER
5 1/2 METERS
1 METER
EXTERNAL TPC
ETA = 1
TOF ARRAY
CENTRAL TPC
ETA = 2
ETA = 3
6 METERS
5.5 METERS
WINDOW FRAME MAGNET VERSION
BNL
RHIC TPC EXPERIMENT PLAN VIEW
C
FILE RHICEXPS.P11
BY FDP REV 1
DATE: 7/24/90
PAGE 1 OF 3

Figure 1

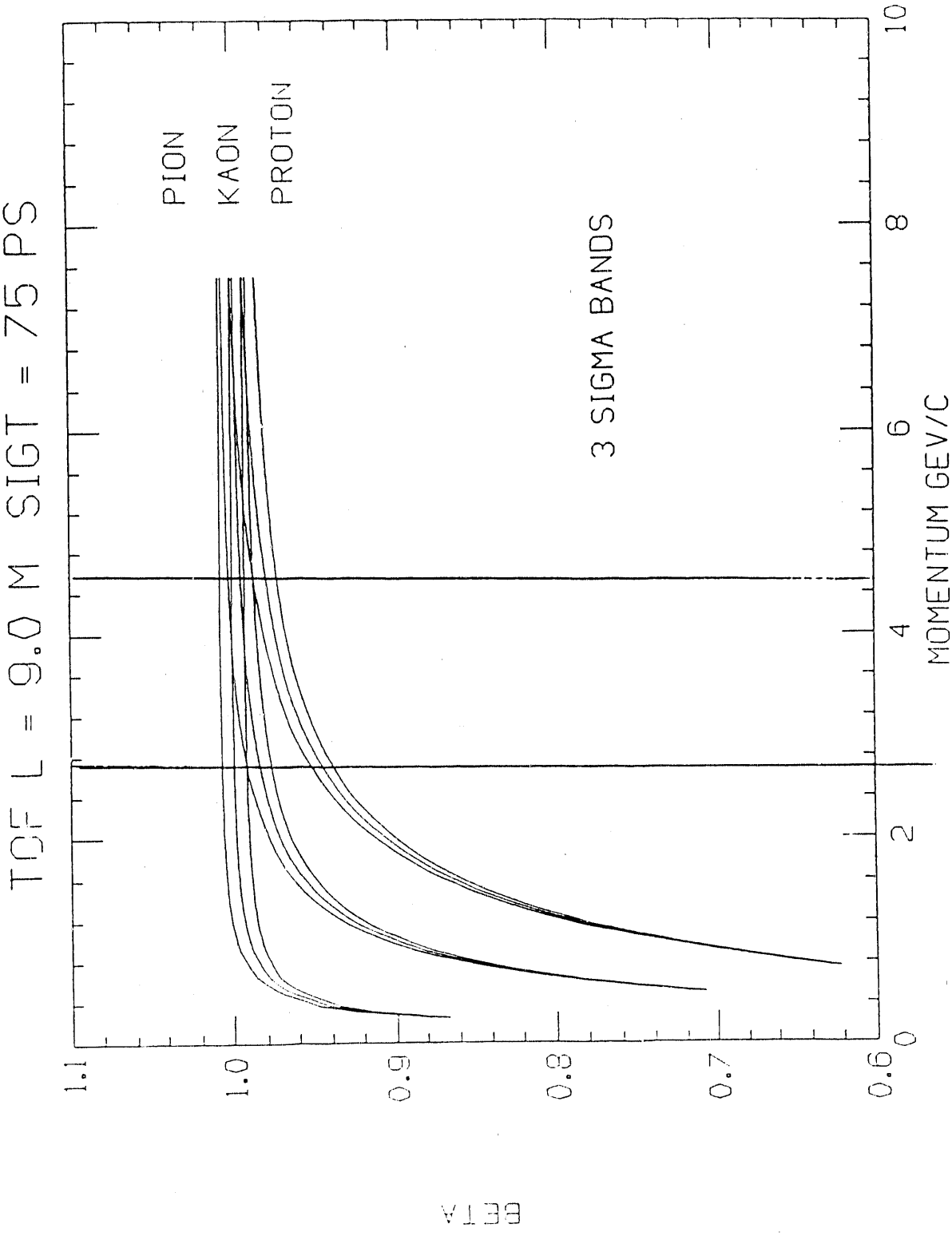
TOF L = 9.0 M SIGT = 75 PS
PION
KAON
PROTON
3 SIGMA BANDS
BETA
MOMENTUM GEV/C
1.1
1.0
0.9
0.8
0.7
0.6
0
2
4
6
8
10

Figure 2

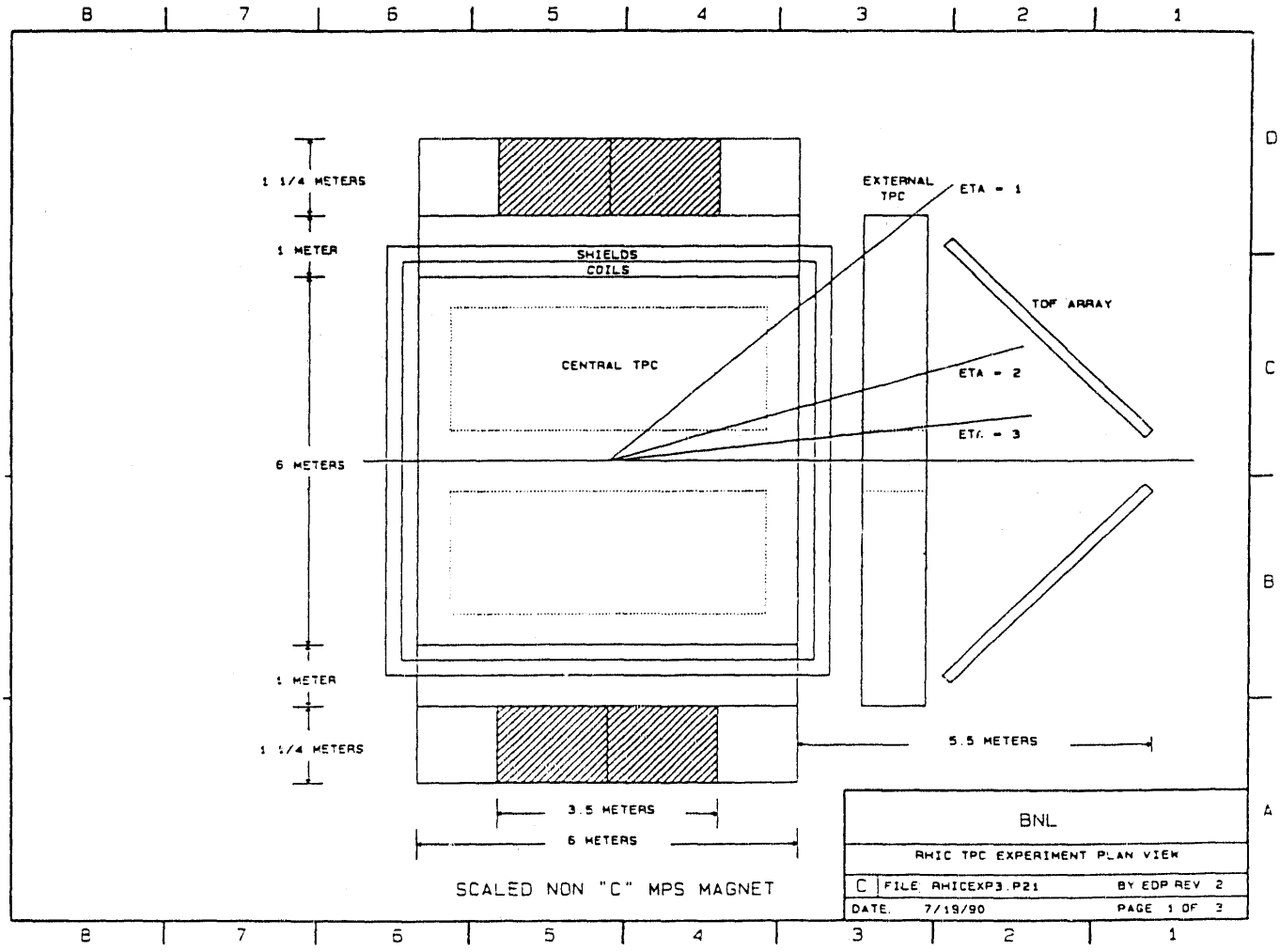
1 1/4 METERS
1 METER
6 METERS
1 METER
1 1/4 METERS
SHIELDS
COILS
CENTRAL TPC
EXTERNAL TPC
ETA = 1
ETA = 2
ETA = 3
TOF ARRAY
5.5 METERS
3.5 METERS
6 METERS
SCALED NON "C" MPS MAGNET
BNL
RHIC TPC EXPERIMENT PLAN VIEW
FILE: RHICEXP3.P21
BY EDP REV 2
DATE: 7/19/90
PAGE 1 OF 3

Figure 3a

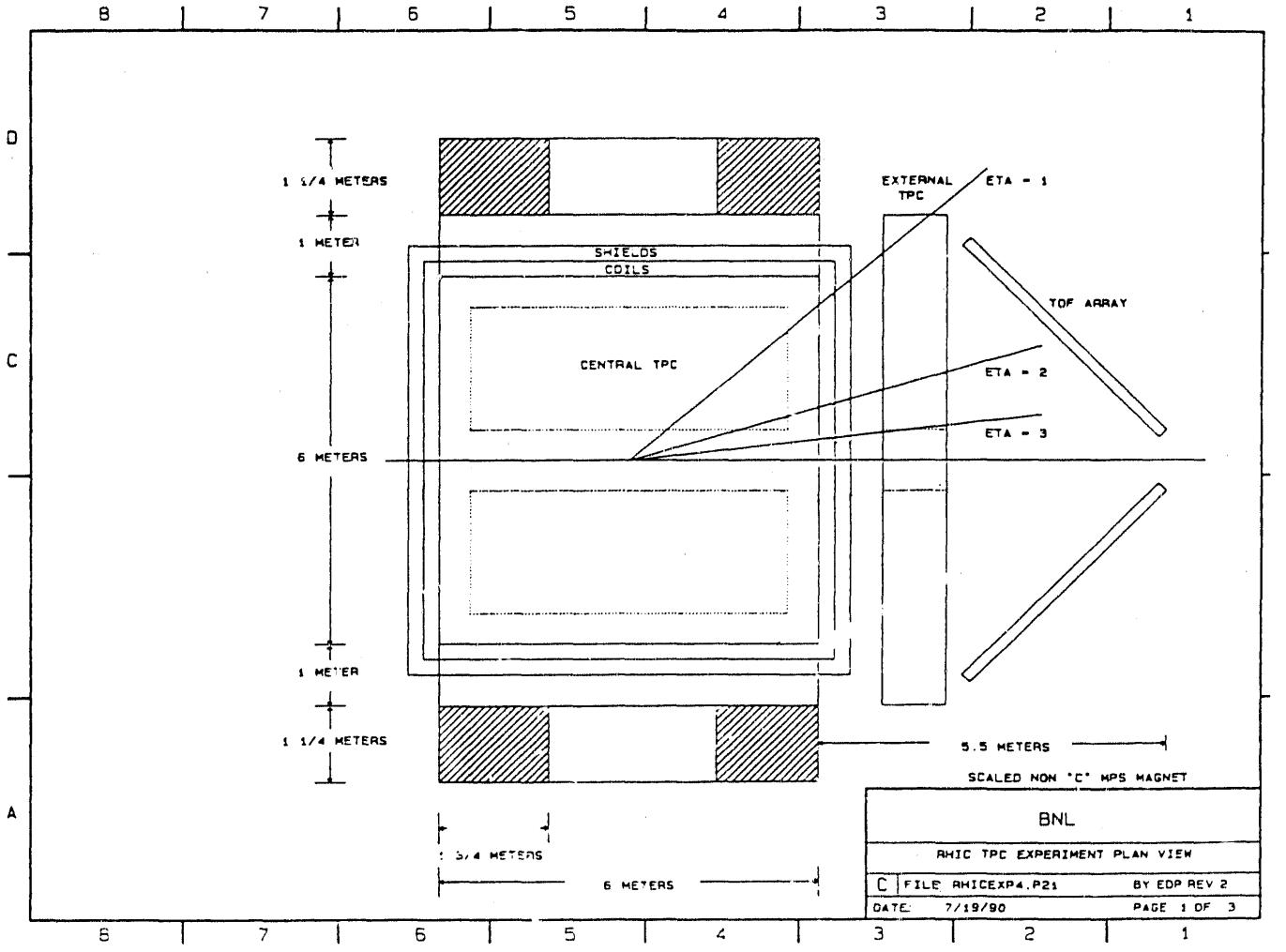
1 1/4 METERS
1 METER
6 METERS
1 METER
1 1/4 METERS
SHIELDS
COILS
CENTRAL TPC
EXTERNAL TPC
ETA = 1
ETA = 2
ETA = 3
TOF ARRAY
5.5 METERS
SCALED NON "C" MPS MAGNET
1 3/4 METERS
6 METERS
BNL
RHIC TPC EXPERIMENT PLAN VIEW
C FILE RHICEXP4.P21 BY EDP REV 2
DATE: 7/19/90 PAGE 1 OF 3

Figure 3b

Available Space for Transverse field detectors

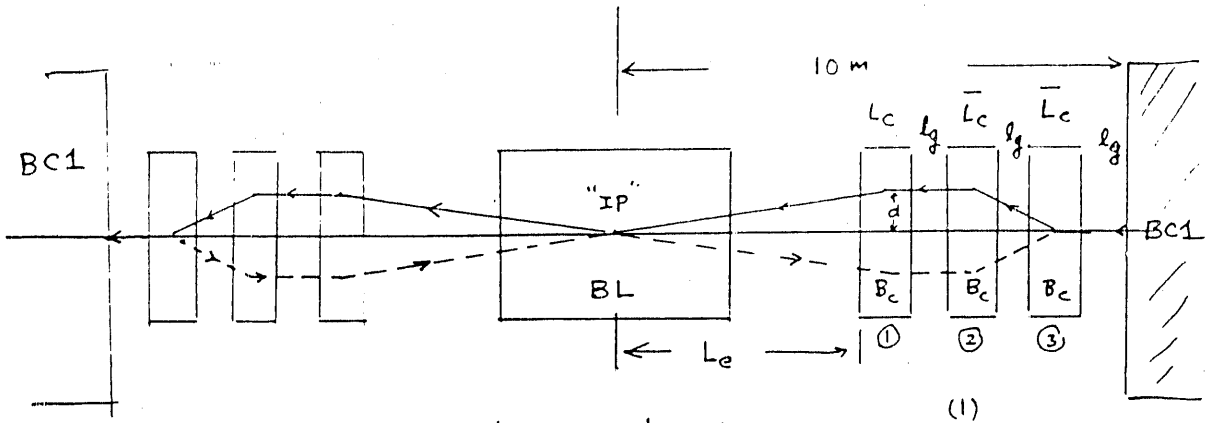

$$B_c L_c = \frac{1}{2} B L \qquad (1)$$

$$d = \frac{1}{2} \frac{BL}{B\rho} * \left(L_e + \frac{1}{2} L_c \right) \qquad (2)$$

$$\frac{B\bar{L}_c}{B\rho} \left(\bar{L}_c + l_g \right) = \frac{1}{2} \frac{BL}{B\rho} \left(L_e + \frac{1}{2} L_c \right) \qquad (3)$$

$$L_e = 10 - 3 l_g - L_c - 2 \bar{L}_c \qquad (4)$$

$l_g = 0.75$ m $B_c = 3.5$ T @ $B\rho = 840.5$ Tm

BL (Tm)	1	1.5	2.0	2.5	3.0
d (mm)	3.8	5.4	6.8	8.1	9.3
L_c (m)	0.142	0.214	0.286	0.357	0.429
$\bar{L}_c$ (m)	0.651	0.82	0.95	1.07	1.17
L_e (m)	6.31	5.90	5.55	5.26	4.99

$$\bar{L}_c^{\,2} + l_g \bar{L}_c = \frac{1}{2} \frac{BL}{B_c} \left(10 - 3 l_g - L_c + \frac{1}{2} L_c \right) - \frac{BL}{B_c} \bar{L}_c$$

Figure 4

ONE RHIC PLASMA EVENT π
6% PLASMA

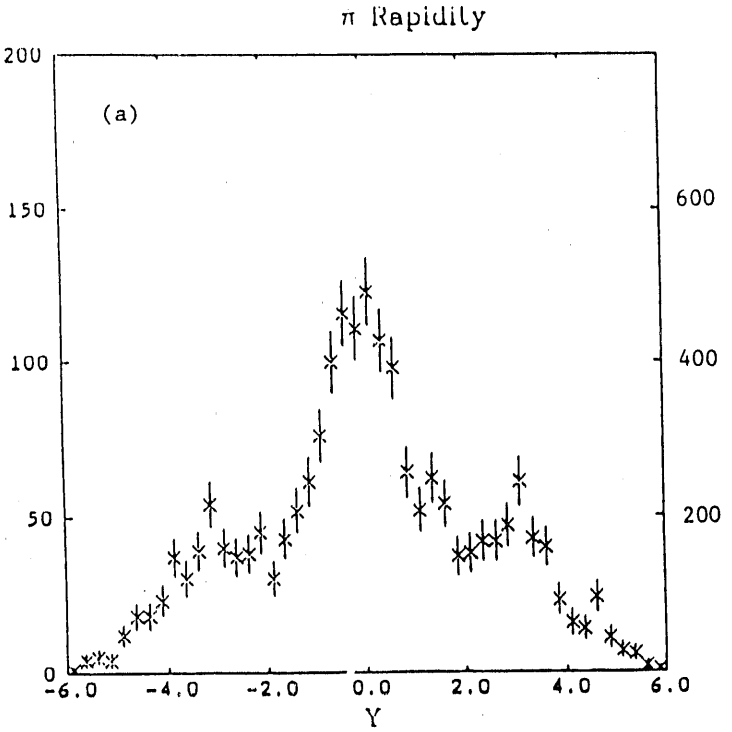

RHIC EVENT

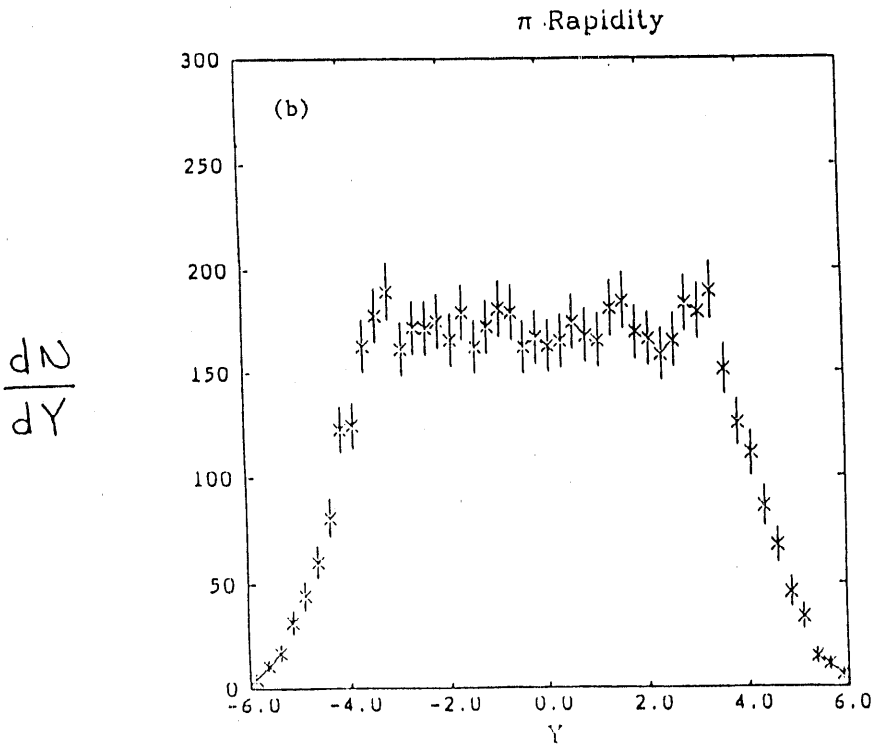

Figure 5

ONE RHIC PLASMA EVENT

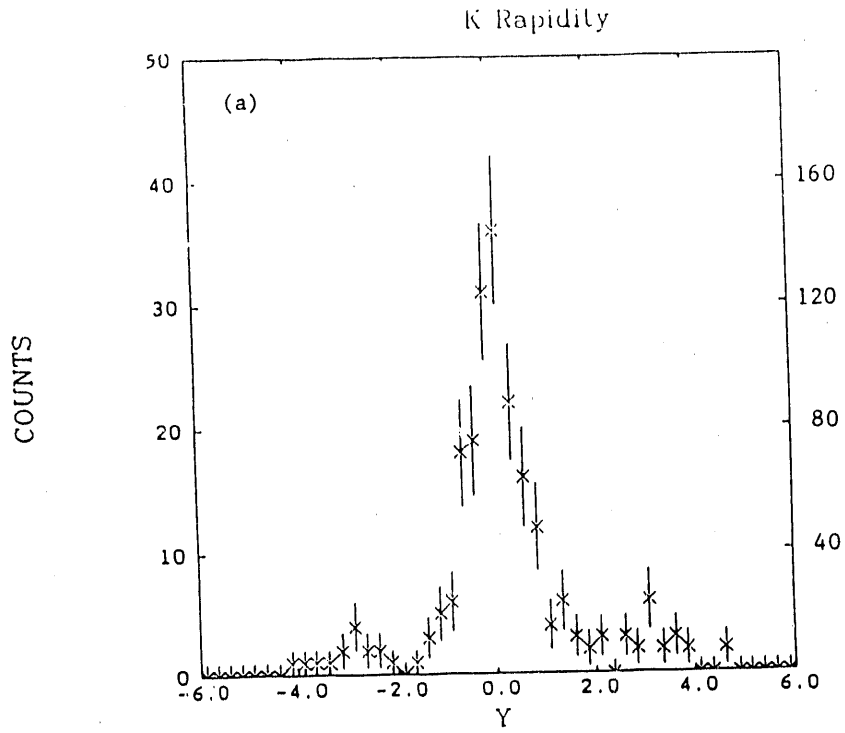

RHIC EVENT

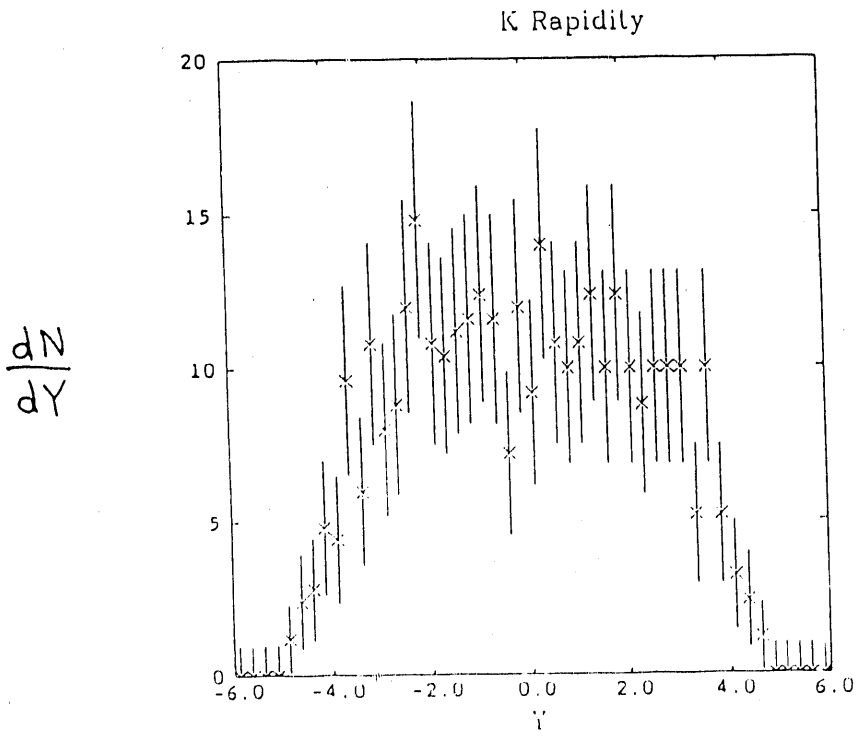

Figure 6

ONE RHIC PLASMA EVENT

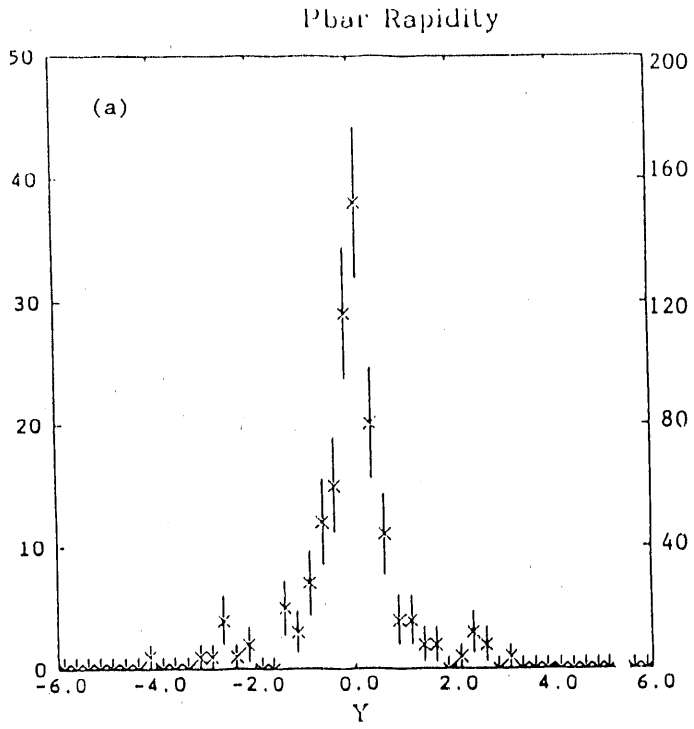

RHIC EVENT

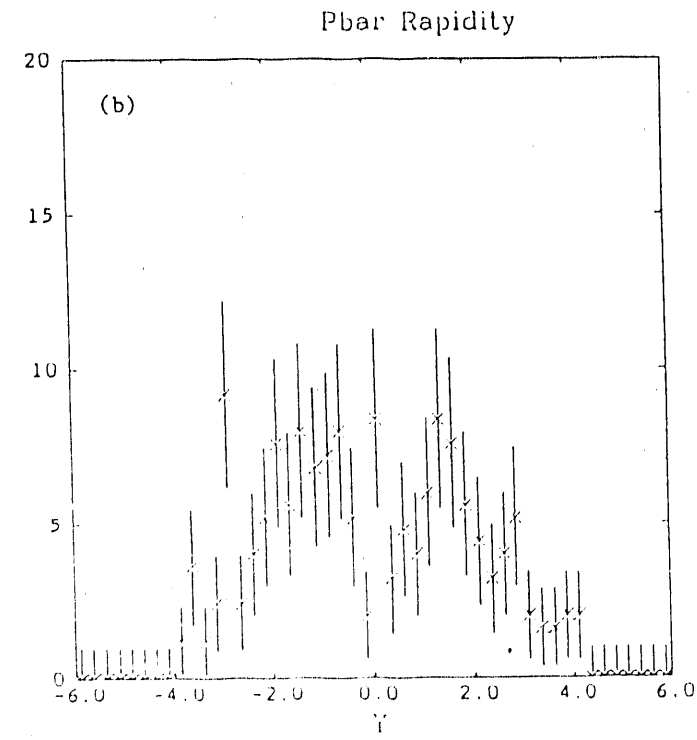

Figure 7

ONE RHIC PLASMA EVENT

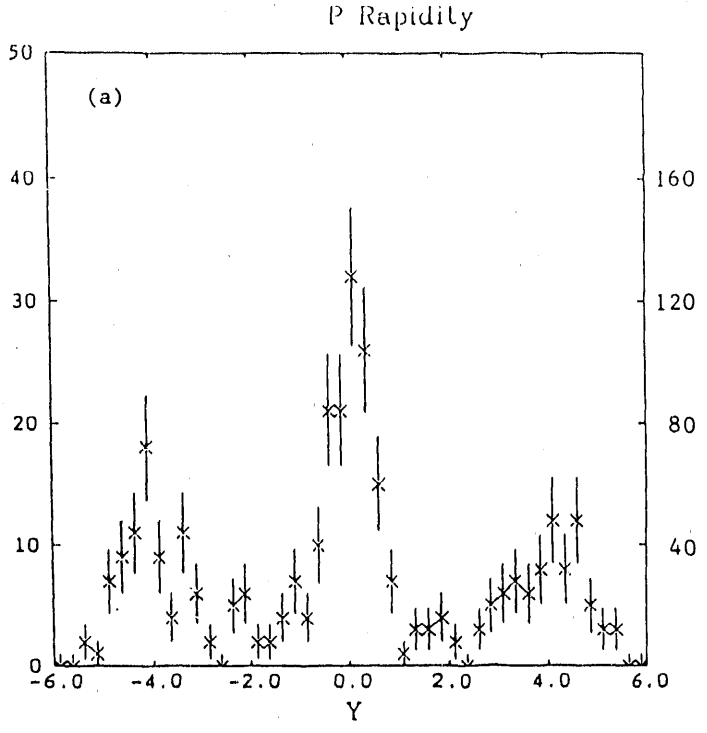

RHIC EVENT

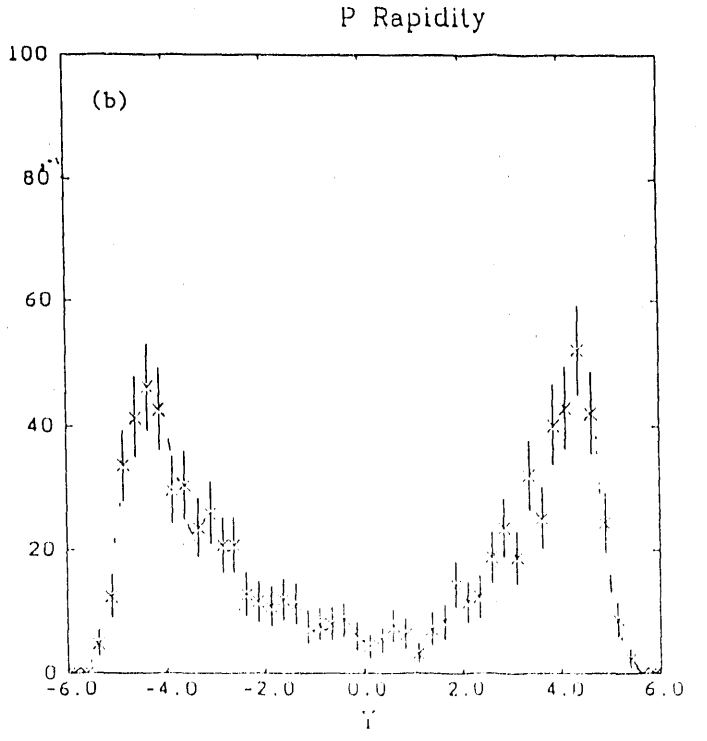

Figure 8

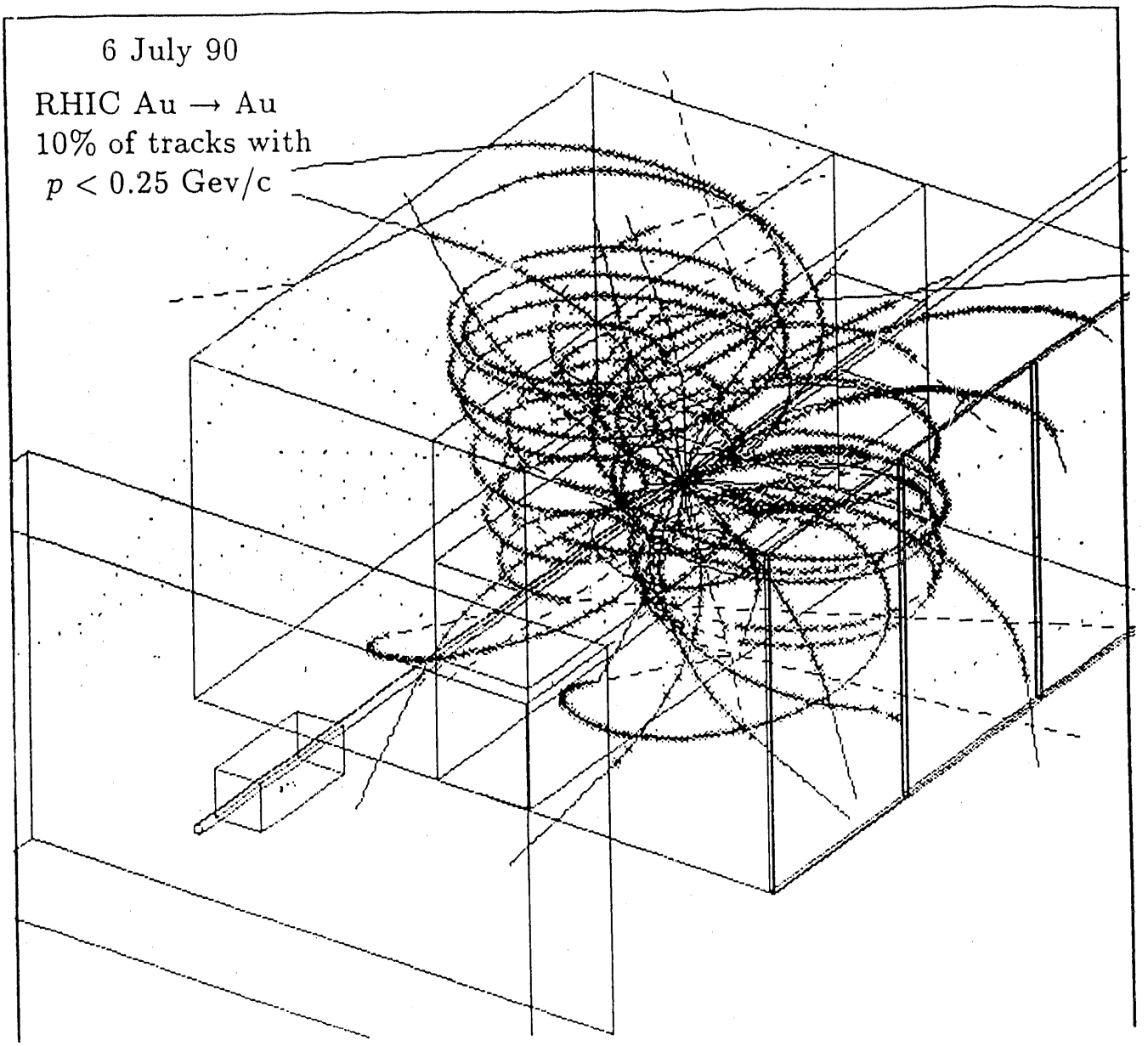

Figure 9

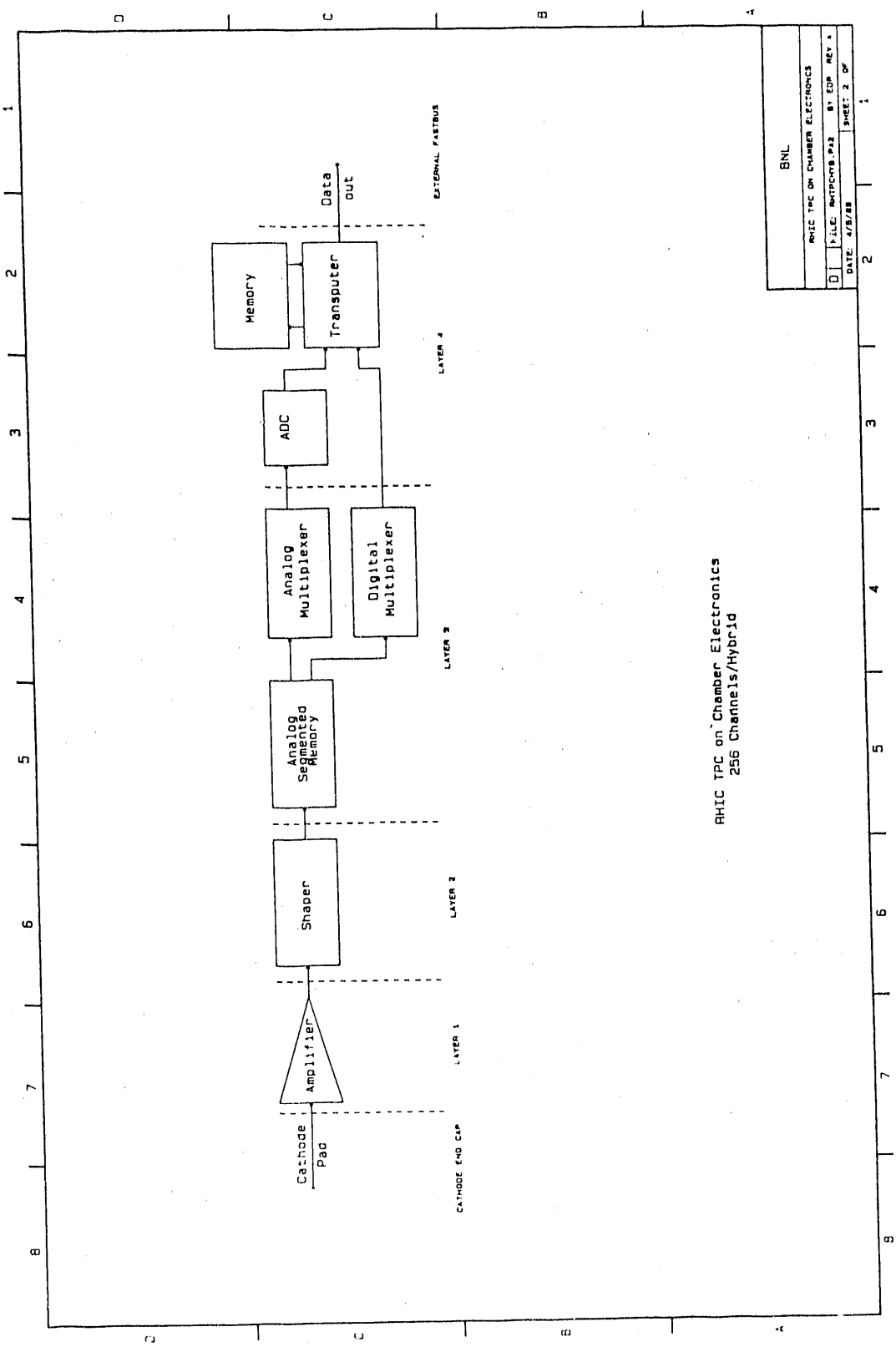
BNL
RHIC TPC ON CHAMBER ELECTRONICS
FILE: RHTPCMB.PAS
BY: EDP
REV: A
DATE: 4/8/88
SHEET: 2 OF
RHIC TPC on Chamber Electronics
256 Channels/Hybrid
Cathode Pad
Amplifier
Shaper
Analog Semaphored Memory
Analog Multiplexer
Digital Multiplexer
ADC
Memory
Transputer
Data out
CATHODE END CAP
LAYER 1
LAYER 2
LAYER 3
LAYER 4
EXTERNAL FASTBUS

Figure 11

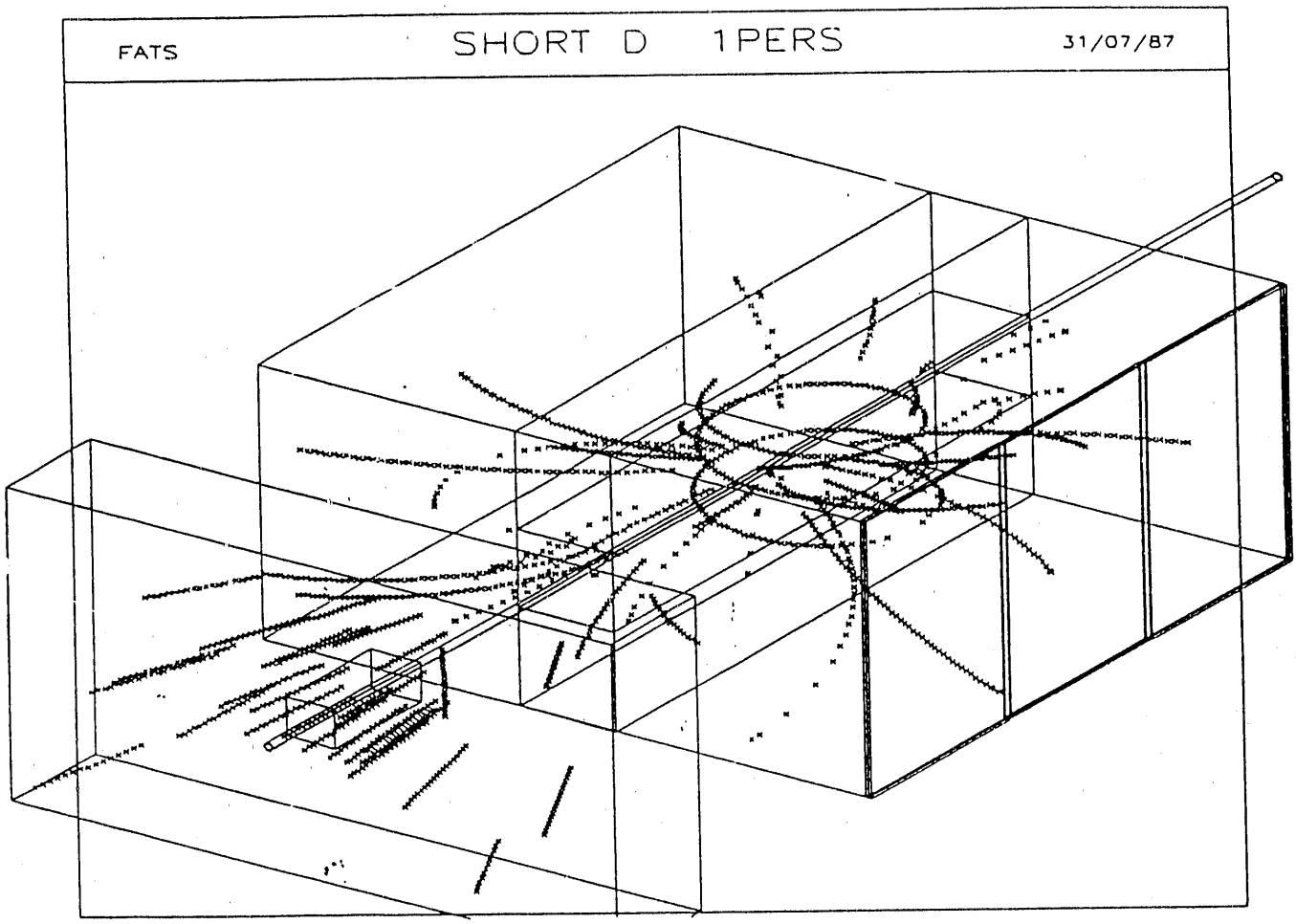

Figure 12

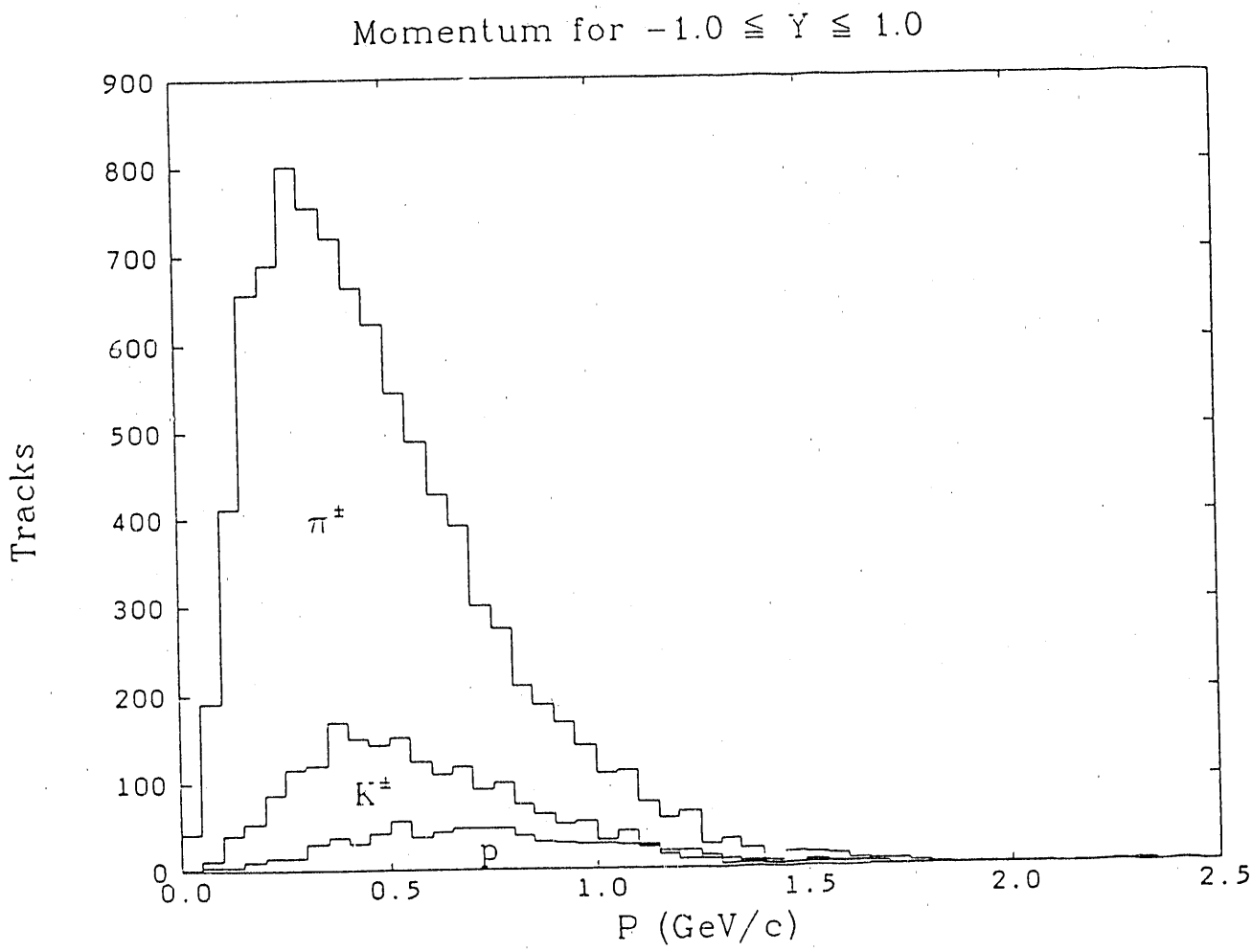
Momentum for −1.0 ≦ Y ≦ 1.0
Tracks
900
800
700
600
500
400
300
200
100
0
0.0
0.5
1.0
1.5
2.0
2.5
P (GeV/c)
π±
K±
p

Figure 13

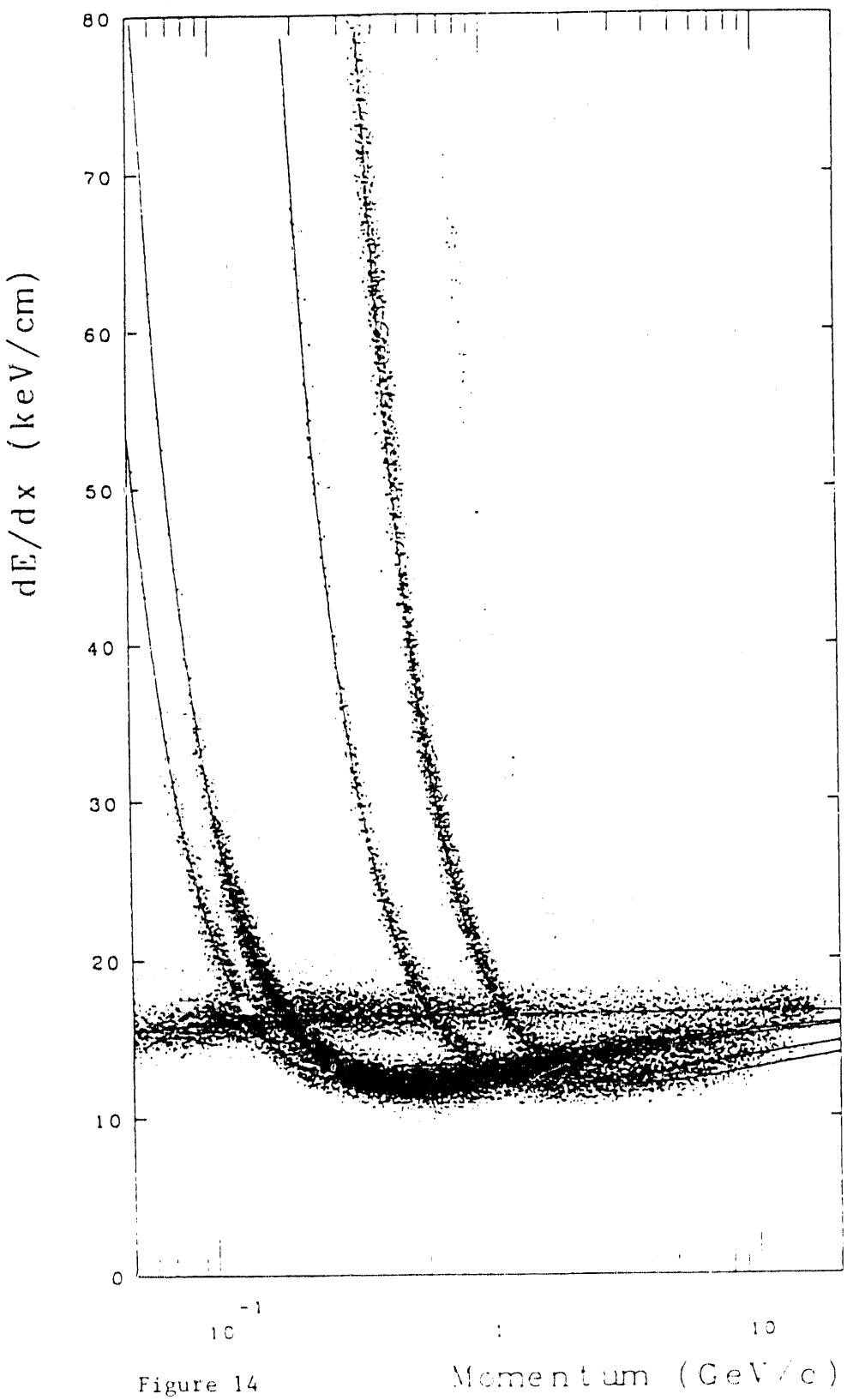
PEP4/9 TPC
dE/dx (keV/cm)
80
70
60
50
40
30
20
10
0
10
-1
1
10
Momentum (GeV/c)

Figure 14

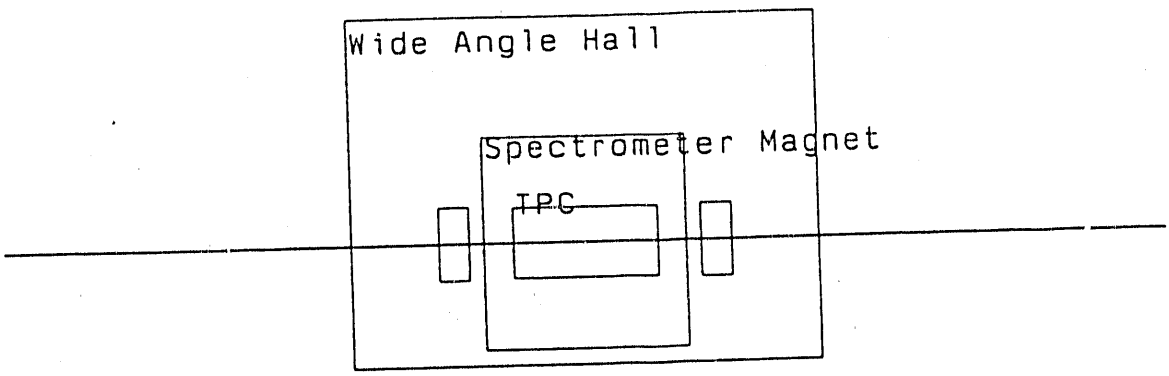

RHIC VIEW YZ

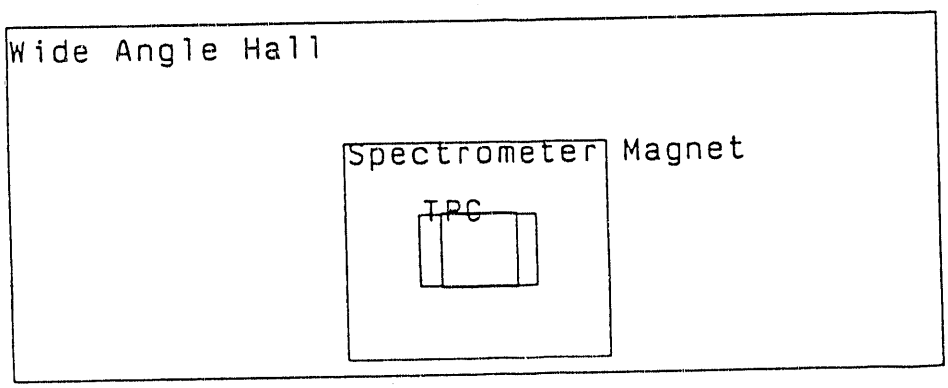

RHIC VIEW XY

Figure 15

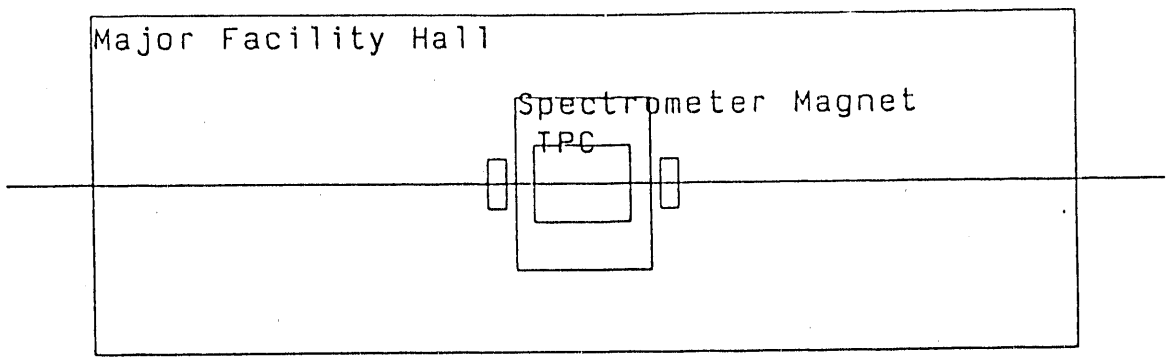

RHIC VIEW XZ

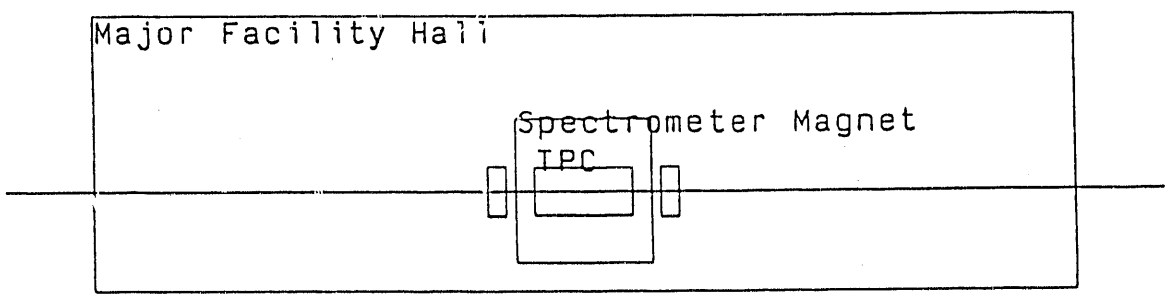

RHIC VIEW YZ

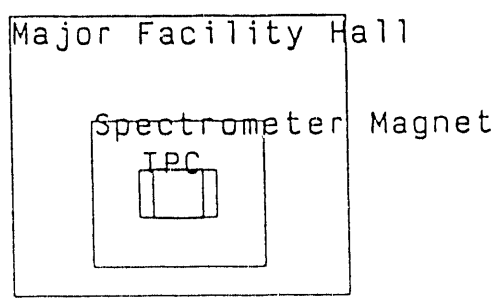

RHIC VIEW XY

Figure 16

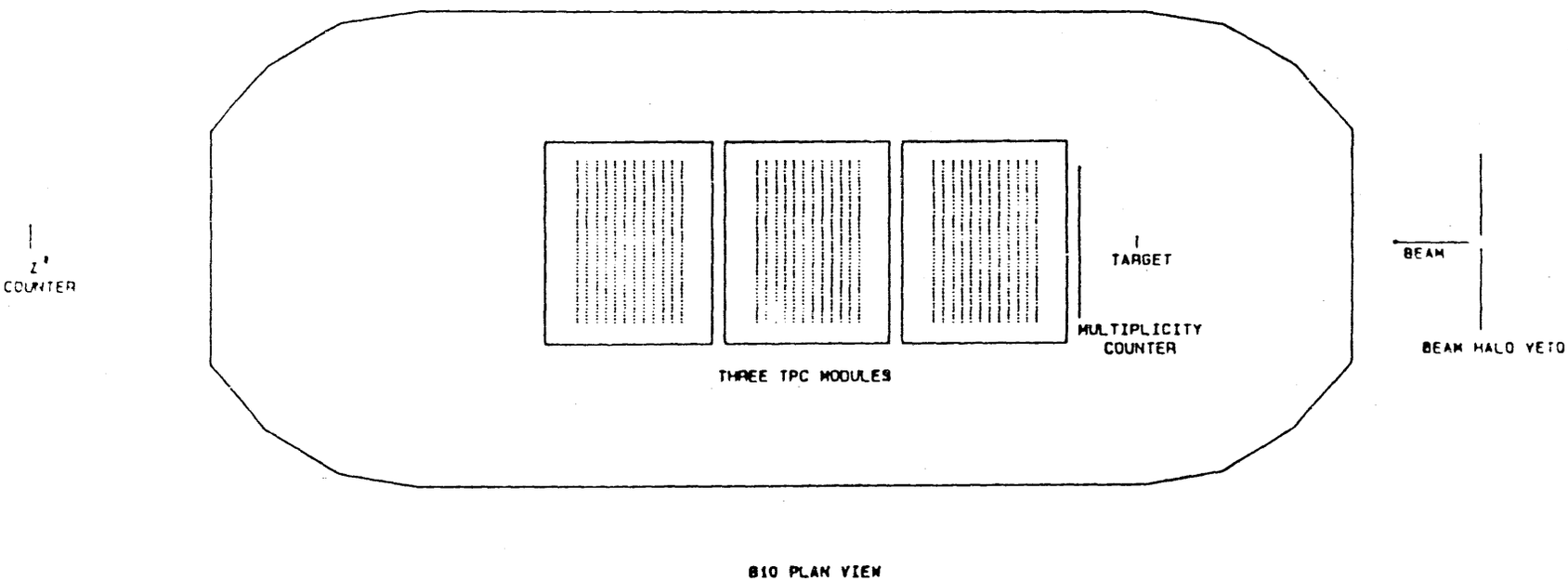

B10 PLAN VIEW

Figure 17

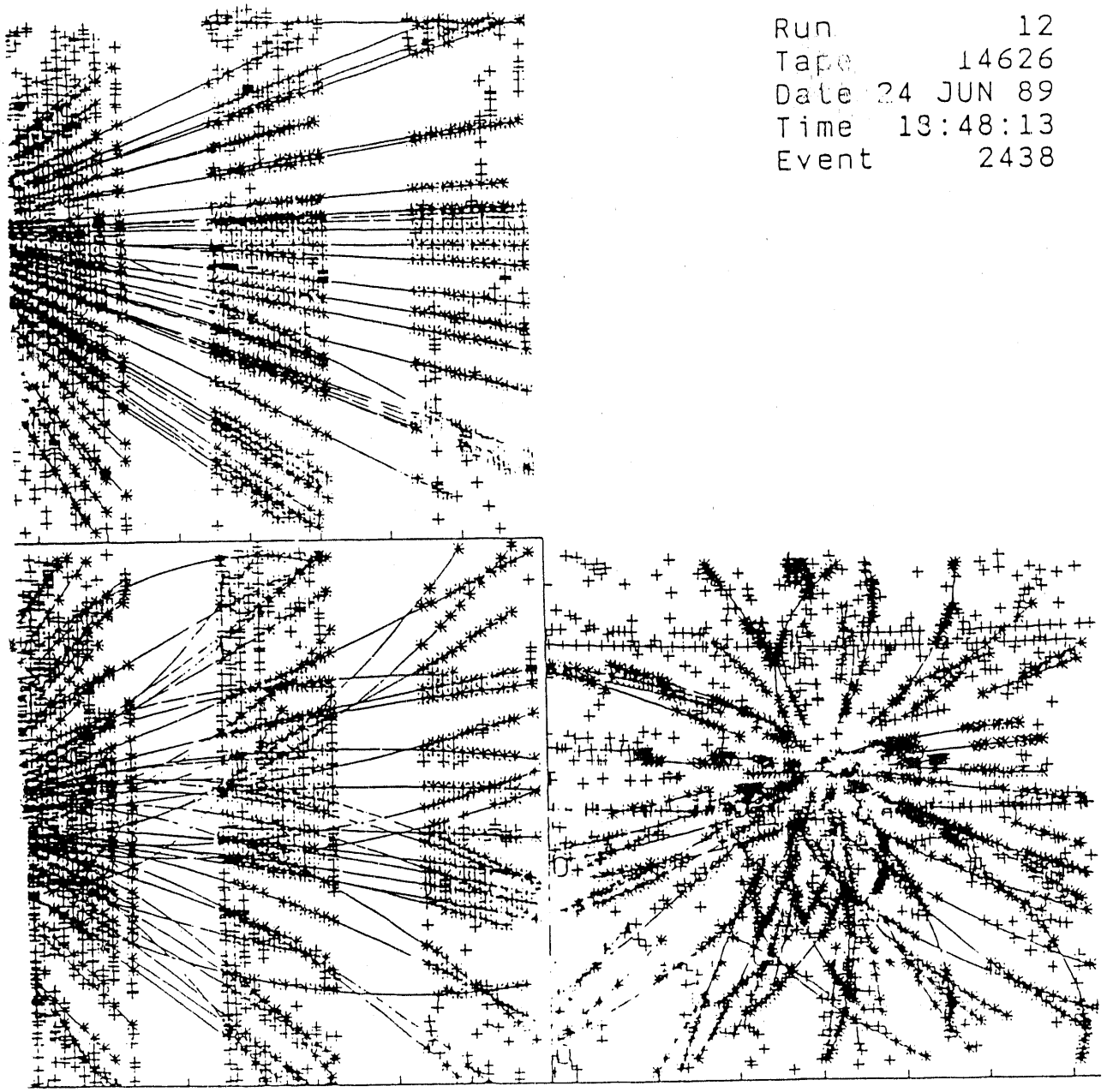

Figure 18a

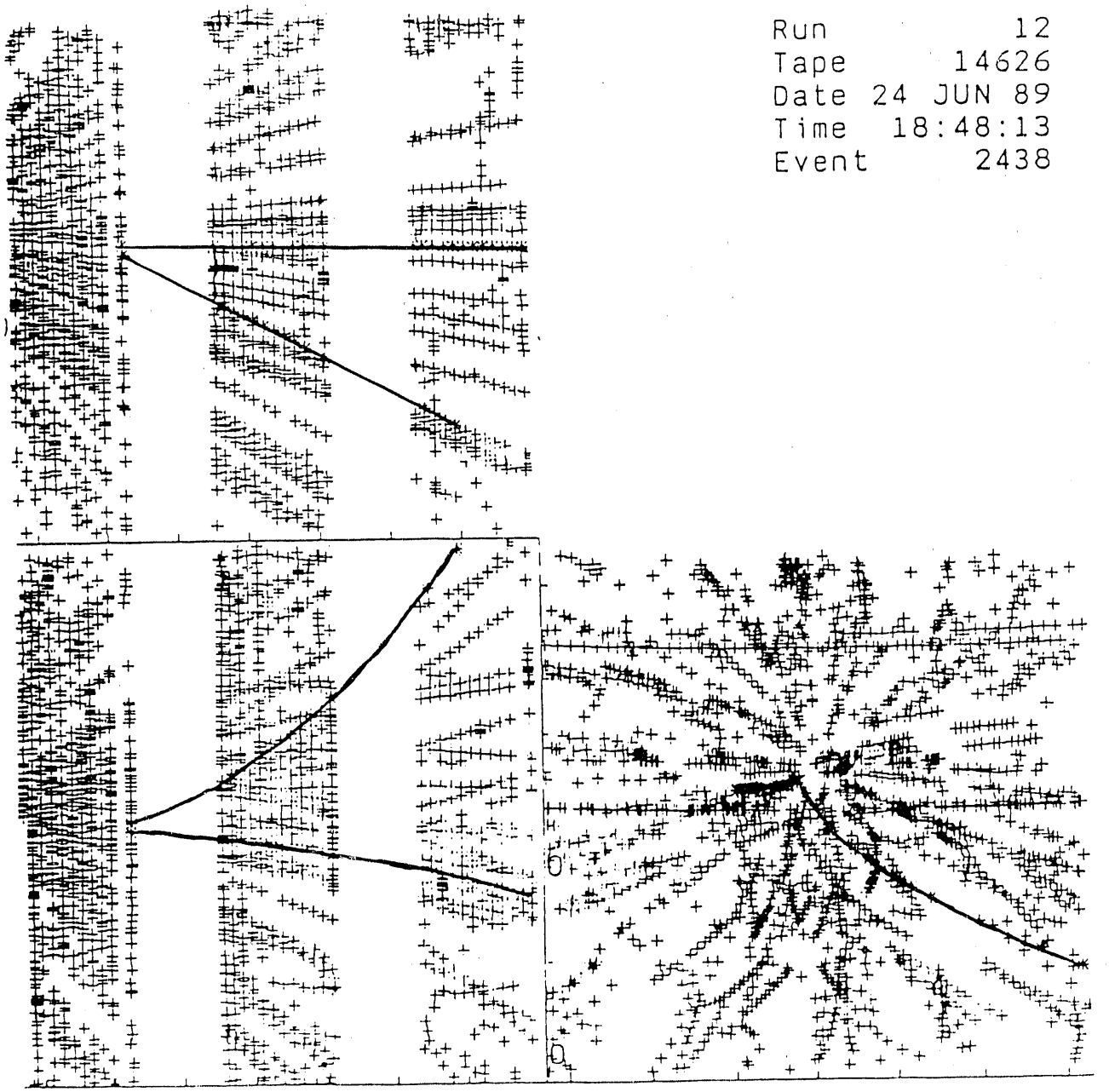

Figure 18b

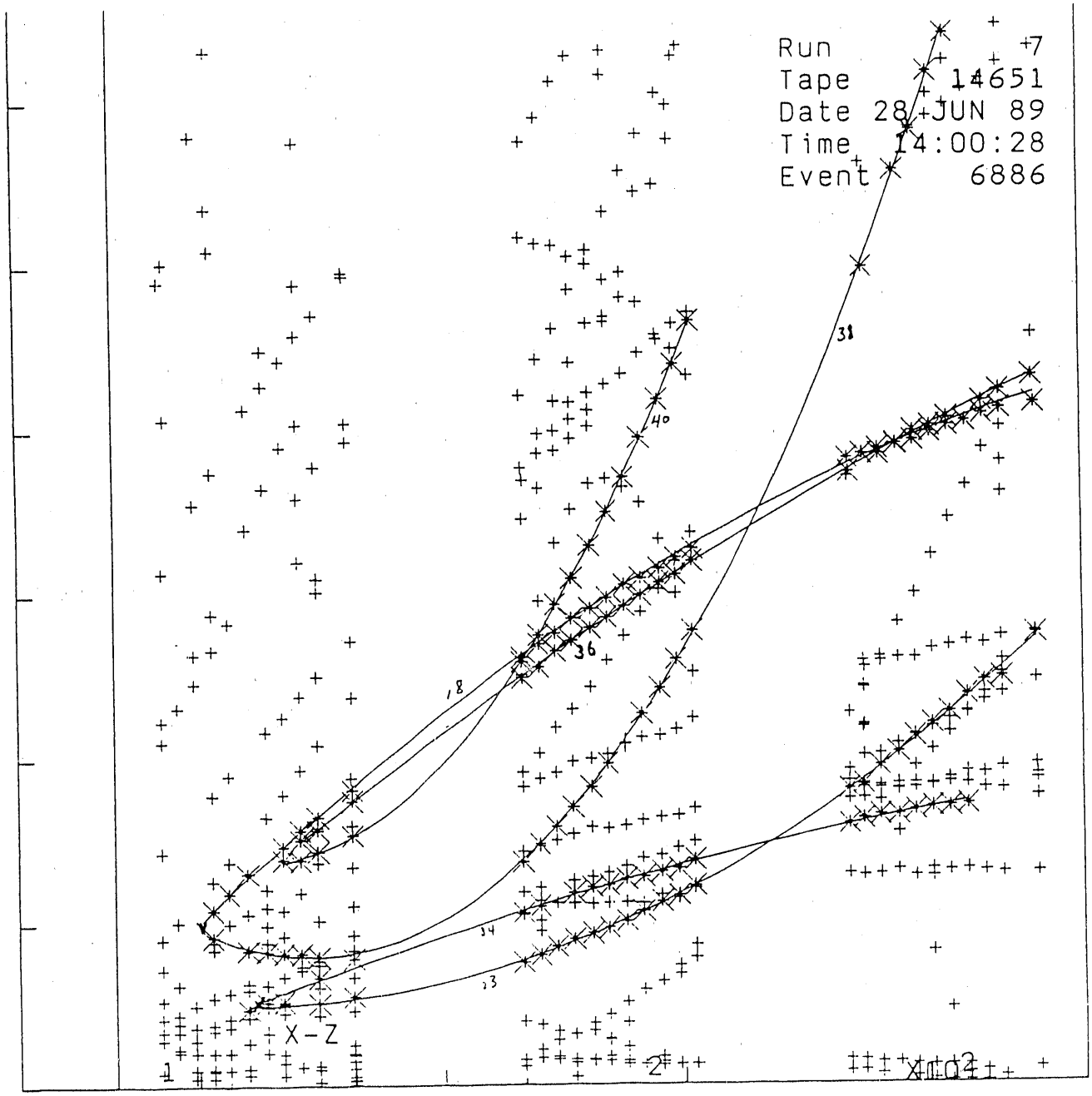
Run +7
Tape 14651
Date 28 JUN 89
Time 14:00:28
Event 6886
31
40
36
18
34
13
X-Z
1
2

Figure 19

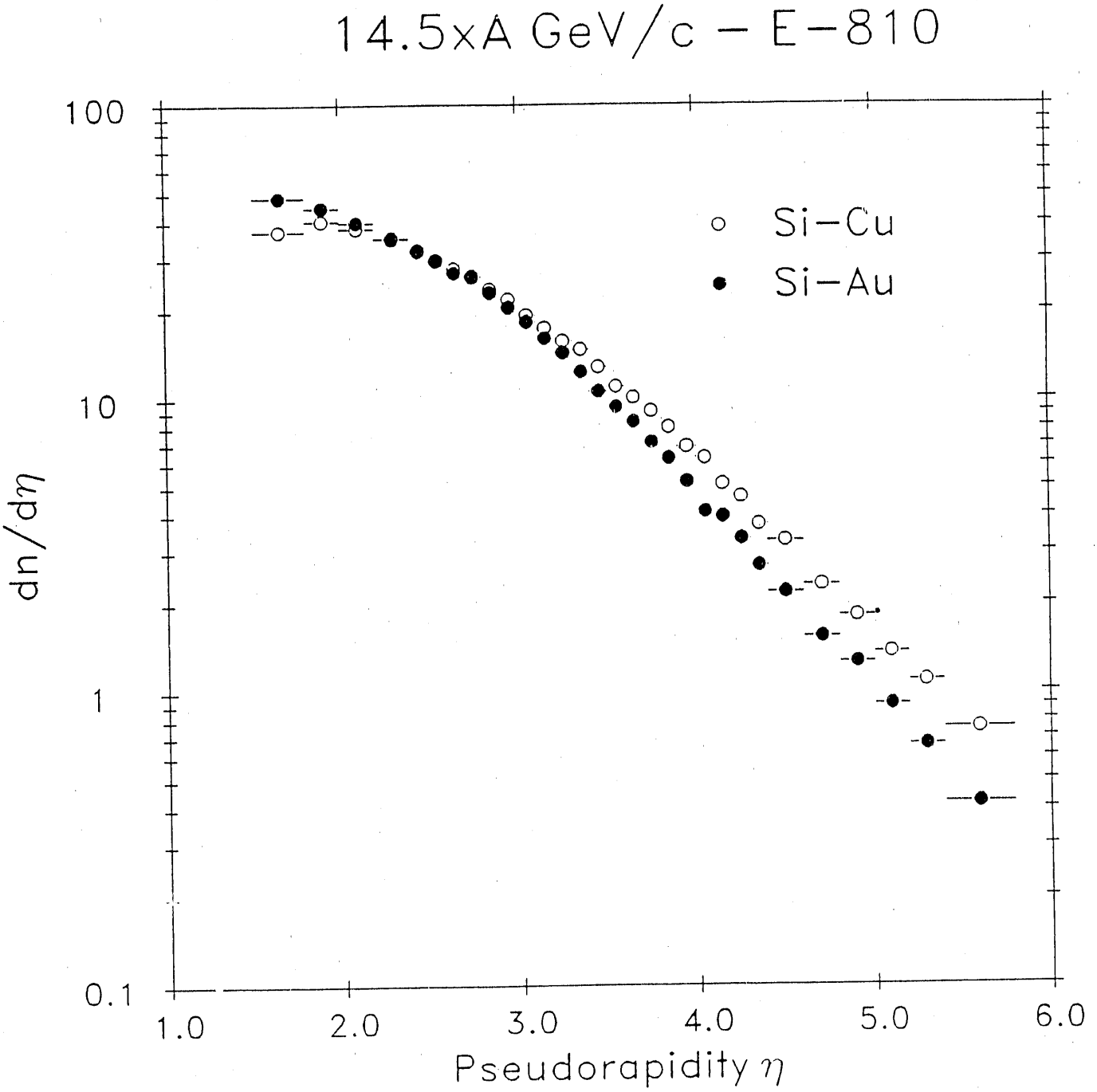
14.5xA GeV/c – E-810
100
10
1
0.1
dn/dη
Si–Cu
Si–Au
1.0
2.0
3.0
4.0
5.0
6.0
Pseudorapidity η

Figure 20

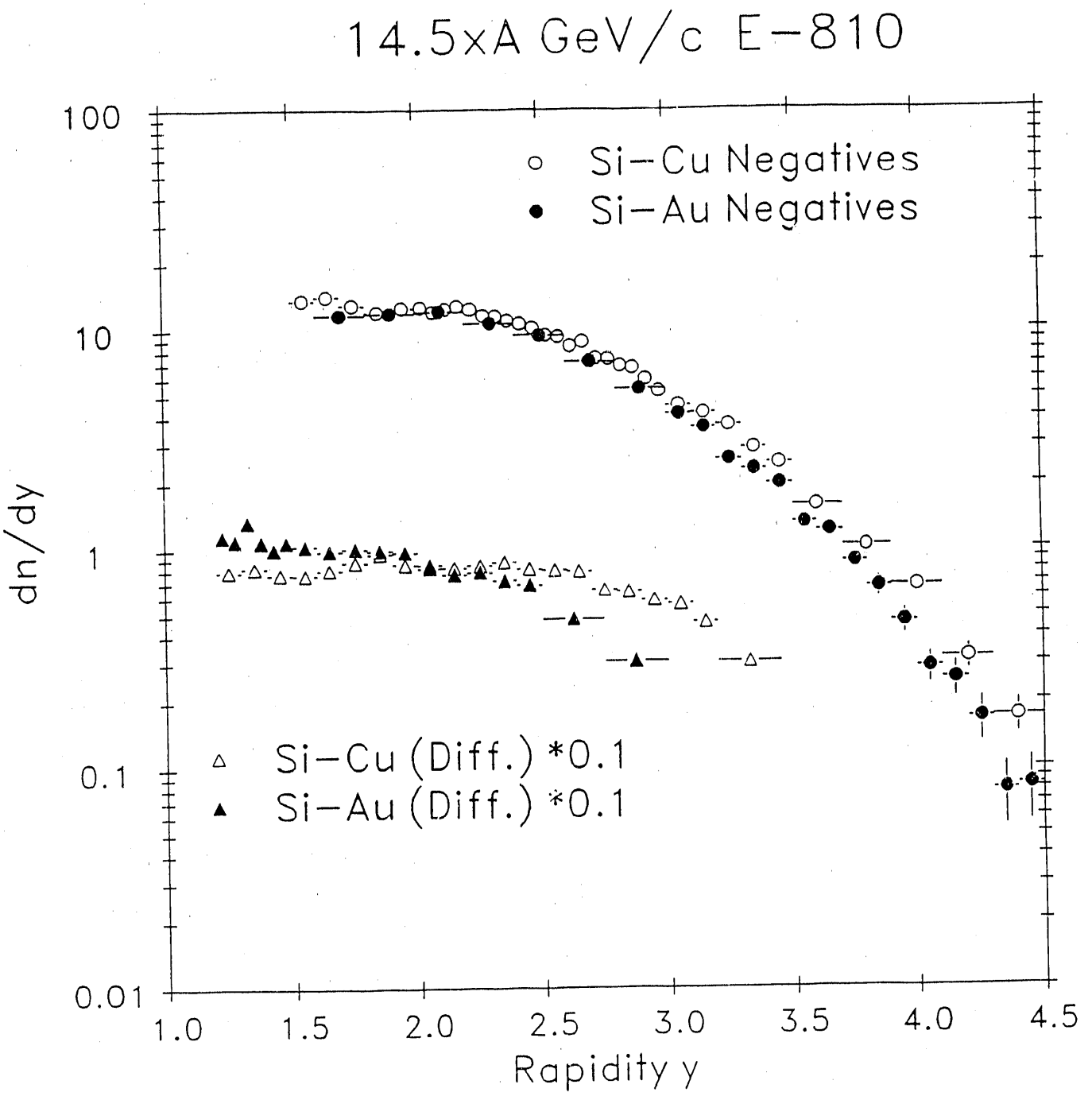
14.5xA GeV/c E-810
Si-Cu Negatives
Si-Au Negatives
Si-Cu (Diff.) *0.1
Si-Au (Diff.) *0.1
dn/dy
Rapidity y
100
10
1
0.1
0.01
1.0
1.5
2.0
2.5
3.0
3.5
4.0
4.5

Figure 21

BROOKHAVEN NATIONAL LABORATORY

August, 1990 BNL –

Hadron Spectroscopy at RHIC

S. U. Chung, W. Kern[a] and H. J. Willutzki

Physics Department, Brookhaven National Laboratory,Upton, NY 11973, U.S.A.

ABSTRACT

A description is given of the physics opportunities at RHIC regarding quark-gluon spectroscopy. The basic idea is to isolate with appropriate triggers the subprocesses pomeron + pomeron → hadrons and $\gamma^* + \gamma^* \rightarrow$ hadrons with the net effective mass of hadrons in the range of 1.0 to 3.0 GeV, in order to study the hadronic states composed of u, d, and s and gluons. The double-pomeron interactions are expected to produce glueballs and hybrids preferentially, while the two-offshell-photon initial states should couple predominantly to quarkonia and multiquark states. A plethora of J^{PC}-exotic mesons can be produced either directly in both types of interactions or in association with a single recoil photon in the final state.

[a] Permanent address: Physics Department,
Southeastern Massachusetts University,
N. Dartmouth, MA 02747

1. Introduction

In this note is described a conceptual design for carrying out a study of quark-gluon spectroscopy at RHIC.

The idea is derived from a douple-pomeron exchange trigger which was successfully implemented in R807 (an ISR experiment at CERN)[1]. The resulting $\pi^+\pi^-$ (see Fig.1) and K^+K^- spectra provided key ingredients in the identification of three $J^{PC} = 0^{++}$ states with masses near 1.0 GeV, one of which may be the scalar glueball[2].

For the trigger to succeed, it is necessary that for $p \times p$ the recoiling beam particles come off at a very small angle, $\theta \leq 2mr$. At RHIC energies this corresponds to installing a set of four 'Roman pots,' two on each side up and down, 10m away from the intersection region. Precision 5x5cm mini-drift chambers and scintillation counters will be installed in each Roman pot to detect and trigger on the scattered beam particles. The intersection region will be instrumented with a 4π-detector consisting of cylindrical drift chambers, ring-imaging Cerenkov counter and lead-scintillator barrel counters, all within a 5.4m-long solenoid magnet with a 3.6m coil diameter, patterned after the Mark III[3] and the ARGUS apparatus.

It was shown in R807 that imposition of momentum balance in the direction perpendicular to that of the beam particles results in pure exclusive events, as follows:

$$pp \rightarrow p\left(\pi^+\pi^-\right)p$$

$$pp \rightarrow p\left(K^+K^-\right)p$$

where the systems shown in the parentheses indicate the particles detected in the central detector. In the proposed RHIC experiment, the central detector will be optimized for charged as well as neutral particles with momenta up to 3 GeV/c, so that the following

reactions can be studied:

$$pp \rightarrow p(\eta\eta)p$$
$$pp \rightarrow p(\omega\omega)p$$
$$pp \rightarrow p(\phi\phi)p$$
$$pp \rightarrow p(\eta\pi\pi)p$$
$$pp \rightarrow p(\omega\pi\pi)p$$
$$pp \rightarrow p(K\bar{K}\pi)p$$
$$pp \rightarrow p(p\bar{p}\pi)p$$

where the parentheses indicate again the central system.

The momentum transfer squared from initial to final protons is given by

$$-t \simeq (p\alpha)^2 \simeq q^2 \simeq 0.025 \text{ (GeV/c)}^2$$

where $p = 250$ GeV/c is the momentum of the initial proton and $\alpha \simeq 2mr$ is the scattering angle of the proton in laboratory and $q \simeq 0.5$ GeV/c is the momentum of the final proton perpendicular to the beam. Since the slope of $-t$ distributions is expected to be around 10 GeV^{-2} at the top end of RHIC energy[4], the value $-t$ is sufficiently small to guarantee a pomeron exchange, and a double pomeron exchange reaction will result if both the final protons come off with $-t \leq 0.025$ (GeV/c)^2. In this case the central rapidity region corresponds in effect to the reaction

$$\mathbf{PP} \rightarrow \text{hadrons}$$

where **P** stands for a pomeron and the $\sqrt{s}$ for this subprocess ranges from 1.0 to 3.0 GeV. The upper limit on the $\sqrt{s}$ is not an inherent limitation; for a study of the states with the c quark, it should be extended to 5.0 GeV.

Let M denote the invariant mass of the total hadronic system, i.e. the $\sqrt{s}$ for the process given above. Then,

$$M^2 \simeq \epsilon_1\epsilon_2 (2p)^2 + t_1 + t_2 - 2\mathbf{q_1} \cdot \mathbf{q_2}$$

where subscripts 1 and 2 denote final deflected beam particles and $1 - \epsilon$ stands for the Feynman x variables[5]. Replacing $-t$ by q^2, one obtains

$$M^2 \simeq \epsilon_1\epsilon_2 (2p)^2 - (\mathbf{q_1} + \mathbf{q_2})^2$$

From this one sees that

$$\epsilon_1 \sim \epsilon_2 \sim \frac{M}{2p} \simeq 4 \times 10^{-3}$$

for $M = 2$ GeV and $p = 250$ GeV/c.

According to S. Y. Lee (BNL), one can choose an insertion mode in which the angular dispersion of the beam can be held to as low as $1.0mr$ at 10m from the intersection. At this point, the deflected particles may range from 10mm to 40mm measured from the beam center. This corresponds to q in the range of 0.25 GeV/c to 1.0 GeV/c for a proton beam at 250 GeV/c. Within the Roman pots there will be a set of four drift-chamber modules and two scintillation counters, each with an active area measuring 50x50mm.

The same experimental setup can be applied to heavy-ion collisions, e.g. those involving gold. M. Rhodes-Brown (BNL) points out that in the extreme low-momentum-transfer region the photon-photon interactions become competitive with the double-pomeron production,

$$\sigma \sim (Z\alpha)^4 \sim 0.1$$

for $Au \times Au$ at 100 GeV/u. The heavy ions of RHIC thus provide an opportunity for a study of two offshell-photon interactions,

$$\gamma^*\gamma^* \rightarrow \text{hadrons}$$

where $\sqrt{s}$ for this subprocess is in the range 1.0–3.0 GeV. Note that the photons involved are highly offshell indeed; the $-t$ corresponding to the photon is given by

$$-t \simeq q^2 \simeq (p \times 1mr)^2 \simeq 20\ (\text{GeV/c})^2$$

where $p = 197 \times 100$ GeV/c and $1mr$ is the allowed angular dispersion of the beam.

The coherent production of hadrons by the two-photon process involves extremely sharp $-t$ distributions. According to A. Skuja and D. H. White[6], the slope of the $-t$ distributions is 700 GeV^{-2} for $Au \times Au$ at 100 GeV/u, indicating that the beams simply pass through undeflected in the region where the cross section is appreciable. The energy loss is also extremely small,

$$\epsilon_1 \sim \epsilon_2 \sim \frac{M}{2p} \simeq 5 \times 10^{-5}$$

for $M = 2$ GeV and $p = 197 \times 100$ GeV/c. It is seen that this loss factor is well within the allowed beam dispersion of RHIC.

It therefore follows that a proper $\gamma^*\gamma^*$ trigger calls for something other than the Roman pots, i.e. it has to rely on a veto on the deflected beam, by a set of four lead-scintillation sandwich barrel counters located at 10m and 40m away from the intersection point. A barrel counter consists of six truncated wedge detectors with widths 5cm and 20cm and 50cm long. Its design is identical to that of the EM calorimeter in the central detector, as described in the next section. Note that each barrel counter covers radial distances down to 5cm radius from the beam line. With this setup, one can span the deflection angles from $1.25mr$ to $5mr$.

It is necessary, in addition, to veto on the diffractive dissociation of the beam. For the purpose, the end iron-plates of the magnet will be cut out at 100cm radius, and a hadron calorimeter will be installed, which consists of 30 iron-scintillation sandwiches, designed to veto hadrons above 10 GeV/c. Additional material on the calorimeter is given in the next section.

The quark-gluon spectroscopy is a study of hadrons with mass in the range between 1.0 and 3.0 GeV, if the constituent quarks are comprised only of u, d and s. The initial state of the double-pomeron production is in reality a flavorless and colorless gluonic bundle. It follows therefore that the final state should be rich in gluonic excitations, i.e. glueballs and hybrids. In contrast, two offshell photons couple preferentially to charged quarks, e.g. $u\bar{u}$ or $c\bar{c}$ if the energy is high enough, leading to the production of quarkonia and multiquark states.

What quantum numbers are allowed for the initial state? Assuming a pomeron to be a $J^{PC} = 0^{++}$ state, one can expect for the double-pomeron initial state $I^G = 0^+$ and $J^{PC} = 0^{++}, 2^{++}, 4^{++}, etc.$ For the two-offshell-photon initial state, one may expect $I^G = 0^+, 1^-$ and $J^{PC} = (0,1,2,3,4,..)^{++}, (0,1,2,3,4,..)^{-+}$. It should be noted that $J^{PC} = (1,3,5,..)^{-+}$ is exotic and cannot couple to quarkonia. Observation of such a state would imply an exotic multiquark state. Study of J/ψ radiative decays proved to be a prolific source of information for hadronic states. One can perform a similar study at RHIC by examining the hadronic system recoiling off a single photon.

2. Central Detector

The central detector consists of a neutral and charged particle detection device with a 4π coverage, all housed in a moderate-size solenoid magnet with an inner radius of 155cm and 540cm long outside. The magnet uses Al coils inside the yoke producing a field strength of 0.5T. It is designed to identify up to a dozen particles with momenta in the range 0.05–2.50 GeV/c, for a study of meson systems with mass 1.0–3.0 GeV. The central detector is thus given the name QGS, for Quark-Gluon Spectrometer (see Fig.2).

The QGS consists of a drift-chamber module surrounding the beam pipe, followed by a ring-imaging Cerenkov counter (RICH), a time-of-flight (TOF) hodoscope and a lead-scintillation sandwich EM calorimeter, all within the magnet coil. Each end of the magnet is instrumented with a hadron calorimeter. These items are described briefly below.

The drift-chamber module is 3.2m long along the beam; it starts at a radius of 5cm and extends to 75cm. The size of drift cells is dictated by the time interval of 225ns between bunch crossings. The whole module is divided into 9 layers, each containing two axial sense wires and two stereo wires at angles from $40mr$ to $80mr$. In all there will be some 9100 sense wires. The rms error on the transverse momentum is estimated to be

$$\frac{\delta p_\perp}{p_\perp} = 1.5 \, , p_\perp (\text{ GeV/c})$$

assuming a measurement accuracy of $200\mu m$ and a field of 0.5T. The angular resolution is, from multiple scattering,

$$\delta\theta = \frac{1.3mr}{p_\perp (\text{ GeV/c})}$$

The particle identification is provided by the dE/dx measurement. Assuming an average of 36 measurements per track, the resolution is expected to be 15% FWHM. This provides a 3σ π/K separation up to about 0.6 GeV/c.

The RICH detector envisaged here is patterned closely after the conceptual design worked out by B. Ratcliff[7]. It extends from a radius of 75cm to 100cm and is 370cm long on the outside. The front segment consists of a 1cm-thick liquid Freon (C_6F_{14}) with an index of refraction $n = 1.277$, so that a relativistic particle produces Cerenkov light of 17cm radius at the end of a 13cm drift region. It is then followed by a 4.4cm-thick photon-conversion region containing C_2H_6 and TMAE (Tetrakis Dimethyl Amino Ethylene). The

readout is accomplished by a system of 2950 10x10cm electronic pads. The drift time is about $25\mu s$, which implies that this RICH counter is not a trigger device. The offline π/K separation is impressive, starting at 0.03 GeV/c and extending to 3 GeV/c.

The TOF system is located at a radius of 100cm and is 3.8m long. It consists of 128 5x5cm scintillation counters, each viewed by two photomultipliers. The resolution is conservatively estimated to be 250ps, providing a 3σ π/K separation from 0.08 GeV/c to 0.6 GeV/c. Thus it can be used as an independent check of both the drift-chamber module and the RICH counter. It can also be used as a component in the charged particle triggers.

The EM calorimeter covers radii from 105cm to 155cm and is 480cm long outside. It consists of 3200 10x10cm towers, each with 84 layers of 6mm lead-scintillation sandwiches (1mm of lead and 5mm of plastic scintillator) for a total of $15X_0$ and viewed by a photomultiplier through a wave-length shifter. A similar device was used by ARGUS[8]. The energy resolution is expected to be

$$\frac{\delta E}{E} = \frac{7\%}{\sqrt{E(\text{ GeV})}}$$

for the photon energy from 0.07 GeV to 3.0 GeV. This device can be used to detect $\pi^0 \rightarrow \gamma\gamma$, $\eta \rightarrow \gamma\gamma$ and $\omega \rightarrow \pi^0\gamma$.

The end caps of the magnet have cutouts with radius 100cm, and two hadron calorimeters with the active areas at radii from 5cm to 100cm will be installed in this space. The calorimeter consists of 30 iron-scintillation sandwiches. Both the iron plate and the plastic scintillator are 1cm thick, and the periphery of the scintillator is edged with a wave-length shifter, which is read out by a photomultiplier. It is estimated that the energy resolution is

$$\frac{\delta E}{E} = \frac{60\%}{\sqrt{E(\text{ GeV})}}$$

so that a 10 GeV/c particle can be measured with an accuracy of about 20%. For the $Au \times Au$ run, the two hadron calorimeters will be used to veto on any particle with energy greater than 10 GeV/c. It is expected that about 90% of all the diffractive dissociation events can thus be eliminated at the trigger level.

3. Triggers

The trigger for **PP** interactions relies on a set of four scintillation counters within the Roman pots. For $p \times p$ runs, two triggers are possible with the Roman pots, 'up-up' and 'down-down.' This means that both of the counters above (below) the beam line at either side of the intersection region are triggered for 'up-up' ('down-down'). The triggers will be augmented with signals from the QGS, utilizing among others the hits in the EM calorimeter. Each hit above the minimum energy threshold, but below the maximum allowed energy, e.g. 10 GeV, is treated with equal weight; a fast microprocessor sums up independently the x, y and z projections of the location of the hit with respect to the midpoint of the intersection region. The trigger requires that the three sums are within a small preset range. This algorithm ensures that an event with a large missing energy in any direction will be eliminated, on the average. Note also that this technique treats charged and neutral particles on an equal footing.

For $Au \times Au$ runs, instead of the Roman pots, the trigger relies primarily on signals from the QGS to pick out two-photon events, accompanied by vetos at two end-cap hadron calorimeters and the four lead-scintillation barrel counters located 10m and 40m away from the intersection region. The vetoes guard against the small-angle beam deflections and the diffractive dissociation of the beams.

A Monte Carlo study is planned to assess the efficacy of the x-, y- and z-projection methods described above in selecting production of low-mass hadrons in the central region.

4. Conclusions

In this note a brief description is given of an exciting opportunity to carry out a hadron spectroscopy experiment at RHIC. The key idea here is that by concentrating on the extreme double-peripheral region at RHIC, the machine is used to produce hadronic systems at low $\sqrt{s}$ in the range 1.0–3.0 GeV.

The subprocesses responsible for the hadronic system in the central region may be expressed either as pomeron + pomeron → hadrons or as $\gamma^* + \gamma^* \rightarrow$ hadrons. The double-pomeron interactions are expected t , produce glueballs and hybrids preferentially, while the two-offshell-photon initial states should couple predominantly to quarkonia and multiquark states. A whole gamut of J^{PC}-exotic mesons $(0^{+-}, 0^{--}, 1^{-+}, 2^{+-}, 3^{-+}, 4^{+-}, ..)$ may be seen either directly in both types of interactions or in association with a single recoil photon in the final state. Another important distinction is that the hadronic system from a double-pomeron interaction has zero net flavor, whereas an $I^G = 1^-$ meson can couple readily to a two-photon initial state.

The salient feature of this proposal lies in the fact that, for the first time, a study of the pomeron-pomeron interactions can be mounted with the same experimental setup as that of the photon-photon interactions.

The authors acknowledge with pleasure the opportunity for learning about the RHIC machine and the experiments being proposed at the 1990 BNL RHIC Workshop. They had useful conversations with S. Y. Lee and M. Rhodes-Brown of BNL during the Workshop.

References

1. T. Akesson et al., Nucl. Phys. B264, 154 (1986);
   P. C. Cecil, Ph. D. Thesis, Cavendish Laboratory, Cambridge, England, Rutherford preprint RAL -T -004 (1984).
2. K. L. Au, D. Morgan and M. R. Pennington, preprint RAL -86 -076 (1986), Phys. Rev. D35, 1633 (1987).
3. D. Bernstein et al., NIM Vol. 226, 301 (1984).

4. K. Goulianos, 'Diffractive interactions of hadrons at high energies,' Physics Reports, Vol. 101, No. 3 (1983).

5. S. U. Chung, 'Kinematics, Phase Space and Phenomenological Amplitudes for Double-Pomeron Exchange Reactions,' BNL Internal Report OG-734 (1983).

6. A. Skuja and D. H. White, 'Two-Photon Phyiscs at RHIC,' RHIC Workshop, BNL-51921 (1985), p. 289.

7. B. N. Ratcliff, Proceedings of the Tau-Charm Factory Workshop, SLAC-Report-343 (1989), p. 940.

8. W. Hofmann et al., NIM Vol. 163, 77 (1979).

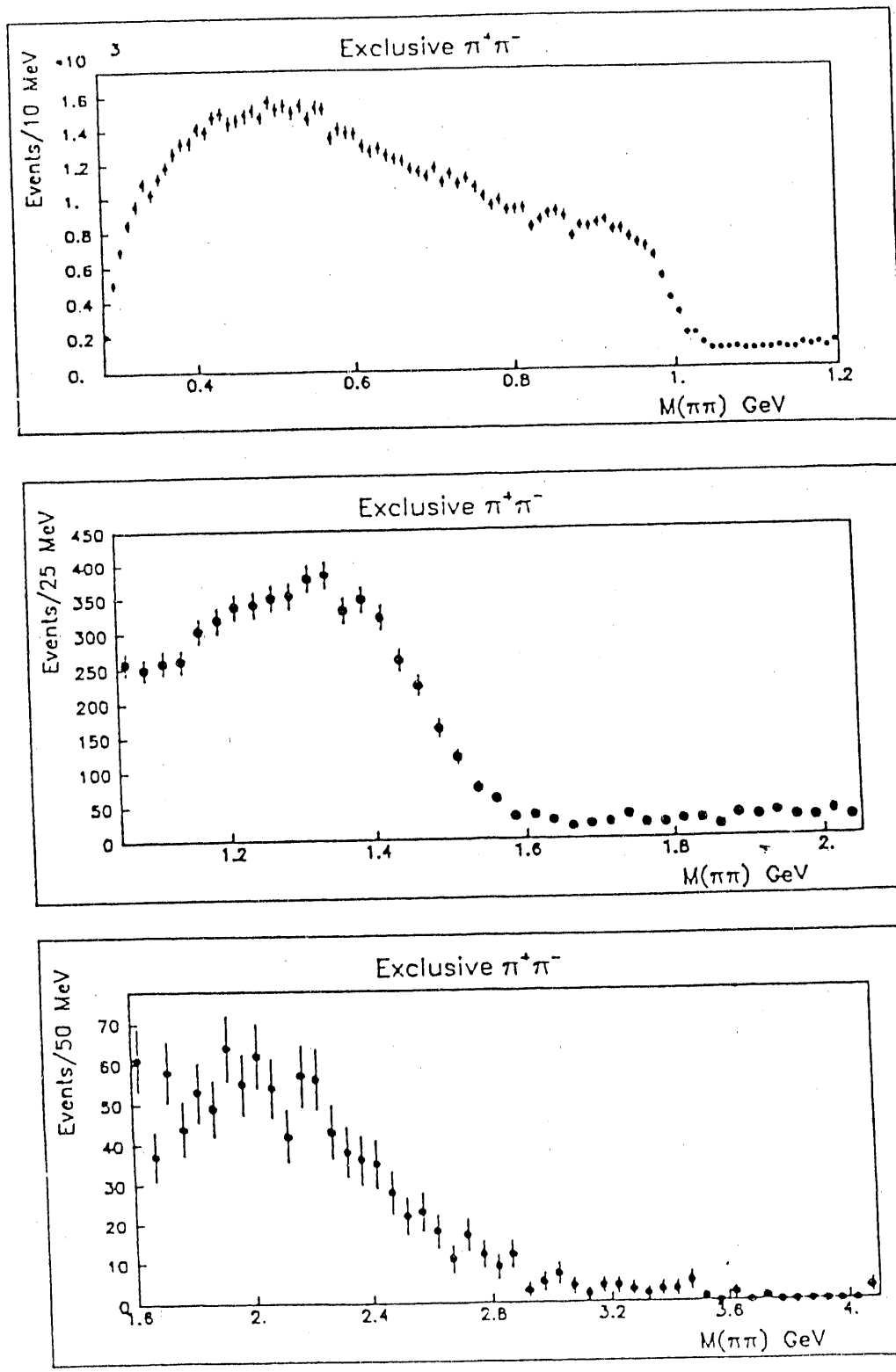

Figure 1: $\pi^+\pi^-$ spectra for $pp \to p(\pi^+\pi^-)p$ at $\sqrt{s}$ =63 GeV.

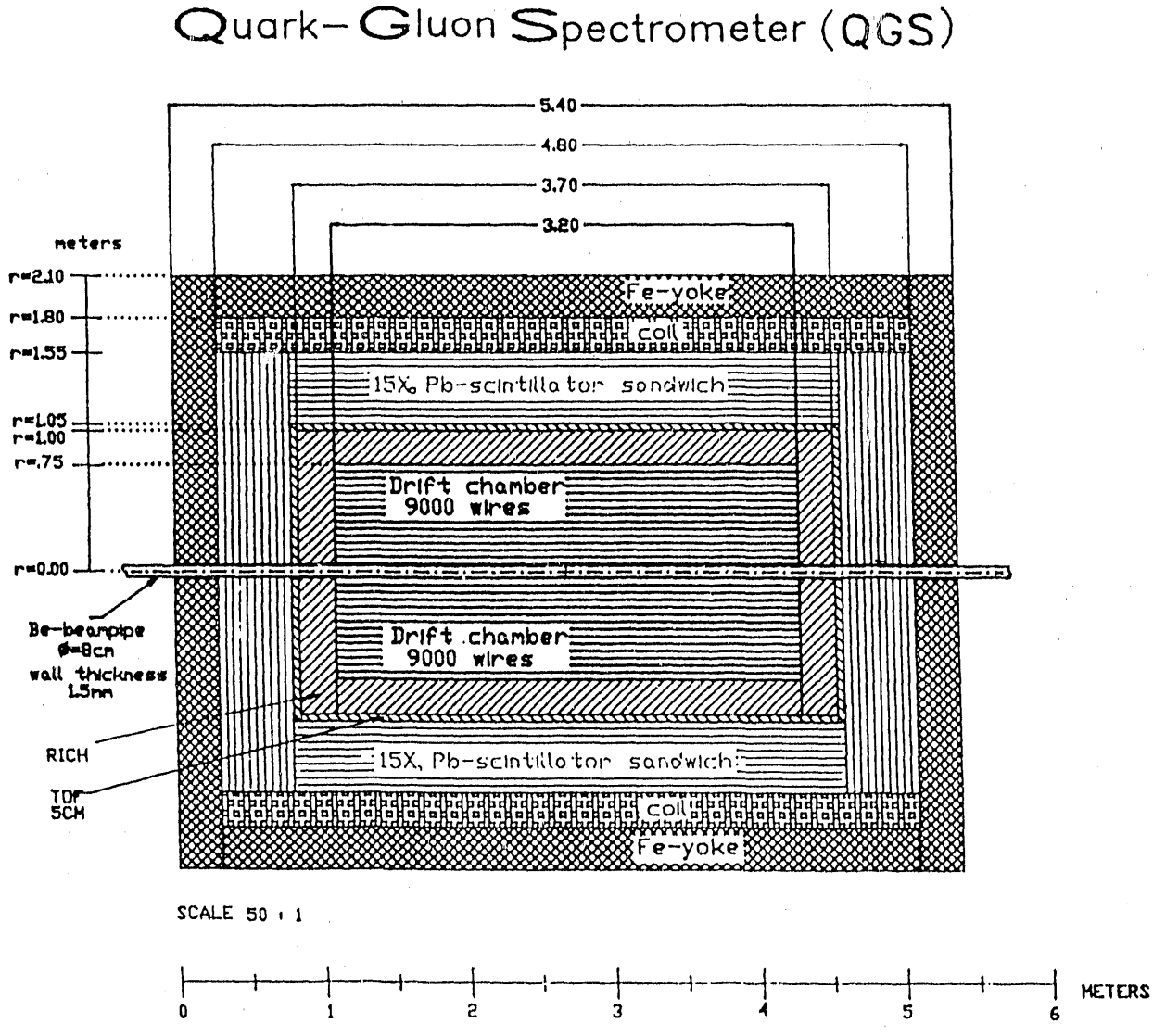

Figure 2: The Central detector: Quark-Gluon Spectrometer (QGS)

Efficiency and Background Simulations for J/ψ Detection in the RHIC Di–Muon Experiment

Charles F. Maguire

Centre de Recherches Nucléaires, Strasbourg, FRANCE
Department of Physics and Astronomy, Vanderbilt University, Nashville, TN 37235

The RHIC Di–Muon experiment[1–4] has for one of its principle goals the investigation of J/ψ production and possible dimunition in the quark–gluon plasma expected to be formed in central collisions. Over the course of an extended period of discussions summarized in Ref. 1–4, the working group has identified the principle obstacles to such an experiment. Essentially the J/ψ production is inherently four orders of magnitude suppressed with respect to pion production in the central collision zone. Since the pions themselves decay to muons, one is faced with the prospect of a fierce combinatorial background from pion decay muons and from pions which cannot be directly resolved from muons. The sole chance of success is to introduce an absorber system which will operate in a delicate balance between filtering out most of the initial pions, but not so effective as to destroy the efficiency and resolution for the soft muon pairs arising from the true J/ψ production.

The working group has presently arrived at a solution which consists of a split, elliptically shaped absorber with its semi–major axis along the beam direction and extending over approximately 15 pion interaction lengths. The transverse, semi–minor axis will cover some 9 pion interaction lengths. The split occurs at 9 interaction lengths in the beam direction, and at 4.5 interaction lengths in the transverse direction. Between the first and second parts of the absorber is to be a 1 to 2 meter magnetic field, momentum analysis region, whose task has been rendered more tractable by the particle suppression afforded in the first absorber.

This contribution reports on the results of simulations for the performance of such an absorber, in particular for the backgrounds arising from combinatorial pairs of tracks emerging from the first absorber. These simulations were carried out using the GEANT detector program[5] into which has been incorporated an accurate representation of the absorber configuration including a small central cavity and 2° conical openings for the beam pipes. Analytic forms for pion and kaon background sources were utilized whose spectra in rapidity and trans-

verse momenta are equivalent to those coming from the HIJET or VENUS reaction codes. The pion and kaon particles were tracked through the first absorber by the GEANT program using the GHEISHA hadronic interaction interface. All particles emerging from the first absorber, including unreacted direct particles, shower products, and decay offspring, had their three–position vector coordinates, four–vector momenta, and particle identification number stored in output files for subsequent kinematic analysis.

An invariant mass is to be constructed for the unlike sign particle pairs exiting first absorber, assuming each partner to be a muon and requiring that each particle have at least 0.3 GeV total energy. The invariant mass construction in turn requires that the four momentum of each particle be reconstituted to its value before entering the first absorber. This is done by calculating the energy loss in an energy and position dependent fashion based on calibration curves developed for muons of specified initial energy and direction. The same procedure was also applied to the true muon pairs arising from the decay of a random J/ψ source having the same rapidity but higher transverse momentum distribution. The peak of the reconstructed true J/ψ invariant masses had a width of 0.13 GeV/c^2 (RMS), so an acceptance window of ± 0.5 GeV/c^2 was chosen as the condition for a background invariant mass to masquerade as a J/ψ.

A total of 500,000 pions and 50,000 kaons (half positive, half negative) were tracked in this simulation, and all their products were regarded as a single ensemble in the invariant mass reconstruction. That is to say, about 7×10^{10} initial pairs are possible. The reaction codes predict an average of 10,000 pions per central event, so here one is looking at the equivalent of 50^2 events, or pairs among 25 million pions taken 10,000 at a time. It can be shown (see Mark Tincknell in Ref. 1) that one should obtain not more than 500 fake J/ψ pairs in such a set in order to have a feasible experiment.

From this background source, some 11,700 particles were seen to emerge from the first absorber, with a particle ID distribution as detailed in Table 1. The 32 million possible pairs available from such a set were not actually calculated, but instead immediate cuts were made in order to reduce the computational effort. The first cut was simply a vertex cut requiring that at the exit of the absorber the particle's position and three–momentum vector be consistent with the original source vertex. The consistency condition, like the invariant mass reconstruction, was developed as an energy and position dependent parameterization based on a study of direct muons of specified energy and initial direction. As seen in Table 1,

the vertex condition reduced the accepted inter–absorber track count by almost 60%, but this still allowed some 66,000 fake J/ψ masses which is far in excess of any feasibility condition.

TABLE 1. Fake J/ψ Rejection from a Set of 500,000 Pions plus 50,000 Kaons
Initial inter–absorber tracks > 0.3 GeV = 11,700 (87% π, 11% μ, and 2% K)

Cut Description	Accepted Tracks	Fake J/ψ Pairs[a]
Vertex Consistency (V)	4700	66,500
Second absorber hadron shower (H) + V	830	10,100
Timing cut (T) of 0.5 ns + H + V	165	237
$-2.2 <$ Y2 — Y1 $< +2.2$ (D) + T + H + V	165	0
V + H + D (no timing cut)	830	15
H + D (no timing or vertex cuts)	2171	562

[a]Invariant mass between 2.6 and 3.6 GeV/c^2

The second cut was on the effect of the second absorber which allows a last chance for emerging hadrons to shower. In spite of the large reduction in accepted inter–absorber tracks, this cut still left over 10,000 fake masses. A third cuts was then introduced on timing. While it has been well known that time–of–flight measurements would be useless to distinguish primary pions from muons of the same energy, it was realized in this simulation study that time–of–flight immediately after the first absorber might serve to discriminate secondary products from primary products even for those secondaries which had by chance escaped the vertex cuts. This is shown to be the case in row three of the table where it is seen that such a cut reduces the fake mass yield by 98% relative to just the vertex and second absorber cuts.

The final cut is not on individual particle parameters, but rather on the rapidity difference of the pair of particles. In Fig. 1 is shown a contour of true J/ψ accepted muon pairs as a function of the rapidity of each partner. The maximum of the yield is seen to lie along the ridge line Y2 = Y1 which just reflects the focussing power of the initial J/ψ rapidity. By contrast, the same contour plot for the fake pairs which had passed all other cuts (see Fig. 2) is seen to peak away from what now becomes a Y2 = Y1 valley line. In Fig. 3 is shown the projection of these respective contour plots along the Y2 — Y1 axis. The true J/ψ pairs have a width of 1.1 (RMS) on this axis, and fall remarkably well within a window left vacant by the fake pairs. Such a cut had been previously recognized by the working group as particularly effective, and

the present results give independent confirmation of that conclusion. For reference, Fig. 4 shows the contributing partners to the fake background before the rapidity difference cut. The particle ID numbers are those of GEANT (5=μ^+, 6=μ^-, 8=π^+, 9=π^-). For further elucidation, the muon particles originating from inter–absorber pion decay are designated by 5.5 and 6.5. It is seen that about 10% of the fake pairs have at least one such decay partner.

The background level is now simply 0 from this set of sources. Hence, one would conclude in this particular regard that the experiment is feasible. (Of course there will be other background sources such as Drell–Yan production and Open Charm semi–leptonic decay combinatorials, but these are expected to be smaller than the J/ψ yield and are intrinsically interesting in themselves.) The remaining rows in the table shows the resolving power of various sub–combinations of these four cuts. It is seen that removal of the time or the vertex conditions, while keeping the rapidity difference and second absorber conditions still allows adequate background rejection, or equivalently the proposed quadruple background rejection scheme is powerfully redundant.

Naturally, such background rejection would be worthless if the true J/ψ yield were itself inordinately reduced. This is not the case. As seen in Fig. 3, the integrated J/ψ efficiency is 44% after all the kinematic cuts, and this goes straightforwardly to 42% after the 2 sigma rapidity difference cut. The differential efficiency, as a function of rapidity and transverse momentum of the reconstructed J/ψ particle is shown in Fig. 5 for $0 < Y < 4$ and $0.3 < P_T < 8.0$ GeV/c. It is seen that the efficiency is at least 20% in all the bins, and this increases to unity with increasing transverse momentum and rapidity.

Summarizing, simulations made with the GEANT program indicate that there will be suffcient kinematic cuts available to reduce drastically, perhaps even to negligible amounts, the combinatorial backgrounds arising from absorber leakage in the RHIC Di–Muon experiment. Such background rejection is completely compatible with very respectable true J/ψ detection efficiency and resolution. It should be emphasized, however, that all of these results are in the realm of simulation, and that a vigorous detector R&D program is required to verify the output of the codes and correct inadequate or even wrong physics assumptions made therein.

The author thanks the members of the RHIC Di–Muon working group for their helpful comments and suggestions, especially Glenn Young, Sam Aronson, and Surrender Saini.

References

1. "Minutes of the Third RHIC Di–Muon Workshop" (Oak Ridge National Laboratory, Oak Ridge, TN, May 21–23, 1990, ed. Glenn R. Young and Felix E. Obenshain)

2. RHIC R&D Proposal 10, "Calorimeter/Absorber Optimization for the RHIC Di–Muon Experiment", S. Aronson, *et al.*, Brookhaven National Laboratory, September, 1988

3. "Status of the RHIC Di–Muon Experiment", S. Aronson, *et al.*, in Proceedings of the Second Workshop on Experiments and Detectors for a Relativistic Heavy Ion Collider (Brookhaven National Laboratory, May 25–29, 1987, ed. Hans Georg Ritter and Asher Shor)

4. "A Detector for Di–Muons Produced in the Relativistic Heavy Ion Collider", S. Aronson, *et al.*, in Proceedings of the Workshop on Experiments for a Relativistic Heavy Ion Collider (Brookhaven National Laboratory, April 15–19, 1985, ed. P.E. Haustein and C.L. Woody)

5. GEANT 3.13, R. Brun, *et al.*, CERN DD Division, Geneva, Switzerland

Figure Captions

1. Contour of rapidity Y1 *vs.* rapidity Y2 for true J/ψ muon pairs after cuts V + H + T (see Table 1).

2. Same contour as in Fig. 1 except the points are for fake J/ψ combinatorial pairs.

3. a) Projection along the Y2 — Y1 axis for the true J/ψ muon pairs shown in Fig. 1; b) projection along the Y2 — Y1 axis for the fake J/ψ combinatorial pairs shown in Fig. 2.

4. Contour of particle identification for the fake J/ψ combinatorial pairs shown in Fig. 2 (key: 5=μ^+, 6=μ^-, 8=π^+, 9=π^-; 5.5=μ^+ from inter–absorber pion decay, 6.5=μ^- from inter–absorber pion decay).

5. Efficiency for true J/ψ muon pair reconstruction as a function of rapidity and transverse momentum (note scale is logarithmic).

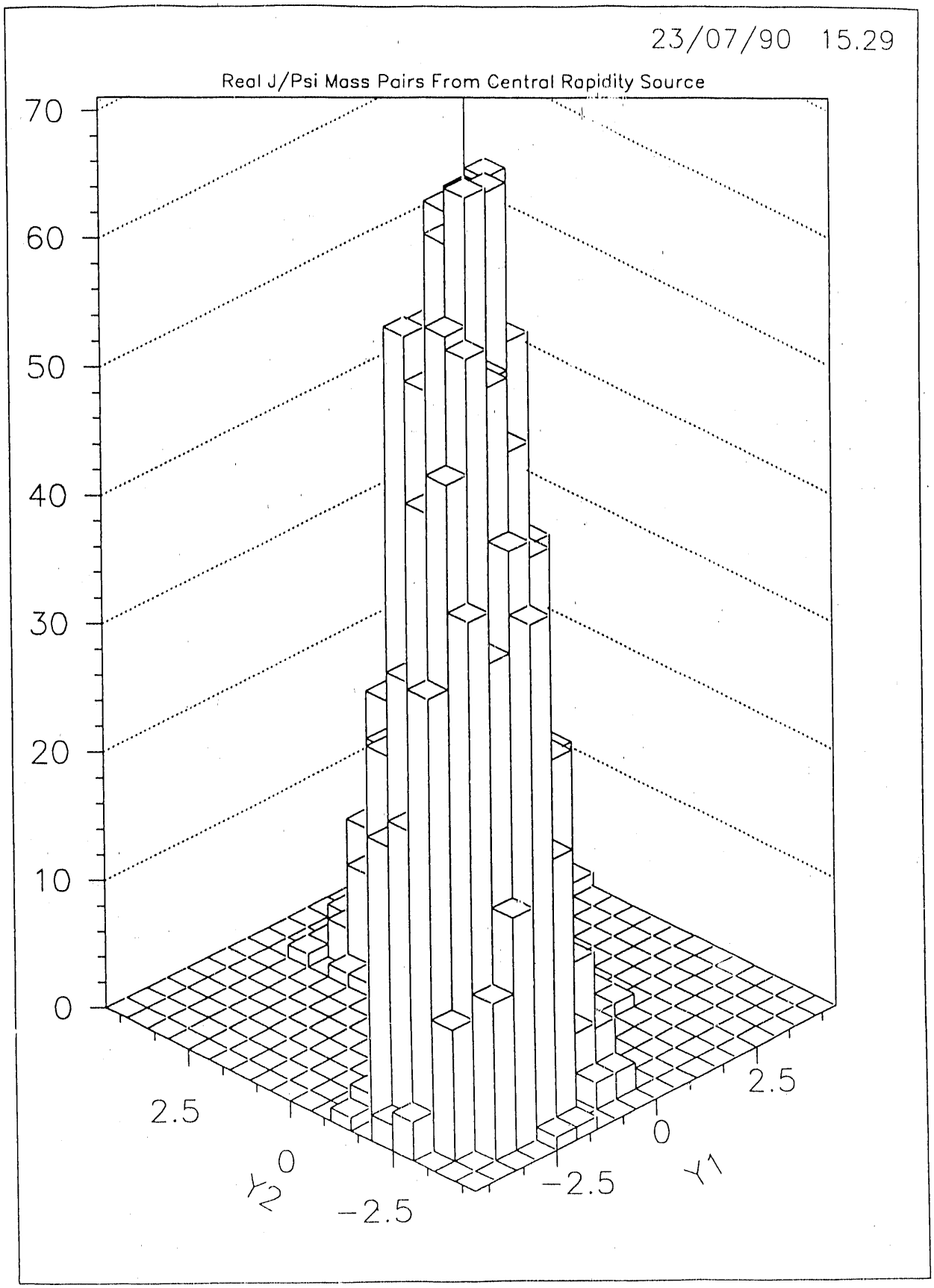
23/07/90 15.29
Real J/Psi Mass Pairs From Central Rapidity Source
70
60
50
40
30
20
10
0
2.5
0
-2.5
Y2
2.5
0
-2.5
Y1

1

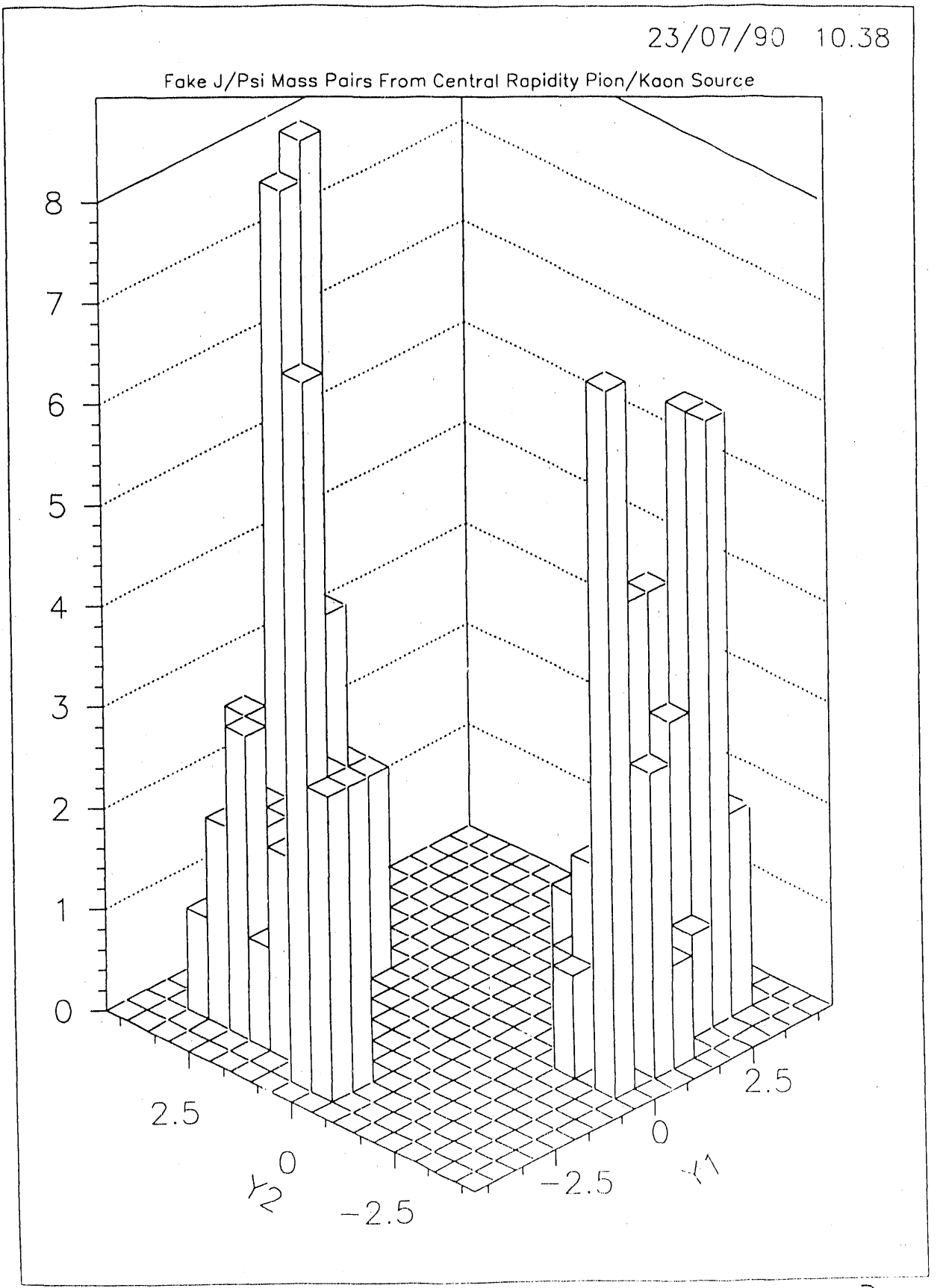
23/07/90 10.38
Fake J/Psi Mass Pairs From Central Rapidity Pion/Kaon Source
8
7
6
5
4
3
2
1
0
2.5
0
-2.5
Y2
2.5
0
-2.5
Y1

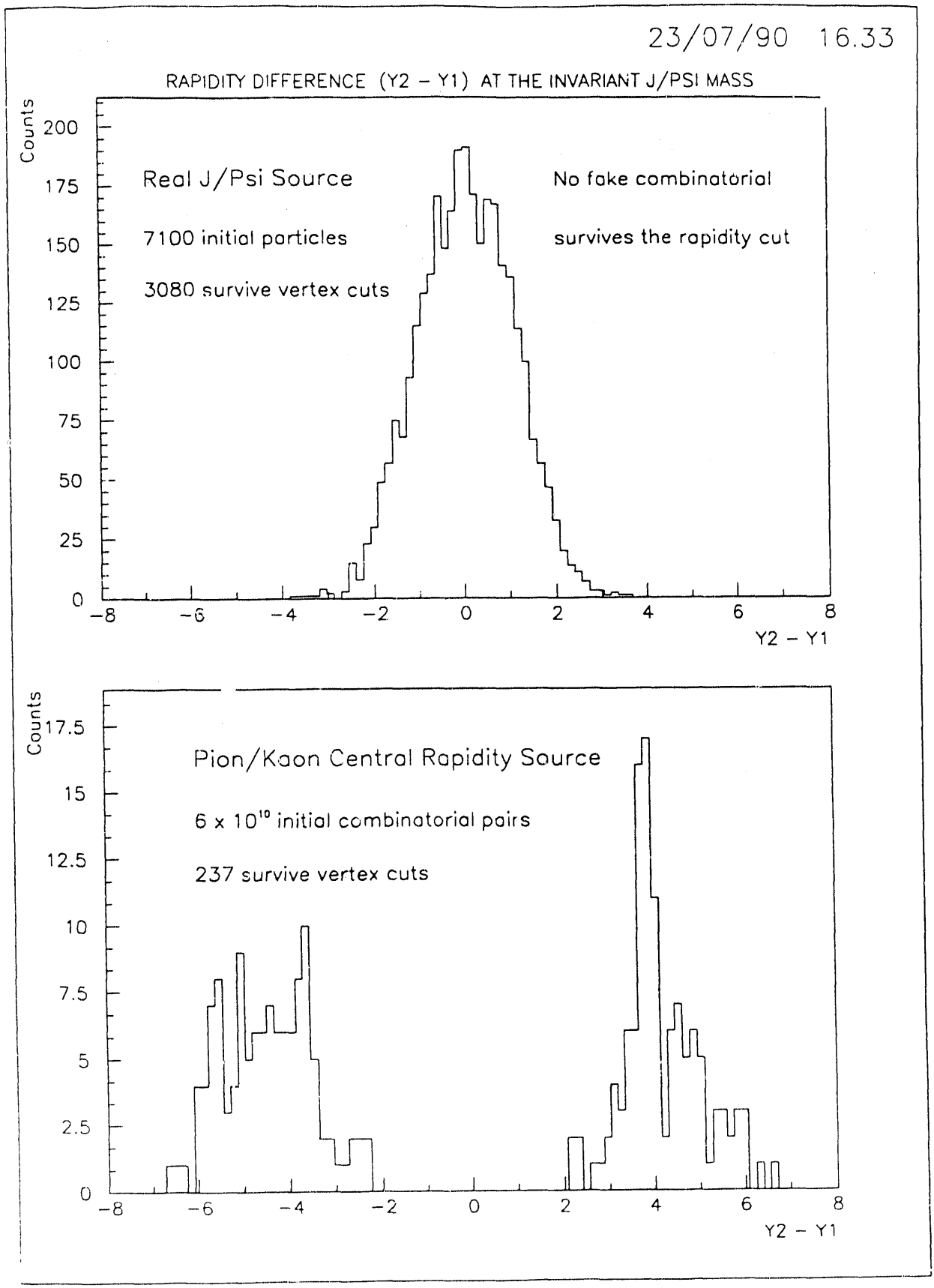
23/07/90 16.33
RAPIDITY DIFFERENCE (Y2 – Y1) AT THE INVARIANT J/PSI MASS
Counts
Real J/Psi Source
7100 initial particles
3080 survive vertex cuts
No fake combinatorial
survives the rapidity cut
Y2 – Y1
Pion/Kaon Central Rapidity Source
6 x 10^10 initial combinatorial pairs
237 survive vertex cuts
Y2 – Y1

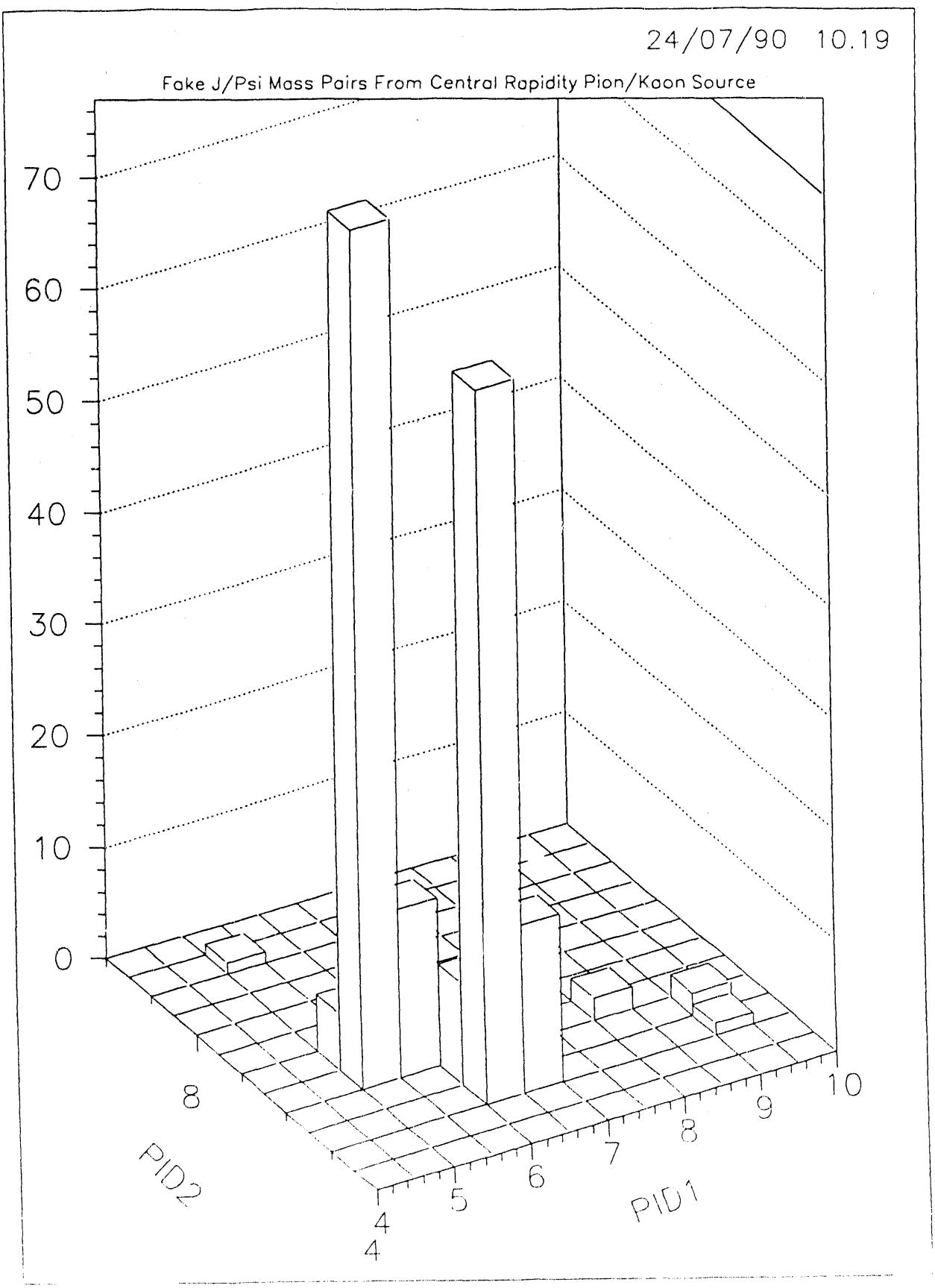
24/07/90 10.19
Fake J/Psi Mass Pairs From Central Rapidity Pion/Kaon Source
70
60
50
40
30
20
10
0
8
PID2
4
4
5
6
7
8
9
10
PID1

4

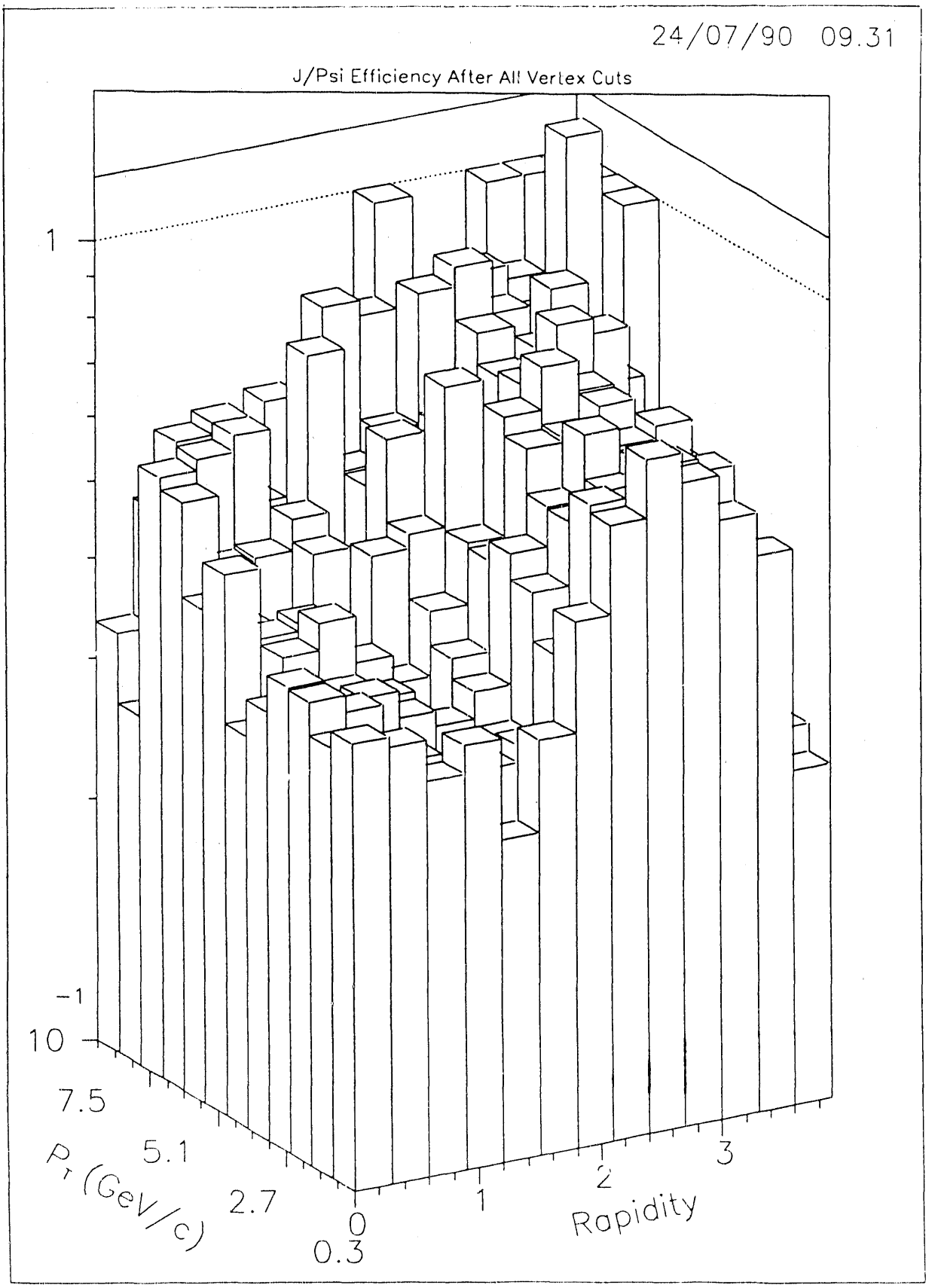
24/07/90 09.31
J/Psi Efficiency After All Vertex Cuts
1
-1
10
7.5
5.1
2.7
0.3
P_t (GeV/c)
0
1
2
3
Rapidity

5

Study Groups

Contents:

STUDY GROUP I

The Collision Regions at RHIC
Beam Crossing Geometries
Layout of Experimental Areas
Radiation Environment

Convenor:
A.Stevens
Brookhaven National Laboratory

Contents:

Collision Regions - List of Participants

D.Beavis,A.Etkin,K.Foley,S.Y.Lee,D.Lissauer,M.Sakitt,A.Stevens
Brookhaven National Laboratory

RHIC WORKSHOP

STUDY GROUP ON COLLISION REGIONS

A PEDESTRIAN'S GUIDE TO

COLLISION REGIONS AT RHIC

Including Information on:

Layout of Experimental Areas

Radiation Environment

Beam Crossing Geometries

D. Beavis
A. Etkin
K. Foley
S.Y. Lee
D. Lissauer
M. Sakitt
A. Stevens

July 1, 1990

LAYOUT OF EXPERIMENTAL AREAS

I. Liaison Mike Schaeffer

II. Simplified Drawings

III. Key Parameters

IV. Concerns/Issues/Recommendations

II. DRAWINGS

8 O'Clock

(Facility Hall)

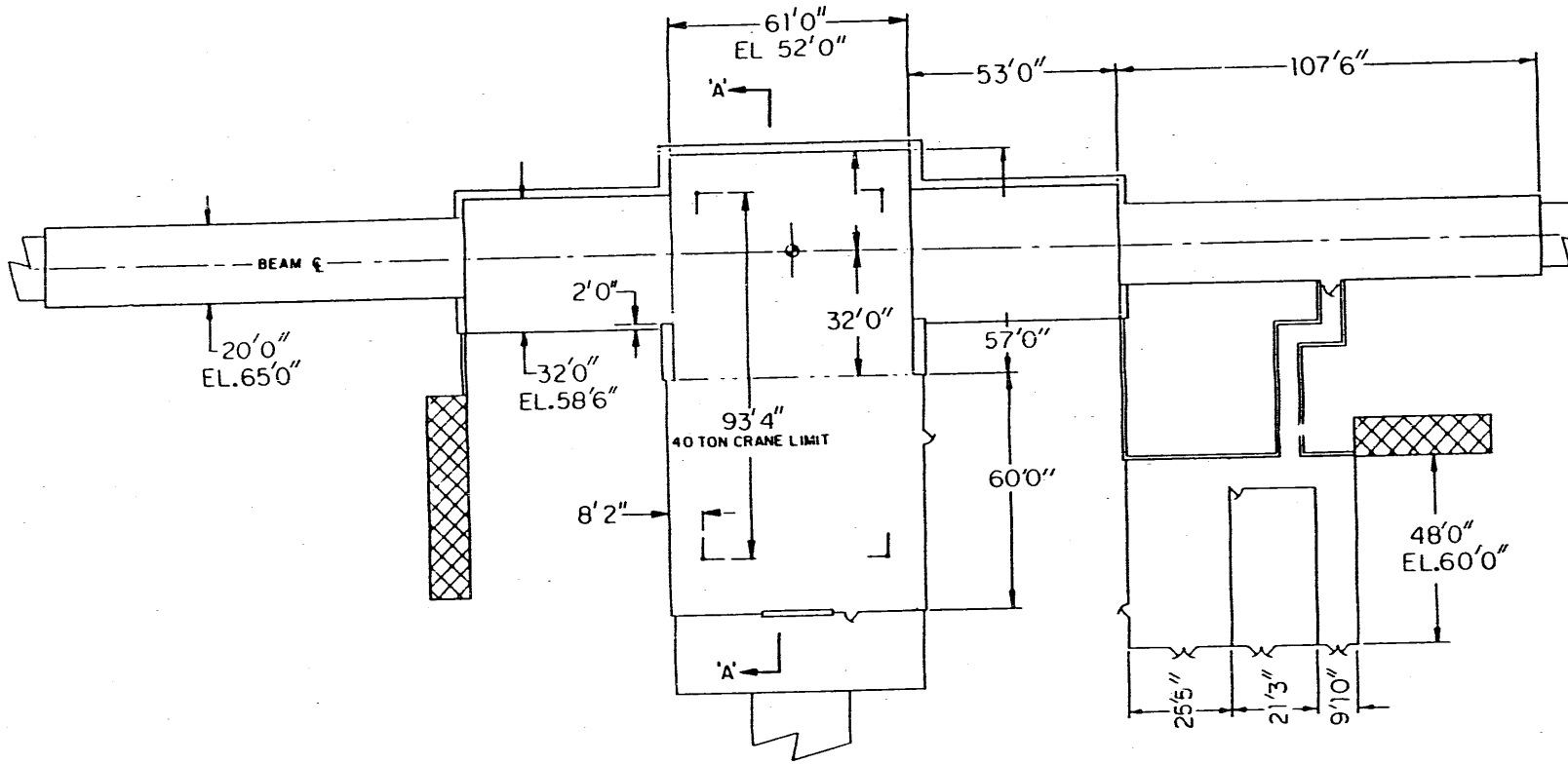

PLAN VIEW

MAJOR FACILITY HALL

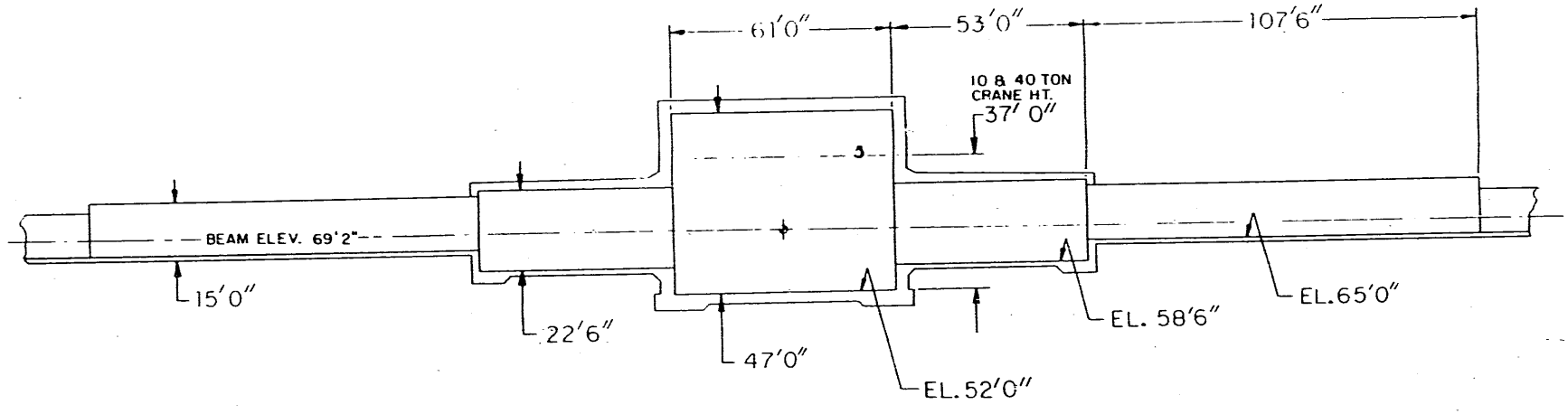

SIDE ELEVATION

MAJOR FACILITY HALL

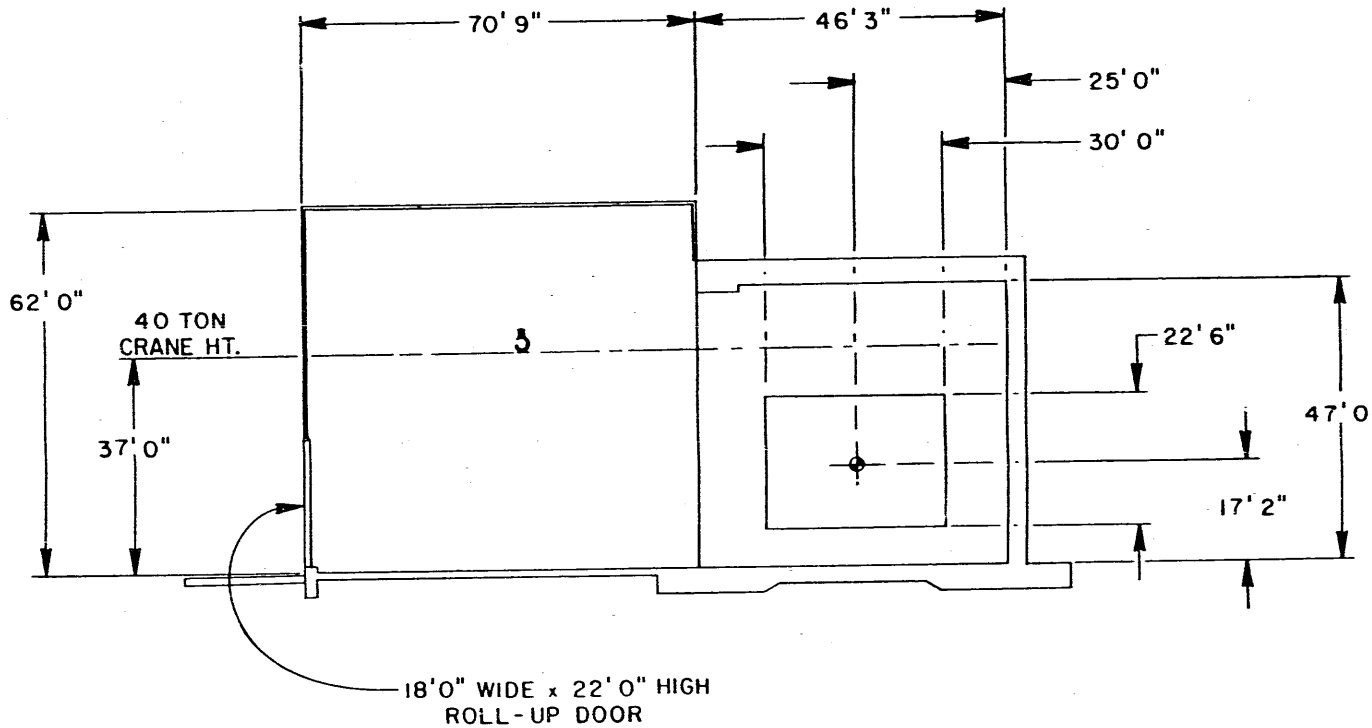

SECTION 'A-A'

MAJOR FACILITY HALL

II. DRAWINGS

6 O'Clock

(Wide Angle Hall)

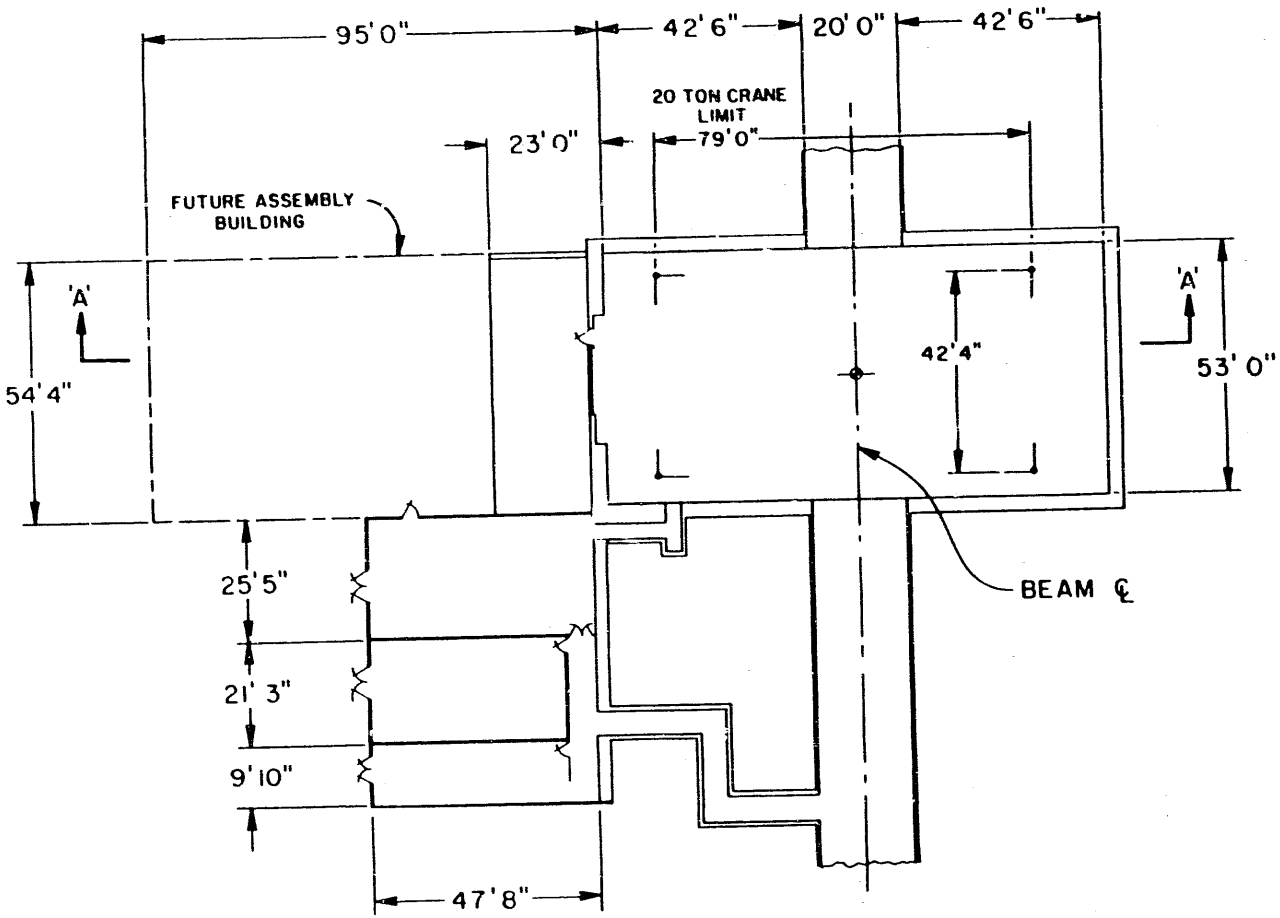

PLAN VIEW

WIDE ANGLE HALL

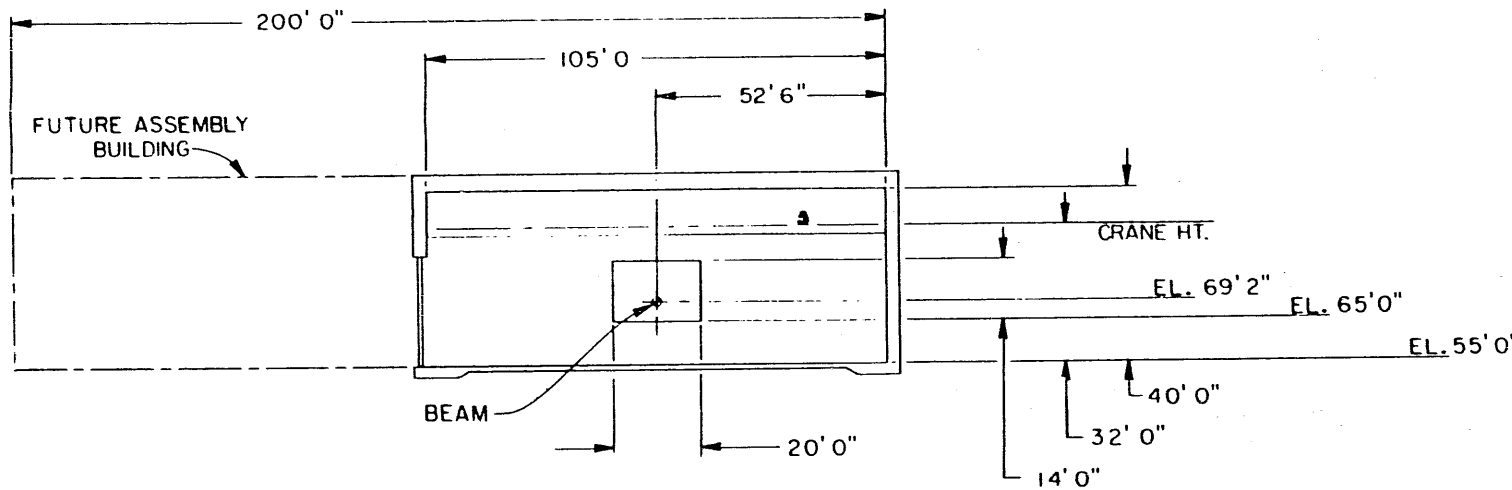

SECTION 'A-A'
SIDE ELEVATION CROSS SECTION

WIDE ANGLE HALL

II. DRAWINGS

2 O'Clock

(Narrow Angle Hall)

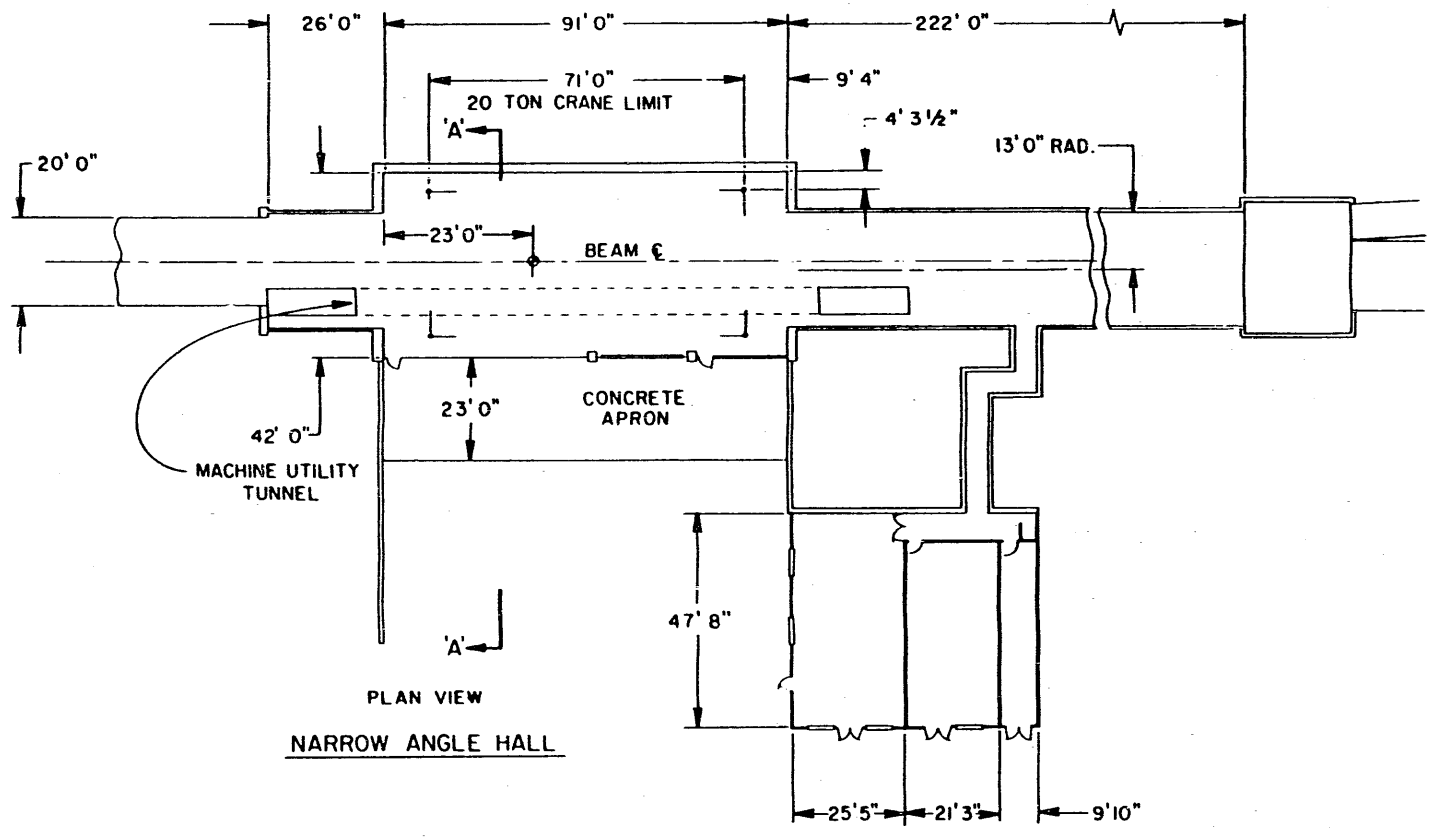

NARROW ANGLE HALL

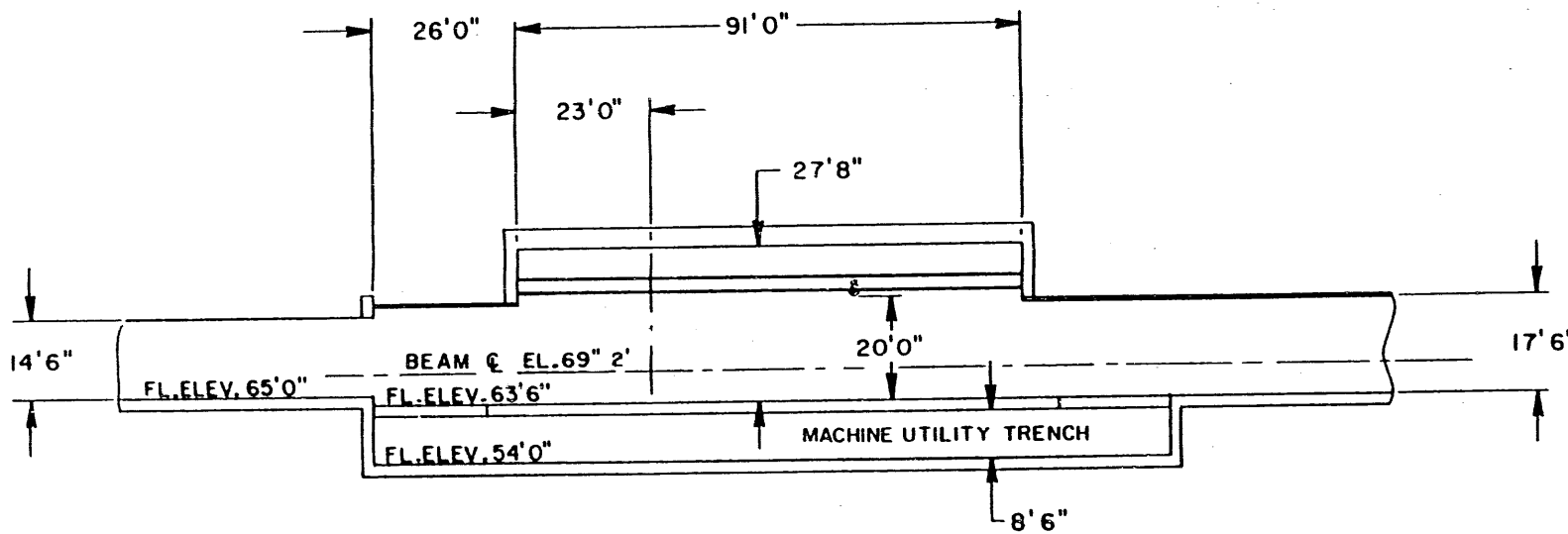

FRONT ELEV. CROSS SECTION

NARROW ANGLE HALL

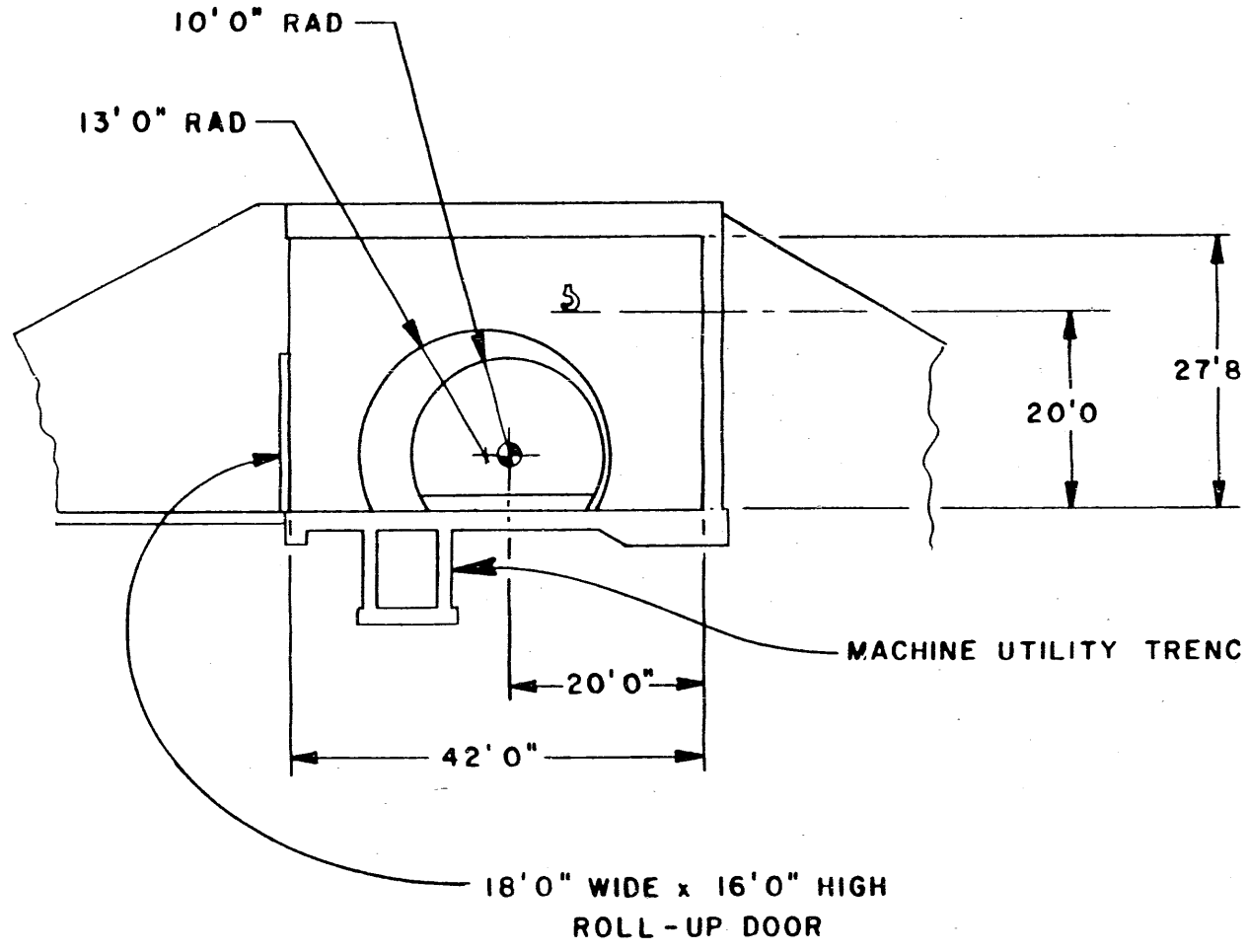

TUNNEL 8 EXPERIMENTAL AREA
SECTION 'A'-'A'

NARROW ANGLE HALL

II. DRAWINGS

4 O'Clock

(Pad Only at Present)

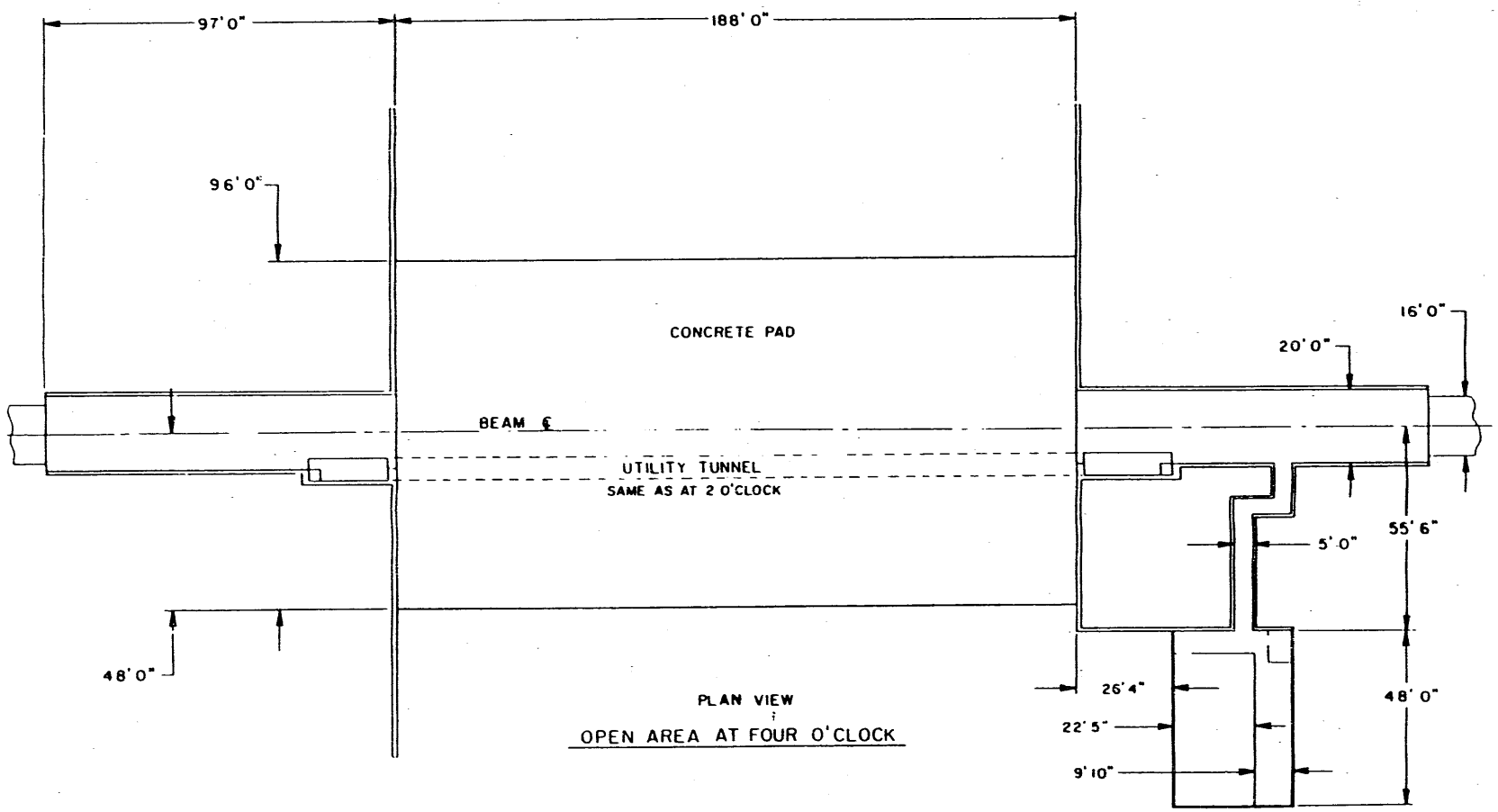
97'0"
188'0"
96'0"
CONCRETE PAD
16'0"
20'0"
BEAM ℄
UTILITY TUNNEL
SAME AS AT 2 O'CLOCK
5'0"
55'6"
48'0"
48'0"
26'4"
22'5"
9'10"
PLAN VIEW
OPEN AREA AT FOUR O'CLOCK

III. Key Parameters

	Facility (8 o'clock)	Wide Angle (6 o'clock)	Narrow Angle (2 o'clock)	4 o'clock
Crane Capacity (tons)	40	20	20	--
Hook Height (ft-above floor)	37	32	20	--
Floor Loading Limit (lbs/sq ft)	6000	6000	6000	6000
Counting House	Std.	Std.	Std.	--
Assembly Bldg	Yes	No	Apron Only	--

Notes:

1. 6 o'clock has rail capacity for second 20 ton crane and "thin wall" for Assembly Bldg addition

2. Standard Counting House ~ 47' x 25' but easily expandable

3. Assembly Bldg at 8 o'clock separated from Expt. Area by shielding blocks

IV. CONCERNS/ISSUES/RECOMMENDATIONS

A. Space Occupied by Machine Utilities (restrictive)

1. Trenches at 2 o'clock, 4 o'clock

2. Ring-outside wall space at 8 o'clock, 6 o'clock

B. Counting Houses (size, locations)

1. Too small in general

2. Distance too far from crossing point if fast signals required (see especially 8 o'clock plan view)

C. Shield wall between assembly area and experiment at 8 o'clock (awkward for access)

D. Dump upstream of 6 o'clock (noise spikes, shielding questions)

E. Recommendations:

1. Do not use trenches

2. Maximize use of vertical space -- rather than lateral space -- for machine utilities where required

3. Put machine utilities passage as far away as practicable for undeveloped areas (10 o'clock, 12 o'clock), and use blocks for shielding here for ease of future hall development

4. Pursue possibilities of counting houses on hall roofs and/or movable shielded counting rooms (see also "RADIATION ENVIRONMENT" section of this document)

RADIATION ENVIRONMENT

I. Liaison ?? [A. Stevens, acting]

II. Method of Calculation

III. Radiation Damage

IV. Shielding Requirements

V. Questions Left Unanswered

II. METHOD OF CALCULATION

A. CASIM

Pick p,n as primaries according to Z/(A-Z) ratio. Weight primary by A.

B. HIJET + CASIM

Primaries read from file created by HIJET run.

C. REFERENCES

1. A. VanGinneken, Fermilab FN-272 (1975)
2. A. J. Stevens, AGS/AD/Tech Note 296 (1988)
3. T. Ludlam, A. Pfoh, A. Shor, BNL 51921 (1985)

III. RADIATION DAMAGE

Calculate rads vs. angle in cavity using HIJET + CASIM for beam-beam collisions at a point. Results given below for Au on Au at $\mathcal{L} = 2 \times 10^{26}$ cm^{-2} sec^{-1}. [Worst case for "Day-1" luminosities about 5 times greater]

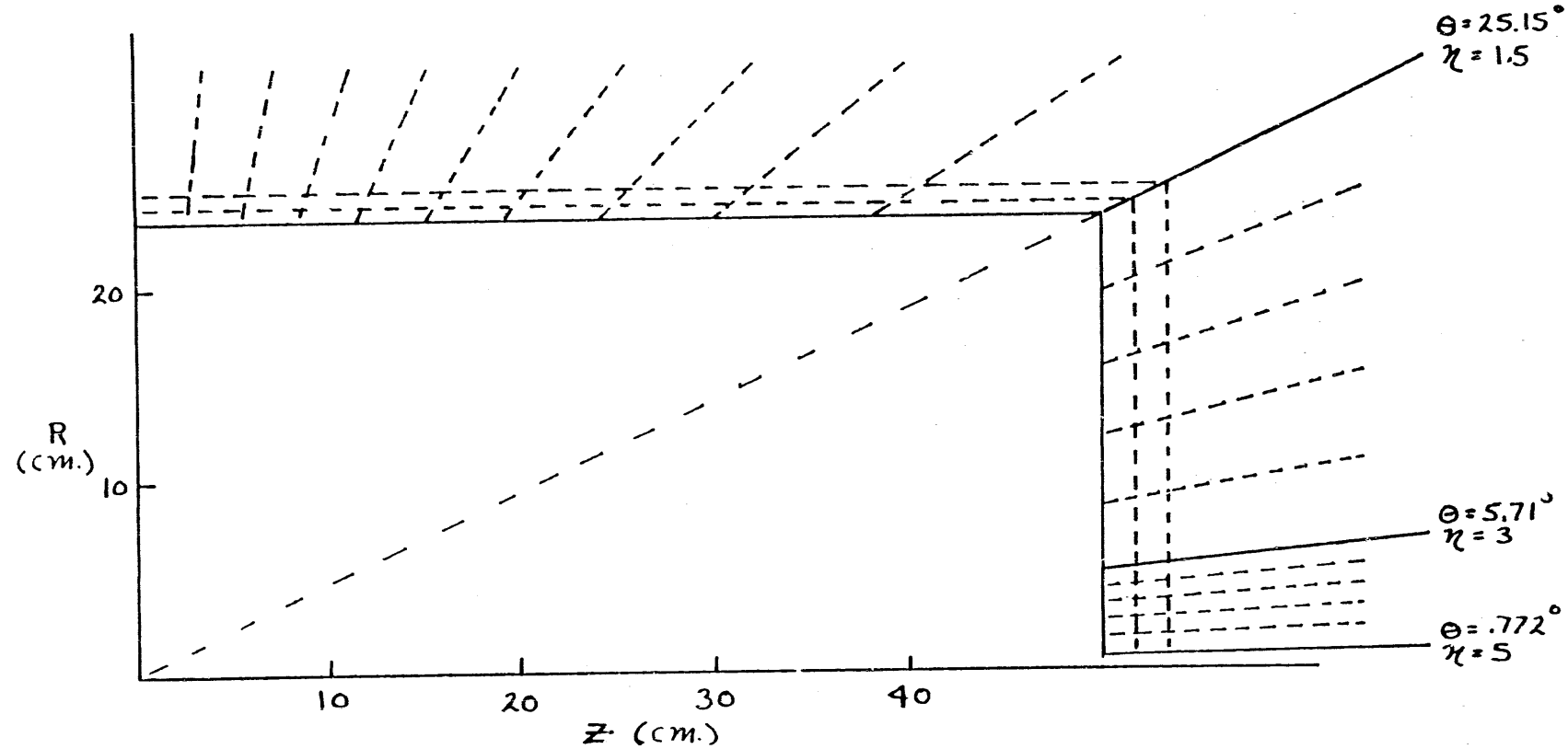

GEOMETRY OF RADIATION
DAMAGE CALCULATION

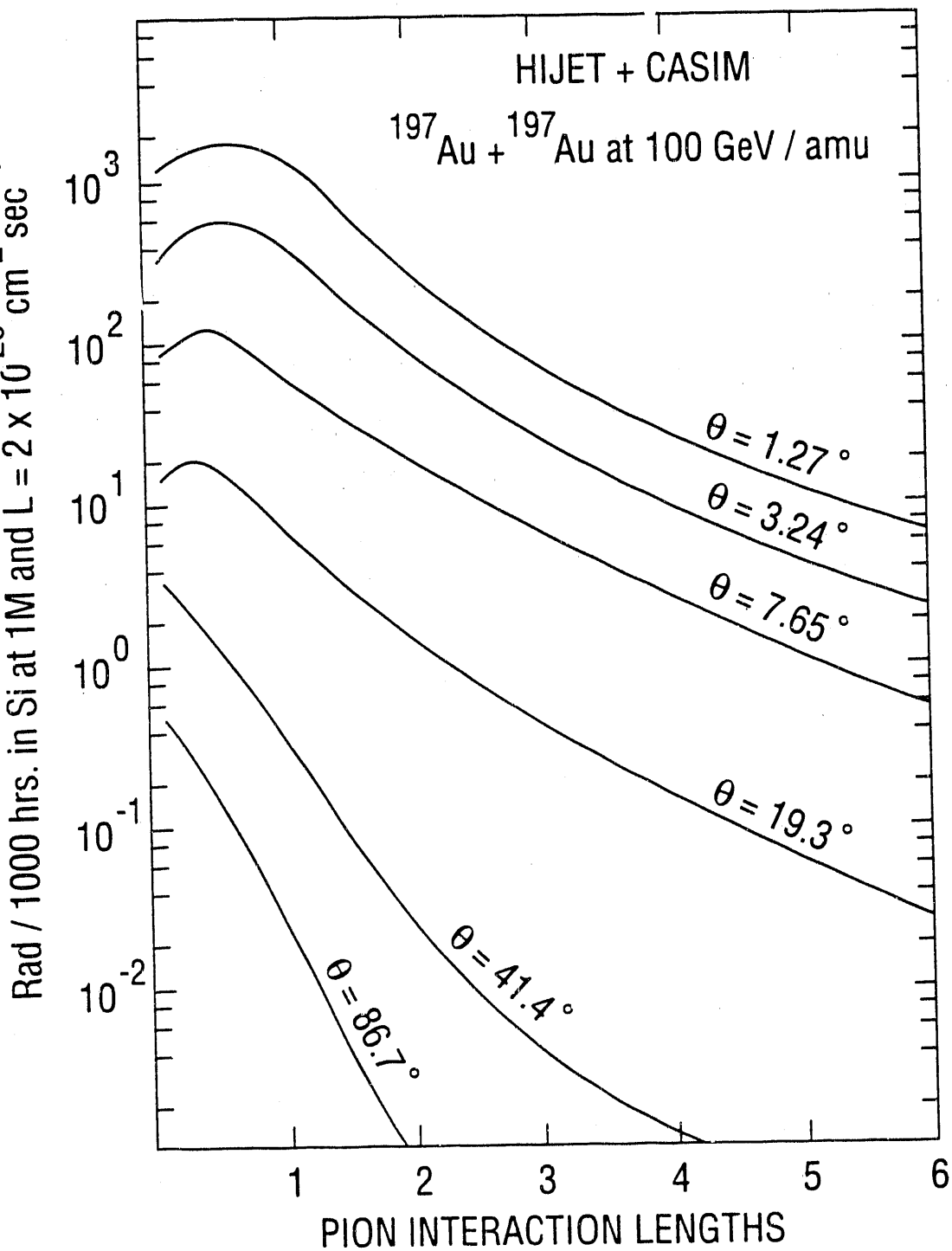

$\lambda = 128\ g/cm^2$

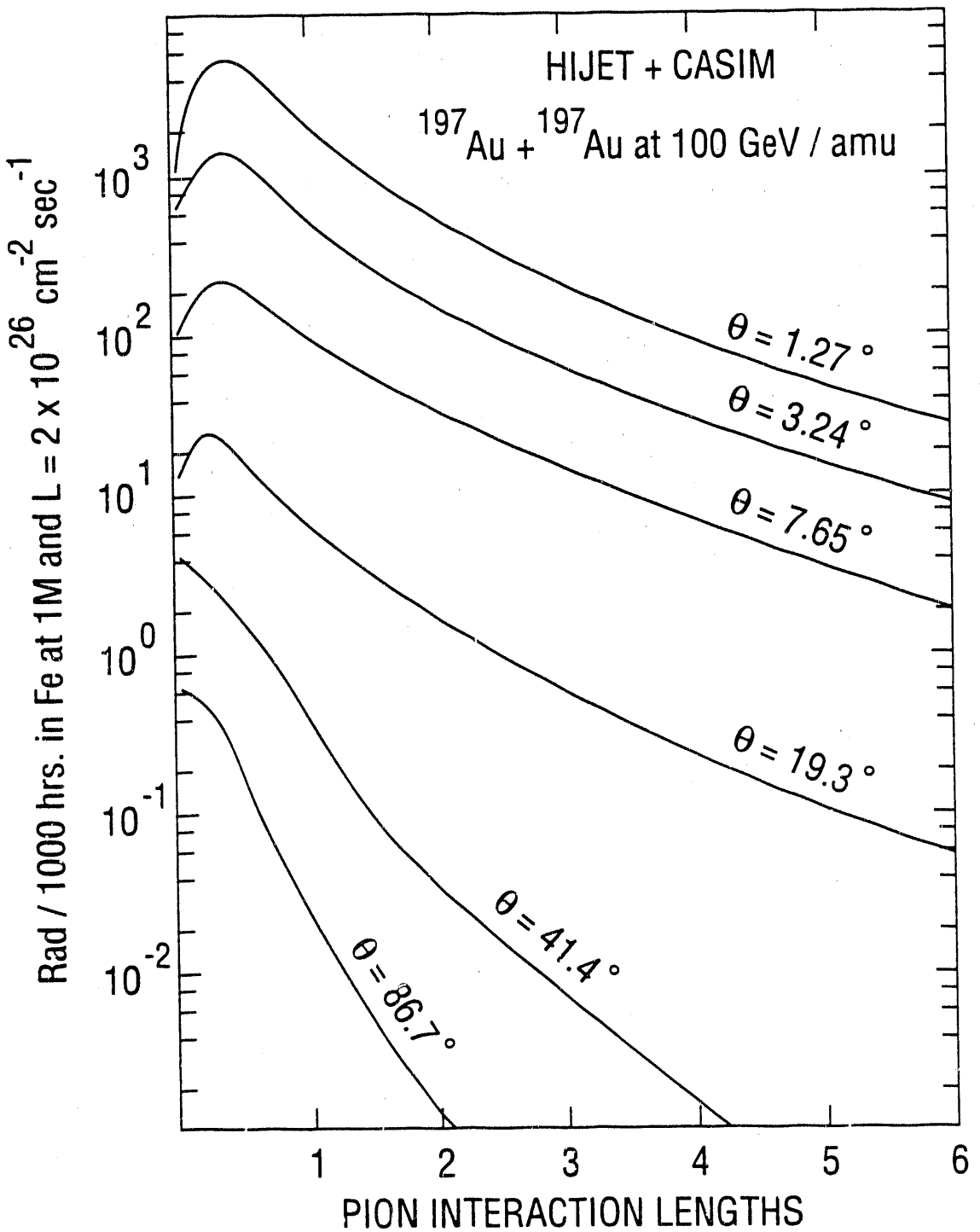

$\lambda = 155\ g/cm^2$

IV. SHIELDING REQUIREMENTS

A. CRITERIA

DOE DESIGN CRITERIA

1. 0.5 mrem/hr in "continuously occupied areas"
2. Less than 100 mrem in an hour for "Radiation Area"
3. Less than 1 rem/year (probable in near future - N. Rohrig)

PROPOSE THE FOLLOWING

1. 0.1 mrem/hr for known loss (beam-beam + beam-gas + dump)
2. 100 mrem per full beam loss fault
3. Possible higher criteria for close in, low occupancy places?

PROPOSED CRITERIA 1 AND 2 ARE CONSISTENT AT ~ 1 FAULT/YEAR. ["FAULTS" ALWAYS A PROBLEM]

B. CALCULATIONS

1. Beam-beam

2. Comment on beam-gas

3. Transverse shielding required for fault. (Full beam loss near experiment.)

4. Forward shielding required for fault. (Full beam loss at upstream high beta location.)

1. BEAM-BEAM

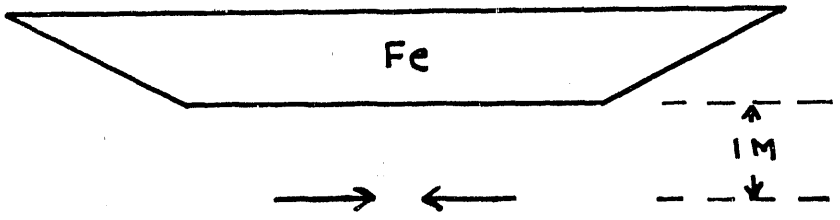

HIJET + CASIM

Result for Au + Au at $L = 2 \times 10^{26}$ cm^2/sec.

$$\text{mrem/hr} = \frac{0.61 \cdot e^{-s/.195}}{R_T^2}$$

where s (thickness), R_T in meters

35 cm. Fe sufficient at 1M for 0.1 mrem/hr

BUT not determining factor

2. COMMENT ON BEAM-GAS

a. RHIC gas mixture gives A (effective)~ 3.55

b. Scale air to 10^{-10} Torr
$\rho = 4 \times 10^{-17}$ g/cc

c. Derive:
Int/cm.-sec = 0.088 (Au)

d. For 100 m. illuminating hall
880 Int./sec
comparable to
1328 Int./sec Au + Au @ 2×10^{26}

CONCLUDE:

1. Serious Exp. Bkgd, but CDR promises 10^{-11} Torr

2. But SMALL compared to loss of full beam in fault

3. TRANSVERSE SHIELDING REQUIRED FOR FAULT

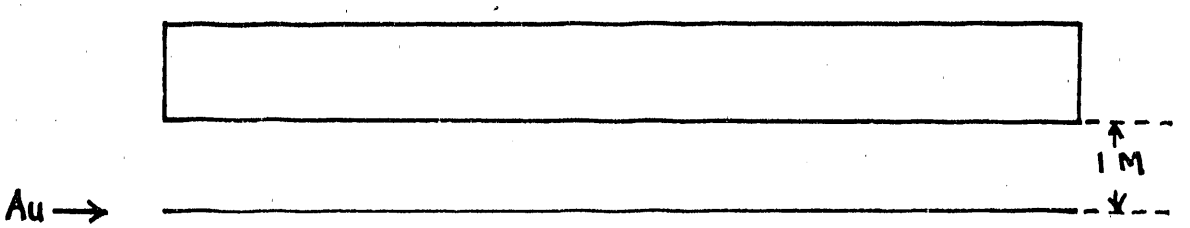

Geometry - Force Interaction on Beam Pipe

Result (see next page)

For Day-1 Intensity (6.27×10^{10} Au ions)

$$\text{mrem/fault} = \frac{6 \times 10^{4} \cdot e^{-s/.188}}{R_T^2}$$

Conclude:

1. Need 0.5-1.0 M Fe equivalent

2. Dominates beam-beam

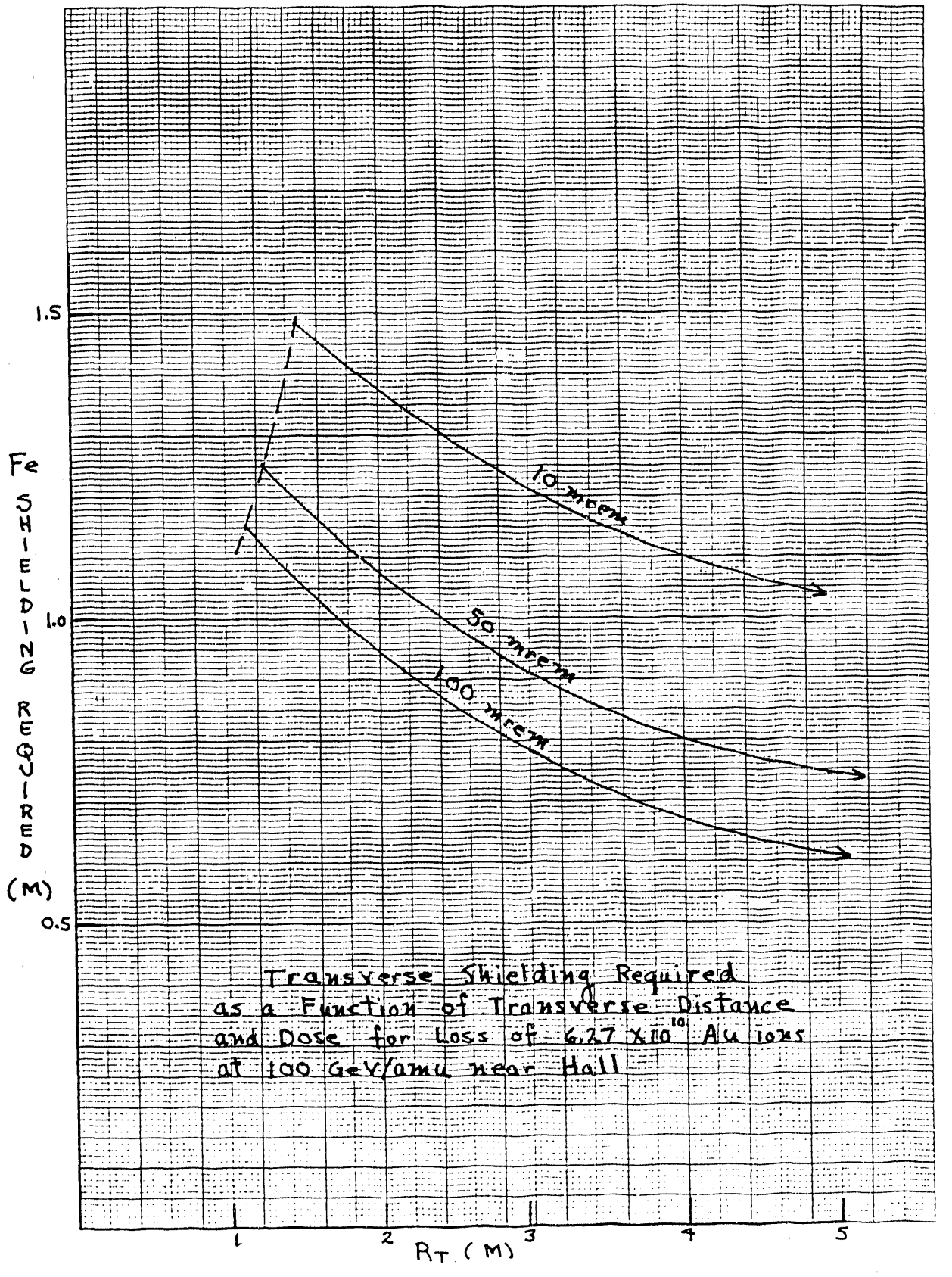

Transverse Shielding Required as a Function of Transverse Distance and Dose for Loss of 6.27×10^{10} Au ions at 100 GeV/amu near Hall

4. "FORWARD" SHIELDING REQUIRED

a. Geometry - see next page
Magnetic field neglected

b. Result - see following page

CONCLUDE:

1. Fault criteria dominate shielding requirements

2. For people at 4 M transverse distance, e.g., need

   ~ 0.7 M Fe equiv. transverse
   ~ 1.6 M Fe equiv. forward

3. More realistic calculations required -- these results a useful guide

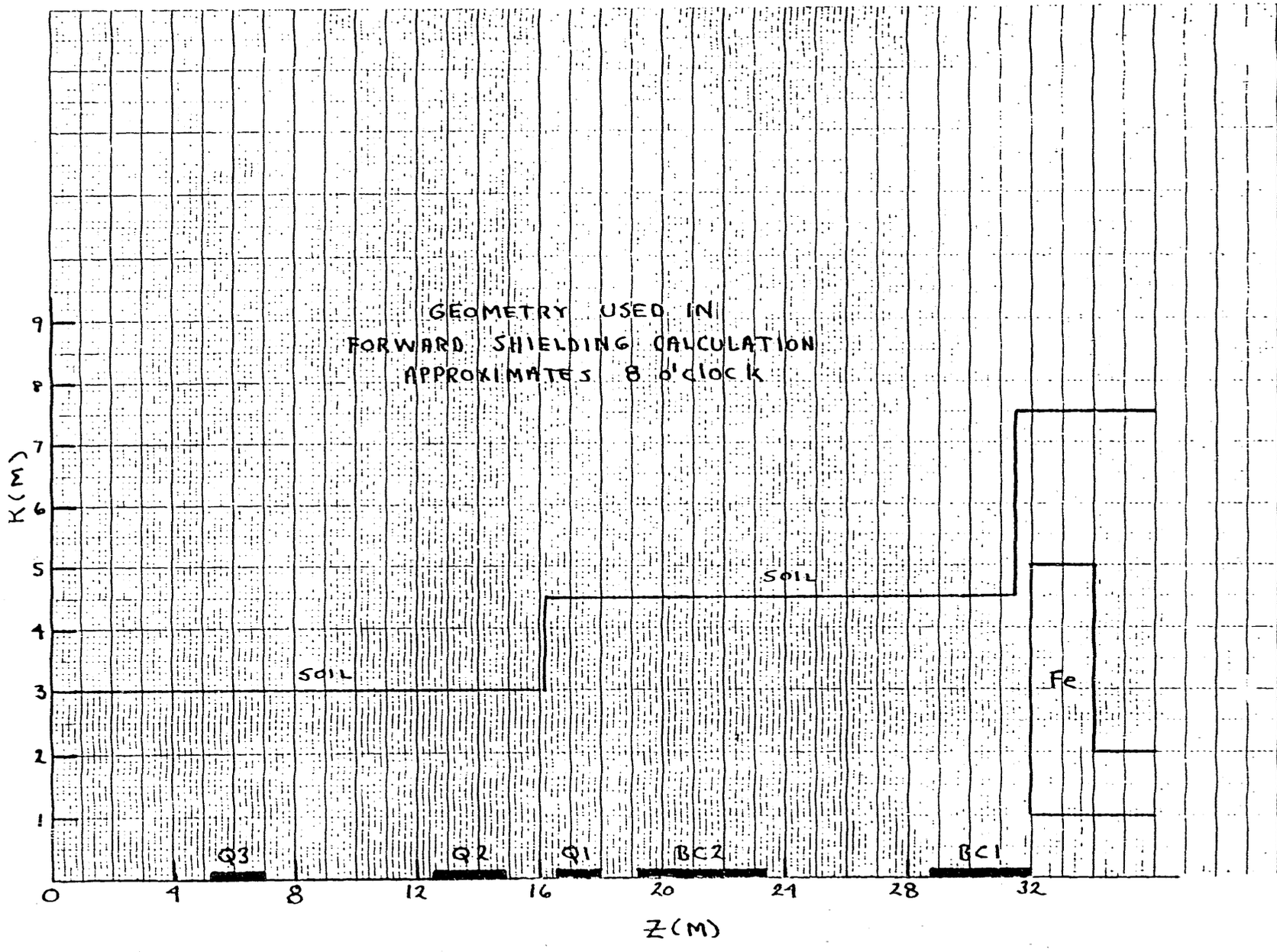
GEOMETRY USED IN
FORWARD SHIELDING CALCULATION
APPROXIMATES 8 o'clock
SOIL
SOIL
Fe
Q3
Q2
Q1
BC2
BC1
K(M)
Z(M)
0
4
8
12
16
20
24
28
32
1
2
3
4
5
6
7
8
9

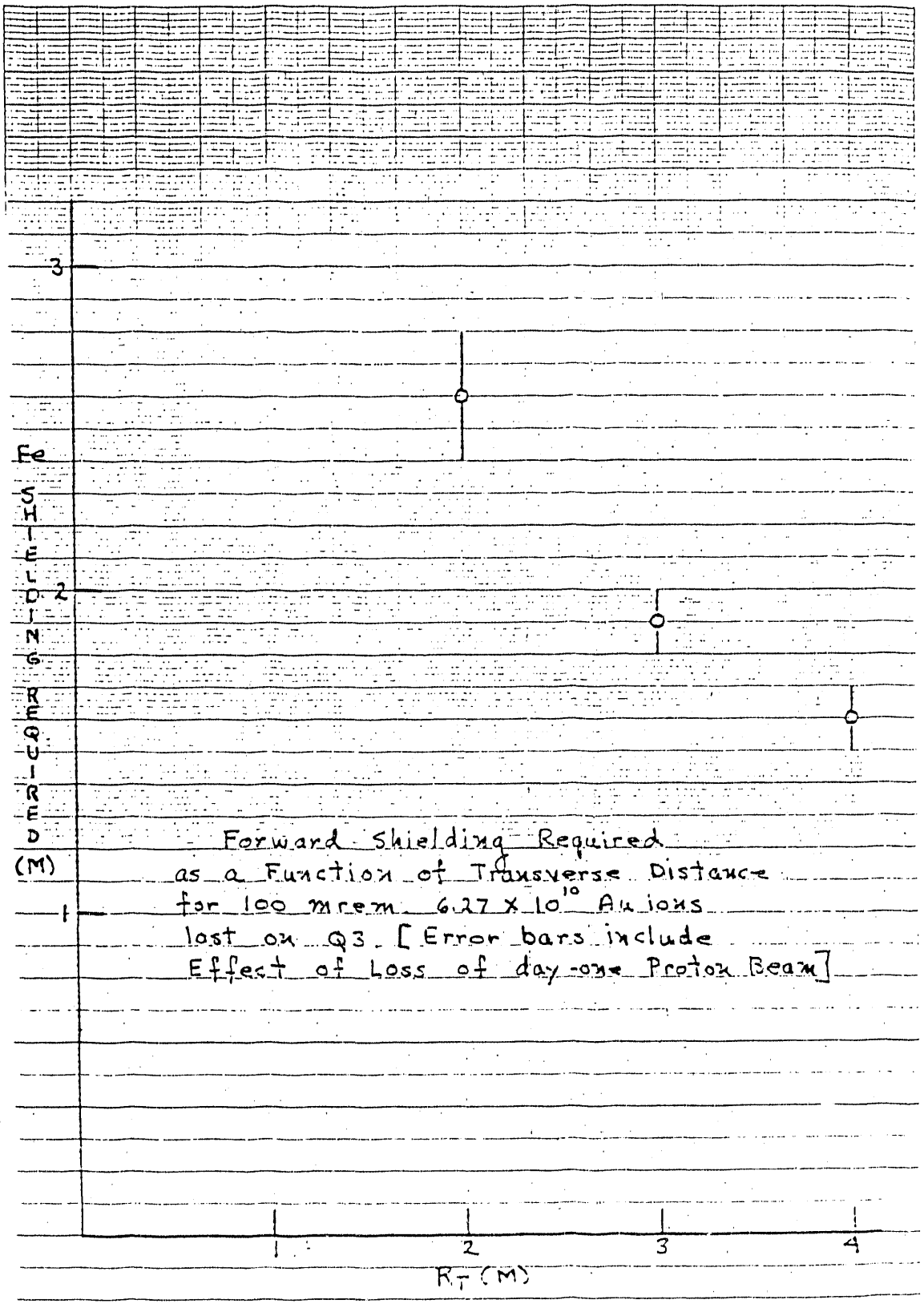
Fe SHIELDING REQUIRED (M)
3
2
1
1
2
3
4
R_T (M)
Forward Shielding Required
as a Function of Transverse Distance
for 100 mrem 6.27 X 10^{10} Au ions
lost on Q3. [Error bars include
Effect of Loss of day-one Proton Beam]

V. QUESTIONS LEFT UNANSWERED

A. What is radiation from dump at 6 o'clock?

B. What muon calculations need to be done?

C. Can Counting Houses be put on top?

D. Is higher allowable dose for low-occupancy (close in) regions acceptable?

E. What else?

BEAM CROSSING GEOMETRIES

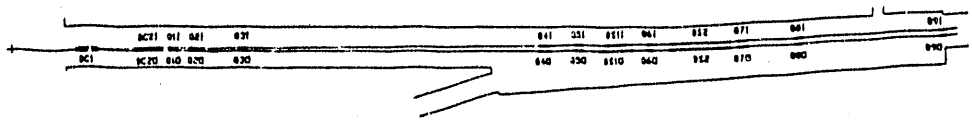

Fig. IV.2-3. RHIC half-insertion at 6 o'clock.

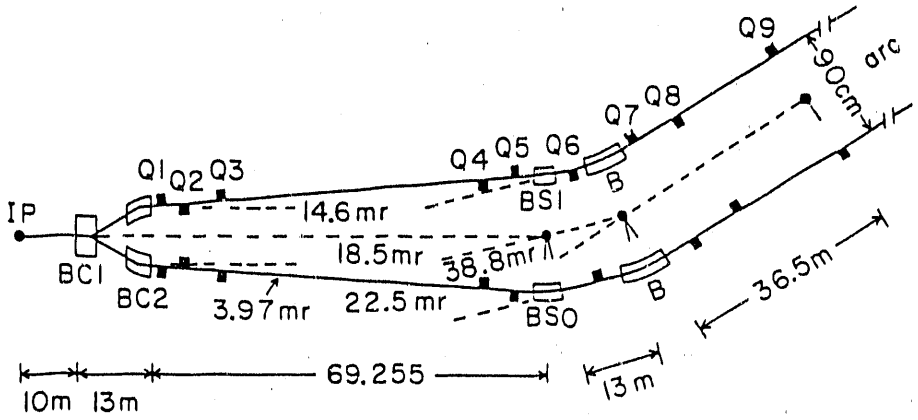

I. Liaison S. Y. Lee

II. Space

III. Diamond Size

IV. Luminosity

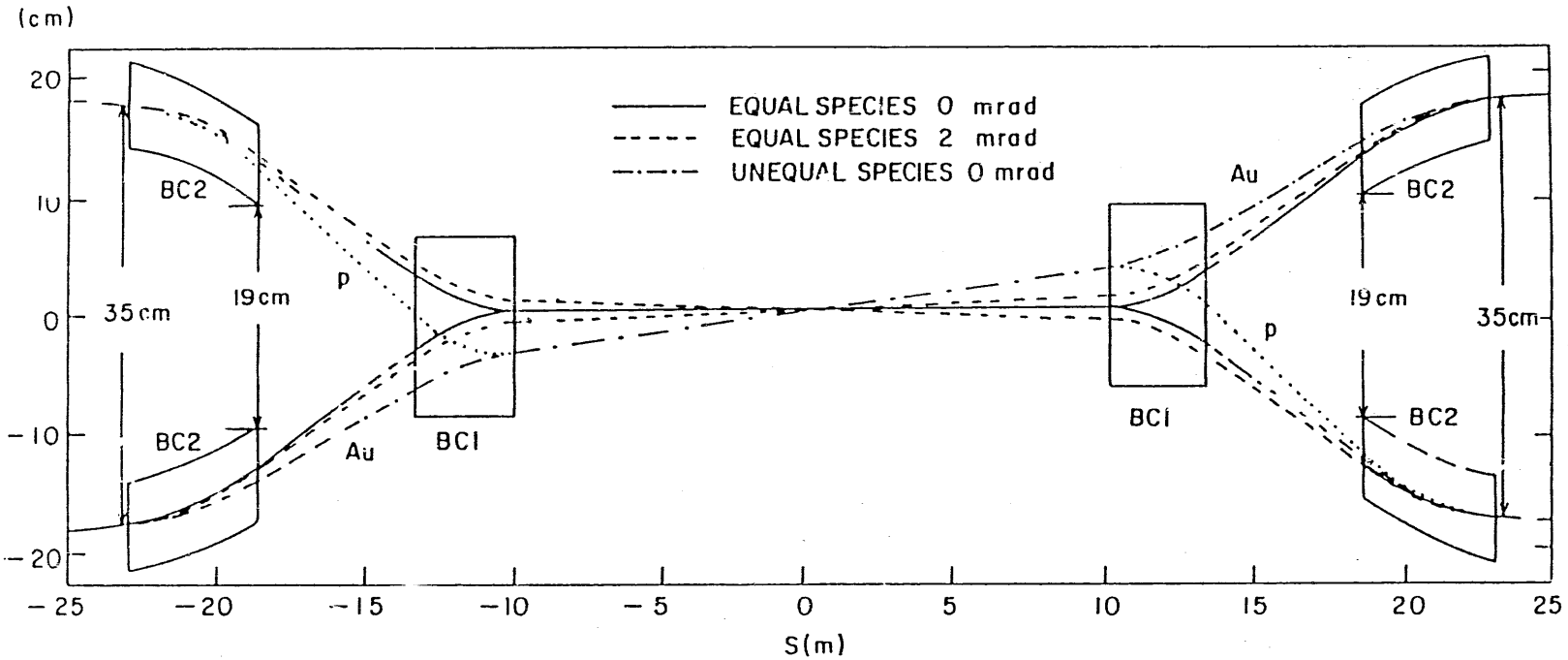

Beam Crossing Region for Present Configuration
Apertures Only Shown

II. SPACE AVAILABLE FOR DETECTORS

A. PRESENT CONFIGURATION

1. Free space ± 9 m

2. B = 57 (number of bunches)
   ⇒ Δt = 224 nsec.

3. "Mini-beta" possible *
   BUT reduces space to ± 4.5 m

B. FUTURE POSSIBILITIES

1. Moves BC1, BC2 closer to crossing point
   a. Permits greater $\mathcal{L}$ *
   b. Reduces space to ± 7 m

2. Special Insertion (example next page)
   a. For small angle tracking/calorimetry
   b. Reduces space to ± 6 m

* Some possibilities for greater $\mathcal{L}$ reduce space (See Section IV below)

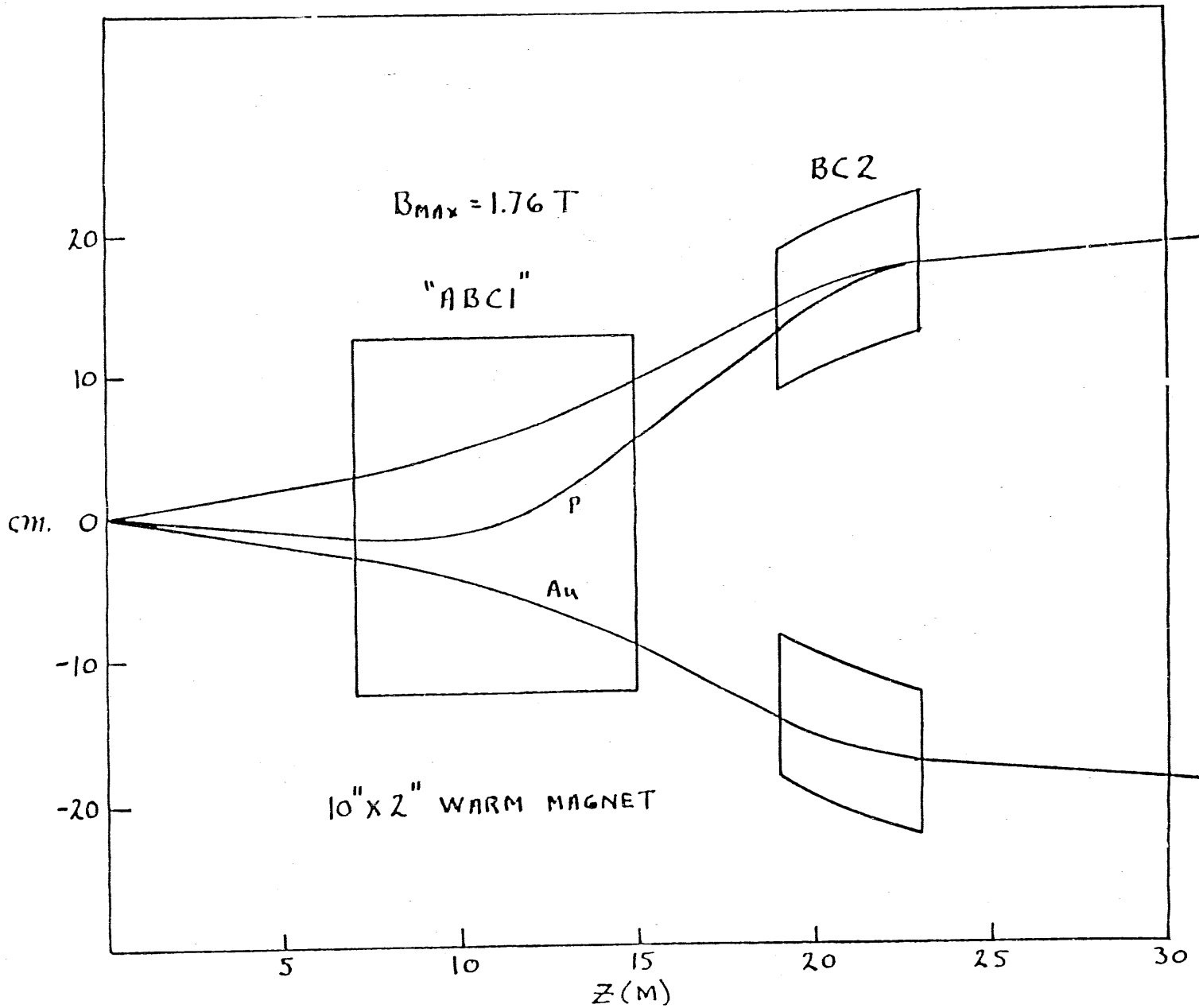

Special Insertion

III. DIAMOND SIZES

A. TRANSVERSE & LONGITUDINAL EXTENT

	Au	P
ϵ_N (mm-mrad)	60π	20π
σ_H (mm)	0.45	.158
σ_I (cm)	22	5.7

where

σ_H = beam size (at $\beta^* = 2$ m)

σ_I = interaction length (at 0^o crossing angle)

Note:

ϵ_N is time-averaged transverse emittance

More RF cavities could make smaller ϵ_N possible for Au where intrabeam scattering is large

B. EFFECT OF FINITE CROSSING ANGLE ON INTERCTION LENGTH (Au)

	α (mrad)	σ_I (cm)	$\mathcal{L}/\mathcal{L}(\alpha=0)$
	0	22	1.0
Probable →	1	16	0.75
Fair Chance →	2	11	0.50
?? →	3	7.8	0.35

Uncertainty due to effects of synchrobetatron instability (longitudinal - transverse coupling)

IV. LUMINOSITY

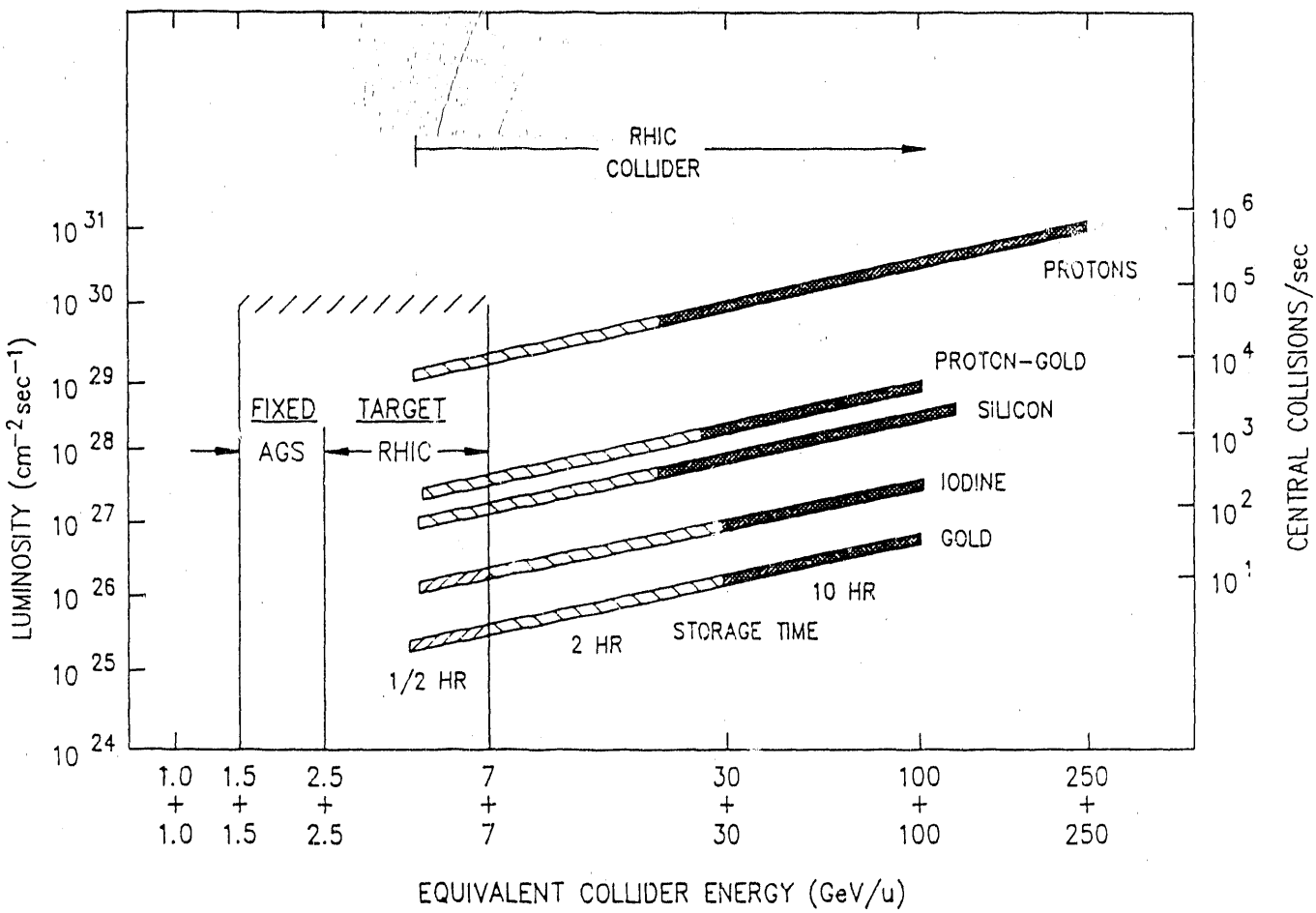

The design luminosity, for various ion masses, as a function of collision energy over the full range accessible with AGS and RHIC. On the right-hand scale, central collisions correspond to an impact parameter less than 1 Fermi.

A. FORMULA FOR Au AT 100 GeV/amu

$$\mathcal{L} = 1.1 \times 10^{27} \cdot \frac{(N_B/10^9)^2 (B/57)}{(\beta^*/2)(\epsilon_N/10\pi)} \qquad (t = 0)$$

BUT performance limited by:

$$\Delta\nu_{BB}(inj) = 2.4 \times 10^{-3} \cdot \frac{(N_B/10^9)}{(\epsilon_N/10\pi)} < 0.025/N_C$$

$$\Delta\nu_{SC} = 0.018 \cdot \frac{(N_B/10^9)}{(\epsilon_N/10\pi)} < 0.03$$

Where:

N_B = Particles/Bunch
B = Bunches/Ring
β^* = Beta at Crossing Point (M)
ϵ_N = Normalized Transverse Emittance (mm-mrad)
$\Delta\nu_{BB}$ = Beam-Beam Tune Shift
N_C = Number of Crossings
$\Delta\nu_{SC}$ = Space Charge Tune Shift

Note:

1. $\mathcal{L}$ above at injection emittance (10π) time-averaged $\mathcal{L}$ much less
2. $\Delta\nu_{BB}$ limitation less for fewer crossings
3. For $N_C = 4$, limition is space charge, but .03 value is uncertain

B. WAYS TO INCREASE $\mathcal{L}$ (given working machine)

1. Instantaneous $\mathcal{L}$ value

   a. Increase N_B (x 4 in $\mathcal{L}$ possible with source improvements)

   b. Reduce β^*

      i. Mini-beta (x 2 possible)

      ii. Move BC1, BC2 (x 1.3 possible)

      iii. Recall these options reduce space

   c. Increase B

      i. B = 114, 171 (x 2, x 3 possible with hardware improvements)

      ii. But Δt shrinks and

      iii. B = 171 $\Rightarrow$ reduced space everywhere to $\pm$ 7 M

2. Problem of time dependent $\mathcal{L}$ (intrabeam scattering)

   a. Increase RF voltage (~ x 3 in $\mathcal{L}$ possible)

   b. Stochastic cooling (~ x 3-4 possible)

      i. Longitudinal only

      ii. Does NOT reduce diamond length

      iii. Addresses same problem as RF (longitudinal emittance growth with time)

C. ULTIMATE $\mathcal{L}$ FOR Au = ?

Calculations indicate tune shift limitations and EM losses will limit Au time-averaged $\mathcal{L}$ to about x 10 beyond "day-1" value of 2×10^{26} cm^{-2} sec^{-1}, but uncertainty large

STUDY GROUP II

Monte Carlo Simulations of
Interactions and Detectors.

Convenor:
O.Hansen
Brookhaven National Laboratory

Contents:

REPORT FROM THE SIMULATION WORKGROUP

Flemming Videbæk
and
Tom Throwe
Physics department
Brookhaven National Laboratory
Upton,NY 11973

1 Introduction

Ahead of the RHIC workshop a Simualtion Group was formed to make available to the participants a set of events from some of the commonly used event generators. The group also met once during the workshop to discuss some of the common problems regarding event and detector simulations.

First, this report discusses how the event format implemented, and how it can be utilized and accessed. Next some comparisons between FRITIOF, VENUS and HIJET are presented. The last section has a summary of the luncheon meeting.

2 Event Generator Format

This section describes the event format implemented for the RHIC workshop used for data files from the event generators FRITIOF, VENUS and HIJET. It also describes the routines needed to read these data files and how to access the programs via DECNET. This document describes in short how these event files can be read without knowing the detailed implementation.

2.1 Event format

It was recommended at the previous RHIC workshop (BNL 1988) that the events should be stored in a ZEBRA bank format. The present layout is somewhat different than was defined then, but was chosen as a practical starting point for an implementation. Each event file has one data record defining the event generator and the reaction kinematics. This is followed by a model dependent record and the event records. The latter are independent of the model. The ZEBRA output format can be either the socalled binary exchange format which will allow data files to be transferred between computers, or the native format, which allows files to be read faster on the local computers.

2.2 Implementation of a sample reading program.

A sample skeleton program and utility subroutines have been set up and are available to read files written in the chosen eventformat. The user supplies three subroutine (or entries) , namely an initialization subroutine (ANINIT) which can define histograms, accept input , an event subroutine (ANUSER) used to analyze each event, and a termination routine (ANFIN) which can output results. The general routines will manage the ZEBRA calls and unpack the information. The access to the description of the particles is done through a common block defined below. The primary parameters stored on tape/disc are the four-momentum ,particle ID and parent/daughter information. The reading routines will (optionally) calculate a set of useful derived kinematic parameters.

The common block has the following information. The complete listing can be found in eg$source:event.inc.

```
maxptl  : maximum number of particles pr event.
nptls   : number of particles in event
nnproj  : # neutrons spectators (in proj)
npproj  : # protons  spectators (in proj)
naproj  : # spectators (in proj)
nntarg  : # neutron spectators (in target)
nptarg  : # proton  spectators (in target)
natarg  : # spectators (in target)
ntry    : # of tries to get an interaction since last call
          This number is needed to get a cross section from
          the number of attempts + the impact parameter
          range.
px(i)   : 4 momentum of each particle
```

```
py(i)    :
pz(i)    :
energy(i)
idptl    : ID for particle (as given by event generator)
ioptl    : Parent sequence number ( 0 if no parent,negative if not
           present)
y        : rapidity
pt       : transverse momentum (GeV/c)
mass     : mass in GeV of particle
theta    : polar angle theta in radians
phi      : azimuthal angle in radians
gtype    : GEANT particle ID.
```

Reaction description

```
atarg    : Target Mass Number
ztarg    : Target Charge Number
aproj    : Projectile Mass number
atarg    : Projectile Charge Number
Nbeam    : Number of beam particles thrown into the
           area defined by bmin->bmax
```

The four-momentum information can alternative be stored in an array p4vec defined in the following way

```
p4vec(1,i) : px for particle i
p4vec(2,i) : py for particle i
p4vec(3,i) : pz for particle i
p4vec(4,i) : energy for particle i
```

This storage way is convenient when using certain CERN library routines in the analysis of the four momenta. The two way are mutually exclusive, and is selected when running the analysis programs.

2.3 Availability of programs.

The programs can be found on the central Brookhaven BNLCL VAX cluster and on the BNL802 VAX cluster. The root directory is presently 2DUA0:[rhicwork] on the BNLCL cluster and bnlhi0$dub2:[eventgen] on the BNL802 cluster. This directory and descendents will contain data files, source codes , command procedures and examples needed to run the event generators and to read the data files.

The source code and the include files are in 2DUA0:[rhicwork.eg.source], object code in 2DUA0:[rhicwork.eg.library] and command files in 2DUA0:[rhicwork.eg.commands]. These files are world readable and can be accessed via the HEP DECNET.

2.4 Data files

Several Datafiles were generated for the workshop, but these will not be available on the BNLCL and BNL802 cluster for extended periods.

As mentioned earlier, the ZEBRA files can be written in a couple of different formats, namely in native mode or in exchange format. The user program controls the selection by means of a namelist input read from the file EGZPAR.PAR.

2.5 Sample reading program.

Two sample user program can then be found in hi0$event:[eg.examples] (eg$examples) namely adummy.for and dndy_ana.for. These programs can be linked using the command file given in eg$commands. If you have a program in your directory named myana the following commands are needed to compile link and run the program

```
$ for myana
$ @eg$commands:link_read myana
$ define z_tape eg$rhic_data:auau_rhic_central.N_zdat_lund
$ create egzpar.par
 $ZPAR
 Z_DOUBLE_OUT     = F,
 Z_BLOCKSIZE      =        3600,
 Z_FZ_OPTION_OUT  = 'O    ',
 Z_FZ_OPTION_IN   = 'I    ',
 Z_FZLOGL         =          -2
 $END
$create USERPAR.PAR
 $UPAR
 NEVENTS =          100,
 P_IN_2D_ARRAY    = F
 $END
$ run myana
```

The standard link command will link the user routines with the standard reading routines and with the CERN libraries npacklib, genlib, and kernlib. If other libraries

and routines are needed a local copy of the link routine should be made and modified. The USERPAR.PAR input file controls the number of events to be analyzed, and the storage of the four momenta. The example will read 100 events and store the event data in the arrays px,py,pz and energy. If the file was generated in exchange format the data definitons would look like

```
$ define z_tape eg$rhic_data:auau_rhic_central.N_zdat_lund
$ create egzpar.par
   $ZPAR
 Z_DOUBLE_OUT    = F,
 Z_BLOCKSIZE     =        3600,
 Z_FZ_OPTION_OUT = 'TXO ',
 Z_FZ_OPTION_IN  = 'TXI ',
 Z_FZLOGL        =          -2
 $END
$ run myana
```

2.6 Event generators

2.7 FRITIOF

The FRITIOF 1.7 code is available in 2DUA0:[rhicwork.lund] as lund_model.exe. This directory can also be accessed by eg$lund_dir once the setup file is executed. A sample input command file is in run_lund_model_example1.com.

2.8 VENUS

The VENUS 3.07 code is available in 2DUA0:[rhicwork.venus] as venus_zebra.exe. This directory can also be accessed by eg$venus_dir once the setup file is executed. A sample input command file is in run_venus_model_example1.com.

2.9 HIJET

The HIJET 3 code is available in 2DUA0:[rhicwork.hijet] as hijet.exe. This directory can also be accessed by eg$hijet_dir once the setup file is executed. This version of HIJET contains rescattering, but this feature should not be used at RHIC energies. A sample input command file is in run_hijet_model_example1.com.

3 Selected results

In this section a few comparisons between the event generator codes are presented. The histograms were generated using the same analysis program. The first set of pictures show the dN/dy distributions for π^+, K^+, P and $\overline{P}$. The VENUS calculation shown as the dotted curves does not include rescattering, an option available in version 3.07. The HIJET results are shown as dash-dots while the FRITIOF results are shown with the full drawn curves. All calculations are for central collisions. The overall rates are quite similar for the three codes, while substantial differences exists for the shapes and the particles ratios. The three models represents extremes in terms of stopping. FRITIOF predicts a baryon free central rapidity region, while HIJET with the largest amount of stopping give rise to a substantial baryon density at central rapidities. In figure 2 the momentum distributions predicted for the three codes are presented. HIJET and VENUS only include the very soft pure exponential distributions while FRITIOF seems to include parts of the hard scattering processes giving rise to a high p_t tail.

4 Workshop discussions

The simulation group held a two-hour luncheon meeting on July 3. The issue of software support from BNL was discussed. The general impressions as summarized by Ole Hansen are

- There was no large demand for having BNL keep banks of events from event-generators. Most groups thought they preferred to create their own events.
- There was a wish for BNL to transfer blueprint information for hardware in the beam crossings to a list of numbers, which can be used in generating a GEANT description for a given detector.
- There was a fairly stong desire to have BNL maintain and document the most commonly used heavy ion event-generator codes, and be a clearing house for such codes.
- There was a strong demand that BNL create a central software group to obtain, maintain, document, and distribute major software libraries and codes in common use in the high-energy heavy-ion field.

The local group has since met and discussed these impressions . It was felt that item 2 could be dealt with fairly easily. Item 3 can be dealt with in a limited way by the

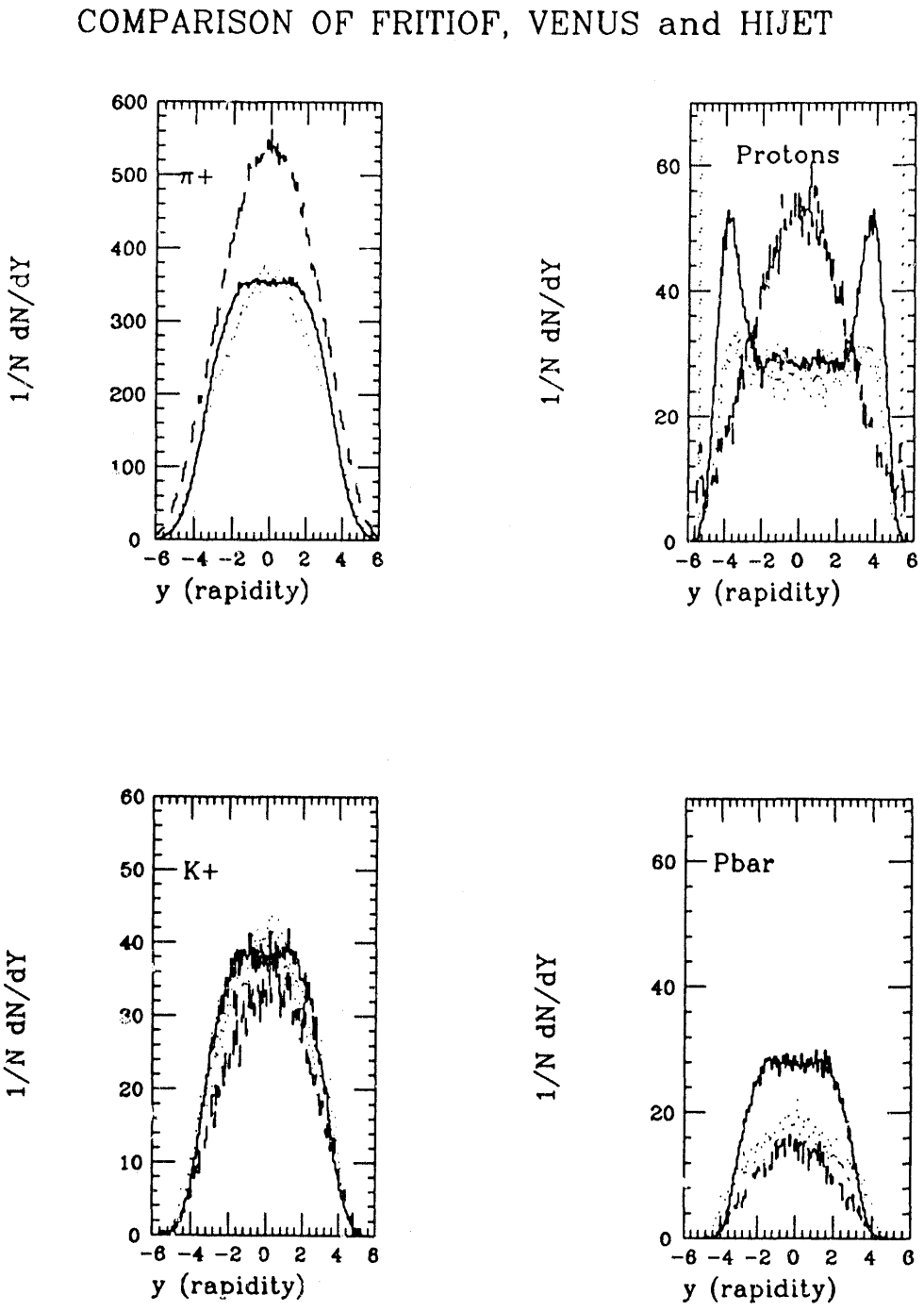

Figure 1: Rapidity distributions for 100GeV+100GeV Au Au central collisions

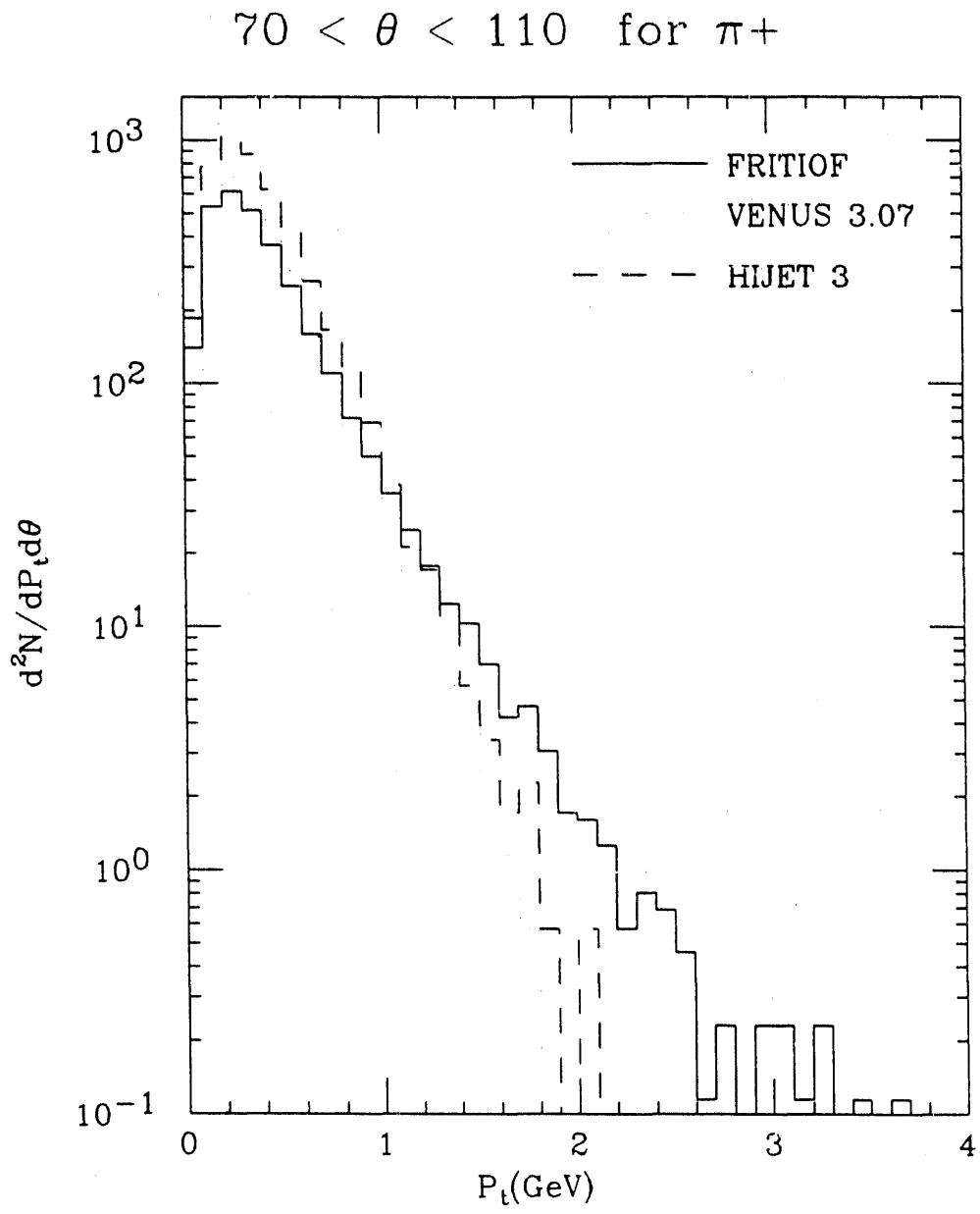

Figure 2: momentum distributions near midrapidity

existing in-house structure as described in the following paragraph. This is partly what caused the specific setup for event-generators described in the second section of this document. Items 3 and 4 are much more than the existing experimental groups can handle in a reasonable way and it will be up to the USERS of RHIC (and AGS) to discuss/recommend how such an infra structure may be created. Clearly there is a strong demand for such a support.

In order to save some duplications of effort, if potetential users of the RHIC machine have written programs (Event generators, jet algorithms, etc) which they feel can be useful to others and which they are willing to share, then they are encouraged to provide a copy of this program with documentation to the simulation group at BNL. The simulation group will then provide copies of the code and documentation to any user requesting it. The simulation group will not convert the code to run on machines other than those for which the author provided code, but rather will collect the codes and make them known and available to others.

STUDY GROUP III

Proton Nucleus Interactions at RHIC.

Convenor:

R.Ledoux

MIT

Contents:

p+A Study Group - List of Participants

J.B.Costales, R.Ledoux
MIT

A.Caroll,M.A.Kramer,A.Sambamurti
Brookhaven National Laboratory

R.Bellwied,M.Muthuswamy
SUNY, Stony Brook

M.A.Bloomer
Lawrence Berkeley Laboratory

P.L.McGaughey
Los Alamos National Laboratory

F.Wang
Columbia University

S.Gavin
University of Helsinki

Report of the Rhic Workshop p+A SubGroup

M.A. Bloomer, R. Bellwied, A. Carroll, J.B. Costales, S. Gavin, M. Kramer, R. Ledoux, P. McGaughey, M. Muthuswamy, A. Sambamurti, X.N. Wang

August 10, 1990

There were two main purposes for the pA subgroup. The first was to identify the design requirements for detectors so that they could be used with as little modification as possible for both p + A and A+A collisions. The second was to determine if there were physics issues that could be particularly well addressed in p+A experiments at RHIC. Both of these topics are discussed in this document. We begin, however, with a brief description of how the accelerator operates in asymmetric collisions.

1 Colliding Laurel and Hardy at RHIC

In the collision of beams of unequal species, the beams must have the same velocity (i.e., the same E/A). This results in a rotation of the line of head-on collisions with respect to the longitudinal center axis of the magnetic optics (beam rotation angle) due to the use of a shared dipole after the intersection region. The beam optics [1] in the intersection region is shown in Figure 1. The luminosities [2] for p+A collisions are obtained by scaling the number of particles in a bunch (i.e., $L(pA) = [L(pp) * L(AA)]^{1/2}$). The beam-beam scattering is large for Au-Au collisions and significantly reduces the luminosity with time. Therefore, the average of the initial and 10 hour luminosities for Au was used. For all other beams, the initial luminosity was used.

Table 1. Luminosities and beam rotation angles for 100 A·GeV/c beams. The luminosity for p+p collisions was taken to be $1.4 * 10^{31}/(cm^2 sec)$.

Heavy-Ion Beam	Heavy-Ion Luminosity	Combined Luminosity	Beam Rotation Angle (mrad)
O	$9.8 * 10^{28}$	$1.2 * 10^{30}$	2.62
Si	$4.4 * 10^{28}$	$7.8 * 10^{29}$	2.62
Cu	$9.5 * 10^{27}$	$3.6 * 10^{29}$	2.96
I	$2.7 * 10^{27}$	$1.9 * 10^{29}$	3.25
Au	$2.0 * 10^{26}$	$5.3 * 10^{28}$	3.40

2 How to make p+A and A+A measurements compatible

There are several considerations which must be carefully addressed if the same detector is to be used in p+A and A+A measurements. Some of these are:

1.) The change in the laboratory angles for the p+A 'center-of-mass'.

2.) The higher luminosities in p+A measurements.

3.) The large dynamic range in detector response and fill factors.

4.) The beam rotation angle.

2.1 Angular Coverage

We begin by considering the necessary coverage in laboratory angle and momentum in p+A collisions. There is no unique definition of a center of mass frame in p+A collisions. However, a useful definition, which also serves as a limiting case, is to consider the kinematics for a collision in which the

proton 'coherently' interacts with the nucleons along its path through a nucleus. Rapidity distributions from the event Monte Carlo VENUS [3] are shown in Figure 2. The rapidity of the center-of-mass is shifted to $y_{lab} \approx 0.8$ in the Au beam direction. (This can be obtained simply by noting that $y_{cm} \approx 0.5 * ln(M/m)$, where $M/m \approx 5$ for minimum bias p+Au.) Pions with a $< p_t >= 0.4$ GeV/c and this rapidity are emitted at 40° in the lab frame. A proton with the same y and p_t is emitted at 20° . The main impact of the shift in the center-of-mass rapidity in the laboratory is that a detector which is designed to measure a similar region of phase space in p+A and A+A collisions must be able measure at more forward angles than may be necessary in A+A collisions alone.

2.2 Luminosity

The inelastic cross sections for p+p, p+A and A+B collisions are approximately $4.5 fm^2$ (extrapolated from ref. [4]), $4.5 A^{0.69} fm^2$ and $6.8(A^{1/3} + B^{1/3} - 1.6)^2 fm^2$, respectively. Table 2 lists the inelastic cross section, interaction rate, mean time between collisions ($< t_{col} >$), and the number of interactions per crossing for p+p, p+Au and Au+Au collisions. There is a factor of 500 decrease in the interaction rate in going from p+p to Au+Au collisions. From a point of view of analog and digital electronics, Au+Au interactions occur at a very low rate . However, if the same electronics are to be used for both A+A and p+A measurements, the electronics must be designed to handle a two orders of magnitude increase in rate (with a possible reduction in optimization for A+A collisions) or the proton luminosity must be reduced.

Table 2: Interaction rates for p+p, p+Au and Au+Au collisions.

	σ_{inel} (mb)	Rate (sec^{-1})	$< t_{col} >$ (sec)	Interactions/Crossing
p+p	45	$6 * 10^5$	$2 * 10^{-6}$	$1 * 10^{-1}$
p+Au	1740	$8 * 10^4$	$1 * 10^{-5}$	$2 * 10^{-2}$
Au+Au	6850	$1 * 10^3$	$1 * 10^{-3}$	$3 * 10^{-4}$

2.3 Dynamic Range

Generally, a detector for which one wishes to preserve the same precision in both p+A and A+A collisions must have a large dynamic range. The mean multiplicity and dn/dy for different particle species for 100 A·GeV/c p+p, p+Au, and Au+Au collisions are given in Tables 3a-c. There is an increase in the negative particle rapidity density at $y_{lab} = 0$ by over two orders of magnitude from minimum bias p+Au to central Au+Au. Therefore, if the precision of a measurement is to stay fixed for all mass systems then the electronics must be designed with either the necessary precision over the full dynamic range or the fullscale range of the electronics must be programmable. This is particularly true for detectors which have fill factors of 10 - 100 particles per central Au+Au collisions.

Tables 3a-c: Mean multiplicities and rapidity densities at $y_{lab} = 0$ for 100 A·GeV/c p+p, p+Au and Au+Au collisions.

3a

p+p minimum bias						
	VENUS 3.07		Fritiof 1.7		Hijet	
Particle	$< n >$	$dN/dy_{y=0}$	$< n >$	$dN/dy_{y=0}$	$< n >$	$dN/dy_{y=0}$
π^+	8.31	1.2	7.65	0.99	9.08	1.23
π^-	7.75	1.2	7.05	0.95	8.40	1.20
K^+	0.80	0.11	0.75	0.11	0.67	0.09
K^-	0.70	0.10	0.64	0.090	0.67	0.09
p^+	1.71	0.076		0.079	1.56	0.06
$\bar{p}$	0.38	0.058	0.43	0.065	0.30	0.04
ϕ	0.0086	0.0015				

3b

p+Au minimum bias						
	VENUS 3.07		Fritiof 1.7		Hijet	
Particle	$< n >$	$dN/dy_{y=0}$	$< n >$	$dN/dy_{y=0}$	$< n >$	$dN/dy_{y=0}$
π^+	20.8	2.8	19.9	2.6	22.9	3.15
π^-	21.3	2.9	20.0	2.7	22.6	3.20
K^+	2.1	0.29	2.0	0.30	1.61	0.22
K^-	1.8	0.28	1.8	0.25	1.59	0.21
p^+		0.17		0.19		0.18
$\bar{p}$	0.88	0.13	1.2	0.19	0.70	0.12
ϕ	0.020	0.003				

3c

Au+Au VENUS		
	Average	Central
Particle	$dN/dy_{y=0}$	$dN/dy_{y=0}$
neg	250	800
p^+	13	30
$\bar{p}$	10	20

2.4 Beam Rotation Angle

The beam rotation angle should have very little effect on momentum and energy measurements of particles except for those at the most forward angles. For p+Au collisions, $\Delta\theta = 3.4$ mrad which results in a $\Delta\eta = 0.2$ at $\theta = 1°$ ($\Delta\eta = (1/\sin\theta) * \Delta\theta$). Even if the reconstruction of tracks does not take into

account the beam rotation angle, the uncertainty in p_t is only 350 MeV/c for a beam momentum particle. The greatest impact will be on experiments with a zero-degree calorimeter after BC1, which is 10 m from the intersection region (see Figure 1). The beam in p+Au collisions is approximately 3.4 cm off center of the front face of DC1 which has an aperture of only $\pm$8.5 cm. Careful consideration in the design of such a zero degree calorimeter will be necessary to accomodate the beam rotation and the space constraints behind BC1. (It should be noted that in the present layout of the beam optics the two BC2 magnets are touching behind BC1.)

3 Physics of p+A Collisions

There are as many possible measurements in p+A collisions as there are in A+A collisions. In this section we have selected from the many possible topics four specific areas of p+A measurements which we considered of interest themselves, as well as being vital for a comparison to A+A collisions. They are:

1.) Baryon distributions.

2.) Identical particle interferometry.

3.) J/ψ and Drell-Yan production via measurements of dileptons.

4.) Jet production.

Many of the measurements we describe here are similar to those which are contemplated for A+A collisions. We will only highlight experimental issues which are relevant to changes incurred in going from A+A to p+A collisions. The reader is encouraged to examine the proposals from various collaborations in these proceedings.

3.1 Baryon Distributions

The available energy in the nucleon-nucleon center-of-mass of 200 GeV for p+A collisions at RHIC is five times higher than the center-of-mass energy presently available at FNAL (which is the highest energy fixed target facility). It is expected that at RHIC energies the central region will be relatively

free from the 'contamination' of projectile fragments, that is, the net baryon number should be close to zero. This expectation is based on the few measurements [5] of baryons within approximately 2 units of the beam rapidity taken at substantially lower energies. These measurements are consistent with a mean rapidity loss of 2 - 2.5 units for protons colliding with a heavy nucleus such as Au. It is very important to directly measure the rapidity loss of the beam rather than assume it is invariant with energy. For these measurements, there are fewer ambiguities in p+A collisions than A+A collisions, since the intial baryon number in the proton beam direction is known without reference to a specific trigger or model.

The distribution of protons and anti-protons from the event Monte Carlo VENUS is shown in Figure 3 for minimum bias p+Au collisions. The difference between these two distributions is proportional to the distribution of the proton fragments. The rapidity distribution in the proton fragmentation region is similar to that from lower energy measurements. VENUS predicts that the ratio of protons to anti-protons is 1.3 at $y_{lab} = 0$, which represents $\approx 30\%$ contribution to the baryon number from beam fragments at mid-rapidity. Examination of Table 3b reveals that this ratio is 1.5 for Hijet and 1.0 for Fritiof calculations. These differences are presumably related to the dynamics used in each model for beam fragmentation. Therefore, measurements of baryons, even at mid-rapidity alone, will strongly constrain these models. To obtain a more detailed understanding of the energy loss mechanism it is necessary to make measurements in a region where the beam fragments actually dominate over baryon pair production. VENUS suggests that this is true for $y_{lab} >$ [illegible]. This corresponds to measurements at angles forward of 5° in the laboratory. These are very difficult measurements and would probably only be performed with a small aperature forward spectrometer.

The study of the transverse momentum distributions for all particles and, in particular, for baryons is also very important. The systematics of the p_t distributions for different particle species as a function system mass, obtained by either changing the mass of the nuclear beam or gating on central collisions, will form the baseline for comparison with those from A+A collisions. The comparison between p+A and A+A collisions will be particularly important for experiments which will study high p_t phenomena, such as jet production, since presumably, the p_t distributions from p+A collisions contain the effects of multiple scattering of the beam and rescattering of

secondaries, but not any 'coherent' effects which may be present in A+A collisions.

There exists a single measurement [6] of the $< p_t >$ of leading baryons in p+A collisions at $\sqrt{s_{NN}} = 20$ GeV. The $< p_t >$ was found to increase with increasing rapidity loss of the leading baryon. Measurements of p+A and Si+A collisions by E802 at the AGS [7, 8] have shown that the $< p_t >$ for baryons is: much higher than for pions and kaons, dependent on rapidity, and increases with increasing system mass. The relatively large separation between the beam fragmentation and mid-rapidity regions at RHIC should help clarify the roles of initial and final state scattering of participant baryons in p+A collisions. A further comparison with A+A collisions should determine if there are collective effects in the baryon distributions for nuclear collisions.

3.2 Identical Particle Interferometry

Identical particle interferometry has been used to infer the space-time extent of pion sources in hadronic collisions. The bulk of the existing measurements, mostly from A+A collisions at the Bevelac, are consistent with a transverse source size approximately equal to the radius of the smaller colliding nucleus. A compilation of data [9], including recent measurements from CERN and the AGS, is shown in Figure 4a.

A transverse radius of about 8 fm (which is twice the radius of the oxygen projectile) has been obtained by NA35 [10] for central O+Au collisions by selecting pairs at the effective center-of-mass. In a simple model [10], the freeze-out radius of the pion source should be proportional to $\sqrt{N_\pi}$. An increase in the pion source size with the event multiplicity has also been reported by Akesson *et al.* [11] for p+p, p+$\bar{\text{p}}$, and $\alpha + \alpha$ interactions. The only existing p + heavy-nucleus measurement (p+Xe) [12] did not observe an increase in source size with pion multiplicity. A compilation [13] of sources sizes as a function of charged particle rapidity density (dn/dy) is shown in Figure 4b.

The use of beams with different energy and mass number in p+A collisions at RHIC will allow for a systematic investigation of the space-time extent of particle sources as a function of particle multiplicity. If the central rapidity region is relatively baryon free, then the interpretation of interferometry results should also be more straightforward at RHIC. The expected charged particle rapidity densities at mid-rapidity in p+Au collisions are ap-

proximately 7 and 10 in minimum bias and central collisions, respectively. As can be seen from Figure 4b, these are very interesting rapidity densities to investigate in p+A collisions since the expected source size is 3 fm based on rapidity density scaling as compared to the proton radius of 1 fm. The relatively high multiplicities should also allow for the measurement of kaon source sizes. The comparison of sources for pions and kaons gated on event topology should help elucidate the dynamics involved in particle production in p+A collisions.

3.3 J/ψ and DY Production

The measurement of the A dependence of dileptons in p+A collisions at RHIC is important for a variety of reasons. One of the foremost motivations is that the suppression of J/ψ production in nuclei has been proposed [14] as a signature of a QGP in RHI collisions. This cannot be quantified until the details of p+A reactions are understood. Since J/ψ production is sensistive to the gluon structure functions in nuclei and possibly initial and final state scattering effects, it is important to study J/ψ production as a function of both Feynmann-x (x_F) and p_t to quantify these effects. The study of higher mass dileptons resulting primarily from Drell-Yan pair production (DY) also probes the quark and antiquark structure functions of nuclei, as has been recently shown [15] by E772 at Fermilab.

Recent results from E772 for high mass dilepton production as a function of target mass at $\sqrt{s_{NN}} = 39$ GeV are shown in Figure 5 for J/ψ and Drell-Yan production. The cross section for J/ψ production is proportional to $A^{0.92}$, which deviates significantly from the $A^{1.0}$ dependence expected for hard processes without initial or final state interactions. The A-dependence for DY is very close to, but not exactly equal to, $A^{1.0}$. It is important to note the high statistics needed to measure the A-dependence of the high mass dileptons, particularly above 4 GeV. Strong A-dependencies in J/ψ production as a function of x_F and p_t have been observed in fixed target p+A experiments [16, 17]. The origin of these effects is not yet quantitatively understood. In addition, D meson production is also strongly A-dependent, indicating that the heavy quark production process (and not just resonance production) may be sensitive to the nuclear medium.

Measurements at RHIC will provide data at a significantly higher center-of-mass energy and will also allow for measurements at low rapidity ($x_F < 0$)

for the first time. The luminosity should be adequate to obtain high statistics for both J/ψ and DY production. For example, assuming for p+Au collisions a luminosity $= 5 * 10^{28}/(cm^2 sec)$, $\sigma_{J/\psi} = 100$ nb/u and $\sigma_{DY} = 0.3$ nb/GeV/u at 4 GeV, yields production rates of 50K/day and 2K/day for J/ψ and DY, respectively.

There is very limited data [18, 19] on the production of lower mass dilepton pairs in p+A collisions. The available data for the cross section of ρ and ϕ production yields an A-dependence of approximately $A^{0.7}$ at $\sqrt{s_{NN}} \approx 20$ GeV. This large deviation from an $A^{1.0}$ dependence is presumably related to the greater importance of initial and final state interactions for low mass resonances. However, there are predictions that the production cross sections and widths of these resonances may be modified in a QGP or hot hadron gas. Given the limited data and theoretical guidance presently available on the effects due to rescattering, it is prudent to study nuclear effects in p+A collisions before looking for collective effects in A+A collisions.

3.4 Jet Production

Jet production in e^+e^-, pp and $p\bar{p}$ collisions has been studied extensively now for over a decade. It has been shown conclusively that jets from hadronic collisions are the result of hard scattering between the parton constituents of the hadrons [20]. Perturbative QCD (pQCD), in conjunction with parton models, has been successful in describing the characteristic features of jet production, such as production rates and angular distributions. Most experimental studies of jets have concentrated on relatively large P_t jet production, but it has been suggested that minijet production [21] becomes increasingly important at $Sp\bar{p}S$ energies and higher. The exact p_t scale at which pQCD can be used to predict minijet production is still a matter of intense debate, but there is experimental evidence of the existence of minijets [22] , and it is believed that minijets will be responsible for about half of the total particle production in central Au+Au collisions at RHIC [23] .

In contrast, jet and minijet production in p+A collisions remains experimentally and theoretically almost unexplored. Fixed-target experiments [24, 25, 26, 27, 28] have been performed at $\sqrt{s_{NN}} = 20$-30 GeV on a variety of targets; some results from the Fermilab E557 Collaboration are shown in Figures 6a-b. The nuclear dependence of the "jet-like" cluster production cross section, σ_{jet}, is plotted in Figure 6a as a function of E_T [26] . The

jet-cluster cross section is parameterized as $\sigma_{jet} = \sigma_o A^{\alpha(E_T)}$, where A is the target mass number and $\alpha(E_T)$ is a function of E_T. These data were taken with a small aperature trigger, which requires a large value of E_T in a small region of a calorimeter, as one might expect for jet production. As has been observed in high p_t production of hadrons at similar beam energies, such as by Cronin et al. [29], there appears to be a nuclear enhancement of jet-cluster production for large values of E_T, signaled by $\alpha(E_T) > 1$. Figure 6b is a plot of the transverse momentum flow in azimuthal angle ϕ, where ϕ is defined relative to the jet cluster axis [28] . These data correspond to events containing "back-to-back" (BB) jet clusters with a combined transverse energy $E_T > 15$ GeV. It appears that jet clusters from p+A collisions are broader than those from p+p collisions.

These data represent the state-of-the-art p+A measurements for jet production. However, several problems still exist:

1.) The beam energies of p+A experiments to date are still too low for a proper study of jets even for $p\bar{p}$ collisions, much less p+A; and

2.) Unlike collider experiments, jets in fixed-target experiments are difficult to identify uniquely. Commonly used triggers in p+A jet experiments may enhance the selection of jet events but it is not certain whether or not they pick out jet events unambiguously.

In contrast, jet production at RHIC energies ($\sqrt{s_{NN}} = 200$ GeV) should be relatively abundant when compared to ISR energies. Jet production at mid-rapidity is more easily measured in a collider experiment than in a fixed-target experiment. Hence, jets at RHIC will offer a new and essentially unexplored probe of nuclear matter in p+A and A+A collisions. The study of jet production in p+A collisions can be easily incorporated into detectors designed to measure jets in A+A collisions.

Jets in p+A collisions merit their own study, and not just in relation to A+A collisions, for the following reasons. A jet is produced in a p+A collision during the brief time that the highly Lorentz-contracted proton and nucleus overlap (when observed in the nucleon-nucleon center-of-mass frame). The time scale during which a hard scattering takes place goes as $1/Q$, where Q is the momentum transfer. Hence, for large P_t jets, the scattered partons materialize very quickly. These partons then propagate through the nuclear matter as they begin to fragment into final-state particles. The nucleus can

be regarded as a filter which can effect the parton's dynamical evolution. One can change the filter by substituting targets with different masses. For jet production, p+A collisions have an advantage over A+A collisions in that jets in A+A collisions will probably be difficult to identify event-by-event. However, the "background" in p+A collisions is small enough that a precision measurement of jet production and jet characteristics can be made. Moreover, the amount of nuclear matter traversed by the jet can be well determined on an event-by-event bases by gating on the distribution of other secondary particles.

A number of interesting effects have been predicted for jet propagation in nuclear matter. One is that a jet loses a considerable amount of energy ($\approx$ 1 GeV/ fm of nuclear matter traversed) due to the "string" flip mechanism [30] . Such "jet quenching" may be already been observed in e^-A collisions performed at SLAC [31] . It has also been suggested that this quenching will be greater for gluon jets than quark jets. Gluon-gluon scattering, as well as minijets, occurs at lower P_t, and hence requires large beam energies, such as at RHIC, in order to be studied efficiently. However, it can also be argued that in the absense of this attenuation, jet production may be enhanced for nuclear targets at large P_t because of the scattering of the initial proton beam, as well as the rescattering of the jet partons, and the particles they fragment into (i.e., the Cronin effect). The discrepancy between these two predictions for jet production can only be resolved by a measurement.

As a result of the nuclear medium, one might expect that not only the jet production rate changes, but characteristic features of jets, such as the jet multiplicity and fragmentation function, well-established by p+p measurements made at the $Sp\bar{p}S$ and the Tevatron, will also be different. Differences between the p+p and p+A data might reveal interesting features of the hadronization process that are difficult to measure any other way.

References

[1] *Proceedings of the Third Workshop On Experiments and Detectors for a Relativistic Heavy Ion Collider (RHIC)*, Brookhaven National Laboratory, July 18-22, 1988.

[2] *Conceptual Design of the Relativistic Heavy Ion Collider (RHIC)*, Brookhaven National Laboratory, May 1989.

[3] K. Werner and P. Koch *Phys. Lett.* **B242**, 251 (1990).

[4] A. Donnachie in *Proceedings of the XXIII International Conference on High Energy Physics, Berkeley, California, 1986,* ed. S.C. Loken (World Scientific Publishing Co., Singapore, 1986) p. 1341.

[5] W. Busza and R. Ledoux, *Ann. Rev. Nucl. Part. Sci.* **38**, 119 (1988).

[6] W.S. Toothacker et al., *Phys. Lett.* **B197**, 295 (1987).

[7] T. Abbott, et al., Phys. Rev. Lett. **64**, 847 (1990).

[8] M. A. Bloomer, Ph.D. thesis, MIT (unpublished, 1990); J. B. Costales (E802 Collaboration) in *Proceedings of the Workshop on Heavy Ion Physics at the AGS,* Brookhaven National Laboratory, March 1990 (to be published).

[9] W. A. Zajc in *Multiparticle Production,* P. Carruthers, ed. (World Scientific Publishing Co., Singapore, 1988); W. A. Zajc in *Proceedings of QM90,* Menton, France, May 1990 (to be published).

[10] A. Bamberger et al., *Phys. Lett.* **B203,** 320 (1988).

[11] T. Akesson, et al., *Phys. Lett.* **B129,** 269 (1983).

[12] C. De Marzo, et al., Phys. Rev. **D29,** 363 (1984).

[13] W. A. Zajc in *Proceedings of QM90,* Menton, France, May 1990 (to be published).

[14] T. Matsui and H. Satz, *Phys. Lett.* **B178,** 416 (1986).

[15] P. McGaughey (FNAL E772 Collaboration), private communication.

[16] S. Katsanevas, et al., *Phys. Rev. Lett.* **60**, 2121 (1988).

[17] J. Badier, et al., *Z. Phys.* **C20**, 101 (1983).

[18] M. Binkley, et al., *Phys. Rev. Lett.* **37** 571 (1976).

[19] J. G. Branson, et al., *Phys. Rev. Lett.* **38** 1334 (1977).

[20] P.D.B. Collins and A.D. Martin in *Hadron Interactions,* ed. D.F. Brewer (Adam Hilger Ltd, Bristol, 1984).

[21] A. Capella, J. Tran Thanh Van and J. Kwiecinski, *Phys. Rev. Lett.* **58** (1987) 2015; K.J. Eskola, K. Kajantie and J. Lindfors, *Nucl. Phys.* **B323**, 37 (1989).

[22] C. Ciapetti (UA1 Collaboration), in *The Quark Structure of Matter: Proceedings of the Yukon Advanced Study Institute, Yukon, Canada, 1984,* ed. M. Jacob and K. Winter (World Scientific, Singapore, 1986), p. 455.

[23] X. N. Wang, private communication.

[24] Bromberg et al., *Phys. Rev. Lett.* **42**, 1202 (1979).

[25] Brown et al., *Phys. Rev. Lett.* 50, 11 (1983).

[26] Gomez et al., *Phys. Rev.* **D35**, 2736 (1987).

[27] Miettinen et al., *Phys. Lett.* **B207**, 222 (1988).

[28] C. Stewart and A. Zieminski (E557 Collaboration), in *Proceedings of the 3rd Conference on the Intersections Between Particle and Nuclear Physics, Rockport, Maine, 1988,* ed. Gerry M. Bunce (American Institute of Physics, New York, 1988) p. 630; C. Stewart et al. (Fermilab E557 Collaboration), "Production of High-p_t Jets in Hadron-Nucleus Collisions", preprint (unpublished).

[29] Cronin et al., *Phys. Rev.* **D11**, 3105 (1975).

[30] M. Gyulassy and Michael Plümmer, LBL-28531 report.

[31] M. Gyulassy and Michael Plümmer, LBL-27605 report.

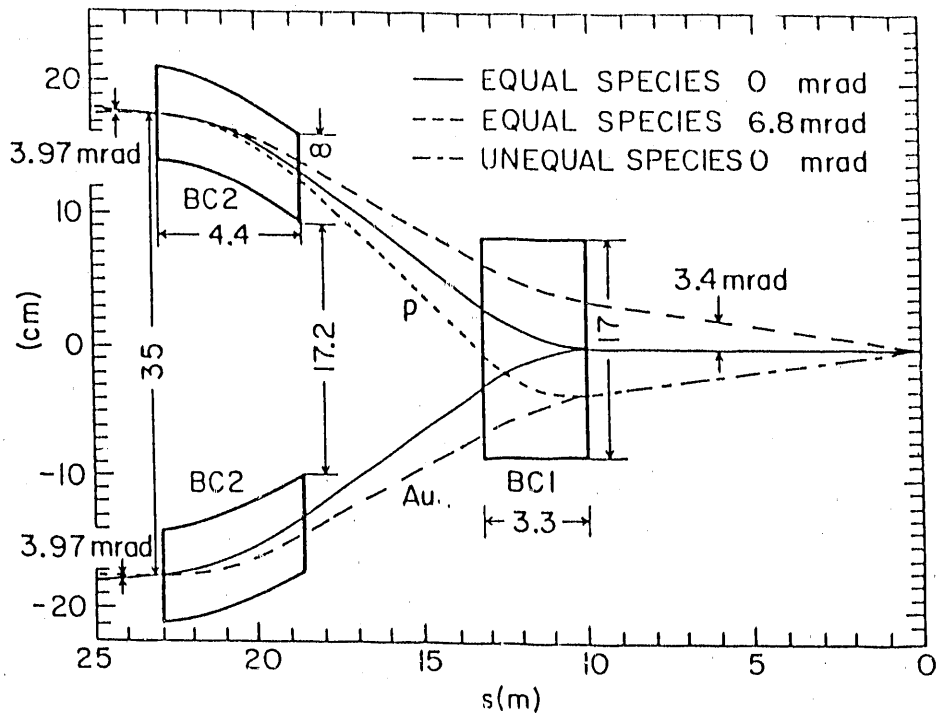

Fig. 1 The beam optics in the intersection region at RHIC [1] .

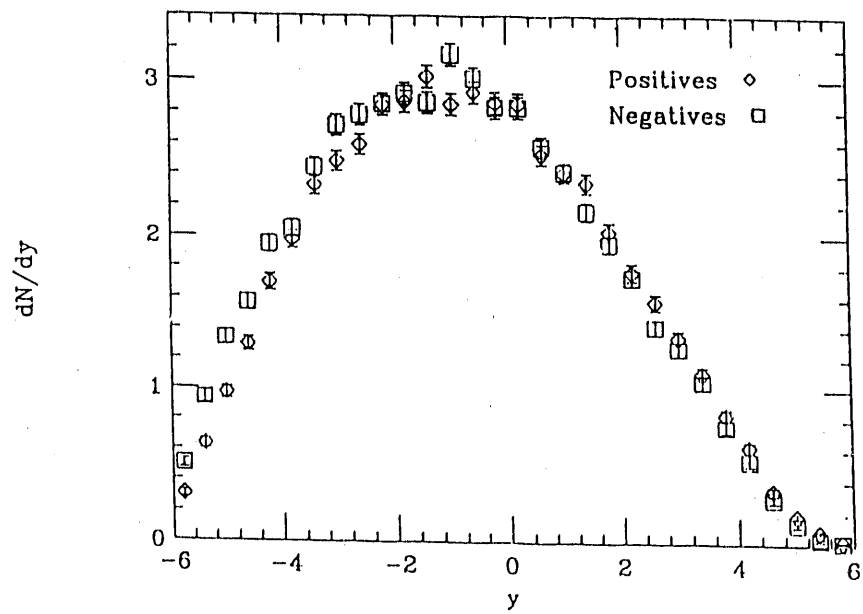

Fig. 2 Rapidity distribution for π^+ and π^- from the Monte Carlo code VENUS for 100 A·GeV/c p+Au collisions.

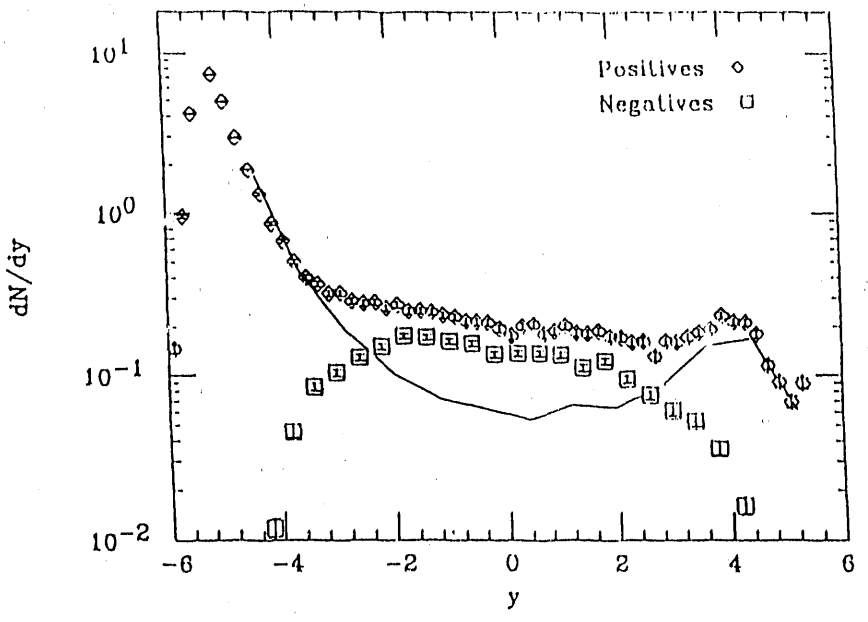

Fig. 3 Rapidity distribution for p and $\bar{p}$ from the Monte Carlo code VENUS for 100 A·GeV/c p+Au collisions. The solid curve is the difference of the p and $\bar{p}$ distributions.

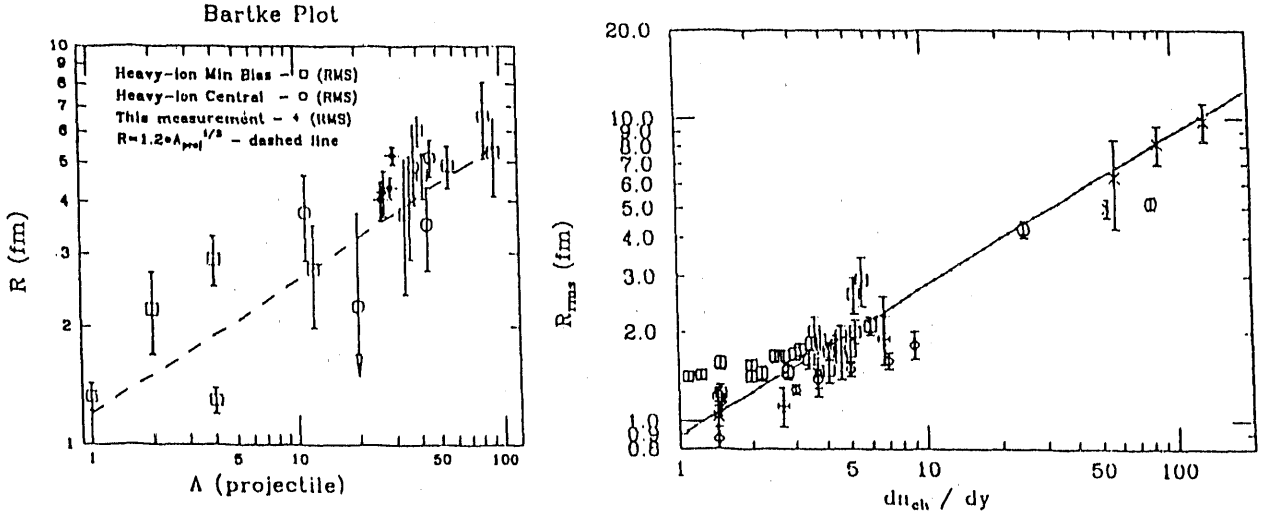

Fig. 4 (a) The rms radius extracted from identical pion interferometry for p+A and A+A reactions versus the atomic mass of the projectile [9]. (b) The rms radius as a function of the charged particle rapidity density [13] . The solid curve is the function $R_{rms} = 0.9 * \sqrt{dn_{ch}/dy}$.

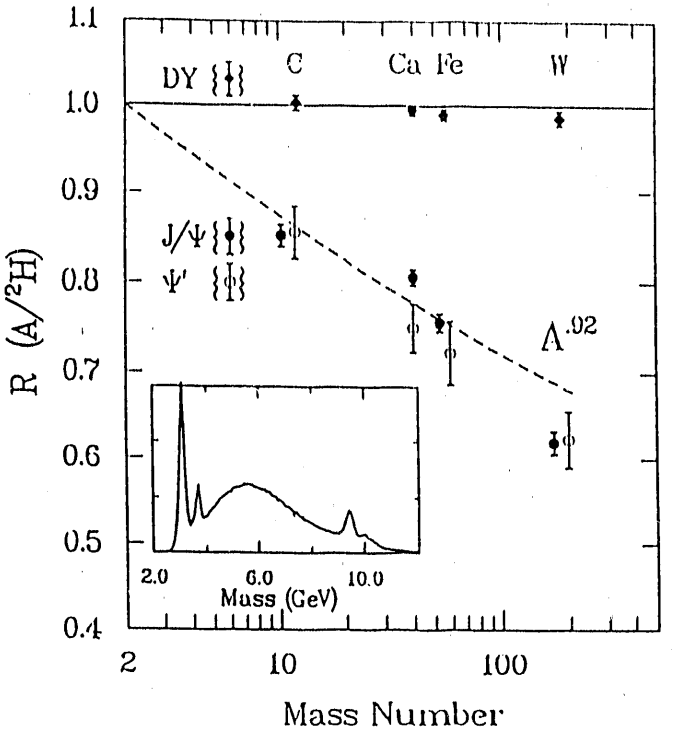

Fig. 5 A-dependence of heavy-mass dileptons from FNAL E772 [15].

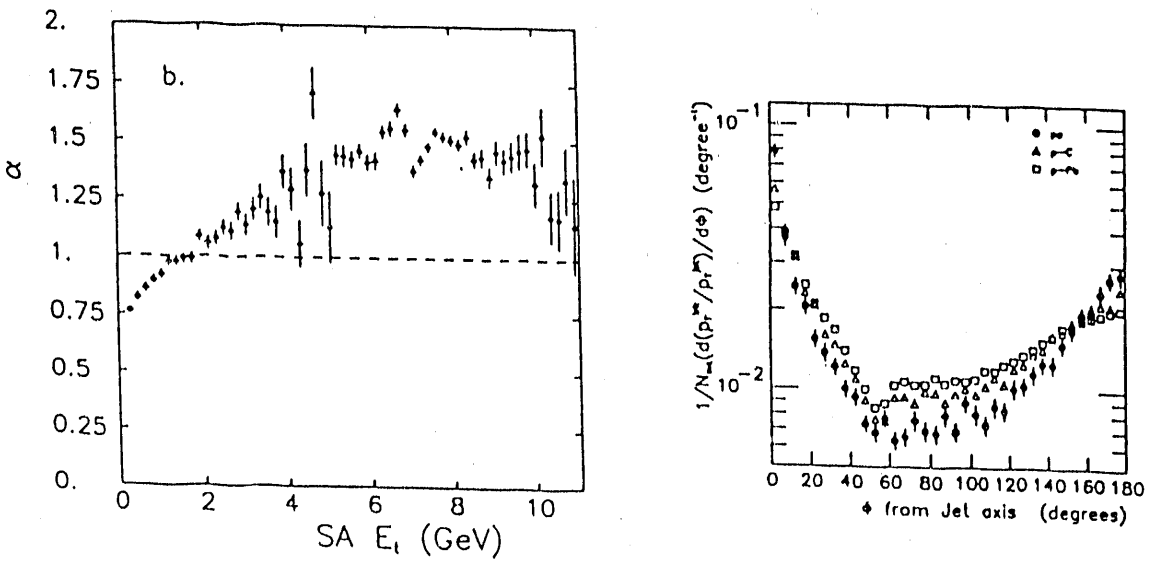

Fig. 6 (a) $\alpha(E_{\rm T})$ versus $E_{\rm T}$ for the small aperature trigger [26] . (b) The azimuthal p_t flow versus the azimuthal angle ϕ, relative to the jet cluster axis, for events with "back-to-back" jet clusters [28] .

STUDY GROUP IV

The Physics of Strong Electromagnetic Fields In Collisions of Relativistic Heavy Ions.

Convenor:

M.Fatyga

Brookhaven National Laboratory

Contents:

QED Study Group - List of Participants.

C.A.Bertulani
Univ. Fed. De Rio De Janeiro

J.C.Hill
Iowa State University

J.W.Norbury
Rider College

J.Wu
Oak Ridge National Laboratory

M.Fatyga,T.Ludlam,M.J.Rhoades-Brown,M.J.Tannenbaum
Brookhaven National Laboratory

A note from the convenor

This summary report is comprised of several separate sections reflecting a variety of activities related to the subject which took place before and during the workshop.

The workshop entitled *Can RHIC Be Used to Test QED?* was held at Brookhaven in April of 1990. This workshop was organized by M.Fatyga, M.J.Rhoades-Brown and M.J.Tannenbaum. Its purpose was to discuss the present status of theory and to identify most interesting areas of investigation in the physics of strong fields which could be explored at RHIC. Perhaps the greatest emphasis was put on non-perturbative aspects of the e^+e^- pair production in a collision of high energy heavy ions, but other aspects of two photon physics at RHIC were also discussed. Two experimental groups presented their current and planned efforts in measuring the yields of e^+e^- pairs produced in heavy ion collisions at CERN, LBL and BNL. The summary of the workshop (prepared by its organizers) is the first item in the report of this study group.

During (and prior to) the RHIC workshop in July 1990 two separate efforts were undertaken. First, the question of e^+e^- pairs as a background in a search for new phenomena in central collisions of heavy ions has been addressed quantitatively by M.J.Rhoades-Brown, J.Wu et.al. Second, a feasibility of the experimental study of strong field phenomena at RHIC has been investigated by M.Fatyga and J.W.Norbury. Results of these two efforts are summarized in separate contributions. All the members of the study group (listed below) contributed to discussions on these two subjects. Individual reports however, are authored by the people who directly contributed to a particular effort.

Finally, I would like to turn the attention of the reader to one more contribution in this issue of the proceedings which is very relevant to our subject but not included in the summary report of this study group. Namely, S.U.Chung et.al discuss a conceptual design of an experiment which is intended to measure a production of low mass mesons and resonances in extremely peripheral collisions of relativistic heavy ions. This subject has also been identified during the April workshop as a very promising field of investigation. Since none of the authors of the paper participated in the QED study group, their contribution has been placed elsewhere in the proceedings.

CAN RHIC BE USED TO TEST QED

Workshop Summary

Mirek Fatyga
Mark Rhoades-Brown
Michael Tannenbaum

The two day workshop entitled "Can RHIC be Used to Test QED" took place on April 20 - 21 at Brookhaven National Laboratory. It was attended by approximately 50 physicists from both the U.S. and Europe. Although most of the attendees were theorists, a large portion of the second morning was devoted to pending experiments and the experimental difficulties associated with strong field electromagnetic phenomena. The workshop was remarkably multidisciplinary in nature, attracting elementary particle, nuclear and atomic theorists and experimentalists.

We note that at RHIC, fully stripped Au ions will be accelerated to beam energies of 100Gev/u in a collider mode. At these energies the S-matrix for single $e^+ + e^-$ pair production violates unitarity bounds, thus implying that multiple pair production will occur. The theoretical language for investigating this phenomena is contained within the so-called virtual two photon representation of the heavy ion electromagnetic fields.

Three general subjects were addressed during the workshop. These subjects were:

1. To understand the validity of the best available descriptions of $e^+ e^-$ pair production in peripheral heavy ion collisions, especially for the domain where this process is known to be non-perturbative.

2. To understand the prospects for using relativistic heavy ions to produce Higgs Bosons or Weak Bosons (Z_0, W+, W-). This production mechanism proceeds through the virtual two photon representation of the heavy ions, and is considered a reason for accelerating heavy ions in both the LHC and the SSC.

3. To study the interference mechanisms between the two processes for hadron production in peripheral heavy ion collisions. These two processes are two photon exchange and two pomeron exchange.

$e^+ e^-$ Pair Production in Heavy Ion Collisions

In addition to the fundamental questions regarding $e^+ e^-$ pair creation and non-perturbative QED, it is important for both detector design and collider performance to understand the pair creation mechanism during the heavy ion beam crossing. The created pairs could be a source of background in the detectors at heavy ion colliders. Of equal importance to the detector background is the so-called capture problem, associated with a heavy ion capturing one of the produced electrons in an atomic orbital. Changing the charge state of the heavy ion by one unit will eventually cause the ion to be lost from the beam. This mechanism is a major component in determining the luminosity lifetime in a heavy ion collider.

As discussed by Brodsky and Strayer, the $e^+ e^-$ pair production cross sections in the lowest order perturbative limit was shown to be 33.7K barns for Au beams at top energy in RHIC. This number came from both exact Monte Carlo evaluation of the perturbative matrix element, and by applying the analytic formula due to Racah (Nuovo Cimento 14 (1937) p. 70). Since the

workshop, it has been shown (C. Bottcher, private communication) that the Racah formula and Monte Carlo calculations for e^+ e^- pair production agree extremely well for Lorentz gamma values spanning nearly 4-orders of magnitude (beginning at $\gamma=2$).

Strayer showed that with modern computers, the multidimensional integrals associated with pair creation can be efficiently evaluated using a million or so Monte Carlo points. Detailed Monte Carlo calculations with nuclear form factors showed that the form factors act to suppress the p_T momentum dependance of the differential cross sections $d\sigma/dp_T$. The total cross section for electron pair creation is not affected by the nuclear form factor. Calculations for the single e^+ or e^- distribution $d\sigma/dp_T$ showed that most of these particles are produced in the forward (or backward) direction along the beam axis, with the perpendicular component of the singles momentum falling several orders of magnitude as p_T grows from 0 to 100Mev. Thus, most of the singles or pairs may be considered soft in nature. Further calculations of the energy distributions and the angular distributions of the singles and pairs are expected to be performed at the forthcoming RHIC workshop (July 1990). Strayer also showed his calculations for mu-pair production, including the interesting result that for invariant mass values M<4Gev, the coherent differential cross section $d\sigma/dydM$ from beam crossing is larger than the Drell Yan background.

For a certain class of detectors at RHIC, the total integrated cross section may not be the most relevant quantity. If the detector gates on a limited range of impact parameters, the pair production probability for these impact parameters might be more relevant. Further studies are needed on this impact parameter question.

The fact that $e^+ e^-$ pair production at RHIC violates unitarity was clearly shown by Brodsky and Baur, the latter stating that the probability for producing a single pair at an impact parameter corresponding to the Compton wavelength is 2.5 for Au beams at top RHIC energies. This result clearly suggests that higher order QED effects, most notably multiple pair production, could be observed at RHIC. Estimates for the number of $e^+ e^-$ pairs per ion interaction varied greatly. Brodsky, using an argument based on counting the number of equivalent photon-photon interactions per unit of rapidity interval for each heavy ion, gave an upper limit of 2000 pairs per interaction at RHIC. Baur, using an analogy of exciting harmonic oscillators by a time dependent force, schematically sums multiple pair diagrams to arrive at a Poisson distribution for the probability of producing pairs of multiplicity N at a given impact parameter. This technique suggests only a few pairs are produced, but after intense discussion, it was suggested (Muller) that the accuracy of neglecting the time ordering in the perturbation series needs to be explored in more detail.

Two theories for understanding non-perturbative QED phenomena were presented. Bottcher described a promising technique for non-perturbative electron pair production, based on the light cone representation of the Dirac equation. This high energy representation takes advantage of the weak coupling between the longitudinal and transverse momenta of the produced pair. For Au beams at RHIC, calculations based on this method indicate a factor of two reduction in the total electron pair cross section from the perturbative result. In contrast, Schied described a coupled-channels calculation for non-perturbative $e^+ e^-$ pair creation. This calculational technique is difficult to implement at RHIC energies, but at lower energies (γ=10), two orders of magnitude enhancement over perturbative estimates were

claimed for the pair production cross section. Enhancements of this order were also shown for the electron capture cross section.

The striking mismatch between theories for the effects of higher order QED was not resolved at the workshop. The light cone approach is probably not applicable at lower energies (γ=10), and the coupled channels technique is technically difficult to implement at higher energies. However, it is important for both RHIC luminosity lifetime questions, and heavy ion collider detector design, to address the questions on "just how important are higher order QED effects?". As discussed by McLerran, this will require evaluation of higher order diagrams, including box diagrams, as well as detailed comparison with experimental data.

Datz and Belkacem described their experimental procedures for measuring pair production and electron capture at CERN (S beams) and Berkeley (U beams) respectively. Although these fixed target experiments are at energies considerably below what will be achieved at RHIC, they will be an essential component in helping to understand some of the above theoretical discrepancies. Within two years, Au beams will become available at the AGS (γ=10), and thus could provide another set of experimental data.

After the workshop, it was suggested (Fatyga) that the impact parameter dependence of the non-perturbative $e^+ e^-$ production could be studied through a coincidence experiment of $\mu^+ \mu^-$ pairs with $e^+ e^-$ pairs. It is expected that perturbation theory will be accurate for the production of the $\mu^+ \mu^-$ pairs. This concept will be further developed in the July 1990 RHIC workshop.

Producing Higgs Bosons and Weak Bosons in Heavy Ion Colliders

Mueller, Couture, Brodsky, Strayer and Smith discussed in detail the γ-γ physics that would be accessible at the proposed heavy ion colliders (RHIC, plus heavy ions in LHC and SSC). Of particular interest was the probability of producing a Higgs particle or W+ W- pairs via the virtual two photon spectrum of relativistic heavy ions. This mechanism is out of the question at RHIC, because the nuclear size imposes a cut off in the energy of the virtual photon spectra at 3Gev. At LHC or SSC this cutoff extends to 100Gev or 250Gev respectively.

Much of the focus of discussion at the workshop was the then recent preprint of Cahn and Jackson (LBL 28592, 1990). In contrast to the earlier work of Drees, et al (Phys. Lett B223 [1989] 454), Cahn and Jackson used a cutoff in impact parameter space to exclude the finite size of the nucleus. Drees, et al, included this effect through an elastic form factor. Cahn and Jackson showed that for Pb-Pb collisions, production of a Higgs Boson with an intermediate mass of 100Gev is reduced by a factor of 0.14 from Drees' estimate for SSC energies, and reduced a factor of 0.037 at LHC energies. These are discouraging rates, and the workshop left on a pessimistic note that the production rate for Higgs Bosons, using heavy ions, is too low to be experimentally useful.

Since the meeting, preliminary calculations on the Higgs, as shown by Strayer, have been completed. This preprint (Wu, et al, ORNL preprint ORNL/CCIP/90/02) suggests that the results of Cahn and Jackson based on the Weissacker-Williams method were too pessimistic. The Weissacker-Williams method assumes the transverse momentum of the produced pair is zero, an assumption

that is not realistic in this case. Using a Monte Carlo evaluation of the impact parameter dependence of the Higgs production matrix elements, Wu, et al, show that the original calculations of Drees, et al, are reduced by only a factor of 1.9 at LHC energies and a factor of 1.4 at SSC energies, if the constraint that the heavy ions remain intact is imposed. At this time the prospects for producing intermediate mass Higgs Bosons from coherent two photon production appears more promising than at the time of the workshop. At the SSC, Wu, et al, now calculate up to 500 Higgs a year, if a luminosity of 10^{28} cm^{-2} sec^{-1} can be achieved. We note that this value of the luminosity is nearly two orders of magnitude beyond initial RHIC operation values.

Hadron Production from Peripheral Heavy Ion Collisions

Mueller and Brodsky discussed the hadron resonances available through so-called γ-γ physics. Of particular interest at RHIC energies are the η_0, f(1270) and η_c(2980) resonances. As indicated by Brodsky, heavy ion colliders make good γ-γ factories, particularly in the low mass region. It was also pointed out by Brodsky that a heavy ion collider can be very competitive with e^+ e^- machines, if the luminosity can be increased to 10^{28}.

As part of this discussion, Mueller and Brodsky raised the question of a background to photon photon reactions from Double Pomeron Interactions. For intermediate nuclear A and Z values, the γ-γ and p p amplitudes are comparable, resulting in an interference that needs to be taken into account. For very heavy nuclei, the γ-γ interactions will dominate. Thus, an experiment designed to measure hadron resonance production as a function of the mass and charge of the colliding nuclei could, in principle,

study this interference effect. This ability to conduct such a set of comprehensive measurements using the same apparatus and minimal change to the experimental acceptance is a unique capability of RHIC.

Conclusion

The Relativistic Heavy Ion Collider at Brookhaven will be a machine offering some special capabilities in the areas which were discussed during this workshop. One should be able to do comparison measurements of various electromagnetic phenomena with a variety of beams, thus varying the strength of electromagnetic fields in a well-controlled manner. These measurements can be done with a single apparatus and at a fixed value of the Lorentz γ, eliminating many systematic errors due to acceptance corrections or different beam energies. As an example, gold beams can be used to study non-perturbative phenomena in $e^+ e^-$ pair production, with lighter beams providing a reference measurement in which no strong non-perturbative corrections are expected. A search for possible anomalies in the production of hadrons ($q \bar{q}$ pairs) by strong electromagnetic fields can be conducted in a similar manner.

A study of electromagnetic phenomena in extremely peripheral collisions of relativistic heavy ions can become a rich and exciting field that will complement studies of central collisions.

The e^+, e^- Background at RHIC Generated by Beam Crossing†

Mark J. Rhoades-Brown, T. Ludlam

The RHIC Project
Brookhaven National Laboratory
Associated Universities, Inc.
Upton, Long Island, New York 11973

J. Wu, C. Bottcher, M. Strayer

Physics Division
Oak Ridge National Laboratory
Oak Ridge, TN 37831

August 10, 1990

† Talk presented at July 1990 4th RHIC Workshop.

Introduction

At the Brookhaven Relativistic Heavy Ion Collider[1] (RHIC), fully stripped heavy ions will circulate in each of two rings up to beam energies of 250 (Z/A) GeV/u. During the beam crossing, the peripheral electromagnetic interaction between the heavy ions is sufficient to induce copious production of di-lepton pairs. These pairs are a potential source of background for the detectors at RHIC.

In this paper we discuss the expected number of e^+, e^-pairs, given the accepted initial luminosity value L of the collider. More importantly, we also calculate the differential cross sections for the angle, energy, rapidity and momentum distribution of the leptons. Using the luminosity L of the collider, these differential cross sections are normalized to the expected number of leptons per second. We restrict ourselves to e^+, e^-production, a discussion of $\mu^+\mu^-$ and $\tau^+\tau^-$ distributions will be published later. The results are presented for the expected worst case, namely $^{197}Au^{79+}$ions at a beam kinetic energy of 100 GeV/u. This is forseen to be the heaviest ion for high luminosity experiments at RHIC. We note for a given energy, the cross section for e^+, e^-production scales as Z^4, where Z is the atomic number of the ions.

The calculated cross sections correspond to a lepton energy or momentum range up to 1 GeV. For this range the differential cross section falls over many orders of magnitude, and should be adequate to estimate how many leptons will enter the RHIC detectors. On this note, it is expected that the calculations shown here will form the basis of a future peripheral collision event generator for RHIC. In this way, the final angular geometries of RHIC detectors can be used as input parameters to the event generator, thus enabling a selected binning for the differential distributions of the leptons.

Production rate of e^+, e^-pairs

For $^{197}Au^{79+}$beams at top RHIC energies, the total cross section σ_c for e^+, e^-production has been confidently calculated to be[2,3] 33Kb. This value of σ_c corresponds to the perturbative two photon diagram shown in Fig. 1, where this diagram has been evaluated exactly using Monte Carlo techniques[2], or via the analytic expression due to Racah[4]. The

remarkable agreement between these two approaches is shown in Fig. 2 for beam γ values spanning nearly four orders of magnitude.

For the $^{197}Au^{79+}$beam luminosity values at RHIC, the production rate of e^+, e^-pairs is given as $L\sigma_c$ sec^{-1}, where

$$L\sigma_c = 2 \times 10^{26} cm^{-2} sec^{-1} \times 33 \times 10^{-21} cm^2 \equiv 6.7 \times 10^6 sec^{-1}.$$

It is also important to note that at top RHIC energies for $^{197}Au^{79+}$beams, the perturbative calculation corresponding to Fig. 1 violates the unitary bound for the pair production S-matrix element. The amount by which the S-matrix element exceeds unity depends on the choice of impact parameter between the heavy ions. One estimate[5] for $^{197}Au^{79+}$beams at $\gamma = 100$, gives the probability for producing an e^+, e^-pair at an impact parameter of one Compton wavelength (386 fm) as 2.5. It seems clear that multiple pair production will play a role at RHIC, that is for top RHIC energies non-perturbative Q.E.D. effects such as multiple e^+, e^-pair production will be present. The exact nature of these higher order effects is still under investigation, and is one of controversy[3,5]. At this time it would seem that the number of pairs may be a few (3–5) times larger than the $\sim 10^7$ sec^{-1} value above[5,6].

Differential Cross Section for e^+, e^-production

In Figs. 3–12, the differential cross sections for the electrons produced from beam crossing are plotted as a function of various independent variables. The perturbative calculations were performed with a modified version of the Monte Carlo code[2] used to estimate the total cross section for e^+, e^-production. In all the following calculations, the differential cross sections have been scaled with the luminosity value L $\equiv 2 \times 10^{26}$ cm^{-2}sec^{-1} for $^{197}Au^{79+}$beams at RHIC. Thus, for example, the perpendicular momentum $p_\perp$ is rescaled as

$$\frac{d\sigma_c}{dp_\perp}(b/GeV) \rightarrow \frac{dN}{dp_\perp}(sec^{-1}GeV^{-1}) \equiv L\frac{d\sigma_c}{dp_\perp}(sec^{-1}GeV^{-1}),$$

where N is the number of pairs per second. Because of the problem of multiple pair production through higher order Q.E.D. effects, the distribution functions discussed in this section should be considered lower limits on N.

Figures 3–4 show the all important $dN/dp_\perp$ as a function of $p_\perp$ in GeV (velocity of light c put equal to 1). For the pair curve, $p_\perp$ is the perpendicular projection (relative to beam direction) of the total momentum of the produced pair. For the singles, $p_\perp$ is the perpendicular projection (relative to beam direction) of a single lepton momentum value.

The nuclear form factors play an important role in the transverse momentum differential cross sections. Figure 3 shows that the nuclear form factor severely attenuates the differential cross section for $p_\perp \geq 100$ MeV. This attenuation is very evident for the pair distribution. For values of $p_\perp < 100$ MeV, the nuclear form factor has a small effect on $dN/dp_\perp$, however for completeness the results shown in Fig. 4 were calculated with a nuclear form factor. The nuclear form factor used throughout this manuscript corresponds to a Fourier transform of a radial Woods–Saxon density distribution that was fitted to electron scattering data.[7]

Figures 3–4 show how soft the produced electrons are. As $p_\perp$ increases from 0 to 100 MeV, $dN/dp_\perp$ falls nearly six orders of magnitude for the pairs calculated including a nuclear form factor. In spite of the general rapid fall of in $dN/dp_\perp$, some care must be taken with any detector design for the absolute value of $dN/dp_\perp$ is still of considerable magnitude.

In Figs. 5–6, the differential cross sections $dN/dp_\parallel$ are plotted as a function of the longitudinal momentum $p_\parallel$. Once again for the pairs, $p_\parallel$ is the longitudinal projection (along the beam direction) of the total pair momentum, and for the singles $p_\parallel$ is the longitudinal projection of a single lepton. The nuclear form factor has been included in the calculations, but is of negligible importance for this variable. Of course, the curves are symmetric around $p_\parallel = 0$ for this variable. Analogous results in Figs. 7–8 show the differential cross section for the energy variable E.

The angular distributions of the pairs and singles are shown in Figs. 9–10. The angle θ is defined relative to the beam direction. The differential cross section $dN/d(\cos\theta)$ is symmetric with respect to $\theta = 90°$, and is independent of the azimuthal angle. The results show the leptons tend to travel in the forward (or backward) direction, but the total integrated cross section still has contributions for the approximate theta range $0 < \theta \leq 60°$.

The rapidity spectrum is shown in Fig. 11. It can be seen that beyond y = ± 4 units that dN/dy falls exponentially with increasing y.

Discussion

At relativistic energies, the Lorentz contracted Coulomb field between heavy ions in a collider will induce copious amounts of lepton pair production. In this note we have calculated differential cross sections for the produced e^+, e^-particles using exact Monte Carlo evaluation of the perturbative two photon diagram in Fig. 1.

There is some uncertainty in the exact number of pairs that will be produced, because traditional non–perturbative Q.E.D. violates unitarity bounds at RHIC energies. Work is continuing on this more fundamental problem of calculating and summing the Q.E.D. perturbation series.[8]

On a related note, some of the produced electrons (approximately 1 in 440 for $^{197}Au^{79+}$beams) can be captured in a K-orbital of the ion[9]. This mechanism will cause the ion to be lost from the beam, and hence reduce the overall beam lifetime. While reliable perturbative estimates have been made[9], work also continues on this important subject.

This research was sponsored by the Division of Nuclear Physics of the U.S. Department of Energy under contract No. DE–AC02– 76CH00016 with Brookhaven National Laboratory, under contract No. DE–AC05–84OR21400 with Martin Marietta Energy Systems, Inc.

REFERENCES

1 Conceptual Design of the Relativistic Heavy Ion Collider RHIC, May 1989, BNL 52195.

2 C. Bottcher and M. Strayer, Phys. Rev. D39, 1330 (1989).
M. Strayer, invited talk, presented at the workshop "Can RHIC be used to test Q.E.D.?", Brookhaven National Laboratory, Upton, New York, April 1990, BNL 52247.

3 S. Brodsky, invited talk, presented at the workshop "Can RHIC be used to test Q.E.D.?", Brookhaven National Laboratory, Upton, New York, April 1990, BNL 52247.

4 G. Racah, Nuovo Cimento 14, 70 (1937).

5 G. Baur, invited talk, presented at the workshop "Can RHIC be used to test Q.E.D.?", Brookhaven National Laboratory, Upton, New York, April 1990, BNL 52247.

6 M. Fatyga, M.J. Rhoades-Brown, M. Tannenbaum, workshop summary, presented at the workshop "Can RHIC be used to test Q.E.D.?", Brookhaven National Laboratory, Upton New York, April 1990, BNL 52247.

7 R.C. Barrett and D.F. Jackson, "Nuclear Sizes and Structure", Oxford University Press, 1975.

8 C. Bottcher, invited talk, presented at the workshop "Can RHIC be used to test Q.E.D.?", Brookhaven National Laboratory, Upton, New York, April 1990, BNL 52247.

9 M.J. Rhoades-Brown, C. Bottcher, M. Strayer, Phys. Rev. A40, 2831 (1989).

FIGURE CAPTIONS

Fig. 1 Schematic representation of perturbative two photon diagram, including exchange term.

Fig. 2 Comparison of full Monte Carlo evaluated cross section and Racah formula as function of beam γ value. σ_o is a scaling parameter that takes the value 165b for $^{197}Au^{79+}$beams.

Fig. 3 Comparison of $dN/dp_\perp$ as function of $p_\perp$, for both pairs and singles, with and without the nuclear form factor.

Fig. 4 Same as Fig. 3, but for smaller $p_\perp$ scale. Both pairs and singles include the nuclear form factor.

Fig. 5 Plot of $dN/dp_\parallel$ as function of $p_\parallel$, for both pairs and singles, with nuclear form factor.

Fig. 6 Same as Fig. 5, but for smaller $p_\parallel$ range.

Fig. 7 Plot of dN/dE as function of energy E, for both pairs and singles, with nuclear form factor.

Fig. 8 Same as Fig. 7, but for smaller E range.

Fig. 9 Plot of $dN/d(\cos\theta)$ as function of opening angle θ, for both pairs and singles, with nuclear form factor.

Fig. 10 Same as Fig. 9, but for smaller θ range.

Fig. 11 Plot of dN/dy as function of rapidity y, for both pairs and singles, with nuclear form factor.

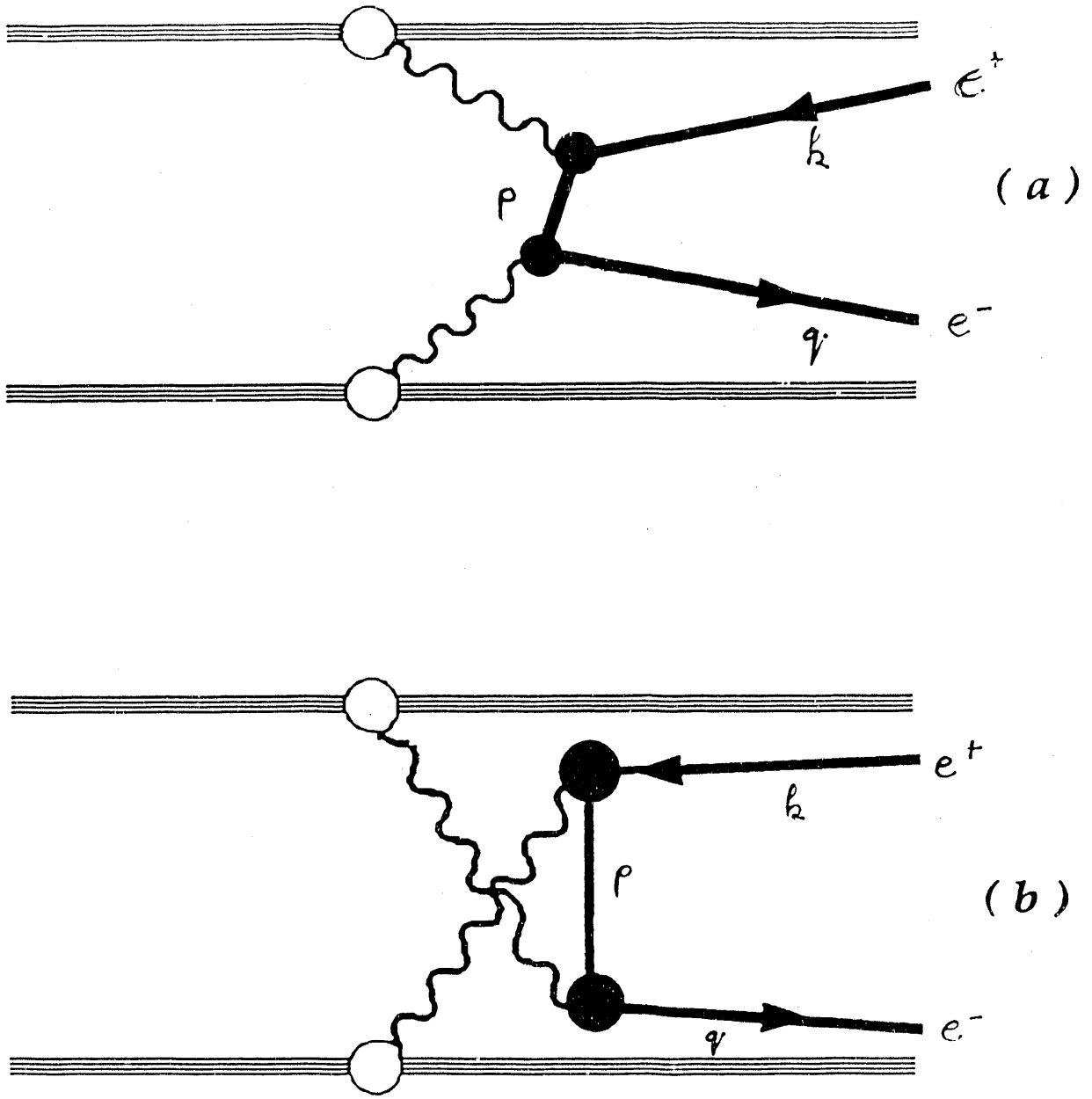

Fig.1

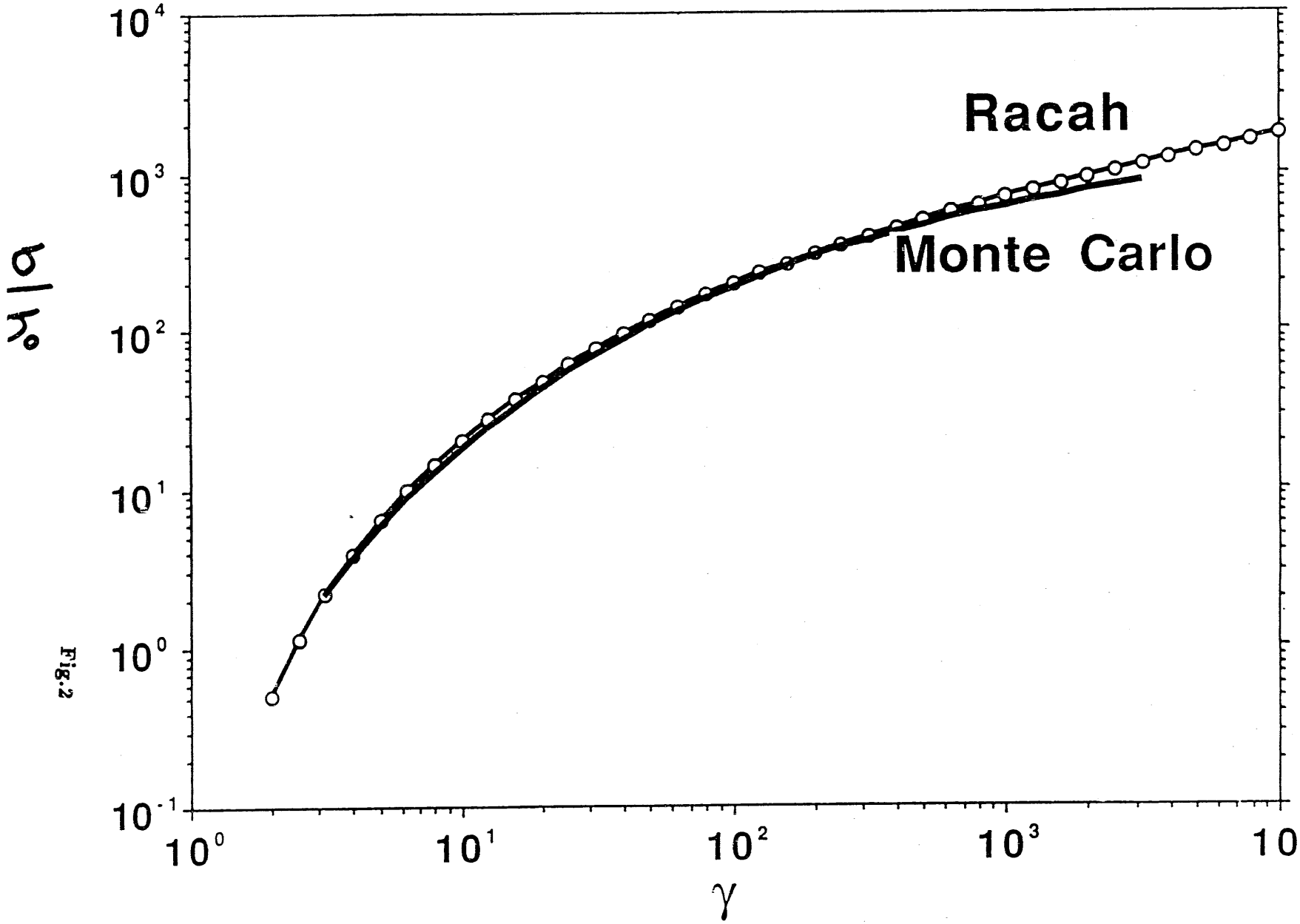
Racah
Monte Carlo
10^4
10^3
10^2
10^1
10^0
10^{-1}
10^0
10^1
10^2
10^3
10^4
γ
σ/σ_0

Fig.2

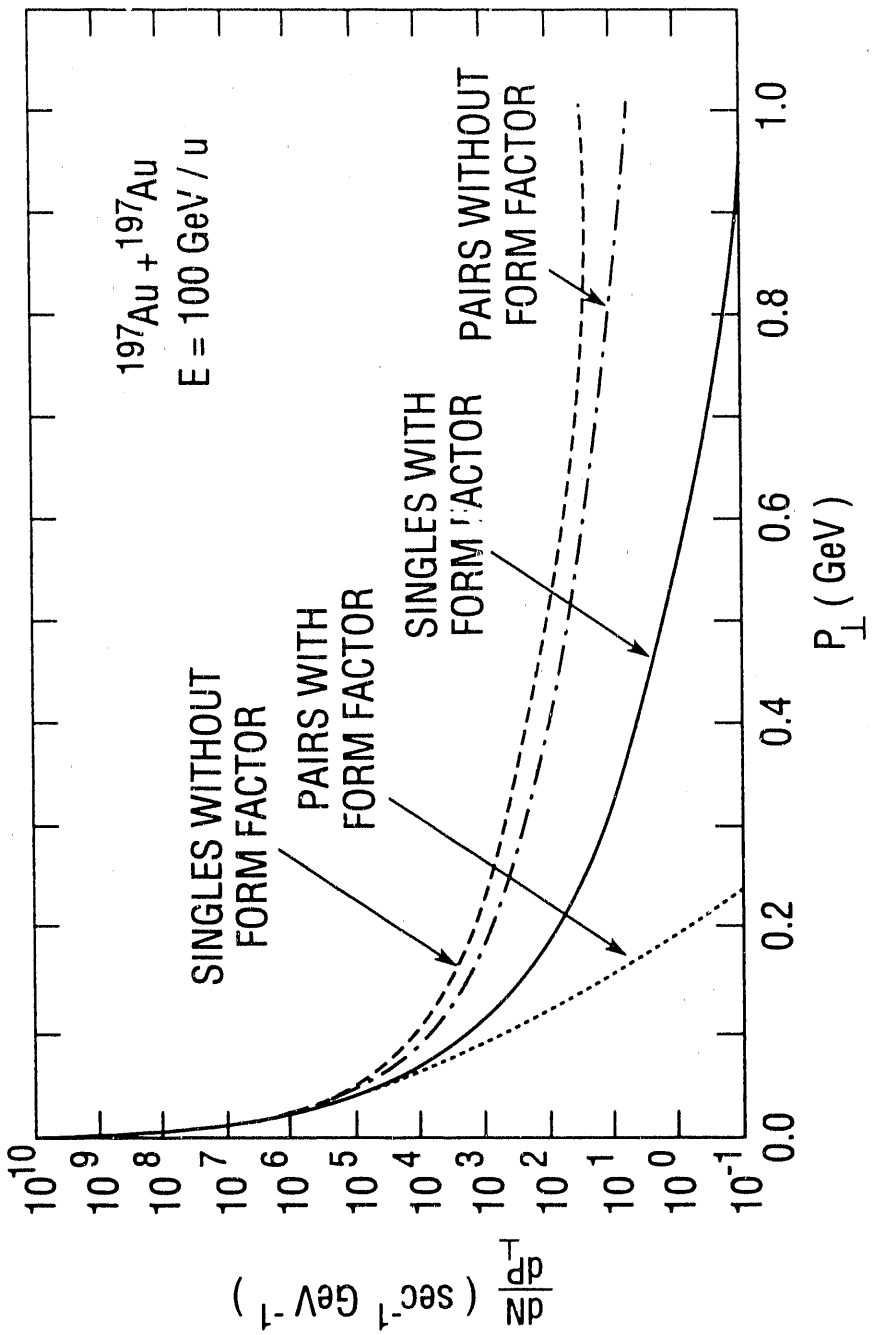
$^{197}Au + ^{197}Au$
E = 100 GeV / u
SINGLES WITHOUT FORM FACTOR
PAIRS WITH FORM FACTOR
SINGLES WITH FORM FACTOR
PAIRS WITHOUT FORM FACTOR
$\frac{dN}{dP_\perp}$ (sec^{-1} GeV^{-1})
$P_\perp$ (GeV)
10^{10}
10^{9}
10^{8}
10^{7}
10^{6}
10^{5}
10^{4}
10^{3}
10^{2}
10^{1}
10^{0}
10^{-1}
0.0
0.2
0.4
0.6
0.8
1.0

Fig.3

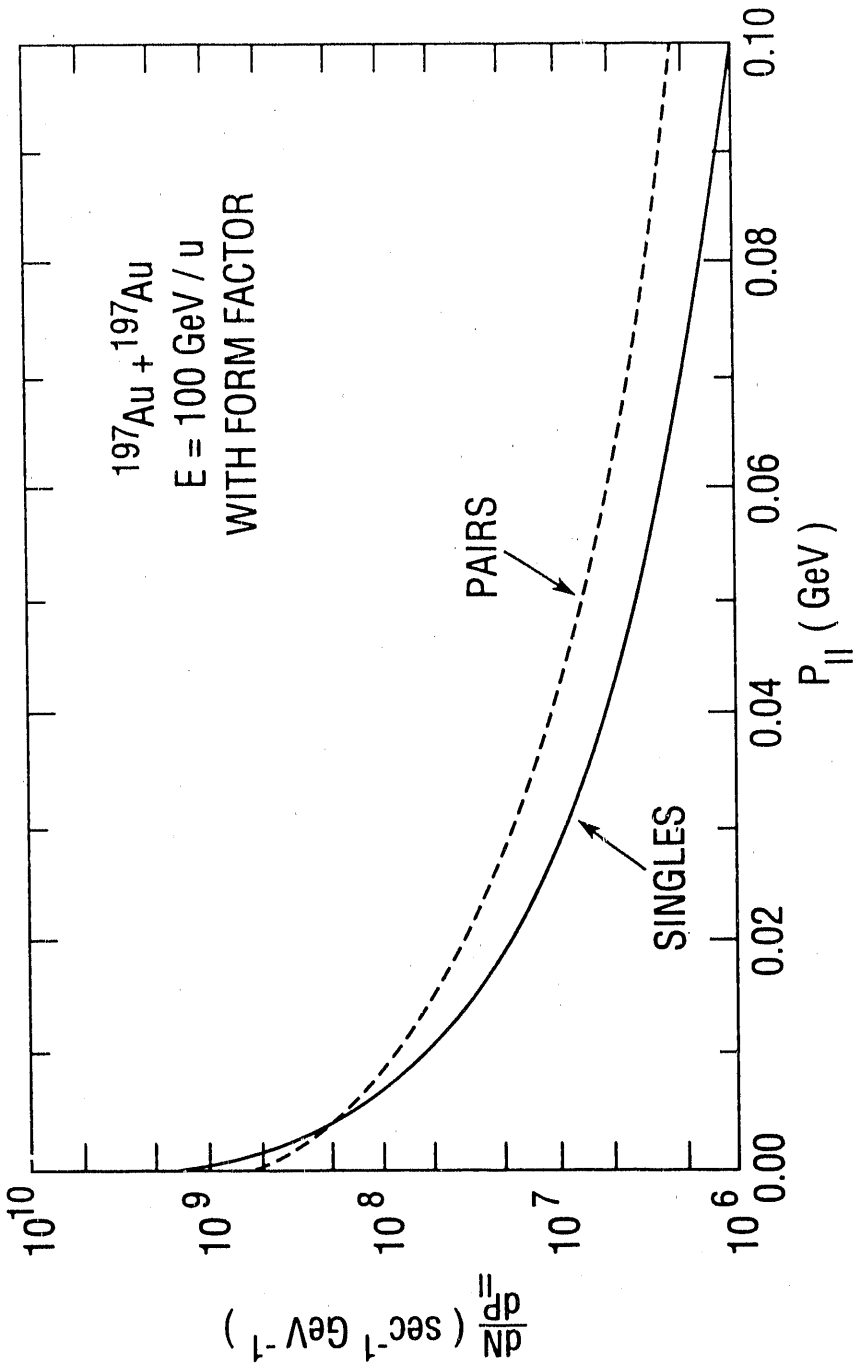
$^{197}Au + ^{197}Au$
E = 100 GeV / u
WITH FORM FACTOR
PAIRS
SINGLES
$\frac{dN}{dP_{ll}}$ (sec^{-1} GeV^{-1})
P_{ll} (GeV)
10^{10}
10^{9}
10^{8}
10^{7}
10^{6}
0.00
0.02
0.04
0.06
0.08
0.10

Fig.6

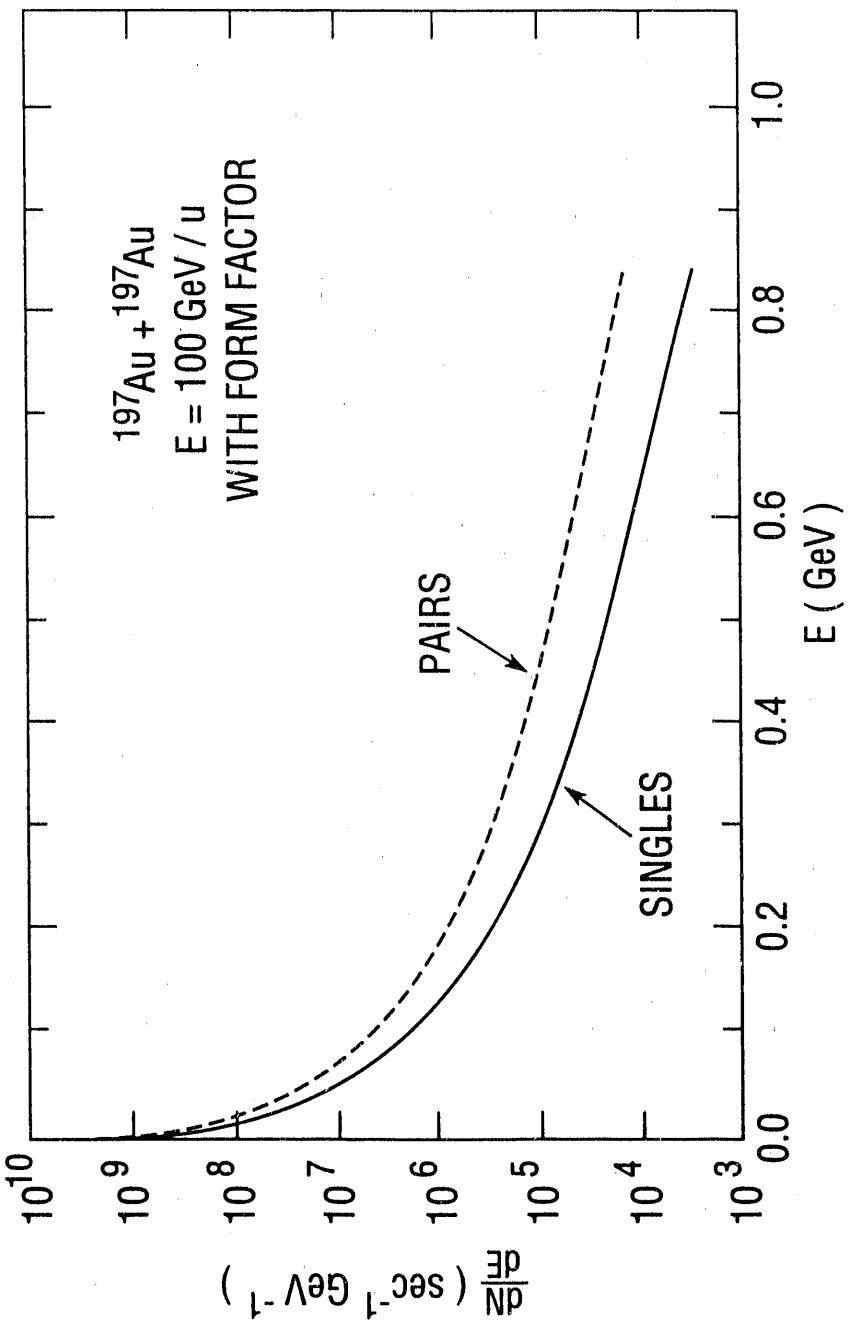
$^{197}Au + ^{197}Au$
E = 100 GeV / u
WITH FORM FACTOR
PAIRS
SINGLES
$\frac{dN}{dE}$ (sec^{-1} GeV^{-1})
E (GeV)
10^{10}
10^{9}
10^{8}
10^{7}
10^{6}
10^{5}
10^{4}
10^{3}
0.0
0.2
0.4
0.6
0.8
1.0

Fig.7

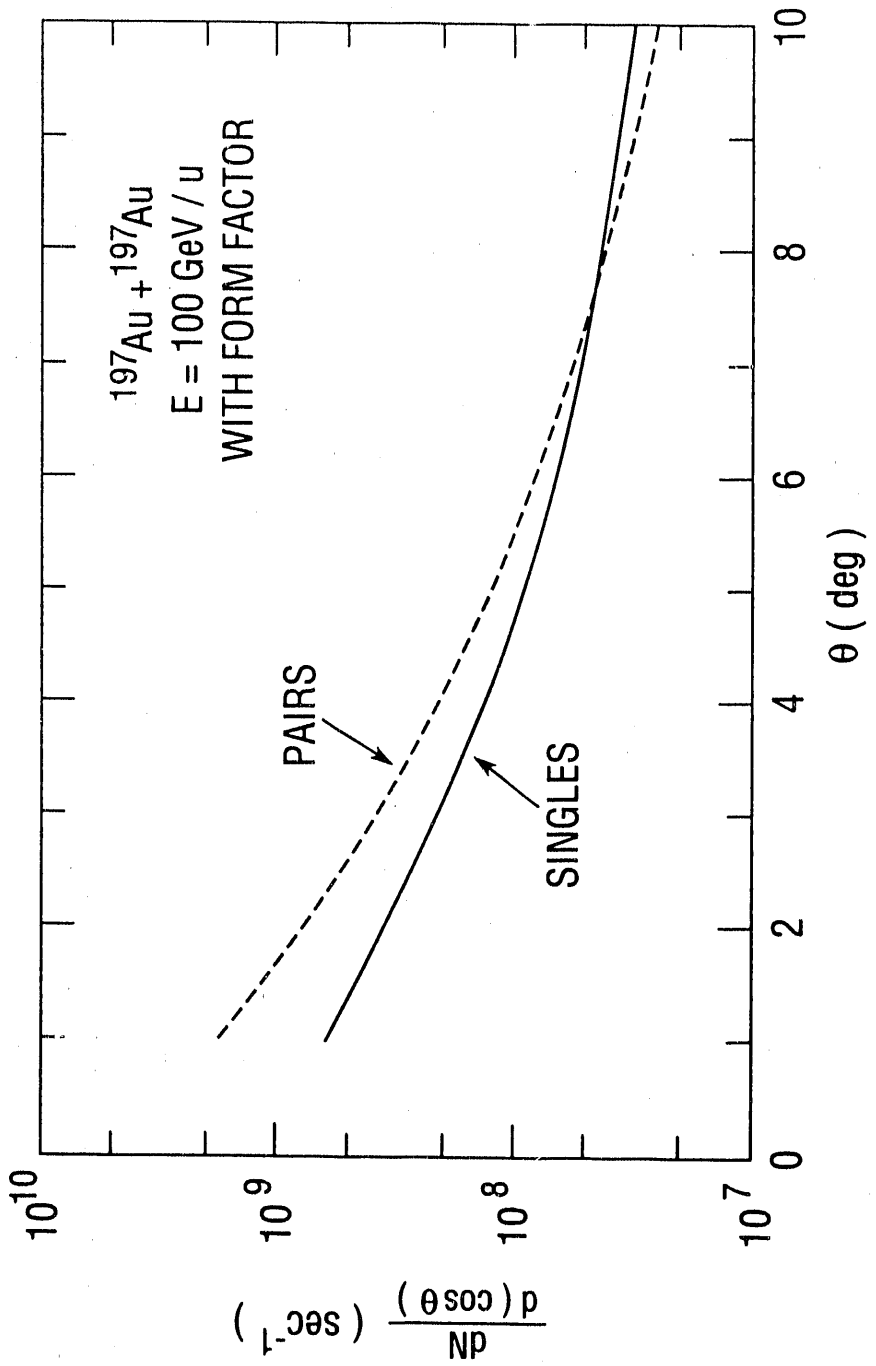
$^{197}Au + ^{197}Au$
E = 100 GeV / u
WITH FORM FACTOR
PAIRS
SINGLES
10^{10}
10^{9}
10^{8}
10^{7}
0
2
4
6
8
10
θ (deg)
$\frac{dN}{d(\cos\theta)}$ (sec^{-1})

Fig.10

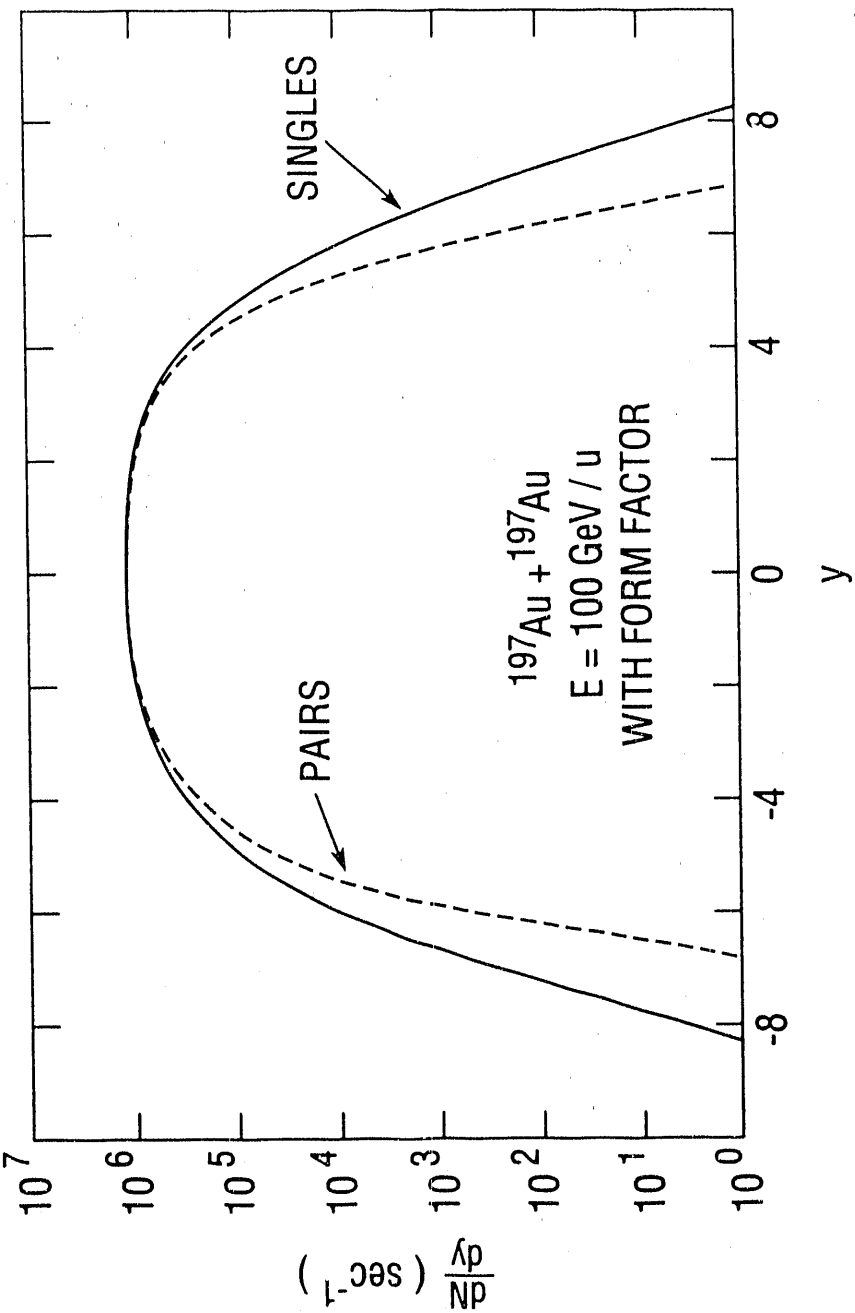
SINGLES
PAIRS
$^{197}Au + ^{197}Au$
E = 100 GeV / u
WITH FORM FACTOR
y
8
4
0
-4
-8
10^7
10^6
10^5
10^4
10^3
10^2
10^1
10^0
$\frac{dN}{dy}$ (sec^{-1})

Fig.11

1. Introduction.

When two high energy heavy ions approach one another to a distance comparable to their nuclear radius, electromagnetic fields of high intensity will be created. The presence of these fields will result in a wide range of electromagnetic processes, involving both the production of particles and photoexcitations of nuclei. The significance of such phenomena for a physics program at RHIC is threefold: first, the production of particles by electromagnetic fields will naturally accompany all central or semi-central collisions. Electromagnetic processes must be carefully considered as a possible background in some investigations of central collisions. Second, two very abundant electromagnetic processes constitute the primary limitation to the lifetime of stored beams at RHIC. One of them is a nuclear decay following the electromagnetic excitation of the giant dipole resonance, and the second one is a creation of an e^+e^- pair accompanied by the capture of an electron in the atomic level of one of the ions. [1] Third, (last but not least) it is of significant interest to study the physics of particle production by strong electromagnetic fields. Even conventional QED calculations indicate that collisions of heavy ions at RHIC will produce unique electromagnetic phenomena which cannot be studied by any other means. Of particular interest seems to be the production of e^+e^- pairs by energetic heavy ions. This process can no longer be described by perturbative methods, since the S-matrix for single e^+e^- pair production violates unitarity bounds. [2] Non-perturbative approaches to QED can be studied in this system through measurements of the pair multiplicity (as well as other properties of pairs) in collisions with small impact parameters. Finally, one must not exclude the possibility that new, as yet unknown phenomena due to strong fields can be observed in collisions of heavy ions. In the remainder of this paper we will present an outline of some experimental concepts which can be used to study the physics of strong electromagnetic fields with relativistic heavy ions.

2.4 Controlling the impact parameter.

The dependence of electromagnetic cross sections on the charge and the energy of a beam is a powerful tool with which one can study some aspects of non-perturbative QED. This tool is likely to be insufficient however, if one wants to search for new phenomena induced by strong fields. Since the electromagnetic interaction is a long range interaction, processes like the production of particles or photonuclear excitations occur within a wide range of impact parameters. To be more quantitative, let us consider again an example of the e^+e^- pair production. In fig.2 we show the dependence of e^+e^- cross section on the impact parameter in U+U and p+p collisions. [4] The impact parameter scale is expressed in the units of the compton wavelength of the electron (385fm). We observe that the calculated cross section in U+U collision is nearly flat (slightly decreasing) in the region 15fm-385fm, while the maximum field intensity must vary by nearly three orders of magnitude in the same interval of b (with weaker fields favored by the phase space). Hence, if one would like to look for effects of strong fields which go beyond the present QED predictions, some method of selecting collisions with a small impact parameter seems necessary.

Conceptually, the most direct method of tagging a collision with its impact parameter would be to measure the transverse momentum transfer to both ions. Since relativistic heavy ions follow essentially classical Rutherford trajectories these two quantities can be related to each other. Unfortunately, a measurement of the transverse momentum transfer in an elastic collision of heavy ions appears to be extremely difficult (probably impossible). The maximum momentum transfered to each ion in gold on gold collisions is approximately 1.1GeV/c, while the incident momentum of each ion is nearly 20000 GeV/c (at relativistic energies the transverse momentum transfer is nearly independent of the incident energy). This means that the maximum deflection angle due to the Rutherford scattering is less than .06mrad, too small to be measured. Some other, more indirect method of tagging collisions with the impact parameter must be found.

In this paper we will discuss an indirect method of measuring an impact parameter which is based on the measurement of a cross section for a coincidence between two electromagnetic processes. Such measurements are not feasible at presently available energies due to prohibitively low coincidence rates. The situation will be far more favorable at RHIC

energies however, as probabilities for some electromagnetic processes approach unity. As a first example let us consider a measurement of the coincidence between $\mu^+\mu^-$ pairs and e^+e^- pairs in a collision of two gold ions at $\gamma = 100$ (a collision without a nuclear contact). Suppose, that we trigger the experiment on a single pair of muons and measure its invariant mass. Having established a trigger, we detect all electrons which were produced in the same event. We can now vary the invariant mass of a muon pair, observing that massive pairs can only be created in a collision with a small impact parameter. To illustrate this point quantitatively, let us assume that we detect a pair with mass M at the rapidity zero. Using the Weizsacker-Wiliams approximation one can estimate the range of impact parameters within which this pair could have been created. The upper limit of this range is given by:

$$b_{max} = \frac{2\gamma hc}{2\pi M} \tag{2.1}$$

If one sets a detection threshold for the minimum mass of

$$M_{min} = 4M_{0,\mu}$$

where $M_{0,\mu}$ is a rest mass of a muon, the maximum impact parameter b_{max} is equal to 95fm. Hence, a trigger pair with the invariant mass equal to $4M_{0,\mu}$ would span the 14fm-95fm range of impact parameters. The lower limit of this range is determined by the requirement of a collision without the nuclear contact. Through the same approximation one can estimate the maximum mass of a $\mu^+\mu^-$ pair to be $2.9GeV/c^2$. A trigger on such massive pairs will therefore select collisions with the smallest impact parameter ($b_{min} = 2R$, where R is a radius of an ion). One should stress, that by requiring a trigger pair of a given mass one does not select a single value of the impact parameter, but a range of impact parameters from the minimum ($b_{min} = 2R$) to the b_{max} which was defined in Eq. (2.1) .

As a second example let us consider an experiment in which $\mu^+\mu^-$ pairs are measured in coincidence with beam rapidity neutrons on either side of the interaction diamond. Beam rapidity neutrons can be emitted in a process of a decay of an excited beam ion. An excitation can be induced electromagnetically or through a nuclear grazing collision. For the purpose of this discussion we will assume that electromagnetic and nuclear components can be accurately separated. Implications of this assumption will be discussed later.

We present calculations concerning two types of events which include beam rapidity neutrons. First, an event in which only one neutron is detected on either side of the interaction region, with no neutron on the complementing side. This type of an event will be denoted as T(1n,0n). Second, an event in which two neutrons are detected, one on each side of the interaction region. This type of an event will be denoted as T(1n,1n). In fig 3 we show probabilities of the both types of events, P[T(1n,0n)] and P[T(1n,1n)], plotted against the impact parameter. We observe two features of these distributions: (a) in collisions with a small impact parameter both P[T(1n,0n)] and P[T(1n,1n)] are large, 50% and 20% respectively. Consequently, these two channels are suitable as an element of a coincidence measurement. (b) Both probabilities depend very differently on the impact parameter. P[T(1n,0n)] changes *roughly* like $\frac{1}{b^2}$, while P[T(1n,1n)] changes like $\frac{1}{b^4}$.
A measurement of $\mu^+\mu^-$T(1n,0n) and $\mu^+\mu^-$T(1n,1n) channels can be viewed as a first step in a separate study of a dependence of the $\mu^+\mu^-$ pair production and electromagnetic excitation of nuclei on the impact parameter. Since both these processes should be calculable within a perturbative formalism, we do not select (or declare) any of them as a trigger process. It is a consistency check, which can nevertheless reveal new phenomena in case a discrepancy is observed. One can go further and study channels T(2n,0n),T(2n,1n),T(2n,2n), etc..... . These channels will introduce even stronger bias towards collisions with a small impact parameter, albeit at the cost of introducing growing experimental problems. First, the absolute value of a probability of inducing a more complex decay will be decreasing, which will decrease the coincidence rate. Second, as the probability of an electromagnetic excitation decreases one must worry more about the background due to the same decay induced in a nuclear grazing collision. These problems should be addressed in future studies (calculations) in order to examine the feasibility of a more extensive program.

2.5 Quality of a trigger.

Several times in the preceding discussion we have referred to possible problems with the quality of a trigger. Before proceeding to describe an experimental apparatus, we will discuss the problem of a trigger quality in more general terms.
A trigger for an electromagnetic process must consist of two parts, the first one to select the desired process and the second one in the form of veto detectors which attempt to

discriminate against hadronic interactions. For example, in the case of $\mu^+\mu^-e^+e^-$ measurement the primary trigger would be defined as two and only two penetrating tracks in the muon region. Veto detectors would probably consist of crude multiplicity detectors covering forward and central regions. The quality of this trigger rests on the identification of muon tracks and a completeness of veto detectors. Although various tests of the performance of such a trigger can be devised, the final test of its quality must be accomplished by measuring the dependence of a trigger rate on the charge of a beam and/or its energy. A precise calculation of the Z dependence of trigger rates should be possible, as long as the rate of a trigger process can be calculated with perturbative methods.

A similar test can be applied to the emission of nucleons from excited ions. The calculation of the dependence of a cross section on the charge of a beam is not as straightforward as in the case of particle production. The main difficulty lies in the fact that the change in the charge of a beam implies simultaneous changes in the nuclear structure which must be taken into account in all calculations. These difficulties are less severe when cross sections are measured as a function of the beam energy, rather than the beam charge. Hence, the dependence of a cross section on the beam energy seems to be the most appropriate test of a trigger quality in this case.

In summary, the issue of a trigger quality definitely requires further study, mainly through Monte Carlo simulations. We note however, that direct experimental tests of this quality can (and should) be performed. Once again, it is apparent that the ability to study the same process with beams of different charge and energy is a very important feature of RHIC.

3. An outline of the apparatus.

The apparatus which will be *sketched* in this section is designed to perform three basic measurements which were discussed in previous sections: massive $\mu^+\mu^-$ or e^+e^- trigger pairs, low energy e^+e^- pairs and beam rapidity nucleons. The actual design of an experiment requires far more work than has been done thus far. In most instances we will simply outline problems which must be studied further, rather than provide ready solutions.

3.1 Low energy electrons.

We begin with a discussion of what seems to be the most difficult task, namely detecting low energy electrons. The kinetic energy spectrum of electrons (positrons) which are produced in a heavy ion collision peaks at energies between 1 and 2 MeV. Hence, a complete measurement of non-perturbative QED phenomena in a heavy ion collision requires a serious effort to detect electrons and positrons down to very low energies. Two features of a collider make it a particularly complicated task at RHIC. First, the length of the interaction diamond (22cm RMS) complicates the geometry and the acceptance of a detector. This length combined with the absence of a target constraint makes tracking of low energy electrons very difficult. Second, due to the stringent vacuum requirements inside the beam pipe ($10^{-10}Tr$) it is very difficult to put detectors directly into the beam vacuum. A silicon strip detector is perhaps the only presently available type of a detector which does not cause a conflict with vacuum requirements. As an alternative solution one can use a thin beam pipe made of a low Z material and position a detector immediately outside the beam pipe. Although the latter choice is probably more practical both solutions should be studied seriously. In fig.4 we show a schematic view of an electron detection region. It consists of an interaction diamond and two adjacent regions of a magnetic field in which more energetic electrons are bent away from the beam and analyzed. One may also consider applying a weak magnetic field to the region of the interaction diamond. The purpose of such a field would be to bend all electrons and positrons out of the beam. Since low energy electrons (positrons) have quite broad angular distributions, it is not clear whether this field is really needed. This question must be studied further. Angular distributions become more focused with respect to the beam axis as the energy of an electron (positron) increases. Hence, one needs two regions of the magnetic field (one on each side of the interaction diamond) to bend more energetic electrons (positrons) out of the beam. The magnetic field will also provide some opportunity for the momentum analysis, albeit an uncertainty due to the absence of a target constraint.

The primary objective of the low energy region should be to measure the multiplicity of e^+e^- pairs and energy distributions of electrons and positrons. It is obviously desirable to measure other kinematic variables like an invariant mass distribution of e^+e^- pairs

or transverse momenta of singles and pairs. The feasibility of measuring an invariant mass spectrum depends to a large degree on the actual multiplicity of pairs. If it is true that multiple pairs are created in a collision, any measurement of the invariant mass will be difficult due to a combinatorial background. It will also be very difficult to measure transverse momenta of electrons (positrons) due to problems which were described above. A detector which is chosen to meet these objectives should have a good granularity as well as a capability to measure the total energy of individual electrons. A simple range detector composed of layers of scintillator tiles (perhaps separated by thin absorber plates) would seem a good choice in the low energy region. Crystals of CsI can be used to detect energetic electrons above 100MeV or so (a trigger pair). The choice of a granularity depends on the expected multiplicity of pairs which is still an object of some controversy (and may remain so until the measurement is done). Consequently, it is difficult to say at this time what granularity is really needed. In fig.5 we show a schematic design of a simple range detector. The design of the low energy electron spectrometer requires much more work than has been done thus far. One of the issues which must be carefully looked at is the feasibility of tracking in the intermediate energy range (5-10MeV). Some less conventional designs of the spectrometer should also be considered.

3.2 A trigger pair.

A trigger pair can be a massive e^+e^- pair or a $\mu^+\mu^-$ pair. There are some technical advantages to the use of an e^+e^- rather than a $\mu^+\mu^-$ pair. These advantages are partially offset by a potential for a combinatorial background when multiple pairs of electrons are produced. This ambiguity can be reduced to an arbitrarily low level however, by imposing a lower limit on the invariant mass of a trigger pair. The probability of producing two massive pairs in a single event will then be very low. The technical advantage of an electron pair is in the fact that the total energy of an electron can be measured in a shower detector. The detector can be relatively small, since electromagnetic showers are both short and narrow. This facilitates both the total energy measurement and a particle identification. The electron can be tracked prior to entering the total absorption detector, giving one more complete and precise information about its kinematic variables than a muon would. It is obviously very interesting to have a capability to trigger both on electron and on muon

pairs and compare the two results in the limit of a high invariant mass of a trigger pair. In f .6 we show a scheme for a combined measurement of a trigger pair and low energy electron-positron pairs. This design is based on the assumption that the transverse momentum of a high energy muon or electron is small when compared to its longitudinal momentum. A high momentum electron (muon) propagates nearly undisturbed through the first region of a weak magnetic field and is analyzed in the downstream region with a stronger field. The detection of an electron should involve tracking backed by a small electromagnetic calorimeter. Muons must be identified by a range detector, perhaps coupled with a detection of a muon decay. At the limit of the invariant mass range of a trigger pair one expects two back to back electrons (muons) with the momentum of the order of 1.4 GeV/c. The identification of an electron above a few hundred Mev poses no problems if one uses a suitable total energy detector (eg. CsI crystals) to identify its electromagnetic shower. A positive identification of muons in this energy range (and particularly their separation from pions) may be difficult. Even so, the suppression of a background due to hadronic interactions should be feasible by requiring two and only two penetrating tracks, one on each side of the beamline. According to our earlier discussion the quality of the trigger can be examined experimentally. One should also mention the fact, that the increase in the invariant mass of a trigger pair is coupled to some broadening of angular distributions of single electrons (muons). Consequently, one may be forced to modify the simple design which is shown in fig.6 to avoid losses of experimental acceptance for high mass pairs. As with most other experimental issues in this paper, the detection of a trigger pair requires further study.

3.3 Detecting beam rapidity nucleons.

Detecting beam rapidity nucleons at RHIC should not be particularly difficult. Neutrons can be detected at zero degrees behind the first bending magnet, while protons will emerge from the beam at twice the bending angle of the beam, also after the first bending magnet. If one assumes a maximum transverse momentum of a neutron to be 400 MeV/c (a conservative assumption), then at a distance of 20 meters from the interaction region all neutrons are still confined within a circle 16cm in diameter. Hence, beam rapidity neutrons remain well focused even at large distances from the interaction region. The most

appropriate technique for detecting a neutron with an energy of 100GeV is a hadronic calorimeter. The main purpose of this calorimeter should be to count the number of neutrons in an event. Even if an overall energy resolution of such a detector is about 20%, one can still count beam rapidity neutrons without much trouble. A two neutron peak would be separated from a one neutron peak by more than five standard deviations, quite enough for a reliable classification of the event. In reality, one should expect the energy resolution to be better than 20%. A good hadronic calorimeter (available today) can offer an energy resolution of 5% at an energy of 100GeV. The fermi momentum distribution will broaden the laboratory energy distribution of a neutron to about 12% of its average value. Hence, even if one assumes that the instrumental energy resolution is a factor of three worse than the 5% quoted above, one still arrives at the overall width of the energy spectrum equal to 19% of the average value. The separation can be further improved if one uses a segmented calorimeter, so that a simple pattern recognition can be used. A similar discussion applies to beam rapidity protons.

3.4 Event rates and multiple interactions per bunch crossing.

The cross section for producing a $\mu^+\mu^-$ pair in an extremely peripheral collision of two gold ions at $\gamma = 100$ is approximately 300 mb. At the design luminosity of $2 * 10^{26} cm^{-2} sec^{-1}$ one expects 60 $\mu^+\mu^-$ pairs per second. Triggering on the invariant mass interval which corresponds to 1% of the total cross section one still expects .6 pairs per second, a respectable trigger rate.

Since the cross section for producing e^+e^- pairs is very large, one must worry about the possibility of multiple interactions per one bunch crossing. The geometric cross section for a passage of two ions within a distance smaller than 385fm is of the order of 5kb, which corresponds to .22 of an interaction per bunch crossing. Hence, the probability of two interactions of this kind in a single bunch is of the order of 5%. In this simple estimate we assume that coherent effects in a crossing of two beam bunches are not important (this assumption needs some further investigation). One should also say, that the 5% estimate is probably somewhat low, since e^+e^- pairs can be produced at impact parameters which are larger than 385fm. The probability to produce a pair drops quite rapidly with the

impact parameter however, making this region of impact parameters less significant. More theoretical work on the impact parameter dependence of the e^+e^- pair production may be needed to improve our estimates. In practice, it will be quite important to compare measurements taken with beams of varying luminosity, to make sure that no significant contamination due to multiple interactions is present.

4. Summary.

4.1 Summary of the experimental program.

In this section we will summarize the experimental program which was outlined thus far.

1. A measurement of the $\mu^+\mu^-e^+e^-$ channel can provide an insight into non-perturbative aspects of e^+e^- pair production, as well as allow one to search for new phenomena in strong fields. All QED calculations predict that the multiplicity of e^+e^- pairs depends very weakly on the impact parameter in a collision, as long as the impact parameter is smaller than 385fm. This result can actually be tested by measuring the multiplicity of e^+e^- pairs as a function of the invariant mass of a $\mu^+\mu^-$ pair. Any significant variation (particularly an increase) in the multiplicity of e^+e^- pairs when the mass of a $\mu^+\mu^-$ pair increases would point to the possibility of new phenomena in e^+e^- pair production. We note, that massive e^+e^- pairs can also be used as a trigger. It would seem very worthwile to repeat the same measurement with $\mu^+\mu^-$ and e^+e^- pairs as a trigger. In the limit of a large invariant mass of a trigger pair both measurements should produce identical results. Any strong field phenomenon should depend very sensitively on the combined charges of beams. Hence, it is essential to repeat this measurement with a variety of beams and study its results as a function of the charge of a beam.

2. A measurement of the coincidence between $\mu^+\mu^-$ or e^+e^- pairs and beam rapidity nucleons can be viewed as a trigger study for the previous experiment, or as an independent study of the dependence of dilepton production and electromagnetic excitation of nuclei on the impact parameter. A coincidence measurement provides a consistency test between the two processes. The failure of this test can be interpreted as a signature of new phenomena in either one of the two processes. Further measurements would be necessary to understand

such a failure. It is again essential to do the experiment with a variety of beams and at several beam energies.

A measurement of the coincidence between two electromagnetic processes provides one with the equivalent of a *minimum bias*, indirect trigger on collisions with small impact parameters. One can interpret a $\mu^+\mu^-$ pair as a minimum bias trigger for the study of e^+e^- pairs. Using this trigger one can study properties of the *average* e^+e^- pair created in a collision with a small impact parameter. If one searches for rare events due to strong fields, this experimental method becomes insufficient. One must then construct a trigger which explicitely searches for such events. Events with an abnormally high multiplicity of e^+e^- pairs can be an example of a rare event.

4.2 Other possibilities.

There are other experiments in the general area of extremely peripheral collisions of relativistic heavy ions which are of interest, but have not been discussed in this paper.

It has been suggested by E.Teller [5] that strong magnetic fields which are created in heavy ion collisions without the nuclear contact can lead to the enhanced production of mesons. His suggestion was motivated by the earlier work of J.Schwinger, [6] who speculated that quarks can have a magnetic charge in addition to their known electric charge. Best candidates for such studies would probably be simple non-flavored mesons like π^0,η,η_c. An anomalous dependence of cross sections for producing these mesons on the charge of a beam could then indicate a new mechanism of meson production due to strong fields. The measurement of a coincidence between mesons and e^+e^- pairs (and/or electromagnetic decays of nuclei) can provide further insights into the impact parameter dependence of meson production.

4.3 Conclusions.

We have discussed some possibilities of studying the physics of strong electromagnetic fields in extremely peripheral collisions of relativistic heavy ions. A physics motivation for these studies ranges from confirming already predicted non-perturbative phenomena in QED processes, to searches for new phenomena due to strong electromagnetic fields. Because of the long range nature of the electromagnetic interaction it seems necessary to

find a way in which an experiment can be triggered on collisions with a small impact parameter. One such method which is based on the coincidence between two electromagnetic processes has been presented in this paper.

It seems that the general area of the physics of extremely peripheral collisions of relativistic heavy ions has a potential to develop into an experimental program at RHIC. This program is quite distinct from the study of central collisions both in terms of its goals and instrumental requirements. Peripheral events have a relatively low multiplicity, with accurate triggering as the main experimental problem. In contrast, triggering is not a problem in studies of central collisions. Backgrounds due to high multiplicities of produced particles are the greatest obstacle in these experiments. Some of the measurements which relate to peripheral interactions can be done parasitically, using detectors which are designed with central collisions in mind. Given the differences in essential requirements however, it would seem most effective to construct modest, dedicated experiments for the study of peripheral interactions rather than attempt parasitic measurements with large detectors. For example, most detectors avoid particle tracking in the immediate vicinity of the interaction diamond due to the background of charged pions. This is a nonexistent problem in peripheral collisions, where some form of tracking close to the interaction region is actually very desirable. For the same reason of enormous charged particle multiplicity, most detectors tend to have high granularity and be located at large distance from the interaction diamond (to reduce the occupancy rate). Again, from the point of view of peripheral interactions such a design is needlessly complex and expensive. Last but not least, physics goals of both programs are quite different, and one probably should avoid mixing them in a single experiment.

We hope that the area of extremely peripheral collisions of relativistic heavy ions will become an integral part of the physics program at RHIC.

References.

1. Conceptual Design of the Relativistic Heavy Ion Collider
   Brookhaven National Laboratory Internal Rep. 52195
   May 1989.
2. Can RHIC be used to test QED? - Workshop Proceedings
   ed. M.Fatyga, M.J.Rhoades-Brown, M.J.Tannenbaum
   Brookhaven National Laboratory Report 52247
   April 20-21, 1990.
3. C.A.Bertulani and G.Baur, Phys.Rep. 163(1988) 299.
4. C.Bottcher, M.R.Strayer, J.S.Wu, A.K.Kerman, M.J.Rhoades-Brown in:
   Can RHIC be used to test QED? - Workshop Proceedings
   ed. M.Fatyga, M.J.Rhoades-Brown, M.J.Tannenbaum
   Brookhaven National Laboratory Report 52247
   April 20-21, 1990.
5. E.Teller, Proc. of the 9th International Conference on the Application of Accelerators in Research and Industry, ed. J.L.Duggan North Holland Amst. 1986.
6. J.Schwinger, Science v165, N3895(1969)757.

Acknowledgments

We would like to thanks all members of the QED study group for useful discussions. In particular we wish to thank Drs. C.A.Bertulani and M.J.Rhoades-Brown.
This work supported in part by NASA Research Grant NAG-1-1134 and DOE contract DE-AC02-76CH00016.

Figure Captions.

Fig.1 A perturbative calculation of the probability for e^+e^- pair production in a collision with the impact parameter 385fm (Ref. 3).

Fig.2 The cross section for e^+e^- pair production as a function of the impact parameter in U+U and p+p collision at RHIC. Colliding beams at $\gamma = 100$ (Ref. 4).

Fig.3 Probabilities of removing a neutron from one ion only (P[T(1n,0n)]) and removing one neutron from each ion (P[T(1n,1n)]) in a collision of two Au nuclei with $\gamma = 100$ (colliding beams). Both probabilities are plotted against the impact parameter.

Fig.4 A schematic view of the low energy electron region.

Fig.5 A schematic view of the low energy electron detector.

Fig.6 A schematic view of the combined measurement of a trigger pair and low energy electrons.

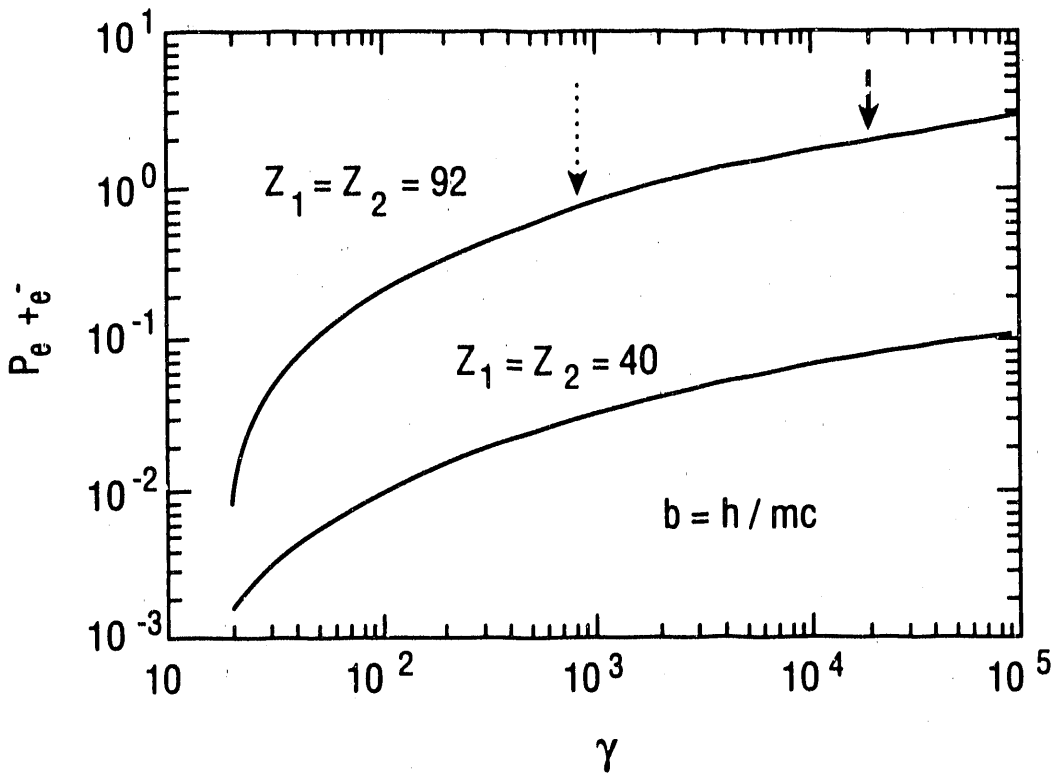

Fig. 1

Fatyga 1a 8/90 IR

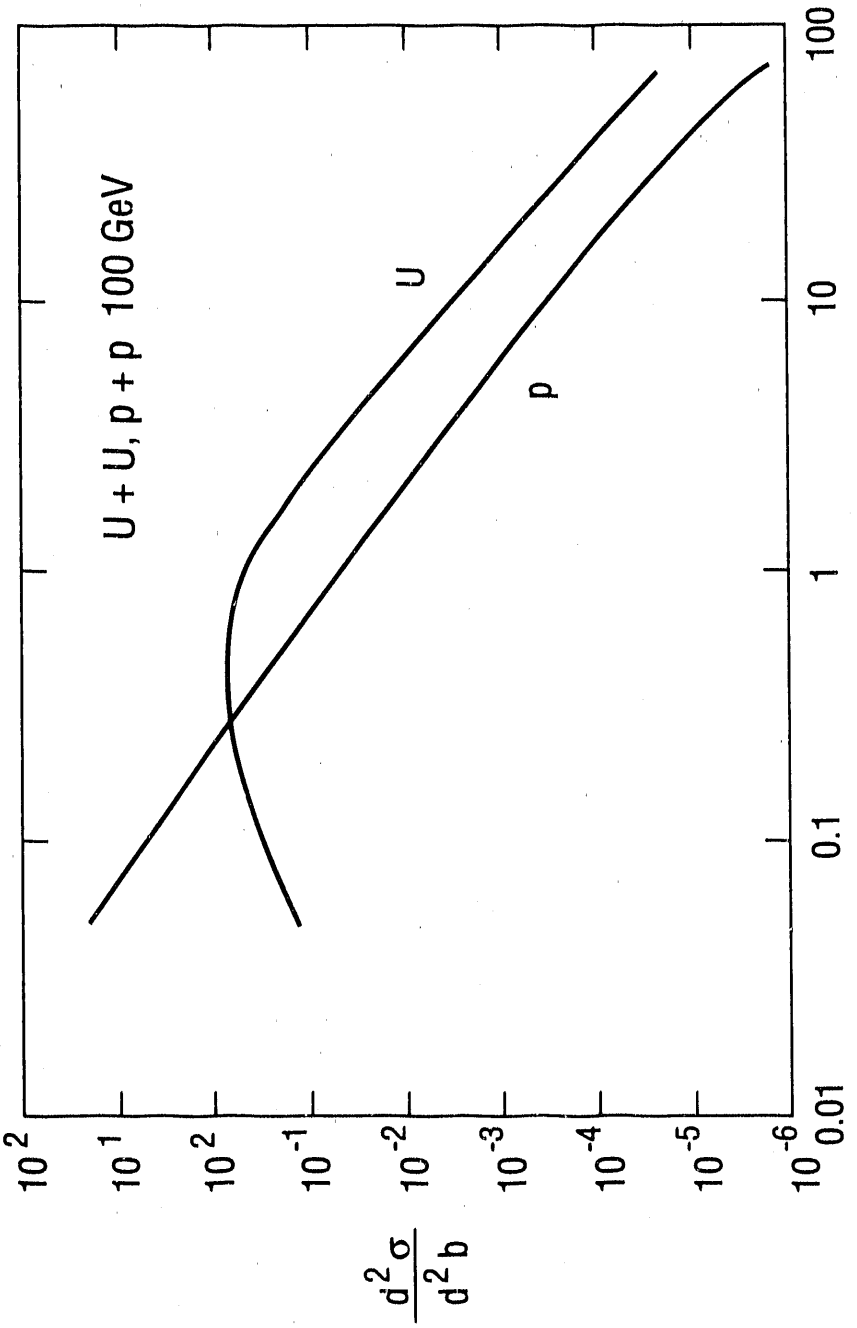

Fig. 2

Fatyga 2-1 8/90 IR

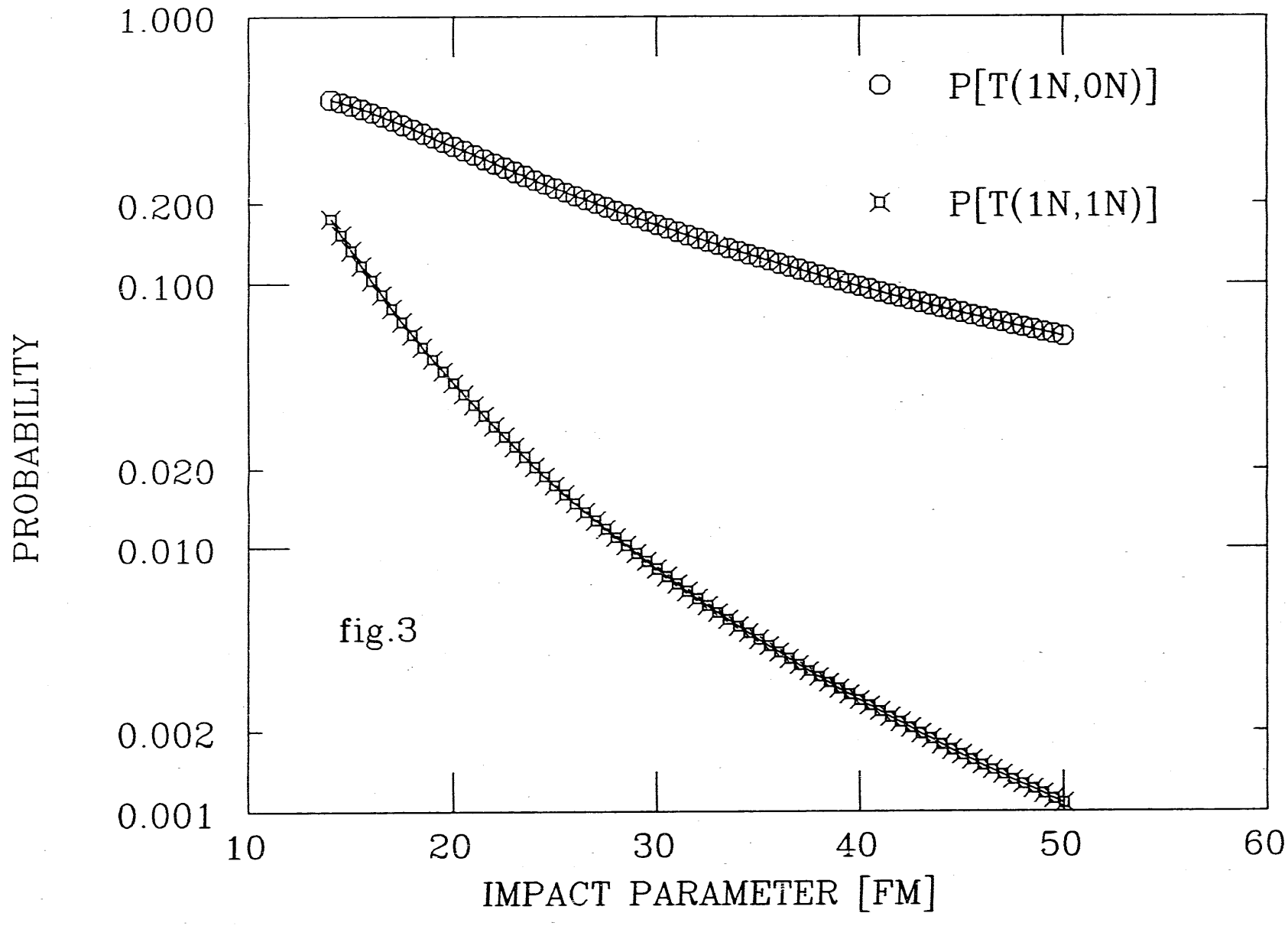
1.000
0.200
0.100
0.020
0.010
0.002
0.001
PROBABILITY
P[T(1N,0N)]
P[T(1N,1N)]
10
20
30
40
50
60
IMPACT PARAMETER [FM]

fig.3

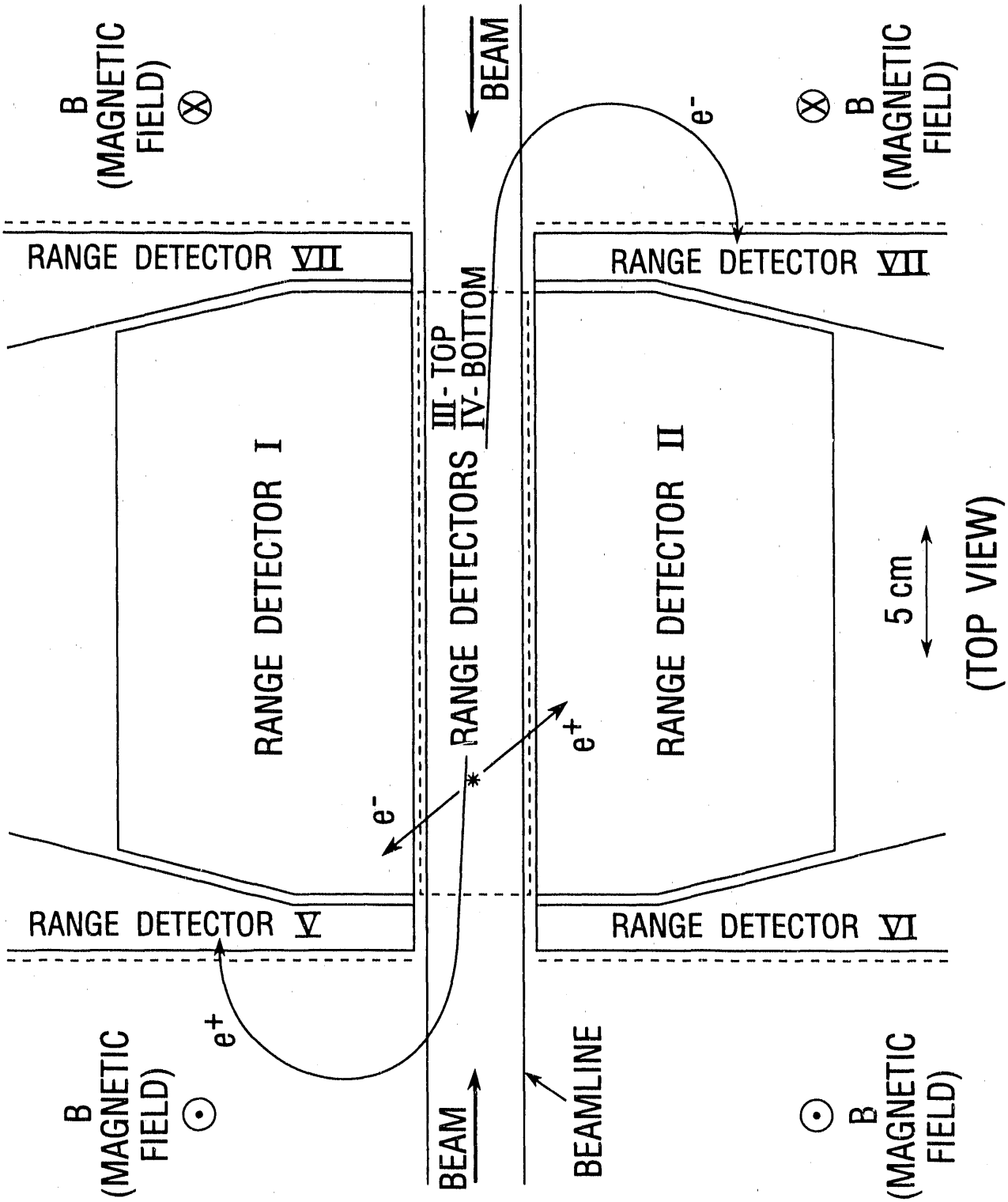

Fig. 4

Fatyga 4-1 8/90 IR

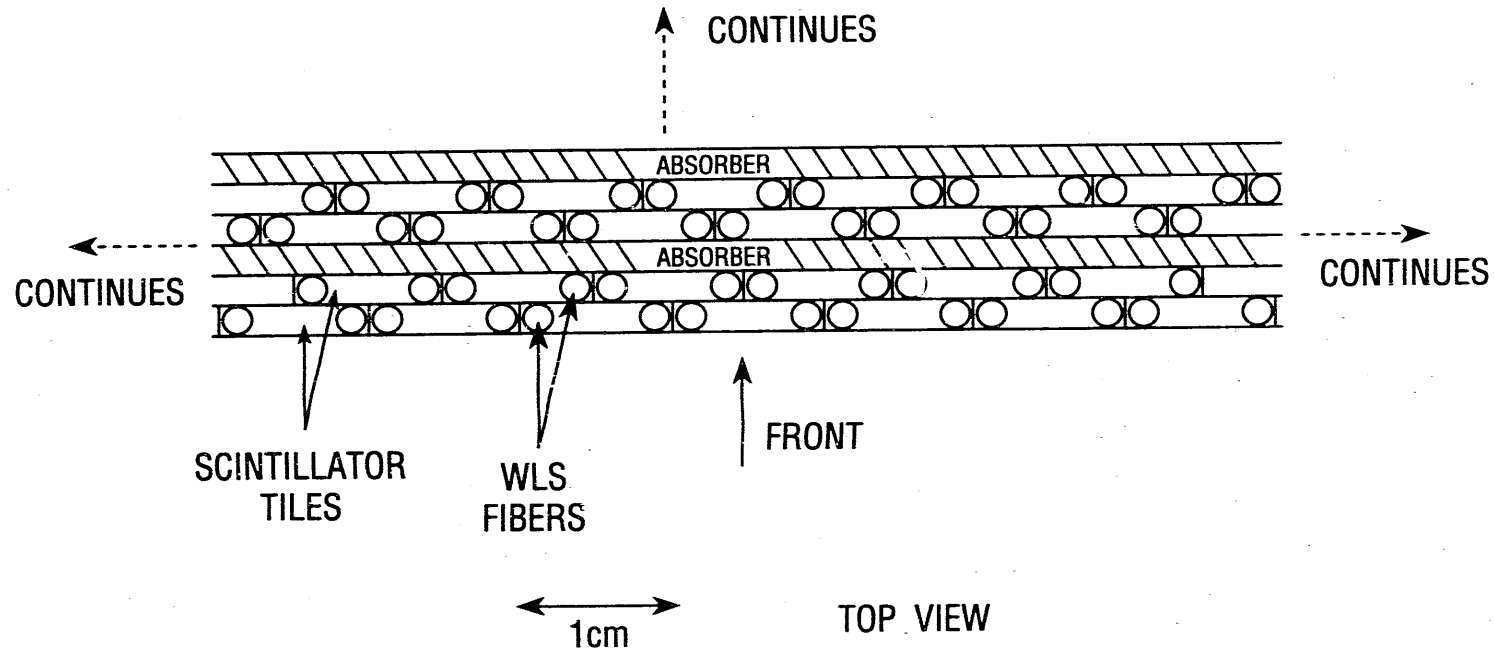

Fig. 5

FATYGA 5-1 8/90 IR

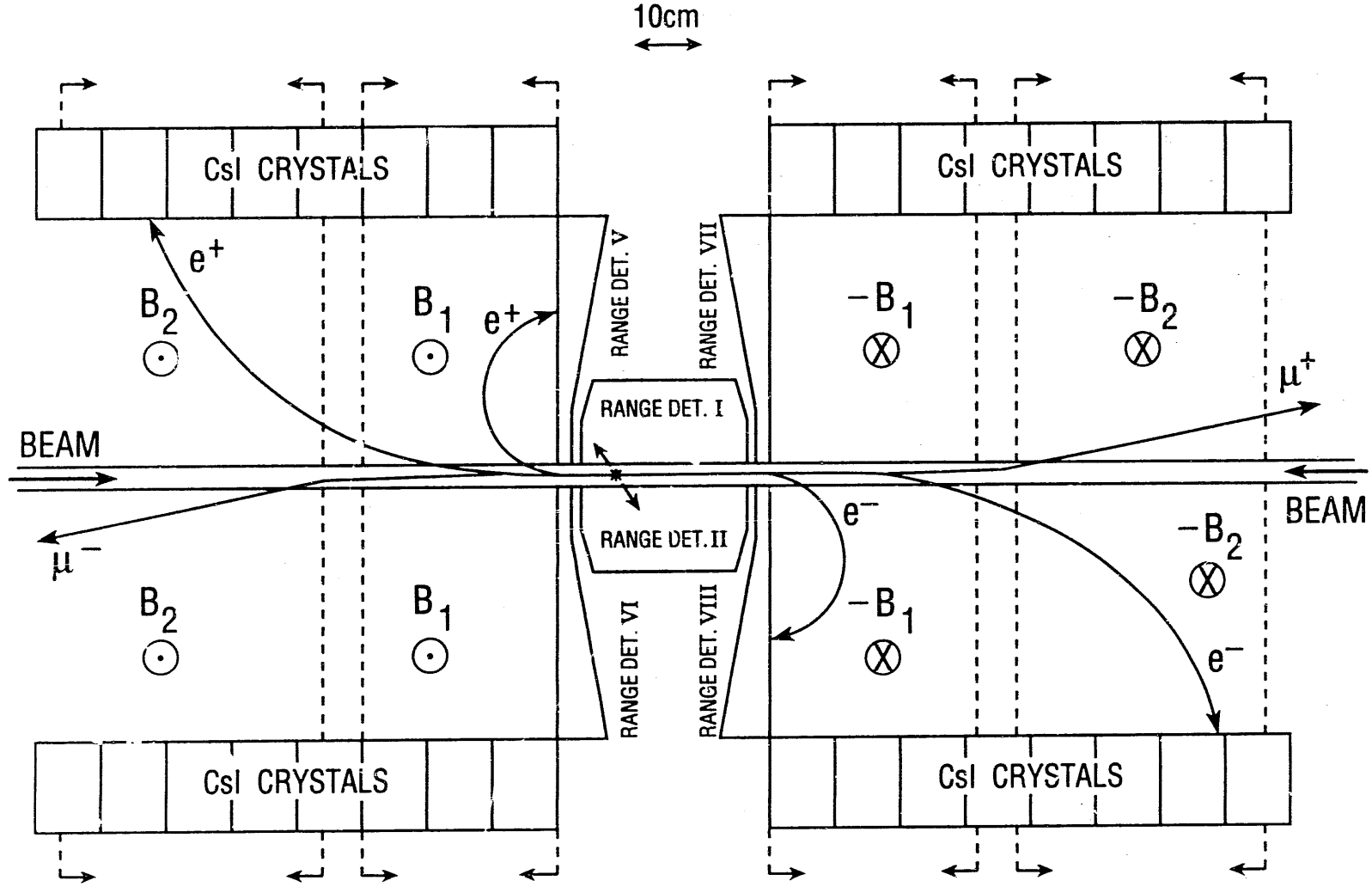

$B_1 = 0.1 - 0.2$ T

$B_2 = 1 - 2$ T

TOP VIEW

Fig. 6

FATYGA 6-1 8/90 IR

Research and Development Projects Related to Experiments at RHIC.

Contents:

A Real-Time Expert System for Experimental High Energy/Nuclear Physics

S. Clearwater[1,2], W. Cleland[1], F. Provost[2], E. Stern[1], Z. Zhang[1]

[1]Department of Physics and Astronomy [2]Department of Computer Science
University of Pittsburgh, Pittsburgh, PA 15260

We are developing a novel real-time expert system to monitor the performance of a triggering system in a high energy/nuclear physics experiment at Brookhaven National Laboratory (Experiment 814). The system runs on an 80386 processor that is completely independent of the data acquisition computer for the experiment. Artificial Intelligence techniques are seen as especially important for the diagnostic capability of the system. In particular, a separation of the diagnostic knowledge from the control procedures facilitates modification of the expert system and hence the diagnostic capability of the overall system. This is highly desirable as changes in the trigger conditions often occur during the course of a physics run. In addition, one of the objectives of this research is to develop a system which is capable of detecting fault conditions in a serial trigger processor and to aid in locating their cause.

1. Introduction

In large physics experiments based on electronic detectors, such as the ones carried out in high energy or nuclear physics, there are two problems which occur frequently:

(1) the systems are sufficiently large that faults which occur with a relatively low probability happen often enough that some form of automated test procedures are needed; and

(2) the duration of an experiment exceeds the length of time than many individuals can commit to a project, so that valuable expertise on a detector or subsystem disappears during the course of the experiment.

We are carrying out a research project which may provide some help in solving both of these problems. Our approach is to develop a real-time expert system for a particular subsystem (the trigger) of an experiment, which will both perform immediate online checks of the trigger logic and will serve as a repository of information obtained by the human experts working with the system. One goal of this project is to determine to what extent useful diagnostic information about an experimental subsystem or detector can be entered into a knowledge base by the human experts in the course of developing the system. In a later stage we plan to also apply machine learning techniques to aid in fault detection.

2. Expert Systems

Artificial Intelligence (AI) is a branch of computer science that seeks theoretical and experimental solutions to problems requiring intelligence to solve. It deals with symbolic, nonalgorithmic methods of problem solving. The problem-solving methods themselves are usually qualitative reasoning techniques rather than mathematical or data-processing methods. AI methods involve heuristics

(e.g. rules of thumb) that, while not guaranteeing a solution like an algorithm would, can reduce the solution time enormously when they work[1]. An expert system can be defined as[2]:

"a computer program that (a) reasons with domain-specific knowledge that is symbolic as well as mathematical; (b) uses domain-specific methods that are heuristic (plausible) as well as algorithmic (certain); (c) performs as well as specialists in its problem area; (d) makes understandable both what it knows and the reasons for its answers; and (e) retains flexibility."

Components of a typical expert system are an interface to the external world (including users), knowledge acquisition system (way to get knowledge), knowledge base (place for storing knowledge), and an inference engine (applying the knowledge). Expert systems have been applied for numerous problems such as data interpretation, monitoring, design, equipment diagnosis, troubleshooting, configuration, medical diagnosis, equipment tuning, network diagnosis and accelerator beam-line fault-finding[3-9].

3. Development of a Workstation for the E814 Trigger Processors

The E814 trigger system, shown diagramatically in Fig. 1, consists of four CAMAC crates, which

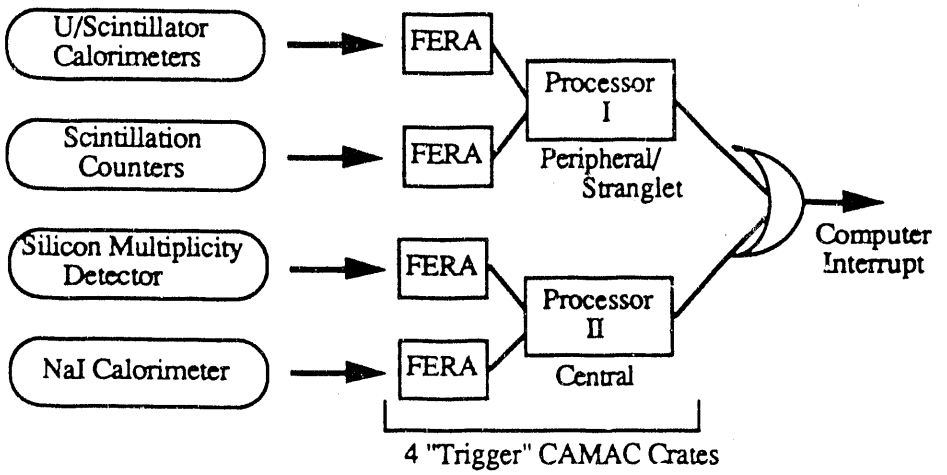

Fig. 1. Schematic diagram of the E814 Trigger system. Information for four major detector systems is digitized by Fast Encoding ADCs (FERAs) and presented to digital arithmetic processors which decide whether to interrupt the computer and read the event. The four CAMAC crates containing the FERAs and the processors provide the data for the real time expert system.

are normally read by the data acquisition VAX, along with the other data for the event. These four crates also contain auxiliary crate controllers which are interfaced to an 80386-based PC (12 MByte RAM, 60 MByte disk) running at a clock speed of 25 MHz. This monitor workstation is organized as a real time expert system. Due to the stringent time constraints from the experiment, certain

tradeoffs in the generality of the software were made in favor of processing speed. This is discussed in more detail below.

3.1 Architecture

The structure of the software for the workstation is shown in Fig. 2. There are two modes of operation of the system: (1) a data collection mode, in which events are read in at high speed and a validation of the trigger decisions is made; and (2) a diagnostic mode, in which anomalous events,

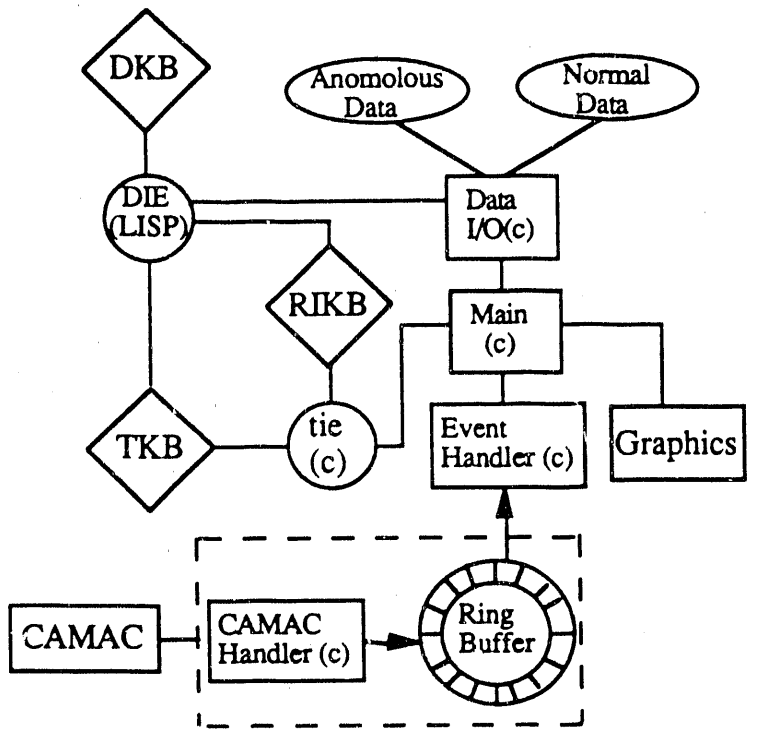

Figure 2. Diagram of the software of the real time expert system. The data are obtained by reading the CAMAC system. Upon receipt of an interrupt, data from the event are placed in a ring buffer. The event handler then calls the trigger checking inference engine (tie), updates the histograms, and writes data out on one of two data streams according to whether the events are normal (trigger decision is consistent with the data) or anomalous. The more general inference engine (DIE) is used to diagnose faults. The files TKB (Trigger Knowledge Base), RIKB (Run Information Knowledge Base) and DKB (Diagnostic Knowledge Base) are used to store information about the trigger system for use by either tie or DIE.

those which for some reason fail the validation criteria, are examined to understand the source of the failure.

The reading of the data is accomplished through an interrupt-driven CAMAC handler, which writes events into a ring buffer. In the data collection mode, subroutine MAIN performs display functions, indicating the state of the system (showing the number of events collected, the fraction of different

trigger types, the number of failures detected, etc.). During this process, it continuously examines the ring buffer pointers to search for new data. When data are available, control is passed to the Event Handler subroutine, where the trigger quantities which were calculated in the trigger hardware are recalculated in software. These quantities, along with the trigger decision words, are then passed to the trigger inference engine (tie), which examines the data, using the logic and parameters contained in the Trigger Knowledge Base (TKB) and the Run Information Knowledge Base (RIKB). The trigger inference engine returns a simple YES/NO flag indicating whether or not the data are self-consistent. Events can be written to two different streams depending on whether the trigger data are consistent with expectations, i.e., one for Normal Data and the other for Anomalous Data. Both event streams are available for histogramming or diagnostic purposes. Both files are written onto RAM disk structures, in order to optimize the speed of the program.

Once a sample of anomalous events has been created, it is possible to enter the diagnostic mode. In this mode, the Anomalous Data and Normal Data files are read by the Diagnostic Inference Engine (DIE). This routine uses the RIKB and TKB as well as a third file, the Diagnostic Knowledge Base (DKB). Diagnostics rules for identifying faults are generated by hand from patterns of previously found faults. These rules are stored in the DKB and used by DIE to compare with patterns in the data. Matches between the rules and the data indicate the likely source of a problem.

The structure described above has been designed to permit the workstation to operate in real time with the experiment. We are striving for a system in which this rate can be as high as 200 Hz when the AGS beam spill is on. The average spacing between events is therefore approximately 5 ms. The CAMAC scan proceeds at a rate of approximately 5 microseconds/word, and the record size will typically be 200 words, giving a read time of about 1 ms. Thus the inference engine which verifies trigger logic must be capable of performing its task in less than 4 milliseconds. For this reason, the code in the trigger inference engine (written in C) must be highly efficient and will therefore be made only as general as necessary to handle rules of the type that are implemented in the trigger hardware. In the diagnostic mode, since the computer will be working only between runs, there is not a stringent speed requirement. Here we would plan to use a much more general inference engine (written in LISP) to handle the possibly very complex reasoning which may occur in fault finding.

The event rate of 200 Hz is realized only in the test runs in which only the trigger data are read into the workstation. For normal data taking runs, the main data acquisition system reads the trigger crates, signals the workstation when it is finished, and then continues to scan the other data from the detectors, which is contained in FASTBUS crates. The workstation then rescans the trigger crates and performs the trigger validation while the data acquisition system finishes its scan of the system. A timing diagram for this mode of operation is shown in Figure 3.

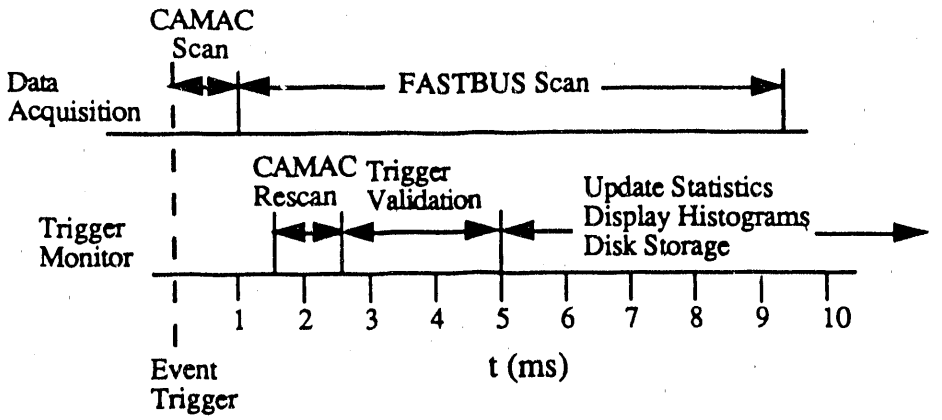

Figure 3. Approximate timing diagram of the reading and testing of trigger data by the workstation, which is carried out while the main data acquisition for the experiment is carrying out the scan of the rest of the data for the event.

3.2 Software

Verification of the consistency of the triggered data is an important function of the diagnostic system. It is convenient to have a database of conditions that each trigger must satisfy since these change frequently, but a "normal" rule processing system would be too slow to be applied for every event. However, the trigger conditions can be reduced to conjunctions of several simple tests of data against thresholds. In order to meet the time constraints and yet retain the desirable characteristics of knowledge-based systems, such as the modularity of the knowledge and procedures that use them, we have developed a fast rule-driven C program. At the start of each run, the list of rules is translated into a compact form for use by the program. For each data event, a C function reproduces the trigger calculations which were performed digitally in hardware. The rule-application program, a very simple inference engine, applies the thresholds and conditions contained in the rule list to the results of the trigger calculations, producing a binary decision. To further speed up the C inference engine it is possible to take into account dependencies among various triggers and order the rules accordingly. For example, if some subset of the rules make a common test then that test can be made first to see if the others should be tested. This arrangement allows for more complex triggers to be tested in less processing time, although the generality of the program is necessarily reduced.

The trigger processor workstation will run within GoldworksII, an inexpensive development environment for the 80386 processor. It contains a LISP compiler, which supports the calling of C subroutines. The use of the C language is important for two reasons: (1) the latest Microsoft C compiler (version 5.0) supports interrupt routines, and (2) for calculations connected with monitoring, the speed of C is an important advantage. The device driver for our CAMAC interface can be called from C.

For the diagnostic task we developed a small LISP inference engine to provide a general means of performing inferences on data using a separate knowledge base of rules. It has the advantage over commercially available "shells" that it is faster and that we have the source code. This inference engine is a simple data-driven rule-based value prediction system, coupled with an evidence gathering mechanism. The evidence-gathering mechanism is used when conflicts arise among the consequents of rules that fire. The inference engine predicts the "best" answer based on one of several user selectable conflict resolution strategies or one defined by the user. More sophisticated reasoning combining data- and goal-driven multiple step inferencing is provided with a general commercial inference engine shell such as Goldworks.

4. Current Status

The monitoring workstation has been installed in Experiment 814, and we have verified that the mode of operation illustrated in Figure 3 works. The rescan time for the CAMAC crates is about 2.5 ms, and the trigger checking requires a similar amount of time, so that the checking process is completed before the FASTBUS scan is finished. The workstation also has one- and two-dimensional histogramming capabilities, and it keeps track of the numbers of events, types of triggers, etc.. A data-taking run for E814 is expected to occur in June 1990, in which the workstation will be used strictly for the purpose of monitoring triggering data and providing online information about the triggering quantities.

The next phase of the project is the development of the diagnostic capabilities of the system. This will be done, as mentioned above, using a slower but more general inference engine, and the input data for this program will the the files of anomalous and normal events generated by the workstation as it is operating in its real-time mode.

5. Discussion

The stringent requirements forced by high data taking rates resulted in several compromises in the system architecture. First, the need to make decisions within a beam spill on an event by event basis means that only very simple inferences can be made. We found it useful both for simplicity and modularity to use a knowledge-based approach but without the overhead (or necessity) of complex inferencing mechanisms. The goal at this level is simply to flag anomalous events for analysis at a later stage. The second step is a more sophisticated analysis that occurs between runs and again uses a knowledge-based approach but this time with much more of the machinery found in expert systems such as forward (data-driven) and backward (goal-driven) chaining of inferences. With the present level of expert system software and the hardware of the experiment this two-level approach to real-time trigger diagnosis seems to be the only viable choice.

In our case, it would also be possible to use a learning program, such as RL4[9], to learn fault conditions in the trigger processors and to locate their probable cause. In the learning mode it may be possible for the program to notice similarities between good and bad data by making various manipulations of the data as it saw fit[10].

Acknowledgements

This work was supported in part by RHIC detector research and development funds.

References

[1] B. G. Buchanan and E. H. Shortliffe, Rule-Based Expert Systems, Addison-Wesley, Menlo Park,1984.
[2] B G. Buchanan and R. G. Smith, Fundamentals of Expert Systems, Ann. Rev. Comput. Sci., 3, 1988.
[3] Proceedings of the First Annual Conference on Innovative Applications of Artificial Intelligence, Stanford University, March 28-30, 1989.
[4] S. H. Clearwater and M. J. Lee, in: Proceedings of the 1987 Particle Accelerator Conference, Washington DC (Mar 16-19, 1987) eds., E. R. Lindstrom and L.S. Taylor, p. 532.
[5] Round, A., The Handbook of Artificial Intelligence, vol. 4, Barr, A., Cohen, P., and Feigenbaum, E., eds., Addisson Wesley, Reading MA, pp493-499, 1989.
[6] A. W. Booth and J. T.Carrol, Computer Physics Communications 45 (1987) 67.
[7] G. Mornacchi, "A Prolog assistant for users of CERN networks", October 1985, CERN DD/85/22 (unpublished).
[8] W. Fabbri, F. Gagliardi, and G.Mornacchi, CERN DD/86/4 (February 1986) (unpublished).
[9] B. G. Buchanan, J. Sullivan, T. P. Cheng, and S. H. Clearwater, in: Proceedings of the Seventh National Conference on Artificial Intelligence, St. Paul (August 21-26, 1988) p. 552.
[10] R. S. Michalski, J. G. Carbonell, T. M. Mitchell, eds., Machine Learning: An Artificial Intelligence Approach (Tioga Publishing Co., Palo Alto 1983).

The Development of Silicon Multiplicity Detectors For RHIC

A PROGRESS REPORT

R. H. Beuttenmuller, A. K. Bhattacharya, W. Chen, J. F. Gannon, H. W. Kraner, Z. Li, D. Lissauer, D. Makowiecki, V. Polychronakos, V. Radeka, L. C. Rogers, D. Stephani, and H. Takai
Brookhaven National Laboratory, Upton, New York 11973.

M. Dris, E. Gazis, H. Rahmani, Th. Papadopoulou
National Technical University, Athens, Greece GR-15773

and

J. R. Hall and D. Wolfe
University of New Mexico, Albuquerque, New Mexico 87131

1. Introduction

A frequently stated common goal of all relativistic heavy ion experiments is the observation of "quark–gluon plasma" (QGP). This postulated state of matter results from the QCD prediction of a phase transition in hadronic matter at sufficiently high energy densities. Several specific signatures indicating the creation of such a state are theoretically predicted and sought in many experiments. These include large soft photon and lepton production, the suppression of J/ψ production, strangeness enhancement etc. In addition to these specific signatures one or both of two experimental observables are used by most experiments for the global characterization of heavy ion collisions. These are the total produced transverse energy (E_T), and the number of the produced charged particles (N_{Ch}). Both observables are closely related to thermodynamic variables commonly used in theory to describe the conditions necessary for the formation of such states. The first

round of experiments with heavy ions both at the BNL Alternating Gradient Synchrotron (AGS) and the CERN Super Proton Synchrotron (SPS) have shown [1] a strong correlation of these variables. Figure 1 shows a $d\sigma/dE_T$ distribution[2] for $^{16}O - Pb$ interactions. In Fig.2a are shown $d\sigma/dN_{Ch}$ distributions for two pseudorapidity intervals. Fig.2b shows a E_T vs N_{Ch} scatterplot [3] which,in spite of the slightly different pseudorapidity intervals, clearly shows the strong correlation. Moreover, due to the large number of produced particles, the correlation is quite narrow even on an event by event basis.[4] For fixed target experiments the total energy flow in the forward direction has also been used as a measure of the produced E_T.

The importance of these observables is further enhanced by the fact that it is relatively simple for either one of them to be used at the trigger level in order to tag the "centrality" of a given interaction. In this development project we are using silicon detectors to measure the total number of charged particles produced in a heavy ion collision as well as to measure their production as a function of pseudorapidity. Unless calorimetric coverage over a large solid angle is necessary for other reasons measuring N_{Ch} instead of E_T is clearly more practical and less expensive.

2. The High Mean Occupancy Technique

Charged multiplicity detectors independently of the technology used are segmented such that the mean occupancy per detector element for the process of interest does not exceed 5-10%. In this way the probability of multiple hits is rather small and therefore the uncertainty in the multiplicity measurement small. This is particularly important for gas detectors where the large Landau fluctuations in the energy loss make it practically impossible to distinguish between one or more minimum ionizing particles traversing a detector element. Typical interactions at RHIC will produce multiplicities of the order of 1000-2000 particles per unit of rapidity. Assuming a mean occupancy of 10% this can lead to a detector with 50-100k channels. The rather large size of the interaction diamond at RHIC would increase this number by at least a factor of 3-5. Our experience, however, with silicon multiplicity detectors in the HELIOS experiment at the CERN SPS shows that in such a detector the Landau fluctuations are sufficiently low to allow one to distinguish

between zero, one, or two particles traversing a detector element. The mean multiplicity per element is measured and an appropriate correction based on Poisson statistics on an event by event basis can be made. Figure 3 shows the pulse-height distribution of one element of such a detector and for a small interval of E_T. The dashed curves represent modified Landau distributions for up to four particles and the solid curve a fit to the sum of these distributions with weights calculated from the mean hit probability using Poisson statistics. A correction thus can be calculated for every element of the detector. Additional corrections at the few per cent level have to be made due to particle decays (mostly K_s) and gamma conversions. This can be accomplished by Monte Carlo techniques using a suitable event generator.

3. The Proposed Program

We have proposed an R&D program which would lead to a multiplicity detector for a RHIC experiment using this technique. Such a RHIC detector could have the following features:

- The detector should be able to cover pseudo- rapidity range of ± 2 units in the c.m. (angular coverage of $\theta, \pm 60$ degrees). Assuming a cylindrical geometry the detector length should be four times the radial position plus the diamond size.
- The system should supply the following information offline:
  - total multiplicity in a given rapidity bin
  - dn/dη , where η is the pseudo rapidity
  - dn/dϕ
- Total multiplicity for a given rapidity bin should be obtained at level 1 trigger (for example ± 1.5 units in pseudo rapidity). An accuracy of 5% for central collisions is needed. The main problem is that because of the relatively large diamond size we can not just add the total pulse height in the detector but need to vary the region of summing depending on the vertex position.

The Brookhaven Instrumentation Division has developed over the last few years the capacity to build Si pad detectors for applications in High Energy/Heavy Ion experiments.

We have used these detectors very successfully in both experiments NA34/Helios at CERN and in experiment E814 at BNL.[5] For the RHIC detectors we will build on the existing experience but the detectors will have different requirements that need additional R&D work:

- use of signals from the detector back plane for Trigger information.
- connection of pads to multiplex electronics
- solve the production problems of a large number of detectors
- radiation damage studies

The proposed detector for RHIC will have approximately 5000-20000 channels. Analog information on individual channels is needed in order to determine the occupancy in each pad. One needs to develop a readout that is compact, relatively cheap and can work in a synchronous machine with 114 n-sec repetition rate. There are two major components to such a readout system which need development.

- Front end electronics based on VLSI technology

  The requirements for such a front end could include:

  - a dynamic range of 8-9 bits
  - 114 n-sec repetition rate
  - radiation resistance
  - packaging compatible with pad design

- A suitable read out system. We propose to start by developing a prototype system that has been designed at CERN by E. Chesi et al. [6] and develop it to a point where it can be used for a basis of a readout system of the multiplicity detector at RHIC.

In addition the necessary tools have to be developed to allow detailed performance studies and optimization of proposed detector configurations. In the following paragraphs we describe the current status of the R&D work as well as plans for the immediate future.

4. Current Status

We have designed and are currently constructing a 512-element detector to be tested later this year at an AGS beam. This detector should demonstrate the practicality of such a device in an environment similar to that which would be encountered at RHIC. To this end we plan to use this detector with AGS Exp. 814 when Au beams are available. The design of this detector is shown in Fig.4. In part a) of this figure the segmentation of the p^+ side (junction side) of the detector is shown whereas in part b) we show the ohmic contact (back plane) of the detector. The optimization of this coarse segmentation which is to be used at the trigger level requires considerable study. The number of segments should be as small as possible but consistent with the required accuracy of the multiplicity measurement at the trigger level assumed at the moment to be of the order of 10%. On the other hand the use of large pads would cause large dead areas in the event of a detector fault. In order to study these questions we have used finer segmentation than thought necessary (16). Several segments can eventually be connected together using ultrasound bonding to form a larger segment or cut off an element of a group to isolate a fault. The technique used to route these signals out of the silicon wafer and eventually to the amplifier motherboard is similar to the one we already used in several detectors for both experiment E814 at the AGS and NA34/NA44 at CERN. It consists of a fiber glass board overlay with traces originating in pads on the perimeter of this board and ending on the periphery of small holes appropriately located throughout the face of the detector and through which they are bonded to the detector pads (Fig.5). The connection of these output pads to matching pads on the preamplifier motherboard is done with a relatively new interconnection technique employing a thin sheet of a polymer (made by Sinetsu Polymer Co. of Japan) which is electrically conducting only in a direction transversely to the surface. This technique eliminates bulky jumper connections resulting in lower input capacitance and therefore lower electronic noise.

For the readout of this prototype detector we will use the AMPLEX chip developed by P. Jarron et al at CERN [7]. Although unsuitable for operation at the RHIC environment because of the lack of a pipeline and the relatively long occupancy times it is nevertheless well matched to our present requirements. This chip built with 3μ n-well CMOS technology

contained 16 channels of low noise charge sensitive amplifiers followed by shapers with integration time of about 500 ns followed by a storage element and multiplexing logic providing one output for all 16 channels. The schematic diagram of one such channel is shown in Fig.6 and its detailed electrical characteristics are provided in Tables I and II. The AMPLEX chip is fully developed and in production. We have joined a recent production run of this device and already have in our possession 250 chips (4000 channels). They are packaged in surface mounted device technology (SMD) allowing a very compact and lightweight readout board. The amplifier motherboard currently under design will contain all the amplifiers necessary to read out 512 channels in a circular band 2 cm wide and about 15 cm in diameter. It has only 5 lines providing power, the single output, and the multiplexing control signals. For the readout of the multiplexed channels we are using the system already mentioned in the previous paragraph. The block diagram of this compact system is shown in Figure 7. One single-width CAMAC module can handle the output of 1024 channels. It has an 8-bit digitizer, and an 8-bit arithmetic logic unit which can be used to subtract prestored pedestals for every channel and also provide zero suppression by comparing the signal of every channel with a programmable threshold level. The address of the element with a signal satisfying the threshold requirement as well as an 8-bit amplitude are store in a memory which is then read out by a conventional data acquisition system. The digitization speed is adjustable with a maximum rate of about 2MHz. We have already set up a stand-alone system capable of reading 1024 channels in order to develop the necessary software.

In parallel and in collaboration with the BNL Instrumentation Division we have started work on the development of the custom monolithics. This is obviously a difficult task requiring resources well beyond the means of most detector development groups. We are taking advantage of a microelectronics development group being formed at the Instrumentation Division and in which some of us are participating in similar efforts for the development of monolithic circuits for the SSC and other RHIC R&D projects. The necessary design and simulation tools have already been obtained and the design team has started working on these tasks. In addition BNL has undertaken a systematic study of neutron and ionizing radiation effects on such devices in collaboration with Argonne National Laboratory. Devices from several radiation hard processes will be irradiated and

measured. The failure mechanism, including the effect of radiation on noise, must be firmly understood. Devices like junction field effect transistors, intrinsically much more radiation resistant than MOSFETs can be built compatibly with MOS devices and may be employed in critical areas of the circuit to improve its radiation resistance.

5. Future Plans

The prototype detector should be completed early this Fall and should be tested as soon as the AGS starts running in FY 1991. In addition we intend to demonstrate the feasibility of this technique in a realistic environment when Au beams are available at the AGS as mentioned already in the previous paragraph. A detector like the one shown in Fig.4 placed at a distance of about 5cm from the target should detect particles with an occupancy rate approaching one.

For the longer term we are starting to consider the systems aspects of such a detector in a RHIC experiment. To this end we have been discussing such a multiplicity detector with a group (of which some of us are already members) thinking of a RHIC experiment employing a semi-open geometry (the Open Focussing Spectrometer). Our goal during this workshop is to arrive at a first order design for such a device and use this to further focus our long range objectives of the microelectronics development effort.

References

1. See for example B. Shivakumar and P. Vincent (ed), Proc. of Third Workshop on Experiments and Detectors for a Relativistic Heavy Ion Collider, BNL 52185 (1988).
2. T. Akesson et al., Phys.C, 38,383(1988).
3. P.Giubellino et. al, NIM A275, 89(1989).
4. J. Schukraft, 19th Symposium on Multiparticle Dynamics, Arles, France, 13-17 June 1988.
5. R.H. Beuttenmmuller et al., NIM, A253, 500 (1987).
6. E. Chesi et al., CERN PS 202 Note (1988).
7. P. Jarron et al., AMPLEX, A low-noise, low power analog CMOS signal processor for multi-element silicon particle detectors, CERN/EF 89-9.

TABLE 1

Filtering parameters of AMPLEX

Poles	Integrating time constants
$p1 = g_{m1}/2\,\pi\,C_{diff}$	$\tau_1 = (1/p1)(C_{det} + C_f)/C_f$
$p2 = g_{m2}/2\,\pi\,C_h$	$\tau_2 = (1/p2)(C_{diff} + C_{fS})/C_{fS}$
$p3 = 1/2\,\pi\,R_{fS}\,C_{fS}$	$\tau_3 = R_{fS}\,C_{fS}$
$p4 = 1/2\,\pi\,R_{SWH}\,C_h$	$\tau_4 = R_{SWH}\,C_h$

Filter input resistance	Differentiating time constant
$R_{diff} = (1/g_{m2})\,(C_h + C_{fS})\,/\,C_{fS}$	$\tau_{diff} = R_{diff}\,C_{diff}$

Transconductances

$g_{m1} = q\,I_{bias}\,(POTA)\,/\,n\,kT$	$g_{m2} = q\,I_{bias}\,(NOTA)\,/\,n\,kT$

TABLE 2

Summary of characteristics of AMPLEX

Gain	5 mV/fC for C_{det} = 20 pF 18 mV/min. ionizing part. in 300 µm Si d .ector (MIP)
Gain uniformity	2% within chip, 5% from chip to chip
Gain versus C_{det}	0.6% gain decrease per pF
Noise	ENC 1000 r.m.s. electrons for C_{det} = 20 pF
Linearity	Better than 2% integral up to 70 fC input charge (corresponds to ~ 20 MIP)
Output DC offset	+ 15 mV
Offset spread	± 10 mV
Maximum acceptable detector leakage current	450 nA
Power consumption	1.1 mW per channel for biasing conditions: $I_{bias\ (POTA)}$ = 50 µA, $I_{bias\ (NOTA)}$ = 10 µA
Peaking time	750 ns

List of Figures

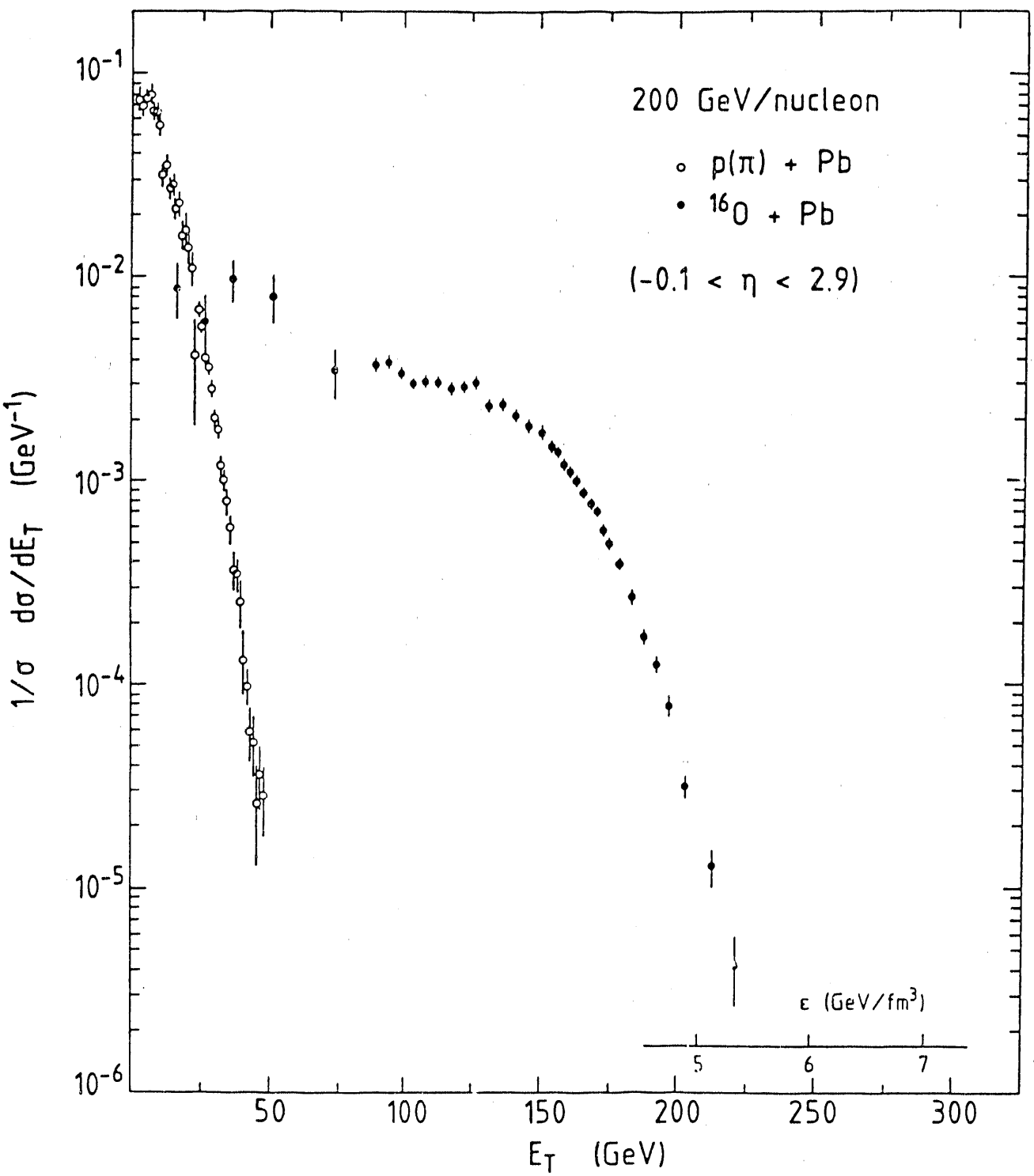
200 GeV/nucleon
o p(π) + Pb
• ^{16}O + Pb
(-0.1 < η < 2.9)
10^{-1}
10^{-2}
10^{-3}
10^{-4}
10^{-5}
10^{-6}
$1/\sigma \; d\sigma/dE_T$ (GeV^{-1})
50
100
150
200
250
300
E_T (GeV)
ε (GeV/fm^3)
5
6
7

FIG. 1

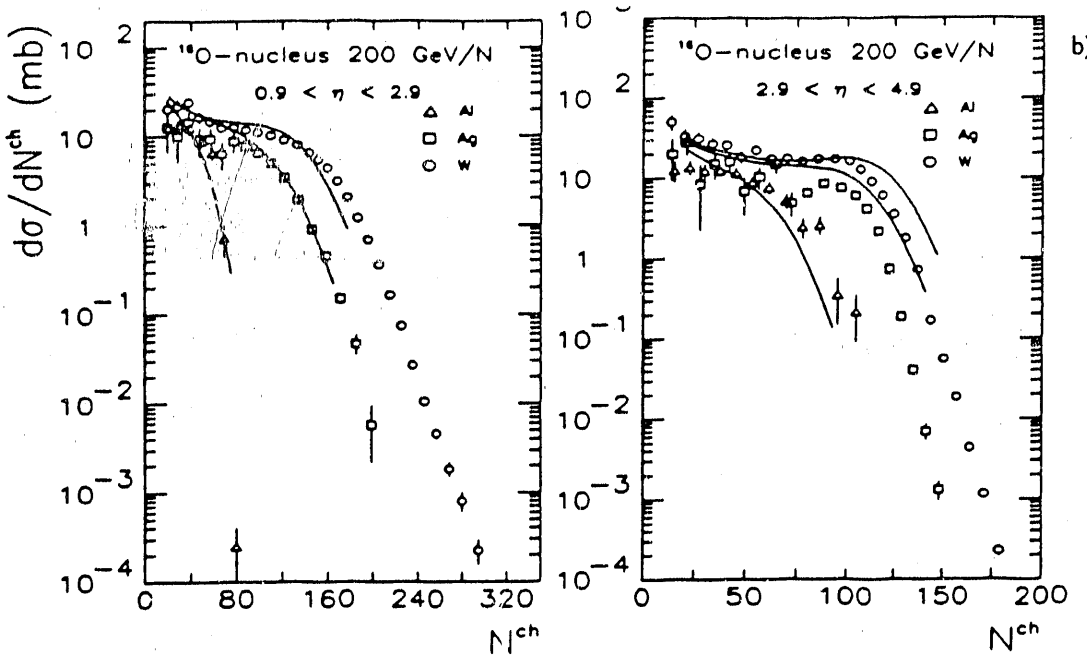
^{16}O–nucleus 200 GeV/N
0.9 < η < 2.9
Al
Ag
W
$d\sigma/dN^{ch}$ (mb)
N^{ch}
^{16}O–nucleus 200 GeV/N
2.9 < η < 4.9
Al
Ag
W
N^{ch}
b)

FIG. 2(a)

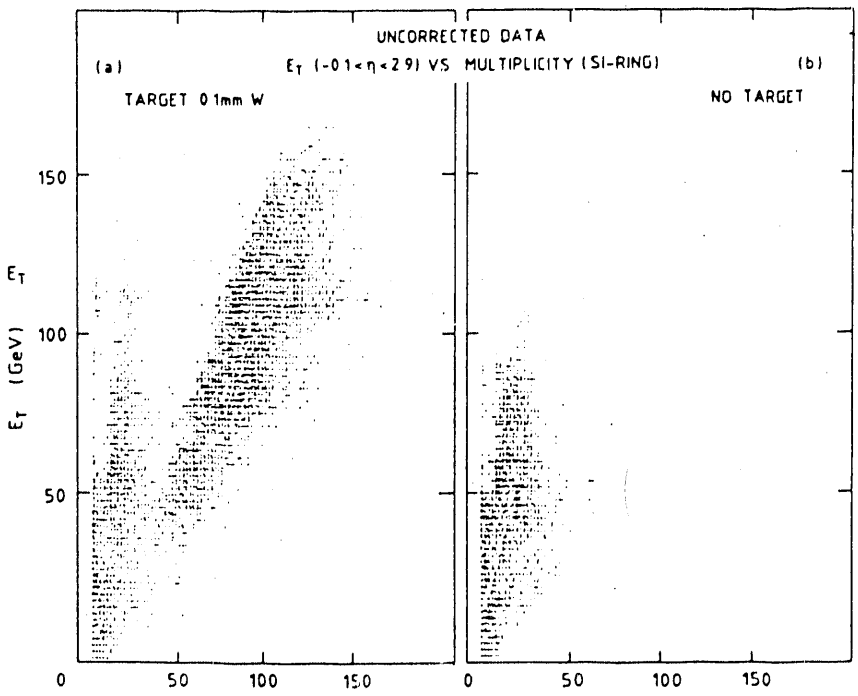
UNCORRECTED DATA
(a)
E_T (-0.1<η<2.9) VS MULTIPLICITY (SI-RING)
(b)
TARGET 0.1mm W
NO TARGET
E_T
E_T (GeV)

FIG. 2(b)

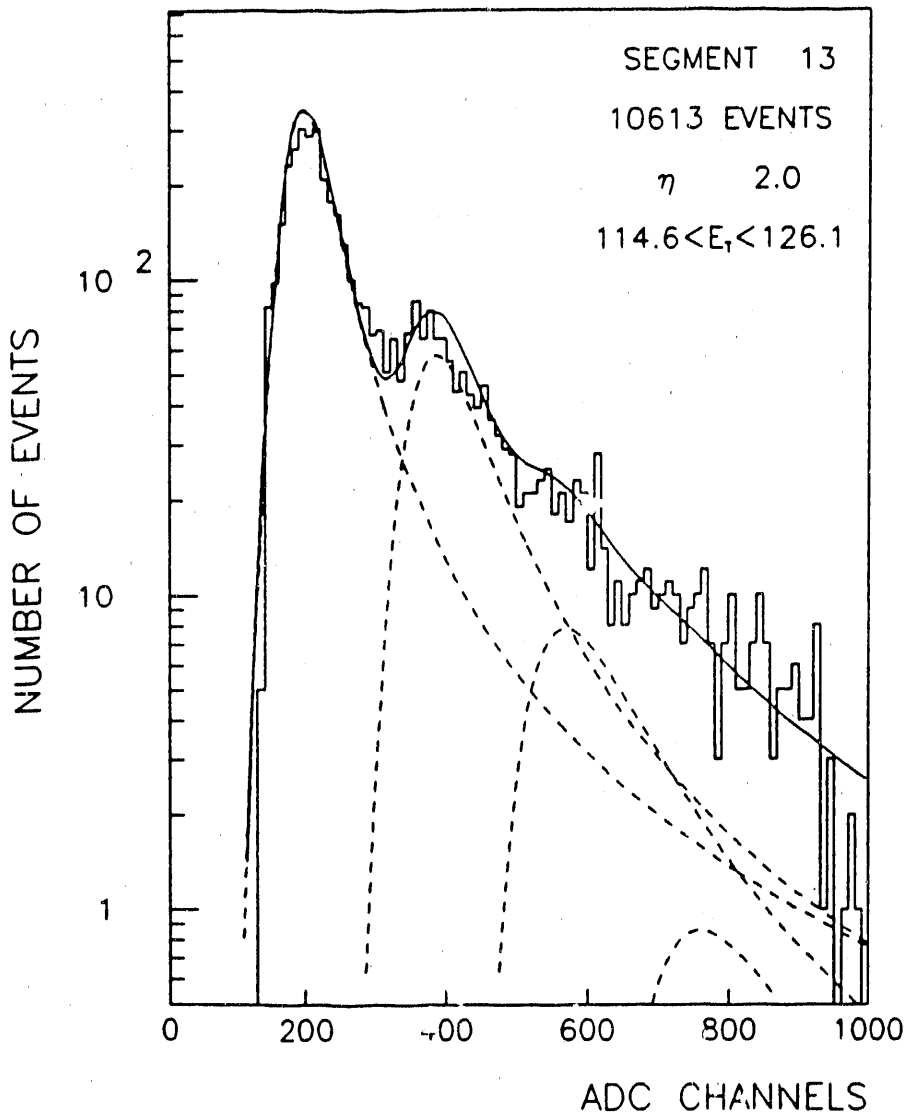
SEGMENT 13
10613 EVENTS
η 2.0
114.6<E_T<126.1
NUMBER OF EVENTS
10 2
10
1
0
200
400
600
800
1000
ADC CHANNELS

FIG. 3

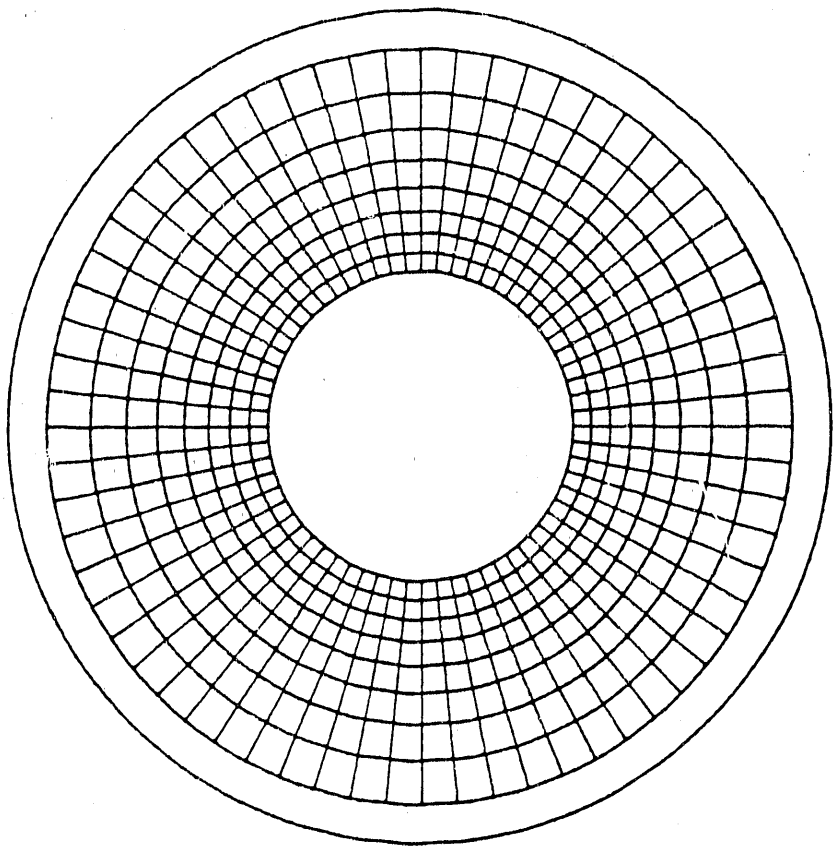

FIG. 4(a)

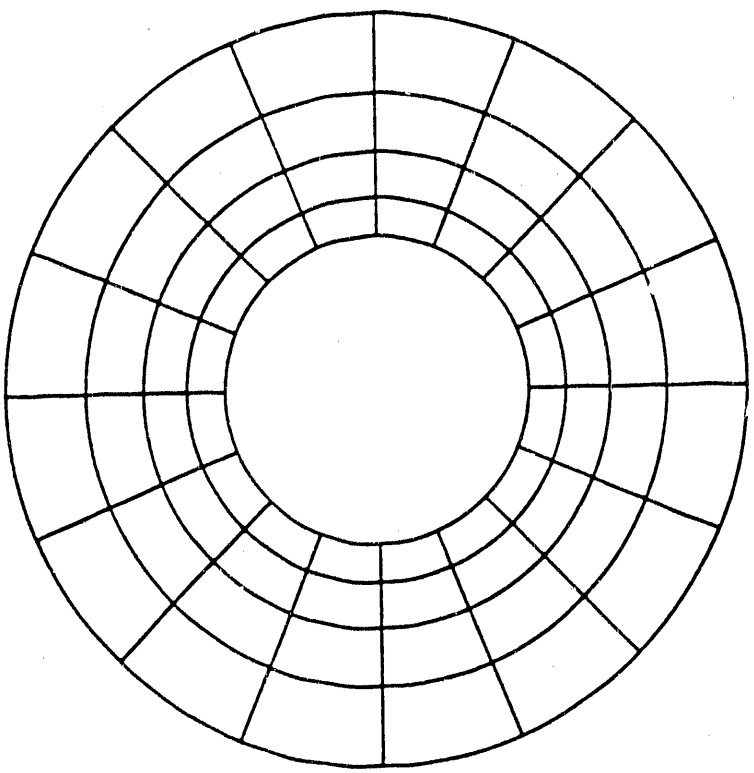

FIG. 4(b)

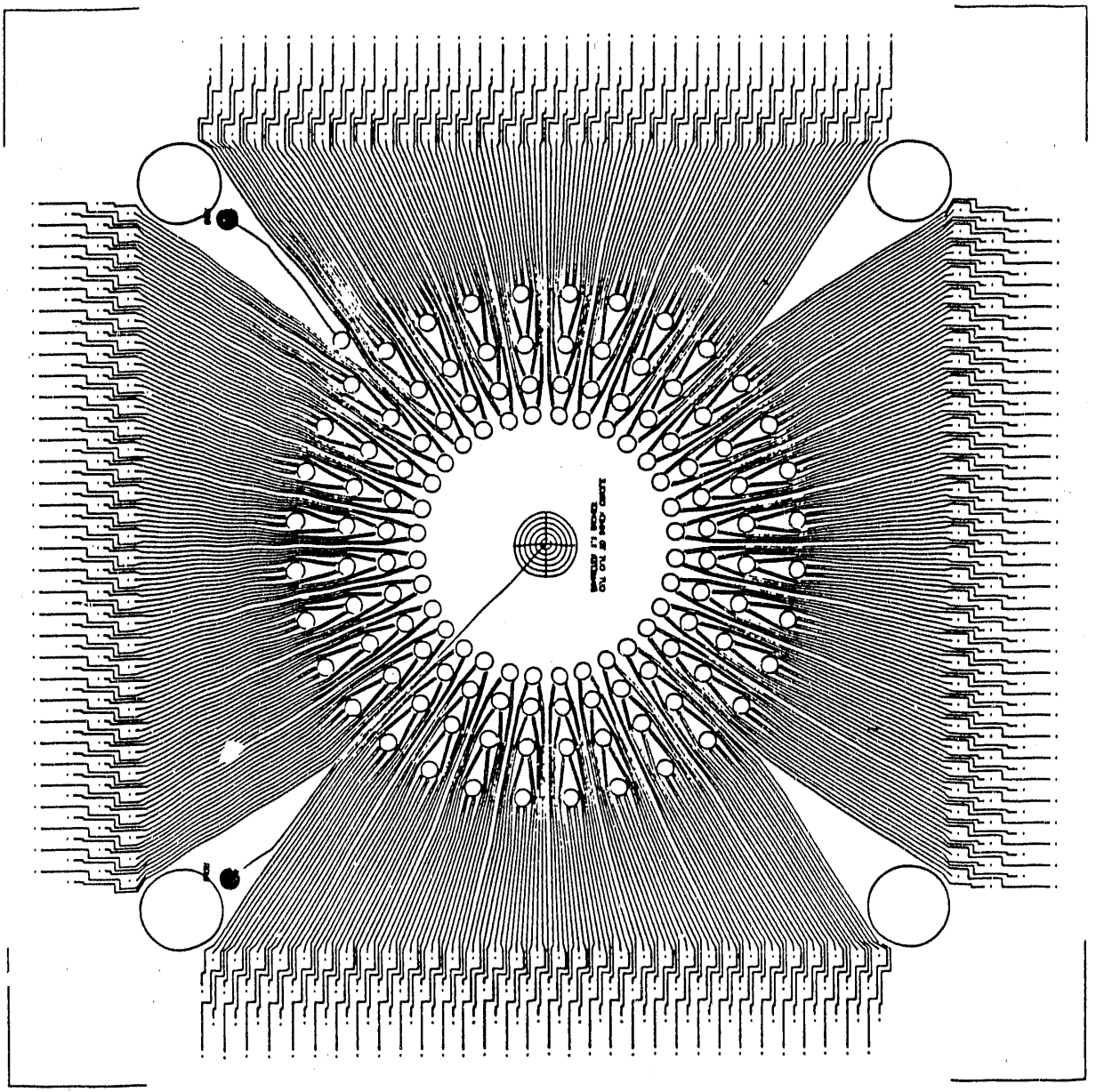

FIG. 5

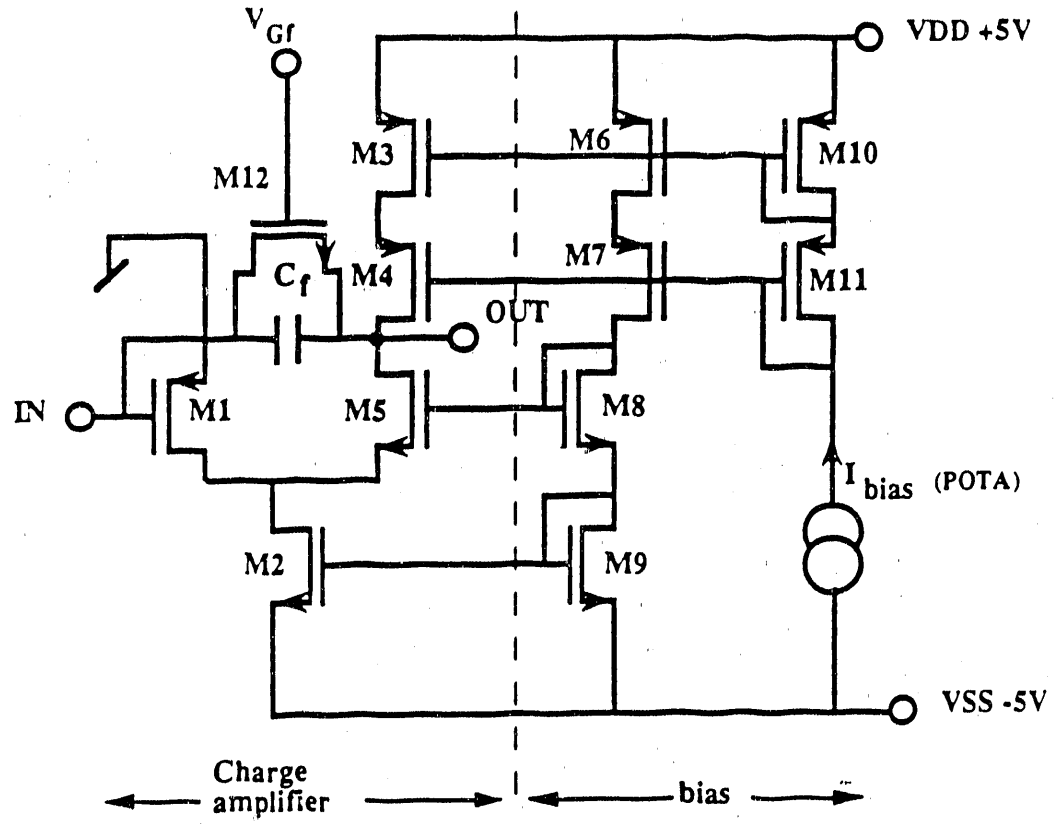
V_{Gf}
VDD +5V
M12
M3
M6
M10
C_f
M4
M7
M11
OUT
IN
M1
M5
M8
I_{bias} (POTA)
M2
M9
VSS -5V
Charge amplifier
bias

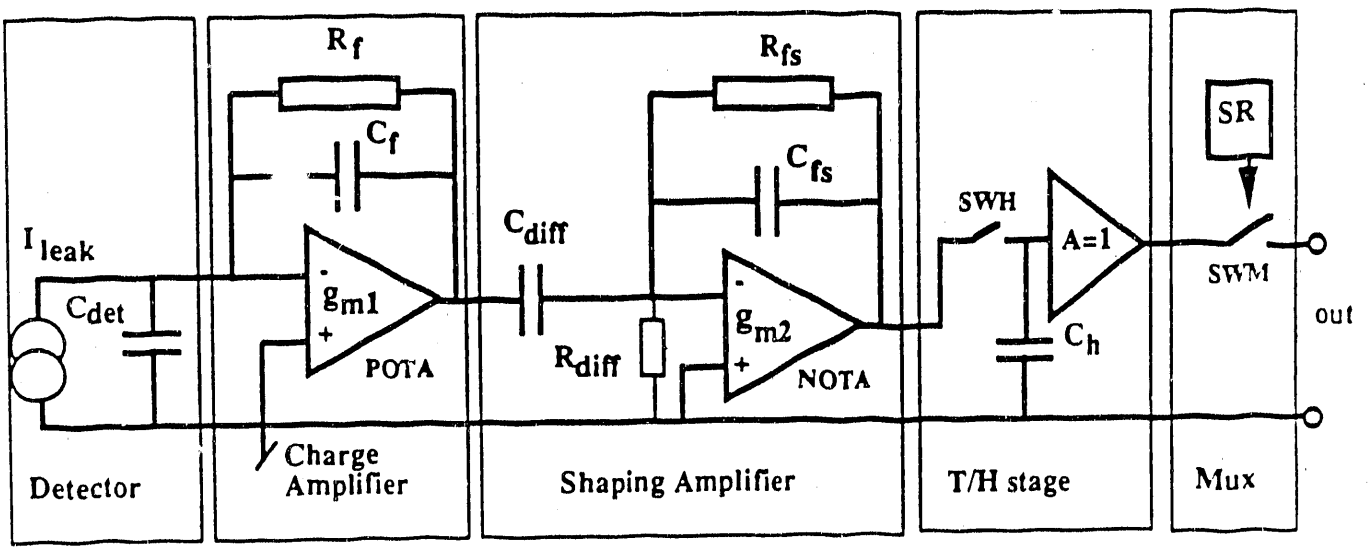
R_f
R_{fs}
SR
C_f
C_{fs}
SWH
I_{leak}
C_{diff}
A=1
SWM
C_{det}
g_{m1}
g_{m2}
out
C_h
POTA
R_{diff}
NOTA
Charge Amplifier
Detector
Shaping Amplifier
T/H stage
Mux

FIG. 6

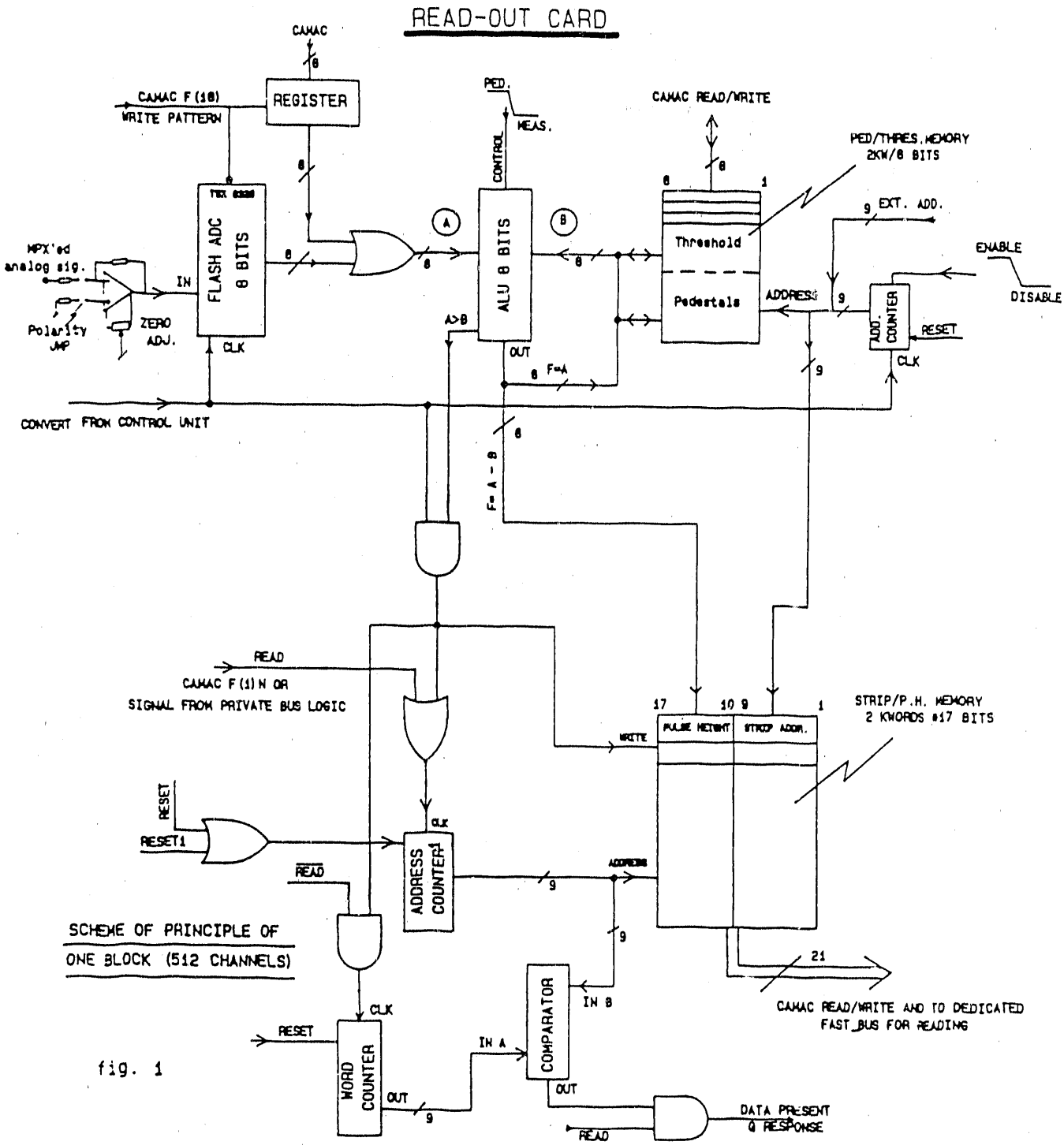
READ-OUT CARD
CAMAC
REGISTER
CAMAC F(16)
WRITE PATTERN
PED.
MEAS.
CONTROL
CAMAC READ/WRITE
PED/THRES. MEMORY
2KW/8 BITS
EXT. ADD.
ENABLE
DISABLE
MPX'ed
analog sig.
IN
Polarity
JMP
ZERO
ADJ.
FLASH ADC
8 BITS
CLK
A
B
ALU 8 BITS
A>B
OUT
F=A
Threshold
Pedestals
ADDRESS
ADD. COUNTER
RESET
CLK
CONVERT FROM CONTROL UNIT
F=A-B
READ
CAMAC F(1) N OR
SIGNAL FROM PRIVATE BUS LOGIC
STRIP/P.H. MEMORY
2 KWORDS x17 BITS
WRITE
RESET
RESET1
ADDRESS COUNTER
READ
ADDRESS
SCHEME OF PRINCIPLE OF
ONE BLOCK (512 CHANNELS)
COMPARATOR
IN B
IN A
CAMAC READ/WRITE AND TO DEDICATED
FAST_BUS FOR READING
WORD COUNTER
DATA PRESENT
Q RESPONSE

fig. 1

FIG. 7

RD-3
R&D Summary
July 1990

A Pad Readout Detector for CRID/Tracking at RHIC

J. Fischer, D. Lissauer, D. Makowiecki, E. O'Brien, V. Polychronakos,
V.Radeka, S. Rescia, G.C. Smith, D. Stephani,P.Z.Takacs,
C. Woody, and B. Yu
Brookhaven National Lab, Upton, New York, 11973

S. V. Greene, T. Hemmick, J.T. Mitchell, B. Shivakumar
Yale University, New Haven, Connecticut, 06511

Introduction

The Physics goals of most RHIC experiments will require detectors able to do particle identification and tracking in a high multiplicity environment. In the search for a quark-gluon plasma, experiments at RHIC will look for signatures such as stangeness enhancement, J/ψ suppression and shifts in the ρ mass[1,2,3]. The experiments will combine tracking in magnetic fields with time-of-flight arrays, Cherenkov counters and calorimetry. Cherenkov ring-imaging detectors will be a useful addition to the particle ID system of any RHIC experiment because of their abilities to operate in high multiplicity environments and do particle ID over momentum ranges difficult for either TOF or calorimetry.

For small impact parameter Au-Au collisions at RHIC we expect mid-rapidity charged particle multiplicites of $0.02/cm^2$ at 1 m in the momentum range of 0-2 GeV/c [3]. Many QGP signatures will require that the experiments have the ability to separate leptons from hadrons, and pions from kaons and protons over a large momentum range. Research by other groups have shown that it is possible for a carefully designed CRID to do $K/\pi/p$ separation up to 30 GeV/c and e/π separation up to 5 GeV/c [4]. The particle identification power of a CRID will be a valuable inclusion in a RHIC experiment.

A CRID may be employed in combination with other detectors for measurements of K/π ratios, HBT of π's and K's, measurement of the ρ mass and detection of $J/\psi \Rightarrow e^+e^-$ signal. The CRID's design would be optimized for either $K/\pi/p$ separation or electron-hadron separation.

Goals

Our group's intention is to build a Cherenkov ring-imaging detector as a prototype of one which could eventually be used in a RHIC experiment. Our prototype will utilize VLSI electronics which will have future applications with both CRID's and Pad tracking detectors. The prototype will be a $K/\pi/p$ CRID that uses a liquid radiator and is proximity focussed. We hope to accomplish the following through our prototype program:

A) Gain experience using VLSI chips mounted directly on the cathode pad plane. The E814 pad detectors use a preamplifier, shaping amplifier and ADC on each channel. As the number of electronics channels increase for RICH experiments the electronics costs could become enormous. A multiplexed VLSI chip containing the preamplifier and the shaping amplifier could greatly reduce the electronics cost/channel. Such schemes have been used successfully elsewhere [4,5,6]. The initial VLSI chips used on the prototype will be commercially available AMPLEX chips.

B) Continue to develop and improve Pad detector technology for eventual use in vertex detectors or tracking spectrometers at RHIC.

C) Employ segmented cathode pad planes to readout UV detector part of the CRID. The cathode pad planes would be based on the successful designs of the tracking pad detectors used in experiment E814 at BNL [7,8].

D) Build up local expertise in the construction, testing and operation of CRID's in anticipation of their eventual use in RHIC experiments.

E) Design and manufacture VLSI chips specifically for RHIC applications. The chips will have 8-9 bit accuracy and be designed for synchronous machines with 100 nsec crossings. Pad detectors, CRID's and silicon detectors all could employ VLSI chips.

Status

Progress has been made in the design and detailing of the CRID prototype. Testing has begun on the segmented pad cathode used in the UV detector of the CRJD. The VLSI AMPLEX chips have been ordered and the design of their motherboard has started. Software tools needed for the design of the dedicated VSLI chips have been purchased.

Prototype Design

The initial prototype design and engineering is finished and draftsman should complete the detailing on the detector in early July 90. The CRID is designed for K/π/p separation. It is proximity focussing and uses a liquid radiator(Fig. 1). It has a 0.39" thick radiator region filled with C_6F_{14}, a 7.9" thick transmission region containing only helium and a UV detector filled with TMAE+He+quencher gas. The outside shell of the CRID is a roughly cylindrical aluminum structure with a radius of 12" and a thickness of 9.75". The entrance to the CRID is a 10" diameter mylar window followed by the freon radiator and then a 3/8" thick quartz window also 10" in diameter. After the quartz window is a He filled transmission region and then a second quartz window, 17" in diameter by 1/8" thick, which serves as the entrance to the UV detector. The UV detector ends with the cathode pad plane where the VLSI chips will be mounted. Finally there follows the exit window made of .020" mylar. The O-ring seals between the UV detector and both the transmission region and the outside will be made of Kalrez which is resistant to deterioration by TMAE. The structures in the UV detector are made of G-10. The quartz windows are Suprasil-II(or equivalent) fused silica.

We expect the machine shop work and purchase of materials for the prototype construction to commence in July.

The UV Detector

The UV detector is the most challenging part of the CRID to make work properly. The UV detector accepts the Cherenkov photon light, converts the UV photons to photoelectrons and drifts the photoelectrons into a detector region with enough gain to make detection of single photoelectrons possible.

The difficulty in detector operation comes because the UV detector must contain both a photosensitive gas such as TMAE and have high gain, and this combination greatly increases the likelihood of electric breakdown in the detector.

Our UV detector combines a multi-step avalanche chamber[9] similar to one used by A. Breskin et al. [10] in the CRID in NA45 at CERN, with a segmented cathode readout adapted from the successful designs used in E814 at BNL [7,8](Fig. 2). The UV detector starts with a quartz window followed by a 3 cm conversion region where the Cherenkov UV photons are converted to photoelectrons. The electrons drift to the preamplification region which consists of 2 parallel stainless steel meshes separated by 3mm. The gain here is of the order of 10^3.

The electrons then travel through a 3 cm long drift region into the final amplification region. The 3 cm drift region contains a pair of parallel stainless steel meshes that are used to electrically gate the drift region closed when photoelectrons from the preamp region are not passing through. The gating technique has been shown to impede the photon feedback process [11].

The final amplification region contains another stainless steel mesh that acts as one cathode plane, a plane of anode wires, and a segmented cathode pad plane. The two cathode planes and the anode wire plane are parallel to one another with the anode plane located about half way in between the two cathode planes and separated from each by approximately 3mm.

The segmented cathode pad plane is a copper-clad multi-layer printed circuit board with a double chevron design etched into the copper cathode (Fig. 3). Anode wires spaced every 2mm run parallel to the direction of the peaks in the chevron shape. The double chevron shape is 4mm wide and 1 cm peak to peak. The 50cm x 50cm cathode plane of the prototype will contain over 6000 indivdual pads.

Our group has constructed a prototype pad detector that has a double chevron pattern etched on the cathode pad and have studied its properties. Using a collimated X-ray beam we have measured the detector's resolution in the anode direction, the reconstructed position error, and the differential non-linearity(Fig. 4). The resolution along the anode wire was found to be on the order of 100μm RMS which is much better than the 1mm resolution we require in our CRID prototype. We have not yet measured the pad detector resolution in the direction perpendicular to the anode wires but we

believe it will also be better than 1 mm RMS. Our group will continue to study resolutions and linearities of the double chevron shape as well as other cathode pad designs as part of our ongoing pad detector R & D effort.

CRID Performance and Design Specifications

Our CRID prototype, designed as specified above, should have some of the following characteristics:

- Based on TMAE quantum efficiency, transmission of Suprasil quartz windows and C_6F_{14} production of Cherenkov light we expect $\sim$ 20 photoelectrons/ ring for a particle above threshold (Fig. 5)[12].
- The Cherenkov ring radii will saturate at 14 cm for particles above threshold. The K/π separation will be better than 3σ at 3 GeV(Fig. 6).
- Based on temperature vs. absorption length curves for TMAE one expects 95% conversion of transmitted UV photons for a 3 cm conversion region and 35° C TMAE(Fig. 7).
- With the UV detector filled with 95% He + 5% C_2H_6+TMAE one expects a drift time of 50 nsec/mm in the 3 cm conversion region [13]. Operated this way the CRID can tolerate an event rate of 600 kHz. As one raises the temperature of the TMAE above 35° C the event rate increases.

Electronics

Based on the design of our CRID prototype we would expect a full scale RHIC CRID to have a pad density of 25,000 channels/m^2. Bringing such a large number of printed traces outside the active area is not a desired solution. The high stray capacitances associated with these traces would degrade the pad detector resolution which is proportional to the total input capacitance. A monolithic chip mount directly on the cathode plane would greatly reduce the stray capacitance problem. If the chip additionally was used to read out many channels through a multiplexing scheme we could also ease the problem of many cables coming into the detector.

Initial work by our group foresees a 16 or 32 channel front end circuit that mounts on the back of the cathode pad plane and contains the charge sensitive preamplifier, the shaping amplifier and the first level analog storage (Fig. 8). Any additional multiplexing would require excessive power dissipation in a region where cooling is difficult. Pedestals could be supressed and events could be selected by the first level trigger at the first analog storage. The sparsified data would then be driven to the next stage of electronics located on the periphery of the detector. Analog storage for the second level trigger as well as the driver that would send the data to the ADC's could be located in this stage of electronics.

Placing the front-end electronics on the cathode plane will virtually eliminate all stray capacitances at the input. The system performance will improve and can fully exploit the small detector capacitance($<$ 2pf/ 10 cathode pads) despite the poorer noise performance of MOS integrated devices. We expect pad detector spatial resolution of $\sigma \approx 100\mu$m will be possible with VLSI electronics.

We have purchased some commercially available AMPLEX chips to incorporate into our early CRID testing. The design of the motherboard to hold these chips has begun(Fig. 9). Our eventual goal is to a VLSI specifically for a RHIC detector with a dynamic range of 8-9 bits and the ability to operate with a synchronous machine at approximately 10 MHz.

Our effort to develop VLSI chips for RHIC detectors will have considerable overlap with the SSC VLSI R & D project also being worked on by members of our group. Much of the design and development equipment purchased for one project will be able to be used for the other. Some of our funds have already gone for computer workstations, CAD software for circuit simulation and physical layout, and IC testing equipment.

Schedule

1990/91:

- Construction of CRID prototype with a Pad chamber readout using existing multiplexed VLSI chip.
- Continue research on Pad detectors

- Continue design and development of VLSI chips for CRID and Pad tracking detectors

- Test CRID at the AGS. With existing VLSI chips.

1991/92:

- Testing of CRID prototype with more advanced VLSI chip(one with an analog buffer).

- Continue VLSI design and development program.

References

[1] Experiments for Relativistic Heavy Ion Collider, P.E.Haustein and C.L.Woody (editors), BNL 51921 (1985).

[2] Proceeding of the Second Workshop on Experiments for Relativistic Heavy Ion collider H.G.Ritter and A.Shor (ed), LBL 24604 (1988).

[3] Proceedings of the Third workshop on Experiments and Detectors for a Relativistic heavy Ion Collider. B.Shivakumar and P.Vincent (ed), BNL 52185 (1988).

[4] D.W.G.S. Leith,*Nucl. Instr. and Meth.* A 265(1988)120.

[5] S.K. Dhawan et al.,*IEEE Trans. Nucl. Sci.*, vol 35 (1988).

[6] V. Ashford et al.,*IEEE Trans. Nucl. Sci.*, vol 34(1987).

[7] J.Fischer et al.,*IEEE Trans. Nucl. Sci.*, vol 37(1990)82

[8] R. Debbe et al.,*IEEE Trans. Nucl. Sci.*, vol 37(1990)88

[9] G. Charpak et al., CERN 78-05(1978)

[10] A. Breshkin et al.,*IEEE Trans. Nucl. Sci.*, vol 35(1988)404.

[11] A. Breshkin et al.,*Nucl. Instr. and Meth.* 178(1980)11.

[12] R.A. Holroyd, J.M. Presses, C.L. Woody, *Nucl. Instr. and Meth.* A 261(1987)440.

[13] A. Peisert and F. Sauli, CERN 84-08(1984)

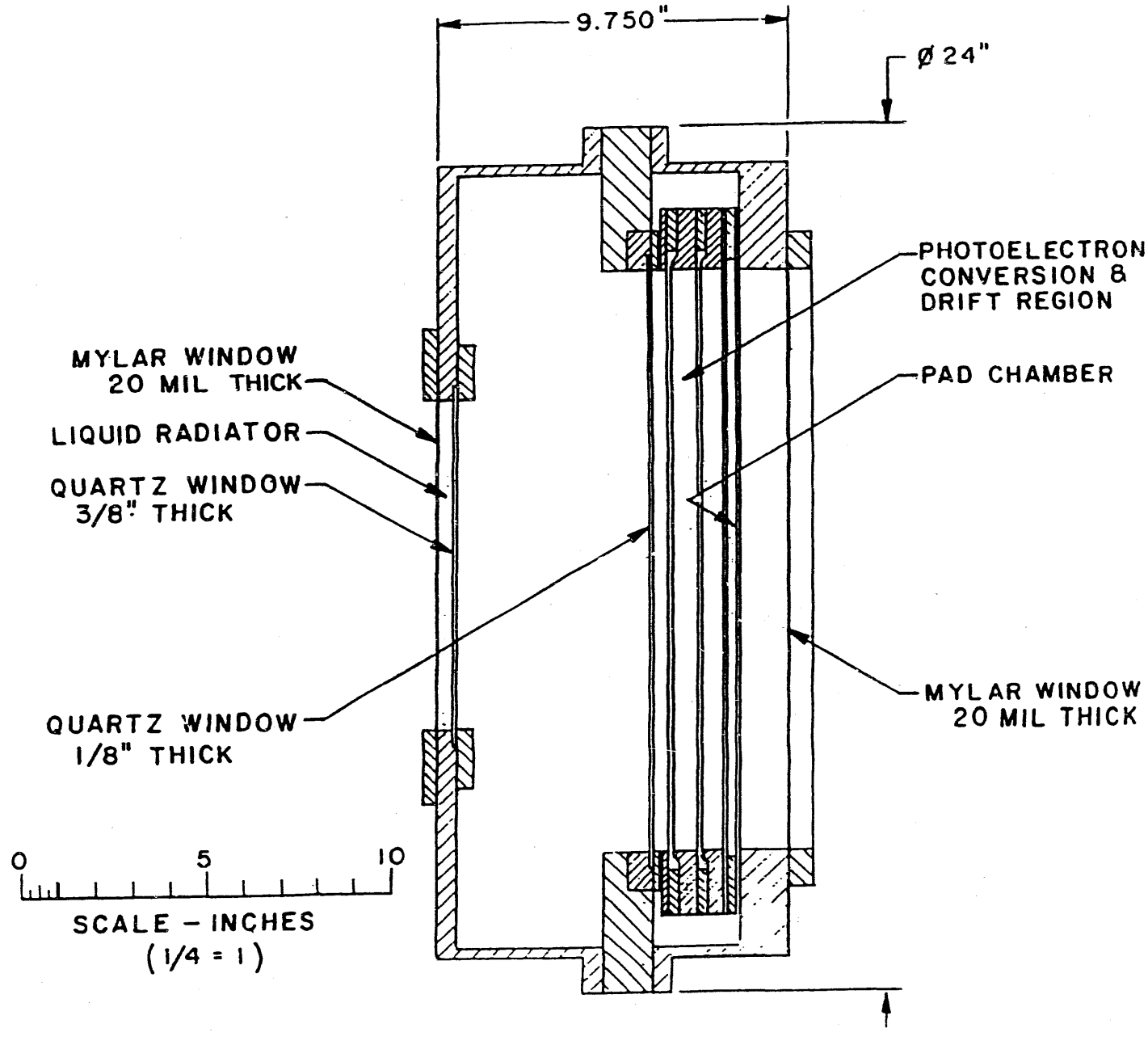

Figure 1: Schematic of the prototype Cherenkov Ring-Imaging Detector

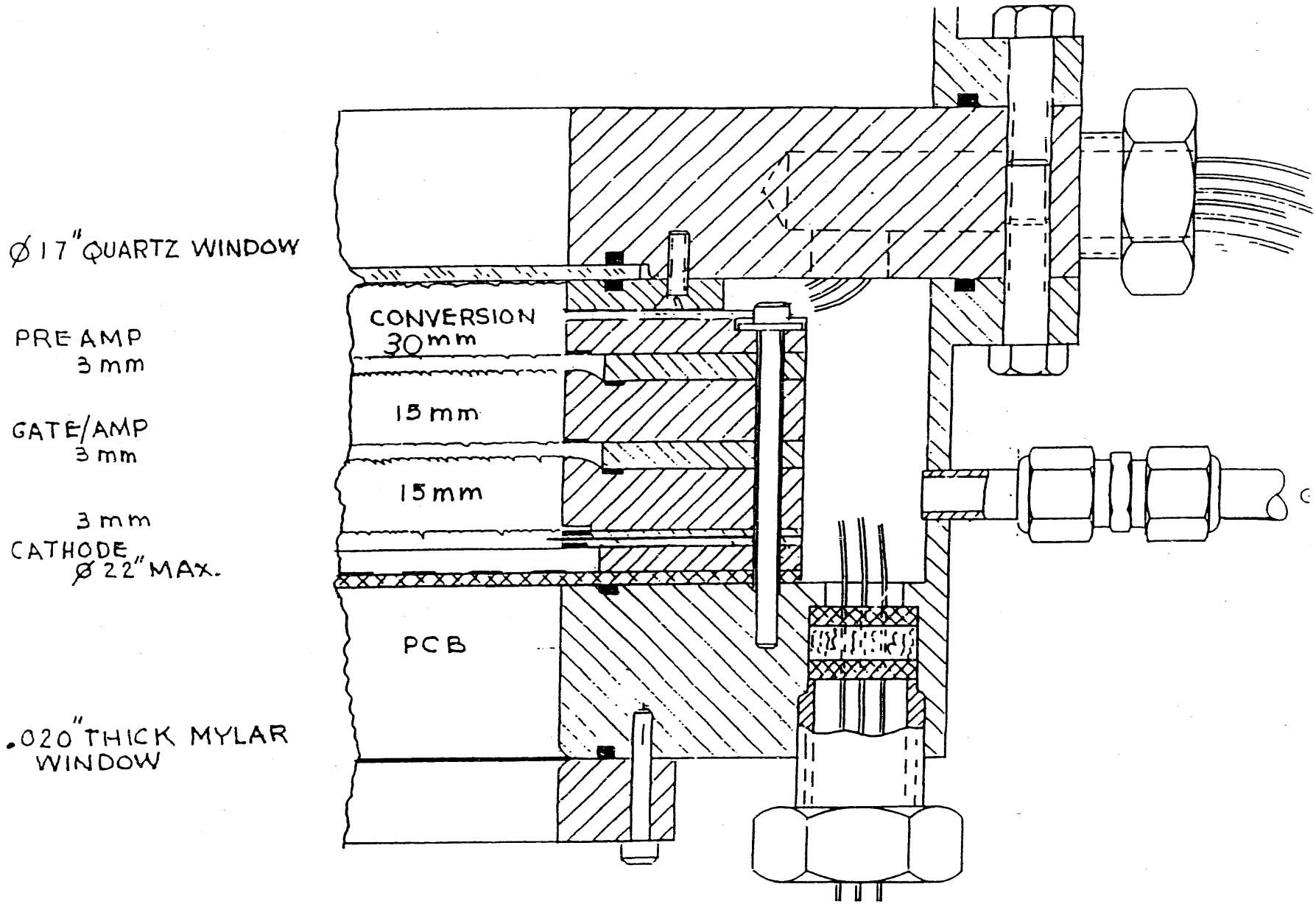

Figure 2: Schematic of the UV detector located in the prototype CRID

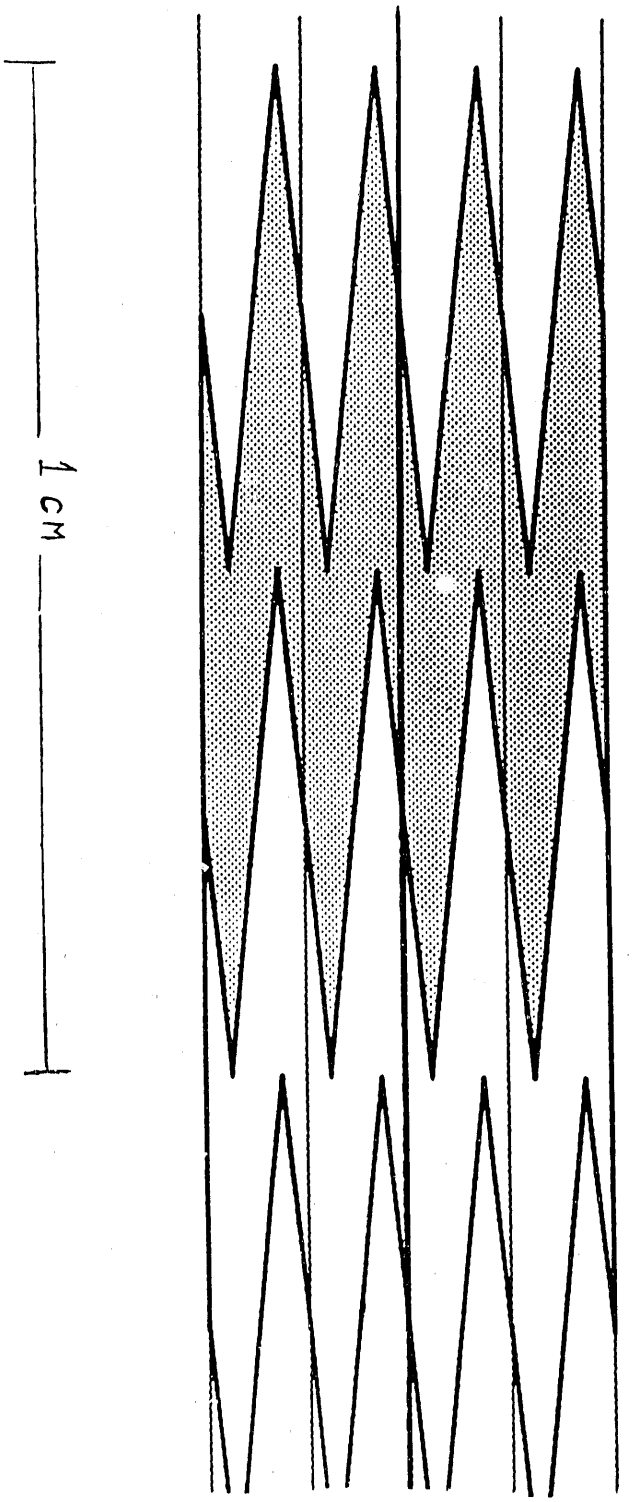

Figure 3: Double chevron pattern as seen on CRID cathode pad plane. The pads are copper and are etched into the surface of a G-10 P.C. board. The dark lines denote the separation between the copper pads. The thin horizontal lines are the anode wires located above the cathode plane.

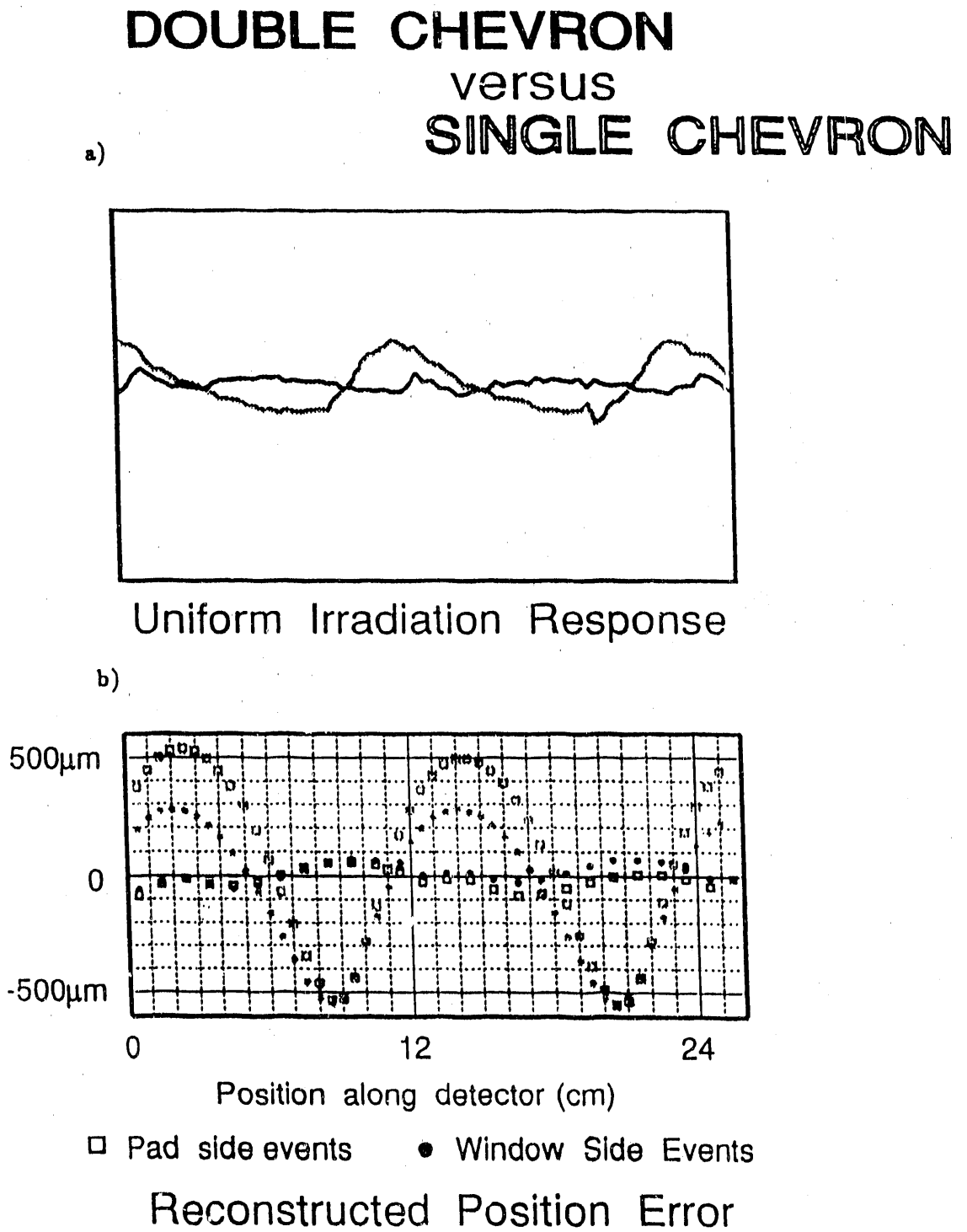

Figure 4: a)The differential non-linearity of the 12mm double chevron(light line) decreases to 10%, as against the 34% value from a 12mm single chevron cathode(dark line).b) The reconst. pos. error of the single cathode exceeds $\pm 500\mu m$. For the double chevron cathode, the position error is less than $\pm 100\mu m$.

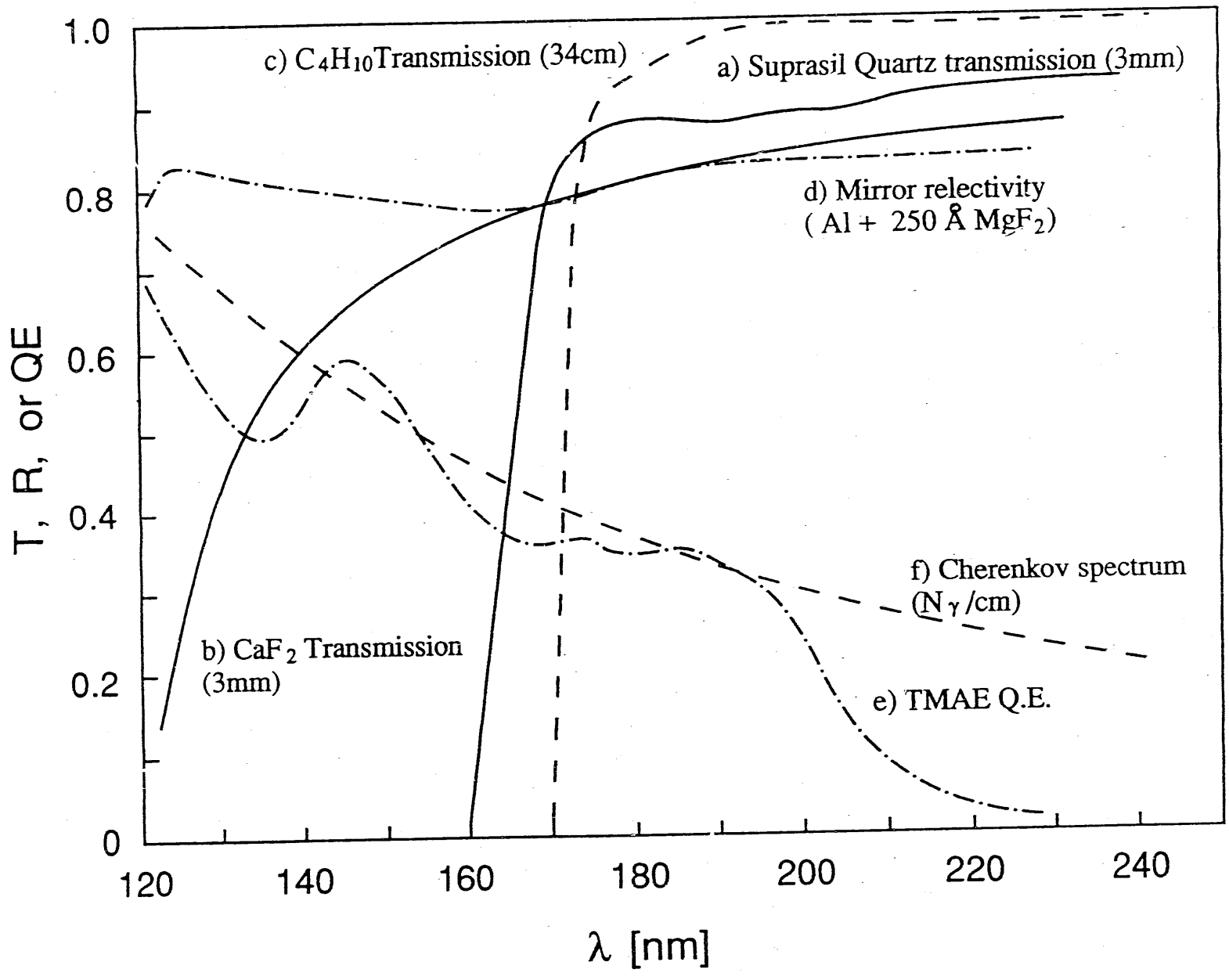

Figure 5: Transmissions, reflectivity and quantum efficiency of various possible components of a Cherenkov Ring-Imaging Detector.

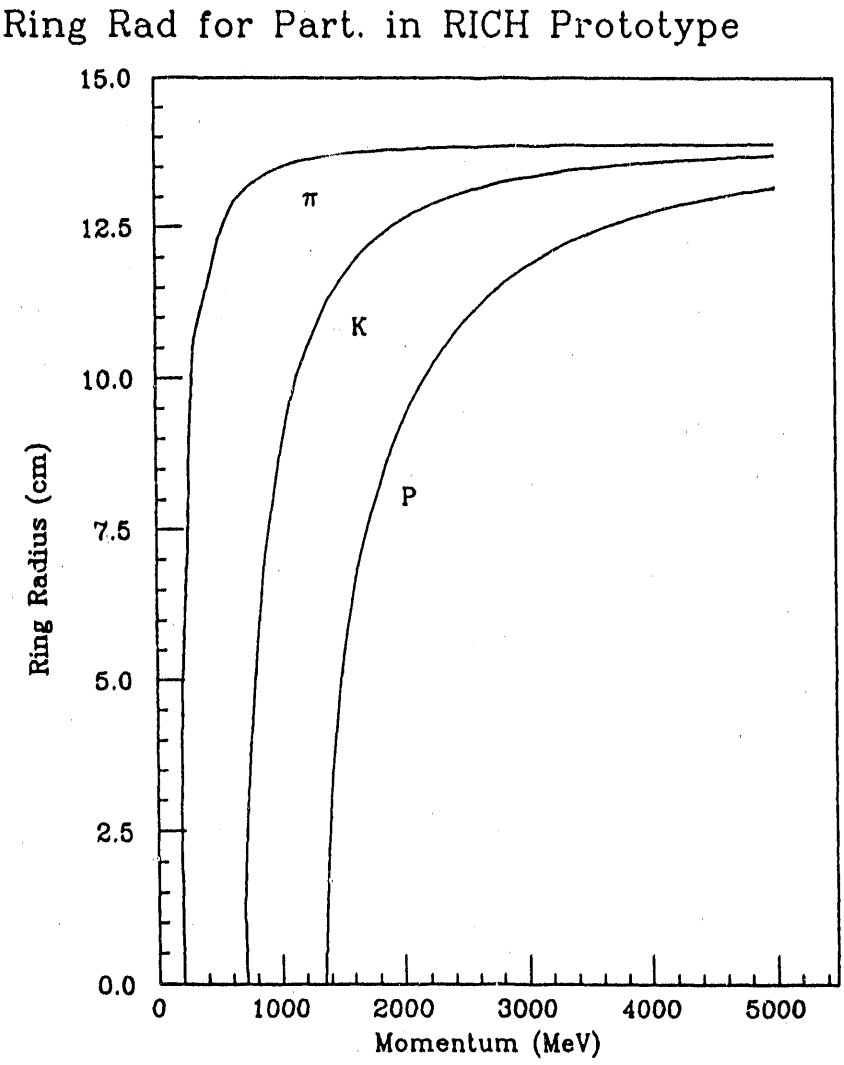

Figure 6: Ring radius vs. particle momentum curve for our prototype CRID

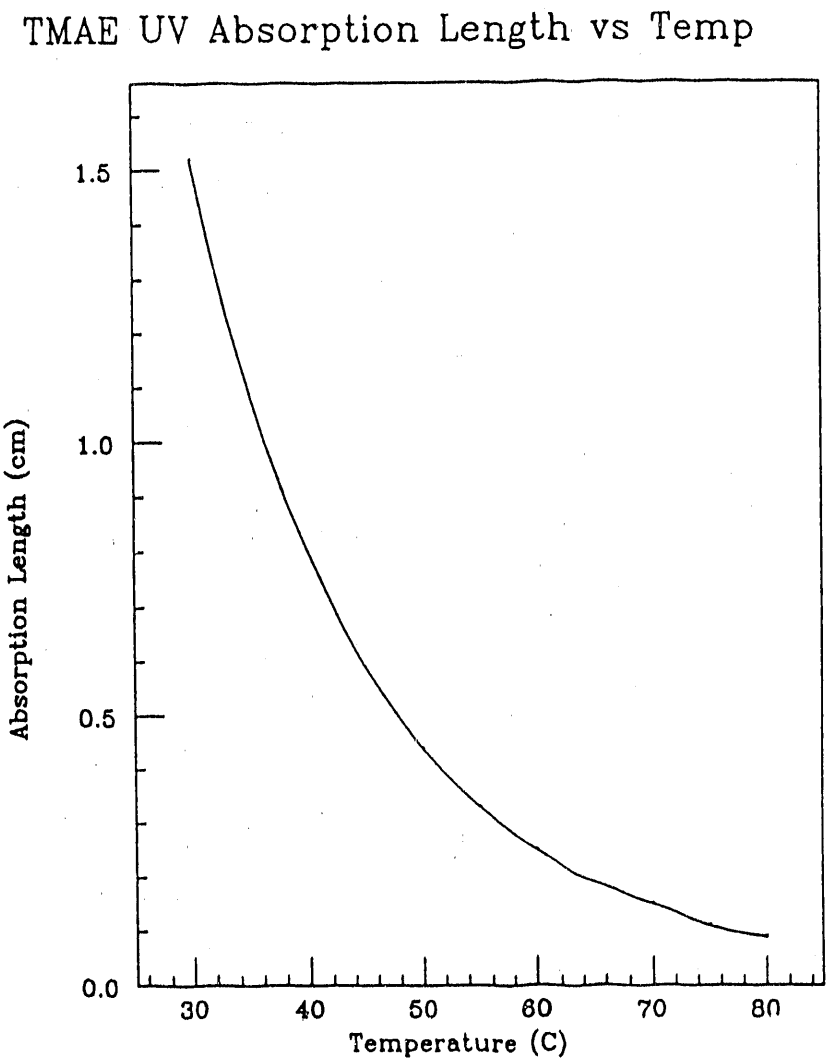

Figure 7: TMAE UV absoprtion length vs. temperature. We expect the prototype to initially run between 35 and 40° C.

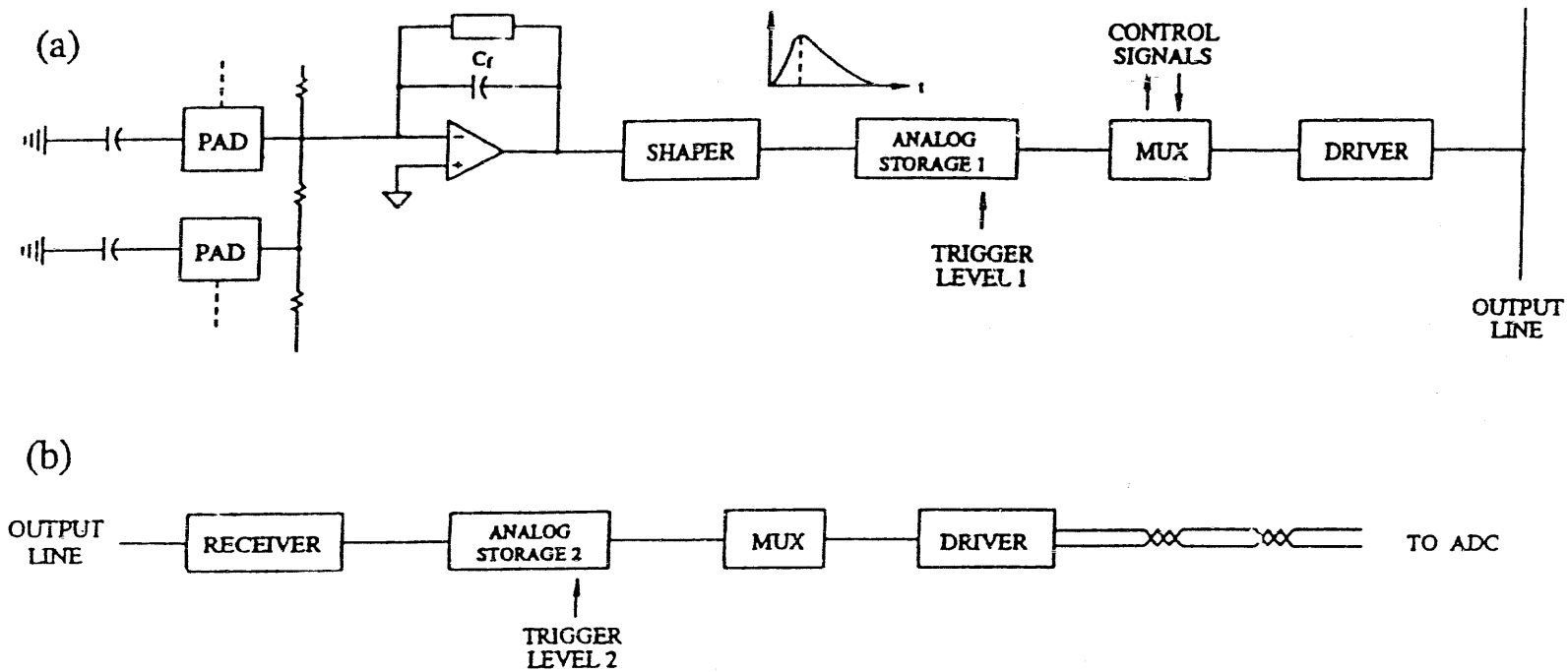

Figure 8: Block diagram of the signal processing chain for the readout of gas chamber with interpolaring pad. A) Electronics to be located on the back of the cathode plane. It will consist of a 16 or 32 channels integrated circuits. B) Electronics to be located on the periphey of the detector.

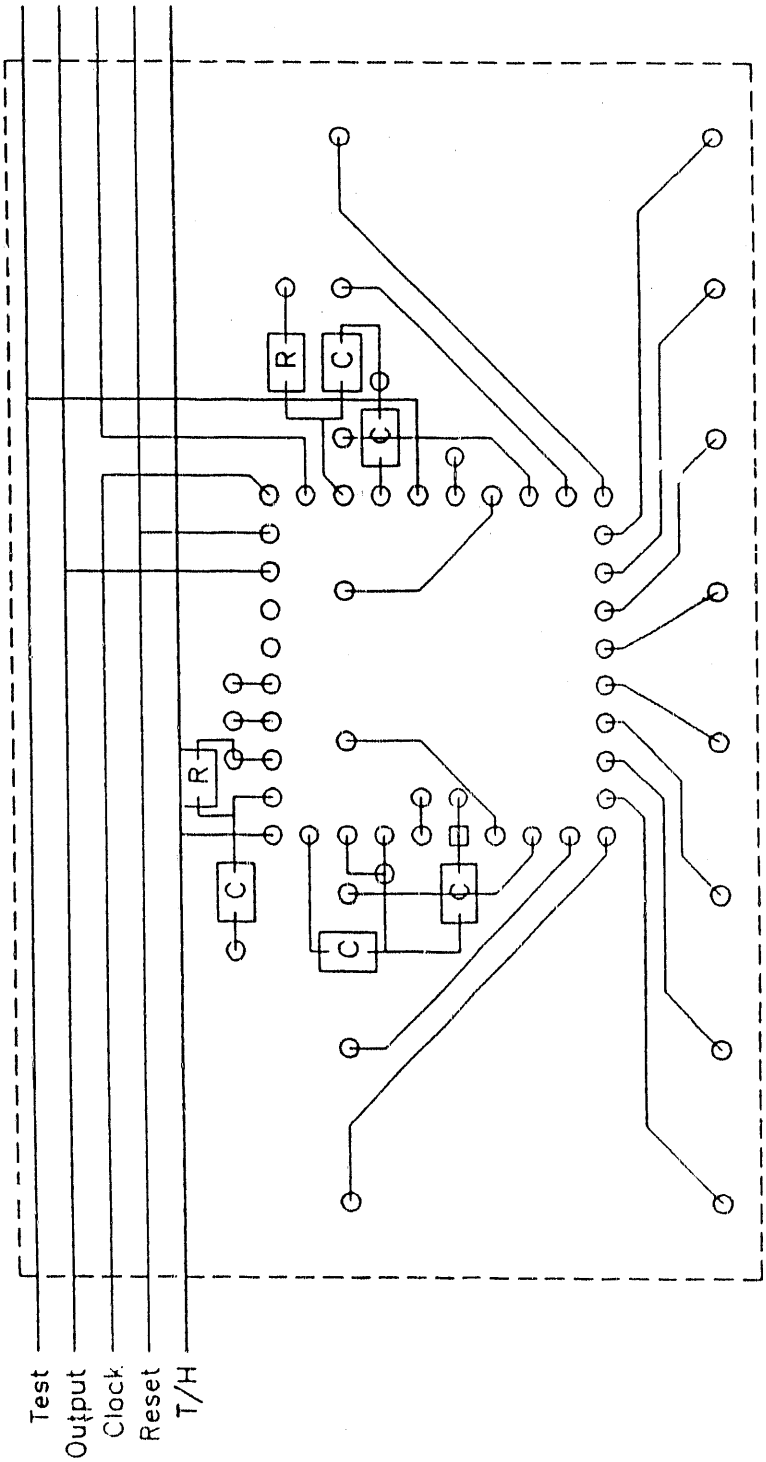

Figure 9: Schematic of AMPLEX chip motherboard to be located on back layer of the segmented cathode pad plane.

RHIC TPC R & D Progress and Goals

G. Danby, S. Eiseman, A. Etkin, K.J. Foley,
R.W. Hackenburg, R.S. Longacre, W.A. Love, T.W. Morris,
E.D. Platner, A.C. Saulys and J.H. Van Dijk

Brookhaven National Laboratory

S.J. Lindenbaum

Brookhaven National Laboratory and City College of New York

C.S. Chan, M.A. Kramer and K. Zhao

City College of New York

D. Nygren and S. Kleinfelder

Lawrence Berkley Laboratory

D.L. Adams, S. Ahmad, B.E. Bonner, J.A. Buchanan, C.N. Chiou,
J.M. Clement, M.D. Corcoran, T. Empl, H.E. Miettinen,
G.S. Mutchler, J.B. Roberts and J. Skeens

Rice University

We have identified eight areas of progress and goals, they are:

1. We have found and tried a method of interconnect that will allow a piggy-back assembly of the several stages of front end electronics described in our proposal This method also provides interconnect to the TPC pads. Our goal is to produce multi-layer printed circuits suitable for mounting the custom IC's for this front end electronics.

2. We have produced the first cathode pad end cap assembly for a test TPC. The goal is to assemble and evaluate the TPC.

3. A gas system has been designed and components ordered. The completion of this gas system will allow a systematic study of gases suitable for a RHIC TPC.

4. We are developing a 3 dimensional electrostatic field simulation software program. We have purchased a 386SX and MATHCAD software to aid in this developement. The execution of this software will require a large dedicated disk connected to the ACP computer farm. The disk has been ordered and we expect soon to start running this simulation program. It is important for us to design the appropriate field shaping structures near the beam pipe.

5. A laser system is under study. This laser-multiplier will allow a critical measurement of field distortions in the TPC.

6. We have been in communication with Dave Dorfan at UC Santa Cruz who is developing a 64 channel amplifier IC suitable for our requirements. The first samples should become available to us in mid July. It is our intention to test these circuits and if necessary, provide input for modification to Dave. The goal is to produce an amplifier-shaper system according to the objectives given in our proposal.

7. Our collaborators in both this R & D project and the forthcoming RHIC experiment proposal, Kleinfelder and Nygren from LBL, have developed a 16 channel 256 sample analog memory IC that will be used on the HISS TPC. It is our intention to modify this device to become a segmented analog memory to satisfy the requirements stated in our proposal.

8. We have designed an IC test facility to evaluate the custom IC's mentioned in items 6 and 7. We are awaiting funding to acquire the necessary equipment. Attached is a partial indication of the set of parametric measurements we intend to do with this system.

Typical Test Requirements for an Analog Memory for a TPC

1. Transfer gain and linearity
2. Offset and stability
3. Rise and fall response times
4. Memory decay time
5. Noise
6. Dynamic range
7. Cross talk
8. Clock to data acquisition timing
9. Sensitivity to supply voltages
10. Sensitivity to temperature

RD-8
R&D Summary
July 1990

RHIC DETECTOR ELECTRONICS R&D PROPOSAL (#RD-8)

DEVELOPMENT OF ANALOG MEMORIES FOR RHIC DETECTOR FRONT-END ELECTRONIC SYSTEMS

PROGRAM SUMMARY
INCLUDING
IMPORTANT GOALS AND CURRENT STATUS

Submitted by Anastasios Konstantinidis
Robert Ledoux, Stephen Steadman,
George Stephans, and Bernard Wadsworth

Laboratory for Nuclear Science

Massachusetts Institute of Technology

22 June 1990

1. INTRODUCTION

Detectors for colliding beam experiments at RHIC will provide 4pi coverage and are expected to contain from 10**5 to 10**6 channels. As the 2 to 5usec required to generate first-level triggers is long compared with RHIC's 114nsec beam crossing interval, there will be a need not only to deal with signals from a great number of channels but also to store and tag these signals over many beam crossings.

We are concentrating our efforts on developing the switched-capacitor (SC) analog memory as the generic mechanism for storing detector signals. Switched-capacitor circuits can be implemented using metal-oxide-semiconductor (MOS) technology; and, for development work, we have relatively easy access to a number of foundries running different MOS processes the choice of which would depend on the exact nature of our application.

Since the late 1970's, MOS SC technology has been dominated by filter applications which in turn have been driven by the telecommunications industry. Only in the last six years or so has there been any interest in applying this technology to storing analog samples, and that mainly for scientific data acquisition. In fact, the development of SC memories has drawn heavily on the large body of literature and engineering practice generated for SC filter applications.

In terms of memory applications, several MOS-based designs have been reported in the literature. Of these, we note three examples:
. A development effort by H.H.Williams and collaborators at the University of Pennsylvania, AT&T Bell Laboratories, and the Catholic University of Leuven, Belgium [1]. This work is directed towards readout systems at fast colliders like SSC and LHC.
. A pipeline SC store developed for calorimetry at Zeus by W.Buttler and collaborators at DESY, Hamburg, and the Fraunhofer Institut IMS, Duisburg, Germany [2].
. The work of Stuart Kleinfelder and collaborators at the Lawrence Berkeley Laboratory on transient digitizers [3].

The second and third examples are more relevant to the development efforts for RHIC detector electronics: the beam crossing time at Zeus is comparable with that at RHIC: 96nsec vs 114nsec; therefore, the tradeoff between speed and precision in the Zeus electronics would be appropriate for the RHIC situation. Indeed, very impressive results have been reported by Buttler et al.: a 13-bit dynamic range has been achieved over a linear range of 4V, at a sampling rate of 10.4Msps. Also, Kleinfelder et al. have achieved the same 13-bit dynamic range in their transient digitizer when s mpling at 10Msps.

MOS technology is generally considered to have advantages over charge-coupled devices in terms of lower power dissipation, lower noise, better linearity, better radiation hardness, and lower cost: all desirable characteristics for a device to be used in a particle detector. However, we have recently learned of new developments in CCD technology at MIT's Lincoln Laboratory, and we find that the advantage of MOS technology over CCD technology, at least in terms of the parameters mentioned above, may not be as marked as once thought. Since CCD's have some interesting features which make them

potentially useful for pipeline trigger applications, if not for the more general storage applications we are considering here, we intend to keep in close contact with this work.

2. GOALS:

Our development work is aimed at providing analog memories specifically tailored for calorimetry and particle identification applications at RHIC. This work will be concentrated in two areas:
. Microarchitecture -- here we are experimenting at the circuit level with different configurations of the switched capacitor array. We expect to achieve at least the 13-bit dynamic range reached by others as mentioned earlier, and we hope to further improve on this. For example, if we improve the dynamic range by another factor of 4, we would be close to the 15-bit dynamic range considered desirable for calorimetry[4]. With such a dynamic range, we could avoid the traditional dual-range solution and reduce the electronics up front by almost a factor of 2. We expect to reduce the systematic sample-to-sample gain and offset variations so that the calibration load is reduced for the more demanding calorimetry applications and perhaps even eliminated for applications like pad chambers and scintillation counters. In this development, we shall be taking full advantage of RHIC's 114ns beam crossing interval in making the inevitable trade-off between speed and accuracy.

. Macroarchitecture -- in this area, we expect to configure analog memory architectures specifically for the physics and particular detector needs at RHIC. While we have given this aspect of our work only preliminary consideration, further work in this area will be undertaken once we have the problems at the circuit level more in hand and the physics and specific detector needs are known in more detail.

By 'macroarchitecture', we mean the manner in which the first- and second-level memories are each configured; the way they interact; the degree of multiplexing involved; and so on. For example, for the pipeline storage required at RHIC, there are two approaches to operating the first-level storage. The first is represented by the 'peristaltic' pipeline ([2], for example) in which the writing process is momentarily stopped if the first-level trigger requires that data be read out to the second-level storage. The second is the 'steady-state' pipeline in which samples can be read (transferred to second-level storage) without having to stop the writing process. Which of these two approaches is used depends on a number of factors including the expected interesting event rate. While the steady-state pipeline requires a more complex bus structure and puts more demands on the bandwidth of the read circuitry, the approach in our opinion has advantages which merit consideration: To obtain the ultimate performance from a switched-capacitor memory requires calibration on a cell-by-cell basis; this in turn requires that each sample which is read to second-level storage be tagged not only with a beam crossing number, but also with a capacitor/cell number. In a peristaltic pipeline, the cell tag (5 bits or more)must be carried through the second-level storage to the point where the calibration can be performed; in addition, the beam tag in this case must be generated and stored commencing with the first-level memory. In a steady-state pipeline, the beam crossing tag can double as the cell tag, and this one piece of information is generated as the associated sample is passed from first- to second-level storage. Also, since there is a fixed delay through the steady-state pipeline, some of the systematic errors introduced in the pipeline are more amenable to calibration.

3. CURRENT STATUS:

. Personnel: We currently have approximately 1.8 person-year equivalents(pye) assigned to this development project. Starting 16 April 90, a full-time design engineer (Konstantinidis) has been working on the layout of the first designs we plan to send to the foundry by 25 July. Two others, Wadsworth and Ross, are spending 25% of their time on circuit design issues and preparing test fixtures. An MIT UROP* student has been hired for the summer to work on the evaluation of two analog circuit simulators, Spice and CAzM.

. Workstations and CAD tools: For IC layout and simulation, we are presently using a VAXstation II/GPX system with two 19-inch color monitors, 16MB memory and 230MB disk to run public domain tools supported by the Massachusetts Microelectronics Center (M2C). The tools include Magic and OCT for schematic capture and layout, and Spice and CAzM for analog circuit simulation. For logic simulation, fault grading and test vector generation, we have been licensed by GenRad to run HILO, a simulator widely used by industry. For printed-circuit board (pcb) design for test fixtures, etc., we are using PCAD Master Designer on a PC(386/25MHz). An hp7595A 8-pen plotter provides color plots of pcb designs and small IC layouts. Larger IC layouts can be produced on a Versatec CE3224 color electrostatic plotter at M2C by transferring files over the network between MIT and the Center. For IC testing, we have a Tektronix LV511 which can be used to evaluate digital IC's in essentially any package style with up to 68 pins.

. IC Fabrication: For foundry services, we have a number of options: At MIT, the Microsystems Technology Laboratory has recently brought on line a 2um BiCMOS baseline process.

At the Massachusetts Microelectronics Center, we have access to a 2um CMOS, n-well, single poly, double metal process suitable for digital logic. The chip size is approx. 4.6mm x 4.6mm; and, for the present, the standard package is a 40-pin DIP. The turnaround time is about 6 weeks.

We have recently signed an agreement with MOSIS -- MOS Implementation System -- a foundry brokering service funded by DARPA and operated by the Information Sciences Institute at the University of Southern California. MOSIS provides access to several different processes from various commercial foundries. The process of particular interest for our initial work is a 2um CMOS, n-well, double poly, double metal process optimized for low-noise analog designs. Four different chip sizes, ranging from 2.22mm x 2.25mm(the so-called 'Tiny Chip') up to 7.9mm x 9.2mm, are available. Turnaround time is 8 to 10 weeks.

. FY'90 Goals and Time-Table: In the time remaining in FY'90, we expect to initiate two foundry runs through MOSIS, one scheduled for 25July90 and the other scheduled for 19Sept90.

For a number of reasons, we have decided to make use of the Tiny Chip option offered by MOSIS. For 550$/design, we get 4 chips of a given design, each in a standard 40-pin DIP package. The packages are delivered with the lids taped in position so the lid can easily be removed to allow internal probing of the chip. Since this is the first time we are using foundry services, we regard this as a very economical way

for us to get started: to become familiar with the protocols involved

* UROP -- Undergraduate Research Opportunities Program.

in the design-fabrication-test cycle; to evaluate some test structures on the chip so that we can characterize some of the process parameters for our own benefit; and to test some individual circuits such as pad buffers and operational amplifiers which will be useful in later chip designs.

Using this Tiny Chip approach, we plan to submit two designs for each foundry run. In July, Chip 1 will carry test structures for characterizing the process; Chip 2 will carry two operational amplifiers including an output pad driver. In September, Chips 3 and 4 will carry examples of various switched-capacitor cell configurations, eight cells of a given type per bus. Unfortunately, because of the 8-week turnaround, we will not be able to feed any information learned in the first run into the design submitted for the second run; experience gained can only be folded in at 4-month intervals. Given the present size of the project team, the length of this 'experience cycle' is not considered to be a major problem.

During the summer, we plan to make a critical evaluation of our two circuit simulators, Spice and CAzM. Spice is said to have a number of problems; the most serious of these for our work is the problem of non-conservation of charge. CAzM is advertized as solving this problem; in addition, it is said to be less susceptible to convergence problems and to execute somewhat faster than Spice. We will be testing both packages and expect to gain some level of confidence and facility in the use of CAzM so that we can explore various options in our designs before they are submitted for fabrication.

In parallel with the above work, we are preparing the test fixturing which will be required by the time the chips from the first run are delivered to MIT in late September.

4. PLANS FOR FY'91:

In FY'91, we will continue with the MOSIS Tiny Chip approach by submitting designs at 2-month intervals for fabrication. Using these particular chips, we will characterize the performance of various bus structures and circuit designs intended to minimize the effect of parasitic capacitances. By June 1991, we will start the design of a larger chip (MOSIS 4.6mm x 6.8mm) which will carry a fullscale single channel memory with the appropriate control and tagging logic.

We expect to spend considerable effort in FY'91 designing and assembling the test fixtures required for evaluating and proving the performance of analog memories with 15-bit dynamic range -- a non-trivial task in itself! We plan to use our Tektronix LV511 tester as the major component of a test fixture which will include a CAMAC-based analog instrumentation system composed of commercially available modules.

5. ACKNOWLEDGEMENTS:

This work is supported by the US Department of Energy through RHIC Detector R&D funds. We would like to thank the personnel at the Massachusetts Microelectronics Center for their help in setting up

VLSI CAD facilities in the Laboratory for Nuclear Science Electronics Facility at MIT, and for their continuing technical support of the CAD tools. We would also like to thank the Dean of Science at MIT for incremental funding in support of this project.

REFERENCES:

1. Front End and Signal Processing Electronics for Large Detectors, L.Callewaert et al., Trans.Nucl.Sci., Vol 36, No 1, 446-457, Feb 89.

2. Design and Performance of a 10MHz CMOS Analog Pipeline, W.Buttler et al., DESY 88-092, 1988.

3. A 4096 Cell Switched Capacitor Analog Waveform Storage Integrated Circuit, S.A.Kleinfelder, Trans.Nucl.Sci.

4. Summary of the Working Group on Readout Electronics, W.E.Cleland et al., Proceedings of the Third Workshop on Experiments and Detectors for a Relativistic Heavy Ion Collider [RHIC], July 1988, edited by B.Shivakumar and P.Vincent. BNL Document No.52185.

R&D STATUS REPORT

RD-10
CALORIMETER/ABSORBER OPTIMIZATION FOR A RHIC DIMUON EXPERIMENT

June 1990

S. Aronson, M. Fatyga, M. Murtagh
Brookhaven National Laboratory

P. Beery, S. Y. Fung, J. H. Kang
University of California, Riverside

H. C. Britt, C. Sangster, J. H. Thomas
Lawrence Livermore National Laboratory

B. Cole, W. Kehoe, S. G. Steadman, G.S.F. Stephans
Massachusetts Institute of Technology

T. C. Awes, R. L. Ferguson, J. Kreke, F. E. Obenshain,
F. Plasil, S. Saini, M. L. Tincknell, G. R. Young*
Oak Ridge National Laboratory

A. Franz, S. P. Sorensen
University of Tennessee

---

* Spokesman

R&D STATUS REPORT

I. GOALS

This project addresses the question of the feasibility of dimuon measurements at RHIC. The principal areas of effort are:

(a) a determination of the level and characteristics of the background behind the hadron calorimeter/absorber in a dimuon experiment

(b) the development of tracking chambers suitable for use in a dimuon experiment at RHIC

(c) the development of a muon identifier for use behind the tracking section of a dimuon spectrometer.

The results will be of use for designing hadron calorimeter/absorbers and muon identifiers for the various experiments in which they have been proposed for RHIC. The ultimate goal of the present effort is to be able to design a workable, dedicated dimuon spectrometer for RHIC. To date the project has concentrated on item (a) above, measuring the background behind a model hadron absorber.

Muons have the property that they can penetrate a quark-gluon plasma, while hadrons do not. Muons can also penetrate thick detectors, while hadrons cannot. This makes it possible to design detectors of large acceptance concentrating on this promising diagnostic of the quark-gluon plasma with little interference from the numerous hadrons produced during the transition back to a hadron gas. This large acceptance makes a dimuon experiment particularly attractive for studying the predicted suppression of the J/ψ and of higher-mass vector mesons in the quark-gluon plasma.[1]

The possibility of performing dimuon measurements at RHIC has been studied at the three RHIC detector workshops.[2,3,4] The use of massive photons to detect the existence of a quark-gluon plasma and subsequently to deduce its properties has been discussed in Refs. 2 and 3 and in other papers referenced therein. Possible designs of dimuon detectors were also given in Refs. 2 and 3. It is the purpose of the present work to obtain basic information about backgrounds involved in a dimuon experiment. This information will be used in the actual design of such a detector. It is fully expected that this future design will evolve considerably from the schematic designs presented in the earlier studies.

The goal of a RHIC dimuon experiment is to detect dimuons over a reasonably broad range of masses and transverse momenta, p_T, that are in the correct range for detecting and diagnosing a quark-gluon plasma. The relevant kinematical regime is quite different from that studied in $\mu^+ - \mu^-$ experiments at large $p - p$ colliders. The conclusions from recent theoretical considerations are that the greatest interest is centered in the intermediate-mass region ($1 \leq M \leq 5$ GeV) and that a broad p_T acceptance, from $p_T = 0$ up to $p_T = 5$ GeV/c, is essential.[3] Events at the high end of the mass range can be studied easily at low rapidities since the relatively energetic muons can penetrate an absorber thick enough to suppress the "sail-through" background. For small values of transverse mass, M_T, dimuons can only be measured at large rapidities so that the muons will have boosted laboratory momenta and be capable of traversing the absorber. In this case, however, angular resolution is very important. Thus, in this region, an absorber with a small ratio of interaction length to radiation length must be used in order to minimize the effects of

multiple scattering on resolution. Problems associated with angular resolution are most severe in the forward regions. Problems associated with tracking a large number of particles and identifying which are muons are also most severe in the forward regions because of the large background of relatively energetic particles and the sharp rise in $dN_{cp}/d\Omega$ with decreasing angle. One must then optimize among competing requirements of low multiple scattering vs. depth to contain hadron showers.

In contrast, in the central rapidity region the problems associated with dynamic range are most severe because the muons receive only a small boost (low rapidity). In this region, a relatively thin absorber shell will help the dynamic range. The general softness of the spectrum of secondaries produced at midrapidity at RHIC makes it feasible to consider a thin absorber, although detailed information on the spectrum of punch-through products is lacking, particularly for the low incident hadron energies that will be encountered in the central region at RHIC. This absorber must still present several interaction lengths, however, to guard against sail-thru hadrons. This requirement motivates the study of absorbers with low Z, because they cause smaller energy loss per lambda than do high Z absorbers.

There is some information in the literature concerning punch-through probabilities for incident hadrons in the range of 5-150 GeV/c. Most of the data are for pions and protons incident on either steel or tungsten. The measurements are at times restricted to simple counts of the number of exiting charged particles that can fire a wire chamber per incident hadron. In many cases, enough information is provided to allow cuts to be made on position and angle matches between the incident and exiting particles. Most measurements were made for a range of absorber thicknesses, though rarely at less than 5 interaction lengths. This is a significant omission for the design of a RHIC dimuon detector because absorbers of less than 5 interaction lengths thickness must be considered, particularly for $y < 2$. Absorbers of mean Z much less than that of steel must be investigated. In addition, information on shower leakage for incident hadrons of $E < 5$ GeV is sorely needed, since such incident particles far and away dominate the spectrum at RHIC. Information on the momentum spectrum of the exiting particles is usually not available, with the significant exception of a series of measurements by the NA3 group, who also used their spectrometer to provide particle ID. A very helpful review is given by Bodek.[5] The lowest energy data he quotes are from Harris et al.[6] The measurements were performed at SLAC with the 20-GeV spectrometer and were made with pions incident on steel at 4.7, 7.7, 10.7, and 15.8 GeV/c.

The initial setup which we have prepared to investigate the background behind a hadron calorimeter/absorber seeks to answer to following questions:

(a) What are the punch-through probabilities for pions, kaons, and protons with incident momenta in the range of 0.5 to 10 GeV/c striking a specific absorber?

(b) How do these probabilities vary as a function of the absorber composition, e.g., carbon, aluminum, concrete or marble, steel, lead, when interleaved with a second material which is suitable active material for a sampling calorimeter? How do the results vary with absorber thickness?

(c) What fraction of the exiting particles can penetrate a second shield and cause a "muon" trigger? How many of the punch-through particles will be rejected by position and angle cuts appropriate to a muon finding analysis program?

In this first round of measurements, the interest is to determine the number and spatial distribution of the leakage particles, with little or no information on the momenta or particle type. This phase is being studied using the detector equipment which was prepared this past year as described below in Section II. The layout of the setup is shown schematically in Figure 1. In this phase the ratio R = (number of particles exiting absorber) / (number of incident particles) will be investigated as a function of the momentum and type of the incident particles (ranging from 0.5 to 10 GeV/c in the AGS A2 test beam line) and as a function of the thickness and composition of the absorber material. Initial tests are being made with a steel-scintillator sandwich absorber/calorimeter. Further tests will be made varying the inert absorber/scintillator thickness ratio and the type of inert absorber (steel, carbon, aluminum, lead). These studies will indicate whether the Monte Carlo calculations which are being made using GEANT or CALOR provide reliable first-order estimates of the leakage and whether a dimuon measurement is technically feasible at RHIC.

It is expected that much of the apparent punch-through background behind the absorber/calorimeter arises from showers that start "late" in the absorber/calorimeter, i.e., after 2-3 interaction lengths. We will be able to investigate this because each depth layer of the absorber/calorimeter sandwich is read out separately. Thus, the location inside the stack where a shower "begins," defined as the layer in which the observed signal exceeds that expected for a minimum-ionizing particle, can be determined for each incident hadron.

II. SUMMARY OF WORK UNDERTAKEN AND PRESENT STATUS

A. Absorber/Calorimeter

We have installed an absorber/calorimeter in the A2 beam line. It allows us to study the shower development and leakage from various materials as a function of beam energy. An engineering drawing of this device is shown in Figure 2. The absorber/calorimeter is constructed from 120 cm x 120 cm x 1.27 cm steel plates and 1-centimeter-thick sheets of plastic scintillator. There are two different scintillator plate designs:

1. The first design consists of 11 slats, each 120 cm x 10 cm x 1 cm, with photomultiplier readout on each end. The strips are stacked up along their 120-cm sides, forming, in effect, a hodoscope between two sheets of steel. Sixteen such "slat arrays" have been installed, with alternating x- and y-orientation. Two are placed at the downstream end of the absorber/calorimeter to give hit information as the shower secondaries leave the stack.
2. The second type of scintillator plate is 120 cm x 110 cm x 1 cm in size. These sheets will be read out using 4 lightguides on each of two opposing sides. The scintillator and support frames have been procured and machined. Prototypes of the new lightguides have been built and tested with the large sheets, and acceptable light collection was observed. Part of the work for FY91 will consist of procuring and installing the new lightguides, followed by installation of the large sheets into the absorber/calorimeter.

The absorber/calorimeter was assembled such that layers of steel and scintillator alternate. Presently there are four 1.27cm thick steel plates for every scintillator array, for a total thickness of 71.1cm of steel. In the final design, every fourth scintillator position will

be of the "slat array" type, as described above, while the other three will be large sheets. As the large sheets are not complete, all scintillator presently installed is in the form of the slat arrays. Successive slat arrays are rotated by 90 degrees with respect to each other. When the large sheets are ready, the scintillator/steel ratio can be doubled. This will be done after a first program of measurements is completed with the array as it is presently set up. All of the slat arrays have been calibrated in beam before being installed.

The total length of the assembly is variable, to a maximum of three meters. The support frame ensures that the plates and scintillator are kept in tight compression to avoid air gaps. This structure was developed to keep the cost of the readout to a minimum while providing periodic information on the transverse profile of the shower in addition to information on the depth at which the shower starts. Even with this arrangement, the structure requires 352 photomultipliers and ADC channels just for the slat arrays. This will increase to 592 channels when all large plates are installed. The absorber/calorimeter is presently read out using a LeCroy 2280 ADC system borrowed from CERN experiment WA80. This ADC system must be returned to WA80. We must therefore find a replacement from the HEEP pool or obtain funds to replace it with a new system, which for cost reasons would be a FASTBUS system. The PMTs used have been recuperated from the liquid scintillator tanks of the calorimeter of BNL experiment E734. Each tube will have the gain stabilized with the light from a pulsed laser system. The laser system is quite similar to one which we use in the CERN WA80 experiment. The laser has been delivered from PRA and brought into service. Light fibers will be purchased next year and the laser system installed.

B. Proportional Drift Tube Array

A first set of tracking chambers has been obtained from BNL experiment E734. These are 4 m x 4 m proportional drift tube arrays. We have installed four double planes of these tubes. Each plane has an x and a y layer. A new support structure was designed for these chambers and installed. Commissioning work to bring the planes back into operation has begun. The custom electronics associated with the chambers has been installed and exercised this spring: this includes the chamber cards, plane controllers, and readout scanner electronics. Some work remains in completing the addressing chains so that the plane controllers can address all the chamber cards. A new readout interface is being implemented to form the data into Ethernet packets which will then be sent to the on-line system. Software development for this has begun.

C. Hodoscopes

Four hodoscope arrays (marked T1, T2, M1, and M2 in Figure 1) have been installed and commissioned. The M1, M2 and T1 arrays were constructed using an existing hodoscope array from an earlier experiment done by LLNL at SLAC. This setup included all PMTs, bases, cables, HV supplies and readout electronics. An LED pulsing system is used to monitor these three hodoscopes. The T1 array consists of 15 horizontal slats and 15 vertical slats mounted in a square array just behind the exit face of the absorber/calorimeter. The T2 array is placed just downstream of the PDT arrays. It consists of 24 slats oriented vertically and 2 sets of 15 slats oriented horizontally with their free ends abutting at the

vertical centerline of the rectangular array. The M1 array is similar to T1 but is 12 x 12 slats in size and is placed just downstream of a 20cm slab of steel which has a larger transverse size. The individual slats in T1, T2 and M1 are all similar and are each 120 cm long x 10 cm wide by 1 cm thick and are read out by fast 2" photomultiplier tubes on one end only. The M2 array was built from existing paddles from Riverside. It consists of 9 of these 120 cm long by 15 cm wide by 5 cm thick paddles oriented horizontally. It is mounted just downstream of the A2 beam line dump, which consists of three feet of steel followed by three feet of concrete shielding block. It is read out with two photomultiplier tubes per paddle, one mounted on each end, again using the photomultiplier tubes recuperated from E734. All the four hodoscopes are interfaced to the online data acquisition system using conventional CAMAC ADCs and TDCs.

D. On-line Data Acquisition System

Our present on-line system is a hybrid put together from three separate entities in order to use existing hardware. The T1, T2 and M1 hodoscopes are read out using local PDP-11 microprocessors housed in the two CAMAC crates housing the ADCs and TDCs for these hodoscopes. Control and diagnostics are provided by video display terminals connected to the PDP-11s. The absorber/calorimeter, M2 hodoscope and all beam-hodoscopes and taggers are read out from three CAMAC crates under the control of a CERN VALET–Plus system. This is based on a 68020 microprocessor in a VME crate with VME interface cards for CAMAC and Ethernet. A Macintosh Plus provides local control and disk storage for the 68020. The PDT arrays will be read out using their existing minicomputers interfaced to Ethernet cards.

All these subsystems transmit their data to a microVAX-II via Ethernet. The microVAX-II is responsible for overall synchronization, coordination, run control, logging of data to tape and error messages to disk and console, and transmittal of data to a VAXstation 2000 via Ethernet for histogram filling and display. This system is straightforward in philosophy and has proved adequate for modest data rates. The present bottleneck is the CERN Remote Proceedure Call software used to handle transferring data via Ethernet between the VALET and microVAX-II. This limits us to no more than 10 events per second (14 per spill during SEB running), which is not a severe limitation for runs triggered only on leakage from the calorimeter backface, but will be a troublesome limitation for runs examining all showers starting in the absorber/calorimeter. The Ethernet link alone has proved capable of 6–10 times greater rates. This will be addressed next year by replacing the VALET software with a much better package from CES Systems that reduces basic cycle times and provides a direct hardware link from the VME crate to the microVAX-II.

This (upgraded) system should be adequate for the early measurements planned for FY91 but will present an increasingly serious limitation for the more extensive readout planned for the new detectors. Accordingly, we plan to set up a more ambitious system, based either on the new WA80 arrangement or the OPAL-type system offered by CES. Both these systems are based on multiple microprocessors in VME with direct DMA connections to a host VAX. The VME microprocessors are responsible for unloading CAMAC and FASTBUS crates and for preparing event streams, while the VAX is used for recording to tape, for file storage, and for human interfacing. We have found the offloading of the

histogramming and display tasks to "satellite" graphics workstations to be a workable solution that permits easy expansion as it becomes possible to acquire more and/or improved workstations for this experimental program. We plan to use much of the software already developed for the parent system we decide to emulate. Code will, of course, be required to match the particular configuration of our test setup.

E. Installation and Operation in A2 Test Beam

The absorber/calorimeter, hodoscope arrays, PDTs and ancillary equipment such as the beam hodoscopes, tagging paddles and veto counter were installed in the A2 test beam area at its north end between December 1989 and April 1990. With the exception of the PDTs, the detectors were brought into operation and tested and/or calibrated with the A2 secondary beam. The online system has been exercised, test data written to and re-read from tape, and online histogramming and monitoring programs tried out.

Unfortunately, operation of the setup to take data fell victim to the AGS interruption to investigate radiation safety faults. An attempt to parasite off of a production target installed in the A-line during heavy-ion running for experiment E858 was not successful due to a factor of 10^4 lower count rate than during normal A2 running with proton primary beam. Data-taking will therefor have to await the FY91 SEB cycle.

F. Tracking Chambers for Background Measurements

We proposed last year to replace the PDT arrays with more suitable tracking chambers as a part of the initial measurement program. We also argued that we needed to employ a set of chambers better matched to both the size of the absorber/calorimeter and to the acceptance of a dipole to be used during the second major phase of this measurement program. In order to determine the momenta of the particles exiting from the absorber/calorimeter, it will be necessary to track the particles through a dipole magnet. This cannot be accomplished with the PDTs due to their large size and large wirespacing. We propose to locate the magnet just downstream of the first hodoscope (marked "T1" in Figure 1). We will place the chambers in 4 packages, two each upstream and downstream of the dipole. A starting point for this work is the (projective geometry) drift chambers built by the MIT group for E802/859. We have begun construction of 32 planes of 100 cm x 100 cm chambers. These are grouped in 4 sets of 8 planes, with each set having x, x, x', y, y, y', u and v planes. Design of these chambers has begun, following the successful design of drift chambers used in E802/E859. The wire spacing (and thus drift cell size) is taken as 4 cm; each chamber will have 25 sense wires, giving a total of 800 sense wires for the 32 planes. Field-shaping wires and the wire preamplifier plus discriminator electronics will follow the E802 design. Readout will be via multihit TDCs, such as the FASTBUS TDCs made by LeCroy.

The design of these chambers has begun. Chamber frame construction, wire stringing and crimping, and electronics construction will continue through the rest of this fiscal year with the major effort occurring in the last three months of the fiscal year. Commissioning of the chambers and preparation of support frames and installtion into the A2 area will occupy several months at the beginning of next fiscal year. We plan to have the chambers running in the test setup by the early part of the next AGS SEB period.

XII. REFERENCES

1. T. Matsui and H. Satz, Phys. Lett. **178B**, 416 (1986).
2. Proceedings of the RHIC Workshop, April 15-19, 1985, Brookhaven National Laboratory Report, BNL-51921.
3. Proceedings of the Second RHIC Workshop, May 25-29, 1987, Lawrence Berkeley Laboratory Report, LBL-24604.
4. Proceedings of the Third Workshop for a Relativistic Heavy Ion Collider (RHIC), BNL-52185.
5. Arie Bodek, University of Rochester preprint UR-911, ER13065-412.
6. F. A. Harris et al., Nucl. Instrum. Methods **103**, 345 (1972).
7. Reinhard Leuchs, Diploma Thesis, RWTH Aachen, October 1982 "Measurement of the Hadronic Background in the Identification of Muons" (UA1 muon background tests) (in German; English translation – ORNL/TR-88/31).

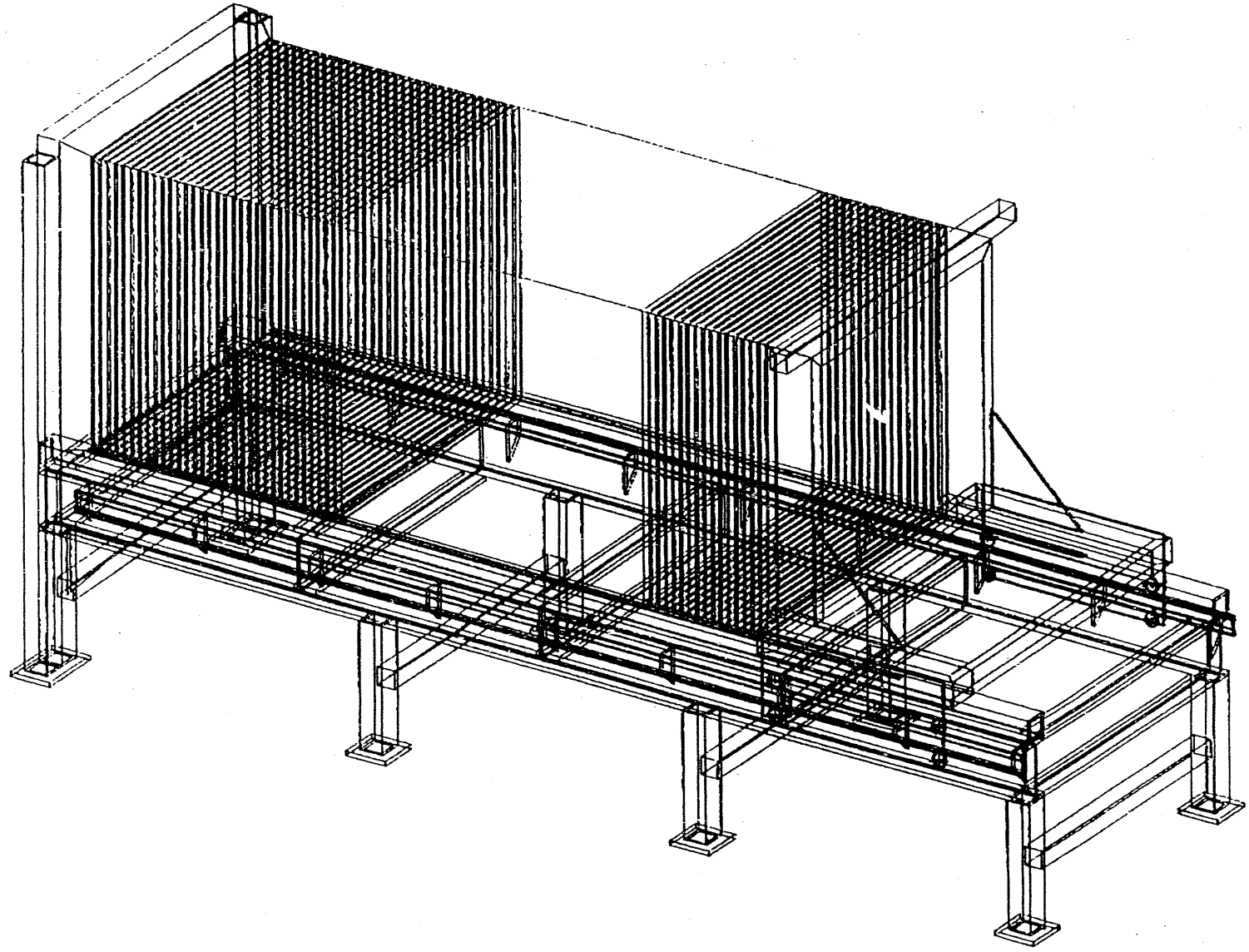

Figure 2. The absorber/calorimeter and support structure are shown. The absorber material is initially steel, and other materials will be substituted. The active layers are plastic scintillator. There are two types of layers: (1) sheets of plastic 1 cm x 110 cm x 120 cm read out from two sides and (2) slats of plastic 1 cm x 10 cm x 120 cm, also read out from two sides. Absorber layers will alternate with scintillator layers, and each fourth scintillator layer will consist of slats. The orientation of the slat layers will alternate between horizontal and vertical.

Construction of a Highly Segmented High-Resolution TOF System

S. Nagamiya†, O. Vossnack,
Y.D. Wu and W. A. Zajc
Nevis Laboratories, Columbia University

C. Chasman and Y. Miake
Brookhaven National Laboratory

J. Engelage
Space Science Laboratory, University of California, Berkeley

†Principal Investigator

1 Introduction

In the construction of a RHIC detector one of the most important efforts is to develop a powerful tracking and particle ID system. During FY90, the present group is focusing on the construction of a highly segmented particle ID device based on time-of-flight (TOF). In later years, we intend to develop a new tracking system to handle high-multiplicity density events.

A typical event in a central Au + Au collisions at RHIC energies will have the following general characteristics:

- $dM_{ch}/d\Omega \sim 300$,
- Momentum of majority of particles < 1.6 GeV/c.

In order to achieve particle ID for these particles, we concluded that a TOF wall with time resolution of $\sigma < 100$ ps with a segmentation of $\sim$ 4cm $\times$ 4cm at a 3 meter distance from the interaction point would do a reasonable job. A straightforward solution is to mount a scintillator directly on a phototube window, as shown in Fig. 1.

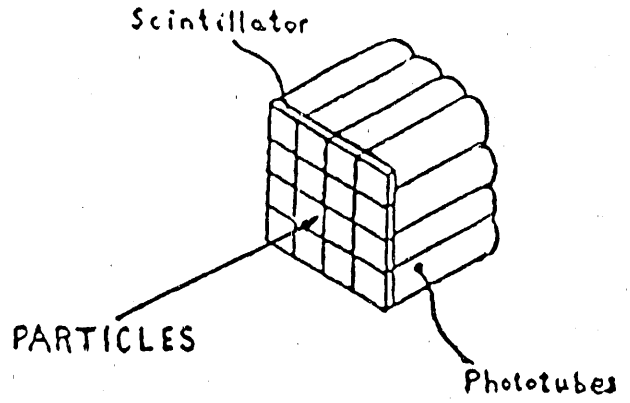

Figure 1: Schematic of a mounting scheme for a segmented TOF wall configuration.

However, this configuration, which we call a "flash-light type" readout scheme, contains a serious problem in that Cerenkov light from the window of the phototube is superimposed on the scintillation light, thereby inducing a timing shift. The outstanding problem then, is to reduce or eliminate this Cerenkov light. One interesting method would be the construction of a new type of phototube which contains a mechanically separated photo-cathode. Before ordering the construction of this type of new phototube, however, we thought that it is important to measure quantitatively the contribution from Cerenkov light so that we clearly specify to the company the thickness of the material on which the photo-cathode should be coated. A Monte Carlo calculation was performed to determine the optimal separation of the photo-cathode from the phototube window. This design is now being fabricated as a prototype by Hamamatsu, Inc.; delivery is scheduled for August 1990.

2 Present Investigations

Before beginning the design a new phototube configuration, we performed a series of measurements on the nature of the Cerenkov light emission in the window glass of the phototube. We have measured the light yield and timing characteristic of the light from the window together with many samples of both scintillator and additional Cerenkov radiators. (Other possible mechanisms are a scintillation light emission, knock-on electron from dynode structures etc.)

2.1 Experimental setup

These tests were made at the AGS A-2 test beam channel, using the experimental setup shown in Fig. 2.

Fig. 3 demonstrates the intrinsic problem found in a "flash-light type" scintillator-tube configuration. A 2cm thick plastic scintillator is mounted 5 cm away from the surface of the tube. For CASE 1, in which the beam hits the center of the tube, the time-of-flight shows a gaussian distribution. (Time-of-flight is obtained from $TEST - (ST1 + ST2)/2.$) However, in Case 2, where the beam hits the edge of the tube, a two peak structure was observed in the TOF distribution. The peak with faster TOF corresponds to the beam hitting the tube and scintillator, while the other case corresponds to the beam hitting the scintillator only. (In CASE2, because of the finite size of the beam defining counter, half of the beam hits the tube and the other half misses the tube.) There is about 1ns timing difference between these cases. It should be noted that this timing jump could not be solved by changing the discriminator threshold levels.

In Fig. 4 , the TOF is plotted as a function of the hit position. The timing jump which occurs when the beam misses the tube can be clearly seen. The effective size of the tube measured by the timing jump agrees very well with the outer diameter of the phototube. Since the dynode structures and photo-cathode has a smaller diameter than the observed distance, we can eliminate the hypothesis that knock-on electrons in the dynode structure are responsible for the shift.

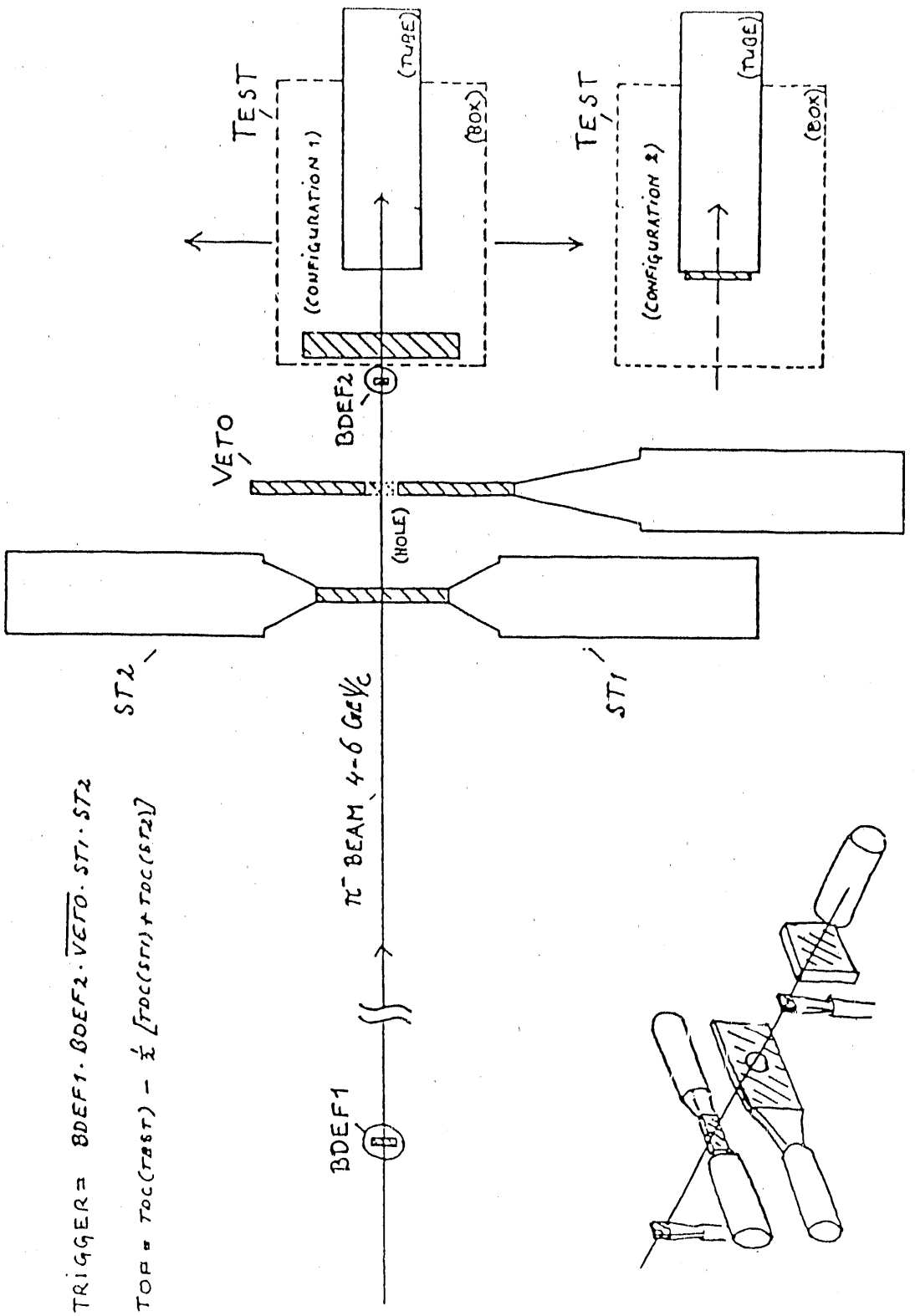

Figure 2: Experimental setup.

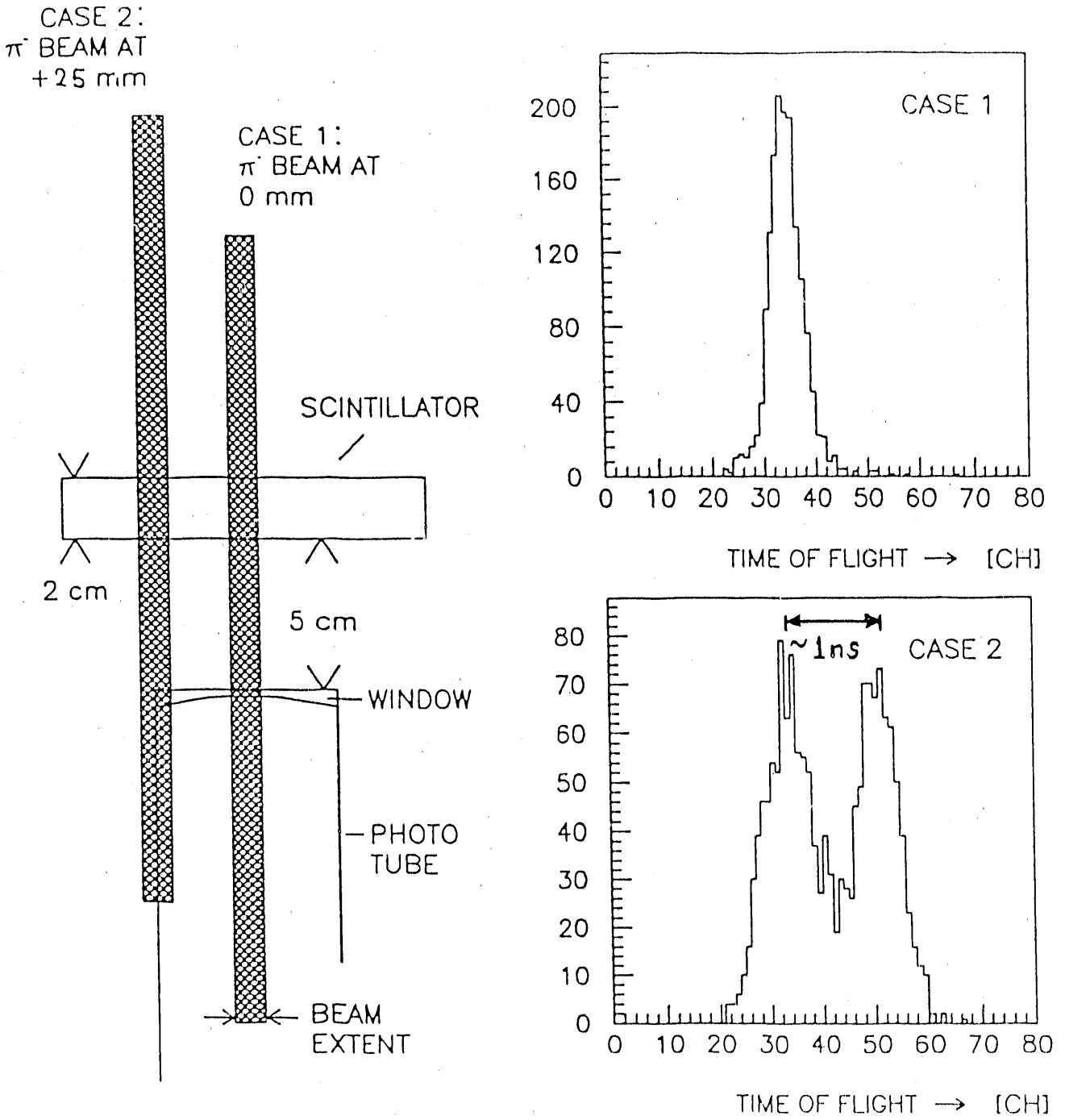

Figure 3: Timing shifts in the "flash-light" configuration. There is ~ 1 ns shift between the signals for those particles which strike both the tube and the scintillator versus those which strike only the tube.

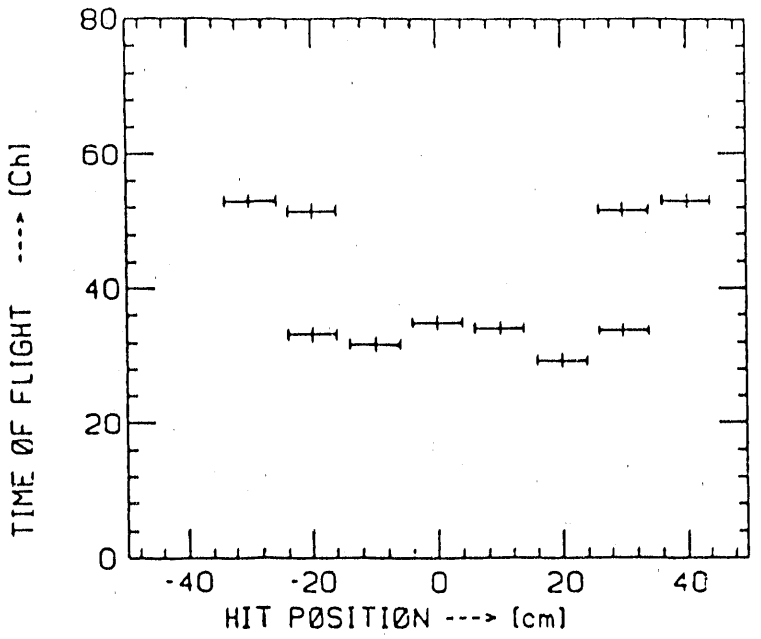

Figure 4: TOF as a function of hit position on the tube.

3 Design of the Prototype

3.1 Light Yield and Width

To study the light emission from the phototube window glass, relative the that from the scintillator, we placed various samples, as listed in Table 1. directly on the tube and measured the ADC and TOF distributions as well as the pulse height (the latter with an oscilloscope). The ratio of ADC's for BC404 and Tube Window respectively is, after normalization to unit thickness, about 20. This value is roughly consistent with the known ratio of Cerenkov to scintillation light emission under these circumstances.

The ratio of ADC value (proportional to the area of the pulse) to pulse height is a measure of pulse width. The pulse width from the Cerenkov light is observed to be a factor of 2-3 times shorter than that from scintillation. We also see from Table I that the Cerenkov light is trapped inside the window glass material if it is placed on the phototube without any optical grease, indicating that total internal reflection provides a possible approach towards suppression of this light.

TABLE 1

Sample	Thickness (mm)	Contact	Pulse Height† (mV)	ADC value‡ (Channel)	ADC/ Pulse Height
Tube by itself	-	-	30	9.3	0.31
Window glass *1	2	grease	50	25.4	0.51
Window glass *1	2	no grease	25	13.2	0.53
Lucite	10	grease	75	44.5	0.59
Lucite	10	no grease	40	20.4	0.51
BC 408	3	no grease	240	266.2	1.11
BC 404	6	no grease	420	370.4	0.88
BC 404	6	grease	800	836.8	1.03

†Pulse height reading on (300MHz) scope after transmission through 200 ft of foamed RG-58.

‡Charge sensitive (current integrating) ADC

3.2 A New Tube with a Separate Photocathode Window

An obvious way to suppress the production of Cerenkov photons in the tube's window is to make it thinner. Also, when the inside surface of the window is flat, virtually all of the Cerenkov light will be reflected from it, as the radiating particle comes in more or less perpendicular to the window and emits its light in a cone with an opening angle that is larger than the critical angle for the glass/vacuum interface. At the same time only part of the scintillation light will be reflected since it comes in from many directions. However, in existing phototubes the inside surface of the window is curved. The idea for a new tube window is sketched in Fig. 5.

From the study described in Section 3.1, if we use 6mm of BC404 scintillator at a distance of 5cm from the phototube window (similar to Fig. 3, then the expected yield will be of order 100-200 mV. If the Cerenkov pulse height can be reduced to roughly 5% of this value we can avoid the corresponding timing shift. This requirement of a 4 mV pulse height (maximum) corresponds to a window thickness of 0.3mm.

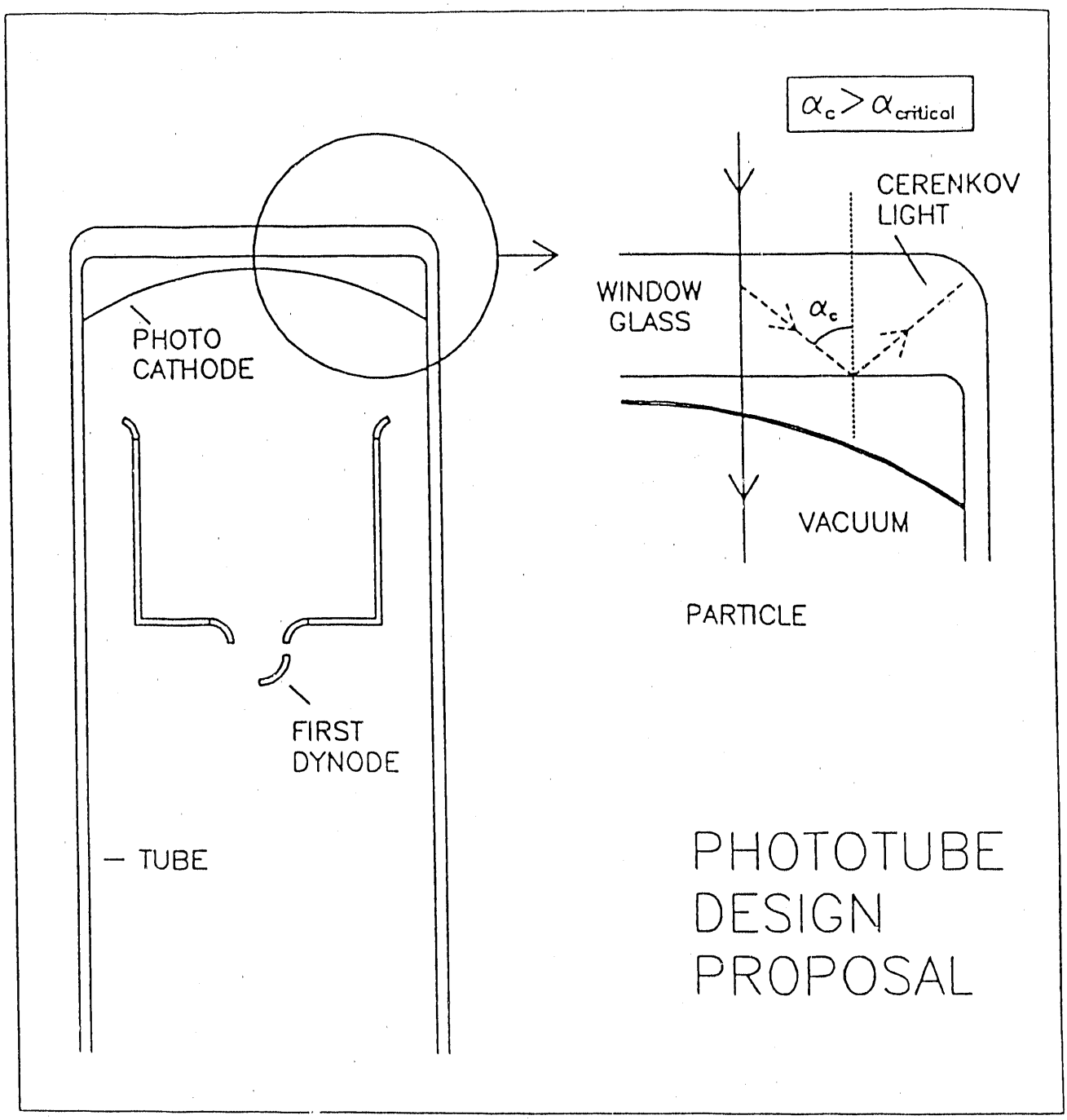

Figure 5: Sketch of proposed phototube design.

The second parameter in the prototype design involves the distance between the phototube window glass and the photocathode. Since the refractive index n of glass is 1.5, Cerenkov light emitted by particles normally incident to the window material will undergo total internal reflection. However, this convenient elimination of the Cerenkov signal is spoiled by non-normal incidence, which is of course to be expected in any realistic detector application. Figure 6 shows the result of a calculation of this effect as a function of the separation d between the window glass and the photocathode. It is clear that a separation of 20mm extends the allowed range of incidence to $\theta \sim 10 - 15°$, which should be adequate for most trajectories encountered at RHIC. This is the value that was selected for the construction of the prototype.

4 Current Efforts and Future Plans

First, a postdoctoral scientist has been hired (T. Nayak), who will concentrate his efforts on the RHIC R&D program at Columbia. He will begin by performing a test of the prototype phototube immediately upon delivery.

One current project involves the development of a constant-fraction discriminator to be mounted directly on the phototube, thereby eliminating the requirement for additional ADC cables in order to perform off-line slewing corrections. This design work in in progress; initial testing will be done with radioactive sources.

A second issue is driven by the question of operating a high-resolution TOF system in a high magnetic field environment. While we attempt to pursue conventional shielding techniques for photomultipliers, we are also investigating alternative systems such as Pestov or multi-channel plate counters that are insensitive to the local magnetic field. These new efforts together with our new initiatives on the electron identification system and a new tracking system will be described in a separate RHIC R&D proposal for FY91.

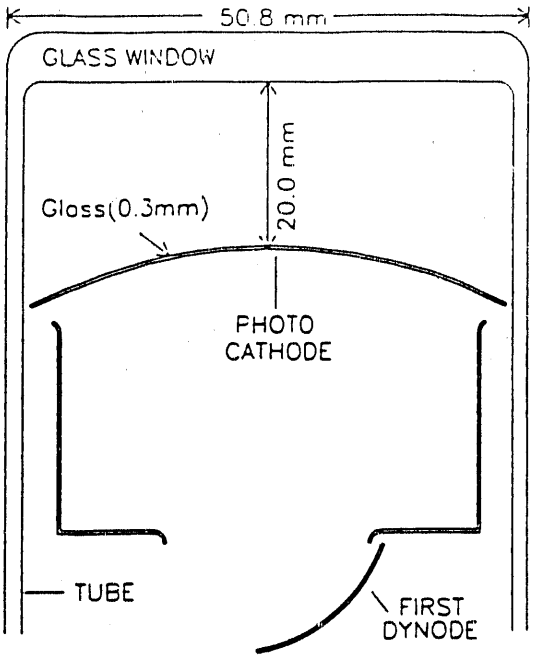

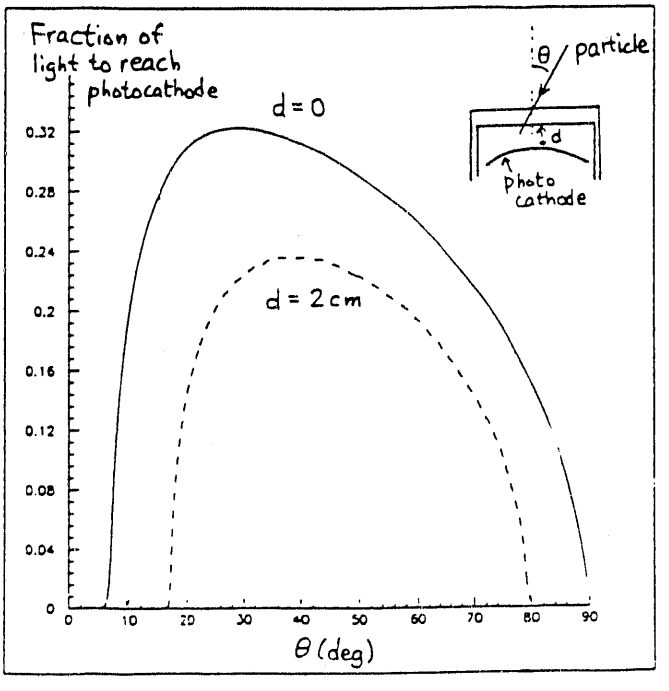

Figure 6: Leakage of Cerenkov light onto the photocathode as a function of incident angle θ. Two different designs are shown; the solid curve corresponds to a photocathode tangent to the window (d=0), while the dashed curve is for d=2mm.

RD-12
R&D Summary
July 1990

June 29, 1990

Progress Report on A Fast, Particle-Identifying Trigger based on Ring-Imaging Cherenkov Techniques

J. Carroll[1], T.J. Hallman[3], G. Igo[1]
P. Jacobs[2], L. Madansky[3], H. Matis[2], C. Naudet[2]
L. S. Schroeder[2] and P. A. Seidl[2]
[1] University of California, Los Angeles, CA 90024
[2] Nuclear Science Division, Lawrence Berkeley Laboratory, Berkeley, CA 94720
[3] Johns Hopkins University, Baltimore, MD 21218

We report progress on the three goals set forth in our proposal: 1. the development of a fast photo-array; 2. the development of a spectrum-splitting mirror; and 3. the development and simulation of fast parallel algorithms for ring finding.

I. Motivation

Experiments which require a large sample of relatively rare events need an efficient (low dead time) trigger that does more than select central collisions. We propose to develop a trigger that will permit sophisticated multi-particle identification on a time scale appropriate for the interaction rates expected at RHIC. The visible component of the ring-image produced by an appropriate Cherenkov-radiator-mirror combination is focussed onto an array of fast photo-detectors. The output of the photo-array is coupled to a fast pattern recognition system that will identify events containing particles of specified types and angular configurations. As a parallel effort, we propose to develop a 'spectrum-splitting' mirror that will permit the ring-image from a single radiator to be used both in this trigger (the visible component of the image) and in a TMAE containing gas detector (the UV component). The gas detector will provide higher resolution information on particle ID and direction with a delay of a few microseconds. This technique will enable nearly optimal use of the information contained in the Cherenkov spectrum.

A fuller statement of the goals of this program is contained in the original proposal, which is attached as an appendix.

II. Progress Toward Stated Goals

We have made a rather slow beginning at the project, in part because of trying to fine tune the administration of the contract to give us the most return for the given number of dollars. Although this effort was successful, we have thus only recently been able to actually spend money. Turning to the individual topics for which support was received -

1. The Development of a Spectrum-splitting Mirror

   We have now received reflectance/transmittance curves for three production trials from Acton Research Corporation, and from the last trial we have received two 6x6" sample mirrors. Examples of these curves and comparisons are shown in Figure 1. To date the achieved 'effective reflectivity' is about 66% with some hope for further improvement. 'Effective reflectivity' is the reflected fraction of those

Cherenkov photons which would be detected in a system limited only by a quartz window (at low wavelengths) and by TMAE's quantum efficiency (at long wavelengths).

The curves from the sample mirrors show some shift toward lower wavelengths at the edges of the plates, probably caused by the source-plate geometry during the deposition process, and thus presumably correctable by using a larger oven. On the other hand it may indicate that mirrors making more more efficient use of the short- wavelength component of the Cherenkov light could be made by tilting the blank during the deposition or by tilting the mirror during use. (These mirrors were designed to be used at incident/exit angles of 45 degrees.)

We will pursue the work with the mirrors in two ways. We will contract for the production of mirrors of even higher effective reflectivity. (We have received indications of interest in this project from a group at Lawrence Livermore National Laboratory which specializes in multi-layer dielectric coatings.) We will also carry out a more extensive characterization of the properties of the sample mirrors that we receive - measure the diffuse reflectivity, the variation of specular reflectivity with position, the figure, etc. We also plan to carry out a test of at least one mirror sample as a part of an operational system with our prototype RICH.

2. The Development and Simulation of Fast Parallel Processing Algorithms for Ring-finding

   Progress toward this goal has been both material and intellectual. On the one hand we have ordered the Vaxstation 3200 that we will use both for simulating various pattern recognition schemes and for data acquisition when we are testing the fast photo-array and prototype RICH - delivery is promised on or before July 24. On the other hand we have significantly improved our knowledge of the field of rapid pattern recognition or "fast classification".

   Rather than focus at the outset on a narrow, specific implementation of a pattern-recognition algorithm, we have chosen to first get an overview of the work being done by others in the field, and then to choose for specific investigation one or more techniques that seem

applicable to our specific problem. Although reading has provided the introduction to the field, we have benefitted most from direct contact with people working full time on pattern recognition. An afternoon spent with the machine vision group at the IBM Almaden Research Laoratory was particularly helpful. In preparation for that meeting we prepared a generalized, low-tech description of our particular problem in order to focus the discussion. This material will be expanded so that we can use it in forthcoming meetings with other specialists.

The survey phase is coming to an end without having found any candidate classification technique that is clearly better than all others, for our specific problem. The general conclusion of the survey is that choice of an optimum technique depends in a highly non-linear fashion on the details of the problem. Even though certain problems have been solved 'adequately', this does not mean that these solutions (or 'similar' ones) are adequate for problems that are superficially similar. One thing that has become quite clear during this investigation is that there is a clear separation between the choice of formal classification technique and its embodiment in hardware, even though some formal techniques may be more easily adapted to particular hardware systems. Also of particular interest to those new to the field is the recognition that 'trainability' is not limited to neural-net implementations but applies to a much wider category of classifiers. Gish and Blanz[1] have made a comparison of three trainable machines for two real-world pattern recognition problems. One of the machines was a 'connectionist' classifier, while the other two were implementations of classical statistical decision analysis methods.

Our plan on how to proceed is to begin with one or more implementations of a modified Hough transform,[2] and then perhaps to try a connectionist or neural-net approach after we have developed some familiarity with those techniques.

3. The Development of a Fast Photo-array.

Heuristic arguments have convinced us that phototubes of approximately 1" diameter will best serve the needs of the tests that we will

be doing, and we are presently arranging for delivery of samples of these tubes that have low noise and good pulse height resolution for single photo-electrons. Some preliminary discussions have been held with the shops about ways of constructing the honeycomb reflector, and this, as well as the bases, will be put into construction as soon as the photo-tube is chosen.

III. Participants

- UCLA -

  J. Carroll, G. Igo ($\approx$ 0.5 FTE)

- UC Lawrence Berkeley Lab -

  H. Matis, C. Naudet, P. Jacobs, L. S. Schroeder, P. A. Seidl

  ($\approx$ 1.5 FTE scientific staff; $\approx$ 0.5 FTE engineering and technician effort)

- Johns Hopkins U. -

  L. Madansky, T.J. Hallman ($\approx$ 0.5 FTE)

- (3 FTEs TOTAL)

References

[1]S.L. Gish and W.E..Blanz, IBM Research Report RJ 6981 (65717) 6-17-89

[2]E.R. Davies, Pattern Recognition Letters 7 (1988) 37-43

MIRROR REFLECTIVITY AT 45 DEG

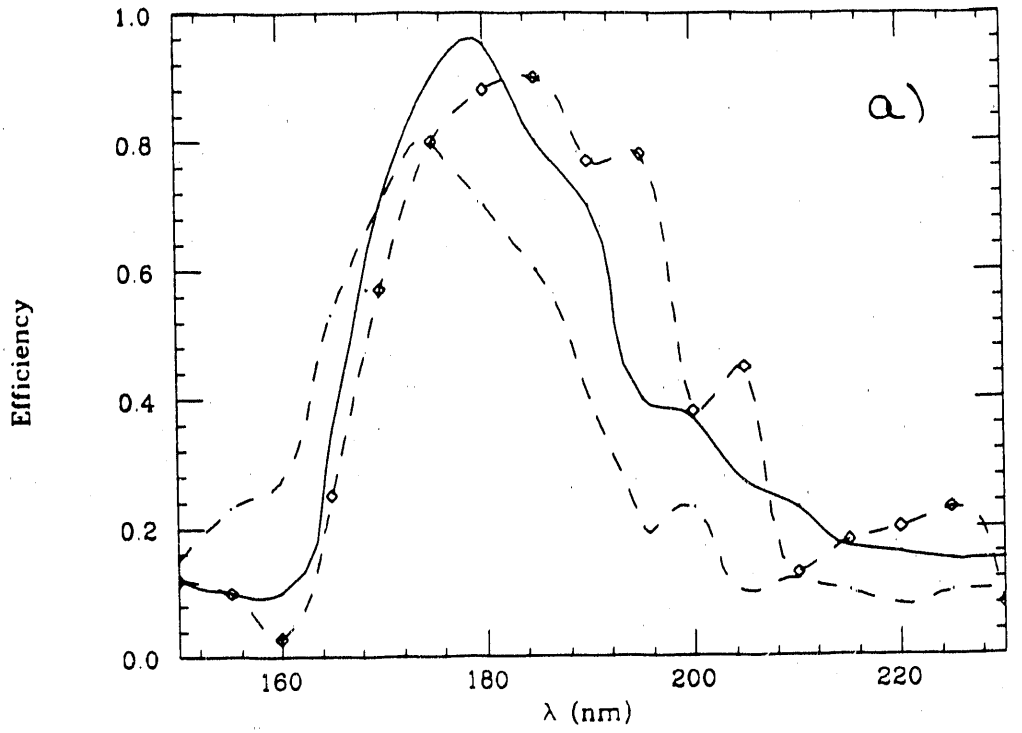

PHOTON SPECTRUM AFTER MIRROR REFLECTION

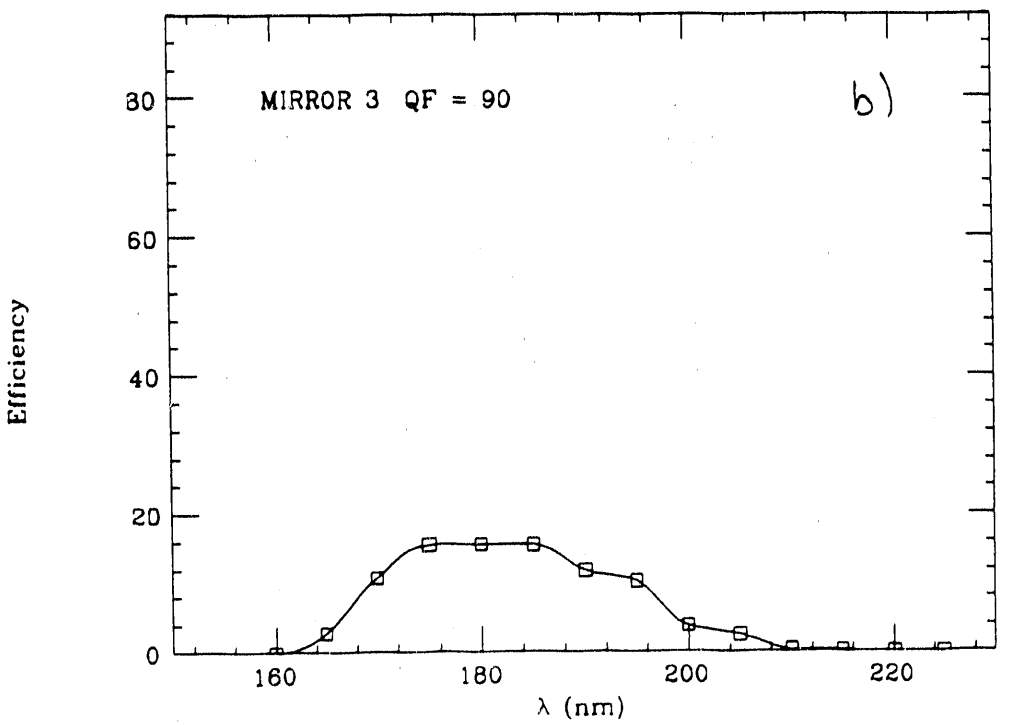

FIG 1 a), b)

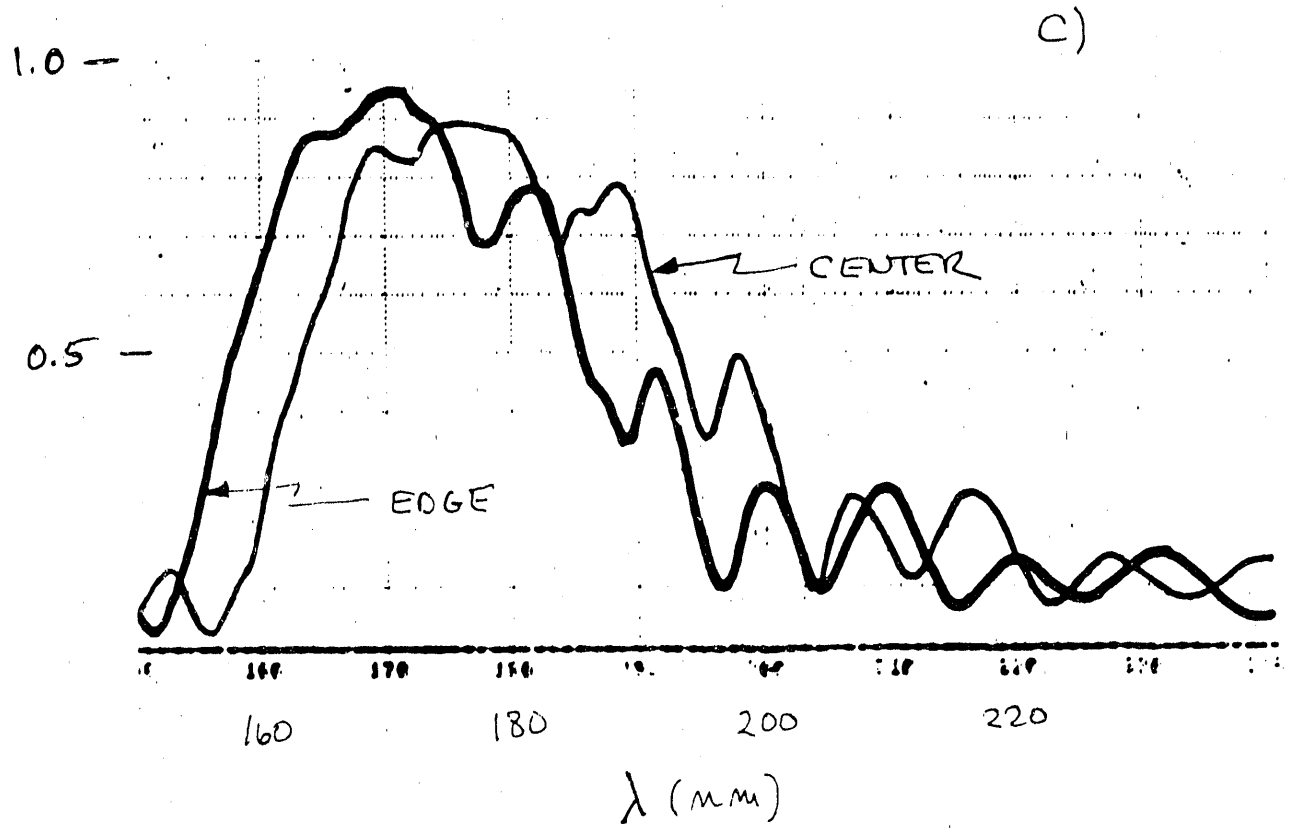

FIG 1 c

Status Report

Highly integrated electronics for a TPC detector RD-13

A.A. Arthur, F. Bieser, B. Hearn, S. Kleinfelder, K. Lee, J. Millaud, M. Nakamura, G. Rai, H.G. Ritter, H. Wieman, Y. Ye

Lawrence Berkeley Laboratory

It is the purpose of our work to develop a complete chain of highly integrated electronics for a RHIC TPC detector. Our long term goal is the production of single integrated circuit that contains several channels consisting of a preamplifier, a shaper and an analog store (switched capacitor array). We proceed by developing and optimizing the individual components separately, using the same process for all three elements so that the integration can be done later.

The RHIC R+D effort has been stimulated by our work on the EOS TPC electronics. For this detector we have developed a preamplifier and a switched capacitor array, components that will be integrated in the RHIC effort, whereas the work on the integrated shaper is funded by the RHIC effort alone. In addition, we can profit from SSC funded development on the switched capacitor array.

Preamplifier

The integrated low noise preamplifier (4 channels per chip) currently being developed for the EOS TPC is the first step towards a completely integrated electronic chain. The noise of each channel is about 700 electrons equivalent rms. It is equipped with a built in channel by channel switchable pulser system for both calibration

and diagnostics. This feature will be included in the fully integrated system.

After several iterations of submissions to MOSIS and subsequent tests and improvements we have established that the preamplifier works and will meet design specifications. We expect to have a production run for the EOS TPC within three months.

Y. Ye is analyzing and studying the design and is preparing a parallel submission to MOSIS with the goal to reduce power consumption and noise.

Analog Memory

During the last year great progress has been made in the development of a switched capacitor array. Prototype chips have been studied and measured in great detail. Since all the specifications for the EOS project have been met, we have gone into production and just received 20 wafers that will be tested extensively. Important device parameters are listed below:

16 signal channels with 256 memory cells each
16 individual outputs plus multiplexed single buffered output
Output impedance 8kΩ
Output swing for positive output 3V
Noise: 0.6mV max
Spatial noise: odd-even effect 25 mV typically, odd-odd or even-even variation <0.6mV rms
Dynamic range: >2000:1
Response to input signal: 16ns
Non-linearity: <10%
Crosstalk: <1%
Write frequency: 10MHz
Output response time: 3.5μs for each channel
Power supply current: analog 20mA, digital 20mA typically
Dynamic shift registers

However, the present design needs improvement, namely the gain bandwidth of the output amplifier could be improved in addition to some modifications to the auxiliary circuits for reset and read-out.

In parallel, development work on the switched capacitor array is being done for future SSC detectors. One project is to modify the shift register so that individual cells can be addressed randomly and to increase the read out speed. Of potentially great benefit for the

RHIC application is another project with the aim to add an ADC to each individual channel.

Shaper Amplifier

The design of a shaper amplifier is complicated since discrete component circuit techniques are not directly applicable to IC design. It is difficult to achieve the precision and consistency for the resistors and capacitors needed for uniformity of the time constants in all channels. We have decided to solve the problem with a simple approach: in parallel to the main capacitors we will use auxiliary capacitors that are switchable via a digital register. This will allow adjustment of individual time constants and to compensate for variations in the process parameters. A simple one stage wide band amplifier, schematically shown below, has been simulated, laid out and submitted to MOSIS. Once this principle works, we still have the choice to design a shaper with all the appropriate poles and zeros or to do only rudimentary shaping and to correct the pulse shape digitally.

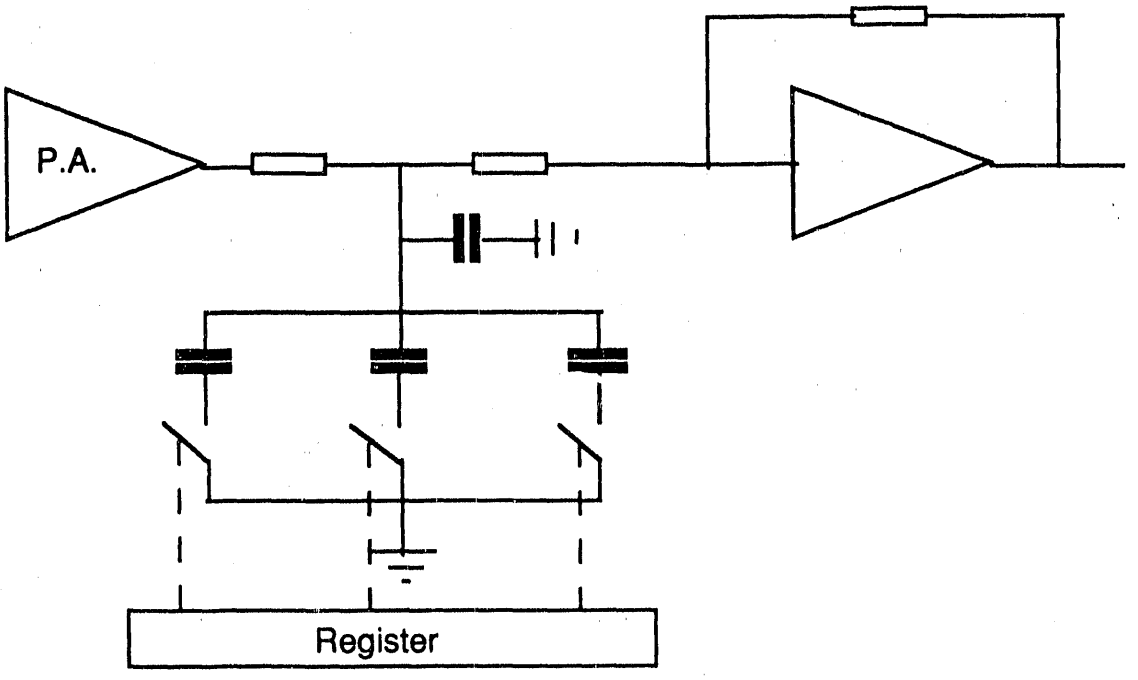

SUMMARY OF RHIC R&D ACTIVITIES IN FY90

Instrumentation & Controls Division
Oak Ridge National Laboratory

G. T. Alley
C. L. Britton
E. J. Kennedy
D. F. Newport
R. A. Todd
A. L. Wintenberg
G. R. Young

This summary highlights accomplishments in RHIC detector electronics development activities conducted at the Oak Ridge National Laboratory since February 1990. Specifically, this work represents the beginning elements of a monolithic readout system that ultimately will be targeted toward readout of streamer tube pads found in the outer muon identifier of the proposed RHIC dimuon experiment. The funding level for this project was $40K. The goal of this work has been to lay the foundation (in terms of system specification, front end circuit development, fabrication process selection, radiation hardness requirements, etc.) for follow-on work that will result in the full implementation of a monolithic readout system, perhaps, applicable to a number of RHIC detector systems. Work has been concentrated in the evaluation and development of appropriate preamp/shaper topologies. A nominal amount of effort has been spent identifying candidate analog memory and ADC topologies for the readout system. The following accomplishments are treated in more detail below:

1.) Fabrication and testing of a CMOS preamp
2.) Design and submission for fabrication of a CMOS preamp with shaping network (submitted on June 27, 1990)
3.) Design of a bipolar preamp using Harris Semiconductor's dielectrically isolated bipolar process (the design is complete, Harris has scheduled the fabrication run in late July)
4.) Evaluation of an existing bipolar preamp for use in RHIC systems
5.) Investigation of candidate analog memory and ADC circuits

I. DESIGN, FABRICATION AND TESTING OF A CMOS PREAMP

ORBIT Semiconductor is offering, through MOSIS, a new "low noise" analog CMOS process for use in non-rad hard prototyping. In order to evaluate this process for RHIC applications, we designed a fast charge sensitive preamp for our pad readout electronics. For a calculated pad capacitance of nominally 10 pF, the preamp noise was targeted at under 1500 e- RMS for a 65 ns CR-RC peaking time. The fabricated preamp had a measured noise of ~5000 e- RMS. This noise appears to be due to a very large 1/f noise contribution (the noise actually had a noise power spectrum of $1/f^{0.8}$). Measured risetime was 3.3 ns and power dissipation was under 3 mW. We have contacted both ORBIT and MOSIS and are presently discussing the noise problem with them. Until this is resolved, no further fabrications will be done using this process.

II. DESIGN AND FABRICATION OF A CMOS PREAMP WITH SHAPER

Our signal processing chain will most likely consist of a charge-sensitive preamp, shaping network (time-invariant), peak detect, analog storage, and ADC together with trigger electronics suitable for the RHIC crossing frequency and trigger decisions. We have designed a preamp/shaper combination as a step toward this eventual configuration. The shaper topology is that of a CR-$(RC)^3$ shaping amplifier with a system charge gain of 0.65 volts/pC, a peaking time of 50 ns, a dynamic range of 10,000, a noise of <2000 e- RMS for a pad capacitance of 10 pF, and a power dissipation of ~4.7 mW (+/- 5 volt supplies). This circuit is being fabricated in ORBIT's 2 micron P-well CMOS technology. The present intent is for a single chip to include four channels of preamplifier, shaper, peak detector, and analog memory with a single ADC servicing all four channels. One four channel CMOS chip will sit at the corners of four pads, process data from those four pads, and send the information out of the detector to the next level of electronics. This circuit was submitted for fabrication on June 27. Parts are expected back in mid to late August.

III. DESIGN OF A HARRIS BIPOLAR PREAMPLIFIER

We have been evaluating the Harris analog design software for the past few months. As part of this arrangement we are going to participate in a run using their rad-hard, dielectrically isolated, bipolar process. Since we had access to this process, we designed a bipolar preamp targeted toward RHIC signal processing electronics. This preamplifier would be used in a somewhat different approach than our all-CMOS design in that the preamp, located on the pads like the all-CMOS version, would send its raw signal out of the immediate vicinity of the detector to a CMOS shaper, peak detector, memory and ADC chip which would be located external to the detector. Comparisons will be made between the bipolar version and the all-CMOS version in terms of noise, power dissipation, and response time. This development is of particular interest since the bipolar process is supposedly rad-hard. The design goals include a charge gain of 0.5 volts/pC, a risetime of ~5ns, and noise at a peaking time of 50ns equal to 1770 e- RMS. The simulations also predict a power dissipation of 12.6 mW (+/- 5 volts). The design is complete and Harris has scheduled the fabrication run in late July.

IV. EVALUATION OF AN EXISTING VTC PREAMP FOR USE IN RHIC SYSTEMS

Several months ago we designed a bipolar preamp using the VTC VJ900 high-frequency complementary bipolar process. As part of our evaluation of various processes and topologies, we configured that circuit as a charge sensitive preamp suitable for RHIC applications. This configuration had a charge gain of 0.5 volts/pC with a measured a risetime of 5 ns using a detector capacitance of 10 pF. Using CR-RC shaping this configuration produced a noise of 5400 e- RMS with a peaking time of 90 ns. The power dissipation was 7.5 mW (+/- 3.5 volts). Tests for radiation effects and high temperature annealing have also been performed. Test data is available.

V. INVESTIGATION OF CANDIDATE ANALOG MEMORY AND ADC CIRCUITS

We have surveyed some of the available literature on analog memories and have concluded that no major development is necessary at this time. We will use some version of a previously published memory that will be customized for our particular system. In particular, the analog pipeline designed for the ZEUS calorimeter appears attractive due to the similar clock speed and technology choice. We are also investigating a parallel run-down (Wilkinson) ADC similar to that being developed for the BVX microstrip detector readout chip. The version used for RHIC would have a clock rate of approximately 10ns and a dynamic range of 10 bits which would result in a conversion time of approximately 10μs. Development of the BVX chip is a joint project between ORNL and FNAL with the ADC development being in an early stage.

END

DATE FILMED

01 / 23 / 91